# FRONTISPIECES

Jan. 27, 1841

'.... it proved to be a mountain twelve thousand four hundred feet of elevation above the level of the sea, emitting flame and smoke in great profusion,.....'

Jan. 28, 1841

'The discovery of an active volcano in so high a southern latitude cannot but be esteemed a circumstance of high geological importance and interest.... I named it "Mount Erebus",..... At 4 P.M. Mount Erebus was observed to emit smoke and flame in unusual quantities, producing a most grand spectacle. A volume of dense smoke was projected at each successive jet with great force, in a vertical column, to the height of between fifteen hundred and two thousand feet above the mouth of the crater,... ... the bright red flame that filled the mouth of the crater was clearly perceptible; and some of the officers believed they could see streams of lava pouring down its sides until lost beneath the snow....'

<div style="text-align: right">Sir James Ross (1847) (p.216-221).</div>

A view of the Inner Crater of Mt Erebus from the main crater floor showing the lava lake discovered in December 1972 by a New Zealand expedition. The lake has increased in size since the discovery and now occupies about half the area of the inner crater. In the present view lava upwelled in the top right-hand area (referred to as the fish tail) and flowed slowly until disappearing down a cave at the bottom centre of the photo. Vigorous strombolian eruptions from the small vent, in the upper right, hurled molten lava to heights of about 500 m, and forced the cancellation of a planned descent into the Inner Crater by a team of French and New Zealand volcanologists. Photo taken in December 1974.
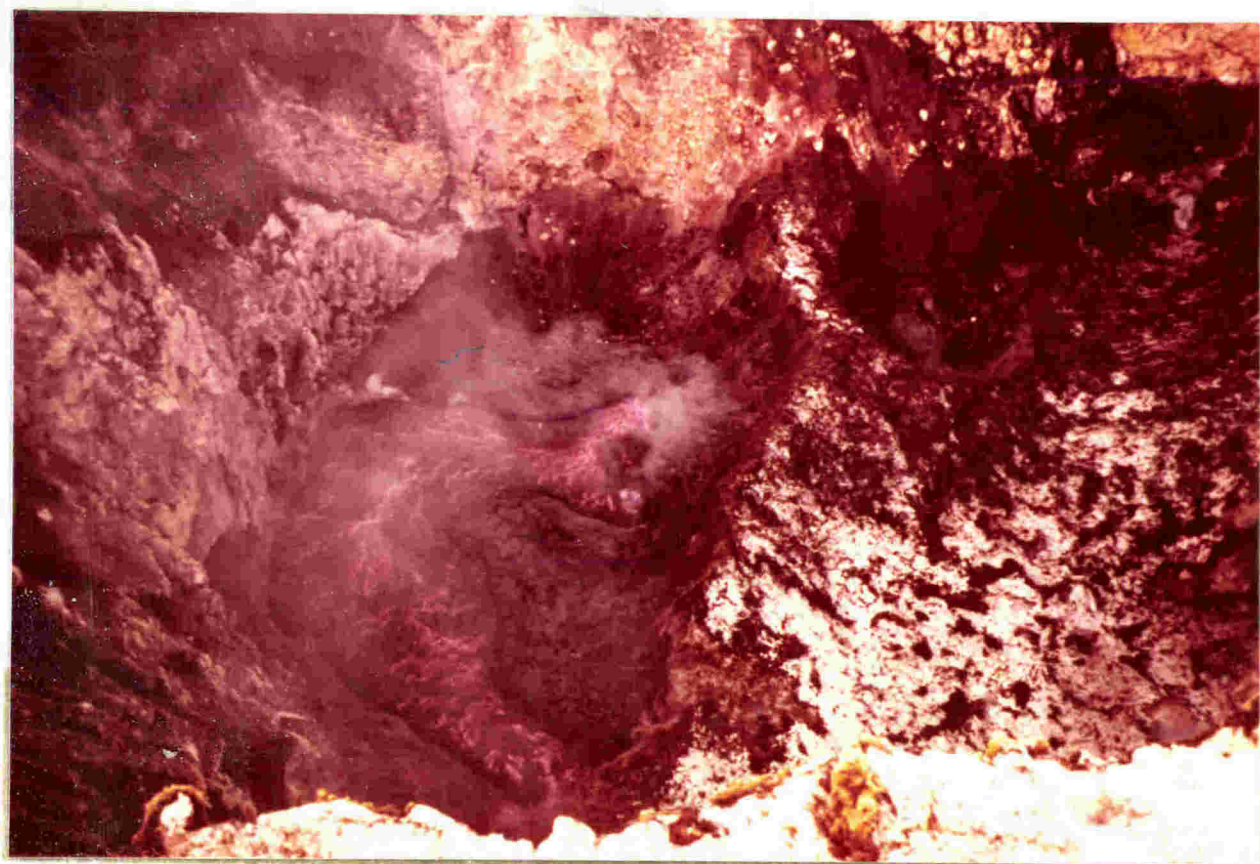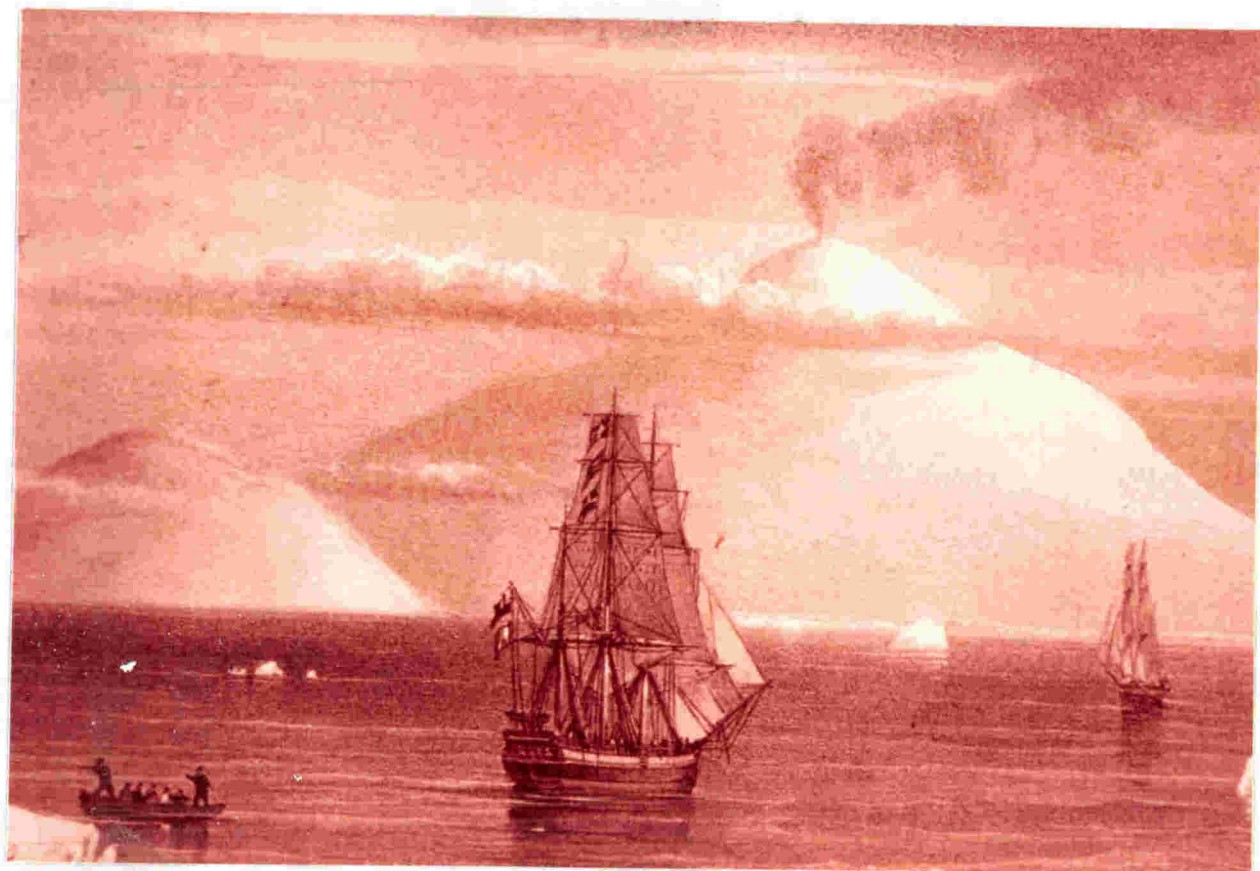
GEOLOGY, MINERALOGY AND GEOCHEMISTRY

OF THE

LATE CENOZOIC MCMURDO VOLCANIC GROUP,

VICTORIA LAND, ANTARCTICA

PHILIP RAYMOND KYLE

A thesis submitted for the degree of

DOCTOR OF PHILOSOPHY in GEOLOGY

at the

VICTORIA UNIVERSITY OF WELLINGTON

FEBRUARY, 1976.

CONTENTS

1972/73

November 1973   62

LIST OF TABLES

LIST OF FIGURES

ABSTRACT

Rocks of the McMurdo Volcanic Group occur as strato-
volcanoes, shield volcanoes, scoria cones, plugs, flows and
volcanic piles up to 4000 m high along the Ross Sea margin
of the Transantarctic Mountains and make up the Balleny
Islands 300 km north of the Antarctic continental margin.
The rocks are predominantly undersaturated and range from
alkali basalt and basanite to trachyte and phonolite. Four
volcanic provinces are recognised; Balleny, Hallett,
Melbourne and Erebus.

The Balleny volcanic province is situated along a
transform fault in the South Pacific Ocean. The rocks are
predominantly basanite.

Hallett volcanic province occurs along the coast of
northern Victoria Land as four elongate piles formed
extensive of hyaloclastites, tuffs, breccias and capped by
subaerial eruptive products. The lavas are a basanite/alkali
basalt-trachyte-quartz trachyte association, and were extruded
over the last 7 m.y.

Melbourne volcanic province stretches across the
Transantarctic Mountains in northern Victoria Land and ranges
in age from 0 to 7 m.y. A Central Suite of intermediate and
trachytic lavas form stratovolcanoes, cones and plugs, while
many small basanite outcrops constitute a Local Suite. Three
lava lineages, resulting from differentiation, are recognised.
1) Lavas at The Pleiades and Mt Overlord consist of a
mildly potassic trachyandesite-tristanite-K-trachyte-
peralkaline K-trachyte lineage. Major, trace and rare earth
element (REE) data suggest evolution by fractional crystallization
of olivine, clinopyroxene, magnetite, apatite and feldspar.
2) A basanite-nepheline hawaiite-nepheline mugearite-
nepheline benmoreite lineage, found at The Pleiades is
believed to result from fractional crystallization of olivine,

clinopyroxene, kaersutite, magnetite, apatite and feldspar.

    3) An oversaturated (Q = 0 to 18%) strongly potassic quartz trachyandesite-quartz tristanite-quartz trachyte lineage occurs at only Mt Melbourne.

    The Erebus volcanic province covers all McMurdo Volcanic Group rocks in south Victoria Land. Mt Erebus itself is still active, but the province includes rocks as old as 15 m.y. Two lava lineages very similar chemically are recognised:

    1) The Erebus lineage consists of strongly porphyritic nepheline hawaiite-nepheline benmoreite-anorthoclase phonolite. Phenocrysts of feldspar, clinopyroxene, olivine, magnetite and apatite are characteristic. The chemistry of the lineage is compatible with fractional crystallization of the phenocryst phases.

    2) A kaersutite lineage consists of basanite-nepheline hawaiite-nepheline mugearite-nepheline benmoreite-kaersutite phonolite-pyroxene phonolite. Clinopyroxene ($Wo_{44-48}En_{40-48}$ Fs_{7-14}) is ubiquitous, kaersutite is common in all intermediate lavas and primary olivine (Fa_{12} to Fa_{26}) is confined to the basanites.
Major element mass balance models for lavas from Hut Point Peninsula suggest formation by fractional crystallization of olivine, clinopyroxene, spinel (includes magnetite and ilmenite), kaersutite, feldspar and apatite. Middle REE show a marked depletion consistent with kaersutite fractionation. REE abundances were evaluated using the mass balance models and published partition coefficients. Calculated REE abundances show excellent agreement with the measured values. Abundances of "incompatible" elements Pb, Rb, Cs, Th and U are not consistent with the models and "volatile enrichment" processes are invoked to explain their abundances.

    Intermediate lavas of the kaersutite lineage are rare in the Erebus volcanic province, occurring only at Hut Point Peninsula and Brown Peninsula. At other areas basanite and phonolite lavas predominate. However these are considered to form by fractional crystallization processes similar to Hut Point Peninsula lavas.

Erebus lineage lavas differentiated at higher temperatures and lower P_{H_2O} than those of the kaersutite lineage, which characterise the periphery of Ross Island. REE abundances and comparison with experimental melting studies indicate DVDP basanite originated by a low degree of partial melting (1-5%) of a hydrous garnet peridotite mantle at pressures of 25-30 kbars. These data suggest that Ross Island is the site of a mantle plume with a diameter of about 100 km and centred on Mt Erebus.

ACKNOWLEDGEMENTS

1.

CHAPTER ONE

INTRODUCTION

Alkali volcanism has been widespread in Antarctica
and its offshore islands during the Late Cenozoic, occurring
in three broad regions (Fig. 1.1):
    i.   the Antarctic Peninsula;
   ii.   Marie Byrd Land;
  iii.   Victoria Land and the Balleny Islands.
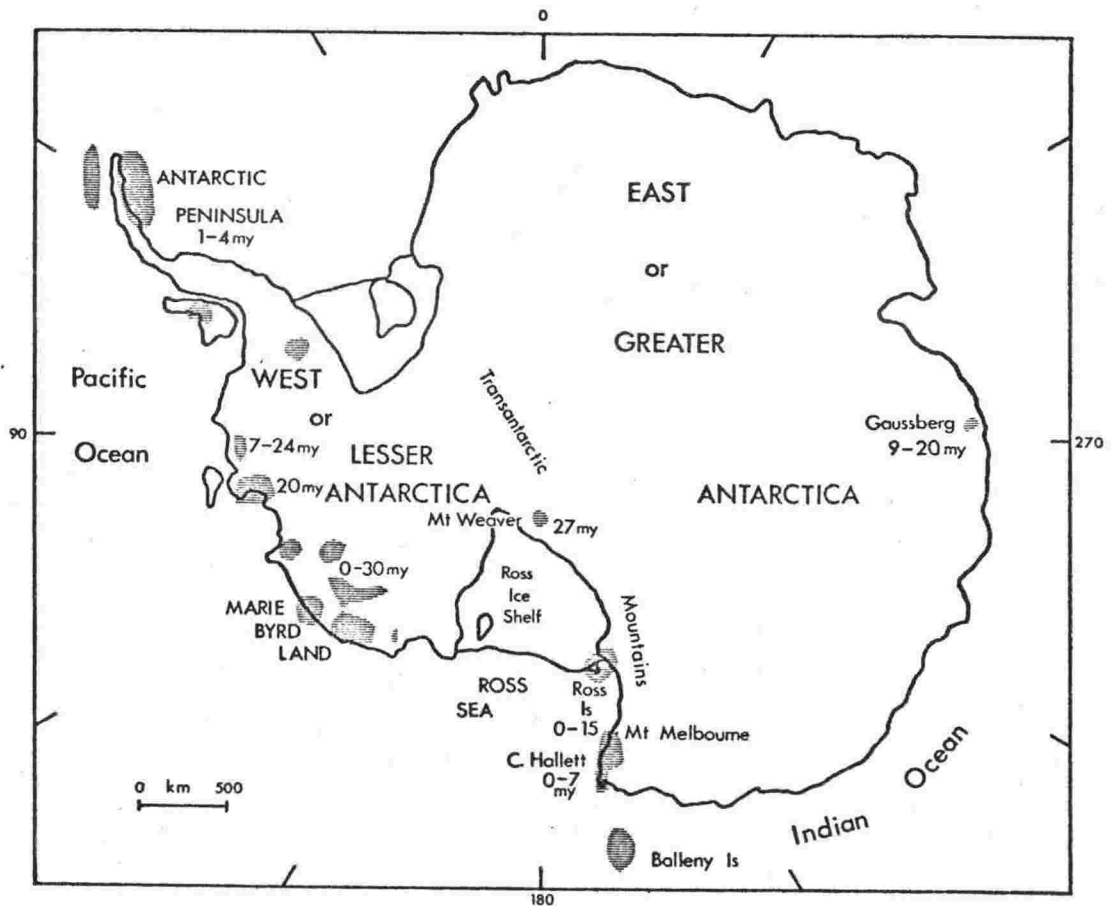
FIGURE 1.1 Distribution of Late Cenozoic volcanic rocks in Antarctica
            (after Craddock, 1972). Radiometric age determinations
            from Armstrong (1975), Bull and Webb (1973), Craddock
            (1972) and LeMasurier (1975 personal communication).

Lavas from the Antarctic Peninsula are mildly alkaline and consist of hawaiite, mugearite and trachyte (Baker, 1972). The Marie Byrd Land and Victoria Land volcanics are chemically and petrographically similar and occur in a similar tectonic environment. They consist of alkaline basaltic to trachytic and phonolitic lavas which are generally more undersaturated than the Antarctic Peninsula rocks. Although the Marie Byrd Land and Victoria Land volcanics are separated by the Ross Sea, Boudette and Ford (1966) consider they are part of one large petrographic province. The crustal structure between the two areas is poorly understood, because of sea and ice cover, but as alkali volcanism is usually associated with tensional environments (Sorensen, 1974), they may be related to a common tectonic feature, such as a zone of rifting.

Late Cenozoic volcanic rocks of Victoria Land, islands in the western Ross Sea and the Balleny Islands constitute the McMurdo Volcanic Group* (Harrington, 1958; Antarctic Lexicon, in preparation). Treves (1967) described small volcanic cones at Mt Weaver in the central Transantarctic Mountains (Fig. 1.1), which he considered were correlatives of the McMurdo Volcanic Group (Goldich *et al.*, 1975). A K/Ar age of 27.3±2.7 m.y. (Bull and Webb, 1973) places them well outside the age range (0-15 m.y.) of the McMurdo Volcanic Group and they are therefore not considered correlatives (Antarctic Lexicon, in preparation). The McMurdo Volcanic Group extends from the Balleny Islands southward for over 1400 km to the strato-volcanoes in the McMurdo Sound area (Fig. 1.2), and contains two active volcanoes - Mt Erebus and Mt Melbourne. The McMurdo Volcanics are one of the larger Late Cenozoic alkali volcanic provinces in the world. In terms of present plate tectonic theory, the volcanics are all intra-plate. The reason for the siting of these volcanoes has not been satisfactorily explained by any plate tectonic model.

It was realised at the beginning of this study that it would be impossible to examine, even in general terms, all areas of the McMurdo Volcanic Group. Several centres were

---

* Referred to elsewhere in this thesis as the McMurdo Volcanics.
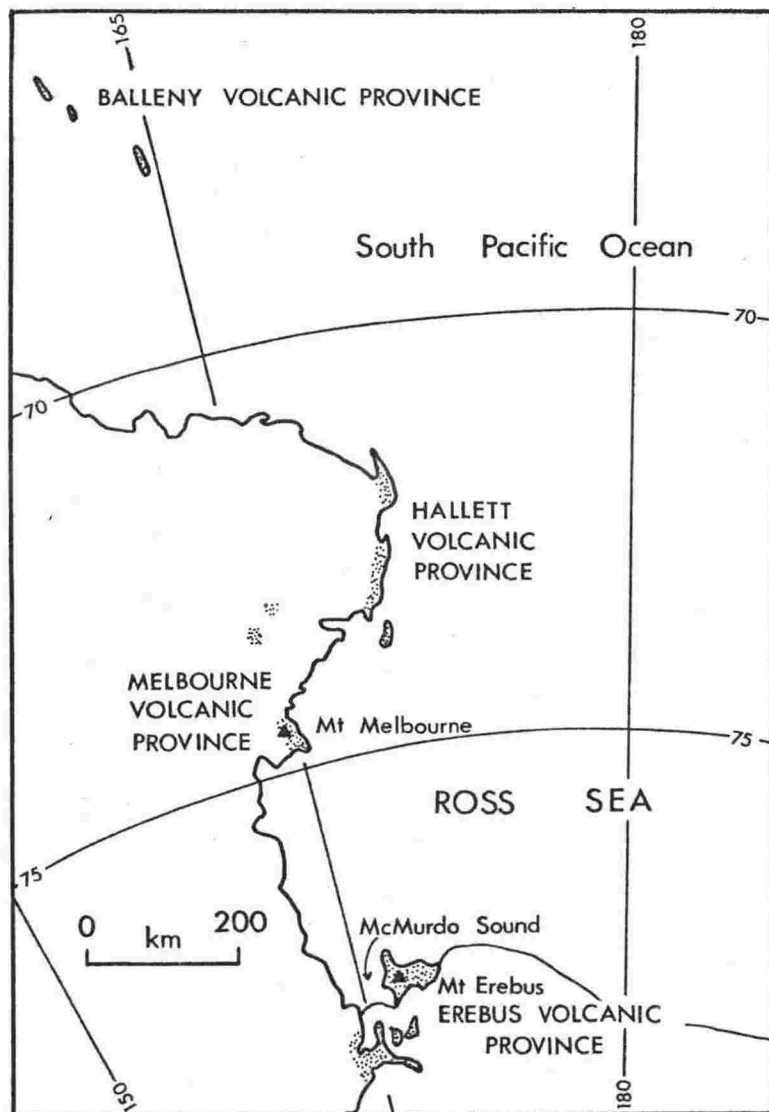
FIGURE 1.2 Distribution of the McMurdo Volcanic Group in Victoria Land, the Balleny Islands and islands in the western Ross Sea.

therefore selected for detailed geochemical and mineralogical investigation to represent the area as a whole. Similarities with the remaining areas were made by comparing the results of the detailed study areas with available data from the other areas. Detailed studies were made of The Pleiades, northern Victoria Land, at Hut Point Peninsula, and to a lesser extent Mt Erebus, McMurdo Sound area.

Considerable areas of exposed McMurdo Volcanics in the McMurdo Sound area are unexplored, and offer areas for future study. Such areas include Mt Discovery, Minna Bluff, Mason Spur, extensive areas of basaltic scoria cones north and west of Koettlitz Glacier and the upper slopes of Mt Morning and Mt Terror (Fig. 3.10).

This study is primarily geochemical and mineralogical, with emphasis on the petrogenesis of the lava sequences in each of the study areas. It has built on the field work and descriptive petrology of earlier workers but also includes additional field work which is described below. A synthesis of old (early 1900's) and new (since 1956) chemical data has been made.

Quantitative mineral chemistry has been interpreted to determine the physical conditions under which differentiation has occurred and as an input for least squares mass balance calculations of differentiation processes. The variation of mineral chemistry with changes in lava chemistry was also examined.

This study has been confined to the volcanic rocks, with only rare exceptions. A large number of highly variable plutonic inclusions, which occur particularly in the lavas from the McMurdo Sound area, have not been examined. No effort was made to examine the use of the McMurdo Volcanics in under-standing the glacial history of Antarctica, but obvious inferences or conclusions have been made.

Field Work

Four consecutive austral summer field seasons from 1971/72 to 1974/75 were spent in Antarctica as a member of Victoria University of Wellington Antarctic Expeditions (VUWAE) 16 to 19. Field work associated with this thesis has been on two main projects:

    i. Dry Valley Drilling Project (DVDP) (McGinnis *et al.*, 1972) as site geologist for holes 1, 2 and 3. 118 days were spent examining and logging core (Treves and Kyle, 1973a; Kyle and Treves, 1974a);

    ii. Erebus Project during which the activity of Mt Erebus was observed (Giggenbach *et al.*, 1973; Kyle, 1975) in three consecutive seasons (total 45 days) from a camp at 3600 m on the summit cone.

Field investigations of the McMurdo Volcanics in northern Victoria Land, Ross Island and Mt Morning totalled only 29 full field days.

In all areas examined exposure was poor and either snow or morainic material predominated. Mapping was difficult because small scale maps (less than 1:250,000) were not available and aerial photography coverage was poor and often confined to oblique photographs. Some vertical photographs from trimetrogon runs were available however. A sketch map for The Pleiades area was drawn using vertical and oblique aerial photographs and radial triangulation.

Previous Work

Previous information has come from the field work and collections made between 1840 and 1916 by the 'heroic era' expeditions, and from the 'post-IGY' (International Geophysical Year 1957-58) polar explorations. The older works are summarised by Smith (1954, 1959), Gunn and Warren (1962) and Stewart (1956); the latter also listed all published chemical analyses.

The most comprehensive studies of the post-IGY period
were made by Harrington *et al.*, (1967) and Hamilton (1972),
on four large piles of predominantly basaltic lavas which
stretch southward from Cape Adare to Coulman Island (Fig. 1.2).
Hamilton (1972) presented field, petrographic and geochemical
data on samples collected during a helicopter reconnaissance of
northern Victoria Land. Thirty four high quality whole-rock
chemical analyses were published, though deductions based on
them must be considered tentative as they represent samples
from an area in the order of 2000 km^2.

The McMurdo Volcanics in northern Victoria Land, from
Mt Melbourne through to The Pleiades (Fig. 1.2), have been
described by Nathan and Schulte (1968) and are discussed in
detail in Chapter 3.

Field mapping and, in some cases, petrographic studies
by Cole and Ewart (1968), Treves (1962), Cole *et al.*, (1971),
Wellman (1964) and the brief summaries of individual areas by
Treves (1967) clearly indicate an alternating basaltic and
phonolitic eruptive sequence in the McMurdo Sound area.
Unpublished B.Sc.(Hons.) projects (Kyle, 1971; Adams, 1973;
Luckman, 1974) have examined some of these eruptive events in
more detail in the field, petrographically and geochemically.

A description of the anorthoclase phenocrysts and a
discussion of the development of peralkalinity in the Mt Erebus
anorthoclase phonolite lavas have been given by Boudette and
Ford (1966) and Carmichael (1964) respectively.

The abundant plutonic inclusions in lavas from Hut
Point Peninsula and basaltic cones along the east flank of
the Royal Society Range (Fig. 3.10) were described by Forbes
(1963), Forbes and Banno (1966) and McIver and Gevers (1970).

Geochemical and mineralogical interest in the McMurdo
Volcanics has been stimulated by activities associated with the
Dry Valley Drilling Project. Although little has been
published the abstracts of McMahon and Spall (1974a, 1974b);
Treves and Ali (1974); Kyle (1974a); Kurasawa (1974);
Browne (1974); Stuckless *et al.*, (1974a, 1974b); Goldich
et al., (1973); Sun and Hanson (1974a, 1974b, 1974c);

Weiblen *et al.*, (1974a, 1974b) indicate a large amount of current research.

During the final stages of preparation of this thesis (September, 1975) a major paper on the geochemistry of the McMurdo Volcanic Group from Ross Island and vicinity by Goldich *et al.*, (1975) was published. Reference to this paper is restricted to discussion in the final part of this thesis.

CHAPTER TWO

Structural Control of Volcanism in the
McMurdo Volcanic Group, Antarctica

by

P. R. Kyle and J. W. Cole

This paper has been reprinted from
Bulletin Volcanologique

Structural Control of Volcanism in the Mc Murdo Volcanic Group, Antarctica

P. R. KYLE and J. W. COLE

Structural Control of Volcanism in the Mc Murdo Volcanic Group, Antarctica

P. R. KYLE and J. W. COLE

Department of Geology, Victoria University, Wellington,
New Zealand

Abstract

Volcanoes of the McMurdo Volcanic Group occur in four volcanic prov-
inces: Balleny, Hallett, Melbourne and Erebus. The Balleny and Hallet provinces
are distributed along the Balleny Fracture Zone and Hallett Fracture respec-
tively. Stratovolcanoes within the Melbourne province may be associated with
north to northwest-trending grabens and faults in northern Victoria Land.
The Erebus volcanic province is located at the intersection of the Rennick
Fault and northeast trending faults along the central Transantarctic Mountains.
Within the Erebus province, volcanic centres around Mt. Erebus and Mt. Dis-
covery possess radial symmetry which may be related to radial fractures at
approximately 120° to each other.

Introduction

The Mc Murdo Volcanic Group (HARRINGTON, 1958; HARRINGTON
et al., 1967; NATHAN and SCHULTE, 1968) consists of under-saturated
alkaline volcanics which form the Balleny Islands, and the strato-
volcanoes and isolated cones in northern Victoria Land and the
Mc Murdo Sound region. The Group forms part of a large Late
Cenozoic alkaline volcanic province which includes the Quaternary
(Byrd) volcanics of Marie Byrd Land (HARRINGTON, 1965; BOUDETTE
and FORD, 1966). The rocks range in composition from alkali olivine
basalt and basanite to trachyte and phonolite, and have been erupted
over the last 15 m years (K/Ar dates from R.L. ARMSTRONG, written
communication). Mt. Erebus, the main volcano of Ross Island, was
recently observed to contain a small lava lake in which frequent
Strombolian type eruptions occurred (GIGGENBACH et al., 1973).

TREVES (1967) has described a few small cones of olivine basalt
and pyroclastic rocks from Mt. Weaver (Lat. 87° S; Long. 152° W) and

1

correlated them with the Mc Murdo Volcanic Group. However because of their limited extent and separation from other rocks of the Group they are not included in this discussion.

For the purposes of the discussion rocks of the Mc Murdo Volcanic Group are divided into four informally named volcanic prov-
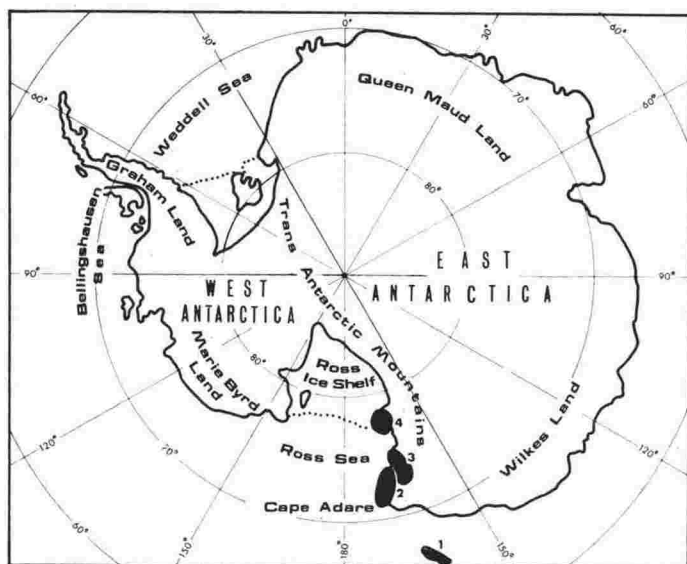
FIG. 1 - Map of Antarctica showing distribution of provinces of the McMurdo Volcanic Group. 1 - Balleny province; 2 - Hallett province; 3 - Melbourne province; 4 - Erebus province.

inces on the basis of their areal distribution (Fig. 1). The Balleny and Hallett Provinces are the same as those designated by HAMILTON (1972), and the Erebus province is renamed from Hamilton's « Mc Murdo » volcanic province to avoid confusion with the Mc Murdo Volcanic Group. A fourth province is proposed for the volcanics between Mt. Melbourne and The Pleiades (NATHAN and SCHULTE, 1968), and is named the Melbourne volcanic province.

Regional Structure

FORD (1972) has reviewed previous literature on the tectonic framework of Antarctica and concludes that Antarctica can be subdivid-

ed into three broad tectonic provinces: a « Pacific margin " Andean " province » in Graham Land; a « Ross-Weddell province » for the west Antarctica-Transantarctic Mountains area, and an « Indian-Atlantic province » for the older cratonic area of East Antarctica. The junction between the last two provinces is along the Transantarctic Mountains front for most of the length but the form of this boundary is a cause of much speculation. We believe that the front represents a major fault or fault zone, but there are few locations where this can be clearly demonstrated. However at the mouth of the Shackleton Glacier, Beacon strata have been downthrown at least 2 km and probably 5 km by a fault subparallel to the mountain front (BARRETT, 1965). Farther north xenoliths of quartzose sandstone comparable to rocks of the Beacon Supergroup exposed in the Transantarctic Mountains occur in volcanic rocks near Cape Royds on Ross Island (THOMSON, 1916), suggesting that Beacon rocks may also have been downfaulted adjacent to Ross Island. On Leg 28 of JOIDES, marbles similar to those outcropping in the Transantarctic Mountains were cored in the Ross Sea (HAYES et al., 1973), again suggesting a major crustal down-warping or fault along the Transantarctic Mountains.

SMITHSON (1972) considers the gravity gradient across Mc Murdo Sound and the Transantarctic Mountains is too large to be explained by faulting alone and that it probably results from crustal thinning from 40 km to 27 km. WOOLLARD (1962) arrived at the same conclusion after considering both seismic and gravity data. SMITHSON (1972) however goes an to explain the crustal thinning by plate-plate collision and subduction along the front of the Transantarctic Mountains in Late Precambrian times. The present authors do not agree with this interpretation but believe that the Ross Sea more likely represents an area of crustal extension possibly due to rifting.

In northern Victoria Land the topographic break on the east side of the Transantarctic Mountains is also pronounced, and is considered to represent the surface expression of the Hallett Fracture (Fig. 2), a major structural break which perhaps developed during the initial separation of Australia and Antarctica.

Evidence of crustal extension also occurs in the Transantarctic Mountains of northern Victoria Land where the Rennick Fault crosses the mountains diagonally and forms the eastern boundary of a graben here termed the « Rennick Graben » (Fig. 2). The Rennick Fault may form a continental extension of the Tasman Fracture Zone proposed

3

by HAYES and CONNOLLY (1972), and, if so, the Rennick Graben may have developed at the same time as the Otway Rift and associated structures of S.E. Australia (GRIFFITHS, 1971; HOUTZ and MARKL, 1972).
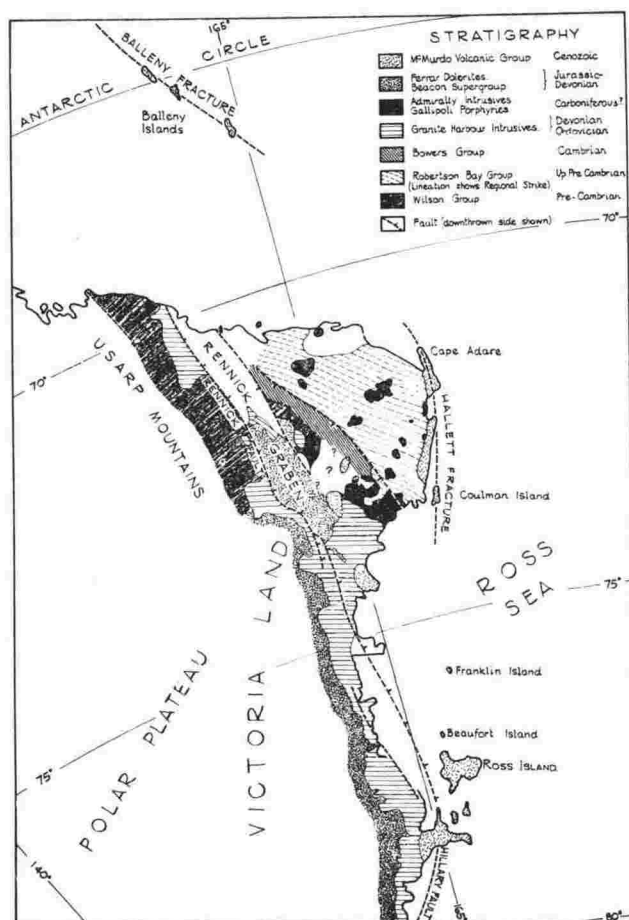
FIG. 2 - Simplified geological map of Victoria Land and the Balleny Islands, to show relationship of volcanism to structure.

Structural Control of Volcanism

Previous syntheses have suggested that the volcanoes of the Mc Murdo Volcanic Group can be related to one major structural trend. HARRINGTON (1965) calls this the Mc Murdo Volcanic Arc; Mc IVER and GEVERS (1970) the Mc Murdo volcanic belt, while GUNN

(1963) related the distribution to the Ross Sea Trough. Reconnaissance mapping (CRADDOCK, 1972) and aeromagnetic surveys (ROBINSON, 1964) however show the volcanics to be discontinuous and they are therefore probably related to several structural trends related to the four volcanic provinces shown in Fig. 1.

Balleny Volcanic Province

Volcanoes of the Balleny Islands are linearly distributed along the Balleny Fracture Zone (FALCONER, 1972), an oceanic fracture which is probably a transform fault offsetting the Indian-Antarctic mid-ocean ridge (GRIFFITHS and VARNE, 1972; FALCONER, 1972). The Balleny Islands are considered by these authors to be situated at the southern end of this fracture which from rates of spreading would suggest a maximum age of 10 million years (GRIFFITHS and VARNE, 1972).

Hallett Volcanic Province

The Hallett province is also a linear feature comprising four elongate volcanic piles along the north-eastern coast of northern Victoria Land (HARRINGTON et al., 1967; HAMILTON, 1972). Harrington et al. (1967) suggest that « tensional rifts in a monoclinal flexure would provide egress for the volcanics » but there is no geological evidence for such a flexure, and it is more likely that the volcanoes are related to a major fracture which is here termed the « Hallett Fracture ». It is possible that it may be the southern continuation of the Balleny Fracture as the northern end has the same trend as the Balleny Fracture. However further bathymetric or magnetic data in the intervening area is necessary to confirm this correlation.

Melbourne Volcanic Province

NATHAN and SCHULTE (1968, p. 943) consider that the volcanoes between Mt. Melbourne, The Pleiades and northwards form a definite curvilinear trend which suggests « a deep-seated crustal rift or tension zone roughly along the main ridge of the Campbell-Aviator Divide », but noted there was no structural evidence of such a zone. The present authors consider that the locations of these volcanoes are primarily controlled by north to northwest trending graben and fault structures in northern Victoria Land (Fig. 2). The stratovolcanoes of

Mts. Melbourne and Overlord are associated with the Rennick Graben, and the volcanoes of The Pleiades and minor eruptive centres to the northeast possibly with the smaller NW trending faults between the Freyberg and Victory Mountains (Fig. 2).

Erebus Volcanic Province

Mc IVER and GEVERS (1970) have suggested that Mt. Erebus may lie at the intersection of a major north-south lineament and a subsidiary east-west fracture which passes through Mts. Terror, Terra Nova, Erebus and the smaller volcanic cones in the Taylor Valley. The present authors consider it more likely that Mt. Erebus and Mt. Discovery are situated at the junction of the southern extension of the Rennick Fault and a NE trending structure which in part may be the northern extension of the Hillary Fault shown by GRINDLEY and LAIRD (1969).

Symmetry of Volcanism in Erebus Volcanic Province

Subsidiary centres and lines of cones on Ross Island have a radial symmetry around Mt. Erebus (Fig. 3), and their distribution may thus be related to radial fractures at approximately 120° to each other. A similar structural relationship occurs around Mt. Discovery with three radial volcanic lineaments corresponding to Minna Bluff, Brown Peninsula and Mt. Morning. This radial symmetry is considered to result from extension of the crust and is comparable to that associated with the basalt shield volcanoes of Hawaii (WENTWORTH and MACDONALD, 1953; MACDONALD, 1965, 1972). Rift zones at 120° to each other surround calderas at Koolau and Waianae volcanoes in Oahu, at Haleakala on Maui, and around Mauna Kea, Mauna Loa and Kilauea on Hawaii. MACDONALD (1972) suggests that radial fracturing on a small scale is due to lateral thrust caused by the weight of a column of liquid magma in the central pipe conduit. He considers this inadequate at Hawaii however and invokes stretching of the volcano by formation of a near-surface magma reservoir and subsequent fracturing. Such a mechanism is supported by the experimental work of Chertkova, who demonstrated that radial fractures form in paraffin wax when subjected to vertical uplift by a round piston (BELOUSSOV, 1962). The fractures produced tend to be sinuous

and become younger away from the centre of uplift. Experiments by CLOOS (1955) with clay models showed that even slight upward movement of a plug resulted in radial fractures which opened into rift structures with increased uplift.

The lavas at Mt. Erebus, Mt. Discovery and the surrounding areas are predominantly alkali basalt and the differentiates, trachyte and
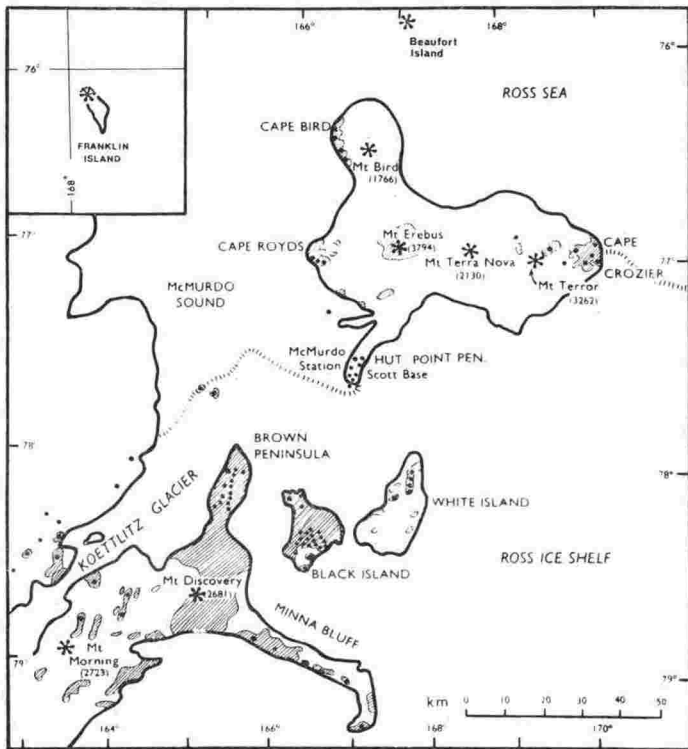
FIG. 3 - Map of Erebus province showing distribution of volcanic centres (indicated by *) and smaller cones (indicated by .). Heights shown in metres.

phonolite. Experimental melting studies on similar alkali basalts suggest that they originate from depths of 50-100 km by partial melting of the mantle (BULTITUDE and GREEN, 1971; GREEN and RINGWOOD, 1967; O' HARA and YODER, 1967). In favourable tensional areas such as a graben or fracture zone the basaltic magma would rise through the mantle into the crust creating pressure and updoming of the

overlying rocks. This updoming would result in the development of radial fractures about the centre of uplift.

In the East African rift valley there is a strong correlation between volcanism and broad topographic domes (KING, 1970). In the Mc Murdo Sound region there are no suitable reference planes older than the main onset of volcanism to determine whether doming has occurred, although submarine lavas (dated at 15 million years) are exposed at an elevation of 400 m near Mt. Morning. WEBB (1972) and VELLA (1969) have described uplift in the region since the commencement of volcanism and this uplift has been interpreted in part as glacio-isostatic and in part tectonic. If the uplift was due in part to the intrusion of magma, it is likely that radial fractures would develop in the upper crust. Magma would travel upwards and along the fractures to form a series of dikes. Where magma reached the surface, stratovolcanoes or lines of cones would form.

Conclusions

The Mc Murdo Volcanic Group is considered to consist of four provinces each of which is uniquely associated with major structural features. Linear basaltic piles in the Balleny and Hallett provinces are associated with major fractures, while the stratovolcanoes of the Melbourne and Erebus provinces appear to be associated with a graben and fault intersection respectively. In the Erebus province crustal doming resulting in radial fractures is postulated to account for the symmetrical radial distribution of volcanic vents around Mt. Erebus and Mt. Discovery.

Acknowledgements

References

BARRETT, P. J., 1965, *Geology of the area between the Axel Heiberg and Shackleton Glaciers, Queen Maud Range, Antarctica, Part 2 - Beacon Group*. New Zealand Jour. Geol. and Geophys., *8*, p. 344-370.

BELOUSSOV, V. V., 1962, *Basic problems in Geotectonics*. McGraw Hill.

BOUDETTE, E. J., and FORD, A. B., 1966, *Physical properties of Anorthoclase from Antarctica*. Am. Mineral., *51*, p. 1374-1387.

BULTITUDE, R. J., and GREEN, D. H., 1971, *Experimental study of Crystal-Liquid Relationships at High Pressure in Olivine Nephelinite and Basanite Composition*. Jour. Petrol. *12 (1)*, p. 121-149.

CLOSS, E., 1955, *Experimental analysis of fracture patterns*. Geol. Soc. Amer. Bull., *66*, p. 241-256.

CRADDOCK, C., 1972, *Antarctica Map Folio Series, Folio 12, Geological Maps of Antarctica*. American Geographical Society.

FALCONER, R. K. H., 1972, *The Indian-Antarctic-Pacific Triple Junction*. Earth and Planet. Letters, *17*, p. 151-158.

FORD, A. B., 1972, *Fit of Gondwana Continents - Drift Reconstruction from the Antarctic Continental Viewpoint*. 24th Intern. Geol. Congr. Montreal, Section 3, p. 113-121.

GIGGENBACH, W. E., KYLE, P. R., and LYONS, G., 1973, *Present Volcanic Activity on Mount Erebus, Ross Island, Antarctica*. Geology, *1*, p. 135-136.

GREEN, D. H., and RINGWOOD, A. E., 1967, *The genesis of basaltic magmas*. Contr. Mineral and Petrol., *15 (2)*, p. 103-190.

GRIFFITHS, J. R., 1971, *Continental Margin Tectonics and the Evolution of South East Australia*. Aust. Petrol. Explor. Assoc. Jl., *11*, p. 75-79.

————, and VARNE, R., 1972, *Evolution of the Tasman Sea, Macquarie Ridge and Alpine Fault*. Nature (Physical Sciences), London, *235 (57)*, p. 83-66.

GRINDLEY, G. W., and LAIRD, M. G., 1969, *Geology of the Shackleton Coast*. In *Antarctica Map Folio Series, Folio 12, Geological Maps of Antarctica* (Ed. Campbell Craddock). American Geographical Society.

GUNN, B. M., 1963, *Geological structure and stratigraphic correlation in Antarctica*. New Zealand Jour. Geol. and Geophys., *6*, p. 423-443.

HAMILTON, W., 1972, *The Hallett Volcanic Province, Antarctica*. U. S. Geol. Survey Prof. Paper 456-C, p. C1-C62.

HARRINGTON, H. J., 1958, *Nomenclature of rock units in the Ross Sea region, Antarctica*. Nature, London, *182* (463), p. 290.

————, 1965, *Geology and morphology of Antarctica*. In *Biogeography and Ecology in Antarctica* (Ed. P. van Oye and J. van Mieghem); Junk, The Hague (Monogr. Biologicae 15), p. 1-71.

————, WOOD, B. L., McKELLAR, I. C., LENSEN, G. S., 1967, *Topography and geology of the Cape Hallett District, Victoria Land, Antarctica*. Bull. Geol. Surv. N. Z., n. s. 80.

HAYES, D. E., and CONOLLY, J. R., 1972, *Morphology of the southeast Indian Ocean*. In *Antarctic Oceanology 2: Australia - New Zealand Sector*. Antarctic Research Series, *19*. (Ed. D. E. Hayes). Amer. Geophys. Union, Washington D. C., p. 125-145.

————, et al., 1973, *Leg 28 deep sea drilling in the southern ocean*. Geotimes, *18* (6), p. 19-24.

HOUTZ, R. E., and MARKL, R. G., 1972, *Seismic profiler data between Antarctica and Australia.* In *Antarctic Oceanology 2: Australia - New Zealand Sector.* Antarctic Research Series, *19.* (Ed. D. E. Hayes). Amer. Geophys. Union, Washington D. C., p. 147-164.

KING, B. C., 1970, *Vulcanicity and Rift Tectonics in East Africa.* In *African Magmatism and Tectonics.* (Eds. T. N. Clifford and I. G. Gass). Oliver and Boyd, Edinburgh, p. 263-283.

MACDONALD, G. A., 1965, *The structure of the Hawaiian Volcanoes.* Koninkl. Ned. Geol. Mijnbouwk, Genoot, Verhandel, *16,* p. 274-295.

————, 1972, *Volcanoes.* Prentice-Hall Inc. New Jersey, 510 pp.

McIVER, J. R. and GEVERS, T. W., 1970, *Volcanic vents below the Royal Society Range, Central Victoria Land, Antarctica.* Trans. Geological Soc. South Africa, *73,* p. 65-88.

NATHAN, S., and SCHULTE, F. J., 1968, *Geology and petrology of the Campbell-Aviator divide, Northern Victoria Land, Antarctica. Part. 1. Post-paleozoic rocks.* New Zealand Jour. Geol. and Geophys., *11* (4), p. 940-975.

O'HARA, M. J., and YODER, H. S. Jnr., 1967, *Formation and fractionation of basic magmas at high pressures.* Scott. Jour. Geology, *3* (1), p. 67-117.

ROBINSON, E. S., 1964, *Regional geology and crustal thickness in the Transantarctic Mountains and adjacent ice-covered areas in Antarctica (Abstract).* Geol. Soc. America Special Paper 76, p. 316.

SMITHSON, S. B., 1972, *Gravity Interpretation in the Transantarctic Mountains near McMurdo Sound.* Geol. Soc. Am. Bull., *83,* p. 3437-3442.

THOMSON, J. A., 1916, *Report on the Inclusions of the Volcanic Rocks of the Ross Archipelago.* Rep. Brit. Antarct. Exped. 1907-9, Geology, *2* (8), p. 129-151.

TREVES, S. B., 1967, *Volcanic rocks from the Ross Island, Marguerite Bay and Mt. Weaver areas, Antarctica.* J.A.R.E. Special Reports, Special Issue No. 1, p. 136-149.

VELLA, P., 1969, *Surficial geological sequence, Black Island and Brown Peninsula, McMurdo Sound, Antarctica.* New Zealand Jour. Geol. and Geophys., *12* (4), p. 761-770.

WEBB, P. N., 1972, *Wright Fjord, Pliocene marine invasion of an Antarctic dry valley.* Antarctic Journal, 7 (6).

WENTWORTH, C. H. and MACDONALD, G. A., 1953, *Structures and forms of basaltic rocks in Hawaii.* U. S. Geol. Survey Bull., *994,* 98 pp.

WOOLLARD, G. P., 1962, *Crustal structure in Antarctica.* In *Antarctic Research.* (Ed. H. Wexler, M. J. Robin and J. E. Caskey, Jnr.). Geophysical Monograph No. 7, American Geophys. Union, p. 53-73.

CHAPTER THREE

VOLCANIC GEOLOGY

Introduction

Rocks of the McMurdo Volcanic Group (excluding the Balleny Islands) are situated along the front or eastern flank of the Transantarctic Mountain range (Fig. 1.2). The only exception is the Melbourne volcanic province where several large stratovolcanoes lie across the range.

The Transantarctic Mountains in the western Ross Sea area consist of a basement complex of deformed Precambrian metasediments which are intruded by Cambrian to Ordovican granitic and granodioritic plutons (Warren, 1969). The plutons are widespread, especially in the vicinity of the Melbourne volcanic province. This basement complex is capped by gently dipping Devonian (?) to Triassic alluvial plain sediments, intruded by Jurassic dolerite sills. In places the tholeiitic magma has reached the surface and formed basalt flows (Warren, 1969). In contrast, at the northern extremity of the Transantarctic Mountains weakly metamorphosed Precambrian geosynclinal sediments form the basement onto which the Hallett volcanic province lavas were erupted (Gair et al., 1969). Nowhere in the Transantarctic Mountains is there a dated terrestrial record from the Jurassic until the commencement of volcanism about 15 m.y. ago.

The rock nomenclature used in this Chapter is explained in Chapter Four.

Balleny volcanic province

The Balleny volcanic province consists of a 150 km chain of three large and several small islands (Fig. 3.1), 250 km northwest of Cape Adare. They lie on the Balleny Fracture Zone,

FIGURE 3.1 Location map of the Balleny Islands (after Quartermain, 1963, and Dawson, 1970).

SOUTH PACIFIC OCEAN

breaks
SEAL ROCK 50'
breaks pinnacle
950'

900'
ice
900'
cliffs
ice
cliffs
300-400 feet
1,000
feet
YOUNG
1200'
ice cliffs
300-400 feet
ISLAND
ice
cliffs
3250'
ice cliffs
100 feet
300-400 feet
700' Conspic. Bluff
600' Conspic. Bluff
ROW ISLAND
700'

BORRADAILE
1250' ISLAND
600'
Beale Pinnacle

NEW
ZEALAND
Wellington
Chatham
Islands
Auckland Island
Campbell
Island
Macquarie Island
Balleny
Islands
Cape Adare
Cape Hallett
Ross
Island

YOUNG
ISLAND
ROW ISLAND
BORRADAILE ISLAND

BUCKLE
ISLAND

SABRINA ISLAND

STURGE
ISLAND
3838

Prominent precipitous bluff
1200'
Penguin Rookery
1700'
600' bluff
2000'
Ice
ice
rocks
cliff
BUCKLE
3100'
3025
pinnacle
600' bluff
2850'
ISLAND
2500'
2000'
Scott Cone
Eliza Cove
1150'
breaks
C. Macnab
Adelie Penguin Rookery SABRINA ISLAND
Monolith
255'

SCALE

0 1 2 3 4 5 6 7 8 MILES (STATUTE)

a transform fault which offsets the Indian-Antarctic ridge (Falconer, 1972; Kyle and Cole, 1974).

All the Balleny Islands are volcanic and probably Late Cenozoic in age (Quartermain, 1963). Reports of volcanic activity on Buckle Island were made in 1839 and 1899 but no activity has been observed this century (Quartermain, 1963; Hatherton *et al.*, 1965). Fine volcanic dust horizons in sediment cores from the south-west Pacific for 4000 km away, are believed to have come from the Balleny Islands. One ash eruption with an estimated explosivity of 20 megatons produced a widespread deposit between 1.8 and 1.6 million years ago (Huang *et al.*, 1974).

Very few landings have been made on the Balleny Islands. The rocks examined in this thesis were collected by B. C. Water-house (New Zealand Geological Survey) in January-March 1965. An unpublished report (Waterhouse, 1965) briefly describes the geology of the islands and gives the sample locations. Little descriptive information on the geology is available. The islands are steeply cliffed and capped by snow and ice. Inter-bedded tuff, agglomerate, scoria and lava flows of alkali olivine basalt, basanite and hawaiite seem to predominate. Several of the small islets may be volcanic necks or plugs (Hatherton *et al.*, 1964).

Hallett volcanic province

Rocks from the Hallett volcanic province (Fig. 3.2) were not examined in this thesis. The following summary from Harrington *et al.*, (1967) and Hamilton (1972) is included to extend the coverage of the McMurdo Volcanic Group.

The rocks of the Hallett volcanic province occur as four elongate offshore piles, that rise to heights of over 2000 metres, along the coast of northern Victoria Land. Three of the piles are joined to the mainland by ice filled troughs, the fourth is an island. The piles form a slightly curved volcanic chain, 210 km in length. Kyle and Cole (1974) believe the chain marks the position of a major crustal fracture which they named the 'Hallett Fracture'. From north to south the piles form the Adare

FIGURE 3.2 Generalised geological sketch map of the Hallett
volcanic province. Compiled from data given by
Harrington *et al.*, (1967), Gair *et al.*, (1969)
and Hamilton (1972).

Precambrian
sediments
and

Paleozoic
granodiorite

168

170 CAPE ADARE

172

ADARE PENINSULA

2·21
Possession Islands

CAPE ROGET

72

72

0   Km   40

● 2·21 K/Ar age
* Cinder cone
✳ Caldera

TUCKER GLACIER

CAPE HALLETT

Northern volcano
6·4

HALLETT PENINSULA

▲ Mt Harcourt
5·35

ROSS

DANIELL PENINSULA

73

Borchgrevink Glacier

Mt Brewster ▲

73

SEA

MARINER GLACIER

▲ Mt Lubbock

CAPE WADWORTH

COULMAN ISLAND

7·0

168

CAPE ANNE
170

172

Peninsula (the longest, 77 km), Hallett Peninsula, Daniell
Peninsula and Coulman Island (the shortest, 33 km). The
piles consist of major overlapping "domes" or shield volcanoes
of elliptical outline and elongated in a north-south direction.
They were formed by eruptions mostly along a crestal fissure
zone. Three domes are prominent on Adare and Daniell
Peninsulas and two on Hallett Peninsula and Coulman Island.
The Hallett and Adare domes were erupted mainly from vents
east of the present peninsula, the eastern half of each vent
has since been eroded away. Daniell and Coulman piles are
symmetrical.

Each pile consists of a thick foundation of palagonitic
breccias (hyaloclastite), pillow breccias, dikes and sills.
Hamilton (1972) believes these were erupted under an expanded
Antarctic ice sheet which had grounded on the Ross Sea shelf.
The piles are capped by a veneer of subglacial flows and tuffs.
Ages of the lavas range from Late Miocene (7.0 m.y.) to Holocene.

Hamilton (1972, p. C43) has estimated the following
abundance of lavas; "70 percent of alkaline olivine basalt
and subordinate olivine trachybasalt, 15 percent of trachyte and
no more than a few percent of basanite, andesine basalt, latite,
phonolite and quartz trachyte". He reported that the
assemblage is strongly bimodal with only a small amount of
rocks intermediate between basalt and trachyte.

Melbourne volcanic province

Introduction

The Melbourne volcanic province was proposed by Kyle and
Cole (1974) for the Late Cenozoic volcanic rocks in northern
Victoria Land forming an arcuate belt inland from Mt Melbourne
that includes Mt Overlord and The Pleiades. At its northern
and eastern extremities the province borders the Hallett
volcanic province (Fig. 3.3). Kyle and Cole (1974) have
discussed the structural setting and believe the centres are
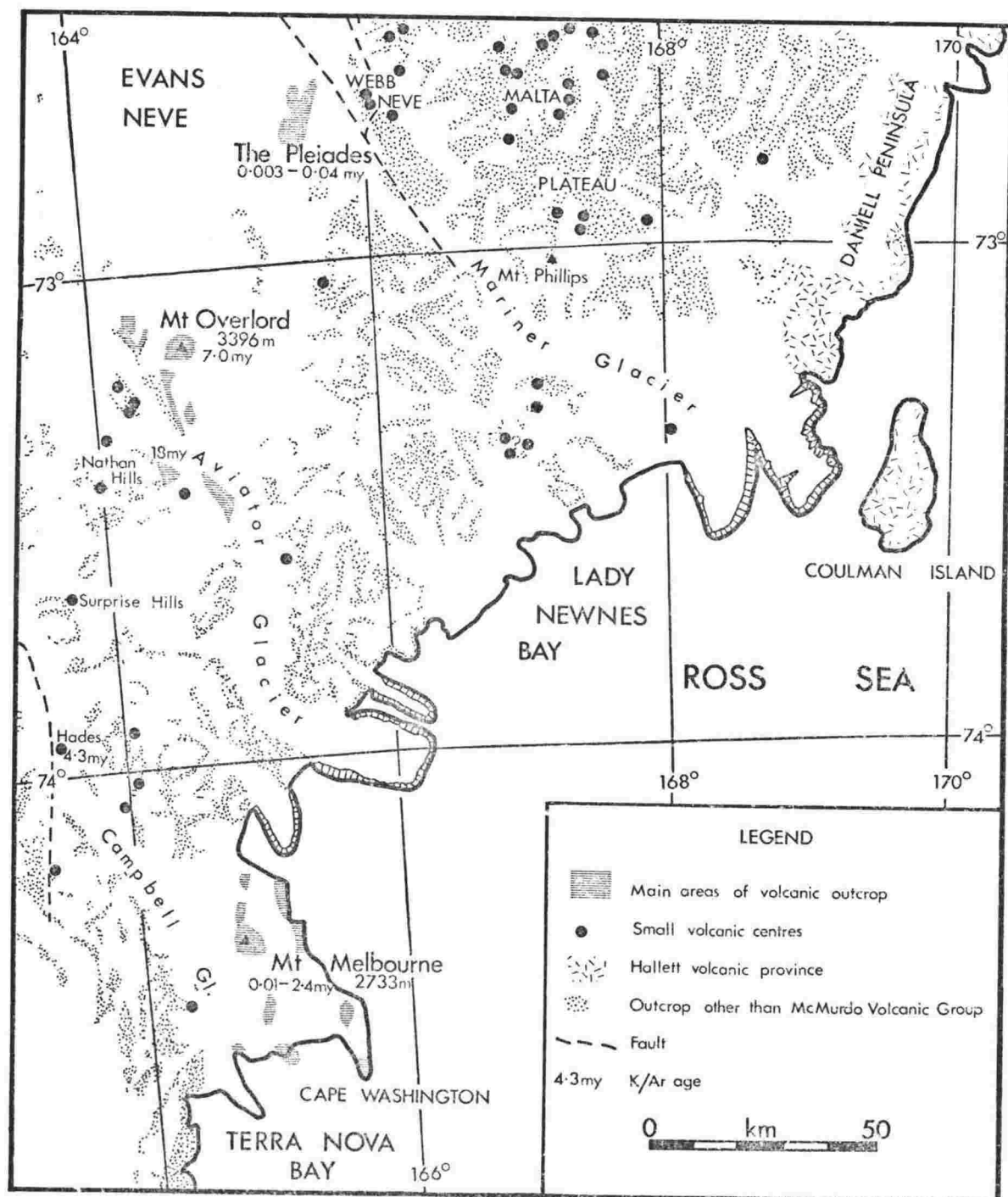
FIGURE 3.3 Location map of the Melbourne volcanic province, showing distribution of eruptive centres. See Table 3.1 for details and source of K/Ar age determinations.

related to northwest trending faults and grabens.

Nathan and Schulte (1968) have described the field occurrences of the volcanic rocks in the area and divided them into a Local Suite and a Central Suite. The Central Suite is the most abundant and consists of the large strato-volcanoes of Mt Melbourne (2733 m) and Mt Overlord (3396 m) and the cones of The Pleiades. Lavas range from basanite to trachyte, with rare nepheline benmoreite; 95% of the rocks have intermediate and trachytic compositions. The Local Suite includes all other occurrences not part of the Central Suite and with two exceptions the rocks are olivine-bearing basanites which generally occur as small outcrops and cinder cones (Fig. 3.3).

The Pleiades

INTRODUCTION

The Pleiades (Lat. 72° 40'S; Long. 165° 30'E) are situated 120 km inland from the northern Victoria Land coast at the head of the Mariner Glacier. They are at an elevation of 3000 m on the Transantarctic Mountains (Fig. 3.3). To the northwest is the Evans Neve, a large accumulation which feeds the Rennick Glacier southeast into the Ross Sea. The Pleiades comprise a series of small cones which extend 13 km in a north-northeast direction, and are dominated by Mt Atlas* in the south, with smaller less prominant cones to the north (Figs. 3.4†, 3.5).

Prior to this study, only two brief visits had been made to The Pleiades in 1966 by Riddolls and Hancox, and Nathan and Schulte. Riddolls and Hancox (1968) described thin sections of a basalt and two trachytes, but no locations for the samples

---

* This cone has previously been referred to as Mt Electra by Nathan and Schulte (1968) but the name was not accepted by the New Zealand Geographic Board, who now recognise Mt Pleiones. The point named Mt Pleiones is not the summit of the cone, so a new summit name, Mt Atlas was submitted for approval.

† In back pocket.
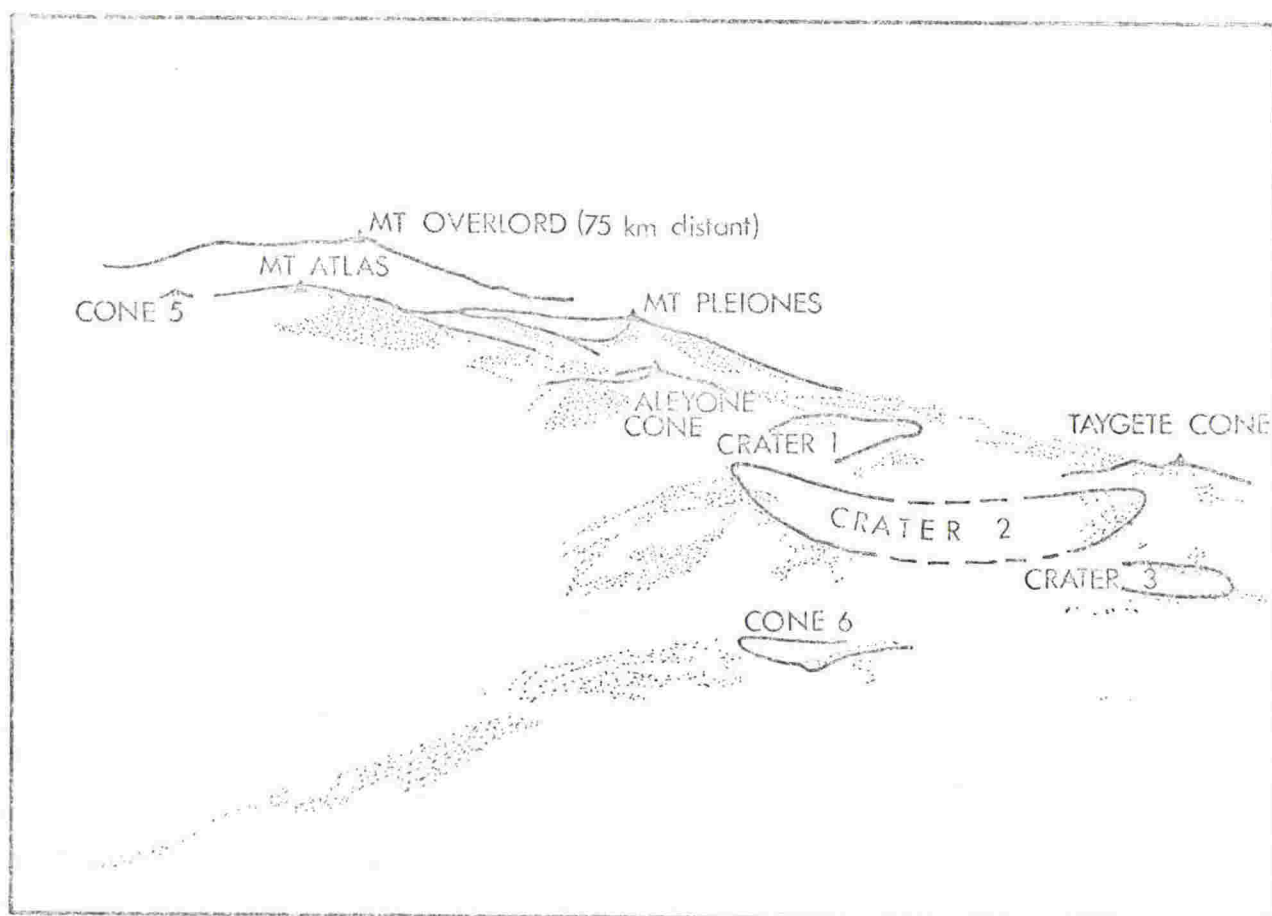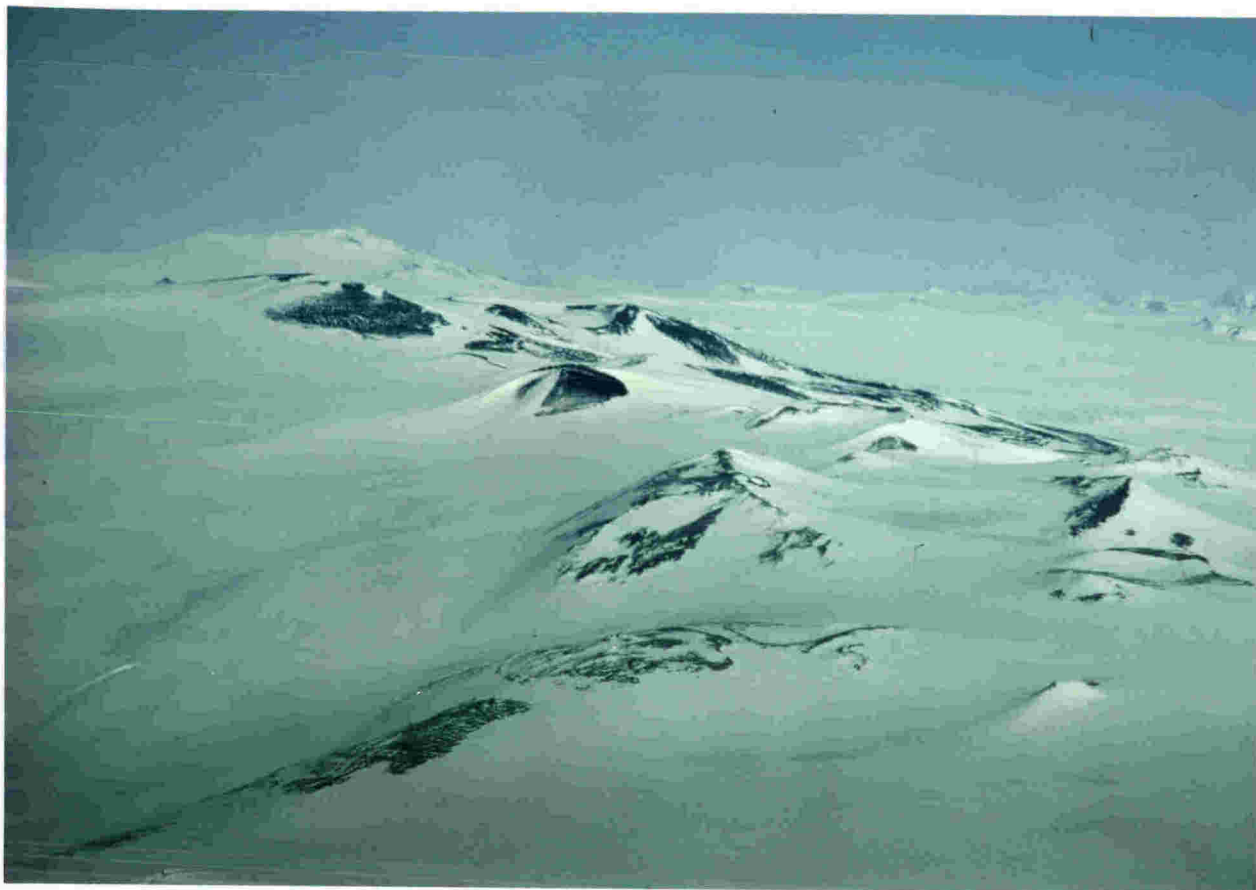
FIGURE 3.5 Aerial view of the southern part of The Pleiades.
Mt Atlas is in the middle distance.

were given. They suggested The Pleiades were formed by at least two periods of volcanism, an early trachytic episode followed by a basaltic episode.

Nathan and Schulte (1968) discussed in detail the geology of the volcanic rocks outcropping between Mt Melbourne and The Pleiades (Fig. 3.3). Several thin section descriptions, a geological map and a discussion of the geology of Mt Atlas were presented.

The present study was undertaken as part of Victoria University of Wellington Antarctic Expedition 16 (VUWAE 16) 1971/72. A total of three days were spent in sampling and mapping the area. Unnamed cones and craters in the following discussion are referred to by numbers (Fig. 3.4).

AGE

Four K/Ar age determinations for The Pleiades rocks (Table 3.1) indicate this volcanic centre is very young. The oldest dated sample from Mt Atlas is 40,000 years old and the youngest 3,000 years old. When the experimental error in the determinations are considered, the ages are not significantly different and can therefore not be used to define stratigraphic relationships.

MT ATLAS

Mt Atlas (3020 m) (Fig. 3.4) rises 500 m above the Evans Neve. It is a stratovolcano, consisting of three main cones, each of which is represented by a crater (Nathan and Schulte, 1968). The oldest and largest cone (no. 1, Fig. 3.4) is 40,000 years old (Table 3.1) and is composed of tristanite (666)* and K-trachyte (667). The latter is exposed on the north side of the crater as oxidised scoriaceous flows. Plutonic xenoliths (663, 668) of essexite up to 0.4 m, but

---

*Sample numbers refer to the petrological collection, Geology Department, Victoria University. All numbers are prefixed by 25__ ; i.e. 666 is 25666. Sample numbers prefixed by P refer to the petrological collection, New Zealand Geological Survey, Lower Hutt.

TABLE 3.1   Potassium-argon age determinations for Melbourne volcanic
            province lavas.

No.	Sample Number [a]	Sample Description and Location [b]	Mean Age [c] 10^6 years BP
1	25706	Peralkaline K-trachyte, south side Taygete Cone, The Pleiades	0.003 ± 0.014
2	P37081	Nepheline tristanite, Cone 2, 1.4 km west of Mt Atlas, The Pleiades	0.012 ± 0.04
3	25671	Trachyandesite dike on northwest side of Cone 3, Mt Atlas, The Pleiades	0.02 ± 0.04
4	25666	Tristanite, Cone 1, 300 m west of Mt Atlas, The Pleiades	0.04 ± 0.05
5	P35412	Glassy trachyandesite, west rim Mt Overlord caldera	6.8 ± 0.14
6	P37085a	Trachyandesite, west rim Mt Overlord caldera	7.2 ± 0.14
7	P35413	Glassy trachyandesite, west rim Mt Overlord caldera	8.1 ± 1.7
8	P34912	Trachyandesite, summit of Mt Melbourne	0.01 ± 0.02
9	P37175	Trachyte, 1 km west Mt Melbourne summit	0.08 ± 0.015
10	P34918	Trachyandesite; parasite cone north flank, Mt Melbourne	0.25 ± 0.06
11	P35422	Trachyandesite; Baker Rocks	0.19 ± 0.04
12	P35425	Basalt; Baker Rocks	0.72 ± 0.10
13	MM1d	Basalt; south of Willow Nunatak	2.4 ± 0.1
14	P35421	Basalt; Hades Terrace	4.3 ± 0.2
15	P35416	Basalt; Nathan Hills	18.0 ± 0.7

(a) Sample number prefixed by P refer to petrological collection of the
    New Zealand Geological Survey, Lower Hutt; MM is field number of
    Simon Nathan (N.Z. Geological Survey). Unprefixed numbers are in the
    Victoria University Petrological collection.

(b) All samples were collected by Simon Nathan except for samples 1, 3
    and 4 which were collected by the author.

(c) All determinations are unpublished results by Dr Richard Lee Armstrong,
    formerly of Yale University, now at University of British Columbia,
    Vancouver, Canada (see reference Armstrong, 1975).

averaging 0.1 to 0.2 m in diameter, are scattered around the rim of the crater.

Cone 2 (Fig. 3.4) is less well defined but exposures along the western side indicate an alternating tristanite-K-trachyte sequence. Tristanite (675) is overlain by K-trachyte and this in turn by tristanite (661, 662, 673) and finally K-trachyte (674). Nathan and Schulte (1968) have described a nepheline tristanite flow (P37081 equivalent to 661) from cone 2 with a 'streaked' texture due to flowage or semi-consolidated lava. K/Ar age determinations on the nepheline tristanite give an age of 12,000±40,000 years (Table 3.1).

The youngest cone (no.3, Fig. 3.4) is composed of tristanite (670), with a near circular unbreached crater. It is cut on the western side by two near vertical trachyandesite (671) dikes, which intrude through oxidised poorly bedded tristanite agglomerate. One of the dikes gave a K/Ar age of 20,000±40,000 years (Table 3.1).

Nathan and Schulte (1968) suggest the two small undissected cones 4 and 5 are the same age as cone 3 of Mt Atlas. The southern cone (cone 4) has a crater 200 m in diameter and is composed mainly of K-trachyte (665). The crater rim is however capped by red oxidised and rare black unoxidised trachyandesite (664) which shows a ropy texture. A few trachyandesite bombs are scattered over the cone.

At the north-northwest base of Mt Atlas, Nathan and Schulte (1968) have described a pattern of semi-circular ridges (Fig. 3.6) which they state "appear to be the remnant of an old trachytic stratovolcano which was presumably eroded down to a low level and later planed off by moving ice". However the ridges are composed of material like that forming moraines the present author has seen in the McMurdo Sound area. The surface of the ridges consist of slightly rounded well-sorted pebbles and cobbles 0.01 to 0.2 m in diameter (Fig. 3.7). The rock types are all volcanic but are diverse and cannot be considered to be in place. The young age of The Pleiades gives very little time for erosion to occur. Processes are also very slow judging from the youthful appearance of 7 m.y. old Mt Overlord (Table 3.1).
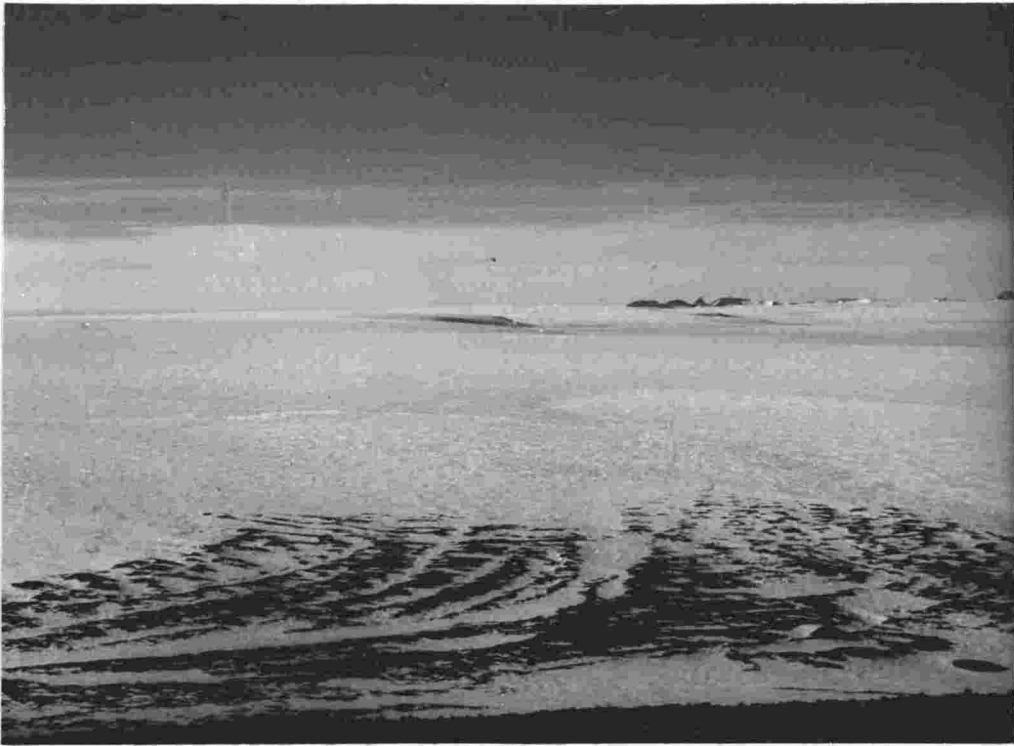
FIGURE 3.6   View of the semi-circular ridges of moraine at the
base of Mt Atlas.

FIGURE 3.7   Close up view of the moraine which makes up the semi-
circular ridges at the base of Mt Atlas.

Several pebbles and boulders of tristanite in the moraine are salt weathered and many have the underside coated with carbonate.

ALEYONE CONE

Aleyone Cone*, 2 km north of Mt Atlas, is only slightly lower in elevation than Mt Atlas, but much smaller in areal extent (Fig. 3.4). On the east side, Aleyone Cone is nearly completely covered in snow, while at the north end there is a large slaggy scree composed of large blocks and bombs of scoriaceous trachyandesite (703). This is only thin however, and at the base of the slope and at the south end of the cone, K-trachyte (701, 702) underlies the trachyandesite. A poorly defined crater breached to the east seems to be the source of the trachyandesite; a thin (~1 m) trachyandesite flow originating from the direction of the crater mantles the trachyte near the summit.

About 100 m north of Aleyone Cone is a low horseshoe-shaped crater (Crater 1, Fig. 3.4), breached to the northeast. It is composed of K-trachyte (705) similar in composition and probably similar in age to K-trachyte (701) from Aleyone Cone. The trachyte is overlain by blocks and bombs, and to the south-southeast by a 1-m-thick scoriaceous flow of nepheline benmoreite (704).

TAYGETE CONE

Taygete Cone* is an endogenous dome of peralkaline K-trachyte (696, 698, 699, 706). It was probably emplaced in part as a consolidated or semi-consolidated plug, as slickensides are well-developed along the south flanks. Slickensides are common within the cone, and this, together with the irregular

---

* Name submitted to the N.Z. Geographic Board for approval.

structure and weakly developed flow banding indicates an
endogenous origin. A K/Ar age determination (Table 3.1),
on the trachyte (706) gives an age of 3,000 years, indicating
the cone is very young, possibly postdating Mt Atlas. Areas of
hydrothermal alteration 3 to 6 m in diameter appear to represent
the most recent activity associated with the cone. There are
at least 5 areas, each showing a zonal distribution of alteration.
The centres are white, strongly bleached, silicified sulphur-
coated trachyte. Around this is a zone of less altered hematite-
stained trachyte (probably a result of alteration of ferro-
magnesium minerals) and beyond this light grey weakly-altered
trachyte. The zonal arrangement and the occasional area of
strong alteration aligned with the slope suggest that the
alteration resulted from a hot spring. Salt weathering of
the unaltered trachyte is very common but the hydrothermally
altered trachyte shows none, indicating that the alteration
is probably recent.

A small semi-circular crater 100 m in diameter is super-
imposed on the eastern side of Taygete Cone. The crater is
mantled on the south and southwest rim by yellow nepheline
mugearite (700) agglomerate. Lava of similar composition to
that forming the agglomerate also overlies the trachyte on the
northern end of Taygete Cone and is probably the same age as
the agglomerate. The areas of hydrothermal alteration discussed
above may also be contemporaneous with the crater development
and associated agglomerate formation.

Northeast of Taygete Cone there is a larger mainly snow-
covered crater (Crater 2, Fig. 3.4). Only the east and west
sides of the crater rim are exposed, with rare outcrops.
Slope material suggests that the crater is composed of a light
greenish-grey trachyte (692). This is cut on the west side by
a small nepheline benmoreite (690) dike, which may feed a few
thin nepheline benmoreite (691) flows. The benmoreite contains
abundant (1-3%) xenoliths of comagmatic(?) syenite and basement
granite. It is overlain by a dark trachyandesite(?). On the
northwest rim there is another small crater (Crater 3, Fig.
3.4) composed mainly of trachyte which is again overlain by
trachyandesite(?).

To the north and west there are a further four eruptive centres. Crater 4 (Fig. 3.4) is mainly snow covered with only the east rim exposed. Although no outcrop occurs, slope deposits indicate the crater is mainly light coloured pumiceous trachyte (681) and peralkaline trachyte (680) which is overlain by basanite (679). A small trachyte (678) flow occurs to the east of crater 4.

Cone 7 (Fig. 3.4), an endogenous dome, is composed mainly of nepheline benmoreite (683) which, like most of the other cones and craters, is mantled by later basanite (682) lava and pyroclastics. The basanite (682) forms a semi-circular crater on the east side of cone 7.

The near circular crater 5 (Fig. 3.4) is the most northern outcrop of The Pleiades. It is breached to the south, and appears to be composed mainly of nepheline hawaiite (685).

Cone 6 (Fig. 3.4) and the slopes leading down to the Mariner Glacier are strongly eroded K-trachyte (687) flows(?) which show strong dog-kennel type salt weathering. The exposure consists mainly of rubbly trachytic slope material containing fragments of dark basaltic rock. Tristanite (688) pyroclastics from an unknown source cover much of the upper part of cone 6.

STRATIGRAPHY

The limited exposure (Fig. 3.5) and diverse chemistry and petrology (Chapter 7) make time relationships between the various cones and craters of The Pleiades very difficult to determine. All vents north of Mt Atlas, except crater 5, are composed mainly of K-trachyte, peralkaline K-trachyte and tristanite which is overlain by later basaltic and intermediate lavas and pyroclastics. Crater 5 is probably part of this final eruptive episode. Mt Atlas shows 3 stages of development and erupted alternately tristanite and trachyte lavas. K/Ar ages for Mt Atlas of between 40,000 years and 12,000 years suggest it predates at least the peralkaline K-trachyte of Taygete Cone which has a very young age of 3,000 years. The error in the

age determinations are however large and the uncertainties in the determinations overlap. The ages do seem to fit the stratigraphic sequence as inferred in the field and at least gives an indication of the youthfulness of the volcanism.

In conclusion, The Pleiades eruptive sequence is one in which trachyte and salic differentiates are the initial eruptive phase followed by more basic rocks. The sequence appears to have repeated itself many times but because direct correlation between cones cannot be made, the number of cycles is unknown.

Mount Overlord

Mt Overlord (3396 m) (Fig. 3.8) has the appearance of a young stratovolcano, but three K/Ar ages give a mean date of
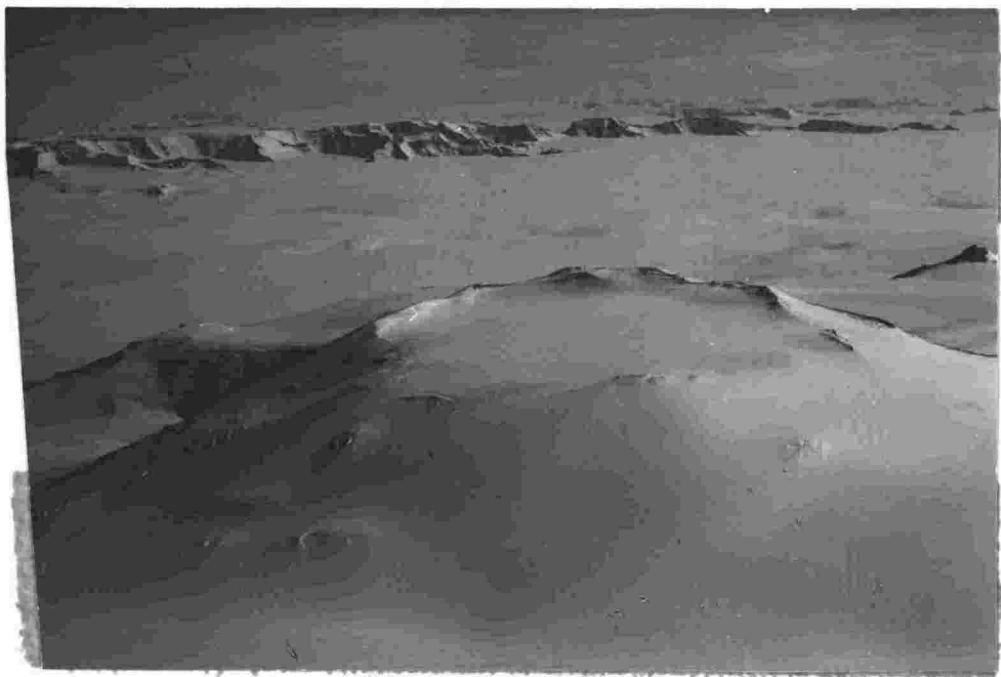
FIGURE 3.8 Aerial view of Mt Overlord (3396 m) looking west towards the head of the Rennick Glacier.

about 7 m.y. (Table 3.1). This surprisingly old age indicates
the very slow rate of erosion, especially at high altitudes away
from major glaciers.

Gair (1964, 1967) was the first to visit and describe
the rocks from Mt Overlord. In a subsequent visit Nathan and
Schulte (1968) prepared a geological sketch map and gave thin
section descriptions additional to those given by Watters in
Gair (1967).

Mt Overlord has a wide (1 km) caldera which is best exposed
on the eastern side as a cliff of trachyandesite (717).
Exposures on the flanks are very poor but surface material
indicates the cone is composed predominantly of intermediate
and trachytic lavas.

Mount Melbourne

Mt Melbourne (2733 m), the largest volcano in the
Melbourne volcanic province, is situated between Terra Nova
Bay and Wood Bay (Fig. 3.3) on the northeast side of the
Campbell Glacier. It is active (Nathan and Schulte, 1967)
with areas of steaming ground and fumarolic ice features (Lyon
and Giggenbach, 1974).

K/Ar age determinations of between 0.01 and 0.25 m.y.
(Table 3.1), give only a general indication of events. A
parasitic cone on the north flank (Fig. 3.9) appears to be
a very young feature and certainly postdates the formation of
the summit lavas. However it has the oldest K/Ar ages, probably
because of a small excess of radiogenic argon.

A 2.4 m.y. age (Table 3.1) for S. Willows Nunatak (Fig.
3.3) suggests that volcanism continued for several million years
in the Mt Melbourne area. Baker Rocks to the north of Mt
Melbourne also gives two ages (0.19 and 0.72 m.y.), both older
than any from the upper slopes of Mt Melbourne.

A breached caldera about 1 km in diameter is the main
feature of the summit (Fig. 3.9). Two small craters with areas
of strong hydrothermal alteration and steaming ground are
superimposed on the south side of the caldera (Nathan and
Schulte, 1968).
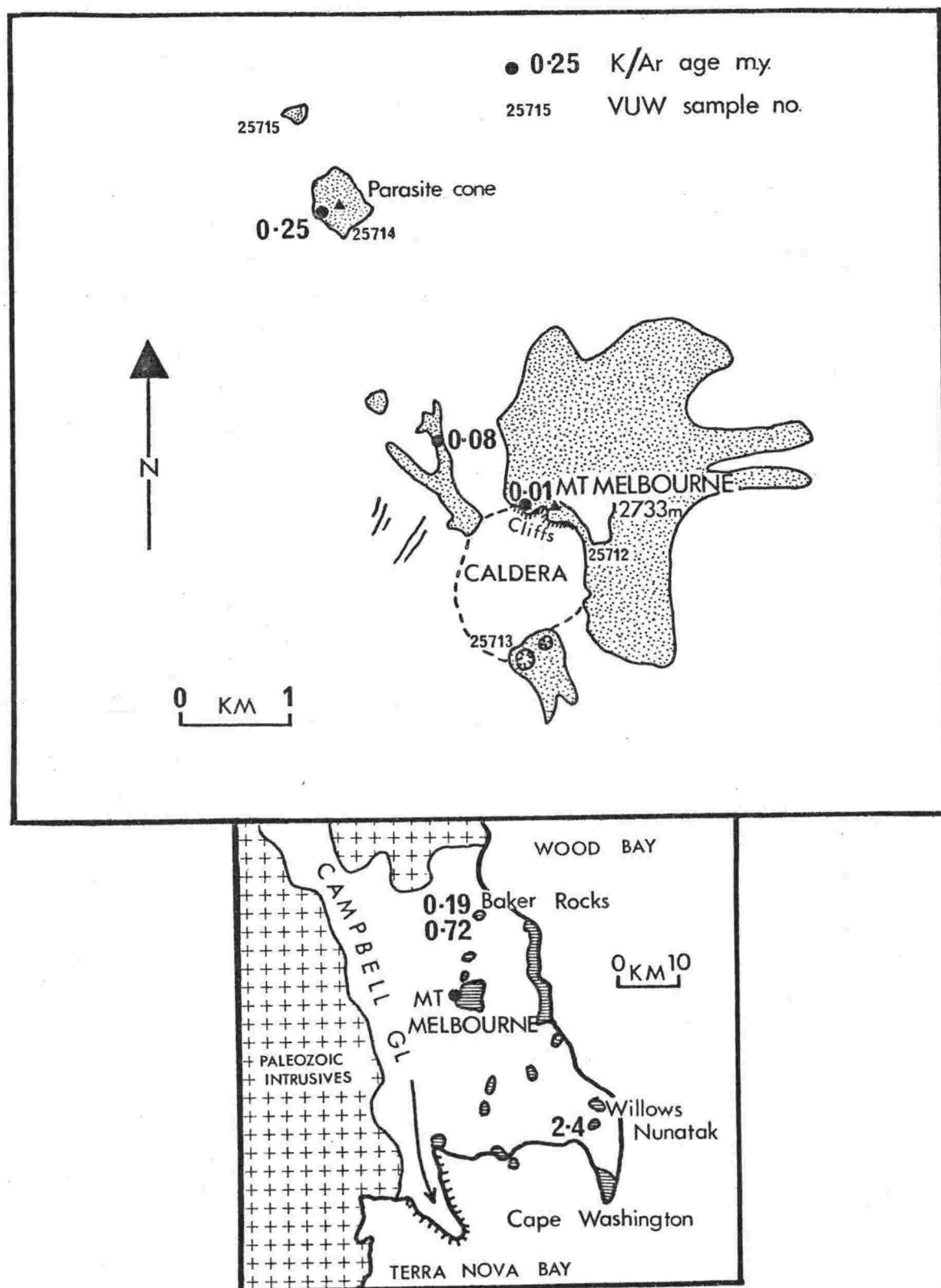
FIGURE 3.9   Geological sketch map of Mt Melbourne (after Nathan
and Schulte, 1968) showing location of analysed samples.

Exposure is very limited, with the snow-free slopes being
mainly scree and slope material. Oxidation has also affected
a high proportion of the rocks. On the north side of the
caldera a good section through the caldera wall shows old
trachyte (712) flows which are overlain by young trachyandesite
(713). Spindle-shaped trachyandesite (716) bombs up to 2 m in
length are common around the summit. A small parasitic
trachyandesite (714) cone on the north slope overlies older
trachyte (715). No basaltic rocks have been found on
Mt Melbourne, but at Baker Rocks, Nathan and Schulte (1968)
have described a sub-horizontal finely stratified basaltic
agglomerate (tuff). The basaltic nature of Baker Rocks suggest
it may be considered part of the Local Suite rather than the
main Mt Melbourne centre.

Small Volcanic Centres

Small centres of the Central Suite are widespread in the
Campbell-Aviator Divide (Nathan and Schulte, 1968) and north
of the Mariner Glacier (Riddolls and Hancox, 1968) (Fig. 3.3).
The outcrops can be divided into cones where a recognisable
cone shape occurs, or mounds when only smears or patches of
scoria occur (Nathan and Schulte, 1968). With the exception
of trachyte at Navigator Nunatak and Surprise Hills all the
lavas are olivine rich basalts (basanites).

Riddolls and Hancox (1968) have described small mounds
of basaltic scoria (P34988) from the Malta Plateau. They believe
the low dome shape of the Malta Plateau may be due to a number
of coalescing shield volcanoes. From a distance the shape
resembles a low angle basaltic shield volcano, and contrasts
with the steeper intermediate and trachytic volcanoes of
Mt Overlord, Mt Melbourne and Mt Atlas. If so it is the only
major basaltic volcano in the Melbourne volcanic province.
Gair *et al.*, (1969) have indicated an extensive area of McMurdo
Volcanic Group rocks near Mt Phillips (Fig. 3.3). Brief
aerial reconnaissance and examination of oblique aerial
photographs have however failed to reveal extensive volcanic
outcrop in either the Malta Plateau or Mt Phillips areas. Until

a ground survey or aeromagnetic survey is made, the presence
or absence of any major volcano east of The Pleiades (Fig. 3.3)
must be held in contention.

Two Local Suite basaltic lavas have K/Ar dates (Table 3.1)
of 4.28 m.y. (Hades Terrace) and 18.0 m.y. (Nathan Hills). Mr
Simon Nathan (personal communication, 1972) reports the cone
at Nathan Hills is extremely fresh and very young in appearance,
and consequently he strongly doubts the validity of the 18 m.y.
date.

There is insufficient dating of the Local Suite lavas,
but it seems likely that there is little time difference between
the stratovolcanoes of the Central Suite and the basaltic
cones and mounds of the Local Suite.

Discussion

The Central and Local Suite of volcanics are probably each
associated with different structural features. Typically the
volcanics of the Local Suite occur as small outcrops and often
seem to be associated with small local faults. In several
places basaltic lavas are extruded along mylonitised fault
zones. The lavas are olivine rich (Nathan and Schulte, 1968)
and so may have risen rapidly from the mantle with only minor
upper crustal differentiation. If the magma had suffered
extensive differentiation the large amount of olivine would
have rapidly settled out. The Central Suite lavas contain
frequent cognate plutonic xenoliths. These indicate the Central
Suite volcanoes are underlain by magma chambers (Nathan and
Schulte, 1968), in which differentiation has resulted in the
range of intermediate and trachytic lavas. The volume of lava
in the Central Suite is many times greater than the Local Suite.

Erebus volcanic province

Introduction

The Erebus volcanic province was proposed by Kyle and
Cole (1974) for all Late Cenozoic volcanics in the McMurdo
Sound area, south Victoria Land, Franklin Island and Beaufort
Island (Fig. 3.10). Hamilton (1972) and Kyle (1971)
independently proposed the names McMurdo Volcanic Province
and Ross Volcanic Province respectively for these volcanics.
However neither of these is here considered acceptable because
of possible confusion with the McMurdo Volcanic Group and the
James Ross Island Volcanic Group of the Antarctic Peninsula
area (Adie, 1969, 1972).

The main volcanic centres of Ross Island, Mt Discovery,
and surrounding areas are situated in front of the Transantarctic
Mountains at a point near a flexure in the trend of the range
(Fig. 1.2). Mt Discovery lies near the apex of the bend where
the Transantarctic Mountains change from a N-S trend to a
NE-SW trend. This is also one of the regions of greatest uplift
along the Transantarctic Mountains of Victoria Land, the Royal
Society Range having an average elevation of about 3800 m.

Smaller basaltic scoria cones and flows are scattered
over much of the Dry Valley area and along the foothills of the
Royal Society Range. These are probably distributed along small
local faults. The large volcanic centres along the coast,
however, are probably associated with major crustal faults
related to rifting (Kyle and Cole, 1974).

In this section the geology of Ross Island will be
described in detail. The areas surrounding Mt Erebus have
similar lithology and are described in the order, Cape Bird,
Cape Crozier, Hut Point Peninsula. A description of lavas at
Mt Erebus and Erebus Bay concludes the section.
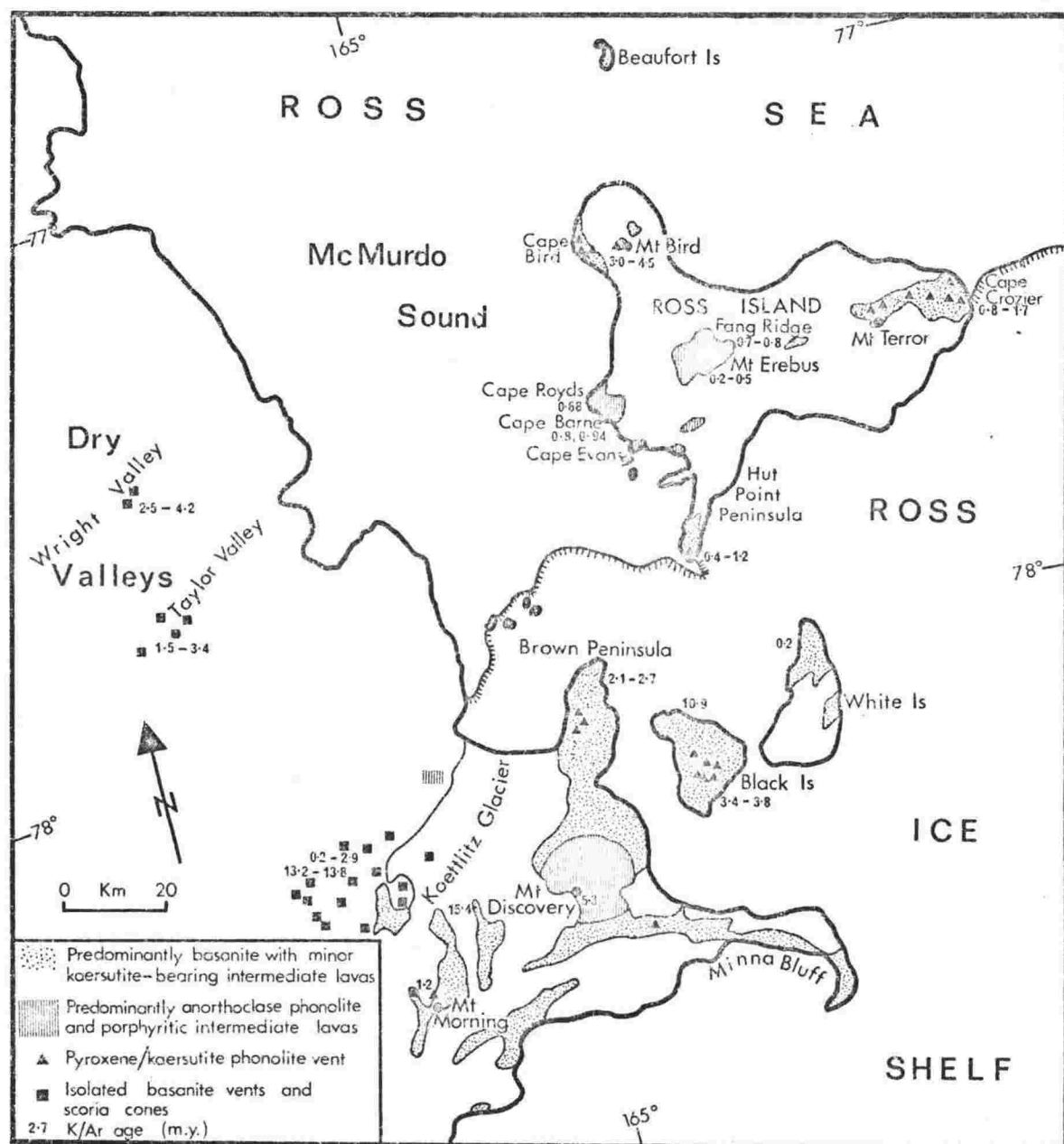
FIGURE 3.10   Generalised geological sketch map of the Erebus volcanic province.
See Tables 3.2 and 3.3 for details and source of K/Ar age
determinations.

Age

A large number of K/Ar age determinations have been made
(Tables 3.2, 3.3), mainly by Dr Richard Lee Armstrong, who
kindly provided his unpublished results. Many of the samples
from the main volcanic centres (Table 3.2) were provided by
the author to determine the volcanic stratigraphy and delineate
ages of individual volcanic centres. Samples from the Dry
Valley area and Koettlitz Glacier (Table 3.3) were, with one
exception, collected by U.S. geologists from small basaltic
cones.

The ages show a range from 0.08 m.y. to 15.4 m.y. (mid-
Miocene), with the majority <5 m.y. Most of the main volcanic
centres seem to be active for 1 to 1.5 m.y. There is no obvious
pattern to the volcanism or evidence of a regular migration of
activity.

Correlation

Very little age overlap in activity between various centres
is apparent. It seems the volcanic vents act individually;
eruptive sequences cannot therefore be correlated between
centres. The formations proposed by Cole and Ewart (1968)
for eruptive events at Black Island, Brown Peninsula and Cape
Bird (Fig. 3.10) and extended to Cape Crozier, White Island
and Hut Point Peninsula by Cole et al., (1971) are not time
equivalents. Although the eruptive sequence of alternating
basanite and phonolite is very similar throughout the McMurdo
Sound area, each eruption is an independent event and should
not be correlated with events at other centres. Where
stratigraphic names are required informal sequence names
restricted to a volcanic centre are recommended (c.f. Hut
Point Peninsula, see page 43).

TABLE 3.2 Potassium-argon age determinations for the main volcanic centres, Erebus volcanic province.

No.	Sample Number [a]	Location	Material Dated [b]	Rock Type and Occurrence	Mean Age 10^6 years	[c] Reference
			ROSS ISLAND			
1	22934	Cape Bird A; Cape Bird	WR	Kaersutite phonolite flow	3.0 ±0.15	1
2	22935	Alexander Hill; Cape Bird	WR	Pyroxene kaersutite phonolite flow	3.15±0.09	1
3	22932	Waipuke Beach, Cape Bird	WR	Olivine augite basanite flow	3.7 ±0.2	1
4	T15970	Summit Mount Bird	WR	Phonolite	4.5 ±0.6	1
5	25778	The Fang, Mt Erebus	WR	Porphyritic plagioclase hawaiite flow	0.73±0.07	1
6	25777	The Fang, Mt Erebus	WR	Porphyritic plagioclase hawaiite flow	0.81±0.02	1
7	25728	Upper northern slope, Mt Erebus	WR	Glassy anorthoclase phonolite flow	0.15±0.05 } 0.18±0.06	1
8	25728	Same sample as 7	Fsp	Anorthoclase separate	0.20±0.07	1
9		Summit crater, Mt Erebus	Fsp	Anorthoclase phenocrysts; lag gravel	0.44±0.09	1
10	T13170	Mt Erebus	WR	Anorthoclase phonolite	0.45±0.2 } 0.5±0.14	1
11	T13170	Same sample as 10	Fsp	Anorthoclase separate	0.55±0.15	1
12		Youngest flow, Cape Royds	Fsp	Anorthoclase phonolite flow	0.68±0.14	2
13	22910	Youngest flow, Cape Barne	Fsp	Anorthoclase phonolite flow	0.94±0.05	1
14	22909	Middle cone Cape Barne	WR	Aphanitic hawaiite flow	0.8 ±0.2	1
15	22907	West cone, Cape Barne	WR	Aphanitic hawaiite flow	9.2 ±1.2	3
16	22892	Black Knob, Hut Point Peninsula	WR	Basanite; small scoriaceous cone	0.43±0.07	5
17	22900	West of Black Knob, Hut Point Peninsula	WR	Olivine-augite basanite flow	0.57±0.03	5
18	22878	Half Moon Crater, Hut Point Peninsula	WR	Augite kaersutite basanite flow	1.0 ±0.15	5
19	22879	Castle Rock, Hut Point Peninsula	WR	Olivine augite basanite dyke in hyaloclastite	1.12±0.4	5
20		Observation Hill, Hut Peninsula	WR	Kaersutite phonolite	1.18±0.03[d]	4
21	T14970	Mt Terra Nova	WR	Basanite	0.8 ±0.5	1
22	22976	Coastal cliff below Post Office Hill, Cape Crozier	WR	Basanite flow	0.8 ±0.14	1
23	22955	The Knoll, Cape Crozier	WR	Phonolite flow	1.29±0.05	
24	22943	Post Office Hill, Cape Crozier	WR	Phonolite flow	1.31±0.04	1
25	22962	Topping Peak, Cape Crozier	WR	Kaersutite phonolite dike	1.71±0.3	3
			WHITE ISLAND			
26	22989	North end, White Island	WR	Olivine augite basanite flow	0.17±0.1	3
			BROWN PENINSULA			
27	21068	3 km west-northwest Mt Wise, Brown Peninsula	WR	Kaersutite basanite flow	2.1 ±0.4	1
28	21094	1.5 km south-east of Mt Wise, Brown Peninsula	WR	Olivine augite basanite flow	2.2 ±0.09	1
29	21047	2 km north-east of Mt Wise, Brown Peninsula	WR	Kaersutite phonolite flow	2.25±0.05	1
30	21001	Rainbow Ridge, Brown Peninsula	WR	Kaersutite benmoreite flow	2.7 ±0.09	1

TABLE 3.2 Potassium-argon age determinations for the main volcanic centres,
Erebus volcanic province (continued).

No.	Sample Number (a)	Location	Material Dated (b)	Rock Type and Occurrence	Mean Age 10^6 years	(c) Reference
			BLACK ISLAND			
31	?1208	3 km east Mt Aurora, Black Island	WR	Olivine augite basanite flow	3.35±0.14	1
32	21208	Duplicate analysis Sample 31	WR		8.2 ±1.0	3
33	21205	2 km north-east Mt Aurora, Black Island	WR	Pyroxene phonolite	3.8 ±0.09	1
34	21205	Duplicate analysis Sample 33	WR		4.3 ±0.5	3
35	21230	4.5 km south-east Mt Melania, Black Island	WR	Olivine augite basanite	10.9 ±0.4	1
			MOUNT DISCOVERY			
36	T15170	Mt Discovery	Fsp		5.3 ±0.14	1
			MOUNT MORNING			
37	25800	2.5 km north of summit of Mt Morning	WR	Phonolite cone	1.15±0.02	1
38	25799	4 km east of Lake Morning	WR	Trachyandesite dike intruding submarine basalts	15.4 ±0.5	1
			FRANKLIN ISLAND			
39	R2C	Franklin Island	WR	Basalt	4.8 ±2.0	1

(a) Sample number refers to petrological collection at Victoria University of
Wellington unless prefixed by T or R in which case the samples were
collected by Dr S. B. Treves, University of Nebraska, and Mr Simon Nathan,
New Zealand Geological Survey, respectively.

(b) WR = whole rock
Fsp = feldspar separate

(c) References

    1. Dr R. L. Armstrong (pers. comm.) formerly of Yale University,
now at University of British Columbia, Vancouver, Canada.

    2. Treves (1967).

    3. Unpublished results by Dr C. Adams (pers. comm.), Institute of
Nuclear Sciences, D.S.I.R., Lower Hutt.

    4. Forbes, Turner and Carden (1974).

    5. Kyle and Treves (1974c).

(d) Mean of 3 analyses.

TABLE 3.3 Potassium-argon age determinations for sample of the McMurdo Volcanic Group from Dry Valleys and Koettlitz Glacier.

No.	Sample Number	Location		Sample Dated	Rock Type and Occurrence	Mean Age 10^6 years	Reference (a)
				WRIGHT VALLEY			
1	LMJ-3	W margin, Meserve Glacier accumulation basin		WR	Basanite cone	2.5±0.3	1
2	LMJ-1	West side of Meserve Glacier		WR	Alpine II moraine, 1 meter depth. Basanite	3.4±0.6	1
3	LMJ-2	Sample as 2		WR	Surface sample, basanite	3.4±0.1	1
4	WV2E	Wright Valley	?Margin at Bartley Glacier?	WR	Basanite	3.50±0.2	2
5	WV3	Wright Valley	?high on S wall?	WR	Basanite	3.75±0.2	2
6	LMJ-4	Second Loop cone, smaller and more westerly of two cones		WR	Basanite cone	4.2 ±0.2	1
7	27	Above Taylor Glacier		WR	Cinder cone partly dissected	1.53±0.06	2
8	22978	South side Lower Taylor Valley		WR	Anorthoclase phonolite in moraine	1.54±0.3	3
9	26	Above Taylor Glacier		WR	Basanite lava cascade from crest ridge	1.84±0.11	2
10	23	E. of Rhone Glacier		WR	Massive basalt flow on cinder cone	1.79±0.13	2
11	20	As 10		WR	Bomb on cinder cone	2.00±0.18	2
12	24	Above Taylor Glacier		WR	Basalt flow capping till	1.94±0.12	2
13	29	Above Taylor Glacier		WR	Basalt lava cascade from ridge crest ≈300 m from 9	2.00±0.06	2
14		Solas Glacier		WR	Basalt scoria pile that antedates and postdates local advances of glacier	2.3 ±0.8	4
15		Snout of Taylor Glacier		WR	Lateral Moraine; sample from volcanic complex up valley	2.6 ±0.2	4
16	10	Solas Glacier		WR	Basalt lava flow in front of glacier	2.66±0.06	2
17		4 km east of Lake Bonney		WR	Basalt complex on a bedrock bench	2.8 ±0.2	4
18	6	Marr Glacier		WR	Basalt lava on steep wall below glacier	2.87±0.15	2
19	3	Hill below Marr Glacier		WR	Basalt flow	2.89±0.10	2
20	1	Probably same as 19		WR	" "	2.93±0.10	2
21	13	West of Solas Glacier		WR	Basalt dike on valley floor	2.95±0.07	2
22	10	Solas Glacier; same as 16		WR	Basalt lava flow in front of glacier	3.00±0.10	2
23	12	West of Solas Glacier		WR	Basalt lava on valley floor	3.11±0.09	2
24	16	Matterhorn Glacier		WR	Basalt lava next to glacier; near highest exposure	3.33±0.10	2
25	19	Near but upvalley from Matterhorn Glacier		WR	Basalt lava overlies till	3.38±0.14	2
26	8	East of Solas Glacier		WR	Basalt dyke exposed by erosion	4.5 ±0.7	2
27	7	East of Solas Glacier		WR	Core of dyke or cinder cone; basalt	4.64±0.12	2

TABLE 3.3   Potassium-argon age determinations for sample of the McMurdo
Volcanic Group from Dry Valleys and Koettlitz Glacier (continued)

No.	Sample Number	Location	Sample Dated	Rock Type and Occurrence	Mean Age 10^6 years	Reference (a)
			KOETTLITZ GLACIER			
28	32	Pyramid Valley	WR	Basalt dome	0.08±0.13	2
29	31a	" "	WR	" "	0.22±0.12	2
30	31b	" "	WR	" "	0.22±0.06	2
31	45	Canyon below Walcott Glacier	WR	Upper units of basalt lava	0.27±0.10	2
32	44	" " "	WR	" " " " "	0.45±0.07	2
33	33	Pyramid Valley	WR	Moderately glaciated basalt cinder cone	0.71±0.16	2
34	50b	Roaring Valley	WR	Basalt lava flow flooding mouth of valley	0.84±0.07	2
35	50a	" "	WR	" " " "	0.90±0.09	2
36	47a	" "	WR	Domes in valley	1.12±0.14	2
37	48a	" "	WR	" " "	1.25±0.10	2
38	47b	" "	WR	" " "	1.35±0.20	2
39	66	Dromedary Platform	WR	Basalt	1.21±0.09	2
40	46	Canyon below Walcott Glacier	WR	Basalt lava flow	1.45±0.15	2
41	40	Top of The Bulwark	WR	Basalt flow-overlies till	1.65±0.3	2
42	30	N summit The Bulwark	WR	Basalt bomb	1.66±0.4	2
43	65	Dromedary Platform	WR	Basalt	1.68±0.08	2
44	35	Pyramid Valley	WR	Basalt lava tongue off The Bulwark, palagontic tuff; mantled by tuff	1.83±0.09	2
45	49b	Roaring Valley	WR	Basalt lava flow down side of valley	1.78±0.19	2
46	49a	" "	WR	" " " " "	2.10±0.09	2
47	63	Dromedary Platform	WR		2.44±0.16	2
48	36	The Bulwark	WR	Massive basalt flow exposed by erosion	2.88±0.15	2
49	37	Near tongue of Koettlitz Glacier	WR	Massive basalt flow associated with pillow agglomerate	13.2 ±0.4	2
50	73	Howchin Glacier	WR		13.8 ±0.2	2

(a) References

1) Fleck, Jones, Behling (1972).

2) Unpublished results by Dr R. L. Armstrong (pers. comm.) formerly of Yale University; now at University of British Columbia, Vancouver, Canada.

3) Unpublished result by Dr C. Adams (pers. comm.); Institute of Nuclear Sciences, D.S.I.R., Lower Hutt.

4) Armstrong, Hamilton, Denton (1968).

Cape Bird

INTRODUCTION

A 15 km ice-free strip of land paralleling the coast at
Cape Bird borders the west flank of the mainly snow-covered
Mt Bird. Mt Bird, a basaltic shield volcano, is circular in
plan with an average slope of about 11 degrees. Cole and
Ewart (1968) described the geology and mapped an alternating
basalt (basanite)-trachyte (phonolite) sequence (Fig. 3.11),
which was correlated with three formations erected by them at
Black Island. A fourth formation, the Trachyte Hill Formation,
was named after rocks at Cape Bird. As discussed above, the
correlation of these formations away from their type location
is incorrect, so the names are not used at Cape Bird in this
account. The use of the Trachyte Hill Formation is also
discontinued.

AGE

Three K/Ar age determinations (Table 3.2; Fig. 3.11)
range from 3.0 to 3.65 m.y. and agree with the inferred
stratigraphy of Cole and Ewart (1968). An age of 4.5 m.y.
from Mt Bird (Table 3.2) indicates a minimum age for cone
building.

PALEOMAGNETISM

Paleomagnetic determinations identified one normal and
seven reversed sites (Appendix A ; Fig. 3.11). Pyroxene
trachyte at Alexander Hill is reversed and 3.15±0.08 m.y. old.
Within the one standard deviation uncertainty of the age, the
reversed polarity agrees with the paleomagnetic time scale of
McDougall and Aziz-ur-Rahman (1972). Polarity of the other
dated lavas also agree with the paleomagnetic time scale
(Fig. 3.11).
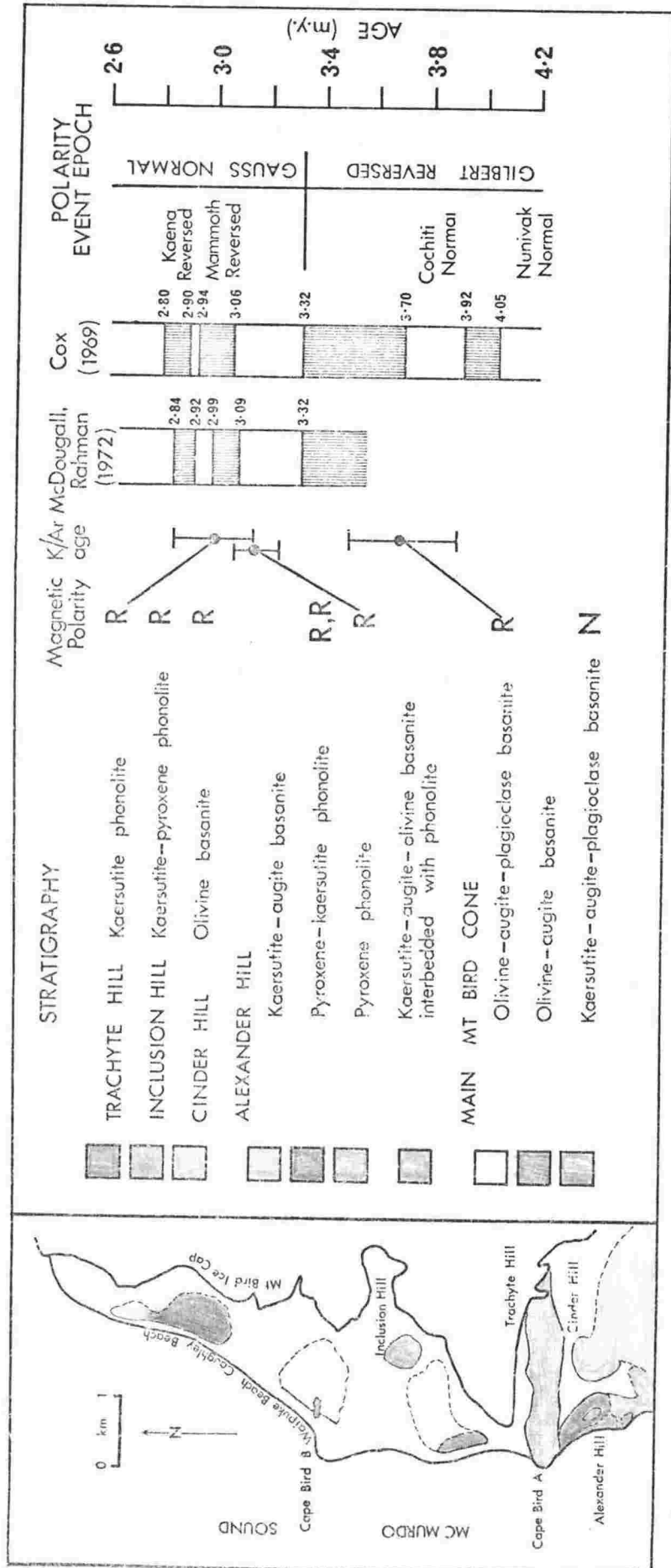
FIGURE 3.11 Geological sketch map of Cape Bird. Geology and stratigraphy after Cole and Ewart (1968), K/Ar age determination from Armstrong (1975).

VOLCANIC GEOLOGY

The geology of Cape Bird consists of basalt* flows
erupted from the Main Mt Bird Cone and later penetrated by
trachyte and basalt plugs and cones (Cole and Ewart, 1968).

Lavas of the Main Mt Bird Cone form a thick sequence of
flows which are best exposed along coastal cliffs. The flows
vary from about 10 m to less than 1 m in thickness and
typically have yellow oxidised scoriaceous tops. Three rock
units were recognised (Cole and Ewart, 1968), the youngest
an olivine-augite-plagioclase basalt has a K/Ar age of 3.65
m.y. The oldest, a hornblende-augite-plagioclase basalt, has
normal magnetic polarity and is older than 3.70 m.y. (Fig. 3.11).

Alexander Hill consists of the eroded remnants of two
complex trachyte-basalt cones in which Cole and Ewart (1968)
recognised four rock units (Fig. 3.11). Basalt is interbedded
in the trachyte with no evidence of lavas intermediate between
basalt and trachyte. Pyroxene trachyte is reversed and 3.15
m.y. old (Table 3.2; Fig. 3.11).

Bright red scoriaceous olivine basalt, containing olivine
nodules, was erupted at Cinder Hill. It is overlain by black
massive olivine basalt flows, containing abundant olivine
nodules, these flows were probably erupted from each of the
ice-free areas (Cole and Ewart, 1968). Large crystals of gem-
quality olivine (peridot) are found associated with these
lavas.

The final events at Cape Bird were the eruptions of
trachyte cones and plugs at Trachyte Hill and Inclusion Hill.
Trachyte Hill lavas are the youngest and have a K/Ar age of
3.0 m.y.

---

*Terminology of Cole and Ewart is used here. Analyses show the
basalts are basanites and the trachytes are phonolites, using
the classification adopted in this thesis. The hornblende
is mainly kaersutite.

Cape Crozier

INTRODUCTION

Cape Crozier borders the east flank of Mt Terror as an ice-free area 10 km long. Outcrop is distributed in a triangular pattern with Cape Crozier the base and the summit of Mt Terror the apex. Mt Terror is a basaltic shield volcano, roughly circular in outline, with a slope of about 9 degrees. Cole *et al.*, (1971) mapped Cape Crozier and described an alternating basalt (basanite)-trachyte (phonolite) sequence which was correlated with formations proposed by Cole and Ewart (1968) at Black Island and Cape Bird. This correlation is no longer valid. K/Ar age determinations indicate the inferred stratigraphy of Cole *et al.*, (1971) is also in error.

AGE

Four K/Ar age determinations (Table 3.2; Fig. 3.12) range from 1.7 to 0.8 m.y. Topping Peak is 1.7 m.y. old, the oldest cone at Cape Crozier, while Post Office Hill and The Knoll are both very similar in age, 1.31 and 1.29 m.y. respectively. A basanite flow exposed in the coastal cliffs is the youngest dated feature at 0.8 m.y.

VOLCANIC GEOLOGY

The geology of Cape Crozier and the slopes of Mt Terror consist predominantly of early basaltic eruptions of lava and pyroclastics which built up the shield volcano of Mt Terror. This early basaltic material is well exposed in the coastal cliffs north of The Knoll (Fig. 3.12). Later activity has peppered the east flank of Mt Terror (and presumably the other flanks, but these are snow covered) with small basaltic cones and phonolitic cones and plugs, the latter appear to have formed by endogenous growth. The cones are too numerous to describe individually and the area too great to map in detail. Based on close-support helicopter reconnaissance the cones on

INFERRED STRATIGRAPHY

Olivine basanite

Olivine-clinopyroxene basanite

Pyroxene phonolite

Kaersutite phonolite

Kaersutite hawaiite

Kaersutite phonolite

Plagioclase hawaiite and intermediate lavas

Olivine-clinopyroxene basanite

Moraine

1·7 my   K/Ar age determination

KILOMETRES

ROSS   SEA

Tuffs

Penguin rookery

0·8 my

Penguin rookery

POST OFFICE HILL
1·31my

N

ROSS ICE SHELF

Interbedded flows
and agglomerate

TOPPING PEAK
1·7my

KYLE PEAK

Cliffs 150 metres high

1·29my
THE KNOLL

Cape
Crozier

BOMB PEAK

IGLOO SPUR

Coastline indefinite

Ice pressure ridges

FIGURE 3.12   Geological sketch map of Cape Crozier. Geology and
stratigraphy revised from Cole *et al*., (1971), K/Ar
age determinations from Armstrong (1975).

the upper slopes of Mt Terror have a similar geomorphic
appearance and are similar in rock type to the cones mapped
at Cape Crozier. The eruptive history of Cape Crozier is
therefore believed to be representative of that of the flanks
of Mt Terror.

The steep coastal cliffs, best exposed north of The Knoll,
are olivine-augite basanite flows with interbedded volcanic
breccia and some tuffs. At the base of the cliffs the lavas
originate from the flanks of Mt Terror, while these are often
overlain by younger flows and pyroclastics from small vents
at Cape Crozier. Rare dikes indicate local vents for some
of the lavas.

Kaersutite phonolite lava from the summit of Topping Peak
is 1.7 m.y. (Table 3.2; Fig. 3.12); thus indicating a
minimum age for the coastal basaltic lavas. On the east
flank of Topping Peak erosion has exposed a section of, from
the base upwards, olivine-augite basanite, trachybasalt,
plagioclase trachybasalt and kaersutite phonolite (Fig. 3.13).
Although no chemical data is available, petrography indicates
the lavas are a differentiation sequence. Kaersutite phonolite
flows which mantle the summit and western flank of Topping
Peak are fed by at least four irregular dikes.

Post Office Hill (402 m) is a steep-sided kaersutite
phonolite cone, which probably formed by endogenous growth. It
has a K/Ar age of 1.31 m.y. (Table 3.2; Fig. 3.12). Cole
et al., (1971) recognised three main rock types on colour and
phenocryst variations. Chemically the lavas are very similar
(see Table 7.9 and Chapter 7).

The Knoll (372 m) is another steep-sided cone and is
composed of pyroxene (aegirine-augite) phonolite. The lavas
at Kyle Peak are identical to those at The Knoll and were
probably erupted at or about the same time. At Kyle Peak,
kaersutite basanite underlies the phonolite, while at The Knoll
two flows of olivine-augite basanite mantle and phonolite.
The Knoll basanite flows were erupted from a small circular
crater near the sumit.
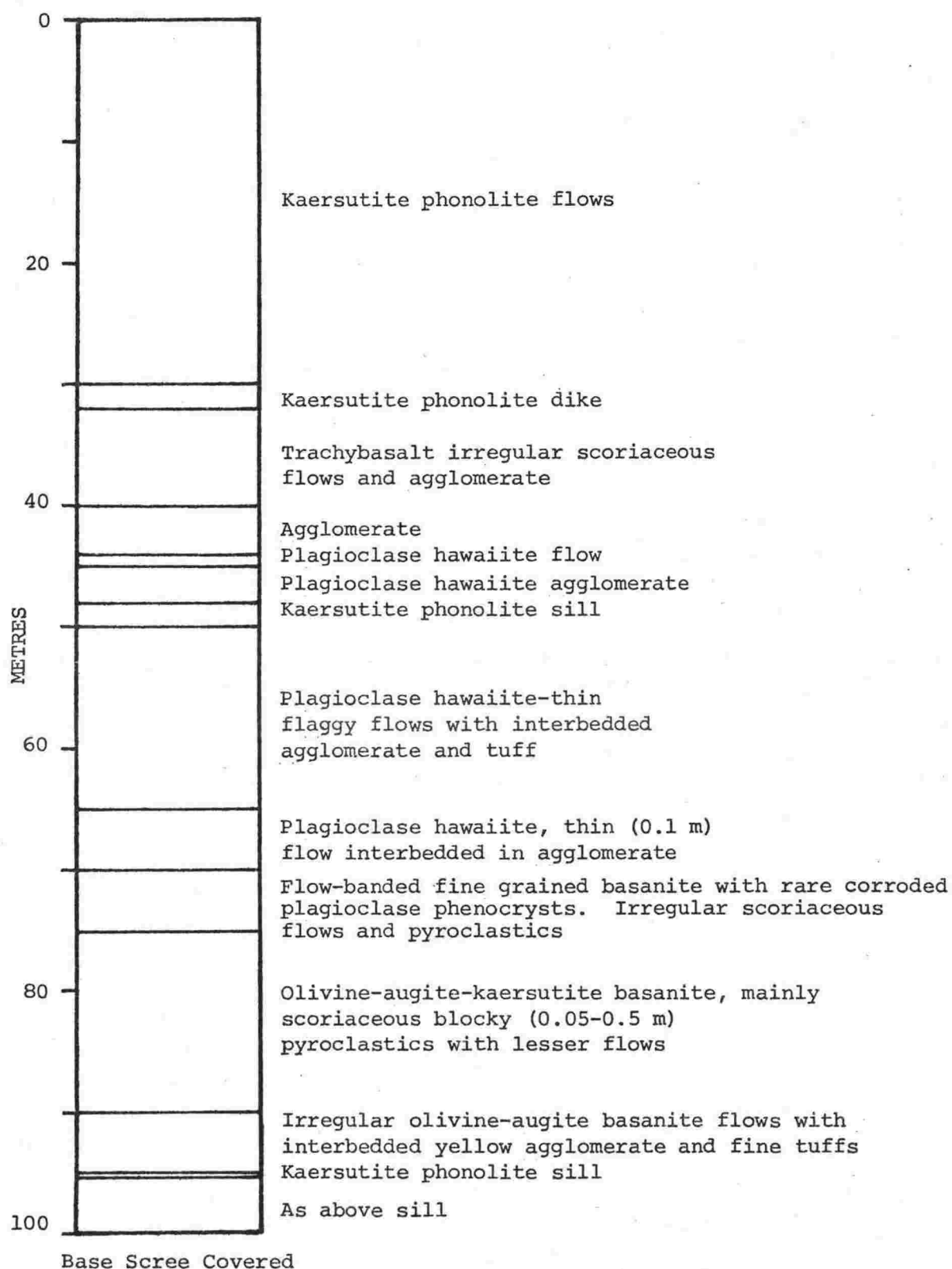
FIGURE 3.13   Generalised geological section of the east flank
of Topping Peak, Cape Crozier.

Olivine-augite basalt similar to that at The Knoll appears to be the final eruptive product at Cape Crozier. It forms a large strongly oxidised scoriaceous cone at Bomb Peak and numerous other outcrops in the Cape Crozier area (Fig. 3.12).

Hut Point Peninsula

INTRODUCTION

Hut Point Peninsula is about 20 km long and 2 to 4 km wide. It consists of a series of en echelon lines of volcanic cones that extend in a south-southwest direction from Mt Erebus (Fig. 3.10). The cones are composed of basanite and basanitoid lavas with lesser amounts of hawaiite and phonolite. Most of the volcanic cones of Hut Point Peninsula are on the western side of the peninsula where they constitute a well defined lineament. A subparallel, older and less well defined lineament occurs to the east and is traceable from a point just east of Castle Rock to Cape Armitage (Fig. 3.14). The youngest lineament, however, is transverse, from Black Knob through Twin Crater to Crater Hill. Wellman (1964) describes it as a fault.

Cole *et al.*, (1971) and Kyle and Treves (1973) briefly describe the geology of Hut Point Peninsula. This updates and expands those earlier reports. The results discussed below have been reported by Kyle and Treves (1974c).

CHRONOLOGY AND STRATIGRAPHY

The volcanic sequence at Hut Point Peninsula is inferred from geologic mapping, K/Ar dates, paleomagnetism and geomorphic evidence. The surface flows have been divided into five informal sequences. An earlier, preliminary eruptive sequence (Kyle and Treves, 1973) has been modified to accord with analytical data. K/Ar age determinations (Table 3.2) indicate

FIGURE 3.14 Geological sketch map of Hut Point Peninsula.

that the volcanic activity that built Hut Point Peninsula occurred over a period ranging from 0.4 to more than 1.2 m.y. ago.

Crater Hill sequence

The Crater Hill sequence is the oldest and consists of olivine-augite basanite. These lavas show a moderate amount of erosion and are overlain by phonolite lavas of the Observation Hill sequence at The Gap and at Cape Armitage (Fig. 3.14). Crater Hill lavas are normally polarised (Appendix A; Fig. 3.14). Since they are older than the reversed lavas, 1.18 m.y. old at Observation Hill, they may have been erupted during the Gilsa Event (Fig. 3.15).

Observation Hill sequence

The Observation Hill sequence (Fig. 3.14) consists of kaersutite phonolite and older nepheline benmoreite-nepheline mugearite lavas. The latter have little surface expression but are abundant subsurface, as shown by cores from DVDP holes 2 and 3 (Kyle and Treves, 1974a). A K/Ar age of 1.18 m.y. (Table 3.2) for the phonolite is consistent with the reversed magnetic polarity (Appendix A).

Castle Rock sequence

The Castle Rock sequence consists of olivine-augite basanite hyaloclastite outcropping at Castle Rock and Boulder Cones. A K/Ar age of 1.12 m.y. (Table 3.2) was determined on an olivine-augite basanite dike at Castle Rock, which was probably a feeder at the time of the hyaloclastite formation. Hyaloclastite at Boulder Cones underlies the augite-kaersutite basanite at Half Moon Crater, and therefore must predate it.

Aeromagnetic surveys (McGinnis, 1974 personal communication) show Castle Rock as a positive anomaly possibly indicating eruption in time of normal polarity. This suggests eruption in the Jaramillo Event (0.89 to 0.95 m.y. ago), similar to the Half Moon Crater sequence.

Half Moon Crater sequence

Augite-kaersutite basanite from Half Moon Crater (Fig. 3.16) has been K/Ar dated at 1.0 m.y. (Table 3.2) and shows normal magnetic polarity (Appendix A; Fig. 3.14). It is suggested that the Half Moon Crater volcanism occurred during the Jaramillo Event (0.89 to 0.95 m.y.) (Fig. 3.14).

Twin Crater sequence

The Twin Crater sequence consists of the younger olivine-augite basanite (Fig. 3.14) which shows little erosion and has normal magnetic polarity (Appendix A). Black Knob lavas are 0.43 m.y. (Table 3.2) and are probably the youngest volcanic rocks of the area (Wellman, 1964). The paleomagnetic data and the age determinations indicate the rocks of this sequence were erupted between 0.43 and 0.69 m.y. ago.

Paleomagnetic measurements (McMahon and Spall, 1974a) and petrographic examination (Treves and Ali, 1974) of DVDP 1 core show the normally polarised olivine-augite basanite of Twin Crater is only superficial and is underlain by reversally polarised kaersutite bearing lavas.

Dry Valley Drilling Project Holes 1, 2 and 3

Details of the geology and petrography of three holes drilled at Hut Point Peninsula by the Dry Valley Drilling Project (DVDP) (McGinnis et al., 1972) are given elsewhere (Treves and Kyle, 1973a, 1973b; Kyle and Treves, 1974a, 1974b; Treves and Ali, 1974; Kyle, 1974a).

Erebus Centre

INTRODUCTION

The area which includes Mt Erebus and its flanks and the Dellbridge Islands is referred to as the Erebus centre. It is

dominated by Mt Erebus (Fig. 3.15) which rises to 3799* m.
Young flows with distinct levees are well exposed on the
steeper upper slopes of the volcano. Exposure around the
flanks of the volcano is limited and good outcrop is restricted
to the coastal areas of Capes Royds, Barne and Evans and the
Turks Head area (Fig. 3.15).

Lavas from the Erebus centre are distinctive with a
predominance of anorthoclase phonolite (kenyte) and porphyritic
plagioclase-rich lavas (nepheline hawaiite and nepheline
mugearite). Other lava types are rare. This contrasts with
the surrounding areas of Ross Island which are predominantly
olivine-augite basanites with minor kaersutite and pyroxene
phonolites (mineralogically unlike the anorthoclase phonolite
of Mt Erebus).

The oldest available K/Ar age determination for the centre
is 0.95 m.y. and it is likely that all activity from the centre
has taken place in the last 2.0 m.y. Mt Erebus is still active
and the summit crater contains a small lava lake.

AGE

Twelve K/Ar age determinations of Erebus centre lavas are
available (Table 3.2). The oldest dated lavas, 0.8 and 0.94
m.y. are from Cape Barne. An age of 9.2 m.y. (Table 3.2 no. 15)
is considered unrealistic and in conflict with the other two
dated samples above. There is no geomorphic or geological
evidence to support such an old age and it is therefore not
regarded as the time of crystallization of the lava.

Porphyritic plagioclase hawaiite flows at The Fang have
a mean age of 0.77 m.y., based on two determinations. This is
considerably older than samples from the upper slopes of
Mt Erebus which are all younger than 0.5 m.y. (Table 3.2).

---

*New height determination by J. Rothery and J. Williams of
New Zealand Department of Lands and Survey, December 1974.
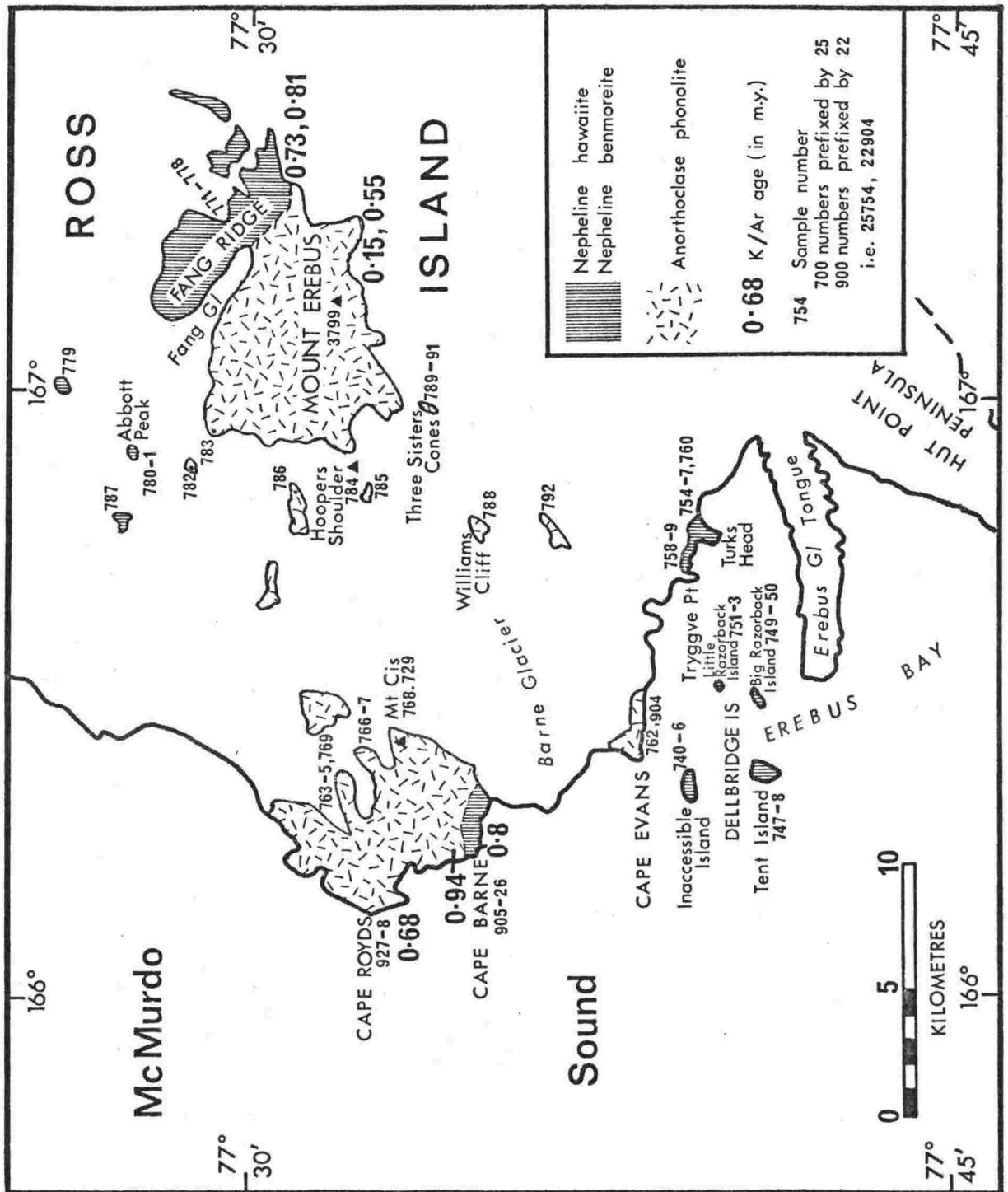
FIGURE 3.15 Location and geological sketch map of the Erebus Centre, Ross Island and Erebus Bay.

DELLBRIDGE ISLANDS

The field geology and physiography of the Dellbridge
Islands (Fig. 3.15) is discussed in detail by Debenham (1923)
and summarised by Smith (1954). Porphyritic andesine-bearing
nepheline hawaiite and nepheline mugearite lavas predominate,
although rare phonolite is also present. Anorthoclase phonolite
(kenyte) is absent in outcrop, although ice-rafted erratics do
occur.

Inaccessible Island, the most northerly in the group, is
composed of many irregular flows that dip from 10° to 30° to
the north and northeast. These are well exposed in coastal
cliffs along the south side of the island, but the dip slope
on the northern side is scree covered. Agglomerate and
tuffs are the oldest exposed material and are also commonly
interbedded with flows. Highly irregular plugs of porphyritic
plagioclase hawaiite and mugearite intrude the flows at the
east end of the island. The basal lavas, about 60 m thick,
are fine grained, of intermediate and phonolitic (745) composition.
These are overlain by about 60 m of porphyritic andesine-rich
nepheline mugearite (742).

Tent Island (Fig. 3.15) is about 1 km south of Inaccessible
Island. The lower part of the island is composed mainly of
pyroclastics which are well exposed around the coast. Flows
of porphyritic andesine nepheline mugearite (747, 748), cap
the island and also are occasionally exposed along the coast.
The flows in general dip about 10° eastward. Along the east
side of the island there is good exposure which shows massive
unbedded agglomerate and volcanic breccia. Bombs and blocks
of porphyritic mugearite averaging 0.2 to 0.4 m but occasionally
1.5 m in diameter, are welded in a light brown ash and lapilli
matrix.

Big and Little Razorback Islands appear to be part of the
same structure and probably represent part of a now eroded cone
(crater) that had a centre to the east of the islands. On Little
Razorback Island 15 to 20 flows range from 1 to 5 m thick, each
flow is separated by a distinct, rubbly, scoriaceous zone. The

flows dip to the northwest. Weakly porphyritic andesine-pyroxene (751, 752) and strongly porphyritic andesine (753) intermediate rocks occur. Big Razorback is similar in form to its smaller counterpart and is composed of numerous thin flows of fine-grained nepheline mugearite (749, 750) lavas. At the southwestern end of the island a turret-shaped intrusive body probably represents a vent. Most of the flows on the island originate from the east.

Lavas from the Dellbridge Islands are of unknown age and may represent the oldest vents in the Erebus centre. Certainly they have been moderately eroded and their eruptive vents are now below sea level. Because the islands are subject to marine erosion an age of <2.0 m.y. is inferred. At Cape Barne hawaiite cones <1 m.y. in age are strongly eroded, indicating the erosional power of the sea.

TURKS HEAD AND TRYGGVE POINT

These two distinct promontories, on the coast, south southwest of Mt Erebus (Fig. 3.15) are composed of hyaloclastite, pillow breccia and palagonitic tuffs. Luckman (1974) described the geology and believed the hyaloclastites are a product of both submarine and subglacial eruption. Porphyritic andesine-rich nepheline hawaiite is the main rock type. The rocks are of unknown age but are considered to be about the same age as the Dellbridge Islands. Anorthoclase phonolite lavas from Mt Erebus overlie the hyaloclastite at Turks Head.

CAPE EVANS

The geology of Cape Evans (Fig. 3.15) has been described by numerous early workers and is summarised by Smith (1954). Anorthoclase phonolite is the only rock seen in place, and forms two flows which reach up to 15 m in thickness (Treves, 1962). The flows originate from the direction of Mt Erebus. Numerous erratics of a variety of volcanic rock types litter the surface and form debris mounds in front of the Barne Glacier.

CAPE BARNE

Three small fine-grained hawaiite cones, K/Ar dated at
0.8±0.2 m.y. (Table 3.2) occur in a line along the south coast
at Cape Barne. The cones are of similar composition and
appear to have been erupted at about the same time. Erosion
has removed over half of the west cone, exposing the consolidated
central feeder vent, which now forms the striking Cape Barne
pillar. Flows within the cone can be seen radiating out from
the pillar, which is composed of volcanic breccia, massive
hawaiite and cut by several dikes. The cones themselves are
built of pyroclastics; mainly volcanic breccia and agglomerate,
with thin interbedded flows.

Two flow banded anorthoclase phonolite flows, younger than
the basalt, make up the remaining area of Cape Barne. The younger
flow has a K/Ar age of 0.94±0.05 m.y. Locally the flows thicken
to over 20 m and appear to follow irregularities in the terrain,
that existed prior to their eruption. Where the flows have
travelled down valleys or depressions, well developed radial
joint patterns occur (Fig. 3.16). From a distance the pattern
suggests a volcanic dome, but on closer inspection, the flow
alignment of the large anorthoclase phenocrysts, and the
obvious lateral extent of the lava shows it originated as a flow.
The source of the flows is in the direction of Mt Erebus.

Above Cape Barne, about 250 m above sea level, is a 6 m
high K-trachyte mound, Mt Cis. This small outcrop has received
attention because it contains sandstone xenoliths (Thomson, 1916)
believed to be of Beacon Supergroup sediment. The xenoliths
indicate down-faulted rocks, similar to those in the Trans-
antarctic Mountains, underlying Ross Island and McMurdo Sound.
The chemistry of Mt Cis K-trachyte is unusual in having very
low alkalis and high silica content in comparison to other
McMurdo Sound lavas, but this may be due in part to contamination
by the xenoliths.
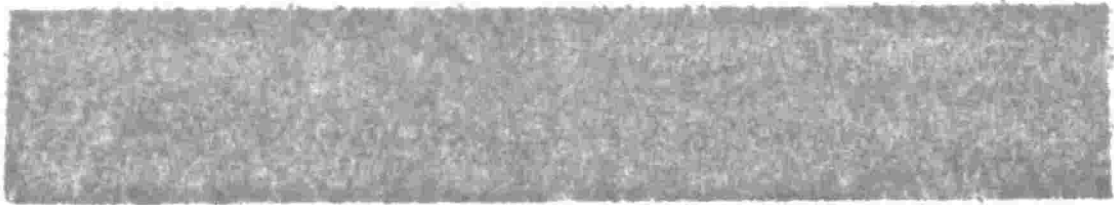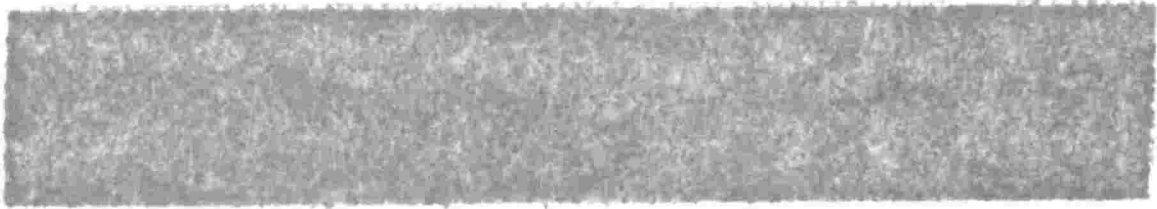
FIGURE 3.16   Anorthoclase phonolite lava flow, on the west side
              of Deep Lake, Cape Barne, showing radial joint pattern.

CAPE ROYDS

Three anorthoclase phonolite flows are exposed along the coast at Cape Royds. The youngest flow is 0.68±0.14 m.y. (Table 3.2) (Treves, 1967) and therefore younger than the flows at Cape Barne, to the south. Early workers (summarised by Smith, 1954) have described in detail the geology and rocks at Cape Royds.

Many small outcrops above Cape Royds, on the slopes of Mt Erebus have been described by early workers to be anorthoclase phonolite cones. Most of the outcrops are in fact small debris cones (resulting from glacial action) or lava flows from higher up the mountain. No source for the flows at Cape Royds or Cape Barne were found. Anorthoclase phonolite lava probably has a high viscosity (in the order of 10^4 to 10^5 poise), and therefore are unlikely to flow for long distances down low slopes. It is therefore difficult to imagine the thick flows at Cape Royds and Cape Barne being erupted from the present position of Mt Erebus, 20 km away. Walker (1973) has however suggested that provided sufficiently large volumes of magma are erupted, then highly viscous flows can travel large distances. Until further evidence is found it is assumed that the flows along the coast of Mt Erebus were erupted from a vent that is now overlain by the younger lavas of Mt Erebus.

MOUNT EREBUS

Fang Ridge

Fang Ridge (the summit, called The Fang, is 3159 m above sea level) is a prominant feature paralleling the northeast slope of Mt Erebus, but separated from it by the Fang Glacier. The north and northeast slopes have an average dip of over 45 degrees and are composed of scree and ribs of rubbly flows and pyroclastics. The Fang Glacier side of the ridge has steep, in places vertical, cliffs greater than 150 m in height. Large, deep windscoops separate the glacier and ridge

making access to the ridge difficult.

Fang Ridge is 4 km long and trends in a northwest-southeast direction. It consists of thin bedded tuffs and agglomerates with scoriaceous flows and is intruded by thin (1-3 m) ramifying dikes. The dikes are contemporaneous with the uppermost flows and probably acted as feeders. Irregularities in the bedding of the tuffs and small (0.5 m) faulted offsets seen in some dikes suggest post-depositional consolidation and compaction. The lavas are strongly porphyritic and commonly show good flow banding of the andesine phenocrysts. Chemically the lavas can be classified as nepheline hawaiite and nepheline mugearite. Olivine basalt has been reported (Smith, 1954) from the lower west end of Fang Ridge, but it was not found in the upper part of the ridge.

Two samples have K/Ar ages of 0.73 and 0.81 m.y. (Table 3.2), in agreement with the samples' relative stratigraphic positions.

Debenham (1923) regarded Fang Ridge as a huge remnant of the oldest crater rim of Mt Erebus. Certainly it represents part of an old cone, most of which is either covered by the younger flows of Mt Erebus or eroded away, but it is more likely that Fang Ridge was a vent on the side of a juvenile Mt Erebus. The lavas of Fang Ridge are similar to those at Turks Head and Tryggve Point, but more age determinations are required before any genetic comparisons can be drawn between the two localities.

Lower Slopes

The slopes of Mt Erebus from 1800 m to the caldera rim at about 3000 m are made up of numerous sinuous, irregular rubbly anorthoclase phonolite flows. They are 20 to 70 m wide and usually have well developed levees up to 4 m high, which clearly mark the path of the flow. Collapsed lava tunnels are apparent in places. In most cases the flow itself is covered in snow with only the levee remaining visible. Rarely when the flows are seen their thickness is variable but they usually have a glassy crust 0.2 m thick, underlain by very scoriaceous or vesicular lava.

A young flow on the north side of the upper slopes of Mt Erebus has a K/Ar age of 0.18 m.y. (Table 3.2), which gives an indication of the young age of most of the flows.

Mt Erebus has at least 5 small parasitic vents (excluding the larger Fang Ridge), around its lower flanks. A few small cones are seen low on the slopes of Fang Ridge, these are considered to be part of the Fang Ridge structure rather than Mt Erebus. The 5 cones are Abbotts Peak, Hoopers Shoulder and the Three Sister Cones (Fig. 3.15).

The Three Sister Cones are all less than 50 m in height and extend in a southwest line; each vent is separated by about 100 m. Hoopers Shoulder is very distinct as a black cone on the west flank, rising about 100 m above the surrounding slopes. All 4 vents are composed of black, glassy, porphyritic anorthoclase phonolite which is extremely fresh in appearance and obviously very much younger than the Mt Erebus lavas. The viscosity of the lava was so high that ropy flows 1 m thick, have consolidated half way down the steep walls of Hoopers Shoulder. There is no evidence of any explosive activity associated with any of these vents. The flows forming the cones are extremely irregular and ropy in appearance.

Abbott Peak (1793 m) consists of nepheline mugearite flows that mantle a cone which formed in the main by endogenous growth.

Summit Area

A 4 km wide caldera with its rim at about 3200 m (a.s.l.) forms the summit area. The caldera rim is marked by a change in slope from the steep upper flanks to a gently sloping summit plateau. Only rarely is the caldera rim exposed. Younger flows, small cones and the present active cone overlie the rim to the south (Fig. 3.17). The summit plateau is mainly a chaotic jumble of large sheets of anorthoclase phonolite flows which show no flow orientation, and possibly formed as a skin on lava pools. Subsequent movement of the underlying magma could account for their jumbled appearance and unusual orientation. Fumerolic ice towers and areas of warm ground are

56.
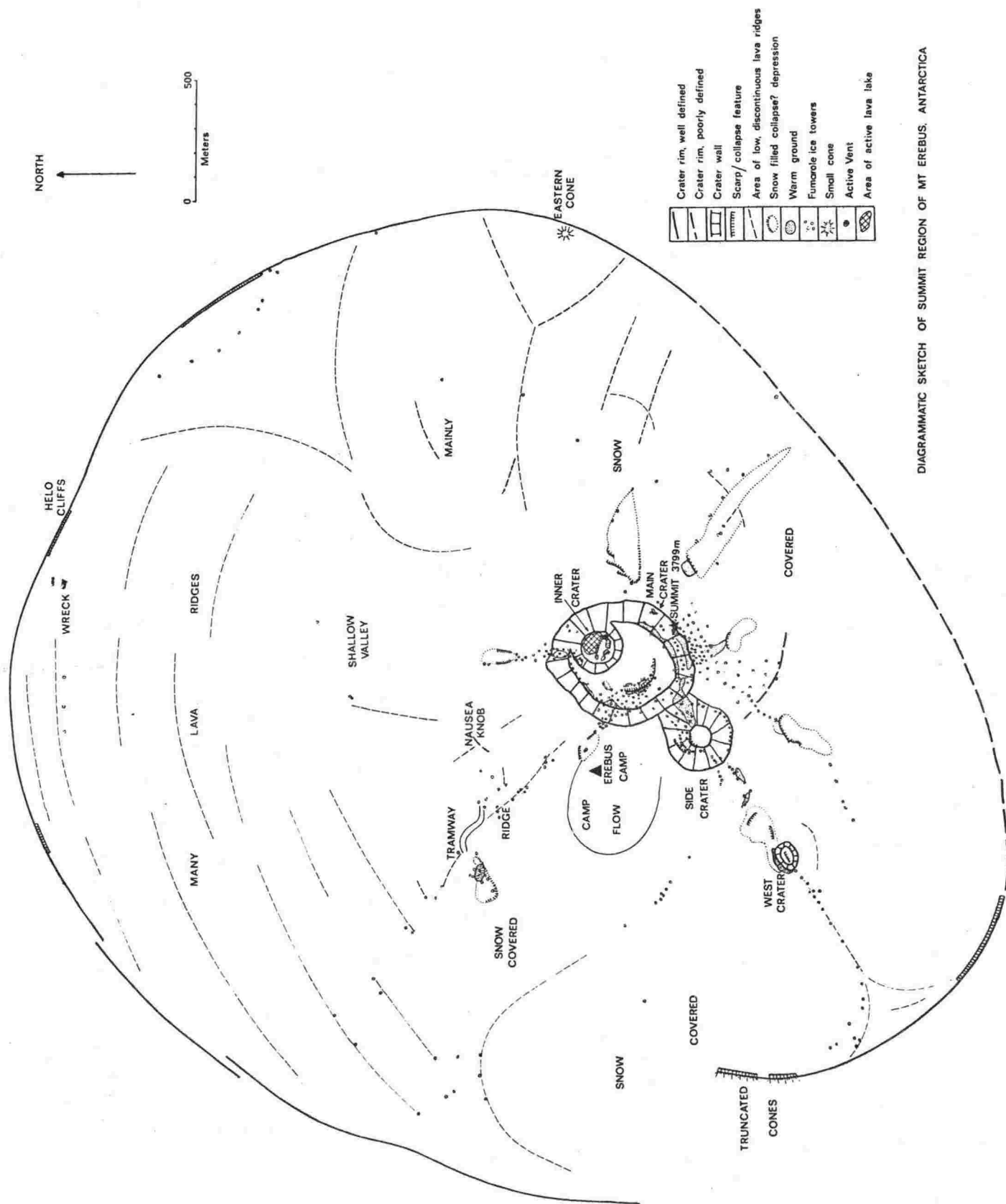
FIGURE 3.17   Sketch map of the summit region of Mt Erebus.
              Drawn by Harry Keys (Victoria University).

scattered around the summit area (Lyon and Giggenbach, 1974).

The summit crater is elliptical ~500 m in diameter east-
west and ~600 m north-south (Fig. 3.18). A small dormant
crater (Side Crater, Fig. 3.18) on the south flank of the summit
crater is described by Beck (1965). The main Mt Erebus crater
floor is ~160 m below the summit, and at the north end the
circular Inner Crater, ~250 m in diameter, is a further ~100 m
below the main crater floor. A northeast-southwest ridge
divides the inner crater in half. In December, 1974, a lava
lake filled most of the north side of the inner crater. The
southern half was covered with snow, sublimates and large bombs
erupted from a ~25 m wide vent (called the Active Vent) on the
southeast quadrant of the inner crater (Fig. 3.18). High
pressure and temperature fumaroles are confined to the southern
side of the inner crater. The main crater floor appears to be
a frozen lava lake. Collapse along semi-circular faults has
produced a 8 m scarp at the southern end of the floor.

The cone is built up of anorthoclase phonolite flows with
minor interbedded pyroclastics. Volcanic breccia mantles the
north and south crater rim.

Geologic History

The following is an attempt to reconstruct the history of
Mt Erebus. It is speculative and based mainly on observations
from the few outcrops described above and available K/Ar age
determinations.

1) The oldest events can only be inferred and must predate
the 0.94 m.y. anorthoclase phonolite lavas at Cape Barne.
Seismic profiling (Northey et al., 1975) has indicated a thick
sequence of Tertiary sediments in McMurdo Sound which underlie
Ross Island. DVDP holes 1 to 3 (Treves and Kyle, 1973a;
Kyle and Treves, 1974a) have shown that eruptions about 1 m.y.
ago were subaerial, for at least 120 m below present sea level,
and that these overlie a hyaloclastite pedestal.

Therefore under Mt Erebus hyaloclastites sit on Late
Cenozoic sediments, these in turn are overlain by subaerial
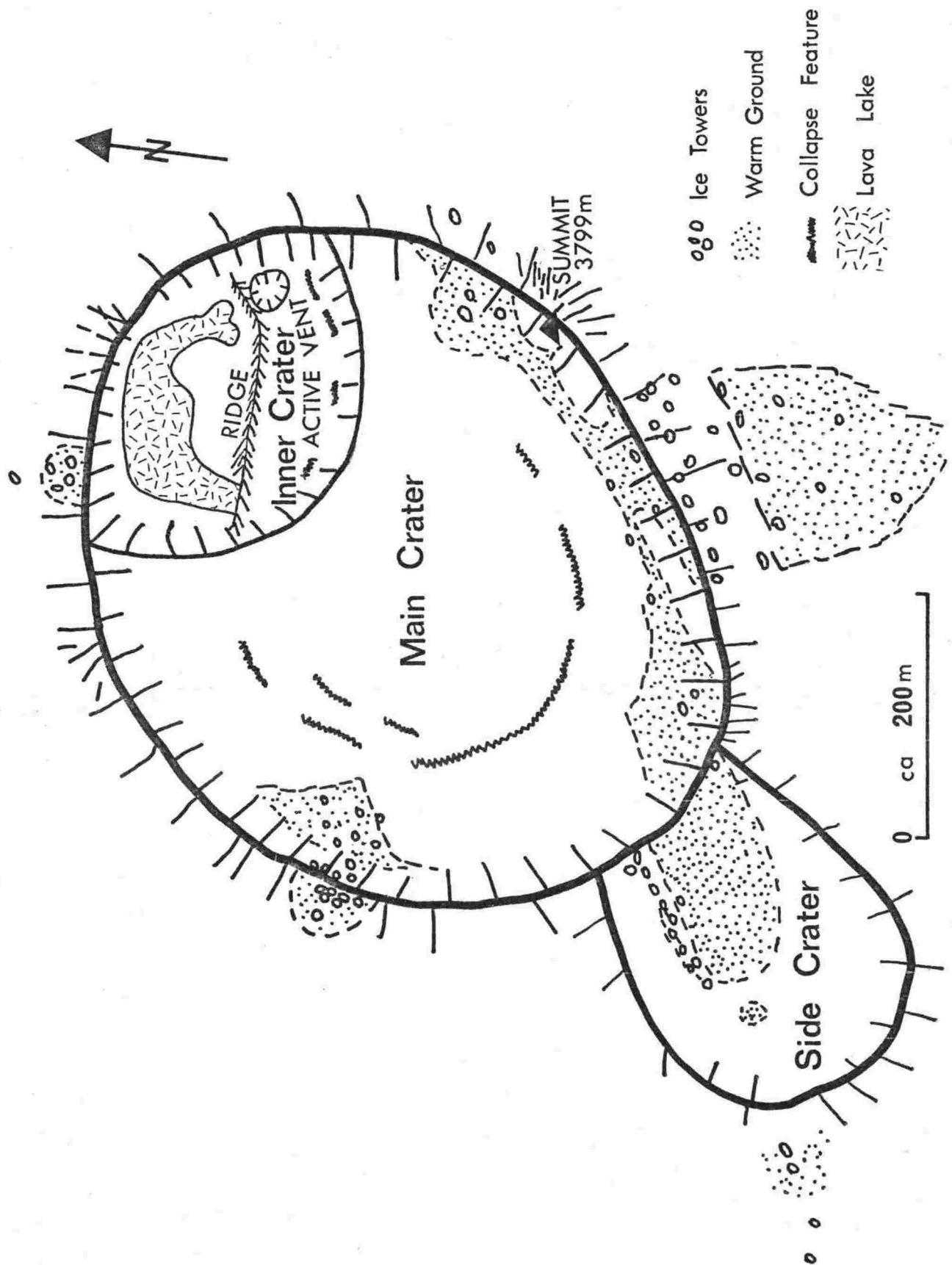
FIGURE 3.18   Sketch map of the crater of Mt Erebus.

flows which extend from about 120 m below present sea level.

2) The oldest recorded event is the eruption of thick flows of anorthoclase phonolite, 0.94 m.y. ago, at Cape Barne. The volume of lava requires a major vent and because of the wide apron of the flows along the coast and their thickness, it may have been a fissure eruption.

3) A volcano, the remnants of which now form Fang Ridge, developed next, beginning prior to 0.81 m.y. and ceasing shortly after 0.73 m.y. ago. The formation of Fang Ridge is difficult to determine without knowing the full extent of this volcano. Although Fang Glacier now occupies a large part of where the former volcano was situated, erosion of the cone by ice is unlikely, because the frozen bases of polar glaciers have little eroding power. Fang Volcano may therefore have collapsed forming a caldera, of which Fang Ridge is a remnant, or it may have been blown apart by an eruption. The latter suggestion is unlikely because of the lack of any tephra that would be associated with such a large eruption. Fang Ridge is situated high (2000 to 3000 m) on the flank of Mt Erebus indicating that by 0.8 m.y. ago the wide lower flanks of Erebus were formed.

4) Eruptions of thick anorthoclase phonolite flows, which commenced eruption prior to 0.94 m.y. ago, probably ceased with the youngest flow, dated at 0.68 m.y., at Cape Royds. Mt Erebus was continuing to grow. Aeromagnetics (McGinnis et al., 1974) show Mt Erebus as a large positive anomaly, thus indicating a high proportion of lavas younger than 0.69 m.y.

5) Erebus continued to grow during the Brunhes Normal Polarity Epoch (<0.69 m.y.), building the upper part of the cone. Flows were probably smaller and shorter and confined to the upper slopes of the volcano.

6) A change in the style of volcanic activity began with the formation of a summit caldera, which filled with lava prior

to 0.20 m.y. ago. Small vents covered the south end of the caldera rim and young flows, dated at 0.2 m.y., were extruded over the flanks of the old cone.

7) The present summit cone developed probably in the last 0.1 m.y. or so. Parasitic cones, Hoopers Shoulder and Three Sisters Cones were erupted during this period.

8) The latest recorded event was the formation of a lava lake sometime between 1971 and November, 1972 (Giggenbach et al., 1973); no doubt lava has been present at other times in the last few thousand years (c.f. Ross, 1847). In December 1974 the lava lake had expanded in size and the associated strombolian eruptions were throwing bombs onto the upper slopes of the cone.

9) During the development of Mt Erebus and Ross Island, and probably still continuing, subsidence due to isostatic loading occurred, so forming a moat around the island (McGinnis, 1973; Northey et al., 1975).

Present Volcanic Activity

<u>1972/73</u>

Present Volcanic Activity on Mount
Erebus, Ross Island, Antarctica.

by

W. F. Giggenbach, P. R. Kyle, G. L. Lyon

This paper has been reprinted from
<u>Geology</u> 1: 135-136.

INTRODUCTION

Active volcanism in East Antarctica occurs mainly in two regions: on Mount Erebus, a constantly steaming volcano on Ross Island, and on Mount Melbourne, in Northern Victoria Land, where fumarolic activity has been observed by Nathan and Schulte (1967).

In the Southern Hemisphere during the summers of 1972 and 1973, members of the New Zealand Antarctic Research Programme spent 2 wk camped near the summit (3,794 m) of Mount Erebus. This report presents observations made then, and later by one of us (P.R.K.) during other visits.

PREVIOUS REPORTS

On January 27, 1841, Sir James Ross sighted the mountain and named it after his ship *Erebus*. On the following day, he reported that the volcano "was emitting smoke and flame in great profusion," and that a "bright red flame filled the mouth of the crater; some of the officers believed they could see streams of lava pouring down its sides" (Ross, 1847).

David and his party, in March 1908, made the first ascent of Mount Erebus (Shackleton, 1909; David and Priestley, 1909, 1914), and observed three well-like steaming openings at the bottom of the crater. Intermittent roaring noises from the depths of the crater indicated strong fumarolic activity (David and Priestley, 1914). Later in 1908, steam eruptions were frequently observed from the expedition base at Cape Royds, 22 km from the summit. Strong outbursts of ash and steam, lit up from below by a bright-red glow, were seen on June 14, 1908, indicating that there was molten lava in the crater at that time.

During David's second ascent, in December 1912, the crater floor was obscured by steam, but an eruption occurred while the party was near the summit (Priestley, 1913, 1962). Blocks of pumiceous lava, containing Pele's hair, were thrown up during the loud explosions. No activity at all was observed in January 1924, but during January 1935, the crater was reported to show the usual vapor plume (Berninghausen and van Padang, 1960). Eruption of lava may possibly have occurred in 1947, also (Hantke, 1951).

A third ascent was made in January 1959, but Beck (1965), in describing the summit regions, recorded no eruptions. A glow, however, had been reported in 1957 and 1958 by observers in aircraft (D. C. Thompson and G. Warren, personal communs.); high temperatures were noted by Burge and Parker (1969) after an aerial infrared survey. No lava lake was observed during two brief visits to the crater rim on January 3 and 5, 1972; steam, how-

ever, prevented a complete view of the inner crater. The fumarolic activity was similar to that encountered in January 1973: strong hissing sounds were emitted from unidentified vents within the inner crater. Photos taken during the 1972 visits showed a small, dark band of ash extending from the inner crater to the southwest along the main crater floor, indicating that explosive activity was occurring at that time.

GENERAL DESCRIPTION OF SUMMIT AREA

Mount Erebus, the most active volcano on the Antarctic continent, is the largest of the four volcanic cones that form Ross Island (Fig. 1). Reports of the elevation of the highest point on Mount Erebus, located on the southeast part of the main crater rim, are conflicting. A height of 3,794 m for the summit, as reported by Warren (1969), is adopted here.

The cone, which is now active, rises 200 to 300 m above the southern half of the summit plateau, bordered by the rim of a filled-in older crater or caldera (Fig. 2). The height of the relatively even and almost circular main crater rim varies between 3,720 and 3,794 m; the diameter is 500 to 600 m. The floor of the main crater lies ~ 150 m below the summit and probably represents the surface of a frozen lava lake. Withdrawal of the lava column feeding this lake is presumed to have caused the semicircular fault that dissects the main crater floor (Beck, 1965). Further collapse caused the formation of the cylindrical pit of the inner crater, ~100 m below the main crater floor and ~200 m in diameter (Fig. 2). In the top third of the vertical, and, in places, overhanging wall of the inner crater, the solidified layers of the old lava lake are exposed. An east-west ridge, studded with fumarolic vents, divides the floor of the inner crater into two distinct parts, with most of the activity concentrated in the northern half, at the foot of the main crater wall; only a few weak fumaroles are scattered over the snow-covered southern half.

The predominant rock type on Mount Erebus, and the only one outcropping in the summit area, is anorthoclase phonolite (Antarctic kenyte; see Smith, 1954). It is characterized by large (up to 10 cm

Present Volcanic Activity on Mount Erebus, Ross Island, Antarctica

Werner F. Giggenbach
Chemistry Division,
Dept. Scientific and Industrial Research,
Wellington, New Zealand
Philip R. Kyle
Victoria University,
Wellington, New Zealand
and
Graeme L. Lyon
Institute of Nuclear Sciences,
Dept. Scientific and Industrial Research,
Wellington, New Zealand

long) anorthoclase phenocrysts in a generally glassy groundmass containing microphenocrysts of olivine, augite, opaques, and occasional incipient nepheline.

K-Ar ages (Treves, 1967; R. L. Armstrong, personal commun.) indicate that Mount Erebus and lavas originating from it have been erupted from 1 to <0.15 m.y. ago. No age determinations have been made for lavas from the youngest craters, but these are probably younger than 0.15 m.y. Aeromagnetic studies (McGinnis and Montgomery, 1972) show Mount Erebus as a single, broad, positive magnetic anomaly of 5,000 γ, indicating formation of the main cone in a period
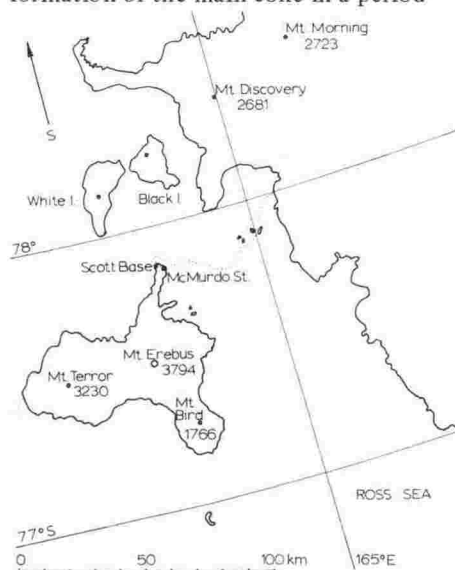
Figure 1. Map of Ross Island, showing Mount Erebus and surrounding volcanoes; altitudes in meters.
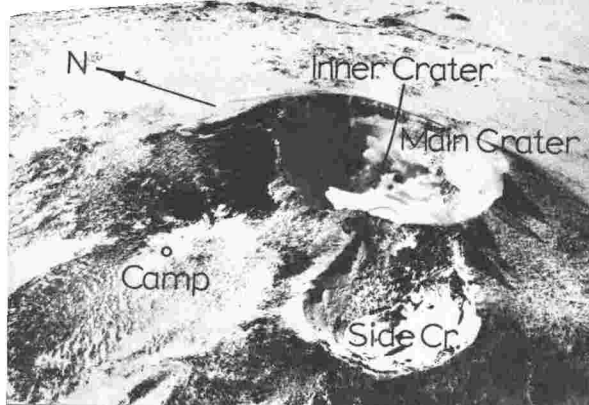
Figure 2. General view of summit area of Mount Erebus. (Photograph provided by the U.S. Navy.)

of normal magnetic polarity which K-Ar ages show to be the Brunhes period which began 0.69 m.y. ago (Cox, 1969).

PRESENT VOLCANIC ACTIVITY

Thermal activity outside the inner crater consists exclusively of gentle emission of steam from patches of warm ground or fumarolic ice towers; high-temperature activity is restricted to the northern half of the inner crater, where incandescent material was observed in at least four areas. A permanent glow was emitted from roughly circular vents on several hornito-type cones with diameters of 2 to 3 m, in the broken crust of what appeared to be a partly frozen lava lake, and an intermittent glow came from two active lava pools 20 to 30 m in diameter. During frequently observed quiet eruptions from these pools, the highly viscous gray surface material started to bulge before breaking and exposing the underlying bright-orange melt; this activity was accompanied by faint splattering and puffing noises. Thereafter, the glowing gap closed again, with a deep furrow marking the location of the event. An intermittently audible strong hissing noise could not definitely be associated with any of the features observed.

In contrast to the quiet eruptions, only 1 of the 35 explosive eruptions heard during the 2-wk period was witnessed from the crater rim; steam, however, precluded direct observations. The time of ~6 sec taken by the ejected material to hit the ground indicated that the height reached by the ejecta was ~50 m. More violent eruptions, however, are indicated by fresh volcanic bombs around the main crater rim, ~250 m above the lava pools. These bombs range in diameter from several tens of centimeters to ~2 m. One such spindle-shaped bomb had a diameter of ~0.8 m and was ~1.5 m long. It disintegrated after an attempt to move it and revealed a hollow, black interior partly filled with Pele's hair; the outer shell consisted of a vesicular, glassy matrix, embedding the ubiquitous anorthoclase crystals. The relatively small number of bombs found outside the main crater rim or detectable by use of bino-

culars on the floors of the main and inner craters suggest that not much material is ejected during these eruptions. Snow on the floor of the southern half of the inner crater indicates low ground temperatures, and only a few relatively mild fumaroles are scattered over this part.

On February 4, 1973, however, an eruption considerably stronger than those observed during December and January occurred in the southern part of the inner crater; it lasted for ~45 sec and sent ash and debris up to the floor of the main crater.

A very strong roaring noise developed for ~10 sec, during which the inner crater filled with steam; it was followed by the emission of a black, ash-charged cloud from a small vent on the eastern wall of the inner crater. Several large blocks landed on the floor of the main crater. They did not appear to be molten lava, but rather secondary material derived from the vent or vent wall. The ash cloud continued to grow for ~30 sec, while the loud roaring noise persisted. The cloud reached a height of ~150 to 200 m above the vent. Judging from the trajectory of the blocks and the direction the ash cloud was emitted, the vent must have been inclined and could be dipping at 70° or less to the east.

During this visit, the red-hot fumarolic vents and the lava pools were in a state very similar to that observed a month earlier; thus, the eruption witnessed in February does not appear to have affected the activity in the northern part of the inner crater. The loud, continuous roaring noise of this eruption was in strong contrast to the short, sharp bangs associated with the eruptions observed earlier. It seems probable that the February eruption represents a vent-clearing process, resulting from a gas build-up at depth due to blockage of conduits feeding the southern part of the inner crater.

Figure 3 shows frequency and duration (in sec) of the explosive Strombolian-type eruptions heard during the 2-wk observational period. During the first week, the average interval between eruptions was 6 hr; thereafter, the average time between eruptions increased to 16 hr, and the average duration decreased from ~3 sec to 2 sec. Seismographic and barometric recordings taken 40 km away, at Scott Base, did not indicate any event that could be associated with activity on Mount Erebus, nor did there appear to be any correlation between eruptive fre-

quency and barometric pressure.
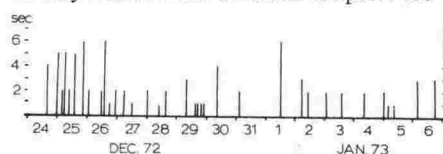
REFERENCES CITED

Beck, A. C., 1965, A note on Mount Erebus, Ross Island, Antarctica: New Zealand Jour. Geology and Geophysics, v. 8, p. 180–185.

Berninghausen, W. H., and van Padang, M. N., 1960, Catalogue of the active volcanoes of the world, including solfatara fields; Pt. X, Antarctica: Naples, Internat. Volcan. Assoc., 32 p.

Burge, W. G., and Parker, D. C., 1969, Infra-red survey in Antarctica: Imagery analysis: Ann Arbor, Michigan Univ. Willow Run Labs. Rept. 1160–9–F.

Cox, A., 1969, Geomagnetic reversals: Science, v. 163, p. 237–245.

David, T.W.E., and Priestley, R. E., 1909, Notes in regard to Mount Erebus, in Shackleton, E. H., The heart of the Antarctic (Vol. 2): London, William Heinemann, p. 308–310.

—— 1914, British Antarctic Exped., 1907–1909, Repts. on scientific investigations: Geology, v. 1.

Hantke, G., 1951, Übersicht über die vulkanische Tätigkeit 1941–1947: Bull. Volcanol., v. 11, p. 81.

McGinnis, L. D., and Montgomery, G. E., 1972, Aeromagnetic reconnaissance and geologic summary of the Dry Valley region: Dry Valley Drilling Project Bull., v. 1, p. 61–90.

Nathan, S., and Schulte, F. J., 1967, Recent thermal and volcanic activity on Mount Melbourne, Northern Victoria Land, Antarctica: New Zealand Jour. Geology and Geophysics, v. 10, p. 422–430.

Priestley, R. E., 1913, The ascent of Erebus, December 1912, in Huxley, L., Scott's last voyage (Vol. 2): London, MacMillan and Co., Ltd., p. 274–280.

—— 1962, Scott's northern party: Geog. Jour., v. 128, p. 129–142.

Ross, J., 1847, Voyage to the southern seas (Vol. 1): London, John Murray, p. 216–220.

Shackleton, E., 1909, The heart of the Antarctic, being the story of the British Antarctic Expedition 1907–1909 (Vol. 1): London, William Heinemann.

Smith, W. C., 1954, The volcanic rocks of the Ross archipelago: British Antarctic Exped., 1910, Nat. history rept.: Geology, v. 2, no. 1, p. 1–107.

Treves, S. B., 1967, Volcanic rocks from the Ross Island, Marguerite Bay, and Mt. Weaver areas, Antarctica: JARE Spec. Repts., v. 1, p. 136–149.

Warren, G., 1969, Geological map of Antarctica, in Bushnell, V. C., ed., Geology of the Terra Nova Bay–McMurdo Sound area, Victoria Land: New York, Am. Geographical Soc., scale 1:1,000,000.

Figure 3. Sequence and duration of eruptions from December 24, 1972 to January 6, 1973.

November 1973

Volcanic Activity of Mount Erebus,
Antarctica, November 1973

by

P. R. Kyle

Volcanic Activity of Mount Erebus,
Antarctica, November 1973.

Philip R. Kyle,
Antarctic Research Centre,
Department of Geology,
Victoria University,
Wellington.

Abstract

The anorthoclase phonolite (kenyte) lava lake, first
observed in Mt Erebus in December 1972, has grown in size.
On November 11, 1973, a flow 20 m by 4 m was seen feeding the
lava lake from a vent on the east side of the crater. Strombolian
eruptions continue with an increase in duration but a similar
frequency to 1972/73 observations.

Introduction

Mt Erebus (3794 m) is the largest of four volcanoes forming
Ross Island. The summit crater of Mt Erebus is slightly
elliptical ~500 m in diameter east-west and ~600 m north-south.
The main crater floor is ~160 m below the summit. Clear
conditions on November 11, 1973, allowed an excellent view of
the inner crater, which is usually filled with vapour. The
inner crater, which is ~250 m in diameter and ~100 m deep, is
situated at the north end of the main crater and appears to be
the result of collapse. An east-west ridge with a few weak
fumaroles dotted along it, divides the inner crater in half.
The southern half is snow-covered and relatively inactive,
although it contains several high pressure fumaroles and
numerous weak fumaroles. Lava and the majority of the activity
is confined to the northern (active) half of the inner crater.

This report discusses observations made on November 11, 1973, by the author and Dr S. B. Treves (University of Nebraska) and during the following fortnight by the author.

Activity

Major eruptions of Mt Erebus were witnessed by Sir James Ross in 1841 (Ross, 1847) and 1908 and 1912 by members of Shackleton's and Scott's expedition respectively (Shackleton, 1909; Priestley, 1913). Summaries of other previous activity are given by Berninghausen and van Padang (1960) and Giggenbach et al., (1973).

Giggenbach et al., (1973) reported the first observations of a lava lake in the Mt Erebus crater. During observations from December 24, 1972 to January 6, 1973 frequent small Strombolian-type eruptions were heard. The eruptions of 1-6 seconds duration, occurred about every 6 hours during the first week and then about every 16 hours in the second week (Fig. 1). An ash eruption from a fumarole vent on the south side of the inner crater lasting 45 seconds, was witnessed by the author on February 4, 1973 (Treves and Kyle, 1973).

On November 11, 1973 viscous lava was observed flowing from a small vent about 0.5 to 1 m in diameter on the eastern side of the active half of the inner crater. A small flow 15 to 20 m long with a maximum width of 3 to 4 m moved slowly (1 to 2 m per minute) west for 5 m then swung northwest until it entered a convecting lava lake 40 m in diameter. Solidified light greenish-grey lava partially covered the surface of the flow and formed a thin skin on the lava lake. The toe of the flow was solidified ropy lava which formed a well-defined flow pattern. Concentric ropy flow lines were common in the lava lake. Periodically the thin skin on the convecting lava lake would upwell and break revealing the underlying molten lava.

On the northwest side of the inner crater a few glimpses were made of a small 25 to 30 m consolidated lava lake, surrounded by areas of fresh consolidated lava. The area of

FIGURE 1   Frequency and duration of eruptions of Mt Erebus in
            December, 1972 to January, 1973 (from Giggenbach *et al.*,
            1973) and in November, 1973.

of the lava lakes has increased significantly since 1972/73 and the crater floor has risen drowning the small hornitos and the lava lake described by Giggenbach *et al.*, (1973).

Strombolian eruptions similar to those reported in 1972/73 were continuing in November 1973. The duration of the eruptions had noticeably increased while the frequency was variable (Fig. 1). No direct observations of the inner crater during an eruption were made. Giggenbach *et al.*, (1973) recorded ejected material hit the ground 6 seconds after an eruption indicating an eruption height of 50 m, but again no direct observations were made. On November 21, 1973 the inner crater was observed from the south end of the main crater rim, during a 5 second eruption. No material was seen to be ejected above the inner crater rim, and there was only a very slight increase in vapour emission. At other times rapid increases in vapour (weak steam eruptions) occurred without any noticeable eruptive sound.

From November 13 to 15, 1973 a heavy snowfall covered the main crater and southern inner crater floors and walls with fresh snow. Observations on November 18 showed no volcanic ejecta covered the fresh snow. Only a fumarole vent in the southwest sector of the inner crater had a 20 by 10 m patch of tephra covering the snow on the crater wall above the vent. The vent was the same one from which the author witnessed a 45 second ash eruption in February 1973 (Treves and Kyle, 1973). It is likely the 25 second eruption on November 17 occurred from the fumarole and deposited the tephra. The lack of any ejected material (apart from around the fumarole) suggests the eruptions possibly are the result of mild degassing of the lava lake, however until direct observations of an eruption are made no positive conclusions can be reached.

Gas activity was similar to previous visits. Irregularly a loud hissing sound, as if high pressure gas was being ejected, built up over 5 to 10 seconds then persisted for 20 to 50 seconds before dying down. Most of the sound seemed to come from fumaroles in the inactive or southern half of the inner crater and from unidentified sources in the extreme west of

of the active area. No obvious increase in gas accompanied the sound. Strong fumaroles were identified only in the inactive side of the inner crater.

In September 1974 several ash eruptions were recorded and red glows seen in the night sky above Mt Erebus by Scott Base personnel, indicating the continued presence of the lava lake.

Discussion

The activity of Mt Erebus appears to have increased since the initial observations of a lava lake in December 1972. The proven existence of the lava lake for one year and the indication that in September 1974 it still continues, makes Mt Erebus one of only three volcanoes with a permanent lava lake.

Observations and an attempt to sample the lava and gases are planned for December 1974.

References

Giggenbach, W. F.; Kyle, P. R.; Lyon, G. L. 1973. Present volcanic activity on Mt Erebus, Ross Island, Antarctica. Geology 1: 135-136.

Priestley, R. E. 1913. The ascent of Erebus, December 1912; in Huxley, L., Scott's last voyage (vol. 2): London, MacMillan and Co. Ltd, 274-280.

Ross, J. 1847. Voyage to the southern seas (vol. 1); London, John Murray, 216-220.

Shackleton, E. 1909. The heart of the Antarctic, being the story of the British Antarctic Expedition 1907-1909 (vol. 1): London, William Heinemann.

Treves, S. B.; Kyle, P. R. 1973. Renewed volcanic activity of Mt Erebus, Antarctica. Antarctic Journal of the U.S. 8: 156.

Discussion

The description of the Erebus volcanic province has been limited to Ross Island. Other areas have been visited and any generalisations are based on observations made throughout the McMurdo Sound area.

On Ross Island the geology of the three areas Mount Bird, Mounts Terra Nova and Terror and Hut Point Peninsula, which surround Mt Erebus are similar. Each is dominated by basaltic lavas with minor phonolitic cones. At Mt Bird, Mt Terror and Mt Terra Nova, large basaltic shield volcanoes have been built, then an alternating sequence of basaltic and phonolitic cones were erupted on the flanks. Hut Point Peninsula consists of a series of basaltic cones, with only one phonolitic cone.

The lavas of the Erebus centre are very distinct and consist predominantly of intermediate and phonolitic lavas. Anorthoclase phonolite was erupted only from Mt Erebus and small cones around its flanks. Porphyritic plagioclase rich intermediate lavas are very common in the Erebus centre. Although this type of lava does occur throughout the Erebus volcanic province it seems to be abundant only at Mt Discovery and Mt Erebus.

A similar distribution of mainly basaltic lavas surrounding a centre of predominantly phonolitic lavas may occur at Mt Discovery. Mt Morning is a large basaltic shield volcano with only minor phonolitic cones, but abundant young basaltic cones occur around its flanks. At Brown Peninsula and Minna Bluff similarly, there are mainly basaltic cones with lesser intermediate and phonolitic lavas. Mt Discovery, at least in the upper part of the cone, is composed mainly of plagioclase-rich intermediate and phonolitic lavas.

69.

Volcanic Evidence Bearing on Glacial Events

K/Ar AGE DATES

Throughout the McMurdo Sound area there is little evidence of eruptions occurring at times of increased ice or snow cover. If subglacial eruptions occurred the likely eruptive products would be hyaloclastite (see below) as at Castle Rock, Turks Head and Tryggve Point. However the abundance of erratics at various heights around Ross Island and other volcanic centres show the Ross Ice Shelf has in the past been at least 800 m higher (Vella, 1969); assuming no isostatic or tectonic uplift. Many dated samples are from subaerial flows and cones (Table 3.2) collected from near sea level, and these therefore indicate times when these locations were ice-free. At these times the Ross Ice Shelf could not have been in an expanded state. Figure 3.19 shows the frequency of dated rocks erupted
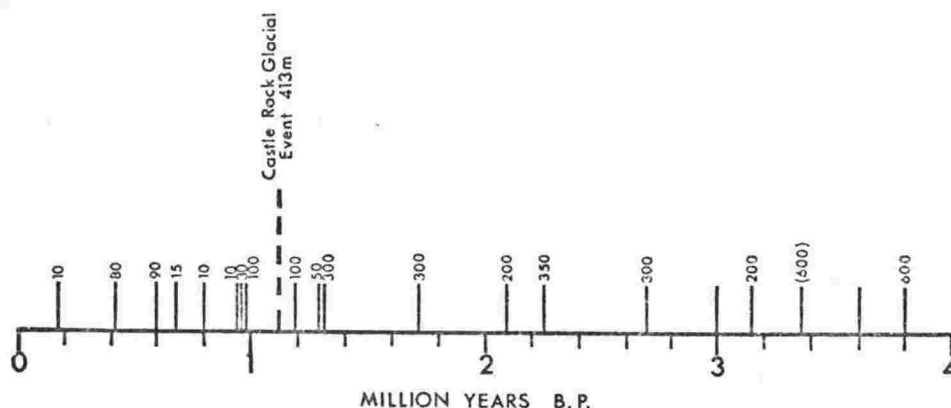
FIGURE 3.19 Frequency of K/Ar dates (see Tables 3.2 and 3.3) of subaerial cones and flows below previous higher ice levels in the McMurdo Sound area. Approximate height of sample site above sea level is shown in metres; S.L. = sea level. See text for discussion of Castle Rock age.

in a subaerial environment below the level of known ice-rafted
erratics (i.e. below the level of previous major ice cover).
The height of the samples above sea level is shown. The only
dated sample indicative of a subglacial eruption is from
Castle Rock (see below) which is 1.12±0.4 m.y. Based on
Figure 3.19 any major expansion of the Ross Ice Shelf was
unlikely to be longer than 0.2 to 0.3 m.y., and in the last
million years must have been even shorter.

ANORTHOCLASE PHONOLITE ERRATICS

Anorthoclase phonolite (kenyte) erratics and moraines
occur over a wide area of McMurdo Sound, including Black Island
and Brown Peninsula (Vella, 1969), Koettlitz Glacier (Blank
et al., 1963) and the Lower Taylor Valley. The only known
vents for these very characteristic lavas are on Mt Erebus.
Lavas from Cape Barne are 0.94 m.y. (Table 3.2), the oldest
K/Ar ages for the Erebus centre, and it would seem that
anorthoclase phonolite lavas from Mt Erebus are unlikely to
be older than about 1.5 m.y. This puts an upper age limit on
the moraines and places constraints on the direction of ice
movement. An anorthoclase phonolite erratic from the Lower
Taylor Valley has been dated at 1.54±0.3 m.y. (Table 3.3),
which is in agreement with the age limits suggested above.

HYALOCLASTITE

Hyaloclastite is generally considered to form in a
subaqueous environment, either submarine or subglacial, and
therefore can be used to indicate former sea or ice levels. In
the Hallett volcanic province, Hamilton (1972) has described
and discussed extensive deposits of hyaloclastite which he
considers are subglacial. Within the Erebus volcanic province,
hyaloclastite is found at Castle Rock, Boulder Cones, Turks
Head area, DVDP holes 1 to 3 and Minna Bluff (Hamilton, 1972).
Castle Rock is composed of poorly bedded hyaloclastite
and the turret shape resembles table mountains (although
smaller in dimensions) in Iceland that are subglacially formed.

If it is assumed that no large amount of isostatic uplift occurred (in fact Ross Island appears to be sinking due to crustal loading), the 413 m elevation of Castle Rock, the shape and the lithology all suggest a subglacial origin. An olivine-augite basanite dike which probably fed lava to the ice contact zone where the hyaloclastite was forming has a K/Ar age of 1.12 ± 0.4 m.y. (Table 3.2). Castle Rock is therefore evidence of an expanded Ross Ice Shelf 1.12 m.y. ago, which was at least 400 m thicker than at present. This period of glaciation could correlate with invasions of the Taylor and/or Wright Valleys by the Ross Ice Shelf. Calkin and Bull (1972) suggest that the Pecten Glaciation of the Wright Valley was between 0.8 and 1.2 m.y. although indirect evidence suggests the Pecten Glaciation may be older than 3 m.y. (Webb, 1972; McSaveney and McSaveney, 1972).

Further studies, particularly radiometric dating of the included clasts within hyaloclastites of the McMurdo Sound area, may help delineate the glacial history of the region.

CHAPTER FOUR

PETROGRAPHY

Nomenclature

The nomenclature of alkali rocks is confusing and subject to considerable debate; in addition, many of the different rock types are rare and restricted to a few localities (Sorensen, 1974; Johannsen, 1939). Classification based on modal compositions (Streckeisen, 1967) is difficult for many reasons, the most obvious being the fine-grained or glassy nature of many volcanic rocks. Consequently many recent classifications have been based on whole-rock chemical analyses and CIPW normative mineralogy.

In their study of rocks from the East Otago Volcanic Province of New Zealand, Coombs and Wilkinson (1969) examined the lineages and fractionation trends, and the associated lava nomenclature in alkali volcanic rocks. Lavas were classified on their chemical and modal compositions and normative mineralogy. The scheme used in this thesis, follows Coombs and Wilkinson (1969) with minor alterations suggested by Price (1973). Field and thin section nomenclature, when chemical analyses are not available, are discussed below.

Alkali volcanic rocks are divided into sodic and potassic series, the former being classically represented by Hawaiian and Hebridean lavas and the latter by Tristan de Cunha and Gough Island lavas. Division into the two series is subjective. Price (1973) and Irvine and Baragar (1971) used the normative orthoclase content whereas Macdonald (1960) and Macdonald and Katsura (1964) used a Na_2O/K_2O ratio of 2. In strongly undersaturated lavas, Coombs and Wilkinson (1969) noted several difficulties with the Na_2O/K_2O ratio; such as the tendency of lava series to show a decreasing Na_2O/K_2O ratio with differentiation. In this scheme the basaltic lavas would belong to a sodic series whereas the rocks with a high differentiation

index (benmoreites, tristanites, trachytes) would be potassic.
Notwithstanding this and other difficulties mentioned by
Coombs and Wilkinson (1969), the division based on a Na_2O/K_2O
ratio has been found convenient in this study. When the bulk
of the lavas from any one region have a Na_2O/K_2O ratio of >2,
then all the lavas are referred to the sodic series, even if
some individual rocks have an alkali ratio of <2, and
conversely, rocks are referred to the potassic series if the
bulk of the lavas have Na_2O/K_2O <2. Once assigned to either
the sodic or potassic series the appropriate nomenclature
(Table 4.1 and Fig. 4.1) may be applied.

TABLE 4.1. Nomenclature, based on normative mineralogy, used to
describe rocks of the McMurdo Volcanic Group.

Sodic Series	Potassic Series	Features and Comments
alkali basalt basanite basanitoid	alkali K-basalt K-basanite –	An >50, Ne <5 An >50, Ne >5 Used synonymously with basanite (see text)
hawaiite nepheline hawaiite –	trachyandesite nepheline trachyandesite quartz trachyandesite	An=30-50, Ne <10 An=30-50, Ne >10 An=30-50, Q>0, D.I. <65
mugearite nepheline mugearite	trachyandesite nepheline trachyandesite	An=10-30, Ne <10, D.I. <65 An=10-30, Ne >10, D.I. <65
benmoreite nepheline benmoreite	tristanite nepheline tristanite quartz tristanite	D.I.=65-75, Ne <10 D.I.=65-75, Ne >10 D.I.=65-75, Q>0
trachyte phonolite – –	K-trachyte phonolite quartz K-trachyte peralkaline K-trachyte	D.I. >75, Ne <10 D.I. >75, Ne >10 D.I. >75, Q>0, Q>Ac D.I. >75, Ac>0, Ac>Q, Ac>Ne

An – normative $\frac{100An}{An+Ab}$,   Ne – normative nepheline.

D.I. – Differentiation Index (Thornton and Tuttle, 1960).

Q – normative quartz,   Ac – normative acmite.

Mineralogical prefixes are used to distinguish some rock types, the phonolites
in particular have been classified as anorthoclase phonolite (equivalent
to the kenyte lavas of the Erebus centre), pyroxene phonolite (for
aegirine-augite bearing phonolites) and kaersutite phonolite.
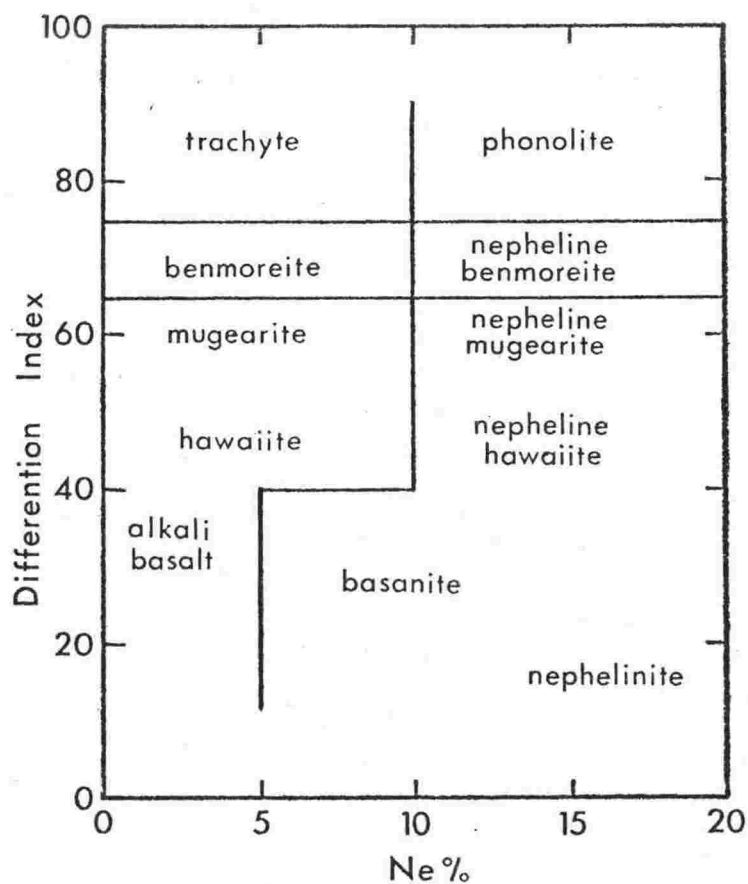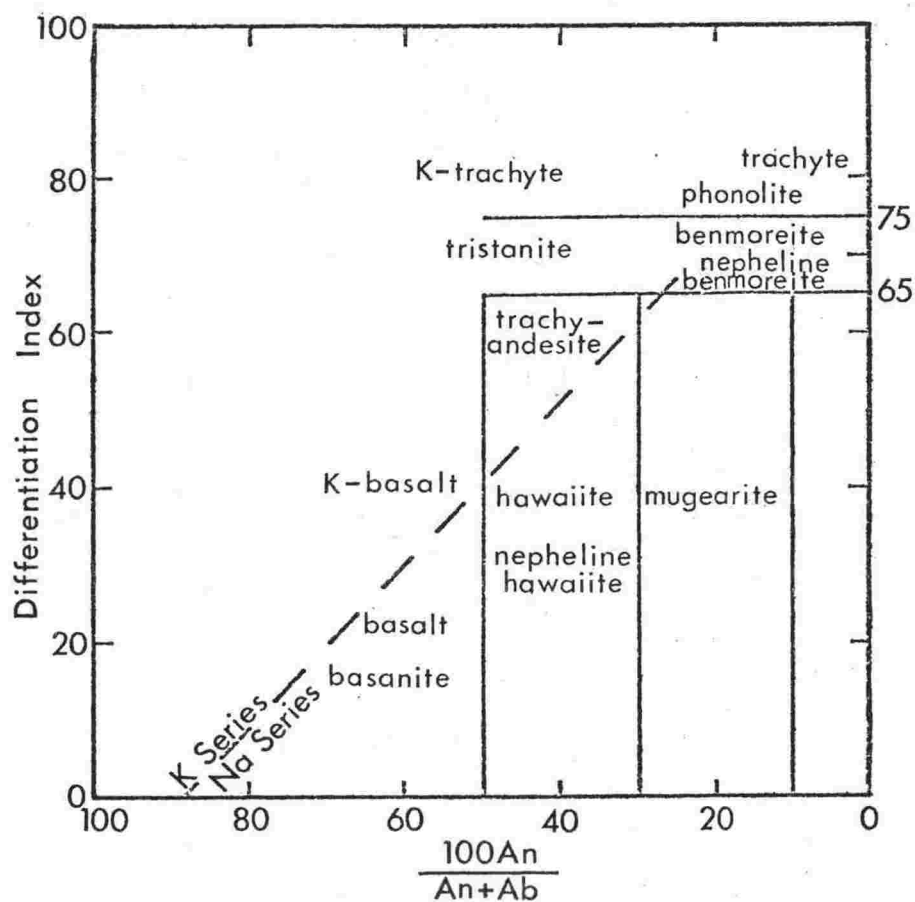
FIGURE 4.1 Plot of differentiation index (D.I.) versus normative plagioclase ($\frac{100An}{An+Ab}$) and D.I. versus normative nepheline (Ne), showing classification scheme used to describe rocks of the McMurdo Volcanic Group.

Several points to note in the classification are the
absence of the term 'trachybasalt' and its replacement by
'K-basalt'; and the use of qualifiers, based on phenocryst
abundances, in the phonolites (Table 4.1). The terms basanite
(modal nepheline present) and basanitoid (no modal nepheline)
are used synonymously, as nepheline is not usually detected in
routine thin section examination but is often found to be
present, particularly in the groundmass, by staining, electron
microprobe or x-ray diffraction studies.

The use of the term 'kenyte' to describe the Mt Erebus
lavas has been discussed by Smith (1954) and Treves (1962).
At Mt Kenya (Africa), the type locality for kenyte, the lavas
contain nepheline phenocrysts; but because it is absent in the
Mt Erebus kenyte lavas, Smith (1954) recommended naming them
Antarctic kenyte. Boudette and Ford (1966) and Treves (1962,
1967) use the less specific names anorthoclase trachyte or
anorthoclase phonolite and this nomenclature is followed in
this thesis. It should be noted however that kenyte is so
strongly entrenched that it remains in use as a field term and
in general descriptive studies.

Throughout this study, the term 'intermediate' has been
used to collectively refer to all rocks of composition between
basalt and trachyte/phonolite, that is rocks classified as
hawaiite, mugearite, benmoreite, trachyandesite and tristanite
and their saturated or strongly undersaturated equivalents.

Field and Thin Section Nomenclature

In the field the rocks were divided into dark or light
coloured and called basalt and trachyte, respectively. These
names were then prefixed, in order of abundance, by the main
phenocryst phases (e.g. olivine-augite-hornblende basalt;
hornblende trachyte). This scheme was also followed in
describing thin sections, when no chemical analyses were
available, and has been used extensively by Cole and Ewart

(1968), Cole *et al.*, (1971), Treves and Kyle (1973a) and Kyle and Treves (1974a). When modal feldspar determinations were made, further refinements in the nomenclature were possible (Table 4.2). Rocks described in hand specimen as basalts, were on analysis found to range from basanite to benmoreite.

An attempt was made to use different nomenclature for samples which are described only in thin section and/or hand specimen, so as to distinguish them in the text from the analysed samples. The use of basalt, trachybasalt and kenyte (Table 4.2) were useful in this respect. There is dual usage of trachyte, but as it was found that the analysed 'trachytic' lavas are almost all phonolites or K-trachytes, the name 'trachyte' generally denotes samples described in thin section and/or hand specimen.

TABLE 4.2.   Field and thin section nomenclature.

basalt   - Dark coloured 'basaltic' rocks containing olivine, augite, kaersutite and plagioclase. Thin sections found to contain modal labradorite.

trachybasalt   - Rocks found from thin section to contain modal andesine or oligoclase.

trachyte   - Light coloured 'trachytic' rocks, with alkali feldspar > plagioclase in thin section.

kenyte   - Field name used for all porphyritic anorthoclase phonolite and anorthoclase trachyte lavas from Mt Erebus.

CIPW Norm Calculations

CIPW weight percent norms are given for whole rock analyses in Chapter 7. Where the iron oxidation state is not determined, norms have been calculated with standard values of Fe_2O_3, using the convention of Thompson *et al.*, (1972):

1) where $Na_2O + K_2O < 4\%$, $Fe_2O_3 = 1.50\%$.
2) where $Na_2O + K_2O = 4-7\%$, $Fe_2O_3 = 2.00\%$.
3) where $Na_2O + K_2O > 7\%$, $Fe_2O_3 = 2.50\%$.

The differentiation index (D.I.) of Thornton and Tuttle (1960) = normative Q+Ab+Or+Ne+Lc.

Descriptive Petrography

Introduction

Excellent petrographic descriptions of McMurdo Volcanic Group rocks, made by previous workers, have provided a useful background to this mineralogical and geochemical study, and only brief additional descriptions are given in this thesis.

Phenocrysts are defined as any mineral grain whose maximum dimension exceeds 1 mm, microphenocrysts are less than 1 mm but are larger than mineral grains in the groundmass.

Balleny volcanic province

The only published petrographic studies are given by Mawson (1950), who described 11 thin sections, mainly of olivine trachybasalt and minor olivine-augite basalts.

Samples examined in this study are olivine and olivine-augite basalts (basanites) and a trachybasalt similar to that described by Mawson (1950).

Olivine-basanite
Usually contains euhedral, seriate phenocrysts and microphenocrysts of olivine, commonly embayed and showing brown iddingsite alteration around the rim and along cracks. The fine-grained intergranular groundmass contains labradorite, olivine, pinkish titanaugite, opaques and minor glass which may be chloritized(?).

Olivine-augite basanite

Typically porphyritic containing varying amounts of seriate olivine and augite phenocrysts and microphenocrysts. Rare augite phenocrysts (up to 10 mm) are rounded and may be partially oxidised together with a few oxidised kaersutite phenocrysts. Pinkish titanaugite phenocrysts are euhedral with weak zoning and have red-brown chrome spinel inclusions. Olivine is colourless and often a little ragged around the edges. The weakly intergranular groundmass contains labradorite laths, augite, cubic opaques and minor glass.

Melbourne volcanic province

Lavas at most centres are adequately described by previous workers, however a wide range of rock types at The Pleiades has been revealed in this study and these are briefly described below. Nathan and Schulte (1967, 1968) have described the lavas from Mt Melbourne, Mt Overlord and the small volcanic centres of the Local Suite; Watters (in Gair, 1967) has described lavas and plutonic inclusions from Mt Overlord.

THE PLEIADES

Basanite

Usually vesicular, with some flow banding and only weakly porphyritic with a few seriate phenocrysts and microphenocrysts of augite (dominant) and olivine (rare). Augite is light brown, euhedral, weakly zoned (occasionally sector zoned) and rarely embayed. Microphenocrysts may form glomeroporphyritic clumps up to 0.4 mm in diameter. Olivine phenocrysts are euhedral and colourless. Microphenocrysts of magnetite and xenocrysts (1 mm) of strongly altered plagioclase are rarely noted. The groundmass is variable but typically dense and intersertal and charged with minute opaque grains. Labradorite laths (<0.1 mm long), rare olivine, stubby augite and opaques are the main groundmass phases.

Nepheline hawaiite

Strongly vesicular and microporphyritic, with microphenocrysts of subhedral brown kaersutite which commonly has a sieve margin studded with minute opaques; completely oxidised pseudomorphs are rare. Inclusions of apatite occur in the larger microphenocrysts. Some kaersutite grains have dark brown, rounded cores otherwise zoning is minimal. The groundmass is vitrophyric with kaersutite, slightly pink augite, plagioclase microlites and opaques.

Nepheline mugearite

Usually only weakly porphyritic with oxidised pseudomorphs (3 mm long) after kaersutite and rare phenocrysts (xenocrysts?) of skeletal magnetite. Kaersutite microphenocrysts are pleochroic from light to reddish brown and show varying degrees of alteration from about half to complete; alteration products consist mainly of pyroxene, plagioclase, magnetite and a very dark brown to opaque mineral not positively identified but possibly rhönite. The hyalophitic groundmass has brown glass with laths and microlites of plagioclase (oligoclase?), magnetite, augite and minor olivine with brown alteration rims.

Nepheline benmoreite

Fine-grained with a pilotaxitic to trachytic texture, they may be microporphyritic with rare fresh-oxidised micro-phenocrysts of kaersutite, pinkish and brownish euhedral augite (often sector zoned), magnetite and alkali feldspar. The groundmass consists of interlocking laths of anorthoclase and sanidine, ragged greenish ferroaugite, magnetite, rare fayalitic olivine and glass.

Trachyandesite

Porphyritic with seriate, euhedral phenocrysts of olivine and augite, and corroded, altered xenocrysts (?) of andesine-labradorite. Rare microphenocrysts of kaersutite occur and in

one slide appear to be xenocrystic. The pilotaxitic to
hyalophitic groundmass contains andesine microlites, olivine,
augite, magnetite and accessory apatite. Hematite occurs in
the groundmass of an oxidised sample.

Tristanite

Mainly microporphyritic with rare phenocrysts, although
a strongly porphyritic sample contains seriate phenocrysts of
andesine, slightly pink augite and olivine. Glomeroporphyritic
clumps of plagioclase with included olivine and augite are also
found in the same sample and may indicate that it is a cumulate.
In the phenocryst-poor lavas, strongly corroded plagioclase,
anorthoclase and augite with large embayments are probably
xenocrysts. In one sample there are microphenocrysts of nearly
completely oxidised pseudomorphs after kaersutite. The ground-
mass is variable and may show a vitrophyric, hyalopilitic and
intersertal texture with andesine prisms,laths and microlites,
very light brown to light green augite, olivine, cubic opaques,
kaersutite (usually oxidised) and glass.

K-trachyte

Usually holocrystalline, fine-grained and typically
showing a trachytic texture, although occasionally rare
microphenocrysts occur. One sample is strongly porphyritic with
phenocrysts of oligoclase, anorthoclase and magnetite and micro-
phenocrysts of biotite, kaersutite, fayalitic olivine and ferro-
augite. The microphenocryst assemblage is anorthoclase,
magnetite, green ferroaugite and accessory apatite. The ground-
mass varies from typically trachytic to orthophyric and consists
of interlocking feldspar (0.1 to 0.3 mm long) with ragged green
ferroaugite and cubic opaques filling the interstices. Fine
brown aegirine (?), rare aenigmatite and minor zircon also occur
in the groundmass.

Peralkaline K-trachyte

Typically holocrystalline and fine-grained with a trachytic texture. Phenocrysts and microphenocrysts of sanidine, anorthoclase and aegirine may make up to 1% of the lava. Interlocking sanidine laths (0.2 mm long) have the interstices filled by cubic opaques and either ragged brown to green aegirine or reddish brown to black aenigmatite. Needles of zircon occur as inclusions in the sanidine.

Essexite

Although only weakly undersaturated (Ne = 0.8 to 1.1%) the chemistry of these inclusions indicates they are cumulates and this partially masks their obvious alkali composition. Two samples (25263, 25268) are hypiomorphic granular with an average grain size of 2 mm. Pink titaniferous augite occasionally subophitically encloses olivine and plagioclase. Olivine is generally altered around its rims and in cracks and is also rounded and slightly smaller in grain size than the other minerals. Labradorite is zoned and has alkali feldspar rims. Late stage titanobiotite and kaersutite are found. An average estimated mode is olivine 5%, pyroxene 39%, biotite and kaersutite 2%, feldspar (predominantly plagioclase) 48%, opaques 3% and mesostasis 3%.

Erebus volcanic province

The meticulous and detailed thin section descriptions of Smith (1954) adequately cover the rock types examined in this thesis. Further descriptions and modal analyses are given by Cole and Ewart (1968), Cole et al., (1971), Treves (1962, 1967), Kyle (1971), Adams (1973), Luckman (1974); DVDP lavas are described by Treves and Kyle (1973a), Kyle and Treves (1974a) and Treves and Ali (1974).

CHAPTER FIVE

MINERALOGY

Introduction

A detailed examination of the mineralogy of lavas and of one plutonic inclusion from The Pleiades, DVDP core samples and Mt Erebus were made by electron microprobe. Analyses and analytical techniques are given in Appendix B.

Olivine

Occurrence and Composition

1. THE PLEIADES

Olivine occurs in all lava types except nepheline benmoreite and peralkaline K-trachyte. Of the 8 thin sections examined by electron microprobe, olivine is present in all samples except K-trachyte 25687 and peralkaline K-trachyte 25699, in these aegirine-augite and acmite are the dominant mafic minerals. Nash and Wilkinson (1970) have shown that fayalitic olivine will not co-exist with acmite, due mainly to the stability of the minerals under different f_{O_2} conditions.

Olivine ranges in composition from Fo_{81} in trachyandesite (25703) to Fo_{46} in nepheline benmoreite (25661). There is then a break in composition with fayalitic olivine (Fo_{22}) in K-trachyte (25702). Analyses are plotted in Figs 5.1 and 5.2.

Within any one sample analyses show little variation and where present is due to normal zoning. Groundmass composition is usually more iron-rich than the phenocrysts or similar to the rims of the phenocrysts. In 25666 a small xenocryst with a reaction rim has a composition of Fo_{48} which differs significantly from the Fo_{77-72} of the phenocrysts.

<div align="center">LEGEND</div>

●   Basanite lavas, DVDP 1 and 2, phenocrysts

○   Basanite lavas, DVDP 1 and 2, microphenocrysts and groundmass

▲   Xenocrysts in DVDP nepheline hawaiite (2-62.41) and nepheline mugearite (2-39.28)

△   Xenocrysts in DVDP benmoreite (1-131.36)

■   All lavas, The Pleiades (Appendix B, Part 1, Table 1)

□   Anorthoclase phonolite, Mt Erebus (Appendix B, Part 3, Table 1)

◆   Peridotite inclusion, Brandau Vent, Royal Society Range (McIver and Gevers, 1970)

      All plots in weight percent.
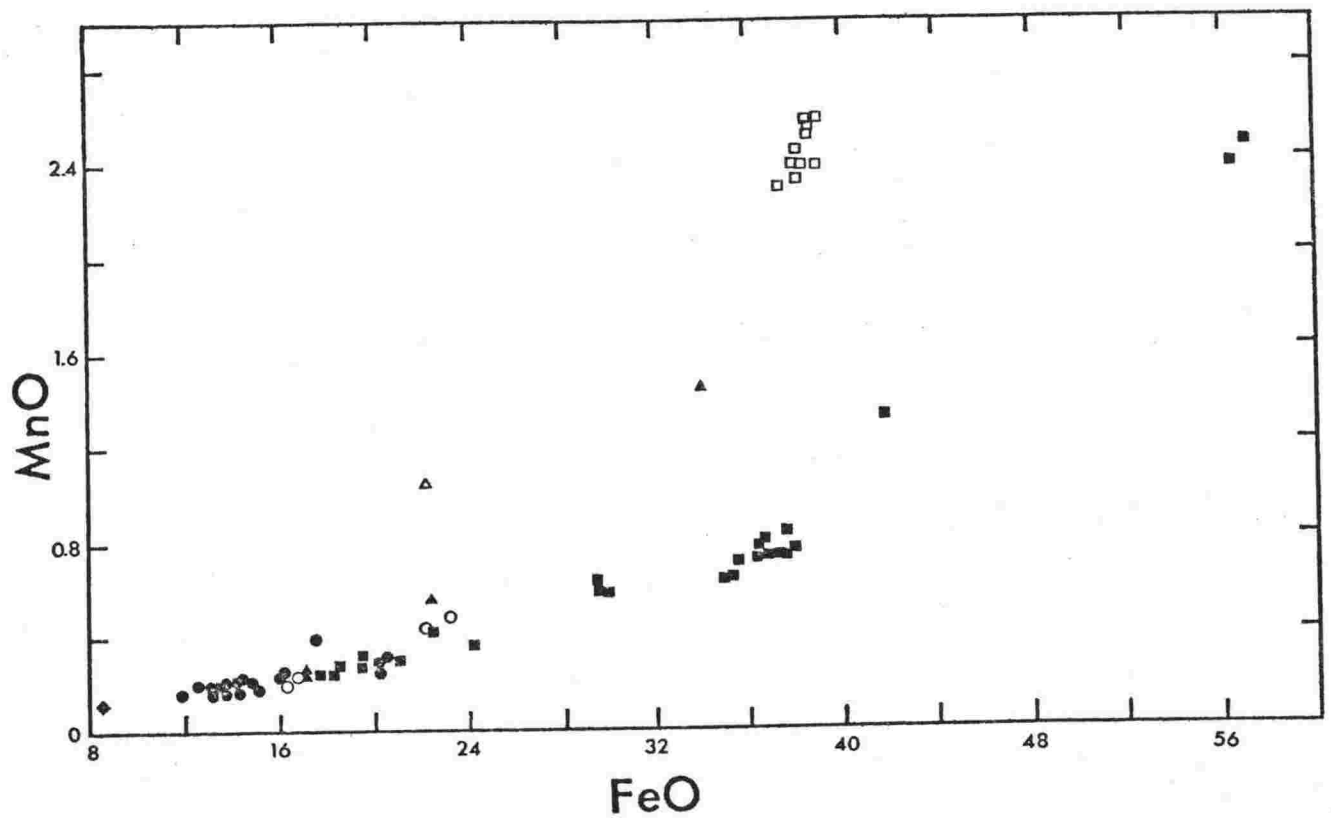
FIGURE 5.1   Variation of MnO vs FeO* in olivine from the McMurdo
              Volcanic Group.   Electron microprobe analyses.
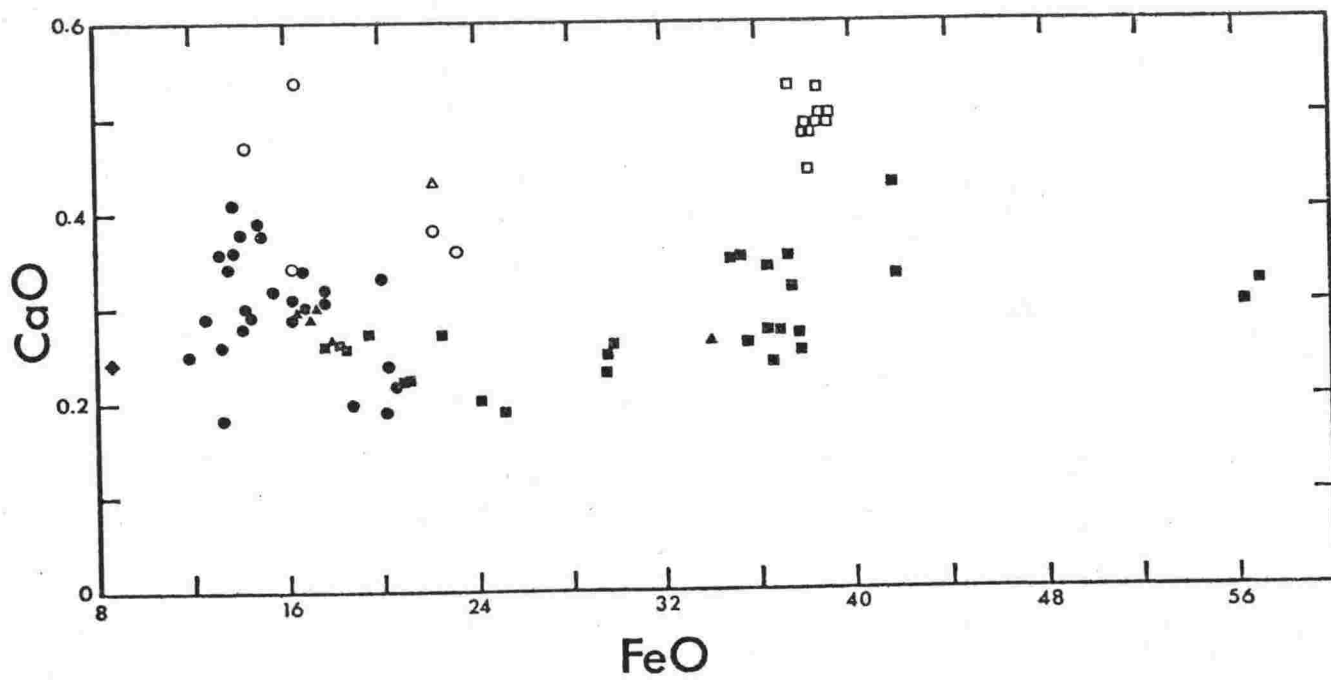
FIGURE 5.2   Variation of CaO vs FeO* in olivine from the McMurdo
              Volcanic Group.   Electron microprobe analyses.

2. DVDP 1 AND 2

Olivine occurs as seriate phenocrysts and as a groundmass constituent in the basanites, but in all other lavas primary olivine is absent. Numerous samples contain rounded resorbed xenocrysts invariably with oxidised kaersutite as a reaction rim around the xenocrysts. The olivine shows only a limited range in composition from Fo_{87} to Fo_{74} (Fig. 5.1) which is typical of basaltic rocks. A xenocryst of Fo_{60} in 2-62.41 is unusual as it is the only iron-rich olivine analysed from the DVDP lavas. The presence of this fayalitic olivine xenocryst suggests a derivation from an intermediate or phonolitic lava, however the hawaiite and benmoreite from DVDP and phonolites from Observation Hill, show an absence of olivine. The origin of this particular grain is therefore unknown. The xenocrysts in the nepheline mugearite (2-39.28) are similar in composition to phenocrysts in the basanites (Fig. 5.2) and are probably derived from that source.

Zoning occurs but is generally only minor, the largest variation noted being Fo_{85} to Fo_{78}. One grain exhibited very weak reversed zoning.

The composition of olivine inclusions in clinopyroxene phenocrysts from basanite 2-99.34 and 2-103.15 is similar to that of the olivine phenocrysts, indicating there was no major compositional change from the earliest forming crystals.

A euhedral microphenocryst of olivine in basanite 2-99.34 shows an unusual symplectic texture of intergrown spinel and magnetite (Fig. 5.3). A microprobe scan (Fig. 5.4) across part of the grain shows the variation in Fe and Mg, resulting from the intergrowths, and also the weak zoning of the olivine towards the rim. Symplectic intergrowths of magnetite + enstatite or hematite + forsterite occur as a result of high temperature oxidation (Haggerty and Baker, 1967). This origin is not applicable to the sample under consideration as it is extremely fresh and spinel is not a product of such oxidation. Minute octahedra and plates of exsolved ferric and chromic oxides are found in some olivines (Deer et al., 1963),
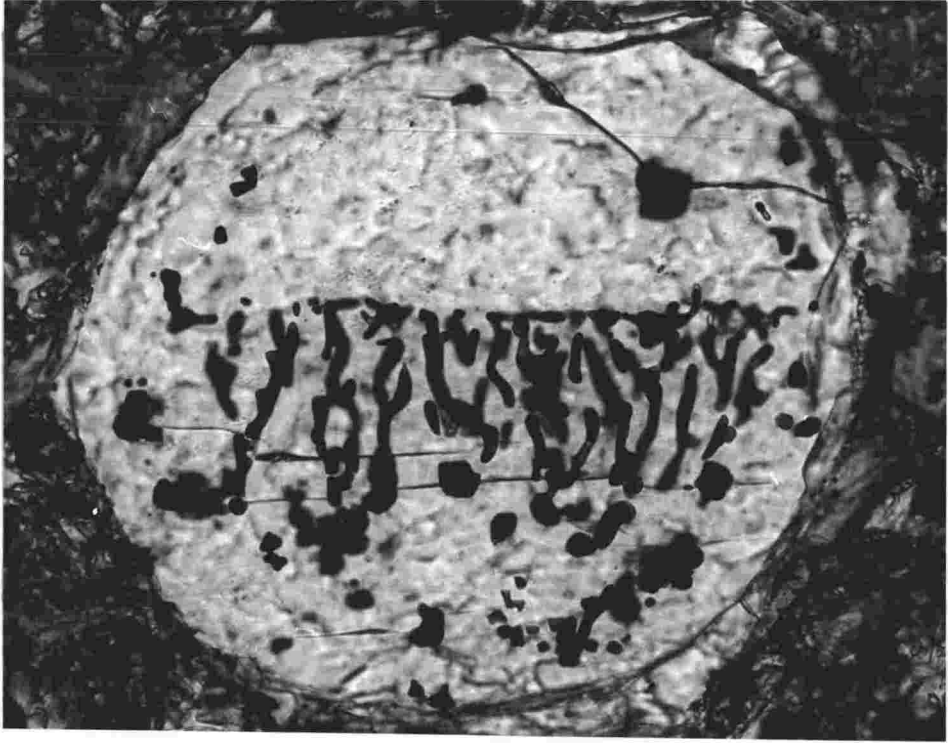
FIGURE 5.3   Photomicrograph of symplectic intergrowth of magnetite
             and spinel in olivine microphenocryst from DVDP basanite
             2-99.34 m.
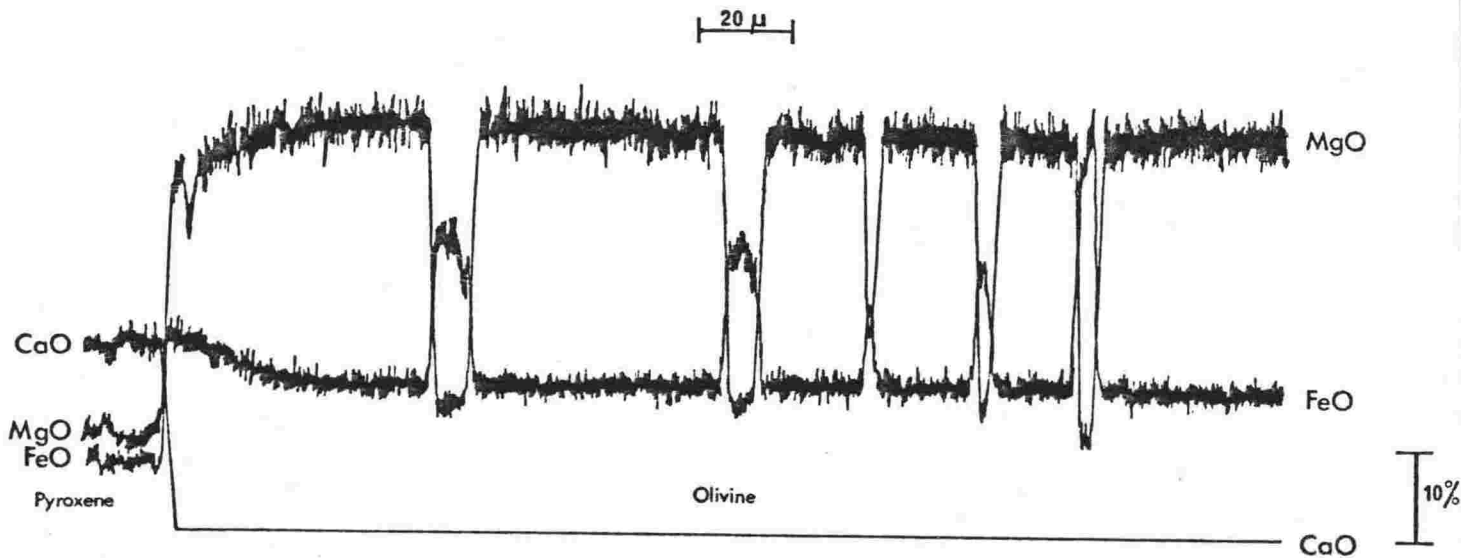
FIGURE 5.4   Electron microprobe scan across part of the olivine figured
             above, showing the variation of MgO and FeO*. Magnetite
             intergrowths have higher FeO* than the spinel intergrowths
             Note the weak normal zoning in the outer 20 μm of the
             olivine.   The olivine is rimmed by clinopyroxene.

however large symplectic intergrowths have not been reported.
The mode of formation for the intergrowths is therefore unknown.

3. MT EREBUS

Fayalitic olivine, which shows only minor compositional
variation (Fo_{49} to Fo_{52}), occurs in anorthoclase phonolite lavas
from Mt Erebus (see Chapter 8).

Minor Element Variation

1. MANGANESE (MnO)

The MnO content of the olivine increases with increasing
FeO (Fig. 5.1). Olivine from Mt Erebus anorthoclase phonolite
contains 2.4% MnO which is noticeably higher than olivines from
other centres. In undersaturated plutonic rocks, Simkin and
Smith (1970) reported olivines with up to 1.9% MnO, while
recently Stephenson (1974) described nepheline syenites from
south Greenland, in which olivine contained 4.8 to 11.1% MnO.
Olivine in trachytes and phonolites from Mt Suswa, Kenya
contain 3.5% MnO (Nash *et al.*, 1969).

2. CALCIUM (CaO)

CaO content is variable within any one rock type, but when
the range of olivine compositions are compared the CaO generally
appears constant with increasing FeO (Fig. 5.2).

Simkin and Smith (1970) showed CaO content is usually less
than 0.10% for olivines in plutonic rocks but exceeds 0.10% for
hypabyssal and extrusive rocks. They suggested that the calcium
content was dependent on pressure. Stormer (1973) has shown that
the entry of calcium into olivine is probably controlled by the
following reaction:

$$CaMgSi_2O_6 = Ca(SiO_4)_{\frac{1}{2}} + Mg(SiO_4)_{\frac{1}{2}} + SiO_2 \qquad \ldots(1)$$
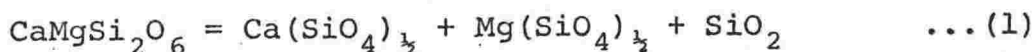
diopside   Ca-olivine   forsterite   liquid

hence

$$K_{(T,P)} = \frac{a_{SiO_2}^{liquid} \cdot a_{Mg(SiO_4)_{\frac{1}{2}}}^{olivine} \cdot a_{Ca(SiO_4)_{\frac{1}{2}}}^{olivine}}{a_{CaMgSi_2O_6}^{pyroxene}} \qquad \ldots(1A)$$

Thus the activity or mole fraction of $Ca(SiO_4)_{\frac{1}{2}}$ in olivine is strongly influenced by the silica activity (the effective thermodynamic concentration of silica) at any given temperature and pressure. Stormer (1973) concludes that if the silica activity remains constant, rapidly rising calcium content in olivine may indicate a pressure drop whereas decreasing or constant calcium content may indicate the dominance of decreasing temperature.

The lack of any widespread scatter of CaO in olivine of the McMurdo Volcanic Group lavas probably indicates decreasing temperature has been important during the crystallization of these lavas.

3. NICKEL (NiO)

NiO wt % decreases as the Fa content increases (Fig. 5.5). Forbes and Banno (1966) examined in detail the nickel-iron content of peridotite inclusions and cognate olivine in basanite samples from Hut Point Peninsula (Fig. 5.5). They showed compositional gaps in the Ni content of olivines from the inclusions compared to olivine in the basanites. A fractionation trend of decreasing Fa was observed in the basanites, but not in the peridotite inclusions (Fig. 5.5). Forbes and Banno (1966) therefore concluded the olivine in the inclusions was not formed from the same parent melt as the basanite olivine.

Olivine from DVDP samples have similar NiO versus Fa trends (Fig. 5.5) to those studied by Forbes and Banno (1966). Olivine cores in the basanite also have similar NiO and Fa contents

.LEGEND

INCLUSIONS

□ Peridotite inclusions, Hut Point Peninsula (Forbes and Banno, 1966).

■ Olivine-titanaugite gabbro inclusions, Hut Point Peninsula (Forbes and Banno, 1966).

◇ Peridotite inclusion, Brandau Vent, Royal Society Range (McIver and Gevers, 1970).

BASANITE LAVAS (all from Hut Point Peninsula)

▲ Phenocrysts (Forbes and Banno, 1966).

● Phenocrysts (this study).

△ Microphenocrysts (Forbes and Banno, 1966).

▽ Groundmass (Forbes and Banno, 1966).

○ Groundmass (this study).

OTHER LAVAS

+ The Pleiades (this study).

Arrows show compositional zoning from core to rim of grains.
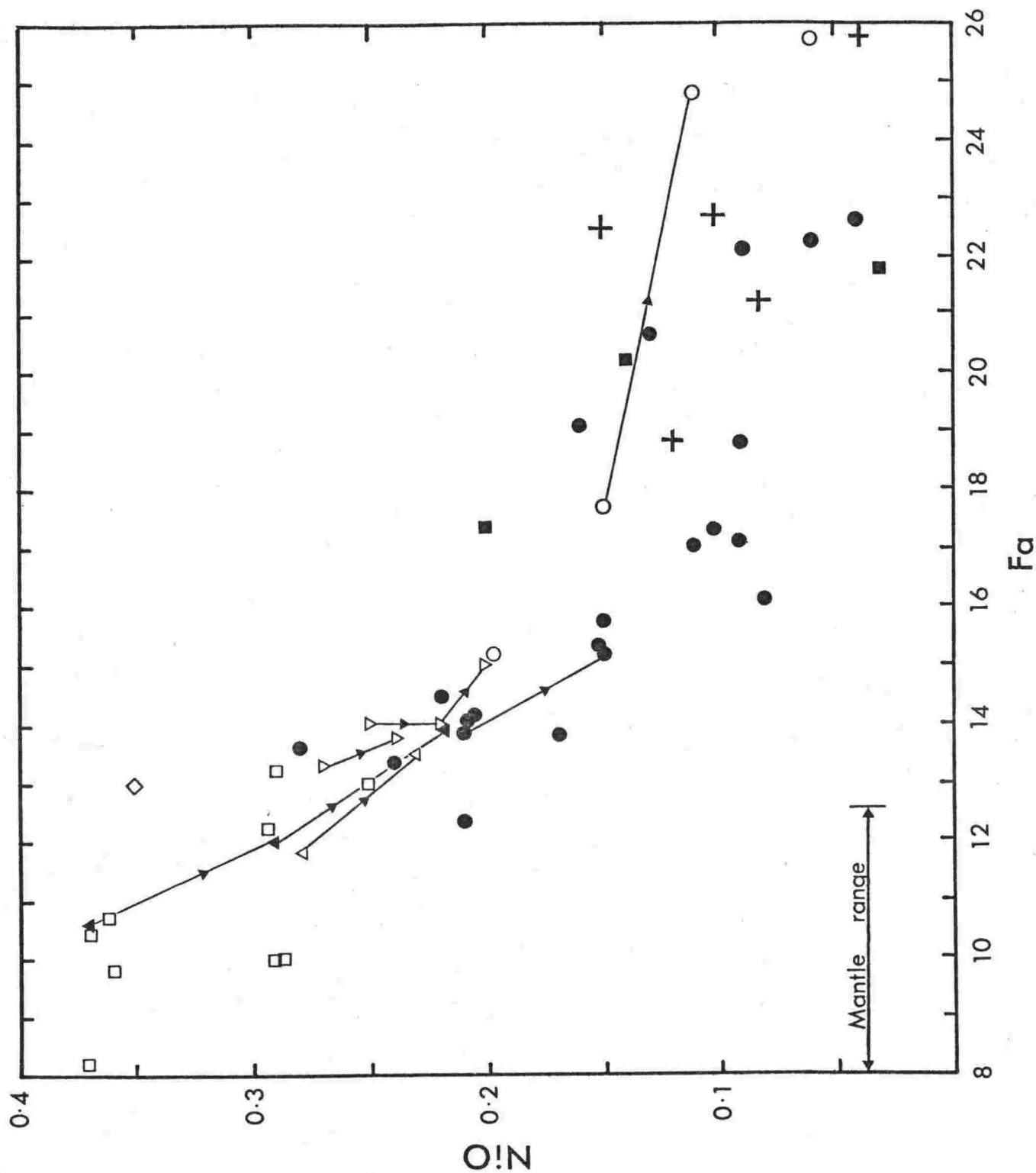
FIGURE 5.5 Variation of NiO (wt %) vs Fa (mole %) in olivine from
mafic and ultramafic inclusions and basaltic lavas from
the Erebus volcanic province. Olivine in intermediate
lavas from The Pleiades, Melbourne volcanic province
also shown.

to olivines from the peridotite inclusions. As the inclusions probably formed under constant pressure and temperature conditions in the upper mantle or lower crust they would be expected to be unzoned (as shown by Forbes and Banno, 1966). Zoning of olivine in the basanites indicates they were formed under varying conditions (such as decreasing temperature - as indicated above by the Ca content) probably as the magma ascended to the surface. One would therefore expect only the cores of the basanite olivines to be similar in composition to the inclusion olivine. This is certainly the case for some of the analysed olivines (Fig. 5.5) and therefore it cannot be concluded that the olivines from the basanites and peridotite inclusions did not form from the same melt.

Olivines in basanites from this study have higher Fa contents than those studied by Forbes and Banno (1966). They overlap in NiO and Fa contents with olivines from titanaugite-olivine peridotite inclusions (Fig. 5.5) suggesting they are autolithic, the inclusion may be high level crystal cumulates.

Pyroxene

Occurrence

Clinopyroxene occurs as phenocrysts, microphenocrysts and in the groundmass of almost all lavas of the McMurdo Volcanic Group. It is absent in occasional phonolites and K-trachytes where the main mafic minerals are aenigmatite or kaersutite.

No orthopyroxene has been found in any lavas, so in the following discussion where the term 'pyroxene' is used it always refers to 'clinopyroxene'.

1. THE PLEIADES

Two groups of pyroxenes can be distinguished in thin section:

i. In the basic and intermediate lavas (excluding the nepheline benmoreites), pyroxene is usually euhedral and occurs as phenocrysts and microphenocrysts, with resorbed xenocrysts rare. It is generally brown to colourless although occasionally it may be pinkish. Sector zoning is common in basanite pyroxenes (e.g. 25679) and normal zoning is present in pyroxenes from all rock types.

ii. In the K-trachyte, peralkaline K-trachyte and nepheline benmoreite lavas the pyroxene is typically green and may be slightly pleochroic. Brownish acmitic pyroxene may be present in the more differentiated lavas. The pyroxene is usually a groundmass constituent, and is anhedral with a ragged outline as it fills the interstices between the flow banded feldspar laths and microlites. Occasional green euhedral microphenocrysts are observed. In a peralkaline K-trachyte (25698), pyroxene is not present, aenigmatite is the main mafic phase.

2. DVDP 1 AND 2

Clinopyroxene is ubiquitous in the DVDP lavas. In the basanites euhedral seriate phenocrysts are present (with the exception of 1-187.64), while microphenocrysts and groundmass pyroxene are always found. Three stages of development are recognised within pyroxenes from the basanites and some nepheline hawaiites. The cores of some phenocrysts are light green to green and often show an irregular outline which suggests resorption (Fig. 5.6). Surrounding this is usually a colourless, or occasionally weak-brown zone of variable width and the grain has a pink to purplish rim (Fig. 5.6). Microphenocrysts and some phenocrysts have colourless cores and purple rims while the groundmass pyroxenes are a uniform purple colour.

Weakly pinkish to colourless phenocrysts, microphenocrysts and groundmass pyroxene occur in the nepheline hawaiite, although rare crystals have green sodic cores similar to
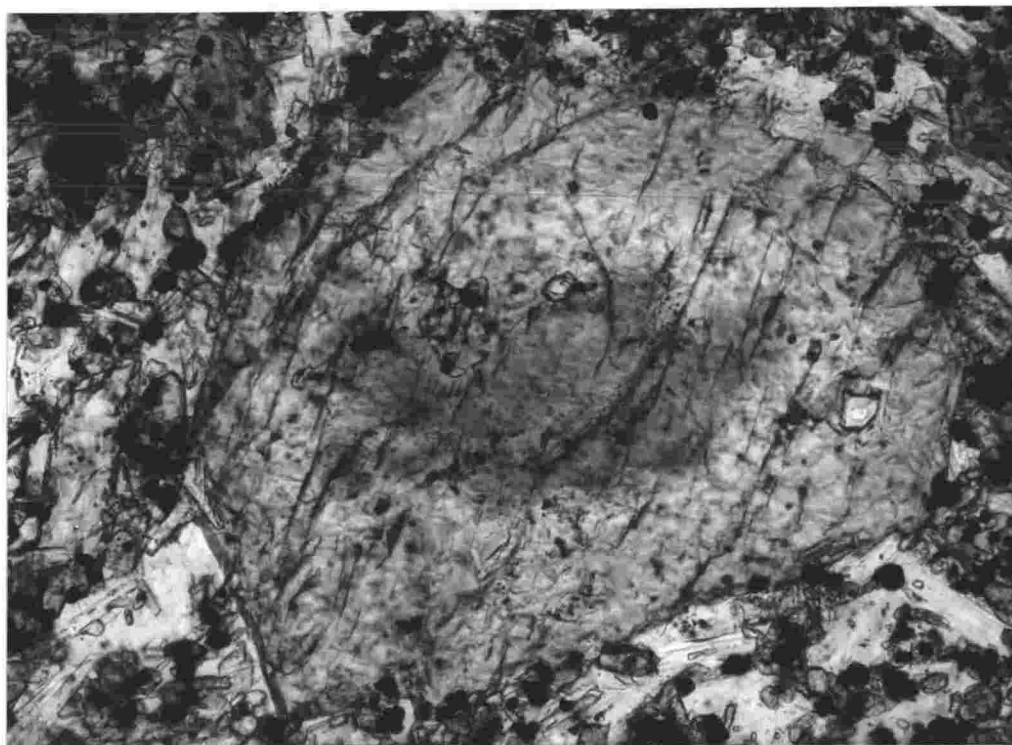
Microphenocryst in 2-103.15; Grain 6 (see Appendix B, Part 2). Grain is 0.5 mm wide.
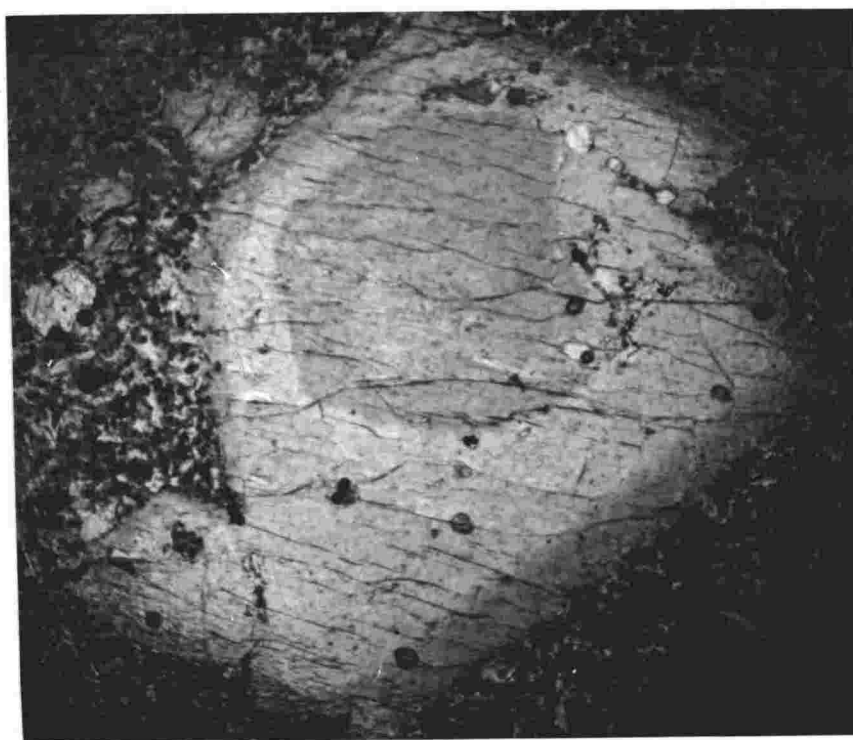
Phenocryst in 2-99.34; Grain 4 (see Appendix B, Part 2). Centre zone is 0.75 mm wide.

FIGURE 5.6 Photomicrographs of clinopyroxene in basanite lavas from DVDP holes, showing zoning from green Na, Fe-rich core to colourless salite. Some grains show a thin purple Ti-rich salite rim.

pyroxenes from the basanites. In the nepheline mugearites
and nepheline benmoreites microphenocrystic and groundmass
pyroxene vary from colourless to very weak brown and light
pinkish.

3. MT EREBUS

Microphenocrysts of brownish resorbed pyroxene are
usually present in the anorthoclase phonolite bombs and lava
from the summit of Mt Erebus (see Chapter 8).

Chemistry

INTRODUCTION

Electron microprobe analyses of the pyroxenes are given
in Appendix B along with their formulae based on 6 oxygen.
Total Fe was determined as FeO, but as the pyroxenes contain
>0.5% Na_2O, a proportion of the Fe must be Fe_2O_3 (particularly
in the more sodic pyroxenes). Several methods of calculating
Fe^{3+} were used;

i. Fe_2O_3 was calculated assuming all sodium occurred
as an acmite component ($NaFe^{3+}Si_2O_6$), in which case the
molecular proportion of Fe_2O_3 equals Na_2O. This scheme was
used by Kyle (1974b)(See Appendix B; Part 2).

ii. Fe_2O_3 was calculated assuming the pyroxene was
charge balanced, the equation given by Papike et al., (1974)
was used;

$$^{VI}Al + {}^{VI}Fe^{3+} + {}^{VI}Cr^{3+} + 2{}^{VI}Ti^{4+} = {}^{IV}Al + {}^{M2}Na$$

Calculations were made using a computer program modified from
a program supplied by Professor J. J. Papike.

Both methods of determining Fe_2O_3 are approximations,
however the charge balance procedure has been used in this
thesis. After Fe^{3+} was calculated theoretical pyroxene

molecules were calculated following a convention given below.

CLINOPYROXENE RECALCULATION

Several schemes for recalculating clinopyroxene analyses have been proposed by Kushiro (1962), and Cawthorn and Collerson (1974). Neither method is satisfactory when dealing with a wide range of clinopyroxenes, particularly of Na-rich compositions, and when Fe^{3+} is calculated by charge balance procedures. Theoretical end-members have therefore been calculated using a scheme based in part on Kushiro (1962) and Cawthorn and Collerson (1974). The scheme is considered applicable to volcanic rocks but is not recommended for use with high-pressure pyroxenes from eclogites and other rocks which contain jadeite or Na and Al rich pyroxenes.

The procedure is;

(1) Combine Na+K, Al+Cr, Mg+Ni, Fe^{2+}+Mn

(2) Form Ca-Ti-tschermak ($CaTiAl_2O_6$); if insufficient Al form Na-Ti-pyroxene [$NaTi_{0.5}(Fe^{2+}Mg)_{0.5}Si_2O_6$] (Papike et al., 1974) with the excess Ti. Formation of the latter pyroxene is very rare and will only occur in Al-poor acmitic pyroxenes.

(3) Form acmite ($NaFe^{3+}Si_2O_6$), if there is insufficient Fe^{3+}, incorporate Fe^{2+} to satisfy the formula.

(4) Form ferri-tschermak ($CaFe^{3+}_2SiO_6$) molecule.

(5) Form calcium tschermak ($CaAl_2SiO_6$) molecule.

(6) Form wollastonite ($Ca_2Si_2O_6$) from remaining Ca after deducting Ca in Ca-Ti-tschermak, ferri-tschermak and Ca-tschermak molecules.

(7) Form enstatite ($Mg_2Si_2O_6$) from remaining Mg after subtracting Mg in Na-Ti-pyroxene.

(8) Form ferrosilite ($Fe_2Si_2O_6$) from remaining Fe^{2+}+Mn after subtracting Fe in Na-Ti-pyroxene and any Fe^{2+} converted to Fe^{3+} to satisfy the acmite component.

Several examples of analyses recalculated by the proposed scheme and those of Kushiro (1962) and Cawthorn and Collerson (1974) are given for comparison in Table 5.1.

TABLE 5.1   Comparison of schemes used to recalculate clinopyroxene analyses.

Sample	2-103.15	25699	2-103.15
Grain	6C	8	16
SiO_2	47.0	50.9	46.3
Al_2O_3	5.66	0.30	8.26
TiO_2	1.08	0.83	3.23
Fe_2O_3	7.16	31.5	1.40
FeO	9.16	0.33	4.17
MnO	0.70	1.68	0.08
MgO	6.54	0.00	12.4
CaO	20.8	1.33	22.7
Na_2O	1.94	12.7	0.61
Cr_2O_3	-	-	0.66
Total	100.04	99.57	99.81

Recalculated clinopyroxene molecules.

	2-103.15 (6C)			25699 (8)			2-103.15 (16)		
	Kyle	Kushiro	C&C	Kyle	Kushiro	C&C	Kyle	Kushiro	C&C
Acmite $NaFeSi_2O_6$	14.5	14.5	0.0	91.2	92.5	95.2	4.4	3.9	0.0
Jadeite $NaAlSi_2O_6$	N.F.(b)	0.0	14.6	N.F.	1.4	1.4	N.F.	0.5	4.4
Ca-Ti-Tschermak $CaTiAl_2O_6$	3.1	3.1	3.2	0.7	0.0	0.0	9.1	9.0	9.0
Ca-Fe^{3+}-Tschermak $CaFe^{3+}AlSiO_6$	N.F.	6.2	N.F.	N.F.	0.0	N.F.	N.F.	0.0	N.F.
Ca-Tschermak $CaAl_2SiO_6$	9.7	6.6	2.5	0.0	0.0	0.0	9.1	9.8	6.9
Fe^{3+}-Tschermak $CaFe^{3+}_2SiO_6$	3.1	0.0	10.5	0.0	0.0	0.0	0.0	0.0	2.9
Wollastonite $Ca_2Si_2O_6$	34.9	34.9	35.3	2.4	2.8	2.9	36.4	35.8	35.8
Enstatite $Mg_2Si_2O_6$	18.8	18.8	19.0	0.0	0.0	0.0	34.6	34.4	34.4
Ferrosilite $Fe_2Si_2O_6$	15.9	15.9	14.9	2.3	3.3	0.5	6.4	6.6	6.5
Na-Ti-Pyroxene $NaTi_{0.5}R_{0.5}Si_2O_6$ (a)	0.0	N.F.	N.F.	3.4	N.F.	N.F.	0.0	N.F.	N.F.

(a)   R = (Fe^{2+}, Mg)

(b)   N.F. = not formed.

Note the breakdown of the Kushiro and C&C calculations for Na, Fe^{3+} pyroxenes (i.e., 25699). Because all the Al is used to satisfy the Na, no Ti component is formed, yet the pyroxene contains 0.83% TiO_2.

CALCIUM, MAGNESIUM, FERROUS IRON (Ca, Mg, Fe^{2+})

The three major end members Ca, Mg, Fe^{2+}+Mn have been recalculated to 100 mole % for all the pyroxenes. When plotted in the pyroxene quadrilateral, some analyses lie above the CaMg - $CaFe^{2+}$ join, due to a large dissolved content of tschermaks molecules. Therefore the wollastonite (Wo), enstatite (En) and ferrosilite (Fs) end-members, calculated by the proposed scheme have also been plotted, these give a more realistic approximation to the pyroxene composition.

1. The Pleiades

Individual analyses are plotted in Fig. 5.7 and summarized in Fig. 5.8.

The most striking feature of the pyroxenes from The Pleiades is their continuous enrichment in Fe^{2+}+Mn with differentiation (Fig. 5.8), a complete sequence from diopside to hedenbergite occurs. A scatter in Fe^{2+}+Mn, Mg and Ca is observed for pyroxenes in the more basic lavas, but this is reduced in plots of Wo, En, Fs (Fig. 5.8). The proportion of Ca and Wo remain constant up to the K-trachyte (25702) and parallel the diopside-hedenbergite join, but they decrease in the acmitic pyroxenes of the peralkaline K-trachyte (25699).

Compositional variation within any one sample is usually small; however in the peralkaline K-trachyte (25699) variation results from Na enrichment and will be discussed below. The largest variation observed is in trachyandesite (25671) where a groundmass grain has the composition $Wo_{42}En_{22}Fs_{36}$ whereas the phenocrysts are $Wo_{44}En_{43}Fs_{13}$.

Zoning within a single grain is in most cases small or non-existent. Except for the peralkaline K-trachyte, the largest degree of normal zoning occurs in K-trachyte (25687) where Fs increases from 17.0 to 22.5. Reverse zoning was noted in several grains from trachyandesite (25703), the largest variation was from $Wo_{43}En_{43}Fs_{14}$ at the core, to
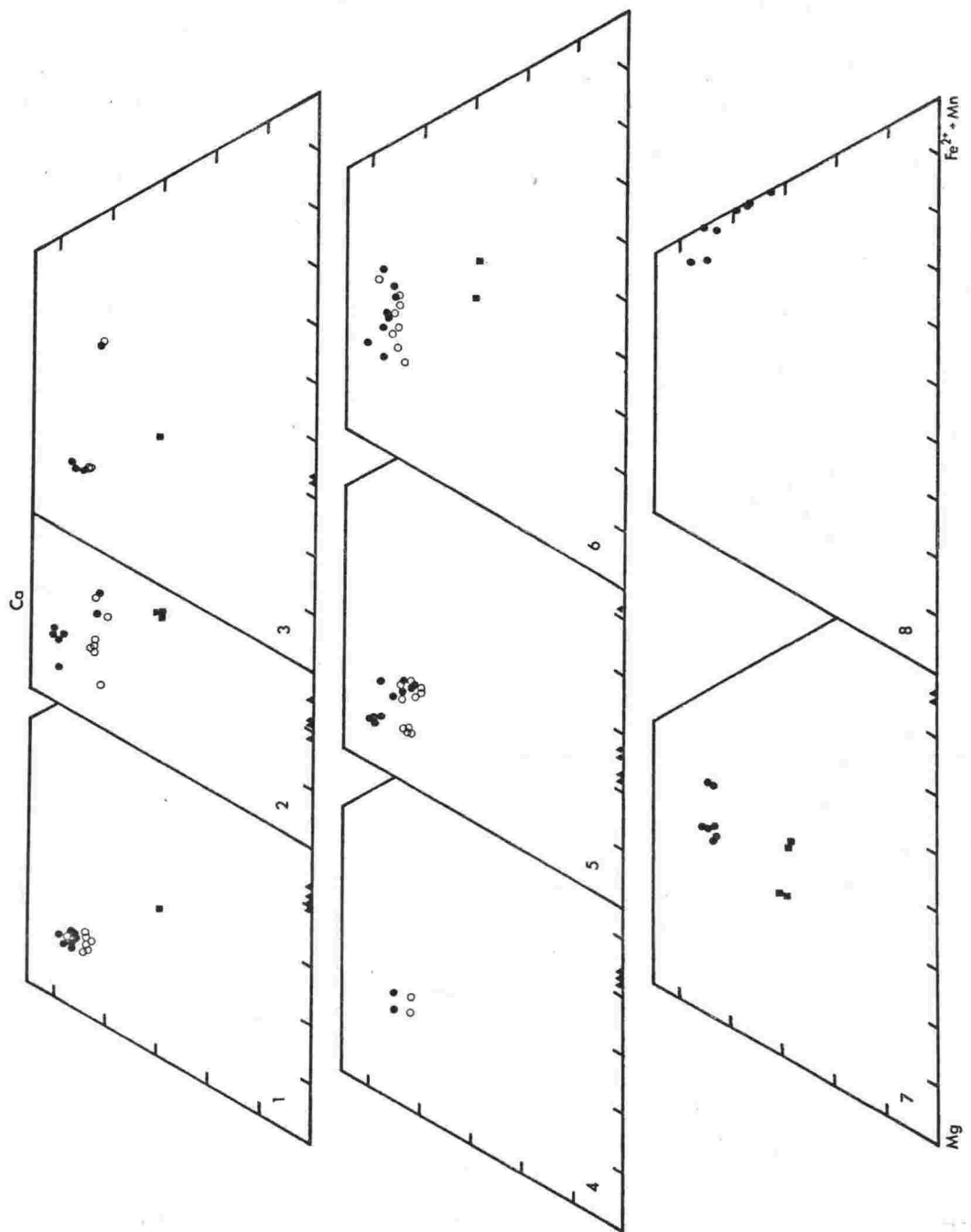
FIGURE 5.7 Composition of clinopyroxene, kaersutite and olivine,
determined by electron microprobe analysis, in rocks
from The Pleiades. Clinopyroxenes are plotted in
terms of Ca, Mg, Fe^{2+}+Mn (mole %) (dots) and recalculated
end-members Wo, Di, Fs (open circles). Olivine (triangles)
is plotted along the base in terms of Fe and Mg (mole %).
Kaersutite (squares) is plotted on the basis of Ca, Mg,
Fe_T (mole %).

1.   25668   essexite inclusion
2.   25703   trachyandesite
3.   25671   trachyandesite
4.   25661   nepheline tristanite
5.   25666   tristanite
6.   25687   K-trachyte
7.   25702   K-trachyte
8.   25699   peralkaline K-trachyte
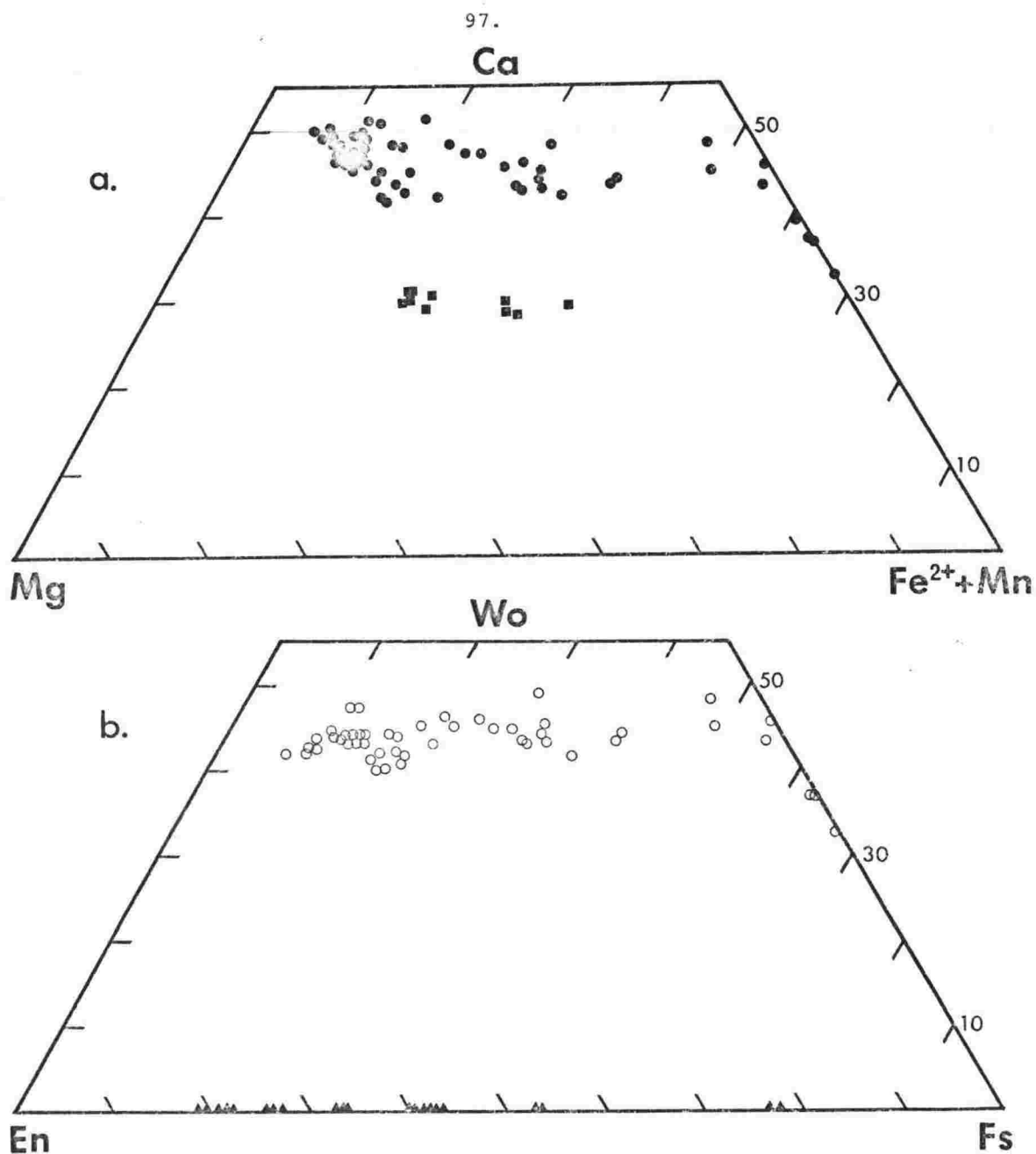
FIGURE 5.8 Compilation of individual microprobe analyses of clinopyroxene,
kaersutite and olivine in rocks from The Pleiades.
a. Clinopyroxene plotted in terms of Ca, Mg, Fe^{2+}+Mn (mole %)
and kaersutite (triangles) plotted in terms of Ca, Mg, Fe_T (mole %).
b. Clinopyroxene plotted in terms of Wo, Di, Fs and olivine plotted
in terms of Fe and Mg (mole %) along base.

$Wo_{42}En_{51}Fs_7$ at the rim, and appears to be related to marked increases in Ti and Al.

2. DVDP 1 and 2

Individual analyses are plotted in Fig. 5.9 and summarized in Fig. 5.10.

The DVDP pyroxenes show extremely Ca-rich compositions, and plots of $Ca, Mg, Fe^{2+}+Mn$ are mainly above the diopside-hedenbergite join (Fig. 5.9). In terms of Wo,En,Fs analyses lie mainly in the diopside, endiopside and salite fields (Fig. 5.10).

The variation of $Ca, Mg, Fe^{2+}+Mn$ in the DVDP pyroxenes is extremely small and even more restricted when the end-members Wo,En,Fs are considered. This is in contrast to the pyroxenes from The Pleiades (Fig. 5.8) which show a well developed crystallization trend. Only one nepheline benmoreite (1-85.35) shows any Fe enrichment while the cores in some phenocrysts from the basanites and nepheline hawaiites also show anomalous Fe enrichment, which is discussed below.

As might be expected from the lack of any crystallization trend, variation within a sample and zoning within a single pyroxene grain is very small. In the pyroxenes with Fe-rich cores, zoning is reversed, this also occurs in the Fe-rich nepheline benmoreite pyroxenes.

3. Mt Erebus

Pyroxenes in the anorthoclase phonolite lavas are plotted in Figure 5.11; they show only minor zoning and no compositional variation between samples. The pyroxenes show almost no enrichment of Fe, even though they occur in a strongly fractionated phonolitic lava. Their composition in terms of Wo,En,Fs are very similar to the DVDP pyroxenes.
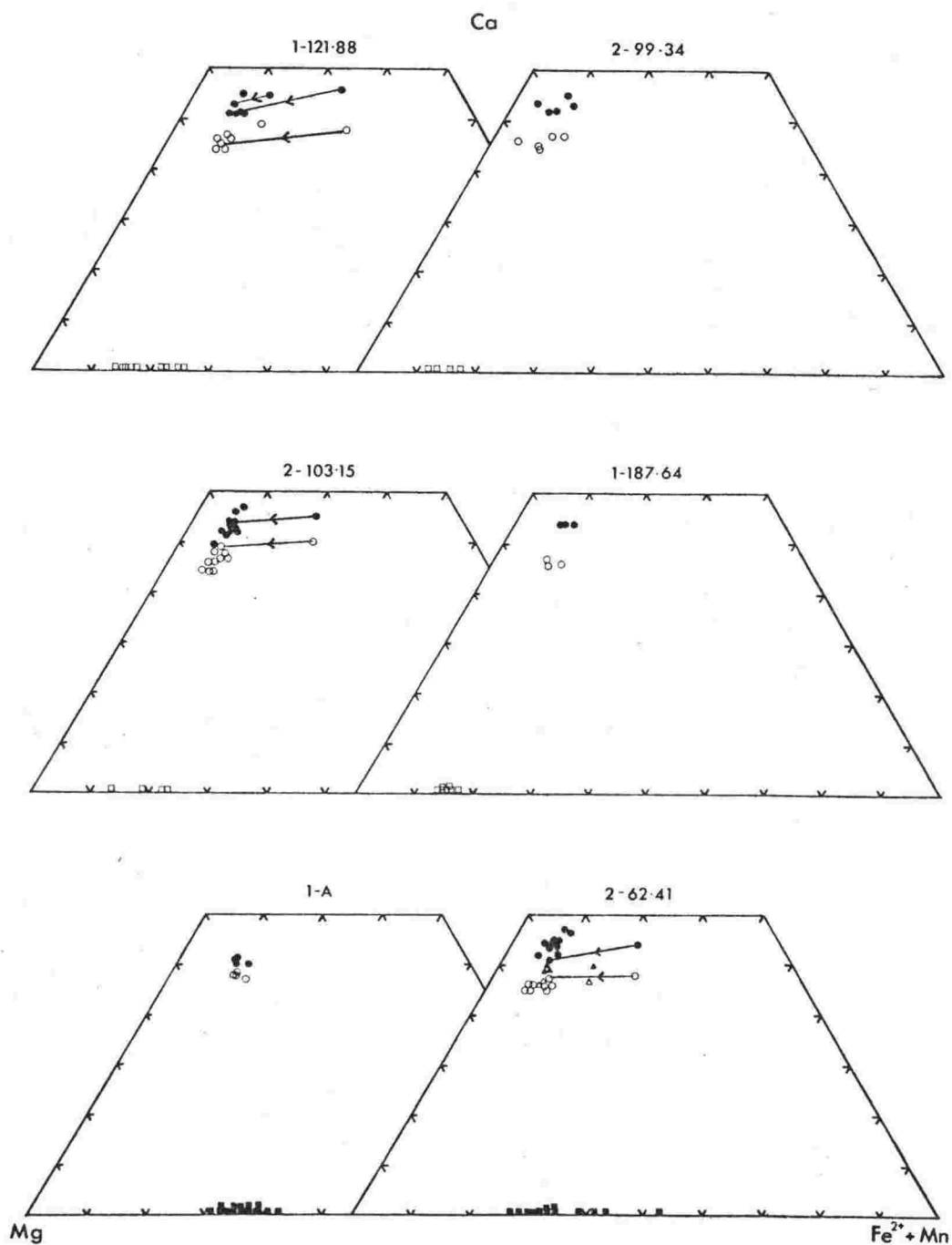
FIGURE 5.9 Composition of clinopyroxene, kaersutite and olivine in
a dike and lava samples from DVDP holes 1 and 2. Clino-
pyroxenes are plotted in terms of Ca, Mg, Fe^{2+}+Mn (mole %)
(dots) and end-members Wo, Di, Fs (open circles),
xenocrysts are also shown (triangles), all analyses
recalculated by charge balance method. Olivine (open
squares) is plotted along the base in terms of Fe and
Mg (mole %). Kaersutite (filled squares) is plotted
along the base in terms of the Mg index ($100Mg/Mg+Fe_T+Mn$).

LEGEND

DVDP (Appendix B, Part 2, Table 2)

●   basanite (1-88.55, 1-121.88, 1-187.64, 2-99.34, 2-103.15)

◪   nepheline hawaiite (2-62.41, 2-70.41)

□   nepheline hawaiite xenocrysts (2-62.41)

△   nepheline mugearite (2-39.28)

▽   nepheline mugearite xenocrysts (2-39.28)

○   nepheline benmoreite (1-57.94, 1-85.35, 2-54.72)
      benmoreite (1-131.36)
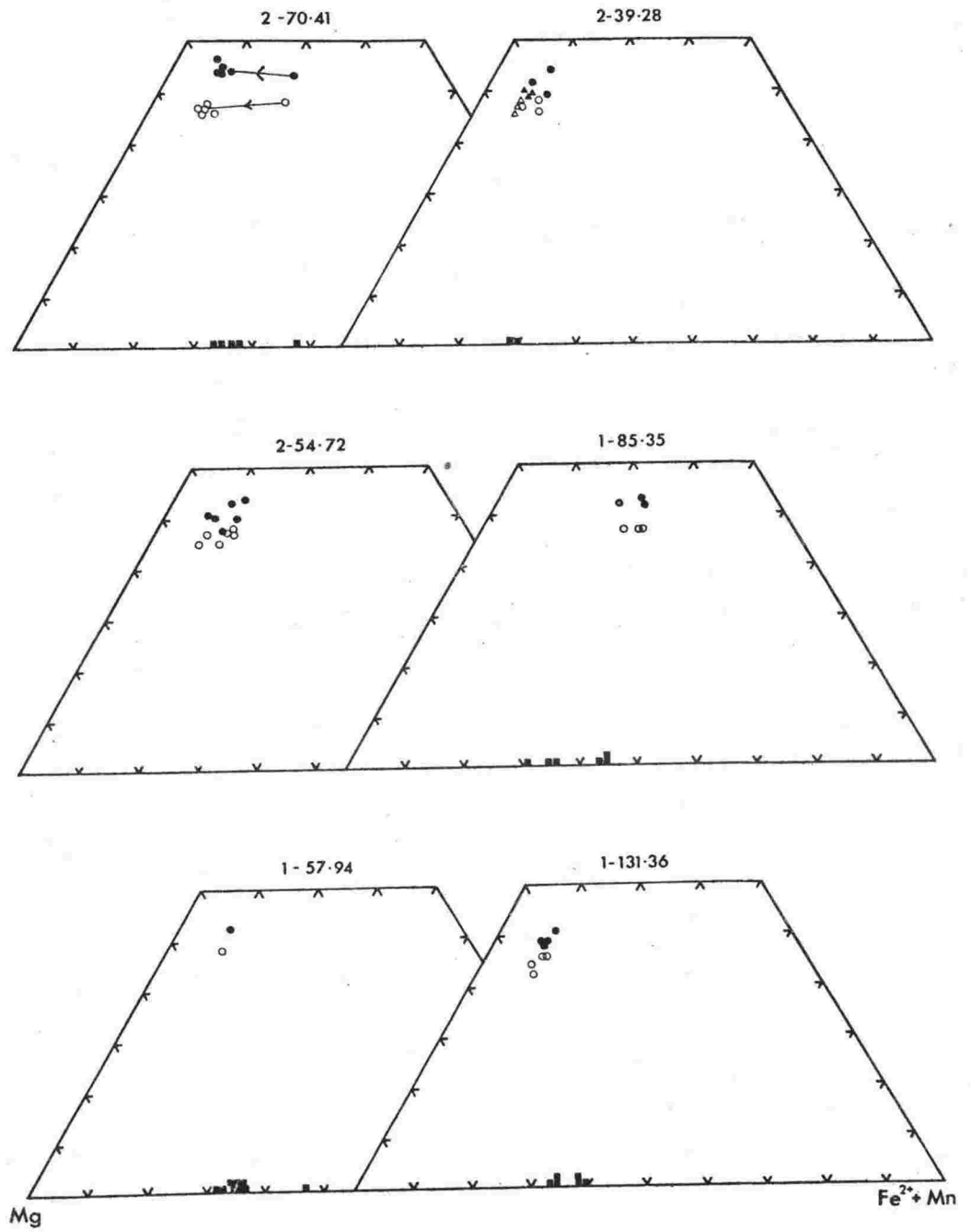
FIGURE 5.9 continued.
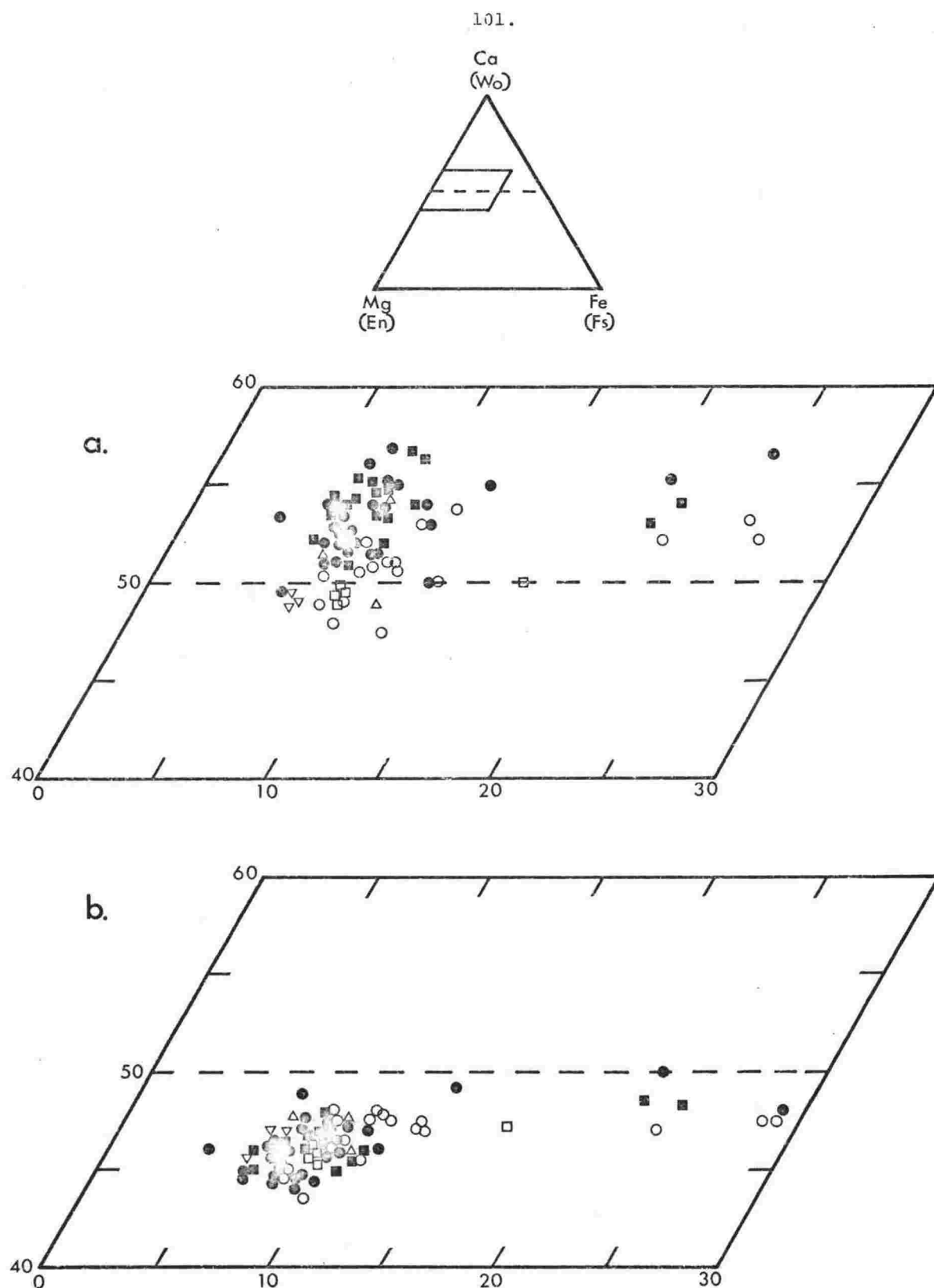
FIGURE 5.10 Compilation of individual microprobe analyses of clinopyroxene in
samples from DVDP holes 1 and 2.
A. Clinopyroxene plotted in terms of Ca, Mg, Fe^{2+}+Mn (mole %).
B. Clinopyroxene plotted in terms of Wo, Di, Fs.
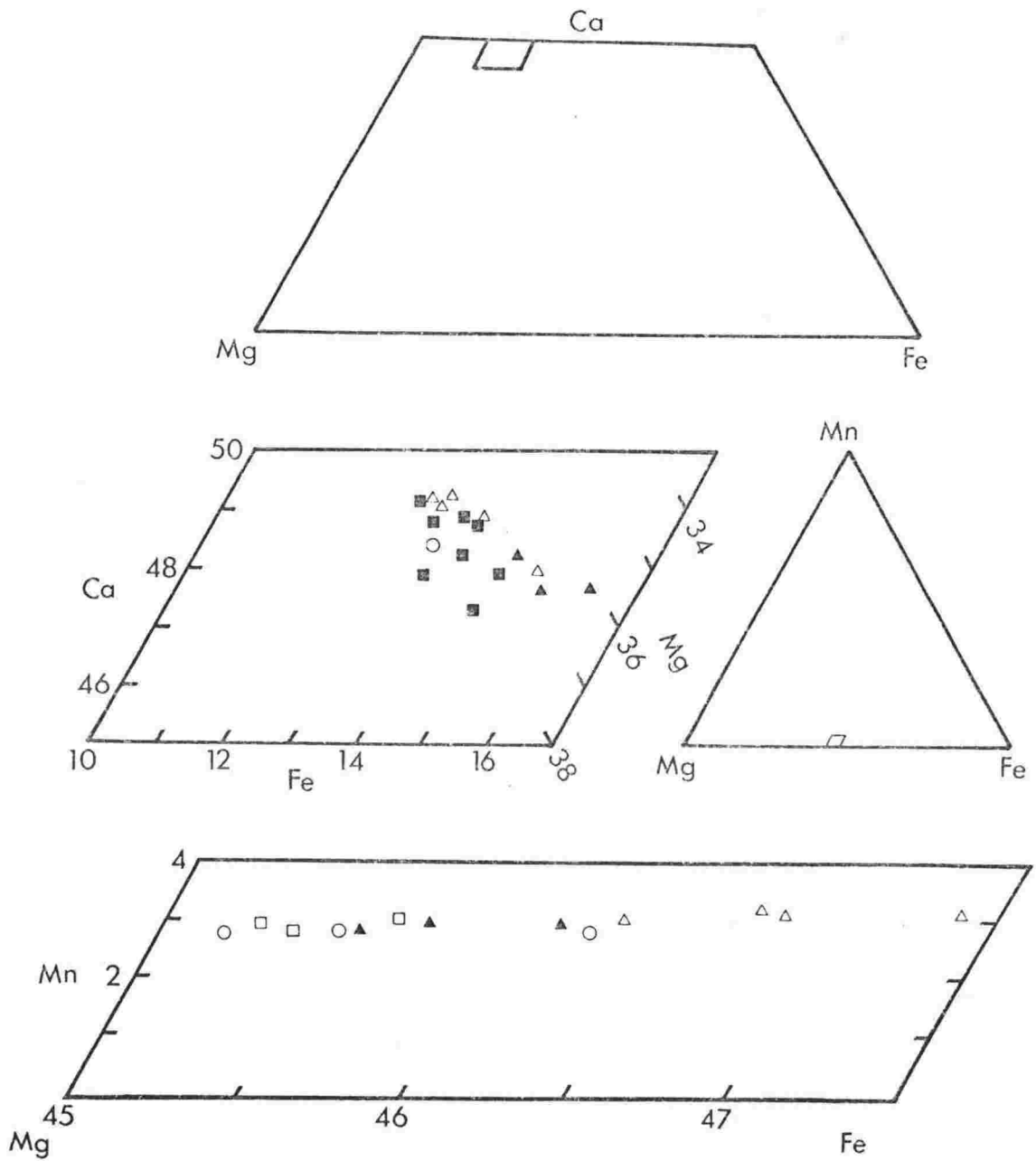
FIGURE 5.11 Composition of clinopyroxene and olivine in recent
volcanic ejecta, Mt Erebus. Lava and bomb samples
25724 (open triangles), 25725 (closed triangles)
25726 (open squares) and inclusions in anorthoclase
phenocrysts-anorthoclase 1 (closed squares),
anorthoclase 2 (circles).

Discussion

Clinopyroxenes in alkali rocks generally show only a
small range in composition, particularly when bulk samples are
analysed; Wilkinson (1974) noted that 'compositions more iron-
rich than Fs_{25} are exceptional'. Gibb (1973) recognised two
clinopyroxene crystallization trends (Fig. 5.12) for alkali
lavas:

i. a calcic augite-calcic ferroaugite-hedenbergite
trend of mildly alkaline basic magmas, e.g. Shiant Isles sill
(Gibbs, 1973) and the Japanese alkali basalts (Aoki, 1964).

ii. a salite-ferrosalite-aegirine trend of strongly
alkaline basic rocks, e.g. Shonkin Sag laccolith (Nash and
Wilkinson, 1970). This trend shows strong Na enrichment and
will be discussed in more detail below.

Both trends contrast strongly with the typical trend
observed for clinopyroxenes in tholeiitic rocks such as
Skaergaard (Fig. 5.12).

Pyroxenes from the McMurdo Volcanics can be considered to
belong to the first crystallization trend listed above, but
can be further subdivided into;

i. a trend of little iron enrichment.

ii. a trend of strong iron enrichment.

Several factors probably control these crystallization trends.
The most significant difference between The Pleiades and DVDP
lavas is their degree of silica saturation, the former is only
weakly unsaturated whereas the DVDP lavas are extremely under-
saturated. Hence silica activity can be expected to play a
dominant control in the trends. Total pressure, oxygen fugacity
and water pressure will also contribute, but these will be
superimposed on the wider differences in magma composition.
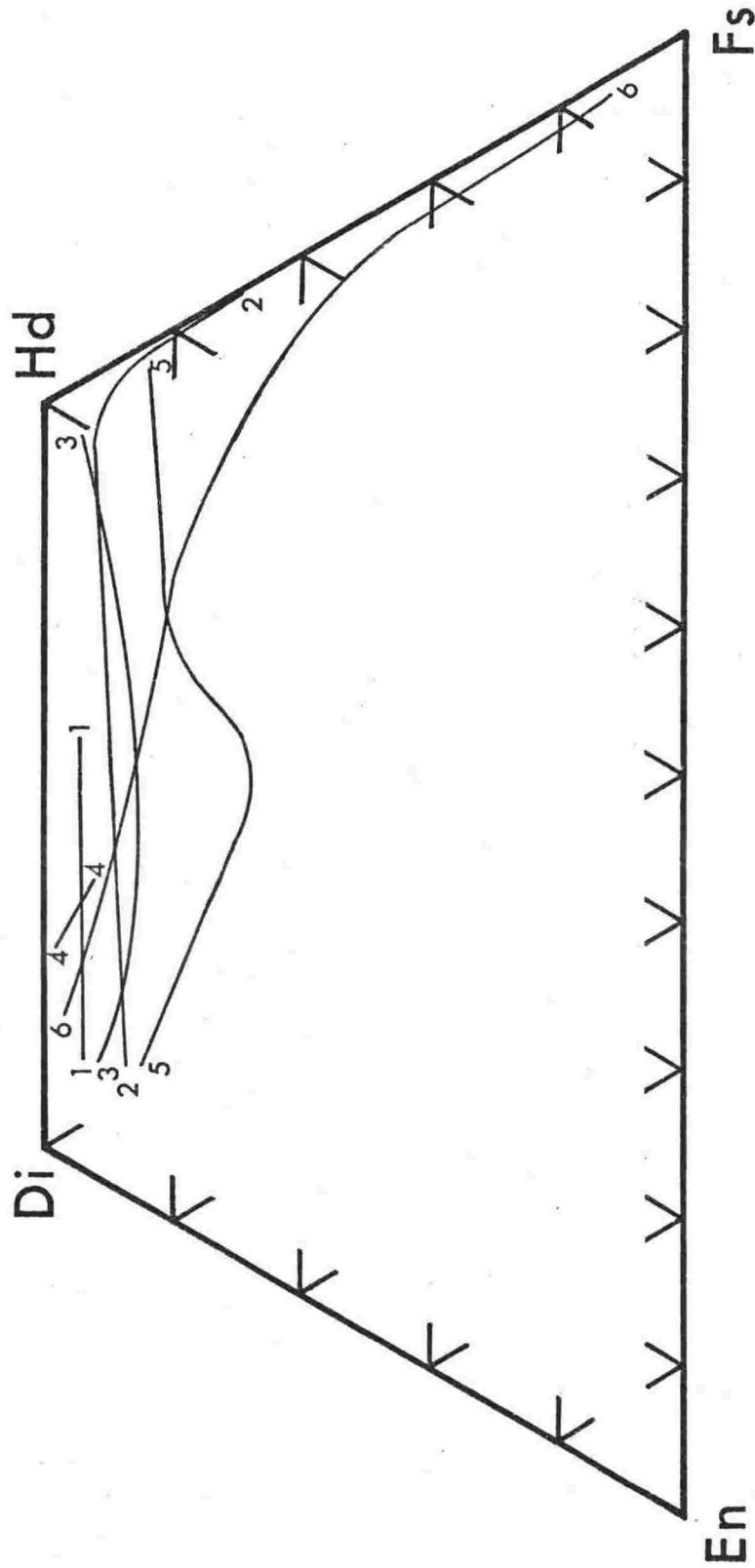
FIGURE 5.12 Generalised clinopyroxene crystallization trends in terms of Di-Hd-Fs-En. 1-DVDP (this study); 2-The Pleiades (this study); 3-Shiant Isles Sill, electron microprobe analyses (Gibb, 1973; 4-Black Jack Sill (Wilkinson, 1957); 5-Skaergaard tholeiitic intrusion (Wager and Brown, 1967); 6-Shonkin Sag laccolith, electron microprobe analyses (Nash and Wilkinson, 1970).

SODIUM (Na)

1. The Pleiades

Although a strong enrichment in Fe^{2+}+Mn is found, Na
shows little variation and is only enriched in the pyroxenes
from peralkaline K-trachyte 25699, where the acmite (Ac)
component ranges from 9 to 91% (Fig. 5.13).

2. DVDP 1 and 2

As might be expected from the lack of Fe^{2+}+Mn enrichment,
Na also shows very little enrichment. When plotted on a
Mg,Fe^{2+}+Mn,Na diagram (Fig. 5.14) the analyses cluster in a
very small field and a short fractionation trend is indicated
by the weakly Fe-enriched pyroxenes from nepheline benmoreite
1-85.35. The trend has a slightly higher Na enrichment than
that for The Pleiades.

Na-rich Cores

In many DVDP basanites and some nepheline hawaiite samples,
occasional phenocrysts and microphenocrysts have irregular
green cores which are Na and Fe rich (Fig. 5.6). The grains
have strong reverse zoning with Fe and Na decreasing outwards
from the core. Electron microprobe scans for Ca, Fe and Mg
(Fig. 5.15) clearly indicate the extreme Fe enrichment and the
sharp boundary with the weakly zoned rims. In basanite
1-121.88 the rim shows weak normal zoning (Fig. 5.15A) while
in the nepheline hawaiite 2-70.41 the rim is reverse zoned
(Fig. 5.15B). Six grains with Na,Fe-rich cores have been
analysed. Charge balance calculations indicate the amount of
Fe^{3+} in the pyroxene exceeds the Na content, so it is therefore
likely that all the Na is present as the acmite ($NaFe^{3+}Si_2O_6$)
component and not as the jadeite ($NaAlSi_2O_6$) component, the
usual high pressure Na pyroxene. The sodic cores were formed
very early presumably at high pressure in the mantle. The

LEGEND

□ trachyandesite   25703

■ trachyandesite   25671

● essexite inclusion   25668

△ nepheline tristanite   25661

▲ tristanite   25666

◇ K-trachyte   25687

○ K-trachyte   25702

▼ peralkaline K-trachyte   25699
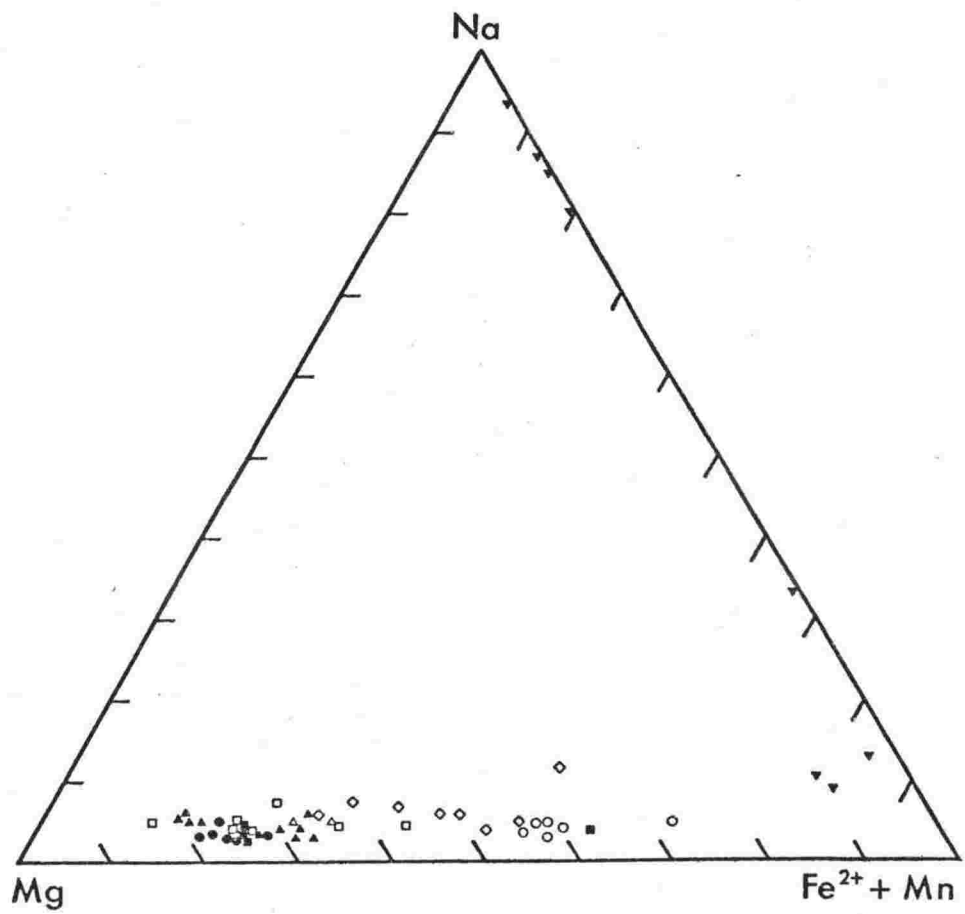
FIGURE 5.13 Na-Fe^{2+}+Mn-Mg (mole %) plot of clinopyroxene from The Pleiades.

LEGEND

DVDP

● basanite

■ nepheline hawaiite

□ nepheline hawaiite xenocrysts

△ nepheline mugearite

▽ nepheline mugearite xenocrysts

○ nepheline benmoreite, benmoreite

Mt Erebus

▲ anorthoclase phonolite
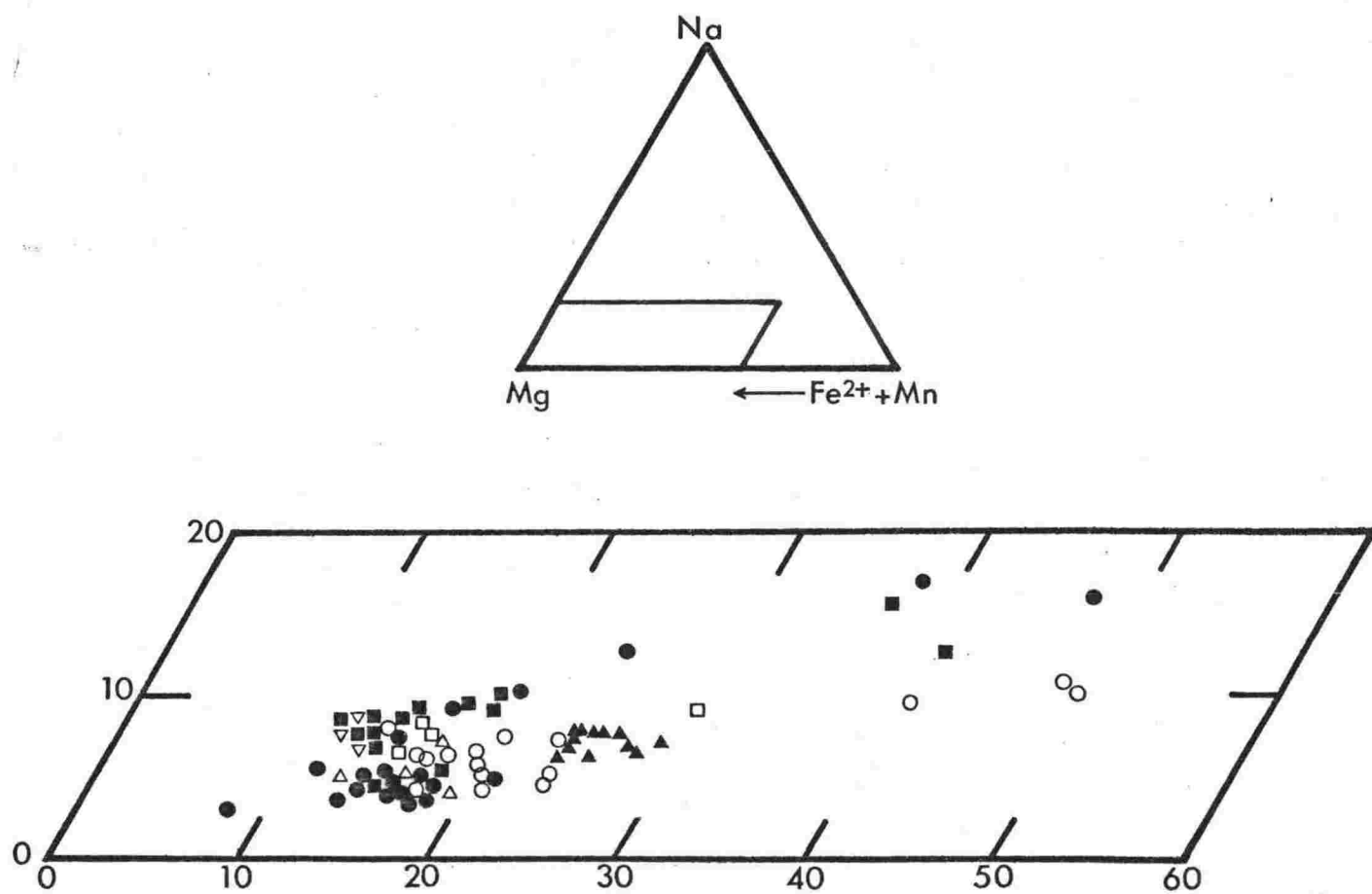
FIGURE 5.14 Na-Fe^{2+}+Mn-Mg (mole %) plot of clinopyroxene from DVDP holes 1 and 2.
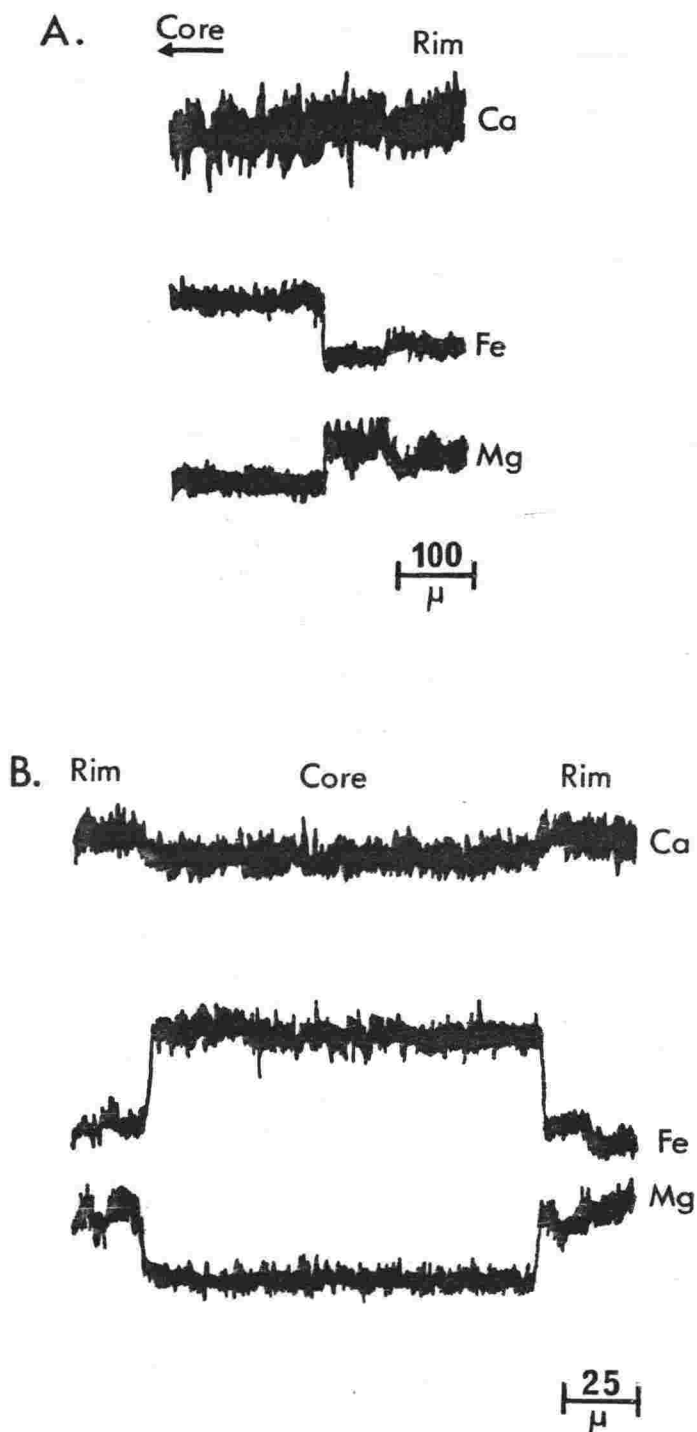
FIGURE 5.15 Electron microprobe scans across clinopyroxene with Na, Fe-rich cores in basanite and nepheline hawaiite lavas from DVDP holes 1 and 2. Note the Fe enriched core and sharp boundary with clinopyroxene of normal salite on rim.

A. Scan across part of DVDP 1-121.88 grain 4.
B. Scan across crystal of DVDP 2-70.41 grain 1.

occurrence therefore of a strong acmite enrichment is difficult
to reconcile with the usual observation of high pressure
pyroxenes being jadeite rich. Unless the Na is present as a
jadeite component, and the Fe^{3+} occurs as ferri-tschermak
($CaFe_2^{3+}SiO_6$) and calcium aluminium ferri-tschermak
($CaFe^{3+}AlSiO_6$) components. Both these latter two components
are generally considered to be of low pressure origin.

A brief summary indicates a few of the widespread
occurrences of Na,Fe-rich cores in clinopyroxenes from alkali
basaltic lavas. Although little has been written on the
conditions of formation, reports on their occurrence are
becoming more numerous. Weiblen et al., (1974b) discussed the
Ross Island examples and indicated they probably were of high
pressure origin. Huckenholz (1973) reported similar pyroxenes,
which he described as fassaitic augite, in nepheline basanite
and alkali basalt from West Germany. High pressure xenoliths
in a Tertiary lamprophyre dike from East Greenland contain
Na,Fe-rich reverse-zoned pyroxenes (Brooks and Rucklidge, 1973).
Dr C. K. Brooks (written communication) has found occurrences
in basanites and related rocks from East and West Greenland
and Sweden. A brief description of green Na,Fe cores in
pyroxenes in alkali basalts from the Canary Islands has been
reported in an abstract by Scott (1969). Analyses of reverse
zoned Fe-rich pyroxenes in plutonic xenoliths from the Canary
Island are given by Frisch and Schmincke (1968) and Borley
et al., (1971). Price (1973) described and figured titaniferous
augite, in an alkali basalt from Dunedin Volcano, New Zealand,
with green Na,Fe-rich cores. The green pyroxene had a mottled
appearance which Price (1973) attributed to late stage alteration,
a conclusion which may be open to reinterpretation in view of
the data presented here.

Experimental studies of the diopside-acmite system
(Yagi, 1962, 1966; Nolan and Edgar, 1963; Bailey and
Schairer, 1966) have only been made at low pressures and relate
to the appearance and stability of acmite in more differentiated
lavas of alkali volcanic series. Gilbert (1969) studied the

LEGEND

Thompson (1974)

     O olivine-rich alkali basalt

     △ transitional basalt

     □ augite leucitite

Bultitude and Green (1971)

     ● olivine nephelinite

     ▲ picritic basanite

     ■ picritic nephelinite

Note. Trend lines for results of Thompson only.

high pressure stability of acmite and found that it melts
incongruently to hematite + magnetite + liquid up to at least
45 kb. An equation for the fusion curve of the reaction was
given as $T(^{O}C) = 988 + 20.87P$ (kb) $- 0.155P^{2}$ (kb). Therefore
acmite is stable under mantle conditions and it seems reasonable
to assume that acmite is also soluble in diopsidic and
salitic pyroxenes under these conditions. It is probable
that the entry of Na and Fe^{3+} (i.e. the acmite component)
into pyroxenes, is dependent on the availability of Fe^{3+}
which in turn may be a function of the oxygen fugacity.

Pyroxenes formed in high pressure melts of alkali volcanic
rocks (Thompson, 1974) and their synthetic equivalents
(Bultitude and Green, 1971) never show any marked enrichment
in Fe, although the effect of f_{O_2} was not investigated in the
experiments. The pyroxenes, which were analysed by electron
microprobe, were however unusual, being mainly of sub-calcic
compositions. The Na content had a strong positive correlation
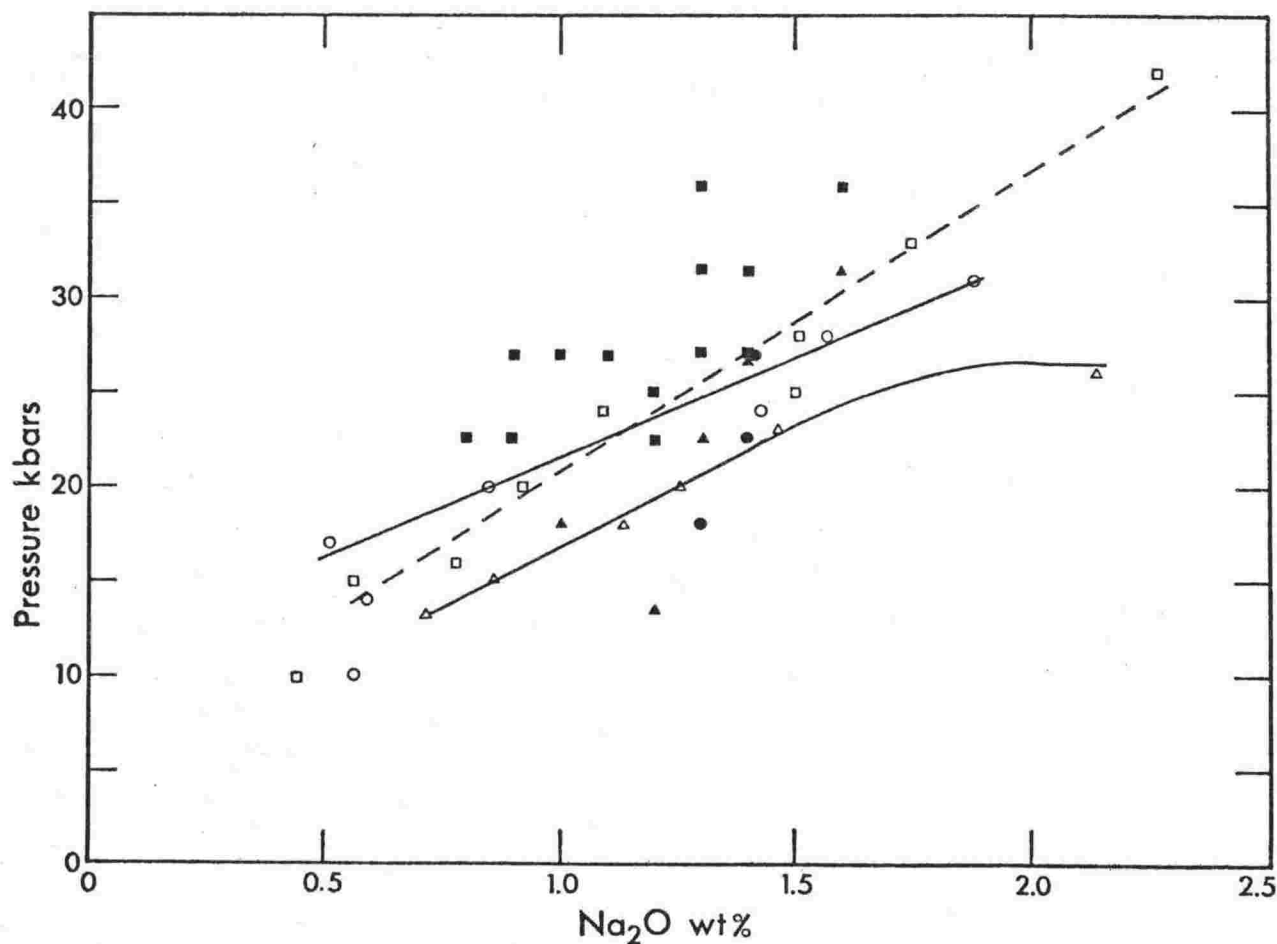
FIGURE 5.16   Variation of Na_2O with pressure in clinopyroxene from high
pressure melting experiments on natural (Thompson, 1974) and
synthetic (Bultitude and Green, 1971) basaltic systems.

with pressure (Fig. 5.16). The data of Thompson (1974) shows
an extremely strong correlation, while the scatter in Bultitude
and Green (1971) data (Fig. 5.16) is probably a function of the
different temperatures and sample capsules used. In these
experiments the Na content was equated as an increase in the
jadeite component. If Na contents of DVDP samples are
compared with the experimental studies it suggests they formed
at pressures of 20 to 30 kbars.

The next question is what conditions in the mantle favour
the formation of Fe^{3+} and the overall enrichment in Fe?
Mysen (1974) partially melted a natural spinel lherzolite at
15 kbars under controlled oxygen fugacity. He found that
Mg/(Mg+Fe) in the resulting pyroxenes decreased when the log
f_{O_2} increased from -10.72 to -4.47 and considered this was
due to a 5% increase in $Fe^{3+}/(Fe^{2+}+Fe^{3+})$. Thus oxygen fugacity
can have some control on the entry of Fe^{3+} into pyroxenes.

Thompson (1974) found that pyroxenes formed in melts
of augite leucitite had cation sums (with total Fe as FeO) which
decreased from about 4.05 at 10 kbars to 4.01 at 28 kbars.
He interpreted this as a decrease in Fe^{3+} content in the
pyroxenes as pressure increased, and showed that it resulted
in a negative correlation with Na. This is the opposite effect
required to form the DVDP pyroxenes. Perhaps oxygen fugacity
may play an important role, although Thompson also noted that
the Fe^{3+}-rich pyroxenes crystallized from a strongly alkalic
and silica-undersaturated melt at the same f_{O_2} as less alkalic
and silica undersaturated basaltic melts precipitated pyroxenes
free of Fe^{3+}. Thompson indicated this supported a suggestion
by Lindsley *et al.*, (1968) that f_{O_2} levels do not vary greatly
in various magma types, but different degrees of oxidation
may be due to changes in the activity coefficients of FeO and
Fe_2O_3.

A factor which has not been discussed and is difficult to
reconcile, is the accompanying enrichment in Fe^{2+}, which
results in a high ferrosilite component in the DVDP pyroxenes.
No explanation can be offered other than to suggest that

perhaps there is a coupled enrichment of both Fe^{2+} and Fe^{3+}. The entry of Fe^{3+} may make it more favourable for the entry of Fe^{2+} than Mg.

A feature of the DVDP pyroxenes is their low values of SiO_2 compared to the pyroxenes of the experimental studies of Bultitude and Green (1971) and Thompson (1974). A jadeite component may not form in the DVDP pyroxenes because Al was entering the Z site (hence the formation of tschermak molecules) to make up for Si deficiencies. In the experimental study of Thompson (1974) the only pyroxene to show Si contents similar to the DVDP pyroxenes were those crystallized from an augite leucitite. In these pyroxenes the Al_2O_3 reached extremely high levels (18% at 42 kbars). The parent rock however had over 15% Al_2O_3 and only 8% $FeO+Fe_2O_3$ whereas the DVDP basanites have 12% Al_2O_3 and 12% $FeO+Fe_2O_3$. Alumina activity may therefore play an important role in the ability of Fe to enter the pyroxene structure in strongly undersaturated magmas.

In summary the early forming Na,Fe-rich pyroxene cores are believed to form at high pressure under oxidizing conditions which favour a high $Fe^{3+}/(Fe^{2+}+Fe^{3+})$ ratio. These conditions may result in the formation of an acmite component, but are unlikely to account for the increase in the ferrosilite component.

3. Mt Erebus

The pyroxene in anorthoclase phonolite lavas from Mt Erebus show no enrichment in Na (Fig. 5.17) and in terms of the Na, Mg, Fe^{2+}+Mn components contain between 6-8% Na. They are very slightly enriched in Fe^{2+}+Mn compared to the majority of the DVDP pyroxenes and lie on the trend line defined by the DVDP nepheline benmoreite pyroxenes (Fig. 5.18).
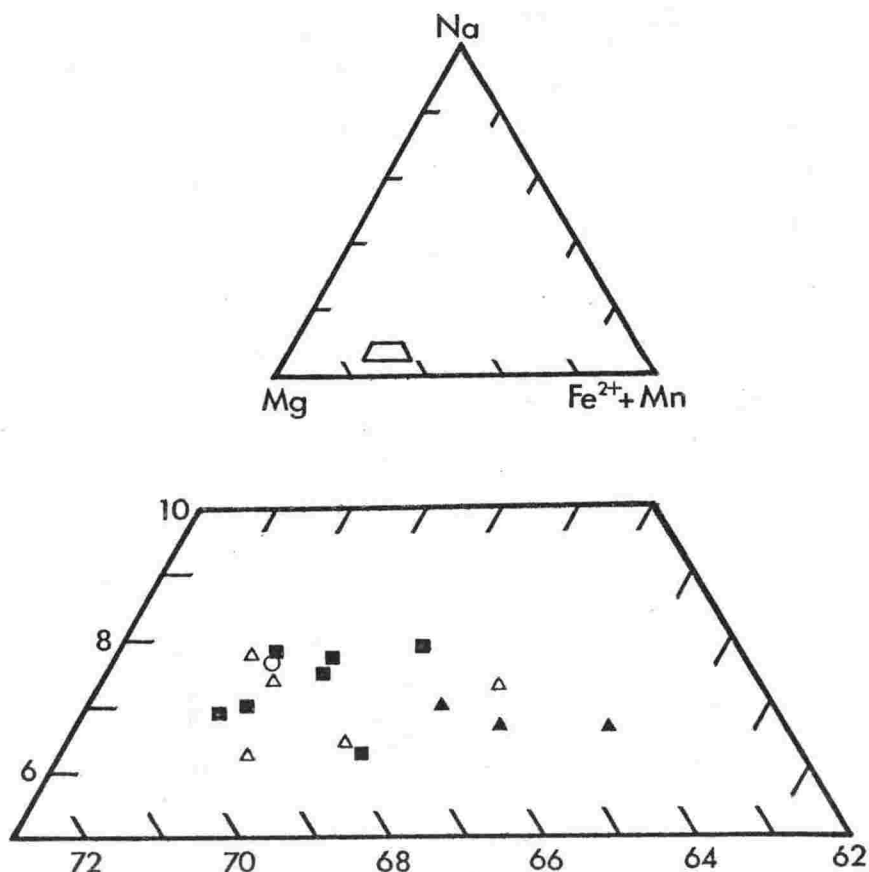
FIGURE 5.17   Na-Fe^{2+}+Mn-Mg (mole %) plot of clinopyroxene in recent
volcanic ejecta, Mt Erebus.   Symbols are the same as
Fig. 5.11.

Discussion

Except for the Na,Fe-rich cores in the DVDP pyroxenes,
the trends for The Pleiades and DVDP-Mt Erebus pyroxenes are
again contrasting.   In general The Pleiades pyroxenes show a
continuous enrichment in Fe^{2+}+Mn with little variation in Na,
until the peralkaline K-trachyte.   The observed trend for The
Pleiades pyroxenes is very similar to that found in pyroxenes
from slightly undersaturated alkali rocks from Dogo, Oki Island,
Japan (Uchimizu, 1966) and generalised alkali basalt-trachyte
series also from Japan (Aoki, 1964) (Fig. 5.18).   It contrasts
strongly with pyroxene trends from Shonkin Sag and other
alkaline differentiation sequences also shown on Fig. 5.18.
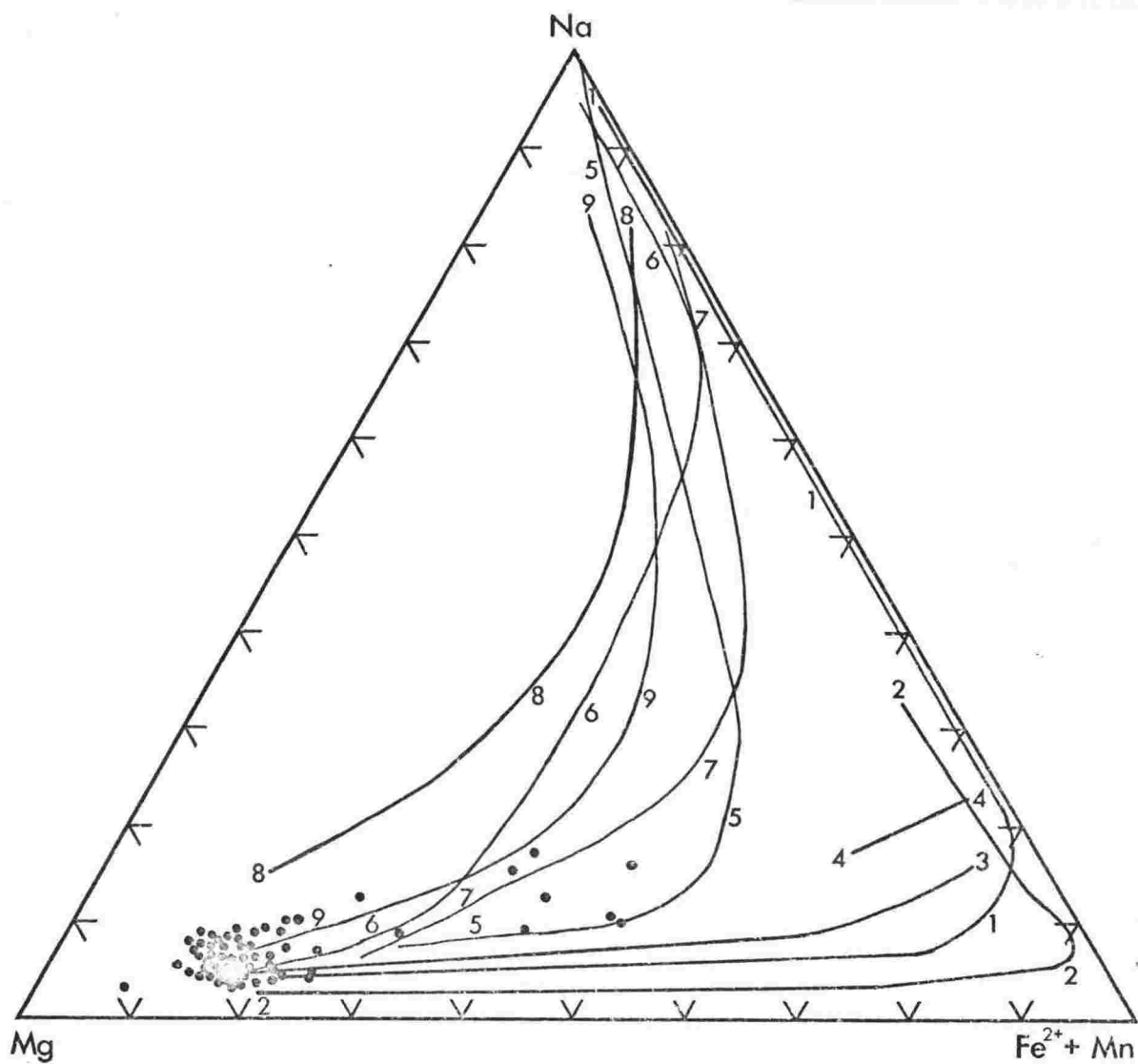
FIGURE 5.18 Clinopyroxene crystallization trend in terms of Na-Fe^{2+}+Mn-Mg. DVDP
clinopyroxenes shown by dots. 1-The Pleiades (this study); 2-Dogo,
Iki Island, Japan (Uchimizu, 1966); 3-Alkali basalt-trachyte series,
Japan (Aoki, 1964); 4-Pantellerite trend (Carmichael, 1962);
5-Nepheline syenite, South Greenland (Stephenson, 1972); 6-Shonkin
Sag, U.S.A., bulk analyses (Nash and Wilkinson, 1970); 7-Morotu,
Japan (Yagi, 1953); 8-Itapiraupua, Brazil (Gomes et al., 1970);
9-Uganda alkali complexes (Tyler and King, 1967).

Na enrichment in pyroxenes results from substitution of $NaFe^{3+}$ for $Ca(MgFe^{2+})$. It has been suggested that Na enrichment may be controlled by high or increasing oxygen fugacity (Aoki, 1964; Yagi, 1966). Nash and Wilkinson (1970) however in their study of Shonkin Sag state "the crystallization of Na-rich pyroxenes does not demand an increase in the fugacity of oxygen, but rather requires that the oxygen fugacity falls less rapidly with temperature than would be the case if olivine and magnetite were present." Olivine and magnetite act as an oxygen buffer according to the reaction

$$3Fe_2SiO_4 + O_2 = 2Fe_3O_4 + 3SiO_2$$

fayalite   gas   magnetite liquid
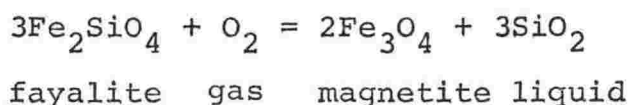
Thus Na-rich pyroxenes occur only when the olivine disappears and is no longer buffering oxygen fugacity. This fits The Pleiades pyroxenes well, as fayalitic olivine persists up to the K-trachytes and only disappears in the peralkaline K-trachyte. It is at this stage that strongly sodic pyroxenes crystallize. The same is also true for pyroxenes at Dogo (Fig. 5.18) where olivine persists throughout the lava series and no Na-enrichment is reported in pyroxene except for one analysis of a slightly sodic groundmass pyroxene.

ALUMINIUM, TITANIUM (Al,Ti)

Introduction

Barth (1931) suggested a coupled substitution of $Ti \rightleftharpoons Mg$ and $Al \rightleftharpoons Si$ occurs in clinopyroxenes. The solubility of Ti therefore increases with the amount of Al present in the tetrahedral Z site (Kushiro, 1960; Le Bas, 1962; Verhoogen, 1962). Ti is usually considered to occur as the Ca-Ti-tschermak molecule ($CaTiAl_2O_3$), and this is followed in the recalculation scheme although in Al-poor acmitic pyroxenes a Na-Ti-clinopyroxene [$NaTi_{0.5}(MgFe^{2+})_{0.5}Si_2O_6$] is also calculated.

Al and Ti are plotted against $Mg/Mg+Fe^{2+}+Mn$ (mg index) (Figs. 5.19, 5.20), a parameter which reflects the degree of pyroxene fractionation.

1. The Pleiades

Al reaches a maximum of 0.449 atoms (on the basis of 6 oxygen) in the pyroxenes from trachyandesite 25703 and is strongly reverse zoned (Fig. 5.19). The mg index increases from core to rim, opposite to the normal trend, but similar to pyroxenes with Na,Fe-rich cores from DVDP basanites. In the other rocks examined Al decreases as the mg index decreases, initially the Al decrease is rapid, but flattens out below 0.6 mg, Excluding the essexite inclusion (25668), the decrease in Al and mg index follows increasing differentiation of the lavas. Pyroxenes in the essexite have very low Al even though the mg index is high. K-trachyte (25687) pyroxenes have a wide range in Al content, varying from 0.379 (atoms) in the phenocryst cores to 0.044 in the groundmass. The very wide spread suggests the pyroxenes with high Al cores may be xenocrystic.

Ti behaves similarly to Al although there is a small enrichment of Ti in the acmites of peralkaline K-trachyte 25699 (Fig. 5.20).

2. DVDP 1 and 2

Pyroxenes with Na,Fe-rich cores from DVDP basanites and nepheline hawaiites are as previously noted reverse zoned with an increasing mg index from core to rim. Al however shows no consistent pattern from core to rim in these pyroxenes (Fig. 5.19), whereas Ti increases in all cases (Fig. 5.20).

A well defined division in Al and Ti content between the basanite + nepheline hawaiite as a group and nepheline mugearite + nepheline benmoreite, is apparent. The former group, in general, have Al and Ti exceeding 0.250 (atoms) and 0.075 respectively whereas the nepheline mugearite and nepheline benmoreite have lower contents (Figs 5.19, 5.20). Xenocrysts in the nepheline hawaiite have low Al and very low Ti.
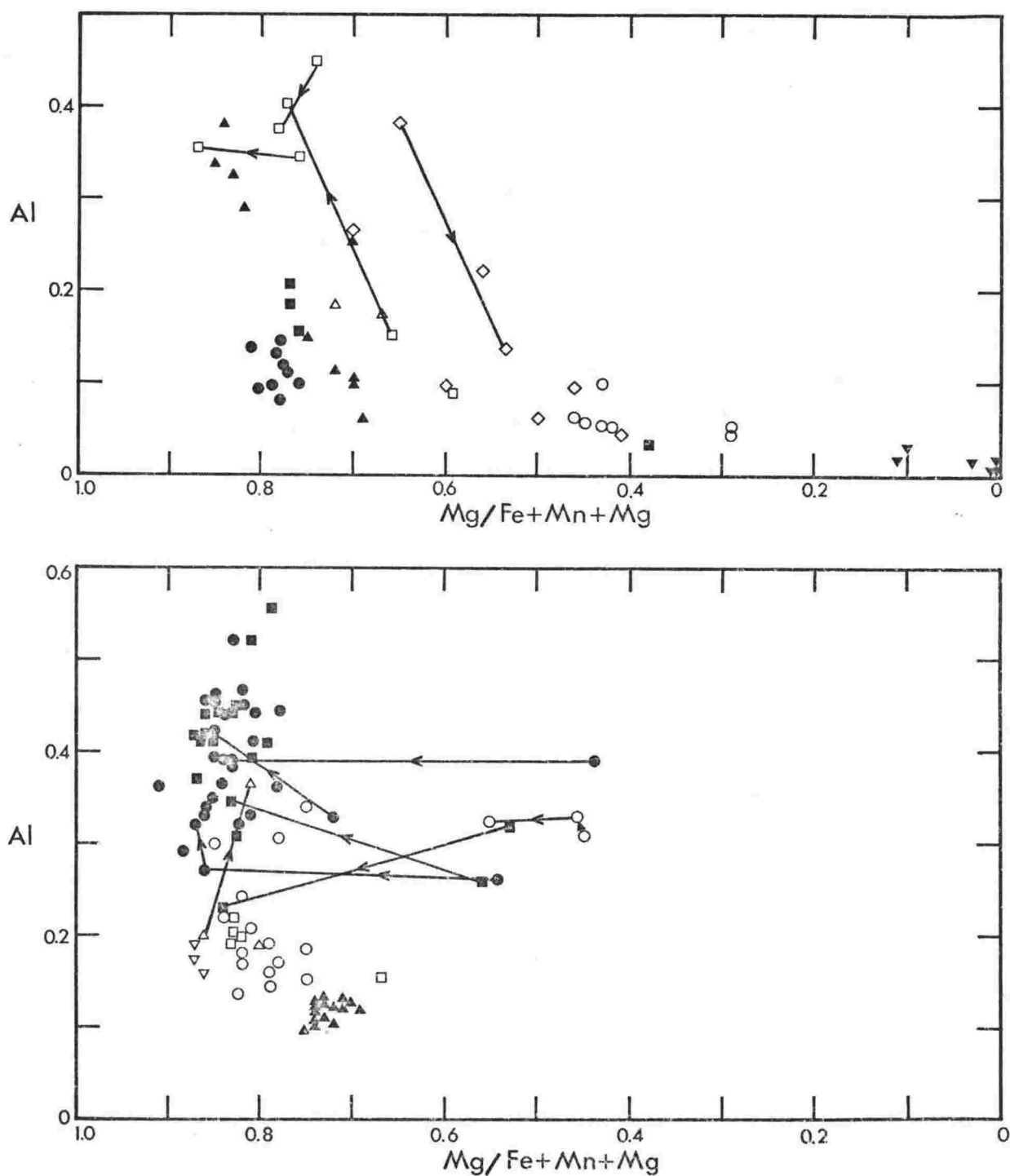
FIGURE 5.19 Variation of Al content of clinopyroxenes
(formula calculated on the basis of 6 oxygen)
plotted against mg index (Mg/Mg+Fe^{2+}+Mn), an
index of fractionation.
A. The Pleiades (symbols as Fig. 5.13).
B. Mt Erebus and DVDP 1 and 2 (symbols as
Fig. 5.14).
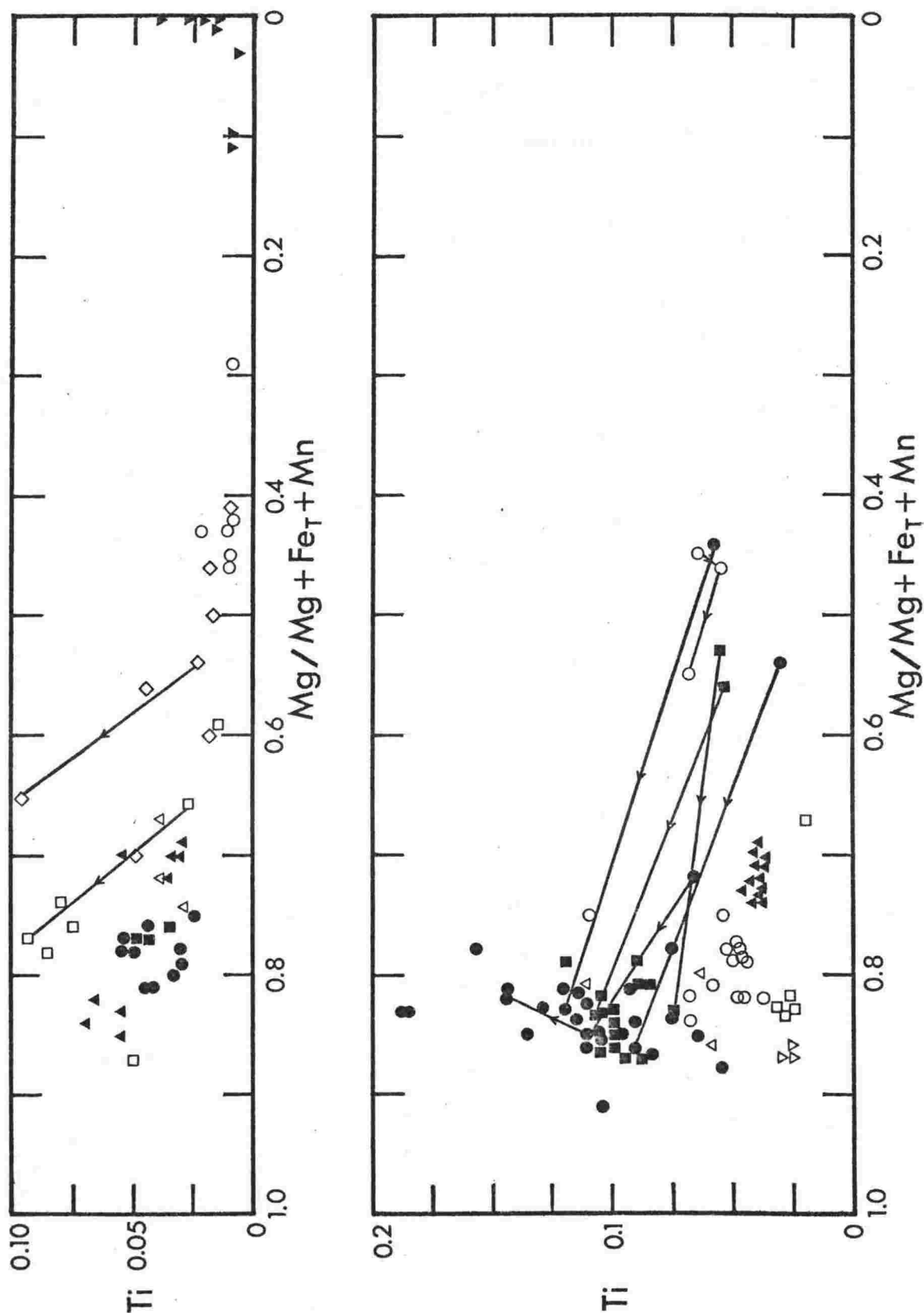
FIGURE 5.20 Variation of Ti content of clinopyroxenes (formula calculated on the basis of 6 oxygen) plotted against mg index $(Mg/Mg+Fe^{2+}+Mn)$, an index of fractionation.
A. The Pleiades (symbols as Fig. 5.13).
B. Mt Erebus and DVDP 1 and 2 (symbols as Fig. 5.14).

3. Mt Erebus

Pyroxenes from anorthoclase phonolites are slightly fractionated (i.e. mg index is lower), and have lower Al contents than DVDP pyroxenes (Fig. 5.19). Ti content is very similar to pyroxenes from DVDP nepheline benmoreites (Fig. 5.20).

Discussion

Introduction

Al content in pyroxenes is controlled by pressure and silica activity. In the recalculation scheme excess Al over that required to form the Ca-Ti-tschermak ($CaTiAl_2O_6$) component forms the Ca-tschermak ($CaAl_2SiO_6$) component (Appendix B). The amount of Ca-tschermak molecule increases with pressure (Aoki, 1968; Aoki and Kushiro, 1968; Kushiro, 1969; Thompson, 1974), so that greater than 5% Ca-tschermaks may reflect pressures exceeding 5 kbars (Munoz and Sagredo, 1974). Experimental studies (Gupta *et al.*, 1973) have confirmed earlier suggestions (Kushiro, 1960; Verhoogen, 1962; Brown, 1967) that the Al and Ti content also vary with the silica activity. The following reaction may be a simple representation of the role of Al_2O_3 in calcium rich pyroxenes (Carmichael *et al.*, 1970):

$$CaAl_2SiO_6 + SiO_2 = CaAl_2Si_2O_8 \qquad \ldots (2)$$

Ca-Tschermak   liquid   plagioclase
pyroxene
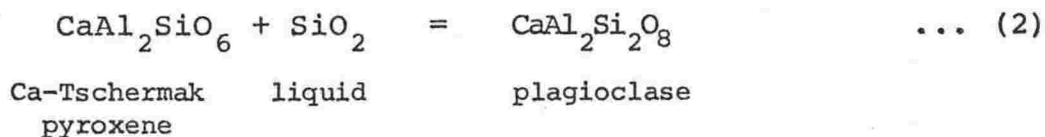
hence

$$K_{(T,P)} = \frac{a^{plagioclase}_{CaAl_2Si_2O_8}}{a^{pyroxene}_{CaAl_2SiO_6} \cdot a^{liquid}_{SiO_2}} \qquad \ldots (2A)$$

In the basanites plagioclase only appears in the groundmass, in the feldspar free situation the following reaction may apply:

$$CaAl_2SiO_6 + \tfrac{1}{2}SiO_2 + \tfrac{1}{2}Mg_2SiO_4 = CaMgSi_2O_6 + Al_2O_3 \qquad \ldots(3)$$

Ca-Tschermak liquid olivine diopside liquid
molecule
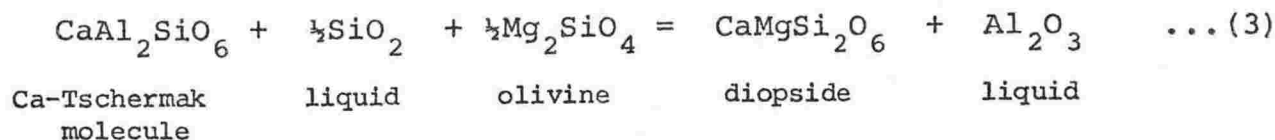
hence

$$K_{(T,P)} = \frac{a^{pyroxene}_{CaMgSi_2O_6} \cdot a^{liquid}_{Al_2O_3}}{a^{pyroxene}_{CaAl_2SiO_6} \cdot \left(a^{liquid}_{SiO_2}\right)^{\frac{1}{2}} \cdot \left(a^{olivine}_{Mg_2SiO_4}\right)^{\frac{1}{2}}} \qquad \ldots(3A)$$

Therefore the entry of Al into pyroxene can be controlled by many factors; pressure, silica activity (a_{SiO_2}), alumina activity ($a_{Al_2O_3}$) and plagioclase crystallization, thus making Al variations in the McMurdo Volcanic Group pyroxenes difficult to understand.

Although Ti shows a coupled substitution with Al it is generally considered to decrease in pyroxenes as crystallization pressures increase. Yagi and Onuma (1967) in a study of the system $CaMgSi_2O_6$-$CaTiAl_2O_6$ found 11% solubility of Ca-Ti-tschermaks at atmospheric pressure, but this was reduced to almost zero at pressures between 10 and 25 kbars and temperatures of $1000^{\circ}C$. On the other hand, Thompson (1974) noted pyroxenes formed in high pressure melts of basalts showed increasing Ti with rising pressure. Thompson (1974) attributed the difference to the greater number of components in the pyroxenes formed from rock melts. Increasing silica activity also decreases the solubility of Ti in diopsidic pyroxenes (Gupta *et al.*, 1973). It may be buffered by the reaction:

$$CaTiAl_2O_6 + SiO_2 = CaAl_2Si_2O_8 + TiO_2 \qquad \ldots(4)$$

Ca-Ti-tschermak liquid plagioclase liquid
pyroxene
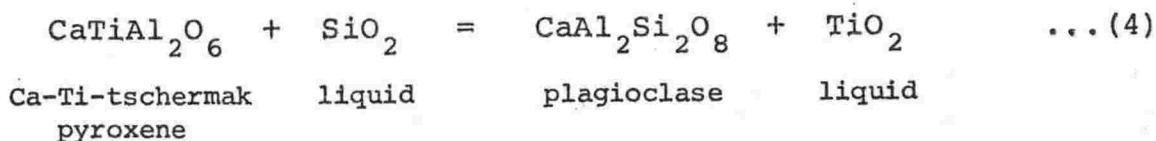
hence

$$K_{(T,P)} = \frac{a^{plagioclase}_{CaAl_2Si_2O_8} \cdot a^{liquid}_{TiO_2}}{a^{pyroxene}_{CaTiAl_2O_6} \cdot a^{liquid}_{SiO_2}} \qquad \ldots(4A)$$

Although there is some evidence to the contrary regarding
variation of Ti with pressure (c.f. Thompson, 1974), the
Al/Ti ratio shows a positive correlation with pressure.
Experimental data (Fig. 5.21) from high pressure melts
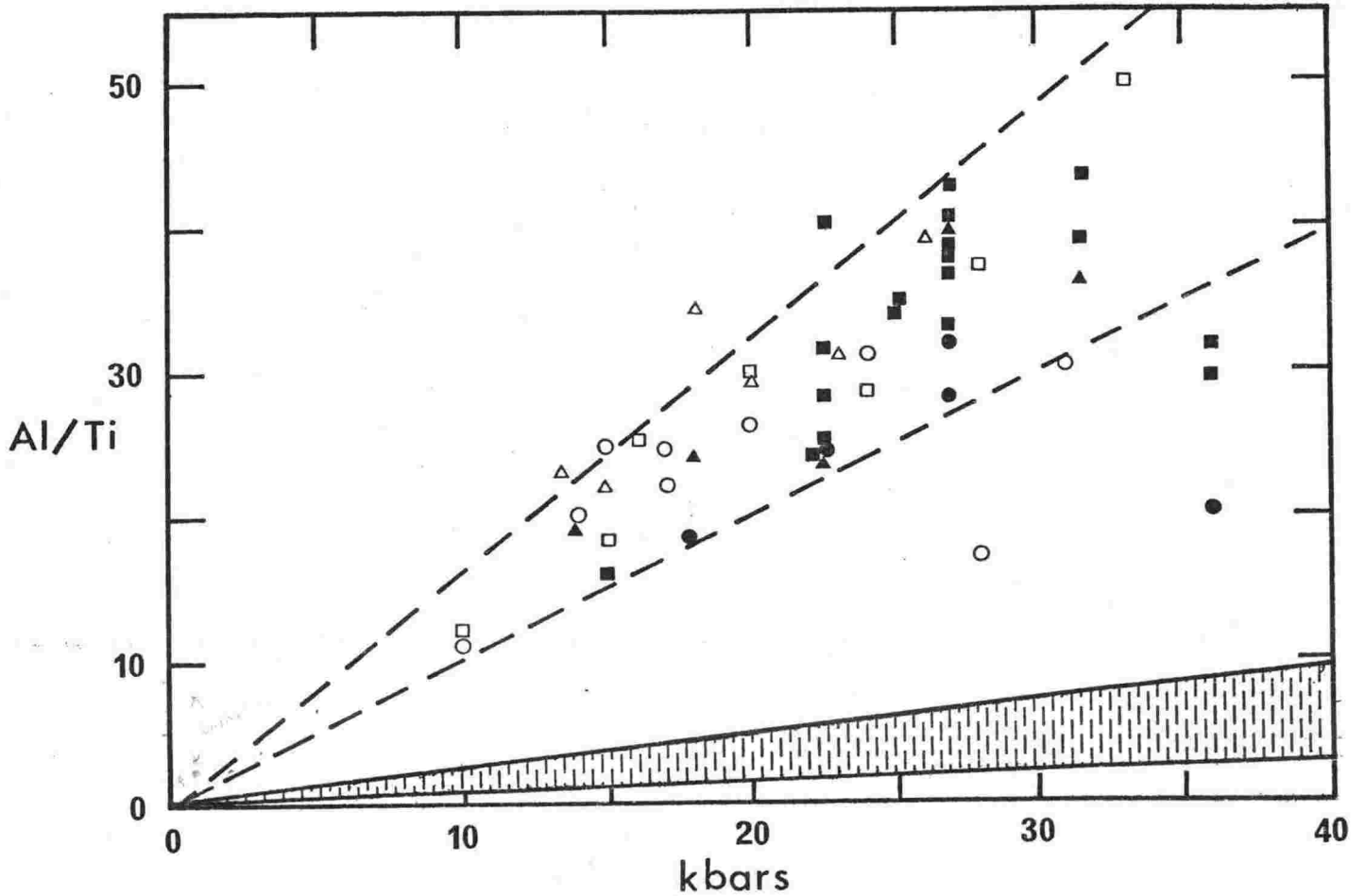
FIGURE 5.21   Variation of Al/Ti ratio with pressure in clinopyroxene
from high pressure melting experiments on natural
(Thompson, 1974) and synthetic (Bultitude and Green,
1971) basaltic systems. (Symbols the same as Fig. 5.16).
Shaded area from partition experiments of Akella and
Boyd (1973).

(Thompson, 1974; Bultitude and Green, 1971) have very high
Al/Ti ratios. Akella and Boyd (1973) examined the partition
of Ti and Al between co-existing silicates in synthetic Ti-rich
melts and also showed a pressure dependence of Al/Ti (Fig. 5.21)
with values that approach those observed in McMurdo Volcanic

Group pyroxenes (Fig. 5.22).

1. The Pleiades

Variations of Al and Ti are erratic in the pyroxenes (Fig. 5.22). Pyroxenes from essexite (25668) have very high Ti and low Al which may indicate low pressure crystallization. The pyroxenes, in terms of Ti and Al, are similar to tristanite 25666. Olivine from the essexite is highly fractionated (Fa_{40-43}) while the chemistry (see discussion on page 194) indicates they are cumulate in origin. The mineralogy thus suggests they are probably high level cumulates associated with fractionation involving the formation of intermediate lavas of tristanite and nepheline tristanite compositions.

K-trachyte (25687) has groundmass pyroxenes similar to those from K-trachyte 25702, trachyandesite 25671 and peralkaline K-trachyte 25699. All have low Al with variable Al/Ti ratios which may be less than 3 and are considered low pressure in origin. Phenocrysts in K-trachyte 25702 are variable their high Al and Ti cores are possibly xenocrysts or alternatively the appearance of feldspar after crystallization of the cores may have resulted in a rapid decrease in Al and Ti.

2. DVDP 1 and 2

DVDP pyroxenes have considerably higher Al and Ti than those from The Pleiades, which probably reflects the extremely undersaturated nature (i.e. low silica activity) of the DVDP lavas compared to those from The Pleiades. Thus as discussed above the lower silica activity favours high Al and Ti in DVDP pyroxenes.

Although a plot of Ti versus Al (Fig. 5.22) for DVDP pyroxenes is scattered the nepheline mugearite, nepheline benmoreite and benmoreite have lower Al/Ti ratios than the basanite and nepheline hawaiite pyroxenes. This is as would be expected and indicates a lower pressure of origin for the pyroxenes from the differentiated lavas. Xenocrysts in nepheline hawaiite and nepheline mugearite have low Al and Ti but high Al/Ti ratios. A high pressure origin could be implied
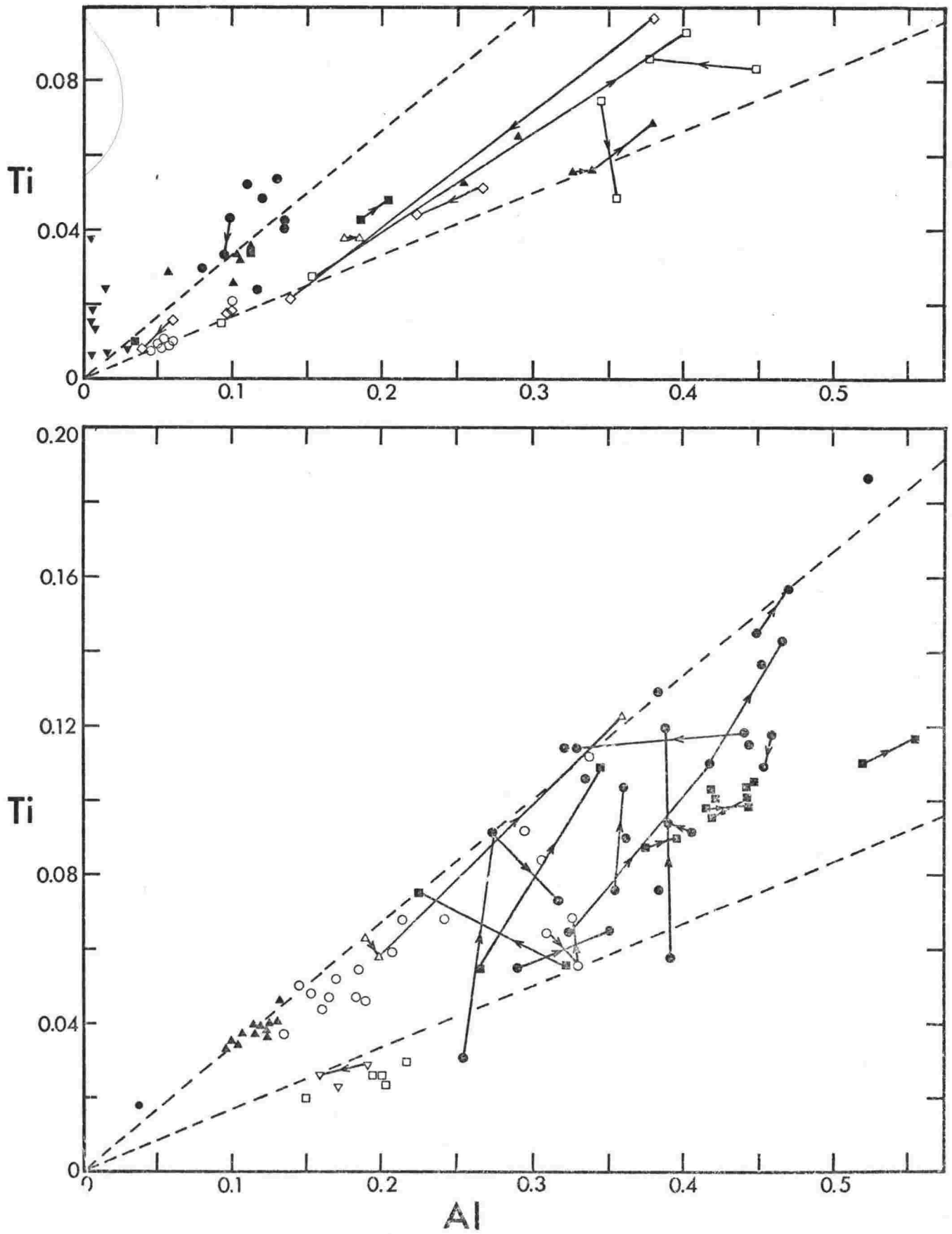
FIGURE 5.22   Variation of Ti versus Al in clinopyroxene (on the basis of 6 oxygen).
A.   The Pleiades (symbols as Fig. 5.13).
B.   Mt Erebus and DVDP 1 and 2 (symbols as Fig. 5.14).

from the experimental data of Akella and Boyd (1973) (Fig. 5.21) on Al/Ti ratios. The Na,Fe-rich cores, as discussed above also have high Al/Ti ratios, usually greater than other pyroxene phenocrysts from the basanites and nepheline hawaiites. By comparison with the experimental work of Akella and Boyd (1973) (Fig. 5.21) a pressure in the order of 25 kbars is implied, this is in agreement with depths inferred from the Na_2O contents (see page 111).

3. Mt Erebus

Pyroxenes from the anorthoclase phonolite lavas have low Al/Ti ratios of about 3 (Fig. 5.22). They probably crystallized at low pressures in the upper crust.

Sector Zoning

Sector zoning (Hollister and Gancarz, 1971) is common in groundmass pyroxenes and is rarely observed in microphenocrysts, particularly on the rims. In DVDP basanite 2-103.15, a sector zoned pyroxene was analysed (Appendix B), the (100) sector is notably enriched in Ti and Al and depleted in Si relative to the (010) sector. As discussed above Al and Ti is dependent in part on the silica activity. Nakamura (1973) has developed a theory of protosite development to explain sector zoning in pyroxenes. In undersaturated magmas the $Si \rightleftharpoons Al+Ti$ substitution is more efficient on the (100) growth surface and when rapid growth occurs the zoning will survive as sector zones.

Further discussion on sector zoning of pyroxenes in a McMurdo Volcanic Group basanite from Ross Island is given by Leung (1974).

Conditions of Clinopyroxene Crystallization

The nature of the clinopyroxenes crystallizing from any magma is dependent on a number of factors such as silica activity, oxygen fugacity, magma composition, temperature and pressure. Although the composition of the magma may be important in defining the crystallization trend (Fig. 5.12), this may not always be so. Barberi *et al.*, (1971) have shown that in rare circumstances a mildly alkalic basalt may crystallize pyroxenes that have tholeiitic affinity.

Clinopyroxenes in McMurdo Volcanic Group lavas show two contrasting trends;

1) a well defined augite → hedenbergite → aegirine (acmite) trend in The Pleiades pyroxenes (Fig. 5.8);

2) a poorly defined diopside → salite trend (Fig. 5.10) in DVDP and Mt Erebus pyroxenes.

Lavas from The Pleiades show a trend towards silica saturation with increased differentiation, whereas DVDP and Mt Erebus lavas are all strongly undersaturated. Silica activity must therefore be a very important factor in controlling the two pyroxene trends. As silica activity decreases not only do the Al and Ti contents in the pyroxenes increase but the degree of Fe enrichment also decreases. Oxygen fugacity controls the entry of $NaFe^{3+}$ in clinopyroxenes, but this is not important in most lavas from the McMurdo Volcanic Group.

Amphiboles

Introduction

Ti-rich hornblende is termed kaersutite when Ti >0.50 in half the unit cell (O=23) and titano-hornblende if Ti <0.5 and >0.25. Kaersutite is subdivided, on the basis of $Mg/Mg + Fe^{3+} + Fe^{2+} + Mn$ (mg), into kaersutite if mg >0.50 and ferro-kaersutite if mg <0.50. Kaersutite is a common constituent in many McMurdo Volcanic Group lavas. It is one of the main mafic phenocrysts in the sodic basanite-phonolite lineages from The Pleiades and in DVDP core samples.

Fe$_2$O$_3$ and FeO contents have been estimated using a method suggested by Aoki (1970). Charge balance procedure used by Papike *et al.*, (1974) to determine the oxidation state of Fe in amphiboles was attempted but mainly indicated total Fe was present as FeO.

Occurrence

1, THE PLEIADES

Kaersutite occurs as one of the main mafic mineral phases in the nepheline hawaiite and nepheline benmoreite lavas, but no analyses have been made. In the potassic series kaersutite occurs in some K-trachytes and as microphenocrysts in the trachyandesites, it also appears along with titano-biotite as a late phase product in the essexite inclusions. Oxidized xenocrysts(?) are seen occasionally in other lavas. In the K-trachyte, kaersutite is oxidized to varying degrees and may be represented by oxidized pseudomorphs.

Eleven electron microprobe analyses of amphiboles from five samples are given in Appendix B, eight are kaersutite and three ferro-kaersutite. Kaersutite was also separated from a plagioclase-kaersutite-apatite pegmatitic(?) inclusion and analysed for major, trace and rare-earth elements (Table 5.2). The major element analysis shows 0.60% P$_2$O$_5$, which is due to inclusions of apatite. The rare-earth element geochemistry is discussed in Chapter 7.

2. DVDP 1 AND 2

Kaersutite is an important mafic mineral in all DVDP lavas except the basanites. Phenocrysts and microphenocrysts of kaersutite in the nepheline hawaiite vary from euhedral grains showing no alteration to grains which are strongly resorbed and oxidised. In the nepheline mugearites and nepheline benmoreites, kaersutite microphenocrysts are invariably

TABLE 5.2   Major and trace element analysis of kaersutite from
            The Pleiades.

	1	Structural Formula[+]			
		Si	5.859		
SiO_2	38.75	Al	2.141		
Al_2O_3	12.78	Al	0.136		
TiO_2	5.20	Ti	0.591		
Fe_2O_3[x]	5.35	Fe^{3+}	0.608	Z	8.000
FeO	9.62	Fe^{2+}	1.217	Y	5.002
MnO	0.22	Mn	0.028	X	2.589
MgO	10.75	Mg	2.422		
CaO	10.90	Ca	1.637	Fe^{3+}/Fe^{2+}	0.50
Na_2O	2.68	Na	0.786		
K_2O	0.87	K	0.166	$\dfrac{100Mg}{Mg+Fe_T+Mn}$	56.6
P_2O_5	0.60	OH	1.982		
Sum	97.72	Sum	17.573		

Trace Elements

Rb	8.2	La	30
Ba	404	Ce	67
Pb	10	Pr	11.5
Sr	657	Nd	58
Y *	69	Sm	15.1
Th	3.9	Eu	3.8
U	n.d.	Gd	14.2
Zr *	160	Tb	1.6
Hf	4.3	Dy	9.7
Sn	1.0	Ho	1.8
Nb	159	Er	4.6
Cu *	34	Yb	3.6
Co *	33	REE	221
Ni *	~3		
Sc *	41		
V *	210		
Cr *	~6		
Ga *	20		
B *	~11		

* Determined by B. P. Kohn using emission spectroscopy, all other
  trace elements and REE by spark source mass spectrometry.

[+] Analysis recalculated to 98% apatite-free, and 2% water added
  to make total 100%. Structural formula based on 24 (O,OH).

[x] Fe^{3+}/Fe^{2+} ratio determined by Mossbauer spectroscopy.

completely oxidized to pseudomorphs composed of small cubic
opaques. In some samples kaersutite may alter to olivine +
augite + plagioclase + magnetite and possibly rhönite.
Groundmass kaersutite is rare and has been observed as brown
strongly pleochroic grains in a few nepheline benmoreites and
a nepheline hawaiite.

Fifty seven analyses of amphibole from DVDP cores were
made (Appendix B, Part 2) and all but five analyses are
kaersutites. Two titano-hornblende and one ferro-kaersutite
were found as reaction rims on xenocrysts in nepheline hawaiite
2-62.41. In nepheline benmoreite 1-85.35, a xenocryst of
titano-tschermakite was analysed.

Chemistry

The kaersutite has a near constant composition, the
greatest variation occurs in the mg index which ranges from
0.54 to 0.73 for the DVDP analyses and from 0.41 (ferro-
kaersutite) to 0.63 for The Pleiades (Fig. 5.23).

Al and Ti show only minor variations and there is a
slight tendency for Ti to increase as Al increases (Fig. 5.24).
Kaersutite from The Pleiades has lower Al and mg index than
DVDP kaersutite. Ti decreases with increased fractionation,
being highest in the nepheline hawaiite and lowest in the
benmoreite (Fig. 5.24). Ti also correlates positively with the
mg index (Fig. 5.23).

Best (1974) has reviewed occurrences of amphiboles in
mantle-derived inclusions. He plotted Ti against Al for a large
number of such amphiboles and showed a wide spread of
compositions (Fig. 5.25). Kaersutites from McMurdo Volcanic
Group lavas usually plot between fields of kaersutites from
shallow crustal intrusions and mantle-derived amphiboles
(Fig. 5.25). Five analyses of kaersutite megacrysts from
basaltic lavas given by Best (1974) overlap with the McMurdo
Volcanic field, but there is no conclusive evidence to indicate
these megacrysts are mantle-derived and they could have

LEGEND (Figs. 5.23, 5.24)

DVDP 1 and 2

    □ nepheline hawaiite

    ■ nepheline hawaiite-groundmass

    ▲ nepheline benmoreite

    △ benmoreite

    ○ The Pleiades
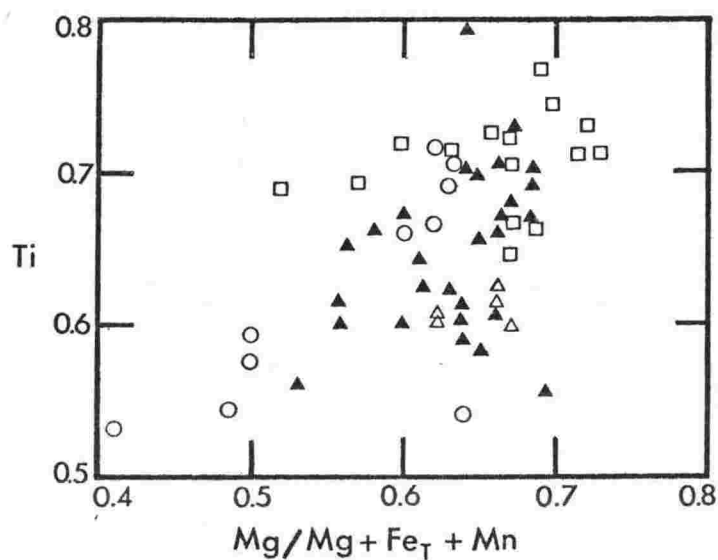
FIGURE 5.23   Variation of Ti versus mg index (100Mg/Mg+Fe$_T$+Mn) in
               kaersutite from DVDP 1 and 2 and The Pleiades.
               Kaersutite formula calculated on the basis of 23
               oxygen.
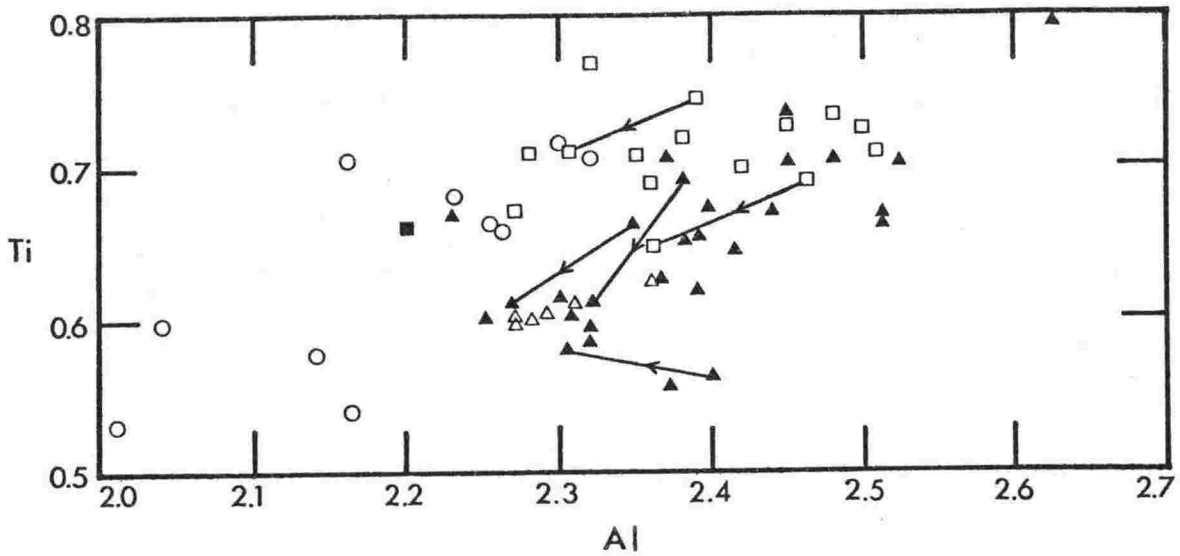
FIGURE 5.24   Variation of Ti versus Al in kaersutite from DVDP 1
and 2 and The Pleiades.   Kaersutite formula calculated
on the basis of 23 oxygen.
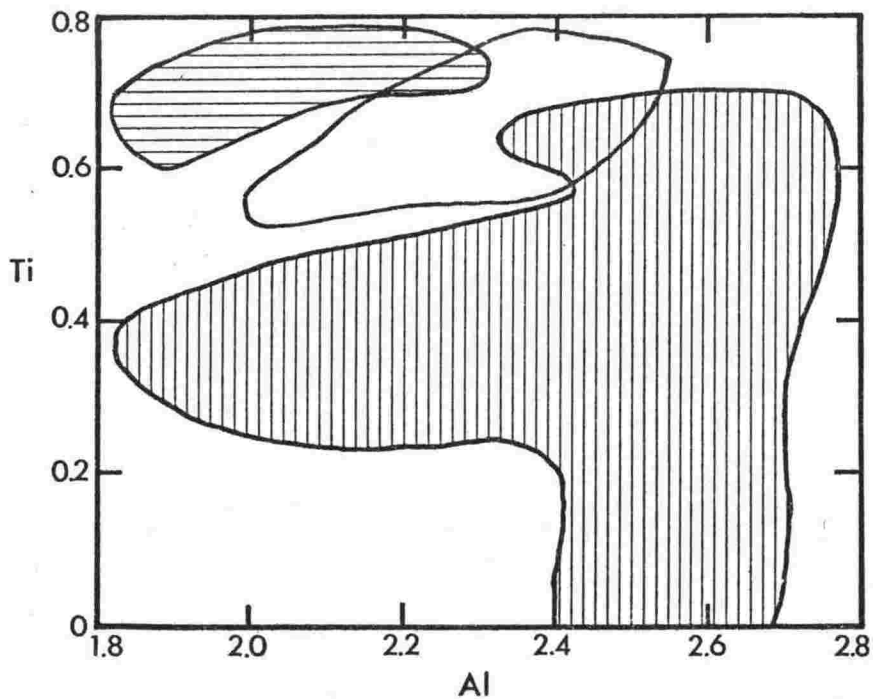
FIGURE 5.25   Variation of Ti versus Al in kaersutite from mantle-
derived amphiboles (vertical shading) and shallow
crustal intrusions (horizontal shading).   Field for
McMurdo Volcanic Group kaersutite is unshaded.
After Best (1974).

crystallized at lower crustal pressures. Excluding these
five analyses there is a general correlation of increasing
Al in kaersutite with increasing depth of crystallization.
A single groundmass kaersutite from a DVDP nepheline hawaiite
has the lowest Al content of any DVDP kaersutite. Al also
decreases from core to rim in phenocrysts, adding further
evidence of possible pressure dependence of Al in kaersutite.

The trace element analysis presented in Table 5.2 is
similar to data on kaersutite given by Kesson and Price (1972)
and Gunn (1972). Because kaersutite has a composition very
similar to the alkali basalt magmas in which it commonly
occurs, it is difficult to show its fractionation effects. A
significant feature is however the high K/Rb of kaersutite,
and its ability, on fractionation, to strongly enrich the
residual liquid in Rb (Kesson and Price, 1972; Gunn, 1972).
Rare-earth elements are the best indication of kaersutite
fractionation, as kaersutite enriches the light and heavy rare-
earths and depletes the middle rare-earths (see Chapter 7).

Discussion

Yagi *et al.*, (1975) has shown kaersutite is stable to
over 20 kbars at temperatures of $700^{\circ}C$ to about $1050^{\circ}C$
(Fig. 5.26). Best (1975) summarized other works pertinent to
kaersutite stability and suggested lower silica activity
(Allen and Boettcher, 1973) and the presence of fluorine
(Holloway and Ford, 1973) may increase kaersutite stability,
otherwise his conclusions were similar to Yagi and others.

As perovskite has not been observed in any lavas in
this study, it is here suggested that the kaersutite crystallized
at pressures of less than 12 kbars and at temperatures below
$1050^{\circ}C$ (Fig. 5.26). Kaersutite would be unstable in the
basanites which presumably crystallized at temperatures of
about $1100^{\circ}C$, but as they ascended from the mantle cooling,
a decrease in pressure and a possible increase in P_{H_2O} would
provide conditions favourable for kaersutite crystallization.
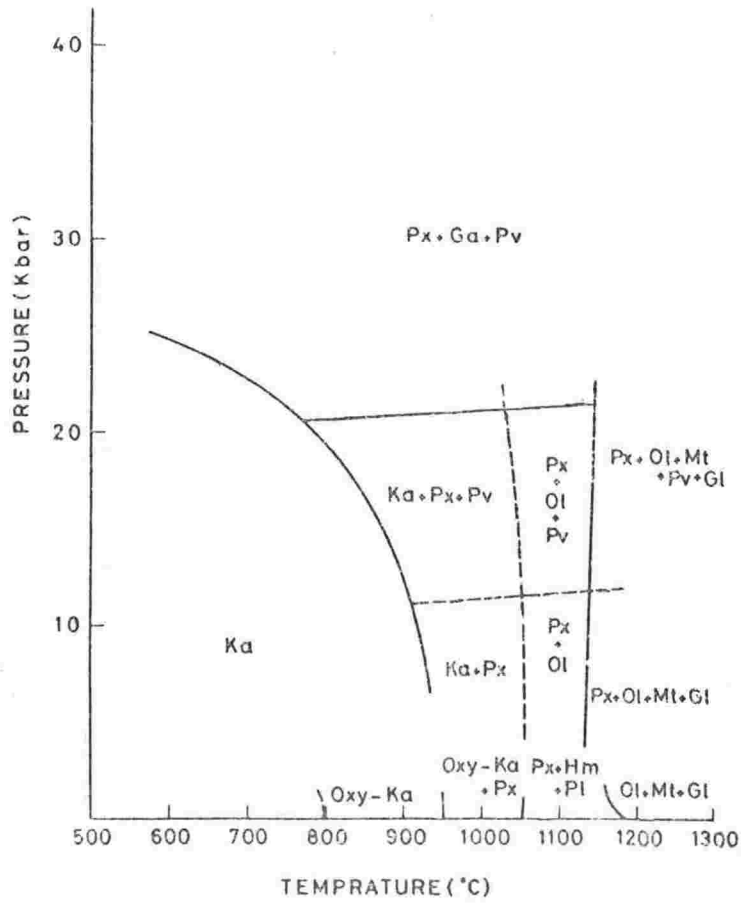
Ka: kaersutite, Oxy-Ka: oxy-kaersutite, Px: clinopyroxene, Pv: perovskite, Ol: olivine, Hm: hematite, Pl: plagioclase, Mt: magnetite, Ru: rutile, Ga: garnet, Gl: glass.

FIGURE 5.26   The stability field of kaersutite (from Yagi *et al.*, 1975).

Kaersutite is easily oxidised and appears to be unstable in most near surface environments. With rare exception it does not occur in the groundmass of McMurdo Volcanic Group lavas. Le Maitre (1969) concluded that kaersutite in plutonic xenoliths from Tristan da Cunha broke down at water pressures below 1.4 kbars. It is likely that kaersutite becomes unstable in the upper crust (<5 km), due to a drop in P_{H_2O} as a magma column degasses.

Kaersutite is therefore an important potassium rich accessory phase in the mantle (Best, 1974) and is also important as a fractionating phase in alkali magmas over a wide pressure range (Kesson and Price, 1972). In the McMurdo Volcanic Group lavas kaersutite is believed to crystallize at temperatures below $1050^{\circ}C$ and at pressures from 1.4 to 12 kbars.

Biotite

Titano-biotite is a minor phase in some rocks from The Pleiades occurring in the essexite inclusions and K-trachyte (25702) (Appendix B). The titano-biotite contains up to 7% TiO_2 which fills any deficiencies in Al and Si in the Z site. There is a marked increase in FeO* and decrease in MgO from the essexite to the K-trachyte; as would be expected from the normal trend of Fe-enrichment of the mafic mineralogy with increased differentiation.

In the essexite, titano-biotite is a late stage constituent and is in equilibrium with kaersutite. With increased crystallization the fluid phase in the essexite probably increased until P_{H_2O} was sufficient to allow biotite and kaersutite to crystallize.

The K-trachyte has microphenocrysts of titano-biotite, indicating P_{H_2O} was high early in the crystallization history. Hydrous minerals are lacking in the groundmass of the trachyte and the biotite microphenocrysts show some resorption. The biotite therefore may have formed under high P_{H_2O} conditions in

a closed upper crustal magma chamber which degassed prior or during eruption of the lava. Other K-trachytes from The Pleiades show little evidence of hydrous conditions (apart from the appearance of kaersutite) during crystallization and differentiation, so that the biotite-bearing trachyte and its implication of high P_{H_2O} is of minor importance.

Rhönite

Occurrences of Rhönite in Alkalic Lavas of the McMurdo

Volcanic Group, Antarctica, and Dunedin Volcano,

New Zealand.

by

P. R. Kyle and R. C. Price

Occurrences of Rhönite in Alkalic Lavas of the McMurdo Volcanic Group, Antarctica, and Dunedin Volcano, New Zealand

PHILIP R. KYLE,

Department of Geology, Victoria University,
Wellington, New Zealand

AND RICHARD C. PRICE[1]

Department of Geology, University of Otago,
Dunedin, New Zealand

Abstract

Occurrences of rhönite are reported in alkalic lavas of the McMurdo Volcanic Group (Hut Point Peninsula, Antarctica) and Dunedin Volcano (New Zealand). Electron microprobe analyses increase the range of composition reported for rhönite, with the Antarctic examples having higher TiO_2, and the Dunedin example higher Na_2O than other terrestrial rhönites. Detectable quantities of Cr_2O_3 (average 0.11 percent) and NiO (0.06 percent) are recorded for the first time. The rhönite shows no compositional variation toward aenigmatite.

Introduction

Rhönite is a groundmass constituent of lavas at Hut Point Peninsula, Ross Island, Antarctica. The mineral was discovered during an electron microprobe investigation of core samples from two holes drilled by the Dry Valley Drilling Project (DVDP) at Hut Point Peninsula (Mudrey *et al*, 1973; Treves and Kyle, 1973; Kyle and Treves, 1974a). This is the first reported occurrence in the McMurdo Volcanic Group and also in Antarctica. In the southern hemisphere the only other previously reported occurrence of rhönite has been in the Otago volcanics, New Zealand, where Benson (1939) reported it as an alteration product after kaersutite. The literature on rhönite has been reviewed by Cameron, Carman, and Butler (1970). Other reported occurrences are in the *Allende* meteorite (Fuchs, 1971) and metaphonolite from Puy de Saint-Sandoux (Grünhagen and Seck, 1972). The crystallography has been discussed by Walenta (1969). As very few analyses of rhönite have been published, the electron microprobe analyses reported here give a further indication of the range in composition.

Occurrence

The Late Cenozoic McMurdo Volcanic Group (Harrington, 1958; Nathan and Schulte, 1968) con-

sists of undersaturated alkaline volcanics which range in composition from alkali olivine basalt and basanite (basanitoid) to trachyte and phonolite. At Hut Point Peninsula the lavas are basanites (basanitoids), nepheline hawaiite, nepheline mugearite, nepheline benmoreite, and phonolite which range in age from 0.4 to greater than 1.2 m.y. (Forbes, Turner, and Carden, 1974; Kyle and Treves, 1974b). Rhönite occurs in unit 37 of DVDP 1, units 12 and 13 of DVDP 2 (Treves and Kyle, 1973), and units 10-15 of DVDP 3 (Kyle and Treves, 1974b). A detailed petrographic examination of surface flows revealed no primary rhönite; however, a fine grained mineral occurring as an alteration product of kaersutite in some of the lavas intermediate in composition between the basanite and phonolite may be rhönite.

Rhönite grains in three samples (DVDP 1-121.88 m; DVDP 2-99.34 m and 103.15 m) of porphyritic olivine (Fo_{77-87})-titan-salite (Wo_{46-53}; Fs_{10-16}, En_{34-40}) basanite (Table 1) were examined by electron microprobe (Kyle, 1974). In DVDP 1-121.88 m rhönite is abundant as euhedral prismatic microphenocrysts which rarely reach 0.2 mm and average 0.1 to 0.05 mm in length. Abundance decreases in DVDP 2 samples where the microphenocrysts are much finer grained (0.01 mm), are irregular and ragged in form, and occur in a subophitic groundmass of plagioclase, pyroxene, and

---

TABLE 1. Analyses and CIPW Norms for Dunedin and DVDP Host Rocks in Which Rhönite Occurs

	Wt Percent			CIPW Norms	
	1	2		1	2
SiO_2	47.57	41.72	Or	12.76	8.80
TiO_2	2.21	4.18	Ab	30.57	3.79
Al_2O_3	16.47	13.03	An	13.78	17.55
Fe_2O_3	4.27	4.25	Ne	8.74	11.84
FeO	7.32	7.66	Di	11.48	26.66
MnO	0.21	0.18	Ol	7.07	15.18
MgO	3.47	12.03			
CaO	6.68	11.47	Il	4.20	7.94
Na_2O	5.52	3.03	Mt	6.19	6.16
K_2O	2.16	1.49	Ap	1.90	1.97
P_2O_5	0.82	0.85	Other	3.40	0.08
H_2O+	2.83	0.08*	Total	100.09	99.97
H_2O-	0.42	-			
S	0.15	-			
Total	100.10	99.97			

1. Nepheline hawaiite; Pulling Point, Otago Harbour, New Zealand.
2. Basanite (mean of 3 analyses); DVDP 1 and 2, Hut Point Peninsula, Antarctica.
* Loss on ignition 1000°C.

opaques. In DVDP 2–99.34 m the rhönite is usually intergrown with or surrounded by groundmass pyroxene. In the Dunedin District, South Island, New Zealand, rhönite occurs within alteration rims on kaersutite crystals which, together with titaniferous augite, olivine, minor intermediate plagioclase, apatite, and titanomagnetite, makes up small (1 cm) coarse-grained xenoliths in a nepheline hawaiite flow at Pulling Point in Otago Harbour. The host rock (Table 1) is composed of a groundmass of plagioclase (An_{40-50}), pale green clinopyroxene, interstitial nepheline, and homogeneous titanomagnetite in which are set phenocrysts of oscillatory and sector-zoned titan-augite, olivine (Fo_{80}), and kaersutite (α = pale yellow, β = pale reddish brown, γ = pale reddish brown).

Grains of rhönite are too small to allow determination of precise optical properties. In standard thin sections it is opaque but in thin sections less than 20 μm thick it shows strong pleochroism from deep greenish brown to opaque, similar to that reported by Cameron *et al* (1970) and Walenta (1969).

Composition

Analyses were made using a JEOL JXA-5A electron microprobe with 15 kV accelerating potential, 2–3 ×

10^{-8} amp specimen current (on periclase) and a beam diameter of 1–2 μm. The empirical correction procedure of Bence and Albee (1968) was used. Standards, alpha correction factors, and analytical techniques are given by Kushiro and Nakamura (1970).

Typical analyses of three DVDP samples and one Dunedin sample, and five previously published analyses of rhönite, are presented in Table 2. With the exception of MgO and Cr_2O_3, electron microprobe scans across grains indicated a uniform composition. Almost all the grains examined contained detectable (detection limit was 0.03 percent) Cr_2O_3 and NiO, which is the first time they have been analyzed in rhönite.

Compared to other terrestrial rhönite the Antarctic samples show higher TiO_2, Na_2O, and lower SiO_2

TABLE 2. Analyses of Rhönite

	1	2	3	4	5	6	7	8	9
SiO_2	23.8	23.7	23.2	28.58	24.82	24.42	30.90	29.8	19.1
Al_2O_3	17.0	16.8	17.4	13.35	17.24	17.25	17.65	13.6	28.9
TiO_2	11.6	11.9	12.0	10.70	9.09	9.46	8.04	10.2	16.8
Fe_2O_3	-	-	-	-	9.48	11.69	6.80	21.2_T	-
FeO	21.3_T	21.0_T	20.9_T	22.49_T	15.98	11.39	15.20	-	1.9_T
MnO	0.19	0.16	0.18	0.17	0.26	tr	-	0.1	-
MgO	12.7	13.05	12.6	12.09	10.67	12.62	9.08	14.4	15.7
CaO	11.8	12.15	12.2	10.23	11.97	12.43	12.20	11.4	17.9
Na_2O	0.96	0.97	0.89	2.11	0.72	0.67	0.76	-	-
K_2O	-	-	-	0.02	0.02	0.63	0.61	-	-
Cr_2O_3	n.d.	0.06	0.15	-	-	-	-	-	-
NiO	0.10	0.04	0.03	-	-	-	-	-	-
V_2O_3	-	-	-	-	-	-	-	-	0.7
P_2O_5	-	-	-	-	0.03	-	-	-	-
H_2O+	-	-	-	-	0.35	-	0.20	-	-
H_2O-	-	-	-	-	0.06	-	-	-	-
Total	99.45	99.83	99.55	99.74	100.69	100.56	101.44	100.7	101.0

Number of Cations on the Basis of 40(O)

Si	6.536	6.484	6.367	7.785	6.674	6.535	8.032	7.608	4.788
Al	5.502	5.417	5.628	4.285	5.464	5.441	5.408	4.092	8.538
Ti	2.396	2.448	2.476	2.191	1.839	1.904	1.572	1.958	3.167
Fe^{3+}	-	-	-	-	1.919	2.354	1.330	4.073	-
Fe^{2+}	4.892	4.805	4.797	5.123	3.593	2.549	3.304	-	0.398
Mn	0.044	0.037	0.042	0.039	0.060	-	-	0.022	-
Mg	5.199	5.322	5.155	4.909	4.277	5.035	3.517	5.481	5.867
Ca	3.472	3.561	3.587	2.986	3.448	3.564	3.398	3.118	4.808
Na	0.511	0.514	0.474	1.116	0.375	0.348	0.383	-	-
K	-	-	-	0.005	0.006	0.215	0.202	-	-
Cr	-	0.013	0.032	-	-	-	-	-	-
Ni	0.022	0.009	0.007	-	-	-	-	-	-
V	-	-	-	-	-	-	-	-	0.141
P	-	-	-	-	0.006	-	-	-	-
OH	-	-	-	-	0.628	-	0.347	-	-
Z	12.000	11.901	11.995	12.000	12.000	11.976	12.000	11.700	12.000
Y	12.591	12.634	12.509	12.332	11.832	11.842	11.163	11.534	10.899
X	3.983	4.075	4.061	4.107	3.829	4.127	3.983	3.118	4.808
Sum	28.574	28.610	28.565	28.439	27.661	27.945	27.146	26.352	27.707

(1) DVDP 1 - 121.88 m; representative analysis.
(2) DVDP 2 - 99.34 m; representative analysis.
(3) DVDP 2 - 103.15 m; representative analysis.
(4) Pulling Point, Otago Harbour, Dunedin, New Zealand; representative analysis.
(5) Big Bend, Texas (Cameron, Carman and Butler, 1970).
(6) Rhön, Germany (Soellner, 1907).
(7) Saint Sandoux, France (Lacroix, 1909).
(8) Haute-Loire, France, electron microprobe analysis (Babkine, et al. 1967).
(9) Allende meteorite, electron microprobe analysis (Fuchs, 1971).

T = total iron expressed as FeO or Fe_2O_3; n.d. = not detected (<0.03%).
- = not determined.

contents. The Dunedin rhönite is noticeably enriched in Na_2O with a related deficiency in CaO, compared with the other analyses. Total iron is slightly higher than previously reported in other rhönites, and the other elements fall within the established limits. Rhönite in the *Allende* meteorite (9, Table 2) differs markedly from the Antarctic and Dunedin samples and from all terrestrial samples, particularly with regard to total Fe.

Structural formulae were calculated on the basis of 40(O) as recommended by Kelsey and McKie (1963) and Cameron *et al* (1970). The ideal formula of $X_4Y_{12}Z_{12}O_{40}$ requires a total of 28 cations; however, rhönites 1, 2, 3, and 4 (Table 1) all have cation totals exceeding 28 with an excess of Y cations, thus indicating that the Antarctic and Dunedin rhönites probably contain Fe^{3+} in the formula. The amount of Fe_2O_3 necessary for the DVDP samples and the Dunedin sample to achieve stoichiometry (*i.e.*, a cation sum of 28) was calculated (Table 3); an average of about 8 percent Fe_2O_3 is indicated for the DVDP samples and about 6 percent for the Dunedin sample. Noticeable, however, is the decrease in the Z cations (Si+Al) while Y still exceeds 12. This implies that there may be a significant amount of Fe^{3+}, as suggested by Cannillo *et al* (1971) for aenigmatite, or Ti in the tetrahedral Z site.

Cameron *et al* (1970) discussed the suggestion of Fleischer (1936) that rhönite and aenigmatite form a substitution series. The rhönite examined in this study shows no evidence of compositional variation towards aenigmatite and thus strengthens the suggestion of Cameron *et al* (1970) that there is only limited solid solution at magmatic temperatures.

Discussion

The crystallization of primary rhönite like the isomorphic aenigmatite (Lindsley, 1970; Hodges and

TABLE 3. Recalculated Fe_2O_3 and FeO assuming Stoichiometry of Rhönite in DVDP and Dunedin Samples

Sample number*	1	2	3	4
Fe_2O_3	7.89	8.45	7.78	6.10
FeO	14.2	13.4	13.9	17.0
Analysis total	100.24	100.68	100.33	100.36
Cation totals				
Z	11.797	11.647	11.758	11.912
Y	12.302	12.366	12.262	12.052
X	3.903	3.989	3.981	4.037

* Same as Table 2.

TABLE 4. Oxygen Fugacity, Temperature, and Silica Activity Calculated for the Groundmass of DVDP Basanites

Sample Number	Magnetite Usp %*	Ilmenite Hm %*	Olivine Fa %	$T^\circ C$	log fo_2	log a_{SiO_2}**
1 - 121.88	68.7	6.2	22	985	- 11.5	- 1.05
2 - 99.34	69.1	6.1	-	970	- 11.8	-
2 - 103.15	61.3	6.7	22	955	- 12.0	- 1.12

* Magnetite and ilmenite electron microprobe analyses recalculated to end members using method of Carmichael (1967).
** Calculated using the reaction
$2/3 \ Fe_3O_4 + SiO_2 = Fe_2SiO_4 + 1/3 \ O_2$ (Nicholls et al, 1971).

Barker, 1973) is probably controlled by such factors as oxygen fugacity, temperature, and the activity of silica and titanium. In the Antarctic samples, estimates have been made of oxygen fugacity and temperature (Table 4) using co-existing groundmass magnetite–ilmenite pairs (Buddington and Lindsley, 1964) that probably crystallized at the same time or later than the rhönite. Silica activity (Table 4) was calculated using the above data and the composition of olivine in the groundmass or at the rim of phenocrysts (Table 4). Both oxygen fugacity and silica activity are typical of basanites and nepheline-rich basaltic lavas (Anderson, 1968; Carmichael and Nicholls, 1967; Carmichael, Nicholls, and Smith, 1970). Crystallization of primary rhönite cannot therefore be explained in terms of unusual temperature, oxygen fugacity, or silica activity.

In the Dunedin nepheline hawaiite, rhönite has obviously formed as a result of reaction between earlier formed kaersutite and the undersaturated host liquid. Groundmass oxides are homogeneous titanomagnetites, indicating generally low fO_2 conditions (Watkins and Haggerty, 1967).

References

ANDERSON, A. T. (1968) The oxygen fugacity of alkaline basalt and related magmas, Tristan da Cunha. *Am. J. Sci.* **266**, 704–727.
BABKINE, J., F. CONQUERE, J. C. VILMINOT, AND P. K. DUONG (1964) Sur un nouveau gaisement de rhönite (*Monistrd-d'Allier*, Haute Loire). *C. R. Acad. Sci., Paris, Ser D.* **258**, 5479–5481.
BENCE, A. E., AND A. L. ALBEE (1968) Empirical correction factors for the electron microanalysis of silicates and oxides. *J. Geol.* **76**, 382–403.

BENSON, W. N. (1939) Mineralogical notes from the University of Otago, N. Z. No. 3: Kaersutite and other brown amphiboles in the Cainozoic igneous rocks of the Dunedin District. *Trans. R. Soc. N.Z. (Geol.)* **69**, 283–308.

BUDDINGTON, A. F., AND D. H. LINDSLEY (1964) Iron-titanium oxide minerals and synthetic equivalents. *J. Petrol.* **5**, 310–357.

CAMERON, K. L., M. F. CARMAN, AND J. C. BUTLER (1970) Rhönite from Big Bend National Park, Texas. *Am. Mineral.* **55**, 864–874.

CANNILLO, E., F. MAZZI, J. H. FANG, P. D. ROBINSON, AND Y. OHYA (1971) The crystal structure of aenigmatite. *Am. Mineral.* **56**, 427–446.

CARMICHAEL, I. S. E. (1967) The iron-titanium oxides of salic volcanic rocks and their associated ferromagnesium silicates. *Contrib. Mineral. Petrol.* **14**, 36–64.

——— AND J. NICHOLLS (1967) Iron titanium oxides and oxygen fugacities in volcanic rocks. *J. Geophys. Res.* **72**, 4665–4687.

——— ——— AND A. L. SMITH (1970) Silica activity in igneous rocks. *Am. Mineral.* **55**, 246–263.

FLEISCHER, MICHAEL (1936) The formula of aenigmatite. *Am. J. Sci.* **32**, 323–348.

FORBES, R. B., D. L. TURNER, AND J. R. CARDEN (1974) Age of trachyte from Ross Island, Antarctica. *Geology,* **2**, 297–298.

FUCHS, L. H. (1971) Occurrence of wollastonite, rhönite, and andradite in the *Allende* meteorite. *Am. Mineral.* **56**, 2053–2068.

GRÜNHAGEN, H., AND H. A. SECK (1972) Rhönit aus einem Melaphonolith vom Puy de Saint-Sandoux (Auvergne). *Tschermaks Mineral. Petrogr. Mitt.* **18**, 17–38.

HARRINGTON, H. J. (1958) Nomenclature of rock units in the Ross Sea region, Antarctica. *Nature (London),* **182**, 290.

HODGES, F. N., AND D. S. BARKER (1973) Solid solution in aenigmatite. *Carnegie Inst. Wash. Year Book,* **72**, 578–581.

KELSEY, C. H., AND D. McKIE (1963) The unit cell of aenigmatite. *Mineral. Mag.* **33**, 986–1001.

KUSHIRO, I., AND Y. NAKAMURA (1970) Petrology of some lunar crystalline rocks. *Proc. Apollo 11 Lunar Sci. Conf.* **1**, 607–626.

KYLE, P. R. (1974) Electron microprobe analyses of minerals in core samples from Dry Valley Drilling Project (DVDP) Holes 1 and 2, Ross Island, Antarctica. *Dep. Geol. Victoria Univ. of Wellington Publ.* **4**, 27 p.

———, AND S. B. TREVES (1974a) Geology of DVDP 3, Hut Point Peninsula, Ross Island, Antarctica. *Dry Valley Drilling Project Bulletin No.* **3** (Northern Illinois University), 13–48.

———, AND ———(1974b) Geology of Hut Point Peninsula, *Antarctic J. U.S.* **9**, 232–234.

LACROIX, M. A. (1909) Note sur la rhönite du Puy de Barneire a Saint-Sandoux. *Bull. Soc. Fr. Mineral. Cristallogr.* **32**, 325–331.

LINDSLEY, D. H. (1970) Synthesis and preliminary results on the stability of aenigmatite ($Na_2Fe_2TiSi_6O_{20}$). *Carnegie Inst. Wash. Year Book,* **69**, 188–190.

MUDREY, M. J., JR., S. B. TREVES, P. R. KYLE, AND L. McGINNIS (1973) A frozen jig-saw puzzle—first bedrock coring in Antarctica. *Geotimes,* **18**, 14–17.

NATHAN, S., AND F. J. SCHULTE (1968) Geology and petrology of the Campbell-Aviator divide, Northern Victoria Land, Antarctica. Part 1. Post paleozoic rocks. *New Zealand J. Geol. Geophys.* **11**, 940–975.

NICHOLLS, J., I. S. E. CARMICHAEL, AND J. C. STORMER, JR. (1971) Silica activity and P_{total} in igneous rocks. *Contrib. Mineral. Petrol.* **33**, 1–20.

SOELLNER, J. (1907) Üeber Rhönit, ein neues änigmatitähnliches Mineral und über das Vorkommen und über die Verbreitung desselben in basaltischen Gesteinen. *Neues Jahrb. Mineral. Beil. Bd.* **24**, 475–547.

TREVES, S. B., AND P. R. KYLE (1973) Geology of DVDP 1 and 2, Hut Point Peninsula, Ross Island, Antarctica. *Dry Valley Drilling Project Bulletin No.* **2** (Northern Illinois University), 11–82.

WALENTA, VON KURT (1969) Zur kristallographie des Rhönits. *Z. Kristallogr.* **130**, 214–230.

WATKINS, N. D., AND S. E. HAGGERTY (1967) Primary oxidation variation and petrogenesis in a single lava. *Contrib. Mineral. Petrol.* **15**, 251–271.

Spinel

Introduction

Magnetite or its oxidation products are the most important spinels found in rocks of the McMurdo Volcanic Group. Chromium and aluminium rich spinels are found in the DVDP basanite lavas.

Most of the magnetites examined contain appreciable titanium and are more correctly termed titanomagnetite. Titanomagnetite is part of a solid solution series between ulvospinel (Fe_2TiO_4) and magnetite (Fe_3O_4). Analyses are given in Appendix B; Fe^{2+}, Fe^{3+} and ulvospinel (Usp %) content in the magnetite has been calculated using the procedure of Carmichael (1967). Any low analytical totals (<98%) after calculation of Fe^{2+} and Fe^{3+}, usually indicate the grains are oxidised (i.e. maghemite). For the spinels other than titanomagnetites, total Fe has been assigned to Fe^{2+} and Fe^{3+} on the assumption of a formula $R^{2+}R_2^{3+}O_4$ with dissolved ulvospinel (Fe_2TiO_4).

Occurrence and Composition

1. THE PLEIADES

Magnetite occurs in most rocks, often however it shows evidence of low temperature deuteric alteration to maghemite (Wakins and Haggerty, 1967) and it may also have oxidation 'exsolution' lamellae of ilmenite (Fig. 5.33); equivalent to Index II or III of the oxidation index of Watkins and Haggerty (1967). In peralkaline K-trachyte 25699, the opaque grains are all titanohematite, while in K-trachyte 25687 most grains are maghemite. K-trachyte 25671 is moderately oxidised and the magnetite contains abundant lamellae of ilmenite (Index III), and was not analysed. In the unoxidised lavas there is no systematic variation of Usp % with increased differentiation.

Magnetite from trachyandesites 25703 and 25661 have high Al_2O_3 (8.9%-2.9%) and MgO (6.5%-2.6%) but this decreases in more differentiated lavas.

2. DVDP 1 AND 2

Magnetite and other opaque minerals (mainly chrome spinels) occur predominantly as microphenocrysts or in the groundmass. In nepheline hawaiite 2-70.41 m, rare resorbed phenocrysts of magnetite occur.

In contrast to The Pleiades, magnetite in DVDP lavas show no evidence of oxidation or ilmenite exsolution. Compositions, particularly in the basanites, are extremely variable and range from spinel to chrome spinel and magnetite (Figs 5.27; 5.28). Recalculated spinel end-members (Appendix B) show a maximum of 44.1% hercynite ($FeO.Al_2O_3$) in basanite 1-121.88 m; 38.2% chromite ($MgO.Cr_2O_3$) in basanite 1-187.64 and 55.1% spinel ($MgO.Al_2O_3$) in nepheline hawaiite 2-62.41 m. With increased differentiation the magnetites move away from the chromite and spinel apex of Figure 5.27 and approach the magnetite-ulvospinel join. As TiO_2 (i.e. ulvospinel) increases, MgO and Al_2O_3 decrease and show a good negative correlation (Fig. 5.29).

In nepheline benmoreite 2-54.72 a groundmass magnetite is similar in composition to magnetite resulting from oxidation of kaersutite. Microphenocrysts are however distinctly richer in ulvospinel and therefore suggest that a proportion of the ground-mass magnetite may not have crystallized from the magma but rather result from kaersutite oxidation at near surface conditions (<5 km, see discussion above on kaersutite stability).

Titanomagnetite in the basanites occur as microphenocrysts or in the groundmass, it may also rim chrome spinel micro-phenocrysts. Electron microprobe scans indicate these Cr and Al-rich spinels are extremely strongly zoned.
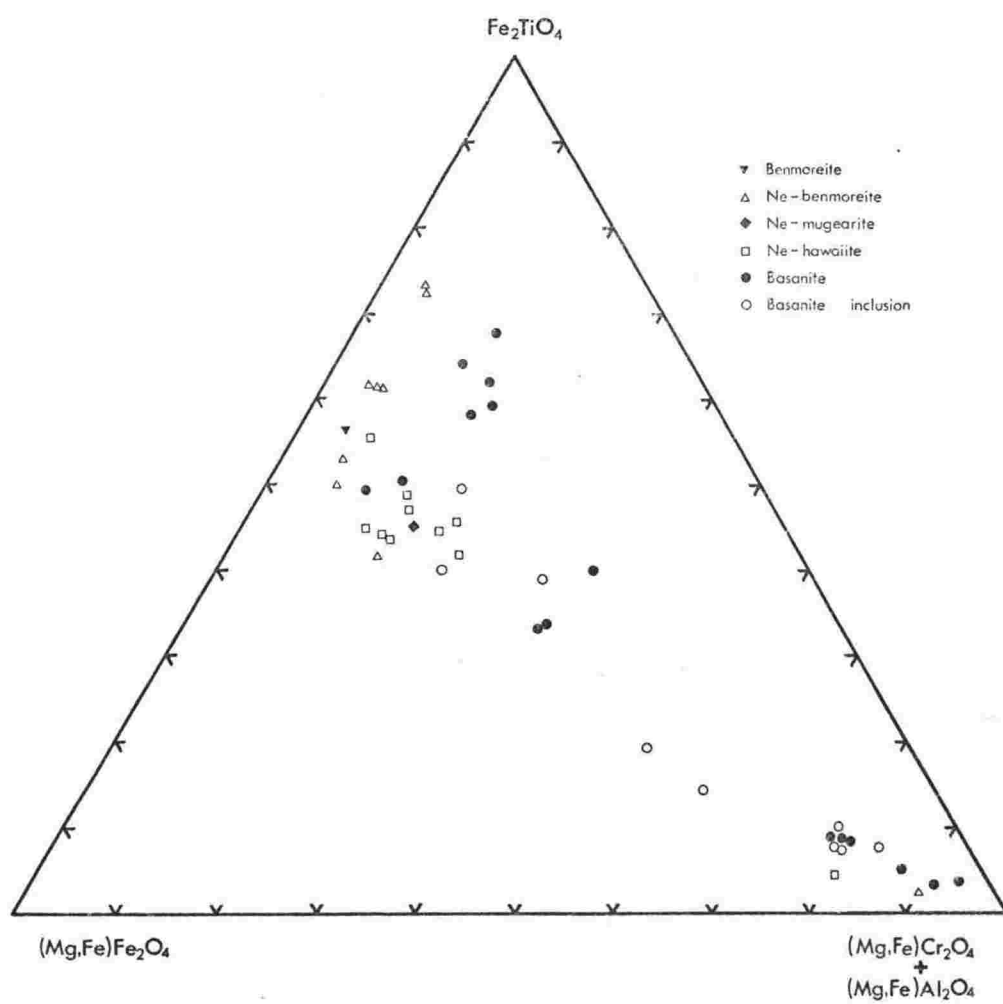
FIGURE 5.27 Plot of spinel analyses from DVDP samples, in terms of recalculated 'end members' (mole %). Fe^{2+} and Fe^{3+} in spinel analyses recalculated assuming perfect stoichiometry.
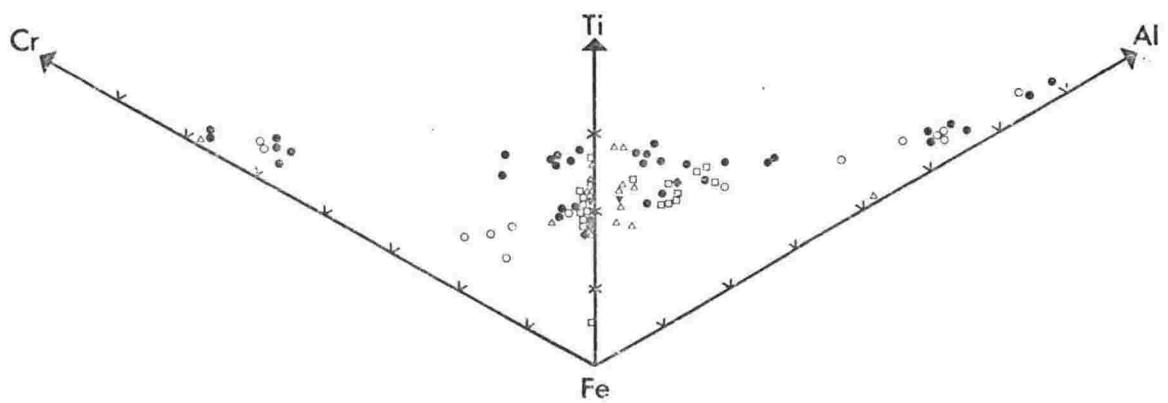
FIGURE 5.28   Variation in Fe, Ti, Al and Cr in spinels from DVDP samples.
Note each point appears twice. For comparative plot of
spinels from other terrestrial and lunar occurrences see
Thompson (1973a). Symbols are the same as Fig. 5.27.

Chrome Spinels

Inclusions of chromite and chrome spinel in olivine are known from many localities. Spinels intermediate between the Cr-rich spinels and Ti-rich magnetites are however rare in lavas and have been interpreted as resulting from reaction between Cr-spinels and the magma as temperature, pressure and liquid composition changed (Gunn et al., 1970; Evans and Moore, 1968; Ridley et al., 1974). Studies of lunar spinels demonstrated an extensive and complex solid solution between chromite and ulvospinel (Haggerty,1972). Hill and Roeder (1974) have shown in melting experiments of tholeiitic basalts under controlled f_{O_2} that there is a compositional solid solution between chromite and titaniferous magnetite. Recent studies of spinels in tholeiitic (Thompson, 1973a) and alkalic (Arculus, 1974) lavas suggest that solid solution in spinels similar to the lunar spinels may also occur in terrestrial lavas.

In the DVDP spinels there is a continuous trend in MgO from 1% to 15% (Fig. 5.29); Al_2O_3 also shows a near continuous trend from 2% to 32% but there is a small hiatus between 16.6% and 22.9% (Fig. 5.29). Cr_2O_3 content has a very bimodal distribution and is restricted between 0% to 11% and 28% to 32% (Fig. 5.29). The large break in the Cr_2O_3 content of the DVDP spinels may indicate reaction between early chromite and clinopyroxene, similar to that suggested by Irvine (1967). Hill and Roeder (1974) found in tholeiitic melts at $f_{O_2} < 10^{-8}$ atm., "the crystallization of early chromite is interrupted by the crystallization of clinopyroxene" but at lower temperatures titaniferous magnetite crystallizes, thus clearly indicating reaction. Continuous trends for MgO and Al_2O_3 in DVDP spinels suggest the opposite and indicate solid solution. It is suggested therefore that solid solution has occurred between ulvospinel and Mg,Al rich spinels, but there may be a field of Cr immiscibility.

An interesting feature is the Cr-poor spinels all occur as inclusions in olivine and pyroxene phenocrysts, while the chrome spinels occur both as inclusions or as microphenocrysts.
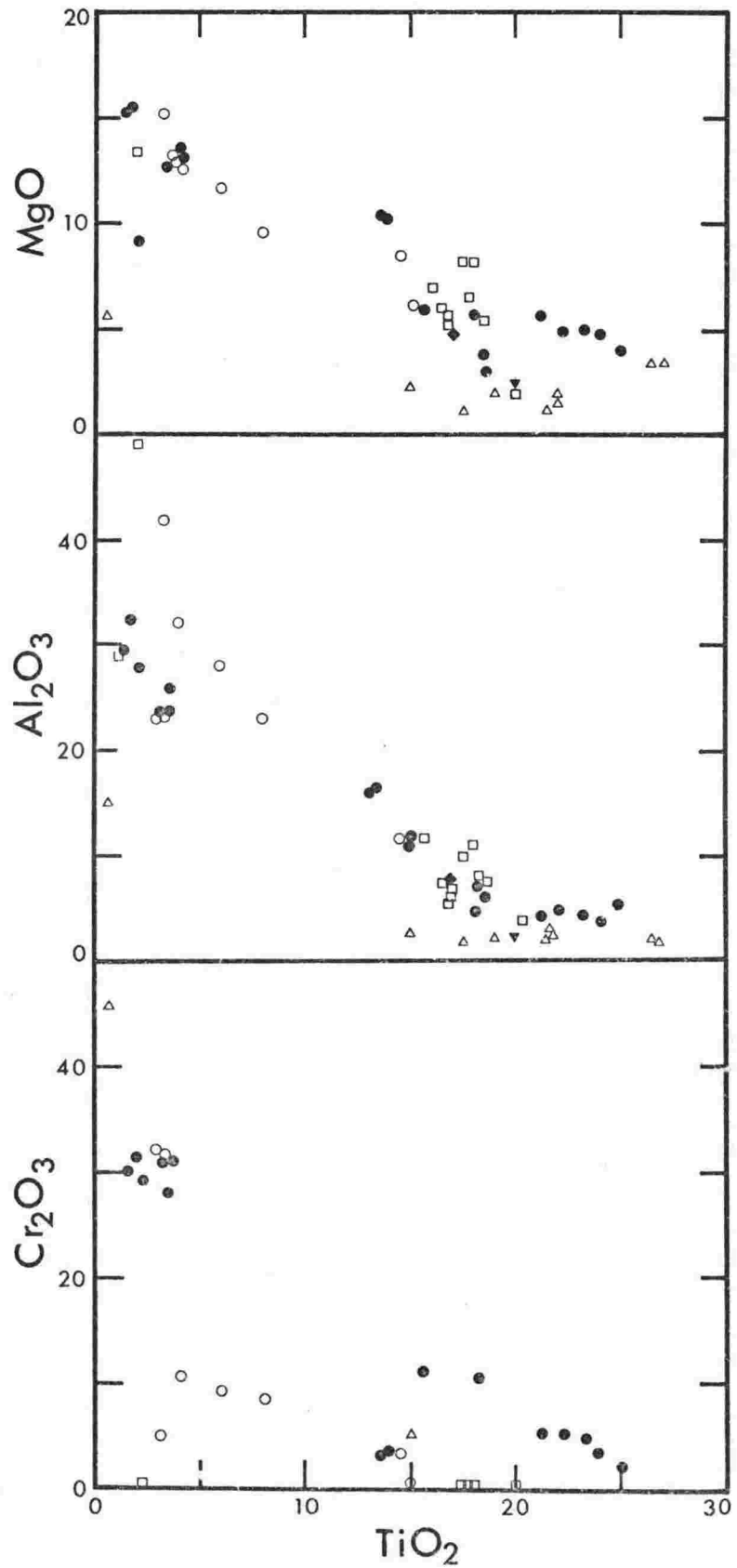
FIGURE 5.29   Compositional variation of spinels from DVDP
samples.   Symbols are the same as Fig. 5.27.

Although the microphenocrysts of spinel are small it does not
necessarily imply they were late in crystallizing, in fact the
opposite is probably the case. Hill and Roeder (1974) suggested
the small size of chromite crystals results because chromium is
enriched by about 1000 in spinel relative to the magma and
therefore it "has to draw from a much larger volume of liquid
to grow to a certain size". Because the Cr-poor spinels have
higher Ti than the chrome spinels, they probably crystallized
later than the chrome spinels, however it is puzzling that they
do not occur as microphenocrysts.

Basu and MacGregor (1975) discussed the chemistry of
chrome spinels from ultramafic xenoliths and concluded that
the ratio $Cr/(Cr+Al+Fe^{3+})$ in spinels increases with pressure
or depth of origin of the xenolith. The Cr-rich spinels from
DVDP basanites are similar in composition to those analysed by
Basu and MacGregor (1975) (Fig. 5.30a,b) and they may have
crystallized at pressures in excess of 20 kbars (Fig. 5.30c).

In summary the spinels are probably the liquidus phase
in the DVDP basanites and show some evidence of solid solution
with ulvospinel. They are believed to have crystallized in
the upper mantle.

3. MT EREBUS

Titanomagnetite is ubiquitous as resorbed cubic euhedral
microphenocrysts of nearly constant composition, averaging
$Usp_{69.5}$ (range $Usp_{70.7}$ to $Usp_{67.5}$). Weak zoning was noted in
only one sample (see Chapter 8).

Ilmenite

Ilmenite occurs as microphenocrysts and in the groundmass
of some basic and intermediate lavas. Oxidised magnetite from
The Pleiades also have ilmenite lamellae. Analyses of DVDP and
The Pleiades ilmenite are given in Appendix B. MgO content is
higher in the DVDP ilmenites otherwise the overall compositions
of DVDP and The Pleiades ilmenites are similar.
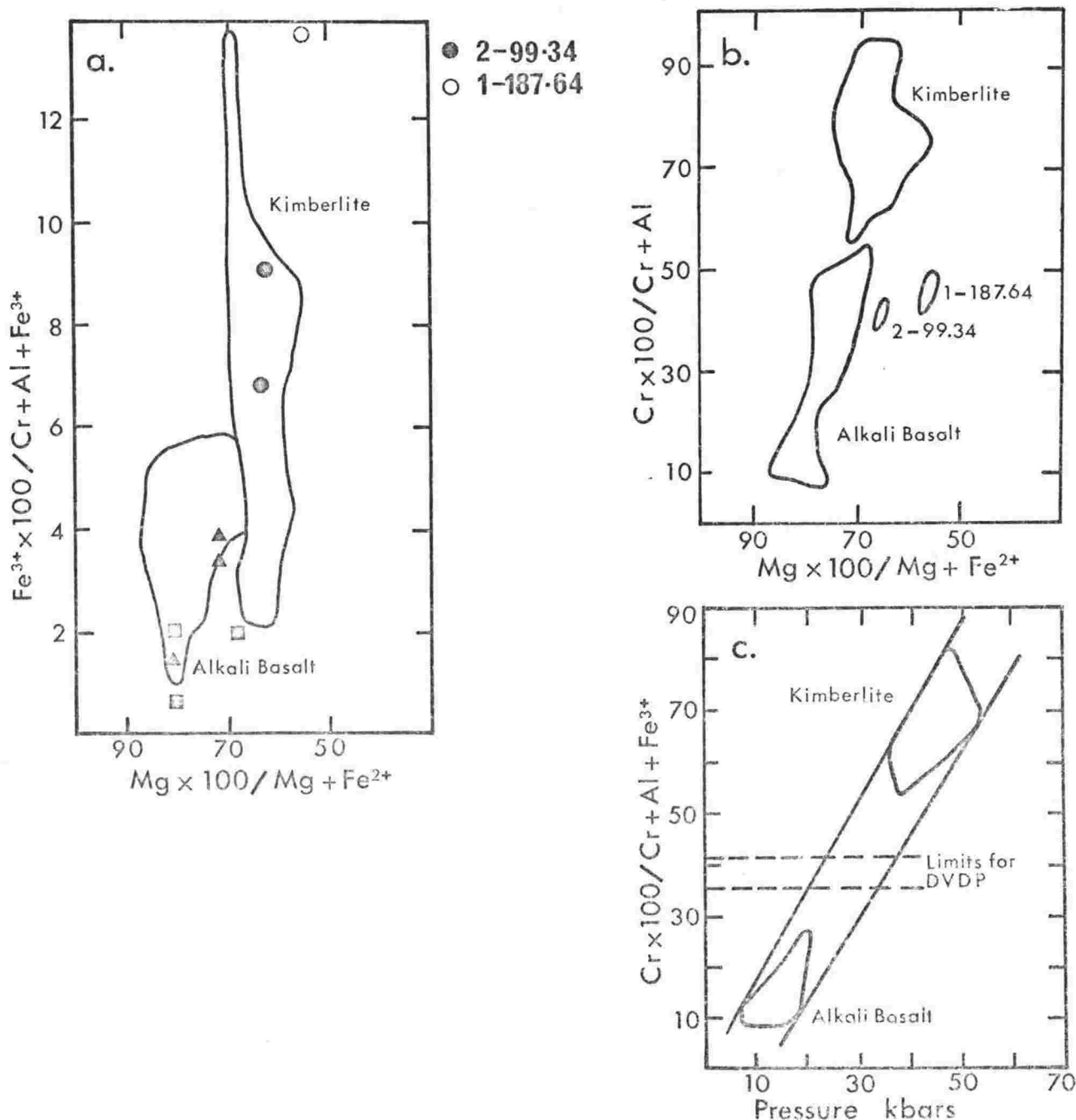
FIGURE 5.30 a) Variation of $Fe^{3+} \times 100/(Cr+Al+Fe^{3+})$ vs $Mg \times 100/(Mg+Fe^{2+})$ in spinels from DVDP lavas and xenoliths in alkali basalts and kimberlites. Spinels in spinel lherzolite (triangle) and garnet lherzolite (squares), average data from Aoki and Prinz (1974).

b) Variation of $Cr \times 100/(Cr+Al)$ vs $Mg \times 100/(Mg+Fe^{2+})$.

c) Plot of $Cr \times 100/(Cr+Al+Fe^{3+})$ in spinels against their estimated equilibrium pressures, calculated from the Al_2O_3 content of the coexisting enstatite. The limits in DVDP spinel compositions suggest equilibration at pressure in excess of 20 kbars. All figures after Basu and MacGregor (1975).

Feldspar

Introduction

Partial electron microprobe analyses of feldspar for CaO, Na_2O and K_2O were made and plotted on feldspar ternary diagrams, a few complete analyses are listed in Appendix B. Often it is not possible to plot all analyses because of the high density of points; representative analyses are however plotted and these indicate the range in compositions.

Occurrence and Composition

1. THE PLEIADES

Plagioclase phenocrysts are rare in the basaltic and intermediate lavas, although in nearly all samples groundmass and microphenocrysts occur. Usually most feldspars are zoned and show normal, reverse and oscillatory zoning, although there is always an increase in Or from core to rim.

Labradorite (An_{50-62}) is the dominant feldspar in essexite 25668, but a very large range of compositions through to potassic sanidine (Or_{81}) (Fig. 5.31) occur as rims and in late stage interstitial patches. A syenite inclusion in nepheline benmoreite 25691 consists mainly of sanidine (Table 5.3).

Trachyandesites (25703, 25671) have labradorite and andesine plagioclase with rare alkali feldspar in the groundmass, normative feldspar compositions have higher Or and lower An components than modal feldspar (Fig. 5.31). Tristanite 25266 has plagioclase ranging from labradorite to oligoclase, but no alkali feldspar. Some of the labradorite is xenocrystic.

Alkali feldspar becomes more dominant in the nepheline benmoreite and K-trachyte and is the only feldspar in peralkaline K-trachyte 25699 (Fig. 5.31). K-trachyte 25687 has andesine (An_{37-41}) phenocrysts, anorthoclase ($An_{19}Ab_{67}Or_{14}$) and sanidine

LEGEND (Normative feldspar compositions)

- ◼ basanite
- ◆ nepheline hawaiite
- ▲ nepheline mugearite
- ● nepheline benmoreite
- ▼ phonolite
- ◇ trachyandesite
- △ tristanite
- ◻ nepheline tristanite
- ▽ K-trachyte
- ○ peralkaline K-trachyte
- E essexite inclusions
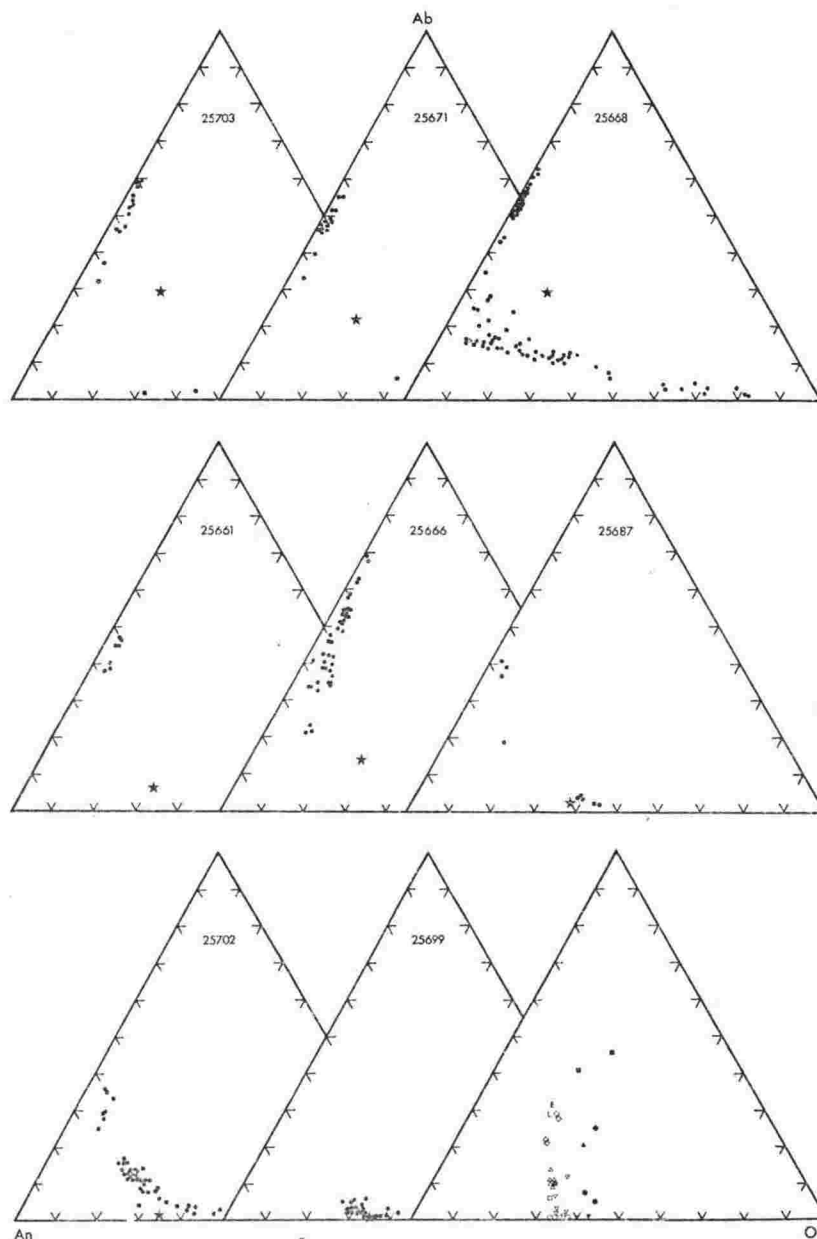
FIGURE 5.31 Partial and complete electron microprobe analyses of feldspar in The Pleiades samples. Normative feldspar composition is shown (star) and summarised, for all analysed The Pleiade samples, in bottom right triangle.

TABLE 5.3   Analyses of feldspar from The Pleiades

	1	2
SiO	67.20	64.85
Al_2O_3	18.94	18.92
TiO_2	0.03	0.03
Fe_2O_3*	0.36	0.15
MnO	0.04	0.02
MgO	0.28	0.16
CaO	0.37	0.54
Na_2O	7.45	6.13
K_2O	5.40	7.57
Total	100.07	98.37

Number of cations on the basis of 32 (O)

	1	2
Si	11.954	11.853
Al	3.968	4.079
Ti	0.005	0.005
Fe	0.050	0.022
Mn	0.011	0.011
Mg	0.075	0.044
Ca	0.075	0.110
Na	2.565	2.175
K	1.218	1.758
Z	15.922	15.932
X	3.999	4.125
	19.921	20.057

Mole %

	1	2
Ca	1.9	2.7
Na	66.5	53.8
K	31.6	43.5

1. Alkali feldspar separated from syenite inclusion in nepheline benmoreite 25691.

2. Alkali feldspar xenocryst in basanite 25682.

Both analysed by standard XRF and AA techniques.

* Total Fe as Fe_2O_3.

(Or_{39-45}) occur in the groundmass; the normative feldspar is however sanidine (Or_{38}) (Fig. 5.31). The other analysed K-trachyte 25702 has feldspar which spread continuously from andesine (An_{36}) through to sanidine (Or_{48}) (Fig. 5.31).

2. DVDP 1 AND 2

Feldspars in the DVDP lavas occur only as microphenocrysts or in the groundmass. It is lacking in many of the glassy basanite samples but when present usually occurs as microlites or incipient groundmass crystals and has a bytownite-labradorite composition (e.g. 1-121.88, Fig. 5.32). Although the nepheline hawaiites (2-62.41, 2-70.41) have normative andesine, their modal feldspars are mainly labradorite (An_{50-60}), there is a short trend towards a more Or rich composition. Nepheline mugearite 2-39.28 and nepheline benmoreite 2-54.72 have microphenocrysts of andesine (An_{40-50}), minor sanidine occurs in 2-54.72. Nepheline benmoreites 1-57.94 and A and benmoreite 1-131.66 have similar andesine (An_{32-44}) which has higher Ab than nepheline benmoreite 2-54.72. There is not a continuous trend of Or enrichment with increased differentiation of the rocks. Nepheline benmoreite 1-85.35 has a differentiation index that lies between 2-54.72 and 1-57.94, yet the feldspars show a much broader range (Fig. 5.32). Pyroxenes also are more fractionated in 1-85.35 than the other benmoreites (Fig. 5.32) and this plus the feldspar development may be related to its occurrence as a dike and its probable longer and slower period of cooling.

3. MT EREBUS

Anorthoclase phenocrysts are the major mineral phase in the glassy anorthoclase phonolite lavas; their chemistry is discussed below (see Chapter 8).

Plagioclase feldspar was separated from porphyritic nepheline hawaiite and nepheline benmoreite lavas from the Erebus centre, analyses are given in Table 5.4.
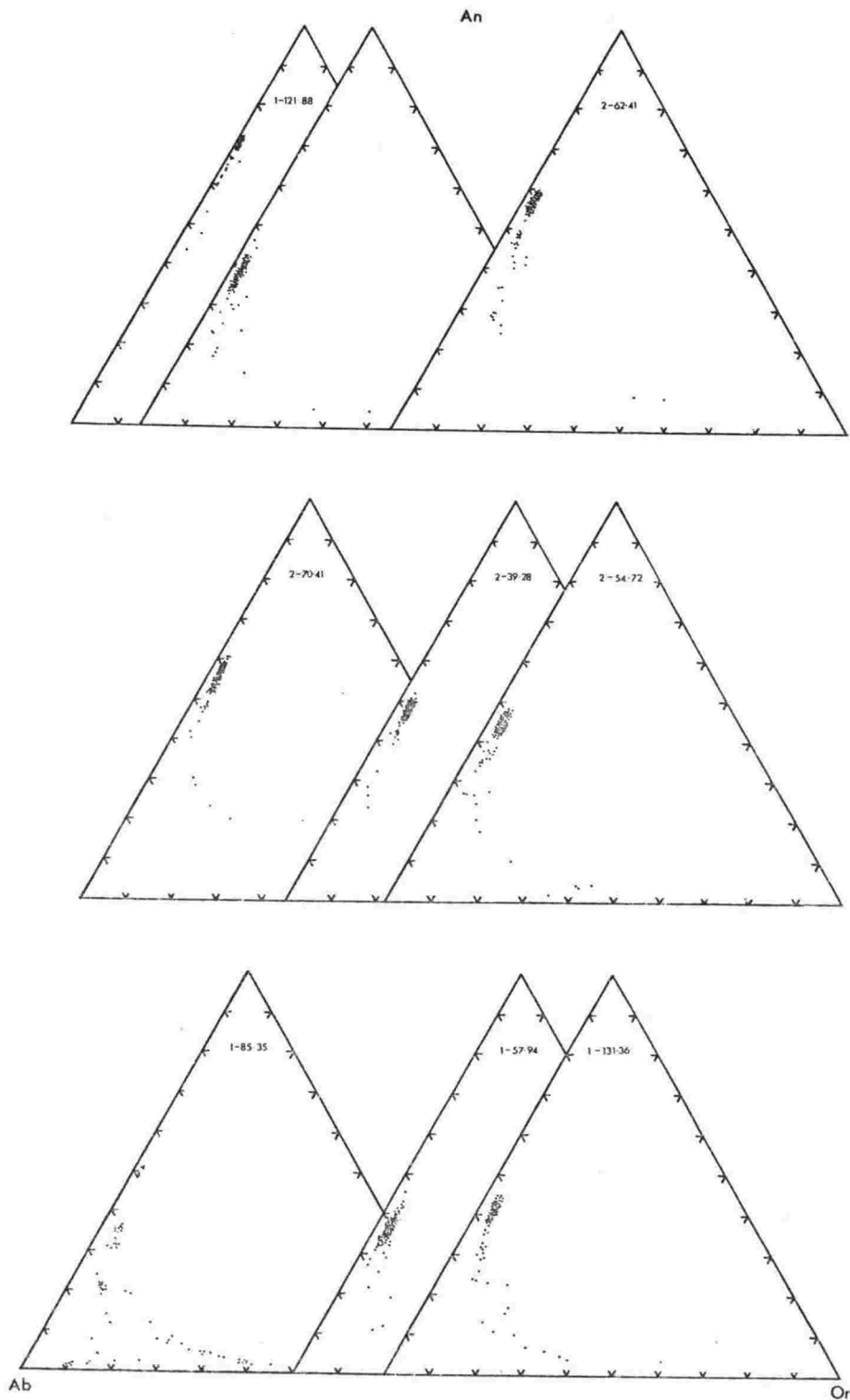
FIGURE 5.32 Partial electron microprobe analyses of feldspar
in DVDP samples. Sample without a label in middle
of top row is a nepheline benmoreite from an unknown
depth in DVDP 1.

TABLE 5.4   Analyses of plagioclase from Erebus centre and Mt Discovery lavas.

	1	2	3	4	5
SiO_2	53.63	53.96	53.57	58.31	59.18
TiO_2	0.29	0.13	0.25	0.18	0.18
Al_2O_3	28.56	28.82	28.57	25.82	25.56
FeO*	0.72	0.34	0.54	0.32	0.33
MnO	0.01	-	-	-	-
MgO	0.17	0.10	0.12	-	-
CaO	10.78	10.84	10.77	7.23	6.55
Na_2O	4.84	4.85	4.90	6.20	6.29
K_2O	0.70	0.50	0.66	1.34	1.39
Loss	0.03	0.04	0.07	-	-
Total	99.70	99.54	99.38	99.40	99.48

Rb		<1
Ba		518
Sr		2913
Zn		8
Cu		10
Ni		<5
V		<2
Cr		<5

Number of cations on the basis of 32 (O)

	1	2	3	4	5
Si	9.764	9.803	9.774	10.516	10.633
Al	6.130	6.172	6.146	5.490	5.414
Ti	0.040	0.018	0.034	0.024	0.024
Fe	0.110	0.052	0.082	0.048	0.050
Mn	0.002	-	-	-	-
Mg	0.046	0.027	0.033	-	-
Ca	2.103	2.110	2.106	1.397	1.261
Na	1.709	1.708	1.734	2.168	2.191
K	0.163	0.116	0.154	0.308	0.319
Z	16.091	16.072	16.068	16.080	16.120
X	3.975	3.934	3.994	3.873	3.771
Sum	20.066	20.006	20.062	19.953	19.891
Ca	52.9	53.6	52.7	36.1	33.4
Na	43.0	43.4	43.4	56.0	58.1
K	4.1	2.9	3.9	8.0	8.5

FeO* total Fe as FeO

1. Nepheline hawaiite dike (25758), Tryggve Point.
2. Nepheline hawaiite (25778), Fang Ridge.
3. Nepheline hawaiite (25754), Turks Head.
4. Nepheline benmoreite (25748), Tent Island.
5. Nepheline benmoreite (P23015), Mt Discovery.

Summary and Discussion

Feldspars in The Pleiades and DVDP suites show a continuous range in compositions from bytownite-labradorite to sanidine. In the intermediate compositions, feldspars overlap in composition, even though their bulk rock compositions differ. Keil *et al.*, (1972) found phenocrysts from Hawaiian tholeiitic and alkali suites also overlapped in composition. Within any one sample the greatest range in feldspar composition occur in the slower cooled intrusive samples, namely a DVDP dike 1-85.35 and The Pleiades essexite 25668.

Feldspar is not an important phenocryst phase in the basic and intermediate lavas from The Pleiades or DVDP and is unlikely to be involved with fractionation processes. In the trachytic lavas from The Pleiades and the phonolites of Mt Erebus, alkali feldspar, particularly sanidine and anorthoclase, are the dominant phases and contribute significantly to the differentiation processes and bulk chemistry of the lavas.

Modal feldspar shows some disagreement with the normative feldspar used to classify the lavas. The trachyandesites and nepheline hawaiites were classified on their normative andesine, however modal plagioclase is typically labradorite. Similarly the nepheline mugearites have normative oligoclase yet modal feldspar is andesine.

Feldspars in McMurdo Volcanic Group rocks are similar to those found in differentiation sequences of alkali volcanics from other areas (e.g. Hawaii, Keil *et al.*, 1972; Dunedin Volcano, Price, 1973).

Apatite

Apatite occurs as microphenocrysts and in the groundmass of basic and intermediate lavas and is often found as inclusions in kaersutite and magnetite. Four analyses from The Pleiades and five from DVDP (Appendix B) show no significant differences. The rapid decrease in P_2O_5 content from tristanite to K-trachyte in The Pleiades suggest apatite is removed during fractional

crystallization. As apatite contains high concentrations of rare-earth elements (REE), its fractionation will have a major effect on the REE chemistry (see Chapter 7).

Baddeleyite and Zircon

Two small (up to 30 μm) grains of baddeleyite which occur as inclusions in a small grain of magnetite from essexite 25668, were found using the electron microprobe (Fig. 5.33). Spectrometer scans indicate the presence of only Zr, Hf, Fe and Ti (Fig. 5.34), the latter two probably result from fluorescence of the magnetite. Baddeleyite is a common accessory phase of lunar basalts and may be more common in terrestrial rocks than the limited number of reported occurrences suggest, but has been overlooked because of its small grain size (Keil and Fricker, 1974).

Zircon ($ZrSiO_4$) was positively identified only in K-trachyte 25702. Minute needles of a mineral that is probably zircon were seen as inclusions and in the groundmass of some nepheline benmoreites and phonolites from the Erebus volcanic province and in K-trachyte and peralkaline K-trachyte from The Pleiades. Zirconium has concentrations in excess of 1200 ppm in most of these late differentiates and would therefore be expected to crystallize as zircon.

Pyrrhotite

Pyrrhotite occurs as small round blebs in magnetite in a wide range of lava types. The only complete analyses are of grains in anorthoclase phonolite from Mt Erebus (see Chapter 8). Other occurrences include in nepheline tristanite 25661 from The Pleiades, nepheline benmoreite 1-57.94, nepheline hawaiite 2-62.41 and several basanites from DVDP. Partial analyses suggest up to 0.56% NiO in the DVDP pyrrhotites whereas those from Mt Erebus are pure pyrrhotite consisting only of Fe and S.
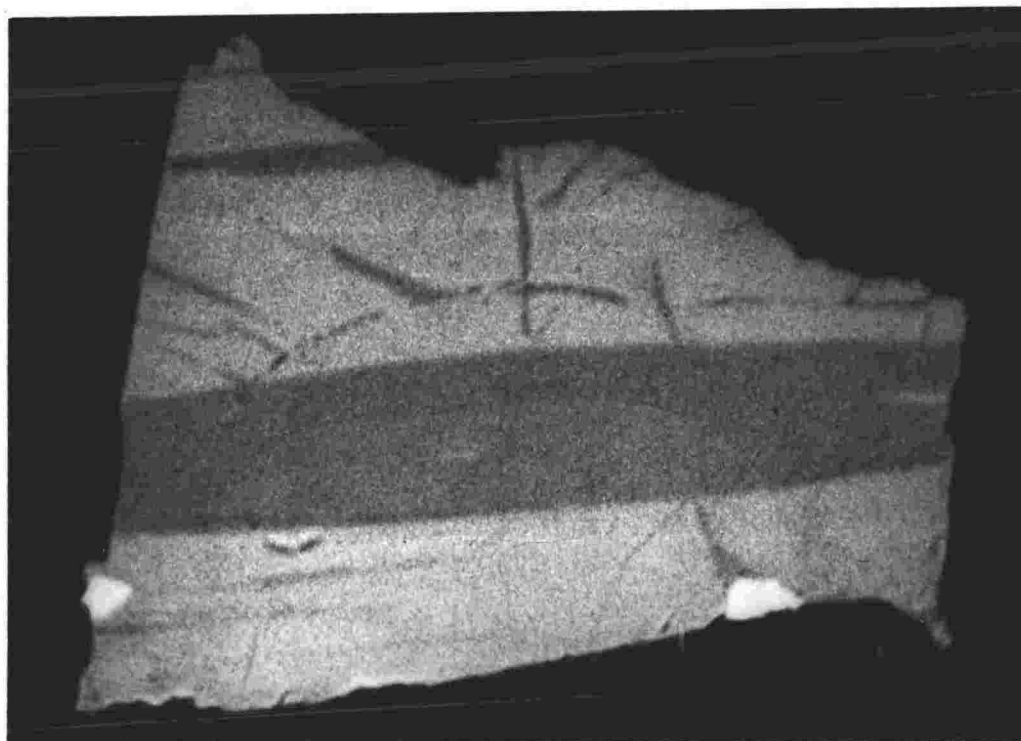
FIGURE 5.33   Electron beam scanning photograph of two small grains of
baddeleyite (ZrO_2) (white) included in a grain of
titanomagnetite (grey) with ilmenite (dark grey) exsolution
lamellae from essexite inclusion (25668), The Pleiades.
Scale 10 mm = 15 μm.
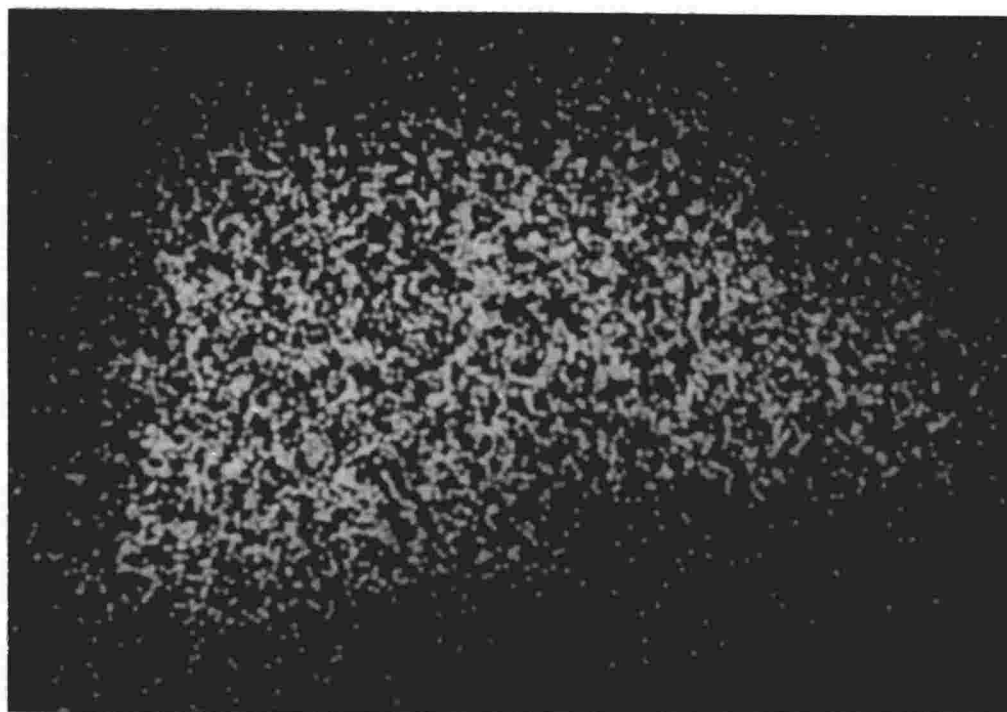
FIGURE 5.34   X-ray scanning image of Zr in the right of two grains of
baddeleyite shown in Fig. 5.33.

Feldspathoids

Most rocks of the McMurdo Volcanic Group are undersaturated and normative nepheline may reach 24%. Feldspathoids have never been positively identified in thin section, although nepheline is often detected by staining, x-ray diffraction or electron microprobe in many lava types. In the nepheline benmoreite dike sample 1-85.35 from DVDP sodalite in the groundmass was partially analysed (Table 5.5).

TABLE 5.5   Partial analyses of sodalite from DVDP 1-85.35

	1	2	3	4
CaO	0.06	0.04	0.05	0.05
Na_2O	25.8	26.2	25.8	23.6
K_2O	0.05	–	0.03	0.05

154.

CHAPTER SIX

PHYSICAL AND THERMODYNAMIC PROPERTIES

Geothermometry

Introduction

In recent years many methods for the determination of
mineral crystallization temperatures have been developed (see
summary in Carmichael *et al.*, 1974 p.78). Temperatures of
several rocks studied have been determined using four mineral
geothermometers. Each method is discussed separately below.

MAGNETITE-ILMENITE GEOTHERMOMETER

Temperature and oxygen fugacity can be determined from
coexisting magnetite-ilmenite pairs using the experimental
calibration of Buddington and Lindsley (1964). This geo-
thermometer has found wide application (Carmichael, 1967;
Anderson, 1968 and others) and has an accuracy of ±30°C
(Buddington and Lindsley, 1964). The magnetite and ilmenite
analyses were recalculated using the procedures of Carmichael
(1967) (see Chapter 5 and Appendix B) and the temperatures
were determined using the calibration curves of Buddington
and Lindsley (1964).

Magnetite is common in the alkali volcanic rocks, but
coexisting ilmenite is rare, and when present often occurs
in the groundmass. Magnetite and ilmenite are readily
oxidised and if this has taken place the calculated temperatures
and f_{O_2} are lower than values obtained for non-oxidised crystals.
In some samples there may be a range in compositions of
magnetite and ilmenite in which case either average compositions
or the compositions of magnetite and ilmenite grains in
contact were used.

1. The Pleiades

Three samples contain both magnetite and ilmenite,
however only one, a K-trachyte (25687) gives a realistic

temperature of 1020°C (Table 6.1). In the essexite (25668), magnetite showed oxidation exsolution (Fig. 5.33) and although these grains were avoided for analysis late stage re-equilibration appears to have affected all grains. Magnetite in tristanite 25666 has been oxidised to maghemite, accounting for the low temperature (Table 6.1).

2. DVDP 1 AND 2

Magnetite-ilmenite temperatures were calculated for six samples (Table 6.1). Three temperature estimates were calculated using groundmass magnetite and ilmenite in the basanites (Table 6.1) and indicate conditions during the final stages of crystallization. Estimated temperatures in the nepheline hawaiites are 880°C and 1010-1020°C (Table 6.1). The lower value of 880°C for sample 2-62.41 probably results from oxidation of the Fe,Ti-oxides, the higher value in 2-70.41 was determined on microphenocrysts and indicate conditions during the later stages of crystallization. A temperature of 1110°C for nepheline benmoreite (Table 6.1) appears very high especially as it was determined on micro-phenocrysts that occur in the groundmass.

OLIVINE-CLINOPYROXENE GEOTHERMOMETER

Powell and Powell (1974) formulated a geothermometer based on the exchange of iron and magnesium between olivine and calcium-rich clinopyroxene and calibrated it against temperatures from magnetite-ilmenite pairs. Because of the rarity of ilmenite in alkali lavas, the olivine-clinopyroxene geothermometer could become very useful, but further calibration may be necessary.

To use the geothermometer the Fe in the clinopyroxene must be apportioned to Fe^{2+} and Fe^{3+}. Powell and Powell (1974) suggested a scheme for doing this and temperatures calculated this way are given in Table 6.2. Temperatures have also been calculated using the Fe^{2+} and Fe^{3+} values determined by charge balance procedures (see page 93). There is exceptionally good agreement in the temperatures obtained for the two methods of pyroxene recalculation (Table 6.2).

TABLE 6.1 Temperature and oxygen fugacity of McMurdo Volcanic Group rocks, calculated using the magnetite-ilmenite geothermometer.

No.	Sample	Rock Type	Magnetite Grain	Usp %	Ilmenite Grain	Hm %	T °C	$-\log f_{O_2}$
THE PLEIADES								
1	25668	Essexite inclusion	13	35.2	10	4.6	735	16.8
			Mean 4	38.7	Mean 4	4.85	760	15.9
2	25666	Tristanite	5-i	13.8	2-i	10.1	635	18.1
3	25687	K-trachyte	2	62.9	1	8.6	1020	10.7
DVDP 1 AND 2								
4	1-121.88	Basanite	4	68.7	1	6.2	985	11.5
5	2-99.34	Basanite	1	69.1	1	6.1	970	11.8
6	2-103.15	Basanite	3	61.3	1	6.7	955	12.0
7	2-62.41	Nepheline hawaiite	Mean 4	41.5	Mean 2	11.8	880	12.2
8	2-70.41	Nepheline hawaiite	Mean 4	42.6	Mean 3	18.5	1010	9.6
			4	47.6	3	17.1	1020	9.7
9	2-54.72	Nepheline benmoreite	1	73.3	1,2	10.4	1110	9.5

Four temperatures have been estimated for each sample using the extremes in compositions. Phenocryst core and either phenocryst/microphenocryst rim or groundmass compositions were used (Table 6.2). Olivine and clinopyroxene from Mt Erebus show no compositional variation, therefore only one temperature was calculated.

1. The Pleiades

Temperatures calculated using rim compositions for two trachyandesites are 1100°C and 1050°C, while tristanite, nepheline tristanite and K-trachyte all have similar rim temperatures of between 990°C and 1000°C (Table 6.2). Core temperatures are generally lower than those calculated using rim compositions.

2. DVDP 1 and 2

Four basanite samples have temperatures of 1010 to 1020°C. These were estimated from rim compositions and are lower than those from the cores of crystals. Magnetite-ilmenite pairs in the groundmass of three basanites give temperatures in reasonable agreement with the rim olivine-clinopyroxene values, although the latter are always higher. The olivine and pyroxene analyses are of rims on phenocrysts and microphenocrysts which probably crystallised earlier and at greater pressure than the groundmass magnetite-ilmenite. This earlier crystallization could account for the slightly higher olivine-clinopyroxene temperatures.

3. Mt Erebus

Olivine and clinopyroxene microphenocrysts are uniform in composition and give six similar temperatures which average 990°C (Table 6.2).

Discussion

The olivine-clinopyroxene geothermometer gives temperature estimates for rim and groundmass compositions that agree reasonably well with groundmass magnetite-ilmenite temperatures.

TABLE 6.2 Temperatures calculated using olivine-clinopyroxene from McMurdo Volcanic Group rocks. All temperatures calculated assuming no pressure correction.

Sample Number	Type	Position	Olivine Grain	Mg/Fe	Pyroxene[a] Grain	Ml-Mg/Fe	Ml-Al	Pyroxene[b] Ml-Mg/Fe	Ml-Al	Temperature T°Ca	°C/5kb	+ Pressure Corr. T°Cb	°C/5kb	Mt-Il T°C
THE PLEIADES														
25703	Trachyandesite	Core	1C	4.304	3C	2.639	0.191	3.221	0.213	1025	27	1021	27	
		Rim	1R	2.868	2	1.501	0.071	1.552	0.078	1054	31	1048	30	
25668	Essexite inclusion	Core	3	1.502	7	3.052	0.093	4.263	0.113	988	28	982	27	
		Rim		1.285	2C	2.587	0.079	3.125	0.103	983	28	985	28	
25671	Trachyandesite	Core	7	1.993	4C	2.655	0.113	3.480	0.146	1007	28	1002	27	
		Rim	4-g	1.982	3-g	0.648	0.053	0.657	0.057	1109	34	1099	33	
25661	Nepheline tristanite	Core	4	1.381	1C	1.723	0.115	2.126	0.151	1007	28	1004	27	
		Rim	3R	1.295	1R	2.037	0.119	2.615	0.156	1002	27	999	27	
25666	Tristanite	Core	1C	3.342	6C	3.022	0.223	5.507	0.267	1018	27	1009	26	
		Rim	1R	1.381	7R	2.199	0.077	2.484	0.096	994	30	994	28	
25702	K-trachyte	Early	Mean 2	0.294	2	0.902	0.057	0.893	0.054	944	29	941	29	
		Late	Mean 2	0.294	6	0.444	0.060	0.439	0.056	991	30	990	30	
DVDP														
1-121.88	Basanite	Core	1C	6.224	6C	3.624	0.248	4.332	0.262	1024	27	1021	26	
		Rim	3-g	2.896	2	3.133	0.234	5.463	0.278	1014	26	1007	26	985
		Rim	3-g	2.896	4R	2.594	0.254	4.605	0.303	1017	26	1010	26	
1-187.64	Basanite	Core	3	6.081	1C	2.919	0.246	4.515	0.283	1027	27	1019	26	
		Rim	4R	4.738	1R	2.492	0.246	3.538	0.280	1025	27	1019	26	
2-99.34	Basanite	Core	1	7.174	3C	2.287	0.243	4.456	0.304	1033	27	1021	26	970
		Rim	2	4.774	3R	3.238	0.218	5.669	0.262	1022	27	1013	26	
2-103.15	Basanite	Core	1	6.556	3C	4.339	0.183	7.417	0.219	1024	27	1014	27	955
		Rim	3	3.418	3R	3.298	0.220	5.925	0.265	1016	27	1008	26	
MT EREBUS														
25725	Anorthoclase Phonolite		1	1.118	1	2.519	0.109	2.561	0.111	989	27	989	27	
25724	Anorthoclase Phonolite		2	1.069	4	2.495	0.110	2.875	0.127	988	27	988	27	
Anorth.1	Inclusions in anorthoclase		2	1.136	1	2.454	0.116	3.106	0.145	992	27	991	27	

a. Pyroxene recalculated using scheme of Powell and Powell (1974).
b. Pyroxene recalculated by charge balance procedures (see Chapter 5).

Good agreement could be expected as the geothermometer was calibrated using groundmass magnetite-ilmenite temperatures (Powell and Powell, 1974).

Calculated temperatures are pressure dependent so that a correction (see Table 6.2) must be applied for the depth of crystallization of phenocrysts. No correction is necessary for temperatures calculated using rim or groundmass olivine-clinopyroxene compositions, as these presumably crystallise at pressures close to 1 bar (i.e. quench conditions).

In the intermediate and trachytic lavas from The Pleiades a maximum pressure for the crystallization of phenocryst cores is estimated to be 10 kbars (i.e. near the base of the crust). When this correction is applied the core temperature in trachyandesite 25671 (Table 6.2) is still lower than the temperature calculated using rim compositions. Further calibration for pressure effects may be necessary.

PLAGIOCLASE GEOTHERMOMETER

Kudo and Weill (1970) developed an empirical geothermometer based on plagioclase-magmatic liquid equilibrium. Subsequently Mathez (1973, 1974 personal communication) has suggested several refinements.

Temperature calculations on McMurdo Volcanic Group lavas have been made using average or core feldspar compositions determined by electron microprobe and the whole rock analysis (i.e. similar to the method used by Stormer and Carmichael, 1970) and these are listed in Table 6.3. For several samples feldspar rim and groundmass or glass compositions of the lavas were used.

In both the dry and hydrated systems there is a general temperature decrease as the lavas become more salic (Table 6.3). Dry system temperatures are extremely high but as the water pressure increases calculated temperatures decrease (an exception is the calculation using the equation of Mathez at 0.5 kbars P_{H_2O}).

Stormer and Carmichael (1970), Brown and Carmichael (1971) and Mathez (1973) considered that temperatures

TABLE 6.3 Temperatures of feldspar crystallization in lavas of the McMurdo Volcanic Group, estimated using the Kudo-Weill plagioclase geothermometer.

Sample	Type	Position	Feldspar Composition	Kudo-Weill Dry	P_{H_2O} 0.5kb	P_{H_2O} 1.0kb	P_{H_2O} 5.0kb	Mathez[a] Dry Basalt	P_{H_2O} 0.5kb	P_{H_2O} 1.0kb	Other[c] T°C
THE PLEIADES											
25703	Trachyandesite	Core	An_{58}	1224	1175	1139	872	1188	1204 1251	1197	
		Gmass	An_{50}	1188	1139	1102	823	1153	1179 1217	1164	1050[d]
25671	Trachyandesite	Core	An_{55}	1216	1166	1129	849	1180	1197 1242	1187	
		Gmass	An_{46}	1169	1122	1084	801	1136	1163 1195	1142	1100[d]
25661	Nepheline tristanite	Gmass	An_{40}	1160	1110	1070	757	1125	1155 1186	1130	1000[d]
25666	Tristanite	Core	An_{51}	1183	1133	1094	792	1147	1175 1213	1157	
25687	K-trachyte	Core	An_{41}	1207	1152	1111	787	1167	1194 1243	1182	1020[e]
25702	K-trachyte	Core	An_{36}	1165	1112	1069	718	1128	1159 1194	1134	
25699	Peralkaline K-trachyte	Gmass	An_{5}	891	852	792	N.S.[b]	875	944 822	776	
DVDP 1 AND 2											
2-70.41	Nepheline hawaiite	Gmass	An_{60}	1278	1225	1190	925	1239	1251 1314	1256	1015[e]
2-39.28	Nepheline mugearite	Gmass	An_{50}	1234	1183	1146	872	1197	1219 1272	1215	
2-54.72	Nepheline benmoreite	Gmass	An_{48}	1231	1180	1143	864	1194	1216 1269	1212	1110[e]
1-85.35	Nepheline benmoreite	Gmass	An_{38}	1183	1135	1097	813	1149	1175 1212	1158	
1-57.94	Nepheline benmoreite	Gmass	An_{42}	1203	1153	1115	830	1167	1192 1235	1180	
1-131.36	Benmoreite	Gmass	An_{46}	1203	1152	1114	820	1167	1192 1237	1180	
MT EREBUS											
25726G	Anorthoclase phonolite	Late	An_{17}	1112	1064	1023	689	1080	1115 1127	1074	
25725G	as above	Late	An_{17}	1096	1049	1007	662	1065	1102 1108	1056	990[d]
25724G	as above	Late	$An_{17.5}$	1114	1066	1024	684	1082	1116 1130	1076	990[d]

[a] For all temperature estimates (except the dry system) feldspar activity coefficients were determined using the data of Orville (1972) and the equations of Mathez (1973).
[b] N.S. - no solution.
[c] Temperatures calculated using other geothermometers.
[d] Olivine-clinopyroxene geothermometer (Table 6.2).
[e] Magnetite-ilmenite geothermometer (Table 6.1).

calculated using the plagioclase geothermometer are almost
invariably higher than expected. Experimental melts of
lavas give an indication of liquidus temperatures (Table 6.5)
and for intermediate lavas these are usually <1200°C (see
discussion below). Many of the plagioclase temperatures for
intermediate lavas of this study (Table 6.3) are higher than
experimental liquidus temperatures and are therefore
considered too high.

OLIVINE-CHROMITE GEOTHERMOMETER

Jackson (1969) outlined a geothermometer based on
co-existing olivine and chromite (chrome spinel). In order
to use the equation of Jackson the Fe^{3+} and Fe^{2+} content of
the chromite must be known, and this has been determined by
assuming perfect spinel stoichiometry. The temperature
calculation is very sensitive to variations in Fe^{3+}/Fe^{2+} ratio
in the chrome spinel, and variations in this ratio may be
responsible for much of the variation in the calculated
temperatures (Table 6.4).

The large range in temperature estimates made using olivine
and chrome spinel in DVDP basanites cannot represent real
crystallization temperatures. Only one chrome spinel was
analysed in samples 1-121.88 and 1-99.34, so temperatures
have been calculated using the maximum variation in olivine
composition. In sample 1-187.64 two olivine grains contain
chrome spinel inclusions and these give temperatures
intermediate between those calculated using 3 other chrome
spinel grains and the maximum variation in olivine
compositions from the same sample. An increase in temperature
is noticeable in all the data as the olivine becomes more
Fe-rich. This is of course contrary to the normal situation
where olivine becomes more Fe-rich as temperature decreases.

Satisfactory temperature determinations were made by
Jackson (1969) and Loney *et al.*, (1971) for intrusive rocks.
Evans and Wright (1972) in a study of chromite in Hawaiian
lavas obtained temperatures of 1762°C to 2490°C and suggested

TABLE 6.4 Apparent equilibrium temperatures determined using the olivine-chromite (chrome-spinel) geothermometer of Jackson (1969).

Sample	Olivine		Chromite					$K_{D_{Mg-Fe^{2+}}}$	T^oC
	Grain	Fe/(Mg+Fe)	Grain	$Fe^{2+}/(Mg+Fe^{2+})$	α	β	δ		
1-121.88	1C	0.138	3C	0.593	0.377	0.539	0.084	9.101	848
	6C	0.153	3C	0.593	0.377	0.539	0.084	8.066	913
	8	0.206	3C	0.593	0.377	0.539	0.084	5.616	1162
1-187.64	5C	0.142	5-i	0.433	0.406	0.447	0.147	4.614	1522
	6	0.146	6-i	0.436	0.415	0.447	0.138	4.522	1609
	1C	0.138	2	0.422	0.358	0.496	0.146	4.560	1456
	1C	0.138	4	0.449	0.405	0.454	0.141	5.090	1436
	1C	0.138	3C	0.451	0.406	0.456	0.138	5.131	1422
	1R	0.170	2	0.422	0.358	0.496	0.146	3.564	1844
	1R	0.170	4	0.449	0.405	0.454	0.141	3.979	1789
	1R	0.170	3C	0.451	0.406	0.456	0.138	4.011	1768
2-99.34	1	0.123	3	0.349	0.353	0.579	0.068	3.822	1469
	2	0.173	3	0.349	0.353	0.579	0.068	2.562	2164

that the equation of Jackson (1969) was not applicable to chromite analysed by electron microprobe in terrestrial volcanic rocks. This suggestion is supported by the calculations made here.

DISCUSSION

Experimental melting of natural rocks at pressures of 1 atmosphere and higher in air and under controlled oxygen fugacity give an independent means of determining liquidus and mineral crystallization temperatures. No such experiments have been made on McMurdo Volcanic Group lavas, but comparison with published results on lavas from other areas are useful (for summary see Thompson, 1972). Liquidus temperatures (Table 6.5) are usually depressed with decreasing f_{O_2} (Thompson, 1973b) and increasing P_{Total} and P_{H_2O}, and therefore represent

TABLE 6.5 Liquidus temperatures of alkaline rocks estimated from 1 atmosphere melting experiments.

Rock Type	Temperature Range ^{o}C	Reference
Basanite	1280-1250	1,2
Hawaiite	1185-1160	1,3
Mugearite	1150-1130	1,4
Benmoreite	1140-1110	1,3,5

References		
	1	Tilley, Yoder and Schairer, 1965
	2	Tilley and Thompson, 1972
	3	Thompson et al., 1972
	4	Thompson, 1972
	5	Thompson, 1973b

a maximum. The mineral geothermometers give a general indication of mineral crystallization temperatures, these will be lower than liquidus temperatures (Table 6.5).

Of the four methods used to determine mineral temperatures the olivine-chromite geothermometer is unsatisfactory and the

Kudo-Weill plagioclase temperatures are believed to be too high. The olivine-clinopyroxene geothermometer when applied to groundmass or rim compositions appears to give reasonable estimates of quench temperatures.

Temperatures estimated using magnetite-ilmenite pairs are considered the most reliable if oxidised samples are excluded. However, phenocrysts of both magnetite and ilmenite are in general lacking; therefore liquidus or near liquidus temperatures are difficult to estimate.

The appearance of kaersutite is believed to indicate temperatures of <1050°C (see page 131 , for discussion). This disagrees with the magnetite-ilmenite temperature of 1110°C estimated on groundmass microphenocrysts in DVDP nepheline benmoreite 2-54.72. A quench or near quench temperature of 1110°C is considered very unlikely in sample 2-54.72 when it is realised that the DVDP basanites give consistent quench temperatures of around 970°C (Table 6.1).

Oxygen Fugacity

Magnetite-ilmenite pairs can also be used to estimate oxygen fugacity f_{O_2} (Buddington and Lindsley, 1964). Most of the magnetite-ilmenite pairs examined have reequilibrated or are oxidised or indicate only groundmass conditions (Table 6.1, Fig. 6.1).

Nicholls et $al.$, (1971) suggested that oxygen fugacity may be buffered in the lavas containing olivine and magnetite by the reaction:

$$\tfrac{1}{3}O_2 + Fe_2SiO_4 = \tfrac{2}{3}Fe_3O_4 + SiO_2 \qquad \ldots\ldots (1)$$

$$\text{gas} \qquad \text{fayalite} \qquad \text{magnetite} \qquad \text{glass}$$
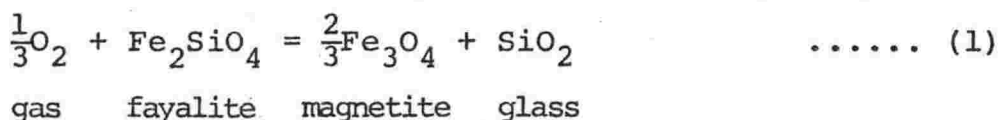
therefore

$$\tfrac{1}{3}\log f_{O_2} = \frac{\Delta G^\circ}{2.303RT} + \log a_{SiO_2}^{liq} + \tfrac{2}{3}\log a_{Fe_3O_4}^{magnetite}$$

$$- \log a_{Fe_2SiO_4}^{olivine} \qquad \ldots\ldots (1A)$$
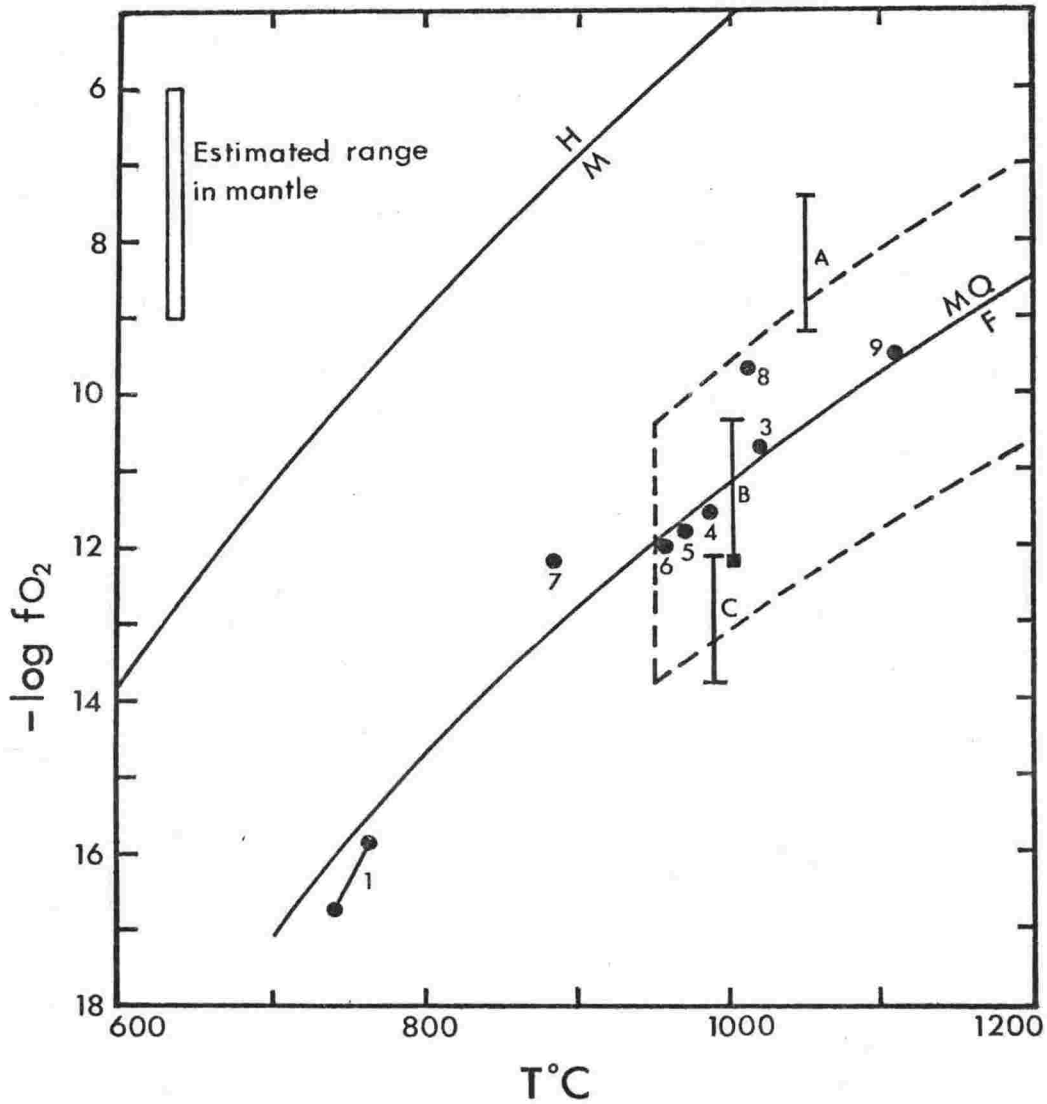
FIGURE 6.1   Temperature and f_{O_2} of coexisting magnetite-ilmenite in
McMurdo Volcanic Group rocks (dots, numbers refer to Table
6.1).   Solid vertical lines show possible range in f_{O_2} of
selected lavas from The Pleiades calculated using equation
(1) and estimated silica activities (Table 6.6), A - trachy-
andesite, B - nepheline tristanite, C - K-trachyte.   E is
calculated f_{O_2} in anorthoclase phonolite from Mt Erebus
(Table 6.6).   Field of conditions in basaltic magmas shown
by dashed line is from Carmichael and Nicholls (1967).   H-M
and F-MQ show variation of f_{O_2} with temperature for the
two synthetic buffers, hematite-magnetite and fayalite-
magnetite-quartz respectively.   Estimated range in f_{O_2} for
basalt source material in the mantle from Sun and Hanson
(1975).

Silica activity (a_{SiO_2}) of alkali volcanic rocks is restricted by:

$$Mg_2SiO_4 \quad + \quad SiO_2 \quad = \quad 2MgSiO_3 \qquad \ldots\ldots (2)$$

$$\text{forsterite} \qquad \text{glass} \qquad \text{clinoenstatite}$$

$$CaTiO_3 \quad + \quad SiO_2 \quad = \quad CaTiSiO_5 \qquad \ldots\ldots (3)$$

$$\text{perovskite} \qquad \text{glass} \qquad \text{sphene}$$
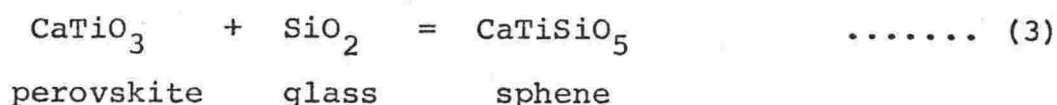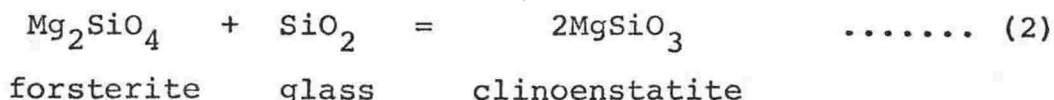
The upper limit of a_{SiO_2} is defined by reaction (2) and the lower limit by reaction (3) (Carmichael *et al.*, 1974) (Fig. 6.2). Although the lavas do not contain modal nepheline most are strongly nepheline normative (Ne > 10%), therefore it is likely that a_{SiO_2} may be closer to that defined by a reaction:

$$\tfrac{1}{2}NaAlSiO_4 + SiO_2 \quad = \quad \tfrac{1}{2}NaAlSi_3O_8 \qquad \ldots\ldots (4)$$

$$\text{nepheline} \qquad \text{glass} \qquad \text{albite}$$
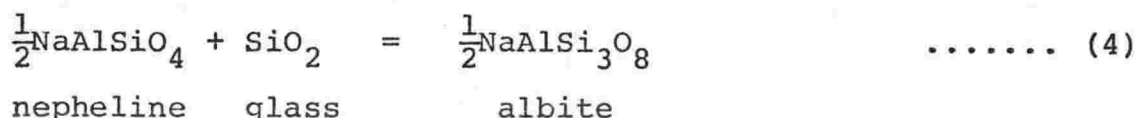
f_{O_2} for 3 lavas from The Pleiades are calculated (Table 6.6) with a_{SiO_2} defined by the buffer reactions (2), (3) and (4), assuming pure mineral compositions (i.e. $a_{mineral} = 1.0$).

For the anorthoclase phonolite from Mt Erebus a_{SiO_2} has been determined using reaction (4) and the appropriate mineral analyses; at $1000^{\circ}C$ the calculated log f_{O_2} is -12.2 (Table 6.6). The anorthoclase phonolite has a similar f_{O_2} to the K-trachyte and nepheline tristanite from The Pleiades, and crystallized under conditions similar to conditions during final crystallization of the DVDP basanites (Fig. 6.1).

Estimates of temperature and f_{O_2} in 3 DVDP basanites (Table 6.1) define a short trend line which parallels, but is slightly lower than, the quartz-fayalite-magnetite synthetic buffer (Fig. 6.1).

The lack of $NaFe^{3+}$ (i.e. acmite) enrichment in clinopyroxenes from DVDP and The Pleiades suggested that f_{O_2} probably remained low throughout the sequence of lavas. This is confirmed by the few available f_{O_2} estimates (Fig. 6.1).

TABLE 6.6 Oxygen fugacity for rocks of the McMurdo Volcanic Group, calculated using buffer reaction (1);

$$\tfrac{1}{3}O_2 + Fe_2SiO_4 = \tfrac{2}{3}Fe_3O_4 + SiO_2$$

gas   fayalite   magnetite   glass

Sample	Type	Olivine Fa %	Magnetite Usp %	Buffer[1]	a_{SiO_2} -log a_{SiO_2}	T °C	-log f_{O_2}
THE PLEIADES							
25703	Trachyandesite	20	48	Fo-En	0.18	1050[2]	7.2
				Ne-Ab	0.63		8.6
				Pv-Sph.	0.76		9.0
25661	Nepheline tristanite	44	58	Fo-En	0.21	1000[2]	10.3
				Ne-Ab	0.66		11.7
				Pv-Sph.	0.83		12.2
25702	K-trachyte	78	58	Fo-En	0.22	990[2]	12.0
				Ne-Ab	0.66		13.3
				Pv-Sph.	0.84		13.8
MOUNT EREBUS							
	Anorthoclase phonolite	46	70	Ne-Ab	0.71[3]	1000[4]	12.2

1 Fo-En $Mg_2SiO_4 + SiO_2 = 2MgSiO_3$

  Ne-Ab $\tfrac{1}{2}NaAlSiO_4 + SiO_2 = \tfrac{1}{2}NaAlSi_3O_8$

  Pv-Sph $CaTiO_3 + SiO_2 = CaTiSiO_5$

2 Olivine-clinopyroxene geothermometer.

3 Estimated from nepheline and alkali feldspar in similar anorthoclase phonolite lavas from Cape Royds, Ross Island (see Chapter 8 and discussion below).

4 Estimated; olivine-clinopyroxene geothermometer indicates 990°C.

Silica Activity

Quantitative estimates and variations of silica activity (a_{SiO_2}) in different magma series have been made by Carmichael and his co-workers (see summary in Carmichael *et al.*, 1974). Unsatisfactory mineral assemblages and the lack of suitable temperature determinations make estimates of a_{SiO_2} during the early stages of crystallization of the McMurdo Volcanic Group difficult.

It is possible to calculate a_{SiO_2} using olivine and clinopyroxene compositions and a buffer reaction:

$$\tfrac{1}{2}Ca_2SiO_4 \quad + \quad \tfrac{1}{2}Mg_2SiO_4 \quad + \quad SiO_2 \quad = \quad CaMgSi_2O_6 \qquad \ldots \ldots (5)$$

$$\text{Ca-olivine} \qquad \text{forsterite} \qquad \text{glass} \qquad \text{diopside}$$
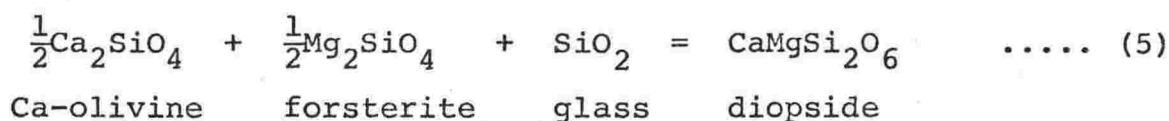
hence

$$\log a_{SiO_2}^{liquid} = \frac{\Delta G^\circ}{2.303RT} + \log a_{CaMgSi_2O_6}^{pyroxene} - \tfrac{1}{2}\log a_{Ca_2SiO_4}^{olivine}$$

$$- \tfrac{1}{2}\log a_{Mg_2SiO_4}^{olivine} \qquad \ldots \ldots (5A)$$

where

$$\frac{\Delta G^\circ}{2.303RT} = \frac{6180}{T} + 1.487$$

(Carmichael, Spera and Wood, in prep.).
Methods and approximations for estimating the activities are given in Table 6.7 and the calculated results are given in Table 6.8 and shown on Fig. 6.2. The calculated a_{SiO_2} may have considerable error, because of the approximations involved in calculating the activities (Table 6.7) and the very small Ca_2SiO_4 component in olivine. The data do indicate the possible range in a_{SiO_2} and also allow comparison between various rock types.

TABLE 6.7 Calculation of activity of components in olivine and clinopyroxene (from Carmichael, Spera and Wood, in preparation).

In the following

X = mole fraction, a = activity, γ = activity coefficient

OLIVINE

a) Ca_2SiO_4

$$a_{Ca_2SiO_4}^{olivine} = X_{Ca_2SiO_4}^2 \cdot \gamma_{Ca_2SiO_4}^2$$

therefore $\frac{1}{2}\ln a_{Ca_2SiO_4} = \ln X_{Ca_2SiO_4} + \ln \gamma_{Ca_2SiO_4}$

where $RT \ln \gamma_{Ca_2SiO_4} = 8651(X_{Mg_2SiO_4}^{olivine}) + 2286$

b) Mg_2SiO_4

$$a_{Mg_2SiO_4}^{olivine} = (X_{Mg_2SiO_4}^{olivine})^2$$

CLINOPYROXENE

$$a_{CaMgSi_2O_6}^{clinopyroxene} = (X_{Ca}\gamma_{Ca})_{M2} (X_{Mg}\gamma_{Mg})_{M1} (X_{Si}^2\gamma_{Si})_t$$

M1, M2, t = M1, M2 and tetrahedral sites of clinopyroxene structure.

$$\gamma_{Ca} \cdot \gamma_{Mg} \cdot \gamma_{Si} = 1 \quad \text{(assumed)}$$

$X_{Ca} = n_{Ca}/(n_{Ca} + n_{Mn} + n_{Na} + n_{Mg}M2 + n_{Fe}M2)$

$X_{Mg} = n_{Mg}M1/(n_{Mg}M1 + n_{Fe}3+ + n_{Al} + n_{Ti} + n_{Cr} + n_{Fe}M1)$

$X_{Si} = n_{Si}/(n_{Si} + n_{Al})$

where n is the number of atoms in the pyroxene formula. Mg and Fe are proportioned between the M1 and M2 sites in the ratio of Fe/Mg so that there is an equal number of cations in each site. $n_{Mg}M1$ is the number of Mg cations in the M1 site.
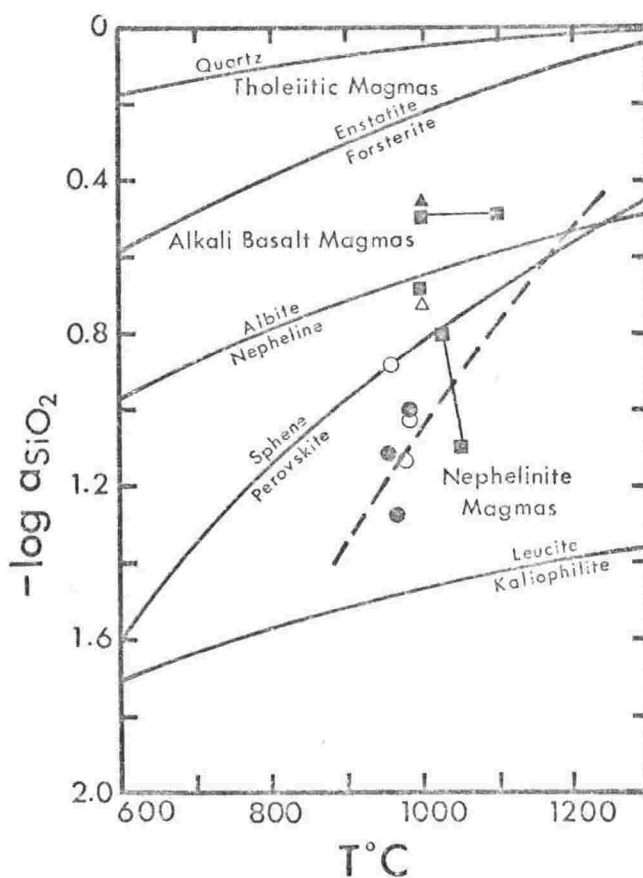
FIGURE 6.2 Variation of -log a_{SiO_2} with temperature, showing calculated a_{SiO_2} of McMurdo Volcanic Group lavas and the inferred fields of 3 basic magma series. Dashed line indicates variation of a_{SiO_2} for a typical DVDP basanite using compositions of phenocryst cores and buffer reaction (5). Silica buffer reactions from Nicholls *et al.*, (1971), magma series after Carmichael *et al.*, (1974).

Reaction (1)

△ Erebus

● DVDP basanites

Reaction (5)

■ The Pleiades

O DVDP basanites

▲ Erebus

1. THE PLEIADES

a_{SiO_2} for three lavas (Table 6.8) are generally similar and plot mainly in the field of alkali basaltic magmas (Fig. 6.2)

2. DVDP 1 AND 2

Quench a_{SiO_2} in the DVDP basanites were calculated using rim olivine and pyroxene compositions (Table 6.8, Fig. 6.2). Calculations were also made using equation (1) (Table 6.9) as T°C and f_{O_2} are known from the groundmass magnetite-ilmenite pairs (Table 6.1). There is reasonable agreement between the values calculated using the different reactions (Tables 6.8, 6.9; Fig. 6.2). Variation of silica activity with temperature in a typical DVDP basanite was calculated using the core compositions of olivine and clinopyroxene and equation (5). The result is shown in Fig. 6.2. The trend lies mainly in the feldspar-free nephelinite magma field as would be expected since the lavas lack feldspar phenocrysts and are strongly undersaturated.

3. MT EREBUS

Anorthoclase phonolite from Cape Royds has a olivine-clinopyroxene temperature of 997°C (Powell and Powell, 1974). This is nearly identical to that calculated for Mt Erebus bombs and lavas (Table 6.2) and as the olivine and clinopyroxene is unzoned the temperature probably approximates to the quench temperature. Cape Royds lavas contain groundmass sanidine microlites (0.464 Ab) and nepheline (0.593 Ne) (Carmichael, 1964). Using equation (4) and the thermodynamic data of Nicholls *et al.*, (1971), quench $(\log a_{SiO_2}^{liquid})^{P=1 \ bar}$ is -0.714 at 1000°C. If $\log a_{SiO_2}^{liquid}$ is known at 1 bar this can be related to higher pressures by using equation (18) of Nicholls *et al.*, (1971),

$$(\log a_{SiO_2}^{liquid})^{P=P \ bars} = (\log a_{SiO_2}^{liquid})^{P=1 \ bar}$$
$$+ [1.34 \times 10^{-6} - \frac{0.0047}{T}](P-1) \quad \ldots \ldots \ (6)$$

TABLE 6.8 Silica activity for lavas of the McMurdo Volcanic Group, calculated using buffer reaction (5); $\frac{1}{4}Ca_2SiO_4 + \frac{1}{4}Mg_2SiO_4 + SiO_2 = CaMgSi_2O_6$

					Ca-olivine	forsterite	glass	diopside

Sample Number	Type	Position	Olivine Grain	X_{Mg}	X_{Ca}	Clinopyroxene Grain	$a_{CaMgSi_2O_6}$	Temp. °C	Geothermometer[1]	log a_{SiO_2}
THE PLEIADES										
25703	Trachyandesite	Core	1C	0.805	0.0035	3C	0.4226	1025	o-c	-0.80
		Core	As above except temperature assumed					1150		-0.55
		Rim	1R	0.73	0.0041	2	0.46	1050	o-c	-1.10
25671	Trachyandesite	Core	7	0.659	0.0035	4C	0.4939	1005	o-c	-0.49
		Core	As above except temperature assumed					1100		-0.31
		Rim	4-g	0.657	0.0035	3-g	0.2817	1100	o-c	-0.49
25666	Tristanite	Core	1C	0.765	0.0030	6C	0.4277	1010	o-c	-0.68
		Rim	1R	0.770	0.0030	7R	0.4766	994	o-c	-0.67
DVDP										
1-121.88	Basanite	Rim	3-g	0.7345	0.0049	4R	0.3324	985	m-i	-1.02
2-99.34	Basanite	Rim	2	0.8189	0.0044	3R	0.3955	970	m-i	-1.12
2-103.15	Basanite	Rim	3	0.767	0.0030	3R	0.405	958	m-i	-0.88
MT EREBUS										
25725	Anorthoclase phonolite	Core	1C	0.505	0.0074	1C	0.5237	1000	o-c	-0.46

[1] o-c = olivine-clinopyroxene geothermometer
m-i = magnetite-ilmenite geothermometer

TABLE 6.9   Calculated quench silica activity (a_{SiO_2}) for DVDP basanites using buffer reaction (1);

$$\frac{1}{3}O_2 + Fe_2SiO_4 = \frac{2}{3}Fe_3O_4 + SiO_2$$

gas   fayalite   magnetite   glass
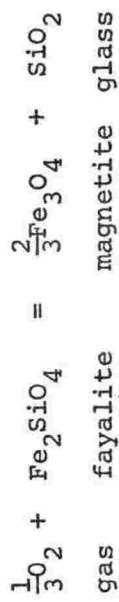
Sample	Type	Olivine Fa %	Magnetite Usp %	log f_{O_2}	$T^{o}C$	log a_{SiO_2}
1-121.88	Basanite	22	68.7	-11.5	985	-1.05
2-99.34	Basanite	17	69.1	-11.8	970	-1.29
2-103.15	Basanite	22	61.3	-12.0	955	-1.12

The anorthoclase phonolite contains large phenocrysts of anorthoclase (0.646 Ab) so if it is assumed these were in equilibrium with the nepheline it is possible to calculate an equilibrium pressure. It must be noted that as anorthoclase crystallised prior to the nepheline then the calculated P_{Total} will be a minimum (Nicholls et al., 1971).

At an unknown pressure the anorthoclase phenocrysts and groundmass nepheline define silica activity, thus (Nicholls et al., 1971):

$$\log a_{SiO_2}^{liquid} = \frac{A}{T} + B + \frac{C(P-1)}{T} + \frac{1}{2} \log a_{NaAlSi_3O_8}^{feldspar} - \frac{1}{2}\log a_{NaAlSiO_4}^{nepheline} \quad \cdots\cdots (7)$$

At 1000°C (1273°K) and assuming the activity equals the mole fraction (a=X), then (Nicholls et al., 1971):

$$\log a_{SiO_2}^{liquid} = -\frac{855}{1273} + 0.012 - \frac{0.0216(P-1)}{1273} + \frac{1}{2}\log 0.646$$

$$- \frac{1}{2}\log 0.593$$

$$= -0.6410 - 16.9 \times 10^{-6}(P-1) \quad \cdots\cdots (7A)$$

Therefore equating equations (6) and (7A)

$$-0.6410 - 16.9 \times 10^{-6}(P-1) = -0.714 + [1.34 \times 10^{-6} - \frac{0.0047}{1273}](P-1)$$

$$P = 5 \text{ kbars (i.e. about 16.5 km).}$$

This is considered a reasonable depth for a magma chamber underlying Mt Erebus.

Alumina Activity

Nicholls and Carmichael (1972) and Bacon and Carmichael (1973) have calculated $a_{Al_2O_3}$ and shown how this combined with a_{SiO_2} can be used to calculate depth and temperature of

equilibrium of basaltic magma with assumed mantle compositions.

For three DVDP basanites in which quench temperatures, f_{O_2} and a_{SiO_2} are known, two $a_{Al_2O_3}$ buffers can be applied (Nicholls and Carmichael, 1972);

$$CaMgSi_2O_6 + \tfrac{1}{2}SiO_2 + Al_2O_3 = CaAl_2Si_2O_8 + \tfrac{1}{2}Mg_2SiO_4 \quad \ldots\ldots (8)$$

diopside   glass   liquid   anorthite   forsterite
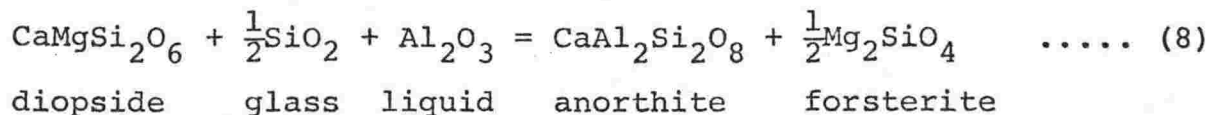
$$\log a_{Al_2O_3}^{liquid} = \frac{\Delta G^\circ}{2.303RT} + \log a_{CaAl_2Si_2O_8}^{plagioclase} + \tfrac{1}{2}\log a_{Mg_2SiO_4}^{olivine}$$

$$- \tfrac{1}{2}\log a_{SiO_2}^{glass} - \log a_{CaMgSi_2O_6}^{pyroxene} \quad \ldots\ldots (8A)$$

and

$$CaMgSi_2O_6 + Al_2O_3 = CaAl_2SiO_6 + \tfrac{1}{2}SiO_2 + \tfrac{1}{2}Mg_2SiO_4 \quad \ldots\ldots (9)$$

diopside   liquid   Ca-Tschermak   glass   forsterite
                                   pyroxene
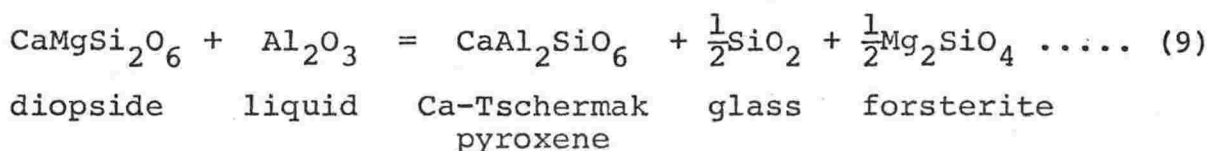
$$\log a_{Al_2O_3}^{liquid} = \frac{\Delta G^\circ}{2.303RT} + \log a_{CaAl_2SiO_6}^{pyroxene} + \tfrac{1}{2}\log a_{SiO_2}^{glass}$$

$$+ \tfrac{1}{2}\log a_{Mg_2SiO_4}^{olivine} - \log a_{CaMgSi_2O_6}^{pyroxene} \quad \ldots\ldots (9A)$$

Methods for calculating activities of the mineral components from their chemical analyses were given by Bacon and Carmichael (1973). They warned that calculation of $a_{CaAl_2SiO_6}$ may be subject to appreciable error, therefore calculations of $a_{Al_2O_3}$ using equation (9) are less reliable than those using equation (8).

$a_{Al_2O_3}$ for three DVDP lavas are given in Table 6.10. Calculations using equations (8) and (9) show reasonable agreement.

The values of $a_{Al_2O_3}$ are currently of little use as there is little or no data available with which to compare. With refinements in the thermodynamic data, however, an increase in the number of calculations of this type can be expected and

TABLE 6.10 Calculated alumina activity ($a_{Al_2O_3}$) for DVDP basanites.

Sample	Type	T°C	log a_{SiO_2}	Olivine Grain	$a_{Mg_2SiO_4}$	Plagioclase $a_{CaAl_2Si_2O_8}$	Grain	Clinopyroxene $a_{CaMgSi_2O_6}$	$a_{CaAl_2SiO_6}$	log $a_{Al_2O_3}$ Equ. 8	log $a_{Al_2O_3}$ Equ. 9
1-121.88	Basanite	985	-1.05	7-g	0.6068	0.60	4R	0.5575	0.3676	-4.079	-3.665
2-99.34	Basanite	970	-1.27	2	0.6839	0.60[a]	3R	0.5281	0.2761	-3.984	-3.901
2-103.15	Basanite	955	-1.12	3	0.5991	0.60[a]	3R	0.5916	0.2227	-4.227	-4.068
							5R	0.5840	0.3206	-4.221	-3.903

comparison will become meaningful. Application of $a_{Al_2O_3}$ in pressure calculations is discussed briefly below.

Pressure Calculations

The activities of components in a magma are useful for determining equilibrium temperatures and pressures between a magma and phenocrysts and xenocrysts and assumed mantle compositions (Nicholls *et al.*, 1971; Nicholls and Carmichael, 1972; Bacon and Carmichael, 1973; Carmichael, Spera and Wood, in preparation).

If a basaltic magma is considered to be derived directly from the mantle without fractionation or modification and if the activity of a component can be defined at known (quench) temperature and pressure then an equilibrium reaction can be set up with an assumed mantle composition. As an example, in DVDP basanite 1-121.88 the reaction

$$
\begin{array}{cc}
Fe_2SiO_4 = & Fe_2SiO_4 \\
\text{liquid} & \text{solid}
\end{array}
$$

gives

$$
\ln a^{lava}_{Fe_2SiO_4} = \frac{\Delta G^{\circ}}{RT} + \ln a^{olivine}_{Fe_2SiO_4}
$$
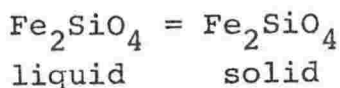
where

$$
\frac{\Delta G^{\circ}}{RT} = -\frac{10468}{T} + 7.008
$$

Using rim compositions of olivine at a quench temperature (determined from groundmass magnetite-ilmenite) $a_{Fe_2SiO_4}$ can be calculated. If the mantle is assumed to contain olivine ($Fo_{90}Fa_{10}$) then the variation of $a^{mantle}_{Fe_2SiO_4}$ with temperature can be calculated. The $a_{Fe_2SiO_4}$ defined by the lava can be extrapolated to higher temperatures and pressures assuming it is in equilibrium with $a^{mantle}_{Fe_2SiO_4}$. A range of P,T values have been calculated (Fig. 6.3) using the procedures of Carmichael *et al.*, (in prep).
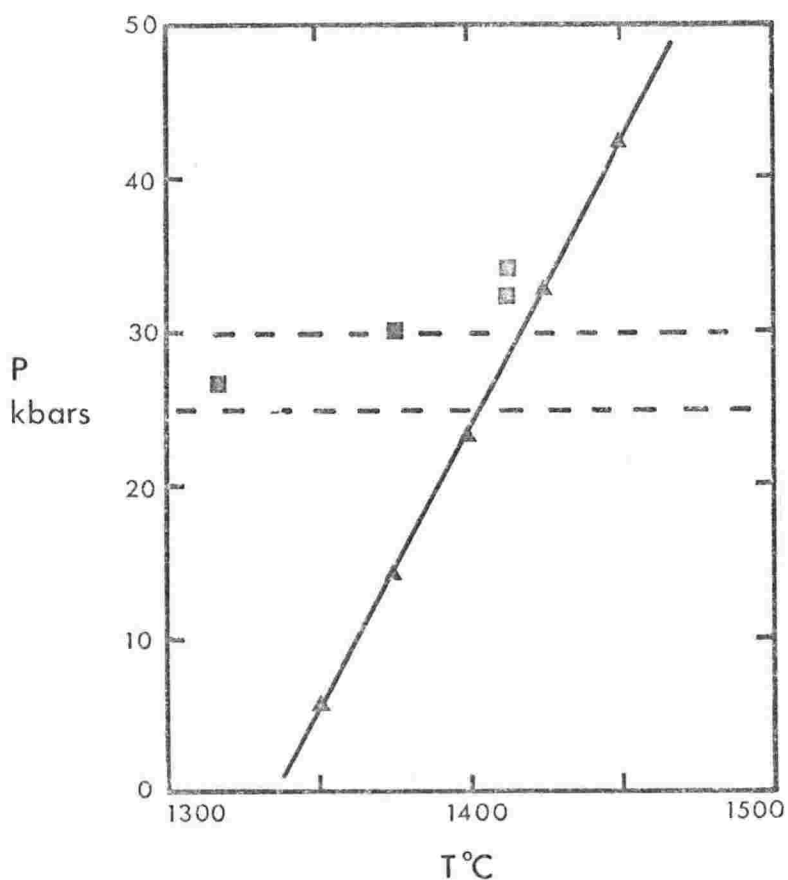
FIGURE 6.3   Equilibrium P,T conditions for Fe_2SiO_4 in DVDP basanite
1-121.88 with assumed olivine ($X_{Fe_2SiO_4}$ = 0.10) in the
mantle.   Dashed lines indicate possible pressure limits
for DVDP basanites.   Squares are calculated equilibrium
conditions, with an assumed mantle, for basanites from
San Quintin, California (Carmichael et al., in prep).

Calculations for several such equilibrium reactions must
be made so that their P,T curves will intersect and define a
unique temperature and pressure. Further calculations using
a_{SiO_2}, $a_{Al_2O_3}$, $a_{CaMgSi_2O_6}$ and the activity of other components
will therefore allow an estimate of equilibrium temperature and
pressure of DVDP basanite with an assumed mantle.

In the DVDP basanites pressures of 25-30 kbars have been
estimated from the mineralogy (see Chapter 5) and by comparison
with experimental melting studies (see Chapter 9). This implies
a temperature of 1400-1425°C using Fig. 6.3; a value that is
high but not unreasonable. Similar equilibrium conditions
were calculated by Carmichael *et al.*, (in prep.) for basanites
from San Quintin, California (Fig. 6.3). The temperature
range of 1400-1425°C at 25-30 kbars is just below the solidus
for estimated mantle peridotite (Wyllie, 1970).

Sulphur Fugacity

Sulphur fugacity (f_{S_2}) can be determined using pyrrhotite
composition if the equilibrium temperature is known (Toulmin
and Barton, 1964; Heming and Carmichael, 1973). Pyrrhotite
is often found as an accessory in lavas from the McMurdo
Volcanic Group, but the only complete analyses are those on
a recent bomb from Mt Erebus (see Chapter 8). At 1000°C
(olivine-clinopyroxene geothermometry gives 990°C) the
pyrrhotite (mole fraction FeS = 0.977) suggests a f_{S_2} of
$10^{-2.7}$ atmospheres (Fig. 6.4).

As $f_{S_2} = 10^{-2.7}$ and $f_{O_2} = 10^{-12.2}$ then f_{SO_2} and f_{SO_3}
can be calculated (assuming P = 1 atm.) using the following
reactions (Heming and Carmichael, 1973)

$$\tfrac{1}{2}S_2 + O_2 = SO_2 \text{ and } \tfrac{1}{2}S_2 + \tfrac{3}{2}O_2 = SO_3.$$
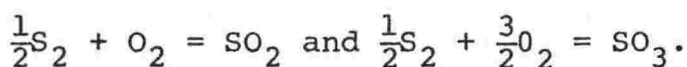
For Mt Erebus lavas $f_{SO_2} = 10^{-2.05}$ and $f_{SO_3} = 10^{-8.88}$ (Fig.
6.4). The values are lower than those reported by Heming
and Carmichael (1973) in pumice from Rabaul, New Guinea and
magmatic gases from Kilauea, Hawaii. Results from Mt Erebus
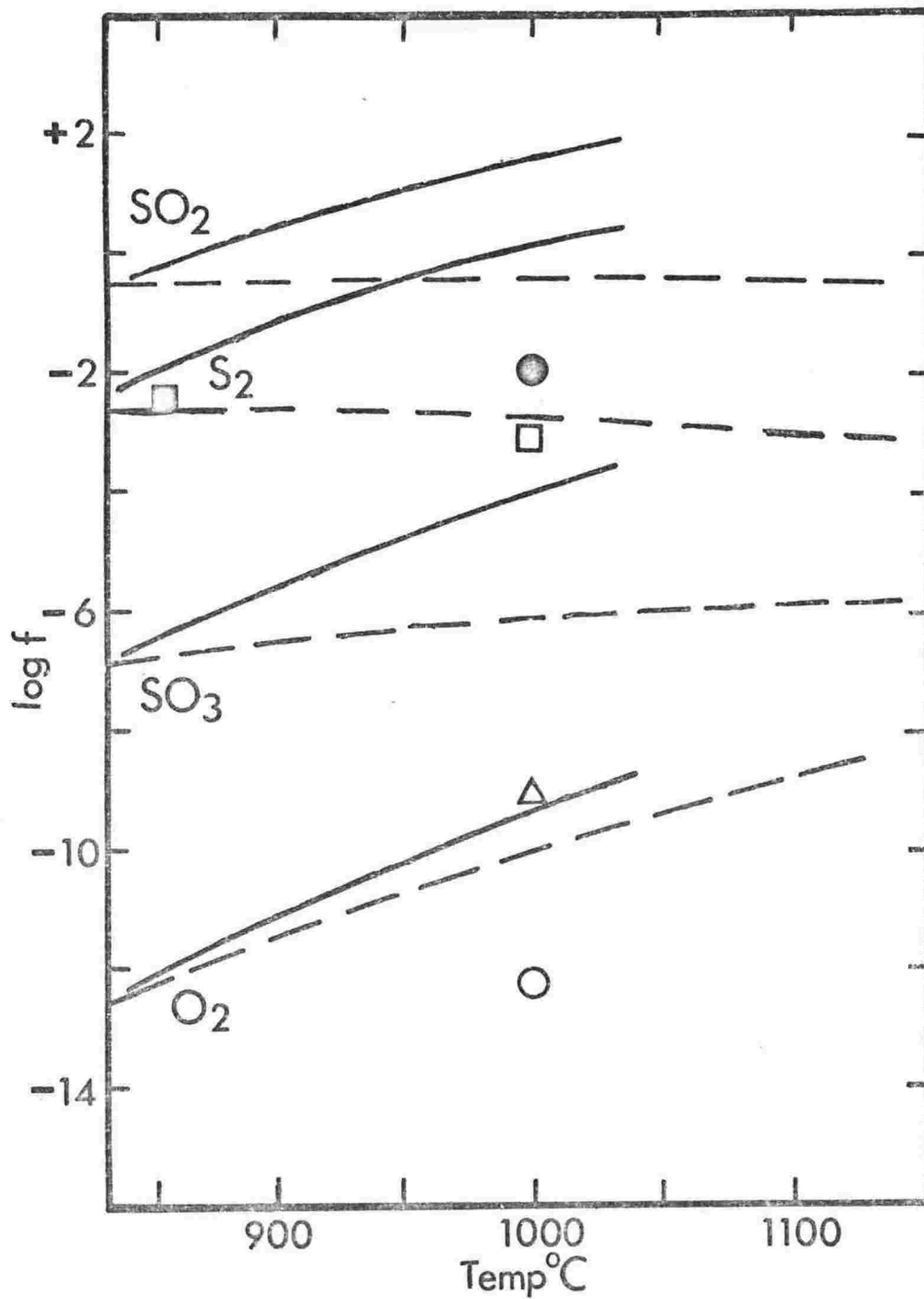
FIGURE 6.4 Calculated fugacity of various sulphur gases and oxygen for anorthoclase phonolite from Mt Erebus. Solid and dashed lines are trends for Rabaul lava samples and Kilauea magmatic gas respectively (from Heming and Carmichael, 1973). SO_2 (dot), S_2 (open square), SO_3 (triangle), O_2 (circle). f_{S_2} measured in magmatic gases from Mt Etna (filled square) (Sato and Moore, 1973).

will have greater significance once f_{S_2}, f_{SO_2} and f_{SO_3} are estimated directly from the magmatic gases, which have not been collected to date.

Sulphur fugacity is probably buffered by the reaction (Carmichael *et al.*, 1974),

$$4Fe_2SiO_4 + S_2 = 2FeS + 2Fe_3O_4 + 4SiO_2$$

fayalite   gas   pyrrhotite magnetite   glass
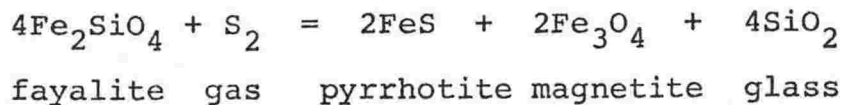
therefore given the appropriate thermodynamic data another reaction is available for calculating a_{SiO_2}.

CHAPTER SEVEN

GEOCHEMISTRY

Introduction

94 major element, 115 trace element and 16 rare-earth element (REE) analyses were made on representative samples from the Balleny, Melbourne and Erebus volcanic provinces. Major and trace element analyses and CIPW norms are listed, by location, in Tables 7.1 to 7.14 and are given in Appendix D. The tables include a compilation of all published analyses from the Balleny, Melbourne and Erebus volcanic provinces. Chemistry of Hallett volcanic province rocks is discussed by Hamilton (1972) and Harrington et al., (1967), and a brief summary is given below. Selected analyses of Hallett province rocks are given in Table 7.15 (Appendix D). A few analyses made in the early 1900's are of doubtful quality, therefore conclusions drawn from inter-pretations of the chemistry are based mainly on modern analyses.

Analytical Techniques

Rock samples were split into 10 to 20 mm cubes using a hardened steel rock splitter, after all weathered and altered surfaces were removed. The cubes were crushed for one minute in a tungsten-carbide 'TEMA' mill, which resulted in a mean grain size of 10 μm (Appendix C). Contamination was limited to tungsten and cobalt. Oxidation resulting from a grinding time of one minute was minimal (Fitton and Gill, 1970).

Major and trace element analyses except FeO, Na_2O, H_2O, and CO_2 were determined by x-ray fluorescence analysis (XRF), using the methods of Norrish and Hutton (1969) and Norrish and Chappell (1967) respectively. A description of the XRF techniques and instrumental settings are given in Appendix C.

Ferrous iron (FeO) was determined by titration with a standard dichromate solution and diphenylamine sulfonic acid indicator after 0.5 gram of sample was decomposed by boiling with $HF-H_2SO_4$ (Shapiro and Brannock, 1962).

Oxidation was overcome by flushing the crucible during boiling with a constant stream of CO_2.

Sodium (Na_2O) was determined using a Techtron AA4 atomic absorption spectrometer (AAS). 100 mg of sample was fused in a flux consisting 1 part $LiCO_3$, 5.52 parts K_2CO_3 and 5.97 parts $Li_2B_4O_7$ at $950^{O}C$ and dissolved in 250 ml of 4% HCl. International rock standards were used for calibration.

When magnesium (MgO) occurred in low concentrations it was determined by AAS using the same solution and method for calibration as Na_2O. Agreement with XRF determinations were excellent (see Appendix C).

Combined water (H_2O+) was in most cases determined in Penfold tubes following the procedure of Shapiro and Brannock (1962). For a few samples, H_2O+ and carbon dioxide (CO_2) were determined by heating one gram of sample, which had been dried at $110^{O}C$ overnight, in a furnace for ½ an hour at $1100^{O}C$. Evolved CO_2 and H_2O were carried by nitrogen gas and collected in absorption tubes containing 'carbosorb' and magnesium perchlorate (Riley, 1958).

H_2O- was determined by heating a sample for 2 hours at $110^{O}C$.

Loss on ignition (LOI) was determined as the weight loss of a sample heated for 1 to 4 hours at $1000^{O}C$.

Geochemical Variations

Introduction

Major element chemistry in combination with CIPW norms have been used to subdivide the lavas into either sodic or potassic series (see Chapter 4). Within these series, a number of lineages can be recognised. Such lineages are more correctly delineated by examining the chemistry of residual glasses, aphyric samples (cf. Thompson *et al.*, 1972), the fine-grained groundmass in porphyritic samples or segregation veins (Coombs and Wilkinson, 1969). Porphyritic samples may contain phenocrysts of cumulus origin and so whole rock chemistry will not represent a liquid in a liquid line of descent. When the present data is plotted it shows a scatter, due in part to porphyritic and altered samples, however generalised trends are obvious. Many of the

samples analysed (except those from the Erebus Centre) contain <5% phenocrysts and are considered to represent liquids, and therefore define fractionation trends.

In the following discussion data has been presented by using Harker variation diagrams. With increased differentiation the lavas generally show a progressive increase in SiO_2. Price (1973) has shown in alkali volcanics from Dunedin Volcano, which are similar to the McMurdo Volcanic Group, that silica is responsible for over 50% of the total variance (Chayes, 1960, 1962). Therefore, Harker-type variation diagrams plotting major element oxide and trace element abundances against SiO_2 are used to visually present the data (Wright, 1974). Other plots are also used to show special relationships or correlations between selected elements. Conclusions on petrogenesis (Chapter 9) and the delineation of fractionation trends are based on all major element and trace element data, any one plot does not uniquely define the position of a lava in a lineage.

Plots of total alkalis ($Na_2O + K_2O$) versus (vs) silica (SiO_2) and K_2O vs Na_2O are used to show the varying chemistry of the provinces.

Balleny volcanic province

Two basanite samples were analysed, making a total of 5 available analyses (Table 7.1). Samples collected from Sabrina Island and vicinity by B. C. Waterhouse are mainly olivine-augite basanites, while one sample described by Mawson (1950) (Table 7.1 analysis 5) from Buckle Island is a hawaiite.

In general the Balleny lavas are similar in chemistry to basaltic lavas from the Hallett volcanic province, but have lower TiO_2 than most basaltic lavas from the Melbourne and Erebus volcanic provinces.

Hallett volcanic province

The Hallett volcanic province is a basanite-trachyte association with rare phonolite. Although 48 analyses (David *et al.*, 1896; Prior, 1902; Harrington *et al.*, 1967; Hamilton, 1972) are available (Fig. 7.1) many of these are of hydrated and/or oxidised samples. If samples showing oxidation (normative hematite - Hm) or hydration and/or large amounts of carbonate (total $H_2O+CO_2 > 1.5\%$ or $CO_2 > 0.5\%$) are ignored only 14 analyses remain (Table 7.15).

The analysed samples have been reclassified using the nomenclature of this thesis and the frequency of rock types is given in Table 7.16. Hawaiites, the largest single lava type analysed, mainly contain <10% normative nepheline (Ne).

TABLE 7.16. Frequency of analyses of volcanic rocks from the Hallett volcanic province

Rock Types	Number of analyses	Number of unaltered samples*	% of all analyses
Alkali basalt	5	1	10
Basanite	6	4	12
Hawaiite	19	4	40
Nepheline hawaiite	3	1	6
Mugearite	1	0	2
Benmoreite	2	0	4
Trachyte	3	1	6
Quartz trachyte	7	3	14
Phonolite	2	0	4

*See text for criteria; analyses given in Table 7.15.
Analyses from David *et al.*, 1896; Prior, 1902; Harrington *et al.*, 1967; Hamilton, 1972.

As many of the lavas are oxidised this causes a decrease in Ne, however with a correction for oxidation some hawaiites become nepheline hawaiites. Basanite dominates over alkali basalt and

several basalts would be classified as basanite if the degree
of oxidation decreased. Even allowing for oxidation, there is
a scatter in the composition of the basaltic and hawaiitic lavas.

Lavas intermediate between hawaiite and trachyte are rare
(Table 7.16), which makes the recognition of possible fractionation
trends difficult (Figs. 7.1, 7.2). The most salic lavas are
trachyte and quartz trachyte (some have >15% normative quartz).
There appears to be a trend toward saturation with increased
silica content, the only exceptions being two analyses (from a
single megapillow) of hydrated phonolite which is extremely
undersaturated (Ne = 30%).

Analyses are plotted in total alkalis vs SiO_2 and K_2O
vs Na_2O diagrams (Figs. 7.1, 7.2). Total alkalis increase
linearly with increasing SiO_2, until 62% SiO_2, but then decrease
slightly (Fig. 7.1). Two samples with 13-14% total alkalis
are from the phonolitic pillow lava discussed above. In Fig. 7.2
the K_2O increases with increasing Na_2O and shows a good trend
to 2% K_2O, however from 2 to 4% K_2O no trend is apparent due
to the lack of analyses of intermediate lavas. The trachytes
show 1% variation in K_2O while Na_2O varies by 2.4%.

In summary the chemistry of the Hallett volcanic province
indicates the lavas form an alkali basalt/basanite-hawaiite-
trachyte-quartz trachyte association.

Melbourne volcanic province

INTRODUCTION

40 new analyses of samples from the Pleiades (32) (Table
7.2), Mt Overlord (3), Webb Névé (1), and Malta Plateau (1)
(Table 7.3) and Mt Melbourne (4) (Table 7.4) are given in this
thesis. Four analyses of lavas from Mt Melbourne have been
published by Nathan and Schulte (1968).

THE PLEIADES

Lavas from The Pleiades are undersaturated and range from
basanite through to nepheline benmoreite and peralkaline K-trachyte.
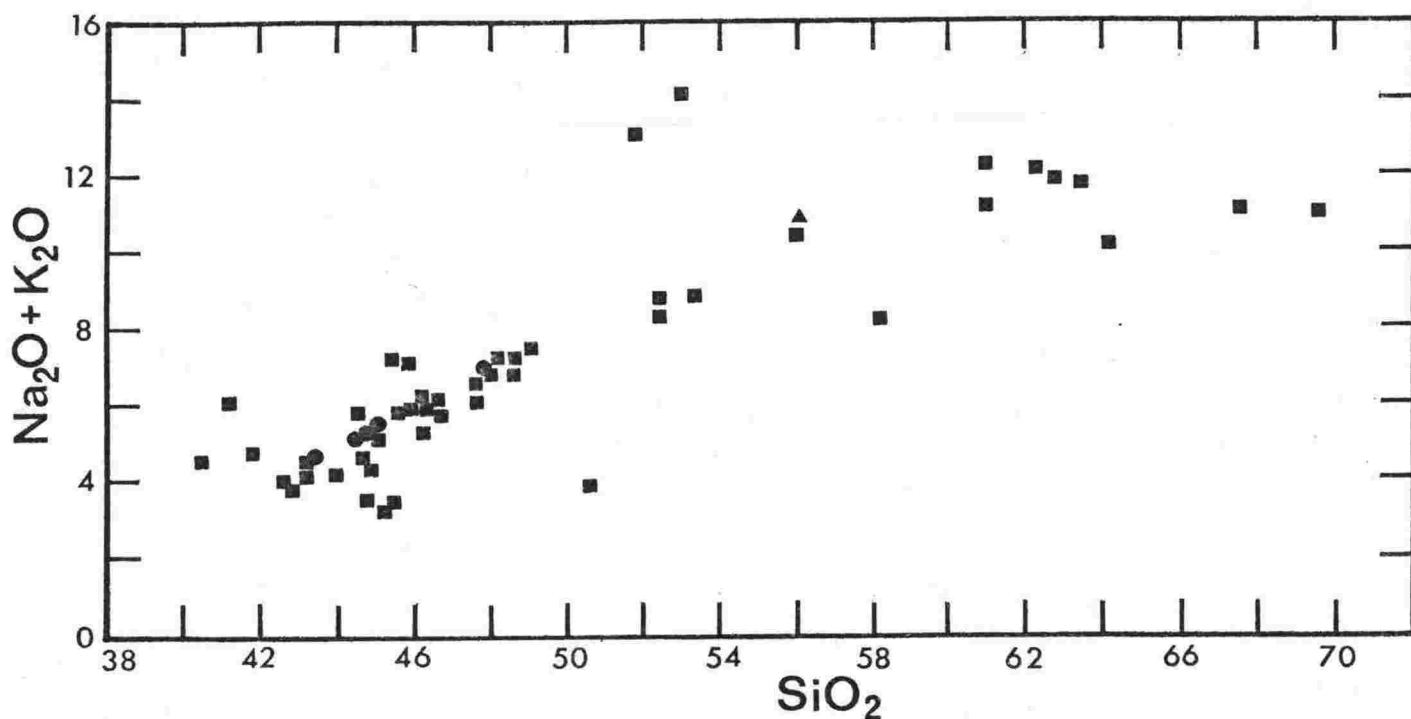
FIGURE 7.1 Plot of Na_2O+K_2O against SiO_2 for Balleny volcanic province ($\bullet$), Hallett volcanic province ($\blacksquare$) and Scott Island ($\blacktriangle$) rocks. See text for source of analyses.
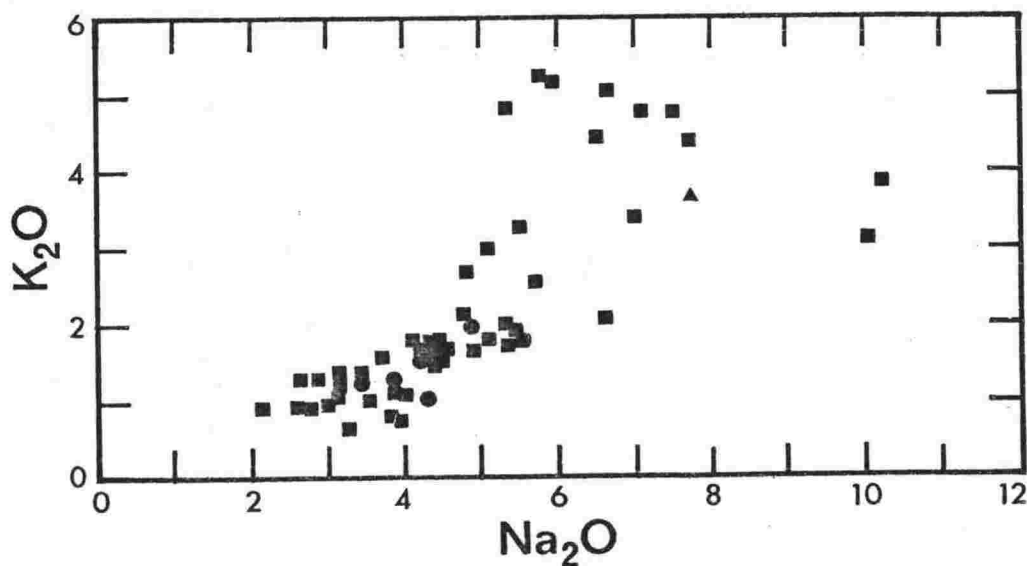
FIGURE 7.2 Plot of K_2O against Na_2O for Balleny volcanic province, Hallett volcanic province and Scott Island rocks. Symbols are the same as Figure 7.1. See text for source of analyses.

Two lava series or lineages can be recognised on the basis of Na_2O/K_2O ratios (Fig. 7.4) and in plots of differentiation index (D.I.) vs normative nepheline (Ne) (Fig. 7.3). The bulk of the lavas have an Na_2O/K_2O ratio <2 (Fig. 7.4) and consist of a mildly potassic trachyandesite-tristanite-K-trachyte-peralkaline K-trachyte lineage. Lavas with Na_2O/K_2O >2 (Fig. 7.4) and a trend of increasing Ne with increasing D.I. (Fig. 7.3) belong to a sodic basanite-nepheline hawaiite-nepheline benmoreite lineage.

On a total alkalis vs SiO_2 plot (Fig. 7.5) the sodic lavas have greater alkali content than the potassic lavas at an equivalent SiO_2 content. Three samples are intermediate between the sodic and potassic lineages (Figs. 7.3, 7.4, 7.5) and may be more sodic variants of the potassic lineage.

Potassic Lineage

SiO_2 variation diagrams of major elements (Figs. 7.5, 7.6) show a reasonably well-defined trend. TiO_2, total iron, MgO, CaO and P_2O_5 all decrease with increasing SiO_2 (Fig. 7.6). Al_2O_3 increases to the K-trachytes and then decreases in the peralkaline K-trachyte. Na_2O increases steadily throughout the lineage, while K_2O is similar but tends to flatten out from K-trachyte to peralkaline K-trachyte. The ratio of K_2O to Na_2O is variable; between 6.5 and 7.0% Na_2O, K_2O increases from 3.5 to 5.0% giving an irregular trend line (Fig. 7.4). Trends for a whole rock-groundmass pair (Fig. 7.6) parallel the whole rock major element analyses, except for TiO_2 which increases with increasing SiO_2. The groundmass was analysed by broad beam (30 μm) electron microprobe analysis. Small microphenocrysts of magnetite were unavoidable during analysis and these probably account for the unusual TiO_2 trend.

Trace element geochemistry is shown on Figures 7.7 and 7.8. Rb, Th, U, Sn, Zr, Hf and Y are enriched throughout the lineage, while Sr steadily decreases. Pb and Ba increase to the K-trachyte but are strongly depleted in the peralkaline K-trachyte. Ni, Cr, V and Cu decrease with increasing SiO_2. Rare earth element geochemistry is discussed below.
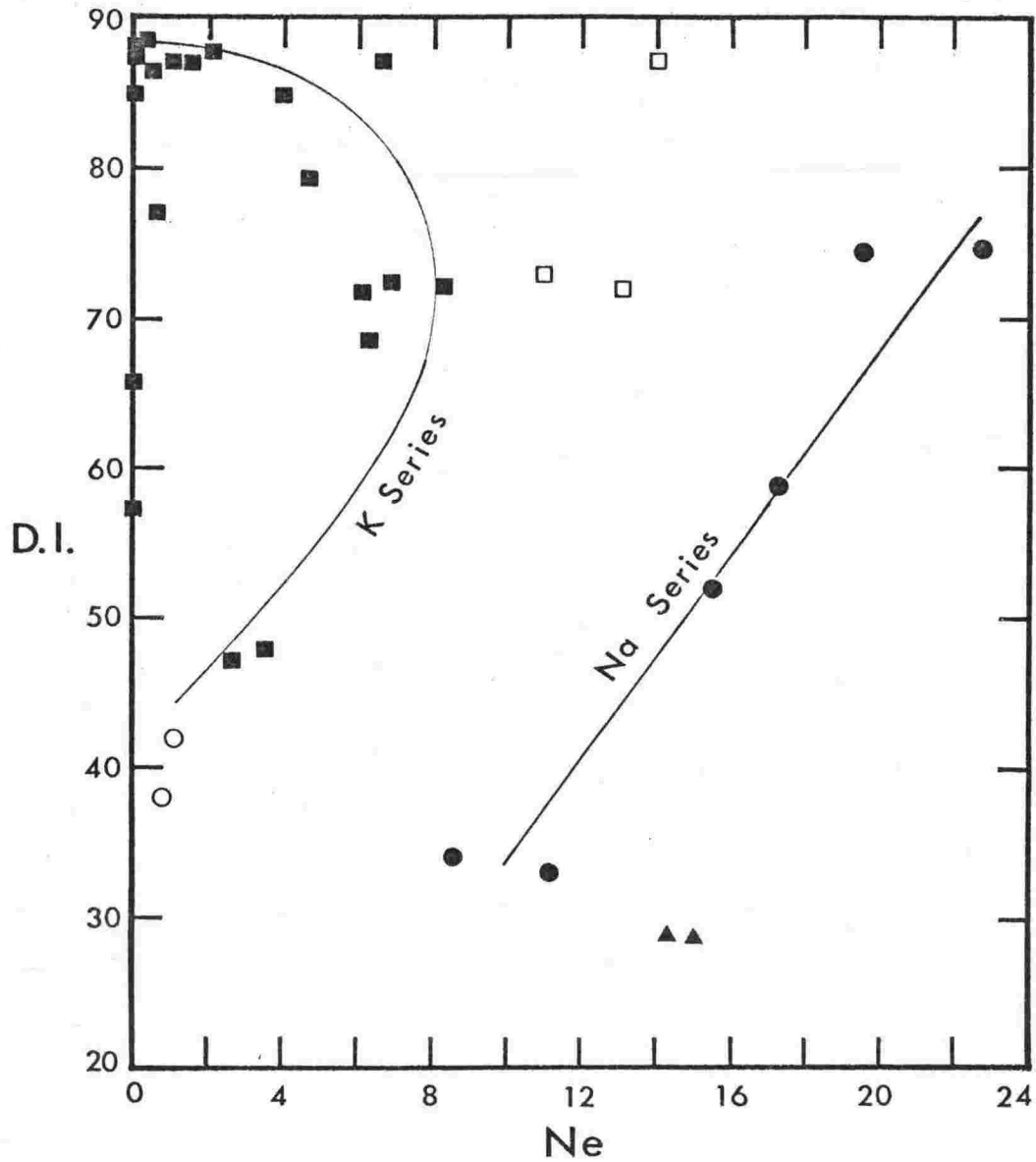
FIGURE 7.3 Plot of differentiation index (D.I.) against normative nepheline (Ne) for rocks from the Melbourne volcanic province, excluding Mt Melbourne. Note the three potassic lineage lavas with D.I. <80 and Ne <1 are oxidised and would contain higher Ne if a correction was made for the oxidation.

SYMBOLS

The Pleiades

■ Potassic lineage

● Sodic lineage

○ Essexite inclusions

□ Transitional

▼ Mt Overlord

▲ Local Suite
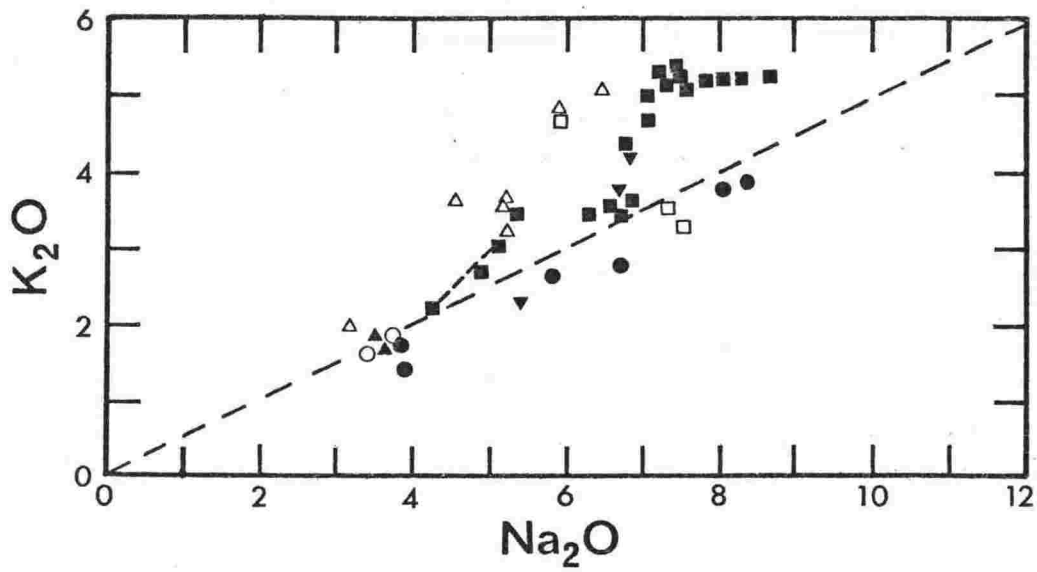
FIGURE 7.4 Plot of K_2O against Na_2O for Melbourne volcanic province
rocks. Symbols are the same as Figure 7.3 with the addition
of Mt Melbourne ($\triangle$). Dashed line indicates Na_2O/K_2O ratio of
2.
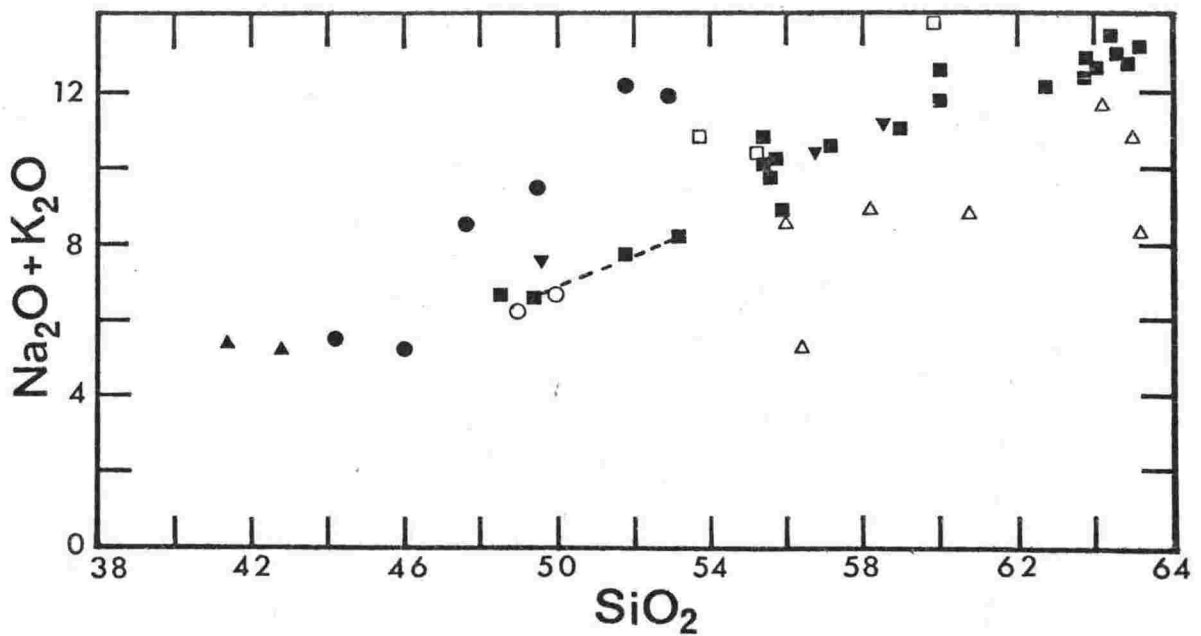
FIGURE 7.5 Plot of Na_2O+K_2O against SiO_2 for Melbourne volcanic
province rocks. Symbols are the same as Figure 7.3
with the addition of Mt Melbourne ($\triangle$).
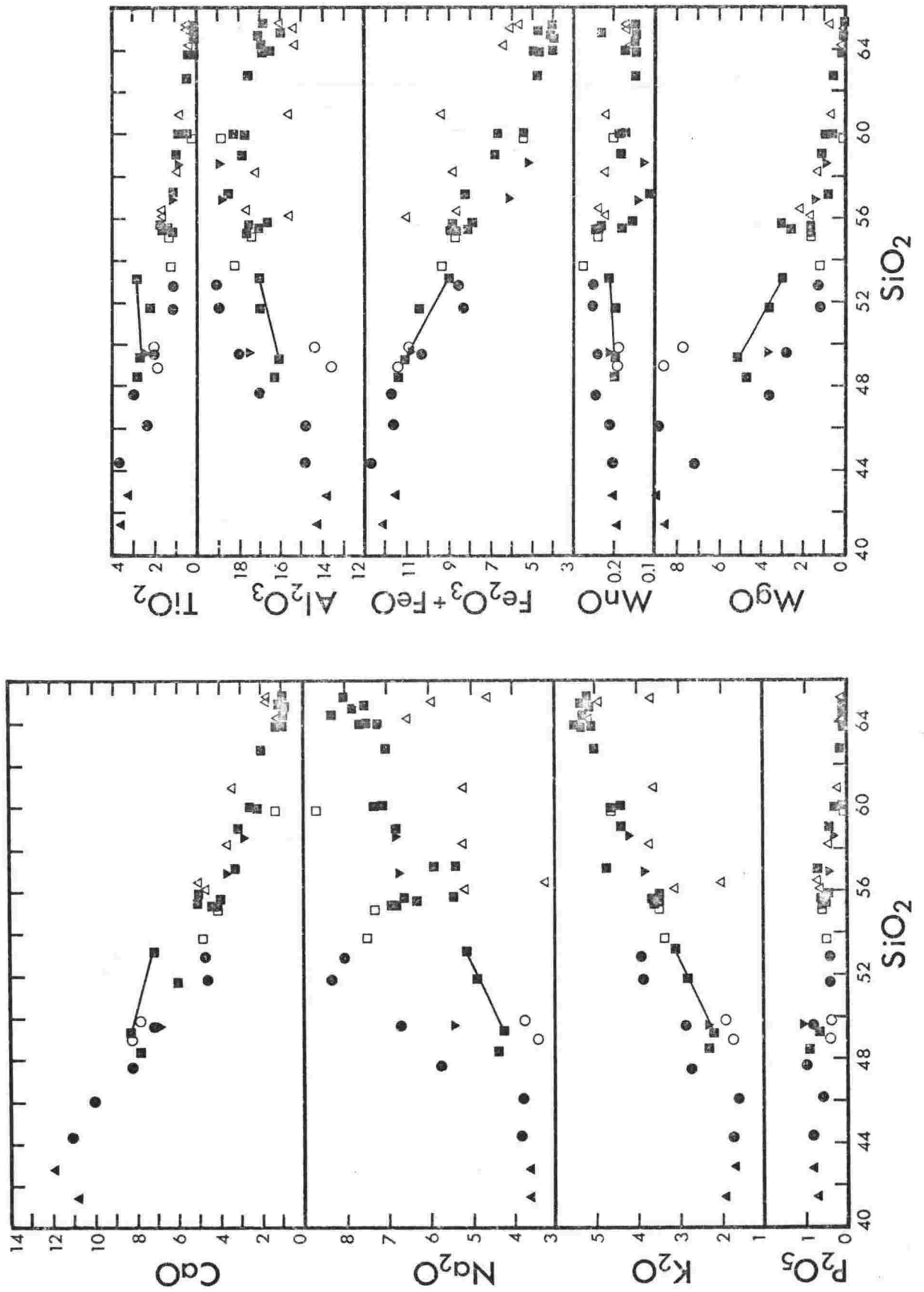
FIGURE 7.6 Major element oxide variations plotted against SiO_2 for lavas and plutonic inclusions from the Melbourne volcanic province. Symbols are the same as Figures 7.3 and 7.4.
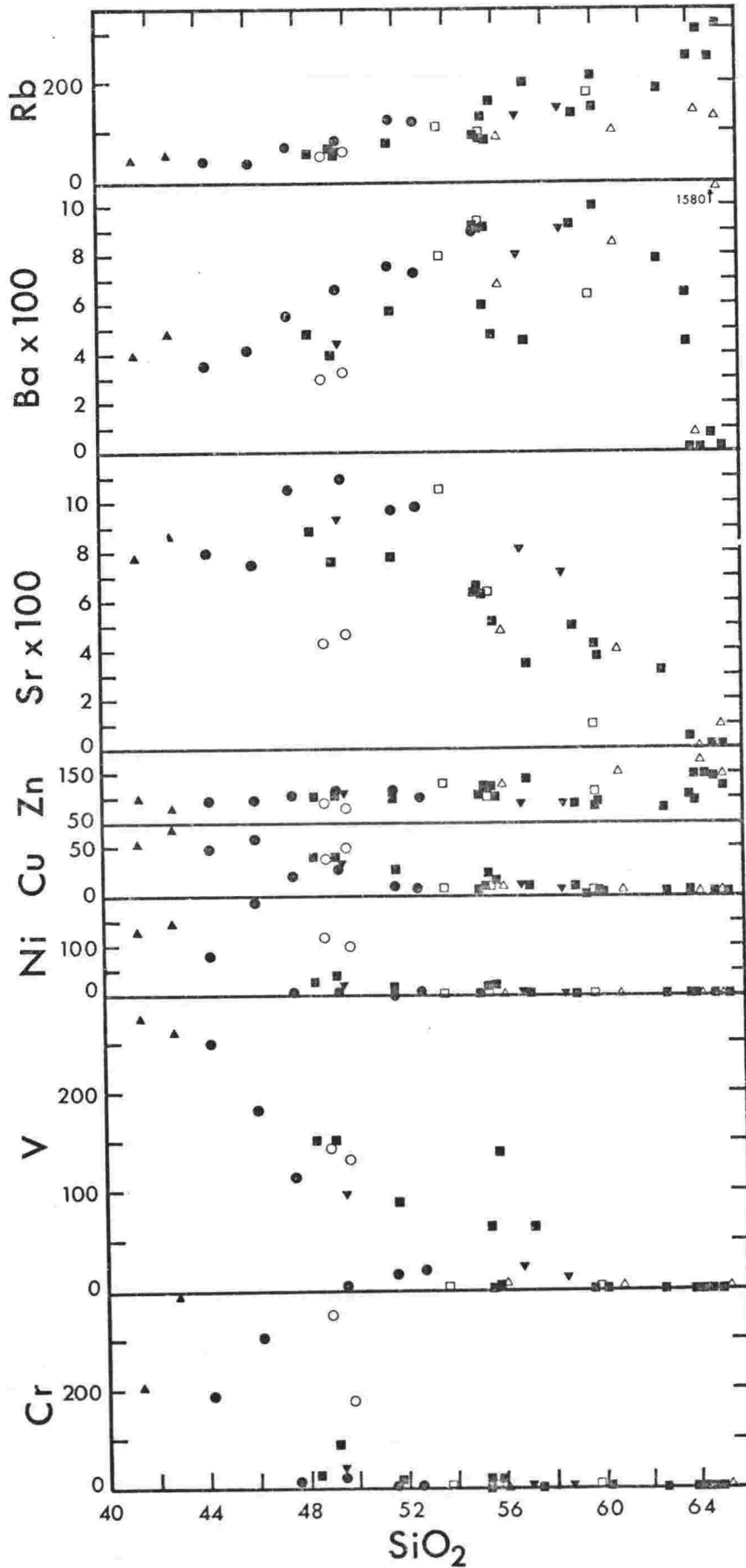
FIGURE 7.7 Trace element variations plotted against SiO_2 for lavas and plutonic inclusions from the Melbourne volcanic province. Trace element concentrations in ppm. Symbols are the same as Figures 7.3 and 7.4.
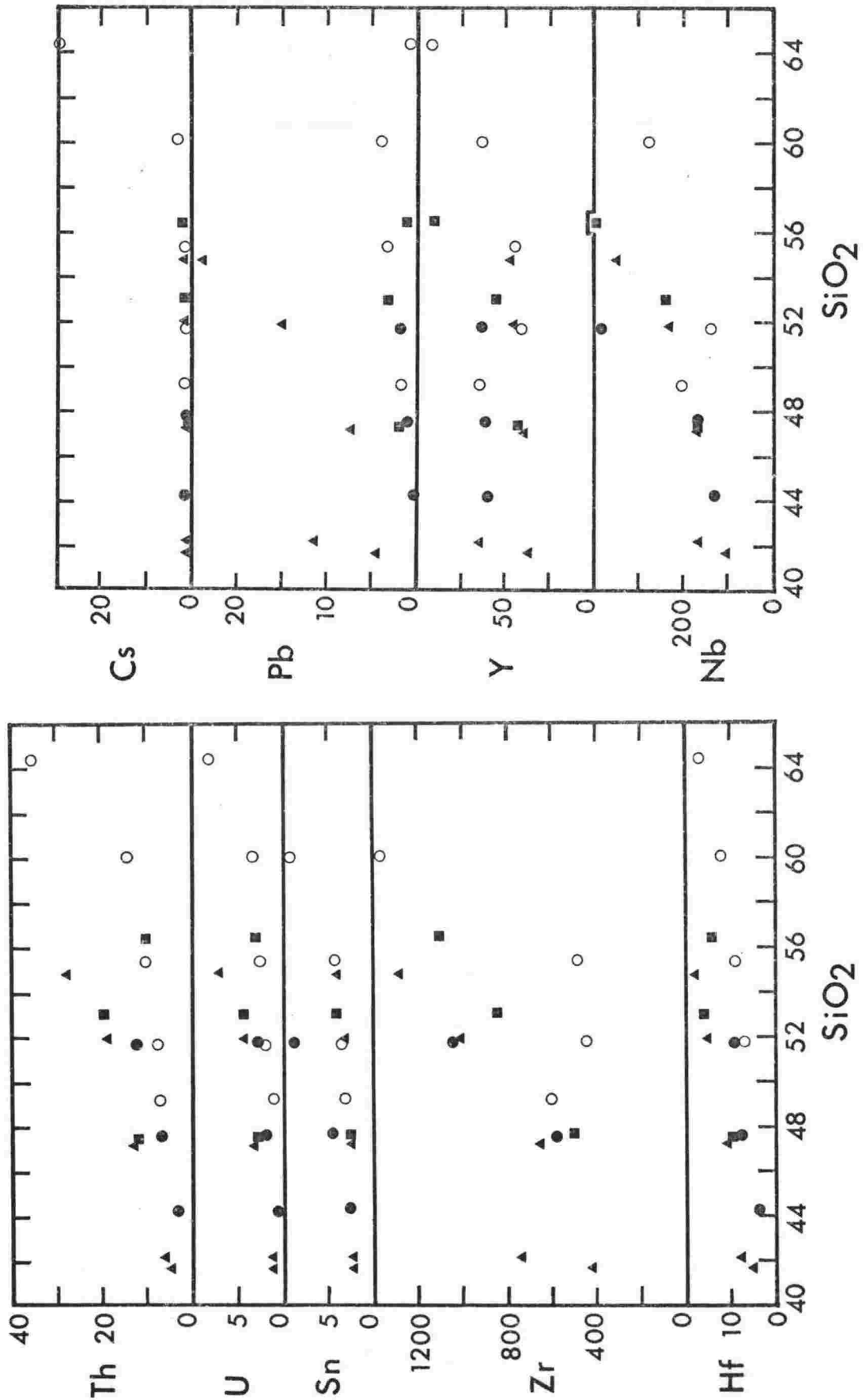
FIGURE 7.8 Variation of trace elements plotted against SiO_2 for selected lava samples from the Melbourne and Erebus volcanic provinces. Trace element concentrations in ppm. Samples from The Pleiades mildly potassic trachyandesite to peralkaline K-trachyte lineage (O) and sodic basanite to nepheline benmoreite lineage (●), also the Erebus centre nepheline hawaiite to anorthoclase phonolite lineage (■) and kaersutite lineage basanite to kaersutite phonolite lavas (▲) from Hut Point Peninsula.

There is some scatter in the major and trace element trends, part of this is due to porphyritic samples, part may be due to contamination. Strongly resorbed xenocrysts are occasionally observed in the intermediate lavas and although every effort was made to remove these prior to analysis, it is likely that some remained.

Commonly associated with the potassic lavas are essexite plutonic inclusions (Table 7.2 anal. 5 and 9). Their chemistry differs from the lavas by having lower Al_2O_3, P_2O_5, Na_2O and Sr while being enriched, relative to the lavas, in MgO, NiO and Cr. The chemistry of the inclusions suggests they are cumulates, formed by accumulation of augite and olivine. This is also reflected in the fractionated chemistry of the mafic minerals (see Chapter 5).

Sodic Lineage

Lavas of the sodic lineage are the final eruptive products at The Pleiades, and constitute about 1% by volume of the lavas. At all outcrops they intrude older potassic lineage lavas. As all the sodic lineage lavas appear to be closely related in time it is suggested their eruption represents outpourings from the same magma chamber. The degree of alkalinity (or degree of fractionation) decreases west and southwestward (Fig. 7.9). Baker (1968) showed a similar systematic composition variation in parasitic bodies and dikes at Saint Helena, from phonolite in the central area, outwards through trachyte to trachybasalt. He suggested a magma chamber with a domed roof was tapped at varying depths and horizontal distances from its centre, and this accounted for the compositional variations. This situation may occur under the northern Pleiades, but with only 6 data points it is not possible to define the shape of any underlying magma chamber.

The major element chemistry of the lineage shows a systematic decrease in MgO, CaO, TiO_2 and total iron while SiO_2, Al_2O_3, Na_2O and K_2O increase regularly (Fig. 7.6). P_2O_5 increases from basanite to nepheline hawaiite and then decreases to the nepheline benmoreite. A K_2O vs Na_2O plot
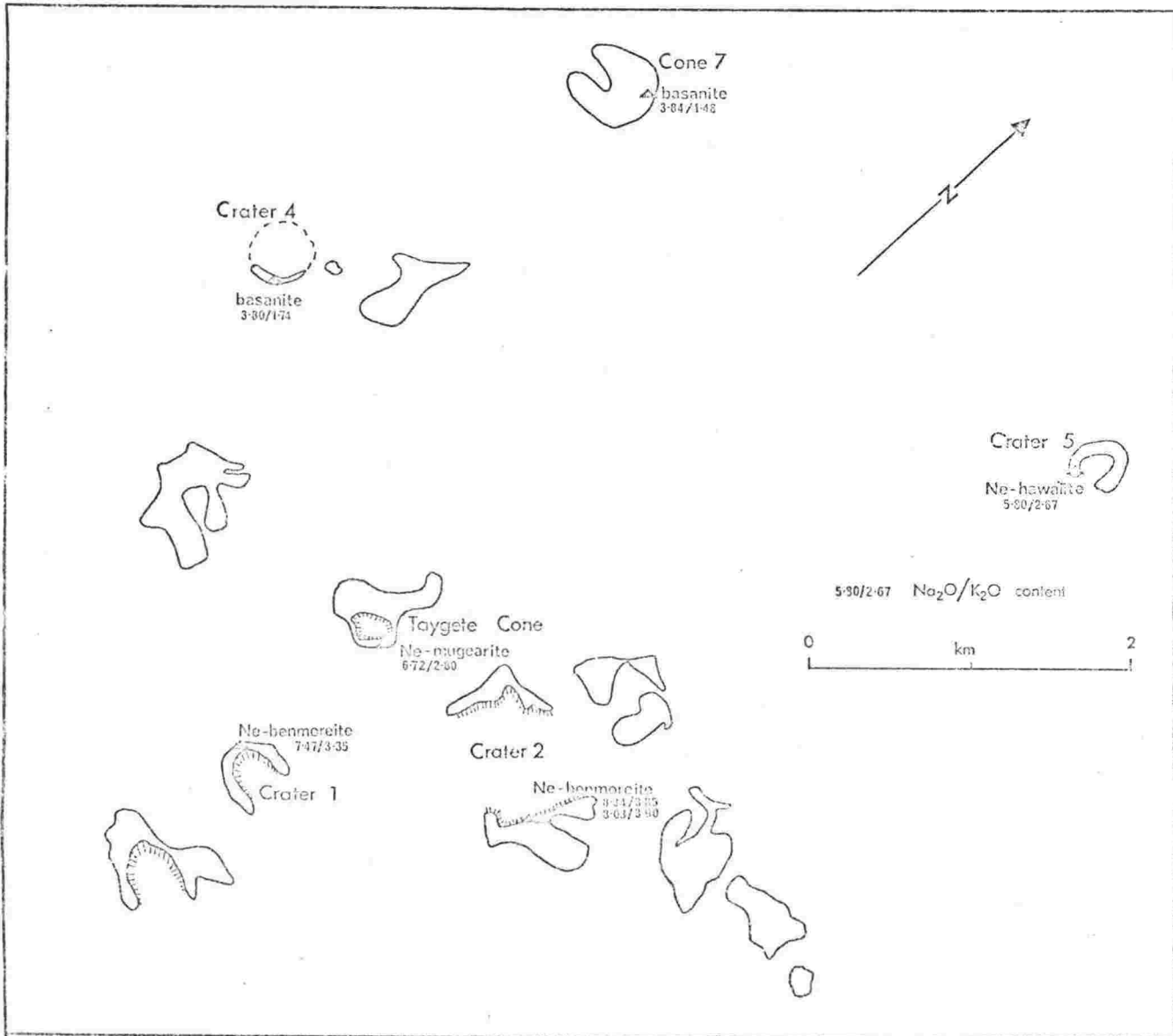
FIGURE 7.9 Distribution of the sodic basanite-nepheline hawaiite-nepheline mugearite-nepheline benmoreite lavas at The Pleiades.

shows a linear trend that differs considerably from the irregular potassic lineage trend (Fig. 7.4).

Trace elements Cu, Ni, V, and Cr are variable with high concentrations in the basanites which decrease to the nepheline hawaiite. A slight increase in some of these elements from nepheline hawaiite to nepheline mugearite, prior to decreasing to nepheline benmoreite, is probably due to the weakly porphyritic nature of the mugearite. Zn and Y remain nearly constant throughout the lineage. The large cations Rb, Ba, Pb, Th, U, Sn, Nb, Zr, and Hf increase with fractionation, while Sr increases to mugearite and is then slightly depleted in the nepheline benmoreite. Rare earth element chemistry is discussed below.

MOUNT OVERLORD

Lavas from Mt Overlord are similar to those from The Pleiades and consist of undersaturated hawaiite, tristanite and K-trachyte (Table 7.3). Hawaiite is intermediate between The Pleiades sodic and potassic lineages; the other lavas are potassic. The only apparent difference between the tristanite and K-trachyte from The Pleiades and Mt Overlord, is that the latter has higher Al_2O_3 and Sr and lower total iron and MnO (Figs. 7.4 to 7.7). This difference could result from the earlier crystallization and fractionation of magnetite in the Mt Overlord magma.

MOUNT MELBOURNE

The Mt Melbourne lavas (Table 7.4) are oversaturated and consist of quartz trachyandesite, quartz tristanite and quartz trachyte. Analyses (Table 7.4) show the lavas have a distinctly lower total alkalis content than any other group of lavas in the McMurdo Volcanic Group (Figs. 7.5, 7.24). The Na_2O/K_2O ratio is also the lowest observed in any group of lavas with the exception of Mt Cis, a small trachyte plug on Mt Erebus (Figs. 7.4, 7.25). No basaltic lavas have been collected from Mt Melbourne, although they do crop out in surrounding areas (Nathan and Schulte, 1968).

Major element variation diagrams (Fig. 7.6) show that variations of TiO_2, MnO, MgO, CaO and P_2O_5 are similar to The Pleiades; Al_2O_3, Na_2O and K_2O being lower while total iron is strongly enriched. The trace elements (Fig. 7.7) are in general similar except for Rb which is lower and Zn which tends to be slightly higher.

LOCAL SUITE

Basaltic lavas are scarce in the Melbourne volcanic province. Small basanite scoria cones and lava mounds, scattered throughout the area, were grouped into the Local Suite by Nathan and Schulte (1968) (see Chapter 3). These Local Suite basanites, along with the two analysed basanites from The Pleiades are the only indication of the parent magma from which the lava lineages were derived. Two basanites were analysed from the Webb Névé and the Malta Plateau (Table 7.3). Their chemistry is similar to that of the basanites from The Pleiades.

DISCUSSION

From the whole rock chemistry it is suggested the Melbourne volcanic province consists of at least three lava lineages:

1) The majority of the lavas from The Pleiades and probably Mt Overlord are a mildly potassic lineage, of trachyandesite-tristanite-K-trachyte-peralkaline K-trachyte.

2) At The Pleiades a late stage sodic lineage of basanite-nepheline hawaiite-nepheline mugearite-nepheline benmoreite has higher total alkalis and the highest Na_2O/K_2O ratio of any Melbourne volcanic province rocks. The volume of the lavas is very small.

3) A strongly potassic quartz trachyandesite-quartz tristanite-quartz trachyte lineage at Mt Melbourne can be distinguished from other Melbourne volcanic province and McMurdo Volcanic Group rocks by being oversaturated and having lower total alkalis and Na_2O/K_2O ratio.

As SiO_2 increases all lineages show a decrease in TiO_2, total iron, MgO, CaO, P_2O_5, Sr, Cr, Ni and Cu; Zn and MnO

remain constant. Rb and the alkalis K_2O and Na_2O are
concentrated in all lineages. In the sodic lineage, Al_2O_3
and Ba are enriched, while in the potassic lineages they are
enriched up to and including the trachytes but then show
depletion in the more salic lavas.

Within the mildly potassic lineage there is a scatter
in the chemistry of any one rock type (e.g. tristanites
25684 and 25670 have 2.66% and 1.60% MgO respectively). It is
likely therefore, that several processes were operating to give
rise to rocks which are broadly similar.

Erebus volcanic province

INTRODUCTION

Lavas from the Erebus volcanic province are the most
extensively analysed in the McMurdo Volcanic Group (Tables 7.5
to 7.14). With rare exceptions the lavas belong to a strongly
undersaturated basanite-phonolite association and are the most
alkali-rich lavas in the McMurdo Volcanic Group (Fig. 7.24).
Two chemically similar fractionation trends are recognised by
their distinctive mineralogy and localised field occurrences:

1) A basanite-nepheline hawaiite-nepheline mugearite-
nepheline benmoreite-kaersutite phonolite-pyroxene phonolite
lineage which is most complete in surface and subsurface
samples from Hut Point Peninsula. Similar lavas, though with
a smaller range in composition, occur at Cape Bird, Cape
Crozier and Brown Peninsula. The lavas are generally fine-
grained or weakly porphyritic and would represent a liquid
in any differentiation sequence. Augite and kaersutite are
the dominant mafic minerals. The lineage is termed the
kaersutite lineage.

2) At the Erebus Centre there is a nepheline hawaiite-
nepheline benmoreite-anorthoclase phonolite (kenyte) lineage
referred to as the Erebus lineage. Samples from Mt Discovery
may also be included in this lineage. Erebus lineage lavas
are mainly strongly porphyritic and contain abundant pheno-

crysts of plagioclase or anorthoclase, and lesser augite, olivine and magnetite. Because of their porphyritic nature, some of the lavas are possibly cumulates and therefore plots of their chemical variations may not represent a true fractionation trend.

A plot of differentiation index (D.I.) against normative nepheline (Ne) (Fig. 7.10) indicates the kaersutite lineage lavas are in general more undersaturated than Erebus lineage lavas (excluding the groundmass analyses). A division at Ne = 17% gives a good separation of the intermediate and phonolitic lavas of the two lineages. The Erebus lineage is essentially one of constant Ne, whereas the kaersutite lineage shows increasing Ne with differentiation (Fig. 7.10).

CAPE BIRD AND MT BIRD

Seven published analyses (Jensen, 1916; Cole and Ewart, 1968; Goldich *et al.*, 1975) of Cape Bird and Mt Bird lavas are given in Table 7.5. The lavas are basanites, nepheline benmoreites and kaersutite phonolites, the petrography of which are given by Cole and Ewart (1968). They belong to the kaersutite lineage. One sample (Table 7.5 analysis 4) has been classified as an alkali basalt, however the very low TiO_2 and high Al_2O_3 suggest a poor analysis. Major element variation diagrams (Figs. 7.11 to 7.13) show the Cape Bird lavas have the same trend as lavas from Cape Crozier and Hut Point Peninsula.

CAPE CROZIER

Twenty analyses of samples from Cape Crozier are given in Table 7.5; five analyses are from Prior (1902, 1907) and Goldich *et al.*, (1975), the remaining major element determinations are from Kyle (1971). The trace element determinations (excluding the three analyses of Goldich *et al.*, 1975) were made as part of this study.

Variation diagrams (Figs. 7.11 to 7.14) show a scatter of points, but generalised trends from basanite containing phenocrysts of olivine and augite through kaersutite-bearing hawaiite and phonolite can be recognised. A hawaiite with

SYMBOLS

KAERSUTITE LINEAGE

- ◆ Cape Bird
- ● Brown Peninsula
- ▲ Hut Point Peninsula and DVDP holes
- ■ Cape Crozier

EREBUS LINEAGE

- ○ Dellbridge Islands, Turks Head
- □ Cape Royds, Cape Evans, Cape Barne
- △ Mt Erebus
- ◇ Mt Cis
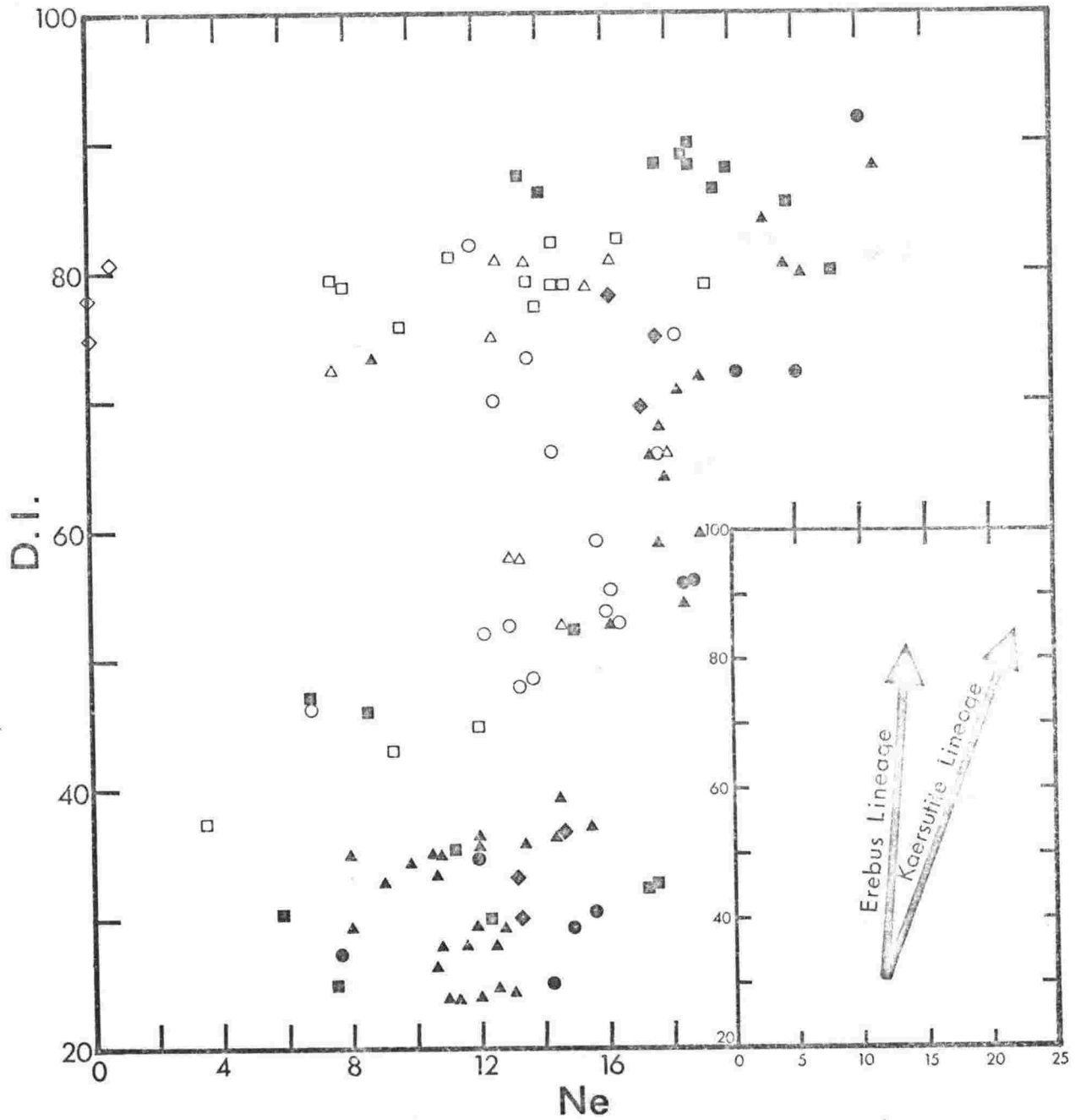
FIGURE 7.10 Plot of differentiation index (D.I.) against normative
            nepheline (Ne) for Erebus volcanic province rocks,
            excluding groundmass and glass analyses of Erebus
            centre lavas.
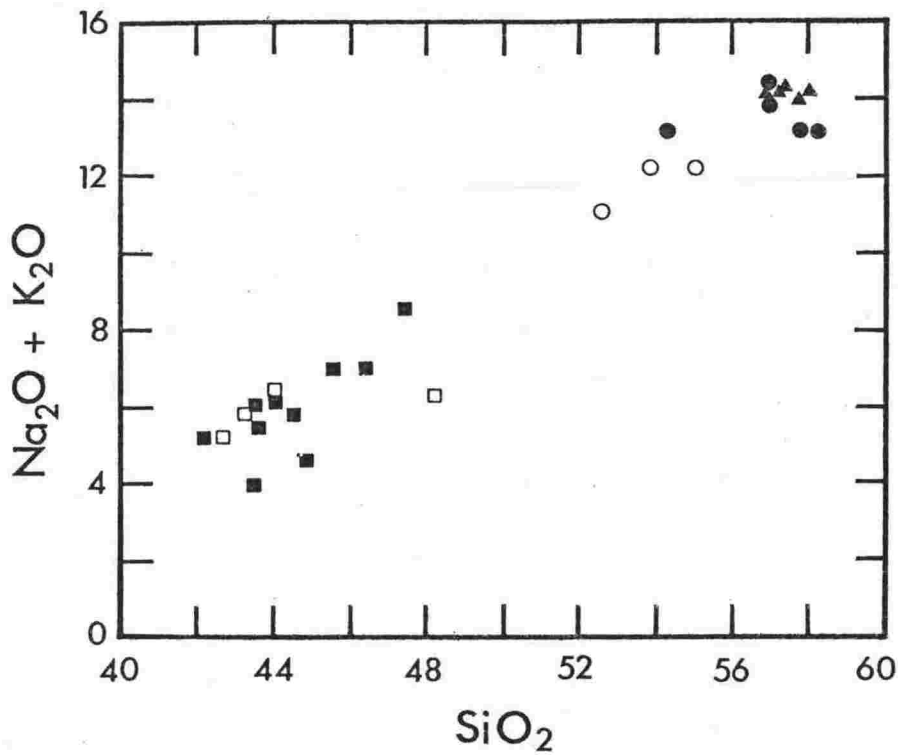
FIGURE 7.11   Plot of Na_2O+K_2O against SiO_2 for Erebus volcanic province lavas from Mount Bird, Cape Bird and Cape Crozier.
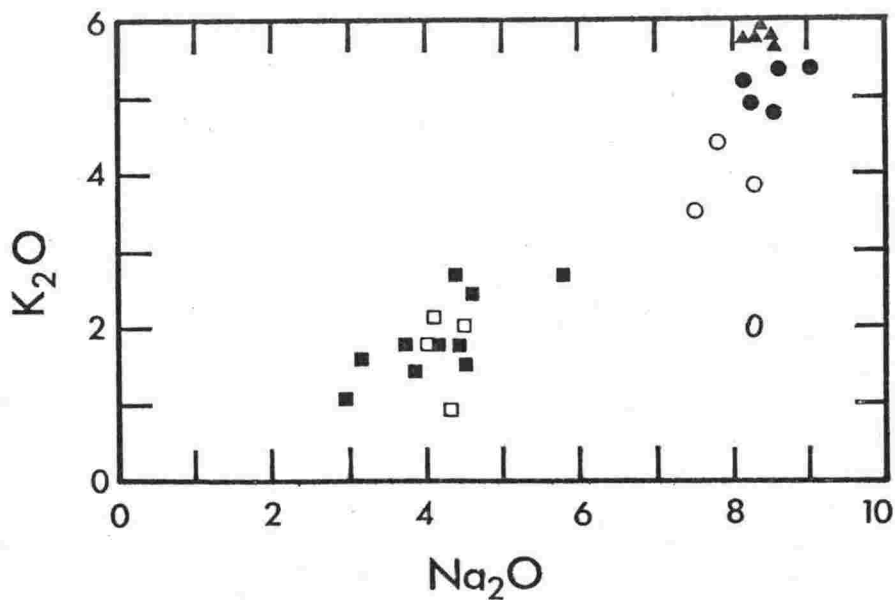
FIGURE 7:12   Plot of K_2O against Na_2O for Erebus volcanic province lavas from Mount Bird, Cape Bird and Cape Crozier.

SYMBOLS

Cape Crozier (Table 7.6)   Cape Bird, Mt Bird (Table 7.5)

■ basanite + hawaiite   □ basanite

● kaersutite phonolite   O benmoreite + phonolite

▲ pyroxene phonolite

SYMBOLS

● Cape Bird and Mt Bird

▲ Cape Crozier

■ Hut Point Peninsula and DVDP 1 and 2

□ Brown Peninsula

○ Erebus Centre

△ Mt Discovery

◆ Mt Cis

▽ Other Erebus Volcanic Province
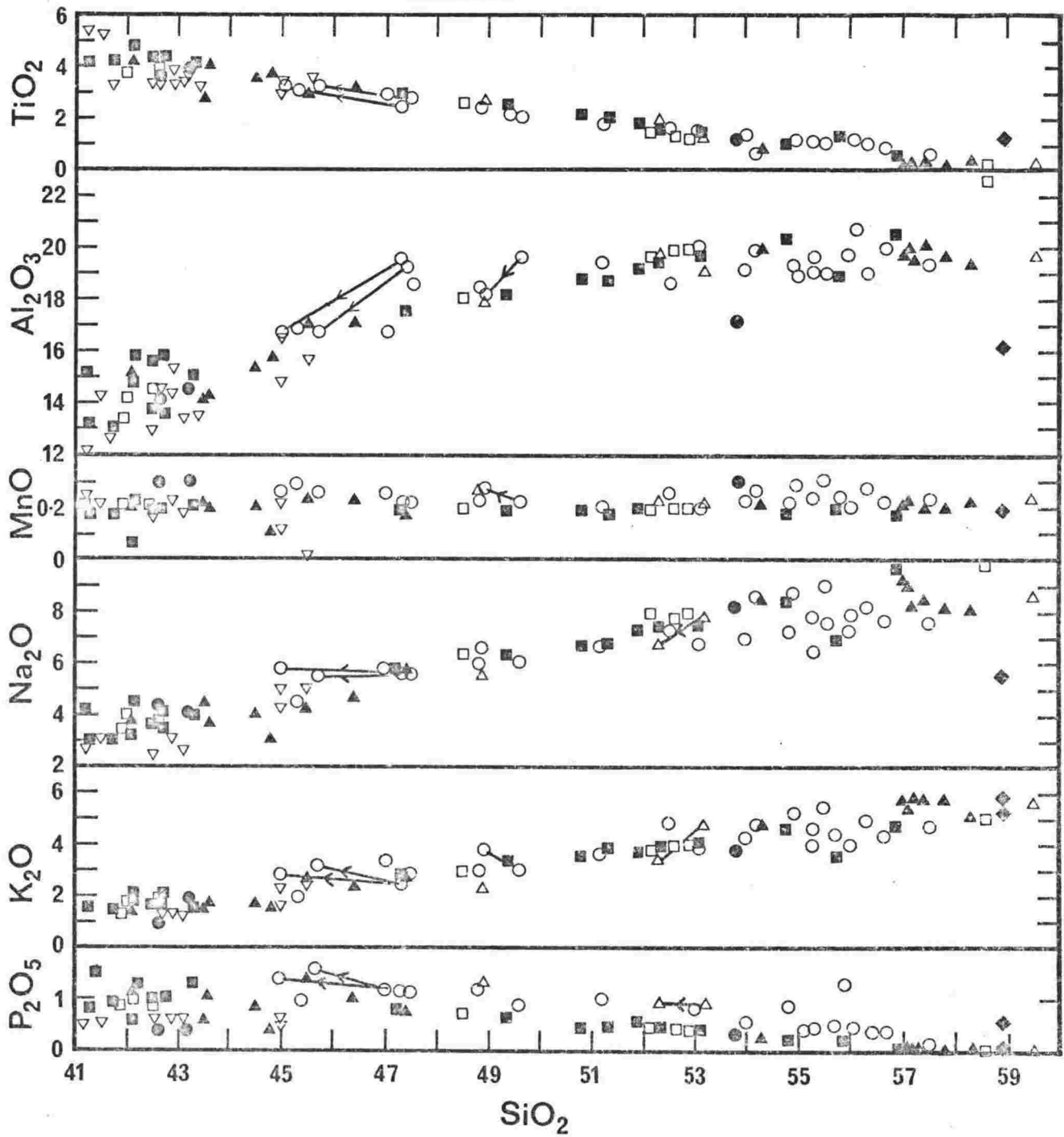
FIGURE 7.13   Major element oxide variations plotted against
SiO$_2$ for Erebus volcanic province samples.
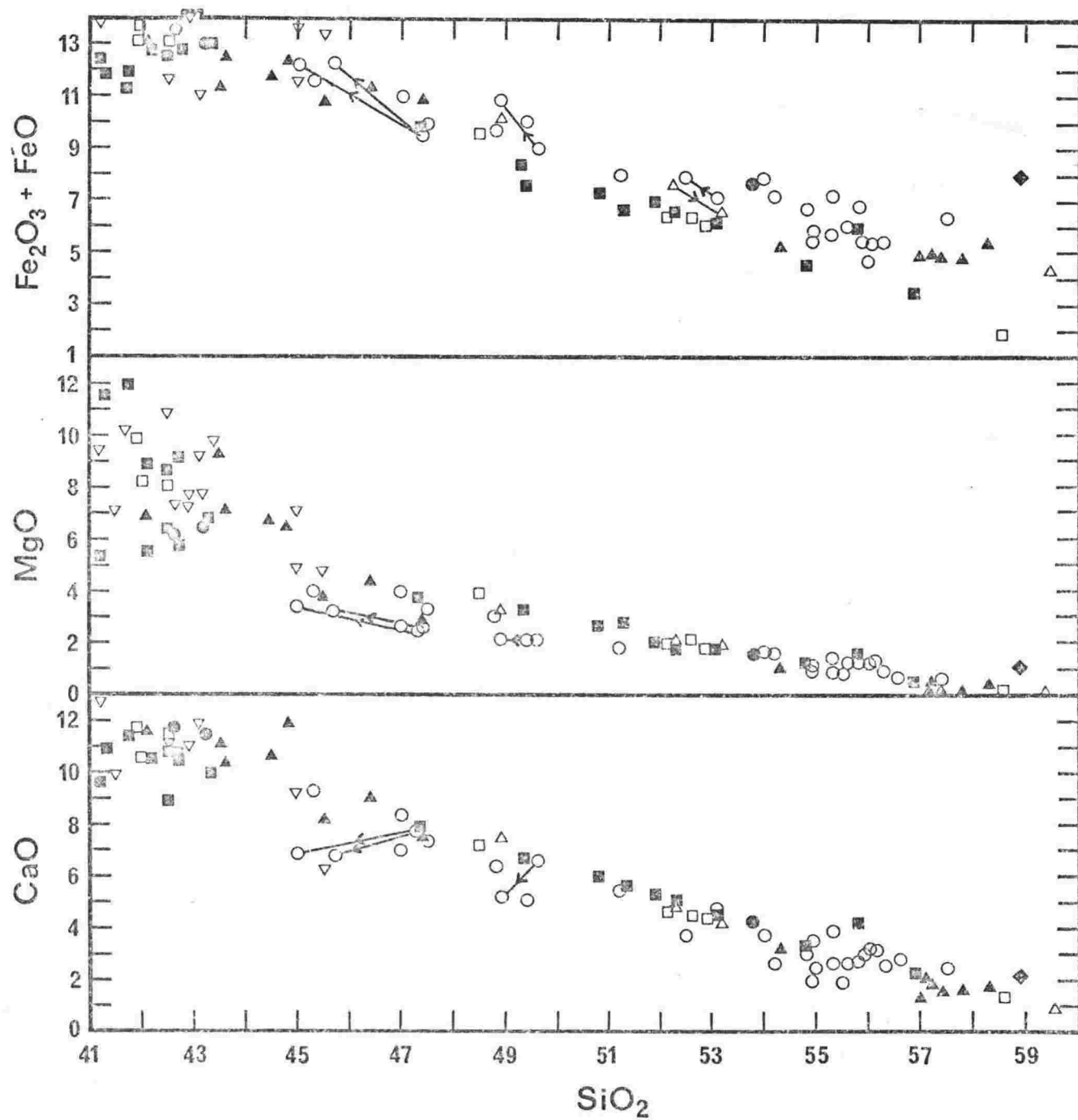
FIGURE 7.13 Continued
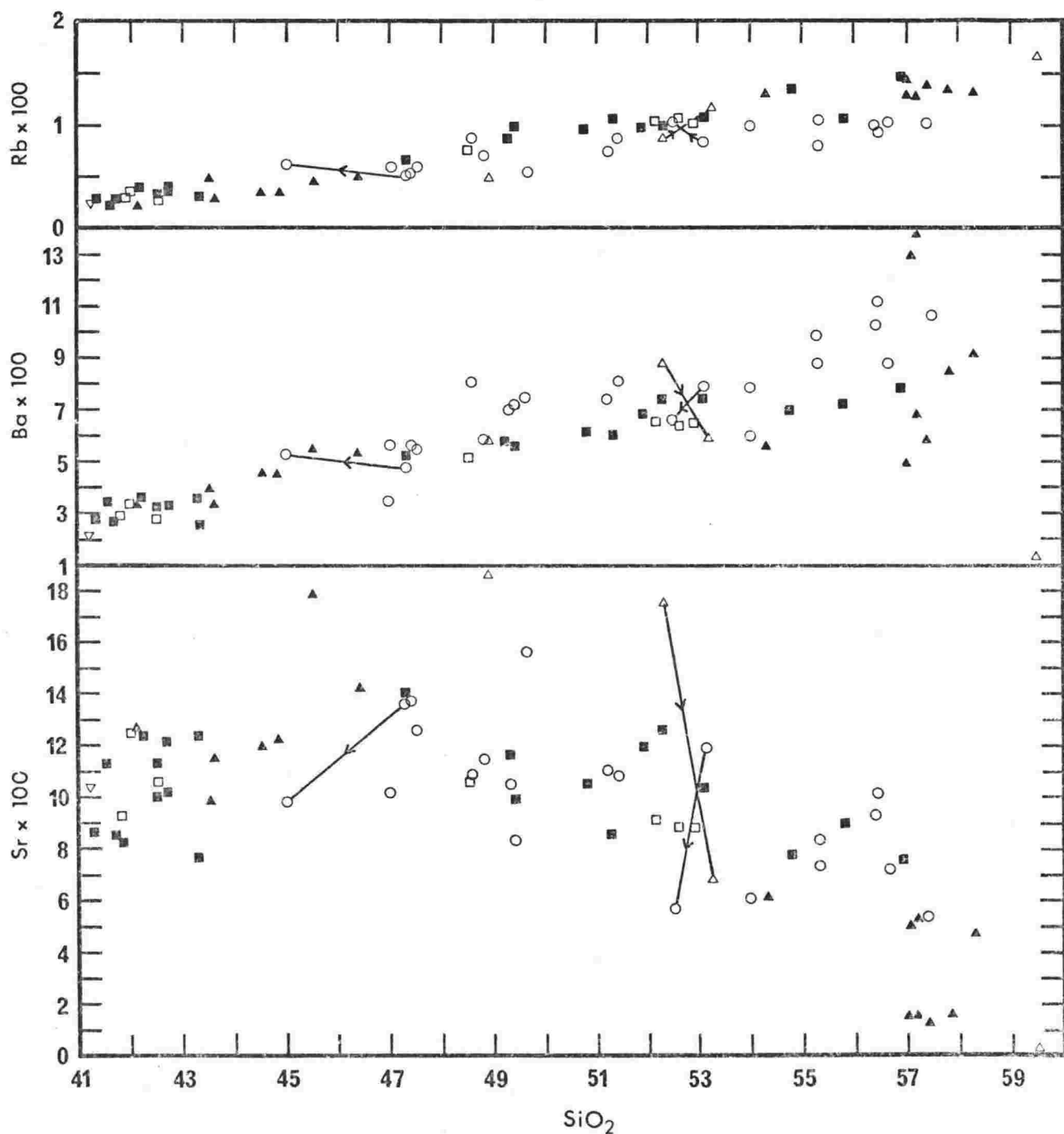
FIGURE 7.14   Trace element variations plotted against SiO₂
                for Erebus volcanic province samples.   Trace
                element concentrations in ppm.   Symbols are the
                same as Figure 7.13.
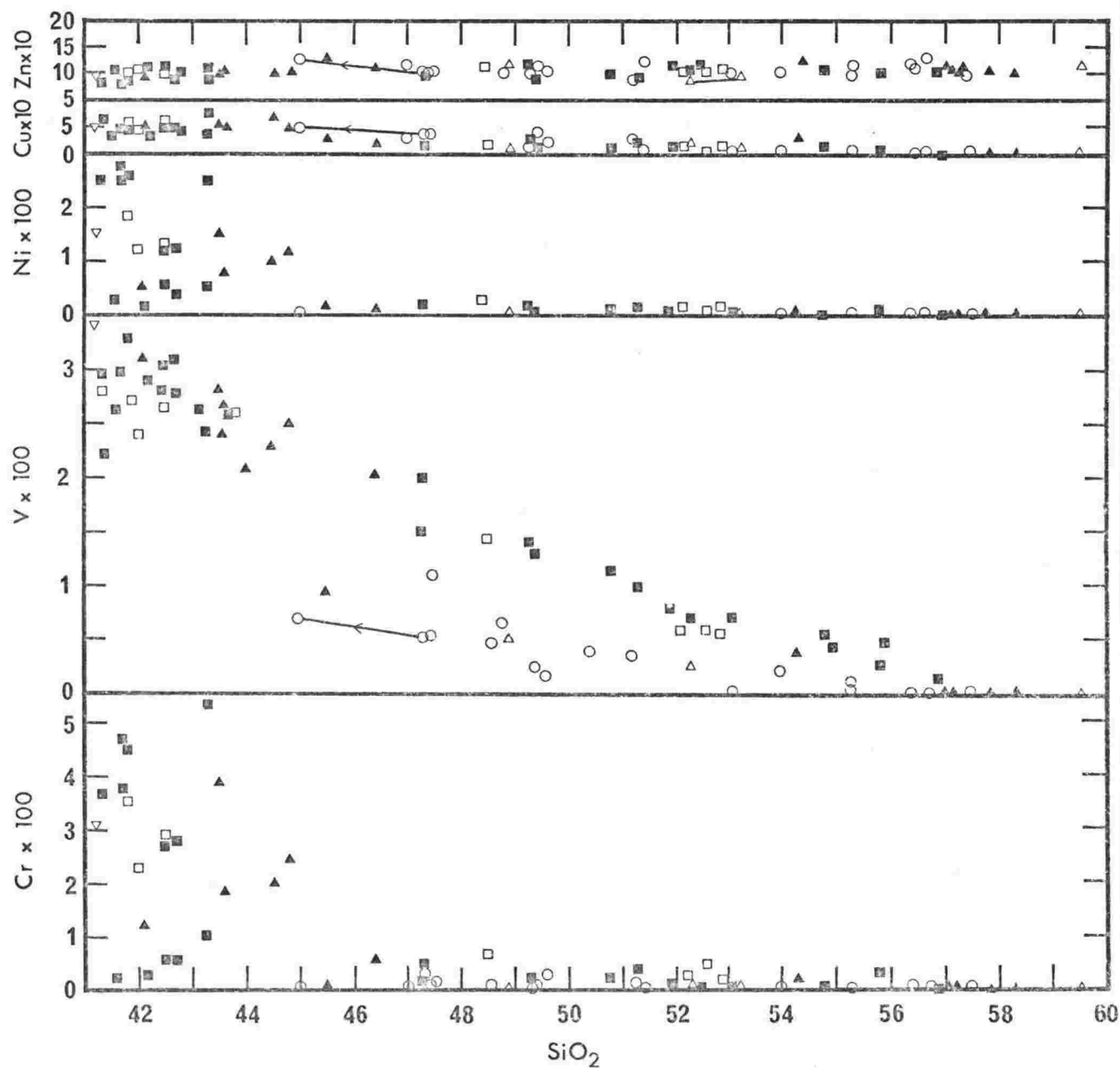
FIGURE 7.14 Continued

andesine phenocrysts has exceptionally high Sr (Fig. 7.14)
and probably contains cumulate plagioclase. The lavas are
considered to represent a differentiation sequence even though
analyses of intermediate compositions are lacking.

Mineralogically the phonolites can be divided into those
containing kaersutite and those with aegirine-augite and/or
aenigmatite. Anorthoclase microphenocrysts occur in both types.
The clinopyroxene (aegirine-augite) phonolites are typically
peralkaline, as shown by acmite in their CIPW norms (Table 7.6),
due to an excess of alkalis over Al_2O_3. They show a marked
depletion of Sr (Fig. 7.14) and enrichment of K_2O (Fig. 7.12)
with respect to the kaersutite phonolite. Compared to other
phonolites from Cape Bird and Hut Point Peninsula the Cape
Crozier phonolites are among the most fractionated, with high
total alkalis (Fig. 7.11) and a strong enrichment of K_2O over
Na_2O (Fig. 7.12).

HUT POINT PENINSULA AND DVDP HOLES 1, 2 AND 3

The most complete sequence of lavas within the kaersutite
lineage is found in surface and subsurface (DVDP holes 1 to 3)
samples from Hut Point Peninsula (Tables 7.7 and 7.8). The
lavas are basanite-nepheline hawaiite-nepheline mugearite-
nepheline benmoreite-kaersutite phonolite; one analysed
sample from DVDP 1 is a benmoreite. Surface samples are
predominantly basanite and minor phonolite (Table 7.7).
The intermediate and most primitive basanites are restricted
to DVDP core samples (Table 7.8). The only chemical discontin-
uity is between basanite (SiO_2 up to 44%) and nepheline
hawaiite (SiO_2 over 47.2%) (Fig. 7.15), otherwise there is
a complete trend from 41 to 57% SiO_2.

A total alkalis vs SiO_2 plot (Fig. 7.15) shows a scatter
in the basaltic lavas, however the intermediate and salic
lavas show a near perfect linear trend. The alkali/SiO_2
trend is almost identical to that shown by intermediate lavas
from Brown Peninsula (Fig. 7.15).

K_2O/Na_2O ratios are very constant and plot along a 1:2
line (Fig. 7.16). The phonolites are similar to a nepheline

SYMBOLS

Dry Valley Drilling Project Holes 1 and 2 (Table 7.8)

■ basanite

▼ nepheline hawaiite, nepheline mugearite

▲ benmoreite, nepheline benmoreite

Hut Point Peninsula (Table 7.7)

● basanite

□ phonolite

Brown Peninsula (Table 7.12)

○ basanite

▽ nepheline hawaiite

△ nepheline benmoreite, phonolite
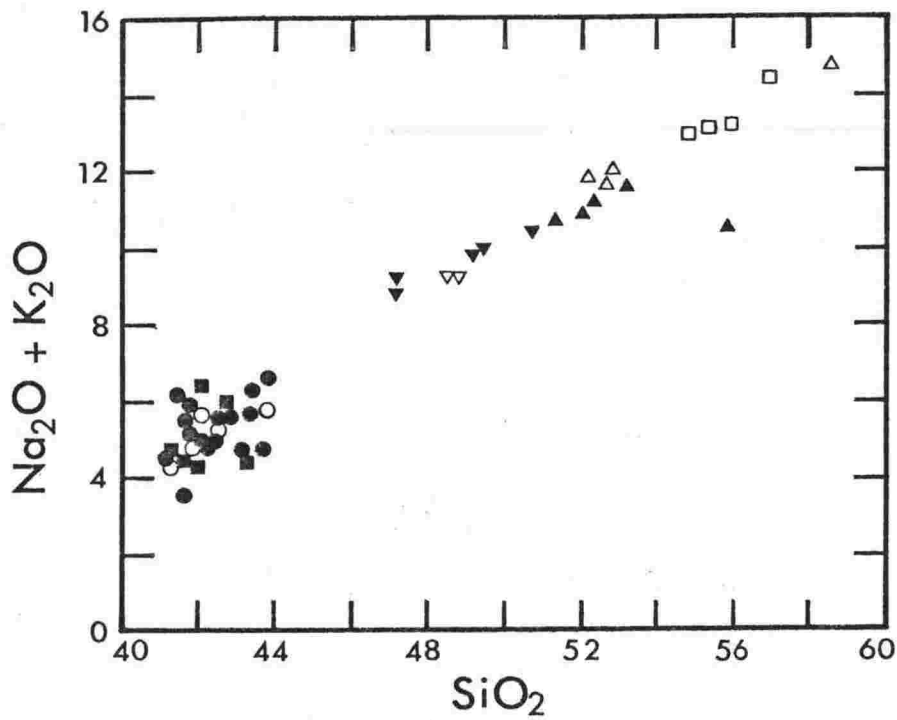
FIGURE 7.15   Plot of Na$_2$O+K$_2$O against SiO$_2$ for Erebus volcanic
               province rocks from Hut Point Peninsula, Dry
               Valley Drilling Project (DVDP) holes 1 and 2
               and Brown Peninsula.
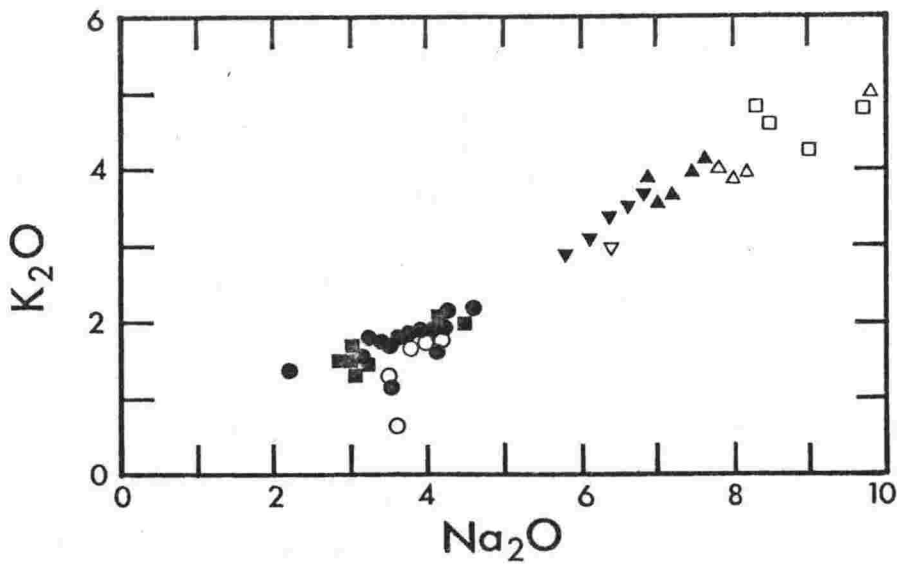
FIGURE 7.16   Plot of K$_2$O against Na$_2$O for Erebus volcanic province
               rocks from Hut Point Peninsula, Dry Valley Drilling
               Project (DVDP) holes 1 and 2 and Brown Peninsula.

benmoreite from Brown Peninsula, but are depleted in K_2O and enriched in Na_2O compared to the Cape Crozier phonolites.

Major and trace element variation diagrams (Figs. 7.8, 7.13, 7.14) show a continuous enrichment of Al_2O_3, Na_2O, K_2O, Rb, Ba, Cs, Pb, Th, U, Zr, Hf and Nb. TiO_2, total iron, MgO, P_2O_5, Cr, Ni and Cu decrease with increasing SiO_2; Mn, Zn and Y remain constant. Sr remains constant, with a mean value of about 1000 ppm, until 52% SiO_2 and then decreases only slightly in the phonolites. Rare earth element chemistry is discussed below. The chemistry is compatible with an origin for the lava sequence by crystal fractionation. Differentiation models are discussed in Chapter 9.

EREBUS CENTRE

Lavas from the Erebus Centre belong to the Erebus lineage and consist of nepheline hawaiite-nepheline benmorite-anorthoclase phonolite.

The only basaltic lava analysed from the Erebus Centre was given by Jensen (1916) (Table 7.10 analysis 1). It is a limburgite, however no field location other than Mt Erebus was given. It has 2.84% total alkalis and 15.01% MgO and is therefore atypical of other analysed lavas from the McMurdo Volcanic Group. Field work has failed to find such a rock and if present it is exceptionally rare; the chemistry suggests it may contain cumulate olivine.

Lavas from Mt Cis (near Cape Barne) are K-trachytes with an unusual composition (Smith, 1954), being saturated and with a higher K_2O/Na_2O ratio (Fig. 7.18) than any other Erebus Centre or McMurdo Volcanic Group lava. The Mt Cis lavas contain numerous inclusions of sandstone which may have contaminated the lava. Their chemistry is plotted on the variation diagrams (Figs. 7.13, 7.17) but because of their atypical chemistry and volumetric insignificance (their occurrence is restricted to a single 7 m high outcrop) the Mt Cis lavas will not be discussed further.

At Cape Barne three small scoria cones of fine-grained nepheline hawaiite are the most basic lavas in the Erebus
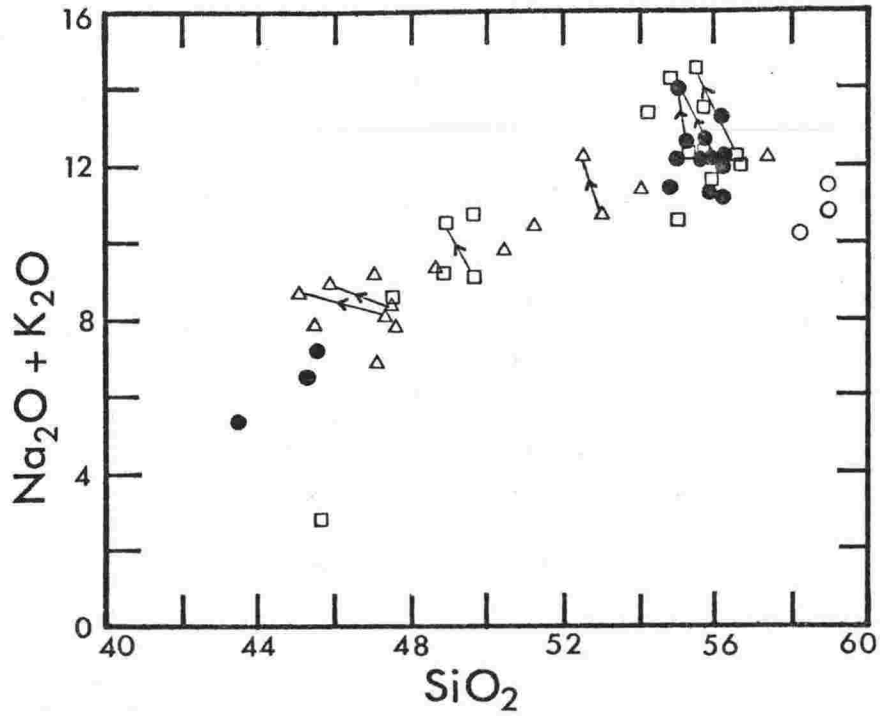
FIGURE 7.17   Plot of Na_2O+K_2O against SiO_2 for Erebus volcanic province rocks from the Erebus centre.
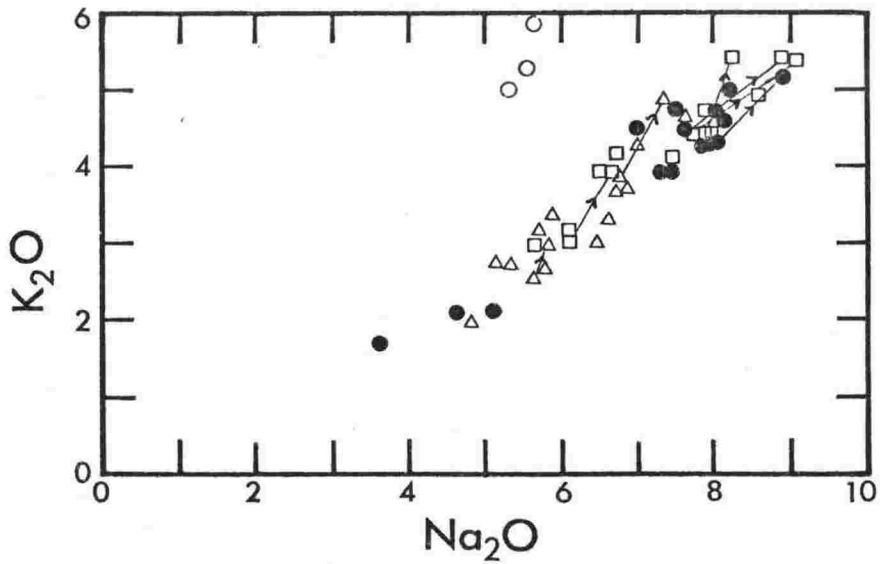
FIGURE 7.18   Plot of K_2O against Na_2O for Erebus volcanic province rocks from the Erebus centre.

SYMBOLS

△ Dellbridge Islands, Tryggve Point, Turks Head

● Cape Royds, Cape Evans, Cape Barne

□ Mt Erebus and Fang Ridge

○ Mt Cis

Centre, with the exception of the limburgite discussed above.

The remaining Erebus Centre lavas are mainly strongly porphyritic and therefore may not represent liquids. This porphyritic character of the Erebus Centre lavas makes delineation of fractionation trends difficult. Plots of total alkalis against SiO_2 (Fig. 7.17) and K_2O against Na_2O (Fig. 7.18) have a scatter which is undoubtedly a function of the lavas' porphyritic nature. The groundmass of four nepheline hawaiite and nepheline benmoreite samples were separated and analysed (Tables 7.9, 7.11). Whole rock-groundmass trend lines are plotted on variation diagrams (Figs. 7.13, 7.14), but they do not follow the trend defined by the whole rock analyses. In most cases SiO_2 decreases, whereas SiO_2 increases with differentiation. The glassy groundmasses do not therefore appear to represent a liquid in the differentiation sequence. The samples must therefore contain cumulate plagioclase or else the whole rock analyses represent a liquid in which considerable low pressure crystallization of plagioclase has occurred.

Rare earth element (REE) analyses of a nepheline hawaiite and a nepheline benmoreite indicate the amount of cumulus plagioclase is probably small (see below). Plagioclase phenocrysts are abundant however (up to 20%) and as they are not cumulate they probably crystallised from a liquid defined by the whole rock chemistry (i.e. the rock was a closed system). Plagioclase was not a major component in any fractionation process during differentiation of the lineage. If it was the differentiation sequence would follow the whole rock-groundmass trend and the REE data would show negative Eu anomalies.

A sample of anorthoclase phonolite from the summit of Mt Erebus has a large positive Eu anomaly (Eu/Eu* = 1.31) which may result from 27% cumulus anorthoclase (see below). Although the nepheline hawaiite and nepheline benmoreite whole rock analyses may represent liquids the whole rock anorthoclase phonolite analyses must be viewed with caution.

If it is assumed the whole rock analyses represent a liquid in a differentiation sequence, a reasonable assumption

for the intermediate lavas, then major element oxide variation diagrams (Fig. 7.13) can be compared. The Erebus lineage is very similar chemically to the kaersutite lineage. TiO_2, total iron, MgO, CaO and P_2O_5 decrease with increasing SiO_2. Al_2O_3 increases but tends to flatten out, while both Na_2O and K_2O increase. MnO remains constant. Trace elements show a scatter (Figs. 7.8, 7.14) as they are more sensitive to effects of cumulus plagioclase. Rb increases but clearly has lower abundances in the nepheline benmoreite and anortho-clase phonolites than the equivalent lavas in the kaersutite lineage from Hut Point Peninsula and Cape Crozier. Ni and Cr are very low while V and Cu decrease as SiO_2 increases. Pb is generally <7 ppm (Fig. 7.8), whereas it may reach 24 ppm in some kaersutite lineage lavas. Ba and Sr tend to increase and decrease respectively (Fig. 7.14) and there is greater scatter in these two elements than any others. Both Ba and Sr are strongly enriched in feldspar, Sr particularly in plagioclase whereas Ba is found in K-feldspar. Variation in their abundances must therefore reflect differences in the amounts of cumulus feldspar.

Considering the data for the whole rock analyses and taking into account the possibility of cumulus effects it is considered the major and trace element variations are consistent with an origin of the lava series by differentiation.

BROWN PENINSULA

The geology and major element geochemistry (Table 7.12) of the Rainbow Ridge area, Brown Peninsula, have been described by Adams (1973). Trace element determinations were made during this study. The lavas are basanite, nepheline hawaiite, nepheline benmoreite and phonolite which are very similar to the kaersutite lineage lavas from Hut Point Peninsula and DVDP (Tables 7.7, 7.8). A phonolite analysed by Prior (1907) is an extremely fractionated lava. Variation diagrams (Figs. 7.13 to 7.16) show identical trends to the kaersutite lineage, with the exception of Sr which is lower in the Brown Peninsula nepheline benmoreite.

OTHER AREAS

Basanites from the Dry Valley and Koettlitz Glacier areas (Table 7.14) show a scatter in chemistry similar to other Erebus volcanic province basaltic lavas (Figs. 7.19, 7.20).

Samples collected by Dr H. J. Harrington from the upper part of Mt Discovery are mineralogically similar to the Erebus lineage lavas, being strongly porphyritic with phenocrysts of plagioclase, olivine, augite and magnetite. Four analyses (Table 7.13), including a whole rock-groundmass pair, show the lavas are hawaiite, nepheline benmoreite and phonolite. The glassy groundmass of the nepheline benmoreite has a phonolitic composition and the trend of the whole rock-groundmass pair, in general, follows the major element variation diagram trends (Fig. 7.13). Trace element data are less conclusive. A Mt Discovery phonolite (Table 7.13 analysis 17) is the most silica-rich lava in the Erebus volcanic province and has anorthoclase phenocrysts (up to 4.5 mm), which resemble (at least in thin section) those from Mt Erebus anorthoclase phonolite. The Mt Discovery anorthoclase phenocrysts are not as large and lack the distinct rhomb shape of those in the Erebus lavas. The resemblance of the lavas from the two areas suggests the fractionation processes and particularly the conditions of crystallization were very similar.

DISCUSSION

All lavas from the Erebus volcanic province are strongly undersaturated and belong to a basanite-phonolite lineage (Coombs and Wilkinson, 1969; Goldich *et al.*, 1975; Smith, 1954). Lavas from Ross Island show two fractionation trends and these can be recognised at other volcanic centres in the McMurdo Sound area. The fractionation trends are only two of a wide spectrum. Each is controlled by the nature and relative proportions of the fractionated minerals which in turn are a function of physical conditions such as T, P, f_{O_2}, f_{H_2O} etc. Further discussion on fractionation processes are given below.

Previous geochemical studies (Smith, 1954; Goldich *et al.*, 1975) of Erebus volcanic province rocks have been hindered by
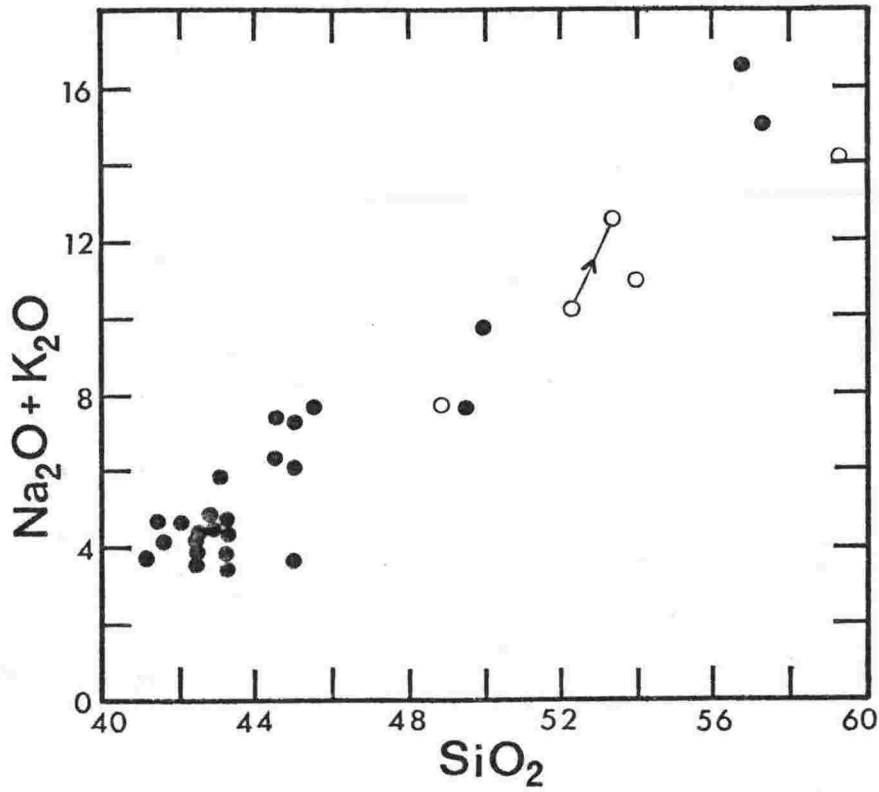
FIGURE 7.19   Plot of Na_2O+K_2O against SiO_2 for Erebus volcanic
province rocks from areas other than Ross Island
(including the Dellbridge Islands) and Brown
Peninsula.
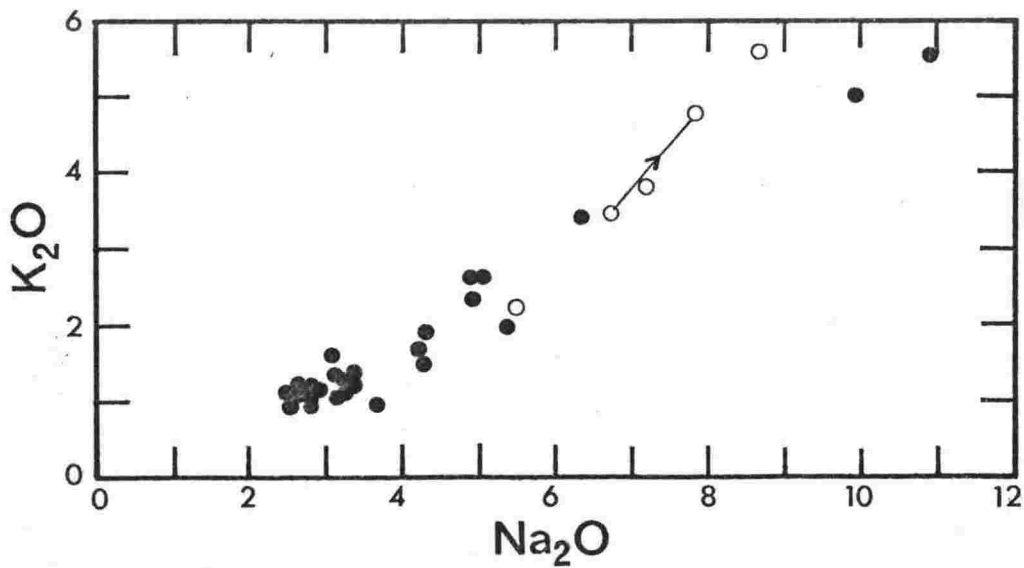
FIGURE 7.20   Plot of K_2O against Na_2O for Erebus volcanic province
rocks from areas other than Ross Island (including
the Dellbridge Island) and Brown Peninsula.

SYMBOLS

O Mt Discovery

● Other areas

the lack of lavas with intermediate compositions. Cole and Ewart (1968) noted this strong bimodal character in both rock types and chemical analyses. It is obvious from this study however that a complete range of intermediate lavas exists, and these help define each fractionation trend.

Variations within a single lineage are apparent and show that several fractionation processes are obviously occurring. In the kaersutite lineage, phonolites from Cape Crozier are rapidly enriched in K_2O whereas phonolites from Hut Point Peninsula and Black Island show a constant enrichment of both K_2O and Na_2O (Fig. 7.25).

Mg Number 100Mg/(Mg+Fe^{2+}) atomic ratio

Roeder and Emslie (1970) and Roeder (1974) have shown experimentally the partition of Fe and Mg between olivine and basaltic liquid is constant and can be defined by:

$$K_D = (\frac{FeO}{MgO})^{Ol} / (\frac{MgO}{FeO})^{Liq} = 0.30$$

which is independent of temperature. Kesson (1973) defined the Mg number [100Mg/(Mg+Fe^{2+}) atomic ratio] and showed, by reference to the above equation, that for assumed mantle olivine composition of Fo_{88} to Fo_{90} a liquid will have a Mg number ranging from 67 to ~77, if it is in equilibrium with such olivine. The Mg number can therefore be used to identify primary mantle magmas (provided rocks of cumulate origin are excluded). An arbitrarily standard ratio of $Fe_2O_3/FeO = 0.25$ was used to correct for any oxidation (Kesson, 1973).

All basanites and basalts from the McMurdo Volcanic Group are plotted in Figure 7.21. Most of the basaltic magmas have a Mg number less than 67, indicating they have fractionated during ascent from the mantle. The few samples with an Mg number >67 are mainly porphyritic with olivine and clino-pyroxene phenocrysts, which could be cumulus in origin. Six

SYMBOLS

▲ Balleny Islands

◆ Melbourne volcanic province

Erebus volcanic province

□ Cape Bird

■ Cape Crozier

● Hut Point Peninsula

○ DVDP holes 1 and 2

▽ Brown Peninsula

△ Koettlitz Glacier area and the
   Dry Valleys
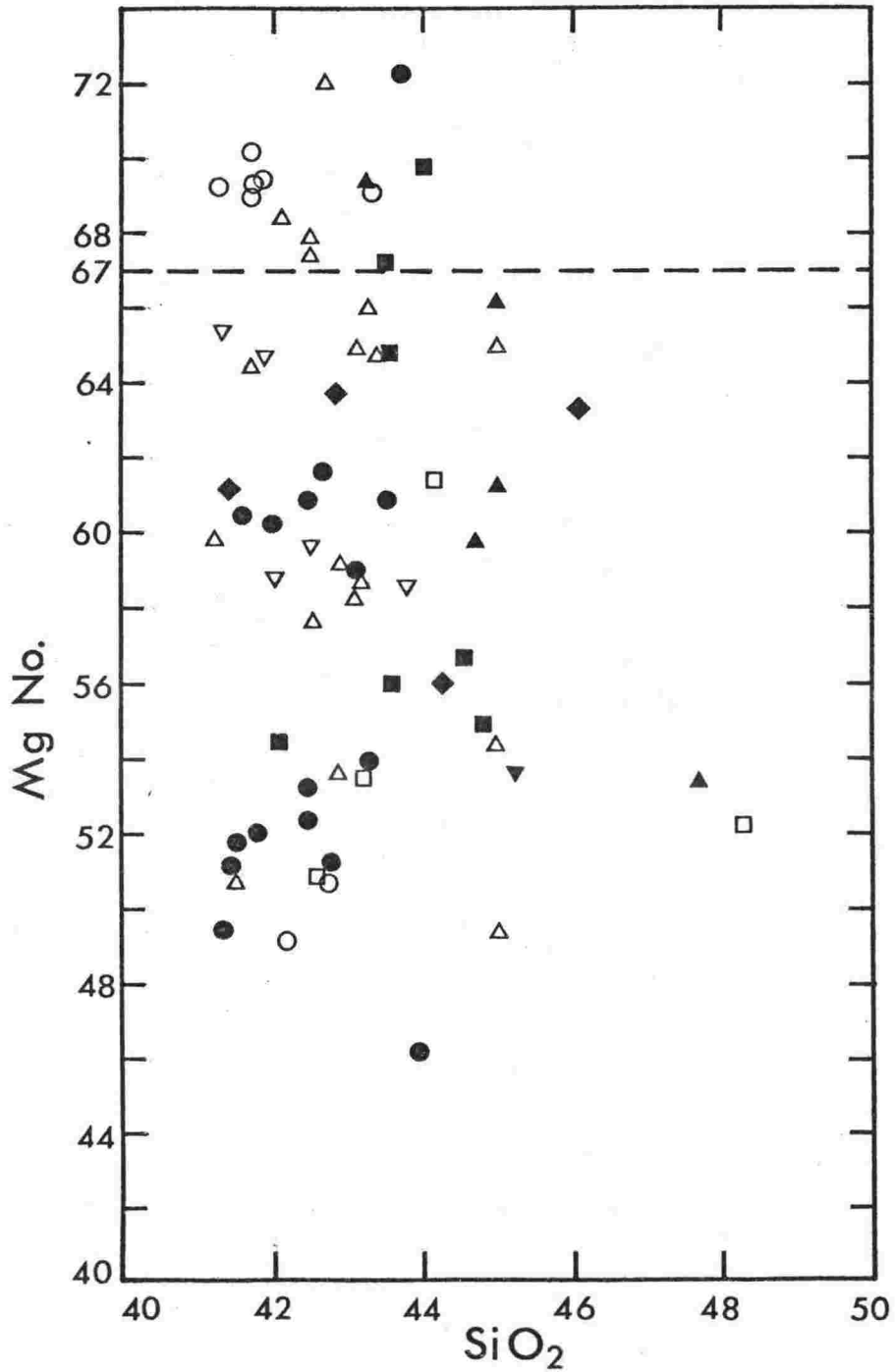
FIGURE 7.21 Mg number (100Mg/Mg+Fe^{2+}, atomic ratio) with Fe$_2$O$_3$/FeO normalised at 0.25 (after Kesson, 1973), in alkali basalts and basanites of the McMurdo Volcanic Group. Plotted against SiO$_2$ (weight percent).
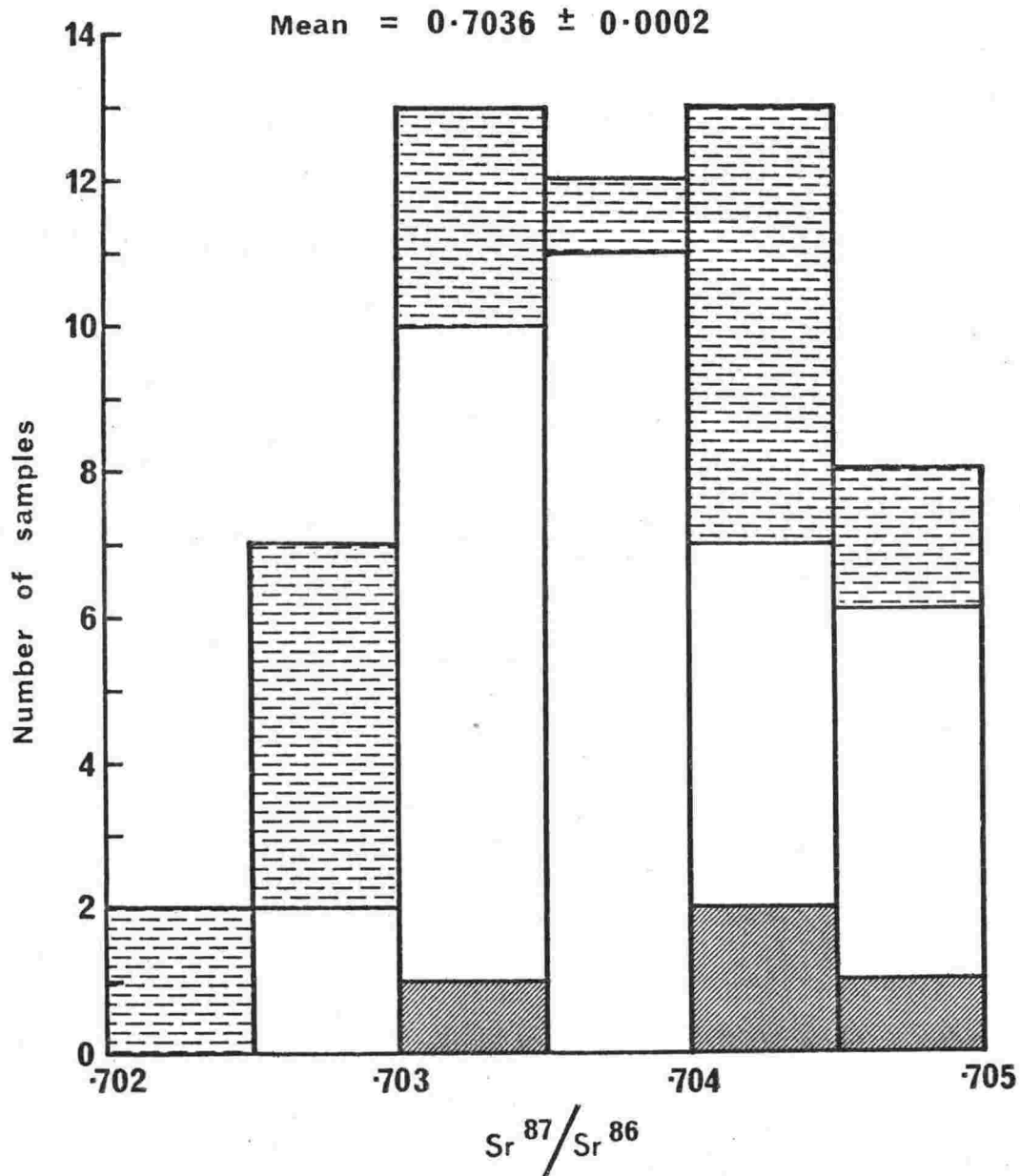
FIGURE 7.22 Frequency histogram of Sr^{87}/Sr^{86} ratios in samples of the McMurdo Volcanic Group. Data from Halpern (1969), Jones and Walker (1972) and Kurasawa (1975). Melbourne volcanic provinces samples are shown by cross hatching, phonolites from the Erebus volcanic province are shaded.
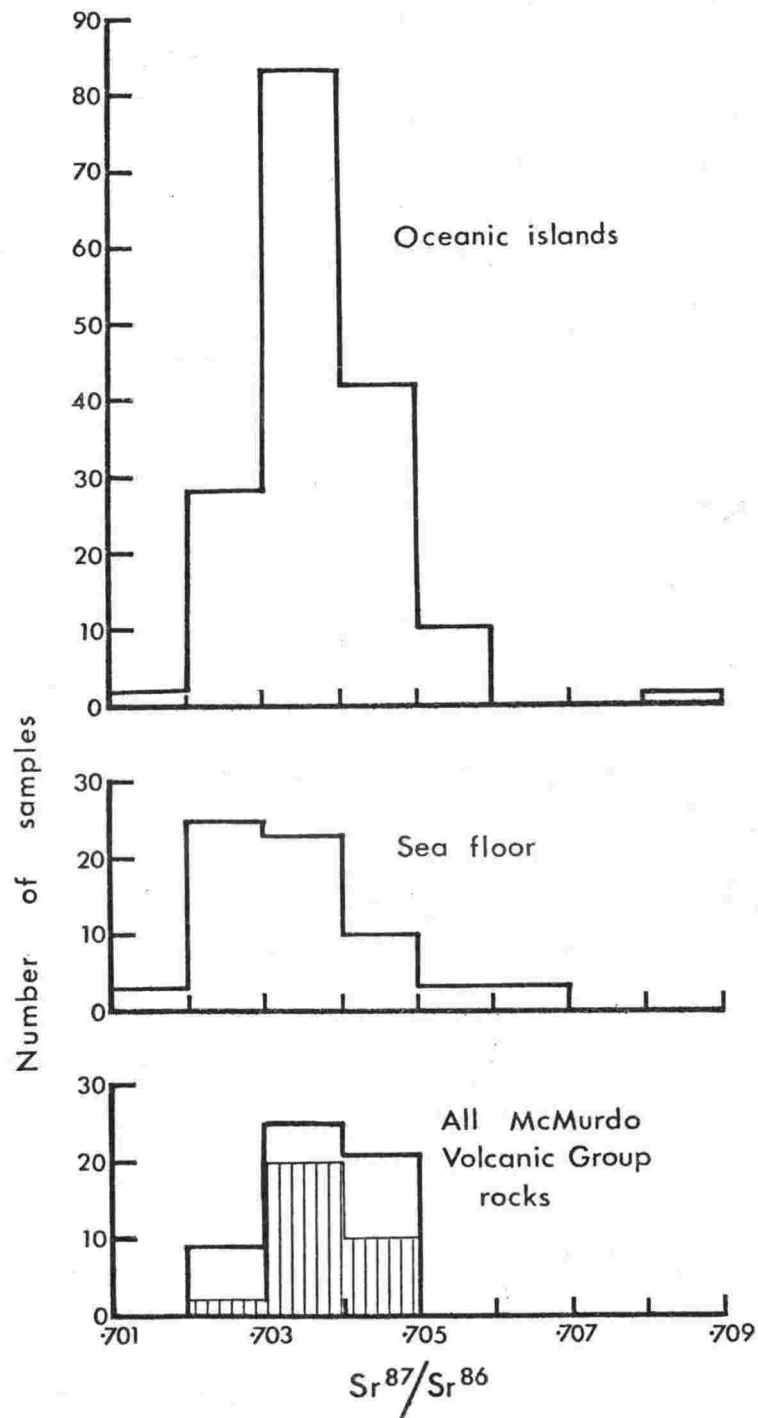
FIGURE 7.23   Frequency histogram of Sr^{87}/Sr^{86} ratios in basaltic lavas
from oceanic islands and the sea floor and all analysed
samples from the McMurdo Volcanic Group.   Basalt data from
Faure and Powell (1972).   Basaltic lavas of the McMurdo
Volcanic Group are indicated by shading.

analysed DVDP basanites have an Mg number >67 and a high
pressure mineralogy (see Chapter 5) and are considered to be
unfractionated and not cumulates. One sample is aphyric,
that is it contains <2% phenocrysts (any crystal >1 mm),
and must therefore represent a liquid. It has a similar
chemistry to the porphyritic DVDP basanites which therefore
validates the assumption that the DVDP lavas represent
unmodified mantle-derived magma.

Strontium Isotope Geochemistry

Strontium isotope measurements on McMurdo Volcanic Group
rocks have been made by Halpern (1969), Jones and Walker (1972)
and Kurasawa (1975). For the Erebus Volcanic Province,
51 Sr^{87}/Sr^{86} determinations have a mean of 0.7036 ± 0.0002 (σ)
and a narrow spread of values from 0.7022 to 0.7048 (Fig. 7.22).
Four determinations of Melbourne volcanic province rocks
average 0.7041 (Fig. 7.22).

Oceanic basalt which is unaffected by possible contamination
from salic crust, has an average Sr^{87}/Sr^{86} of 0.7035 (Fig. 7.23).
Therefore the analysed McMurdo Volcanic Group samples are also
probably uncontaminated by crustal rocks. The overlap of
Sr^{87}/Sr^{86} values for the basaltic and phonolitic rocks
indicates they are comagmatic.

Summary and Conclusions

The four volcanic provinces (Balleny, Hallett, Melbourne
and Erebus) were defined in terms of their distribution
(Hamilton, 1972; Kyle and Cole, 1974). It is also apparent
that there are chemical differences in the lava compositions.
Geochemical characteristics are summarised on total alkalis
versus SiO_2 (Fig. 7.24) and K_2O versus Na_2O (Fig. 7.25)

FIGURE 7.24 Na_2O+K_2O against SiO_2 diagram showing generalised trends
for McMurdo Volcanic Group rocks. A sodic basanite-nepheline
benmoreite lineage, The Pleiades; B basanite-phonolite
lineage (kaersutite lineage), Erebus volcanic province;
C nepheline hawaiite-anorthoclase phonolite lineage (Erebus
lineage), Erebus volcanic province; D mildly potassic
trachyandesite-peralkaline K-trachyte lineage, The Pleiades;
E alkali basalt/basanite-quartz trachyte lavas, Hallett
volcanic province; F quartz trachyandesite-quartz trachyte
lineage, Mt Melbourne. Dashed line G is division between
mildly alkaline and strongly alkaline lavas from southern
Kenya (Saggerson and Williams, 1964). Shaded area indicates
field of differentiation trends for alkaline lavas from
continental, island-arc and oceanic suits (Schwarzer and
Rogers, 1974). Diagonal pattern is boundary between alkaline
rocks and subalkaline rocks proposed by Schwarzer and Rogers
(1974). Averages of Hawaiian alkalic suite lavas shown by
AB - alkali basalt, H - hawaiite, M - mugearite, Bn - benmoreit
T - soda trachyte (MacDonald, 1968).
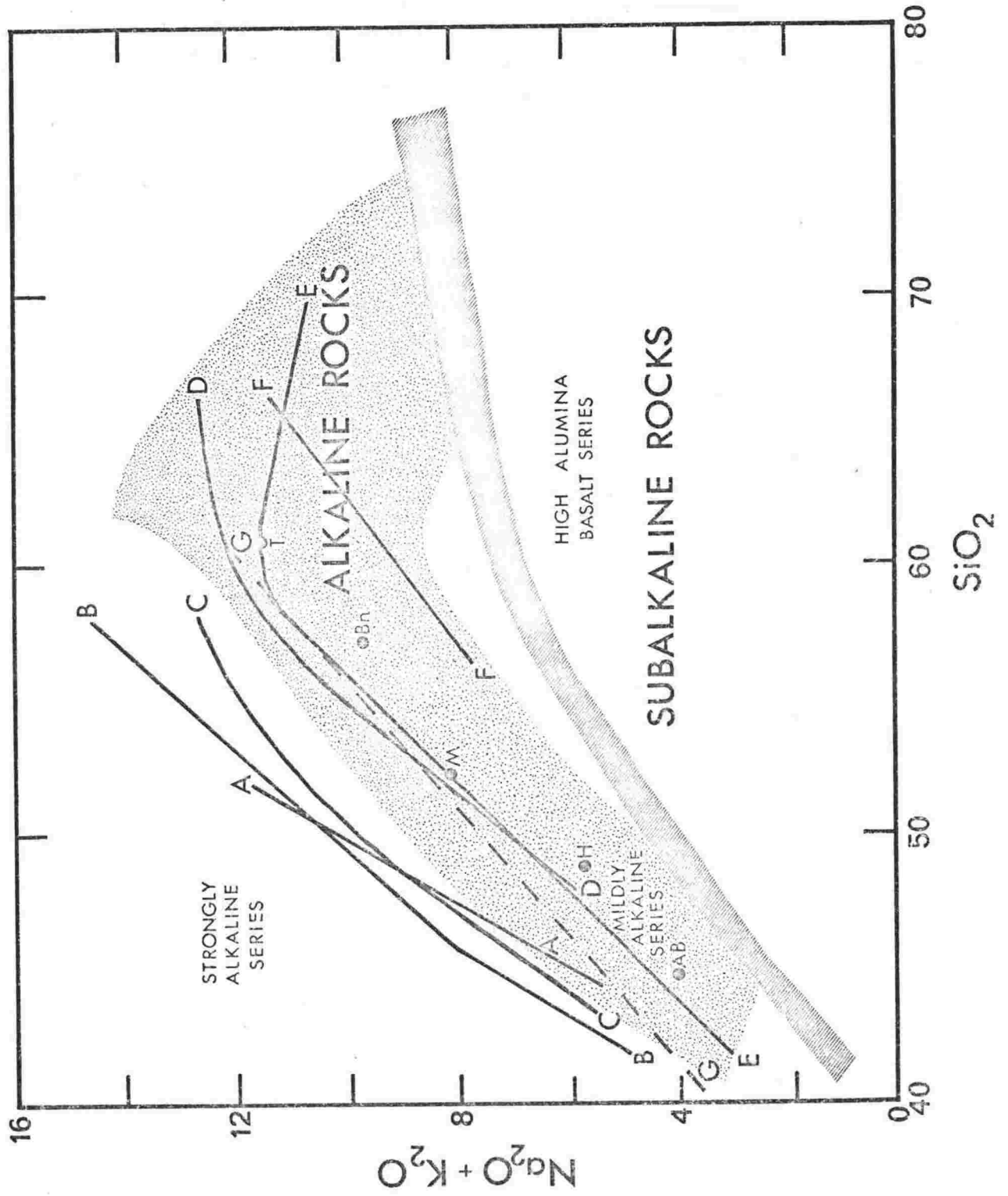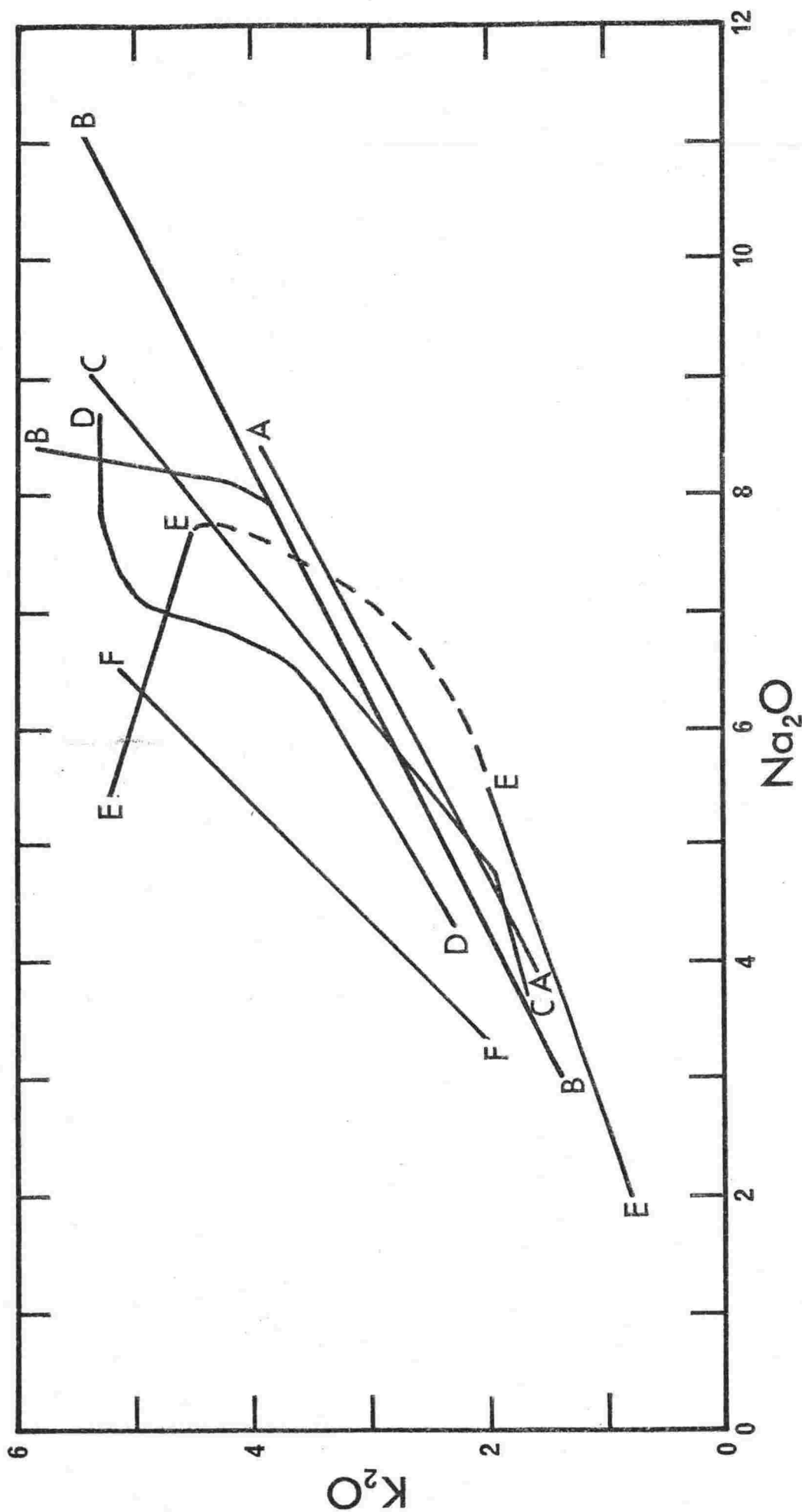
FIGURE 7.25 K_2O against Na_2O diagram showing generalised trends for McMurdo Volcanic Group rocks. Identification of trend lines are the same as Figure 7.24.

The first and most obvious features are the higher total alkalis and lower SiO_2 enrichment in the Erebus volcanic province compared to the Melbourne and Hallett provinces. Erebus volcanic province lavas are strongly undersaturated and consist of basanites to phonolites whereas Hallett and Melbourne volcanic provinces contain alkali basalt/basanite to trachyte lavas (cf. Figs. 7.3 and 7.10). Phonolites do occur in the Hallett and Melbourne provinces but are exceptionally rare. Similarly a benmoreite (in DVDP 1) and a trachyte (Mt Cis) have been found in the Erebus volcanic province, these also are exceptional.

Both the Melbourne and Hallett volcanic provinces contain fractionation trends of alkali basalt/basanite to trachyte. The variation of total alkalis against SiO_2 (Fig. 7.24) for the two provinces are similar up to 60% SiO_2 where they diverge, with Hallett showing a decrease in alkalis. Extreme differentiates at The Pleiades (Melbourne volcanic province) are peralkaline K-trachyte (Ac = 6%) while quartz trachytes (Q = 14%) occur in the Hallett volcanic province. K_2O/Na_2O ratios (Fig. 7.25) in Melbourne volcanic province lavas from The Pleiades and Mt Overlord are considerably higher than Hallett volcanic province lavas. Quartz trachytes from Hallett show an unusual trend with a decrease in Na_2O as K_2O increases.

The saturated and potassic (Fig. 7.25) lavas from Mt Melbourne are unlike any others from the McMurdo Volcanic Group.

The Balleny Islands are too poorly known to make generalisations other than the lavas are mainly basaltic and are chemically similar to those from the Hallett volcanic province. Although trachytic lavas occur in the Hallett volcanic province, basalts and hawaiites are predominant. Melbourne volcanic province lavas are essentially intermediate and trachytic in composition, basaltic lavas are rare. A complete basanite-phonolite lineage occurs in the Erebus volcanic province.

Coombs and Wilkinson (1969) believed there is a continuous series of lineages between alkali basalt-trachyte and basanite-phonolite. They used a variety of plots (i.e. MgO vs $FeO+Fe_2O_3$;

K_2O vs Na_2O and DI vs Ne) to distinguish the various trends.
It is evident that the lineages in the McMurdo Volcanic Group
represent part of this spectrum, with however one difference.
Most of the parent magmas appear to be basanites, so a trend
of basanite-trachyte must be added to those suggested by
Coombs and Wilkinson (1969). A range of basaltic lavas are
generated in the mantle due to varying degrees of partial
melting, differing temperature and pressure and other
processes which are discussed below. Each basaltic liquid
depending on the physical properties influencing it may give
a whole spectrum of differentiate lavas.

McMurdo Volcanic Group lavas are identical to those from
oceanic islands (Borley, 1974) and continental environments
(Sorensen, 1974). Schwarzer and Rogers (1974) compared world
wide occurrences of alkali olivine basalts and their
differentiation trends (Fig. 7.24). All lavas including the
quartz normative differentiates from Mt Melbourne plot above
the boundary between alkaline rock series and subalkaline rock
series proposed by Schwarzer and Rogers (1974) (Fig. 7.24).
The Hallett and Melbourne volcanic province lavas (excluding
the sodic basanite-nepheline benmoreite lineage from The
Pleiades) plot in the field defined by differentiation trends
of alkali olivine basalts and their differentiates from
continental, island arc and oceanic lava suites.

Erebus volcanic province lavas and the sodic lineage
from The Pleiades plot in the strongly alkaline series (Fig.
7.24). Their chemistry and differentiation sequences are
similar to oceanic islands (Ridley, 1970; Schmincke, 1973;
Borley, 1974) and continental areas (Saggerson and Williams,
1964; Abbott, 1969; Coombs and Wilkinson, 1969; Price,
1973; and many others).

RARE-EARTH ELEMENT GEOCHEMISTRY OF LATE

CENOZOIC ALKALINE LAVAS OF THE McMURDO VOLCANIC

GROUP, ANTARCTICA

Philip R. Kyle
Department of Geology,
Victoria University of Wellington,
Wellington, New Zealand.

and

Peter C. Rankin,
Soil Bureau,
Department of Scientific and Industrial Research,
Lower Hutt, New Zealand.

Running Heading: REE in alkali lavas of the McMurdo Volcanic
                   Group, Antarctica

ABSTRACT

Rare earth element concentrations (REE) were determined in 16 Ross Island and northern Victoria Land alkaline lava samples which were representative of four lava lineages of the McMurdo Volcanic Group, Antarctica. A kaersutite and two feldspar mineral separates were also analysed.

Two of the lava lineages, a basanite to nepheline benmoreite and a basanite to phonolite, have similar chondrite-normalised REE fractionation patterns, with a continuous enrichment of light and heavy REE and depletion of middle REE. The patterns result from the fractionation of olivine, clino-pyroxene, spinels, feldspar, kaersutite and apatite. Kaersutite is an important fractionated phase responsible for the middle REE depletion.

Another of the lava lineages is mildly potassic with trachyandesite to peralkaline K-trachyte lavas which have partly overlapping REE fractionation patterns. There is a depletion in REE from tristanite to K-trachyte. Fractionation of olivine, clinopyroxene, feldspar and apatite probably control the REE chemistry of the lineage, greater degrees of apatite fractionation deplete the K-trachyte in REE relative to the tristanite. Feldspar fractionation in the genesis of the peralkaline K-trachyte is shown by a large negative Eu anomaly (Eu/Eu* = 0.10).

A nepheline hawaiite to anorthoclase phonolite lava lineage from the Erebus Centre shows enrichment of REE, although minor overlapping in the middle REE does occur. Anorthoclase phonolite

has a positive Eu anomaly (Eu/Eu* = 1.31) indicating accumulation of anorthoclase. The lineage resulted from fractionation of olivine, clinopyroxene, magnetite and apatite.

INTRODUCTION

Recent studies of rare earth element (REE) abundances in alkali volcanic rocks have been used to elucidate fractional crystallization processes within alkali basalt - trachyte - phonolite sequences (Schilling and Winchester, 1969; Flower, 1971; Nagasawa, 1973; Price and Taylor, 1973). These studies have shown that REE abundances can give a qualitative indication of phases likely to be precipitated and removed during fractional crystallization, while Zielinski and Frey (1970) and Zielinski (1975) showed that when the abundances are combined with computer calculated mass balance computations, quantitative models could be developed.

The origin of alkali basaltic magmas, from knowledge of the distribution of REE, have been discussed by many authors including Gast (1968), Masuda et al., (1971), Kay and Gast (1973), Sun and Hanson (1975), and Shimizu and Arculus (1975). From REE data constraints on the likely composition of the upper mantle, where alkali basaltic magmas are generated, have been deduced.

The Late Cenozoic McMurdo Volcanic Group occurs in four volcanic provinces (Kyle and Cole, 1974): within the Balleny Islands (Balleny volcanic province); northern Victoria Land (Hallett and Melbourne volcanic provinces); and McMurdo Sound

(Erebus volcanic province), Antarctica (Fig. 1). Only lavas from the Melbourne and Erebus volcanic provinces were examined in this study. In these two provinces (Fig. 1) the lavas range from basanite (basanitoid) to trachyte and phonolite, and five lava lineages, arising presumably by crystal fractionation, can be recognised. Four of these lineages (Fig. 2) were examined, by analysing 16 whole rock, a kaersutite (Ti-rich amphibole) and two feldspar mineral separates, to determine the differentiation history and REE variations in each.

Lavas at The Pleiades (Melbourne volcanic province) (Fig. 1) display two lineages (Fig. 2): a mildly potassic lineage of trachyandesite[1] - tristanite - K-trachyte - peralkaline K-trachyte; and a sodic lineage of basanite - nepheline hawaiite - nepheline benmoreite. The potassic lavas are the most abundant and probably account for over 90% of the lavas at The Pleiades. They contain phenocrysts of olivine, clinopyroxene, magnetite, feldspar and biotite (rare). Basanite of the sodic lineage has olivine and clinopyroxene phenocrysts and rare plagioclase xenocrysts, while nepheline hawaiite and nepheline benmoreite are fine-grained with microphenocrysts of kaersutite, minor clinopyroxene and rare magnetite.

---

[1] The major element chemistry, lava nomenclature and details of the lineages will be discussed elsewhere (Kyle, in prep.). Terminology is similar to Coombs and Wilkinson (1969). A Na_2O/K_2O ratio of 2:1 is used to separate the sodic and mildly potassic lineages.
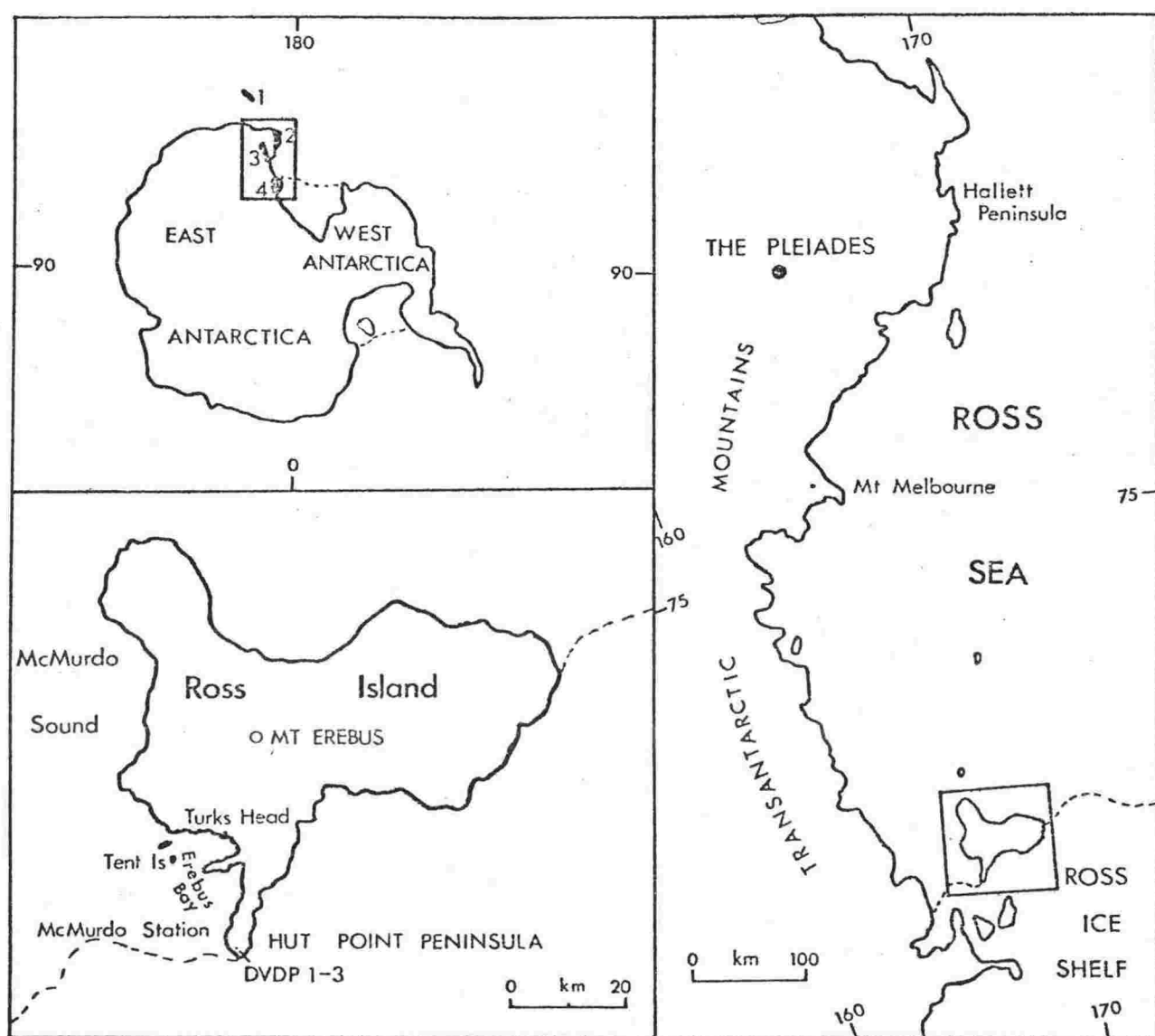
FIGURE 1. Distribution of the McMurdo Volcanic Group and subdivision into
volcanic provinces after Kyle and Cole (1974). 1 - Balleny
volcanic province, 2 - Hallett volcanic province, 3 - Melbourne
volcanic province, 4 - Erebus volcanic province.
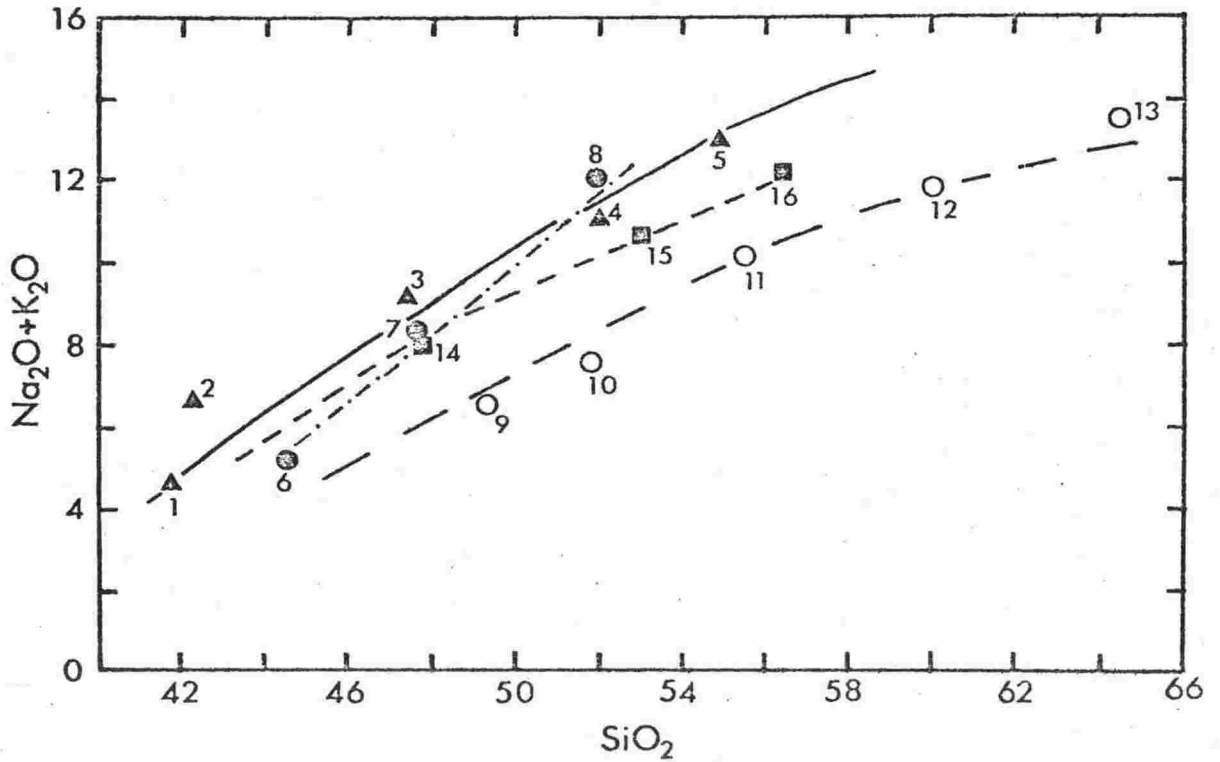
FIGURE 2. Total alkalis versus silica diagram showing generalised trends of lava lineages in the McMurdo Volcanic Group (Kyle, in preparation), examined in this study. Sample numbers correspond to the samples listed in Table 1. Melbourne volcanic province lineages are a mildly potassic trachyandesite-tristanite-K-trachyte-peralkaline K-trachyte (O——, samples 9 to 13) and a sodic basanite-nepheline hawaiite-nepheline benmoreite (●—·——·—, samples 6 to 8). Erebus volcanic province lineages are a sodic basanite-nepheline hawaiite-nepheline benmoreite-kaersutite phonolite (▲————, samples 1 to 5) and a nepheline hawaiite-nepheline benmoreite-anorthoclase phonolite (kenyte) lineage (■————, samples 14 to 16).

The Erebus volcanic province lavas belong to a basanite – phonolite association (Goldich et al., 1975). Two lineages, although very similar chemically (Fig. 2), are recognised by their distinctive mineralogy and localised field occurrences. At Mt Erebus and Erebus Bay (collectively termed the Erebus Centre) (Fig. 1) the lavas belong to a lineage of nepheline hawaiite – nepheline mugearite – nepheline benmoreite – anorthoclase phonolite (kenyte), referred to as the Erebus lineage. The usual mineralogy of the lineage is olivine, augite, magnetite with plagioclase in the intermediate[2] lavas and anorthoclase in the phonolite. The second lineage, termed the kaersutite lineage, is best developed at Hut Point Peninsula in the drill core of the Dry Valley Drilling Project (DVDP) holes 1 to 3 (Treves and Kyle, 1973, Kyle and Treves, 1974); it consists of basanite – nepheline hawaiite – nepheline mugearite – nepheline benmoreite – kaersutite phonolite. Kaersutite and augite are the dominant mafic minerals in the lavas intermediate between basanite and phonolite.

ANALYTICAL TECHNIQUES

All major element determinations except Na_2O and FeO were made by x-ray fluorescence spectroscopy using the fusion method of Norrish and Hutton (1969). Na_2O was determined by atomic absorption spectrometry and FeO by standard wet techniques (Shapiro and Brannock, 1962). Trace elements Rb, Ba, Sr, Zn,

---

[2] Used for rocks of composition between basanite and trachyte or phonolite.

Cu, Ni, V and Cr were determined by x-ray fluorescence spectroscopy, at the University of Montreal.

Rare earth elements (REE) and other trace elements were determined by spark source mass spectrometry, using methods similar to those of Taylor (1965, 1971). The samples were sieved through 50 μm nylon cloth and mixed in a 1:1 ratio with ultra-pure graphite which contained 500 ppm spectrographically pure lutetium oxide as an internal standard. Based on the repeated analyses of international standards, the precision of the method is considered to be 15% for the REE, U, Th, Pb and up to 25% for the other elements. Further description of the technique, and the results of the analysis of two international rock-standards are given by Howorth and Rankin (1975).

RESULTS

Major and trace element analyses for the lava samples are listed in Table 1. REE analyses are given in Table 2. Analyses of kaersutite and two feldspar mineral separates are listed in Tables 3 and 4 respectively. The REE data, normalised to the average abundance in chondrite (Price and Taylor, 1973), is shown in Figs. 3 to 8.

All the samples show a strong enrichment in the light REE relative to the heavy REE, and a very strong enrichment on the chondrite abundances. Many lavas show a depletion of cerium (Ce) relative to the other REE (Figs. 5-8). Dysprosium (Dy) has a small unexplained enrichment relative to the other REE, in the basanite - nepheline hawaiite - nepheline benmoreite

TABLE 1. Major and trace element analyses of McMurdo Volcanic Group rocks.

	1	2	3	4	5	6	7	8	9	10	11	12	13	14	15	16
SiO_2	41.68	42.15	47.27	51.90	54.82	44.26	47.58	51.76	49.26	51.72	55.36	59.98	64.36	47.27	53.09	56.68
TiO_2	4.06	4.66	2.95	1.85	1.16	3.66	2.96	1.15	2.63	2.23	1.31	0.70	0.14	2.43	1.66	1.00
Al_2O_3	12.92	15.84	17.61	19.31	20.41	14.82	16.97	18.96	16.10	16.97	17.57	17.67	16.85	19.31	20.09	19.84
Fe_2O_3	3.06	4.73	3.35	3.01	1.99	4.01	3.53	4.39	4.67	7.17	3.24	5.57	2.34	9.35	7.10	5.18
FeO	8.48	8.27	6.06	3.96	2.52	8.70	8.08	3.86	6.49	3.26	5.55	0.98	1.52	-	-	-
MnO	0.18	0.22	0.21	0.20	0.18	0.20	0.24	0.25	0.20	0.20	0.23	0.17	0.15	0.22	0.19	0.22
MgO	12.13	5.54	3.72	2.07	1.24	7.21	3.51	1.22	5.09	3.50	1.63	0.75	0.08	2.50	1.66	1.06
CaO	11.32	10.60	7.76	5.43	3.46	10.98	8.15	4.58	8.14	5.97	4.14	2.47	0.93	7.78	4.81	2.92
Na_2O	3.16	4.51	6.07	7.26	8.50	3.80	5.80	8.34	4.24	4.86	6.69	7.09	8.26	5.61	6.80	7.88
K_2O	1.48	2.09	3.11	3.70	4.57	1.74	2.67	3.85	2.25	2.78	3.53	4.74	5.24	2.52	3.88	4.45
P_2O_5	0.84	1.30	0.81	0.60	0.26	0.78	0.99	0.39	0.73	0.79	0.60	0.24	0.03	1.19	0.84	0.40
Loss	-	0.10	0.40	-	0.49	-	-	-	0.19	-	0.03	-	-	1.58	-	0.04
Sum	99.31	100.01	99.32	99.29	99.60	100.16	100.48	98.75	99.99	99.45	99.88	100.36	99.90	99.76	100.12	99.67
Trace Elements (in ppm)																
Cs	0.3	0.4	0.5	1.3	1.7	0.9	1.0	2.2	1.8	1.5	1.3	3.7	30	0.5	0.9	2.0
Rb	30	41	72	97	139	40	73	126	71	80	87	154	321	51	84	99
Ba	277	348	545	695	709	356	555	763	396	587	914	986	12	483	789	1027
Pb	4.3	11.5	7.6	15.2	24.2	<1.0	1.1	2.1	1.55	-	3.4	3.8	0.9	1.9	2.9	1.2
Sr	829	1242	1374	1194	782	795	1052	971	758	782	637	386	3	1375	1194	932
Y	37	65	41	44	47	60	62	66	66	40	45	64	93	43	55	91
Th	4.6	6.3	12.9	18.2	26.7	3.4	7.2	11.9	7.0	7.1	10.0	14.0	35.3	11.9	18.7	10.0
U	1.0	1.4	2.8	4.0	7.0	<0.3	2.0	2.7	1.0	1.8	2.6	3.3	7.9	2.8	4.3	2.6
Zr	405	745	654	1014	1288	-	577	1059	599	433	488	1362	-	507	843	1100
Hf	5.4	7.4	10.8	14.6	17.7	3.6	7.7	9.2	-	6.6	9.2	11.6	17.1	9.6	15.7	13.7
Sn	2.0	2.3	2.3	3.0	3.7	2.4	4.9	8.7	2.9	3.3	4.3	9.4	-	2.4	3.9	-
Nb	101	173	166	235	346	133	168	380	206	139	-	279	-	166	239	409
Zn	82	109	111	109	105	96	112	117	105	101	121	90	146	100	99	119
Cu	52	42	29	15	14	52	21	12	41	27	12	8	2	41	11	5
Ni	276	25	22	8	8	78	6	<5	45	17	<5	<5	<5	5	<5	<5
V	300	286	208	77	55	252	115	16	156	90	8	<5	<5	52	23	<5
Cr	469	31	56	15	8	194	8	<5	94	18	<5	<5	<5	30	9	<5

Explanation of Table 1

1. Basanite, DVDP hole 2 - 99.34 m, Hut Point Peninsula.

2. Basanite, DVDP hole 1 - 88.55 m, Hut Point Peninsula.

3. Nepheline hawaiite DVDP hole 2 - 70.41 m, Hut Point Peninsula.

4. Nepheline benmoreite, DVDP hole 2 - 54.72 m, Hut Point
    Peninsula.

5. Kaersutite phonolite (25793)*, Observation Hill, Hut Point
    Peninsula.

6. Basanite (25679), Crater 4, The Pleiades.

7. Nepheline hawaiite (25685), Crater 5, The Pleiades.

8. Nepheline benmoreite (25691) dike, Crater 2, The Pleiades.

9. Trachyandesite (25703), Aleyone Cone, The Pleiades.

10. Trachyandesite (25671) dike, west flank of Cone 3, Mt Atlas,
    The Pleiades.

11. Tristanite (25662), west base of Cone 2, Mt Atlas, The Pleiades.

12. K-trachyte (25665), Cone 4, south of Mt Atlas, The Pleiades.

13. Peralkaline K-trachyte (25706), southwest flank of Taygete
    Cone, The Pleiades.

14. Nepheline hawaiite (25754), pillow lava, Turks Head, Ross
    Island.

15. Nepheline benmoreite (25748), Tent Island, McMurdo Sound.

16. Anorthoclase phonolite (25725), summit of Mt Erebus, Ross Island.

* Sample numbers refer to the petrological collection of the

  Department of Geology, Victoria University of Wellington.

TABLE 2. Rare-earth element analyses of McMurdo Volcanic Group Rocks. (ppm)

| | Basanite-Kaersutite Phonolite Hut Point Peninsula | | | | | Basanite-Nepheline Benmoreite The Pleiades | | | Trachyandesite-Peralkaline-K-trachyte The Pleiades | | | | | Nepheline Hawaiite-Anorthoclase Phonolite Erebus Centre | | |
	1	2	3	4	5	6	7	8	9	10	11	12	13	14	15	16
La	68	110	109	160	184	73	107	165	121	89	103	130	409	97	121	159
Ce	109	201	142	215	273	142	178	255	138	148	>220	177	>220	156	194	208
Pr	15	28	25	26	24	18,3	27	34	27	18,3	22	26	59	23	24	36
Nd	56	104	90	82	70	67	94	100	85	70	78	76	171	86	90	111
Sm	10,4	16,3	13,2	11,8	10,7	14,1	18,6	16,8	12,4	12,7	16,8	13,4	24	16,5	14,0	18,1
Eu	2,5	4,4	3,6	3,3	2,6	4,0	5,5	4,5	3,3	3,4	4,7	3,3	0,6	4,2	4,1	6,3
Gd	8,4	12,6	11,4	9,1	8,4	9,5	12,8	10,7	8,0	9,4	12,4	8,8	15,9	14,3	12,0	12,9
Tb	0,9	1,3	1,1	1,1	0,9	1,0	1,2	1,2	0,9	1,0	1,4	1,2	1,5	1,4	1,5	1,3
Dy	5,0	7,7	6,5	6,4	5,7	7,2	8,7	8,0	5,6	6,0	8,8	7,9	10,3	8,6	8,5	7,2
Ho	1,0	1,4	1,5	1,3	1,4	1,2	1,7	1,3	0,9	1,2	1,6	1,2	2,4	1,7	1,7	1,5
Er	2,0	2,6	3,5	3,2	3,7	3,2	4,4	3,9	2,7	3,5	4,8	3,7	8,8	4,6	5,1	5,1
Yb	1,6	2,4	2,9	3,4	4,4	2,9	3,9	4,7	2,7	3,2	5,0	4,7	7,6	4,1	5,1	6,4
ΣREE	280	492	410	524	590	343	463	605	408	365	>509	453	>930	417	467	576
Eu/Eu*	0,88	0,98	0,97	1,03	0,87	1,09	1,13	1,05	1,05	0,99	1,05	0,96	0,10	0,91	1,04	1,31
La/Yb	42,5	45,8	37,6	47,1	41,8	25,2	27,4	35,1	44,8	27,8	20,6	27,6	53,8	23,6	23,7	24,8

lineage from The Pleiades (Fig. 6). The depletion in Ce and enrichment in Dy appear too large and regular to be an analytical error. Depletion of Ce has been reported in many lavas (Masuda, 1968; Ishikawa, 1974) and may result from the oxidation of Ce to the +4 state (Ishikawa, 1974).

A large negative europium anomaly (Eu/Eu* = 0.10) occurs in the peralkaline K-trachyte (sample 13)[3] from The Pleiades (Fig. 7), and a large positive anomaly (Eu/Eu* = 1.31) is found in the anorthoclase phonolite from Mt Erebus (Fig. 8). The negative and positive anomalies can be attributed to the depletion and accumulation, respectively, of feldspar.

Kaersutite

Kaersutite was separated from a kaersutite - plagioclase - apatite pegmatite(?) inclusion from The Pleiades. Major element analysis shows 0.60% P_2O_5 (Table 3), indicating inclusions and/or incomplete separation of apatite. Prior to REE analysis the sample was further purified using electromagnetic separation and heavy liquids. Grain mounts and x-ray diffraction did not show any apatite.

Nagasawa (1973) reported REE abundances in kaersutite from Oki Dogo Island, Japan (Fig. 3). Abundances from The Pleiades kaersutite show a similar trend, but are enriched overall, especially in light REE. Minor irregularities in the trend for the middle REE are probably due to analytical

---

[3] Sample numbers refer to those in Tables 1 and 2.

TABLE 3. Analysis of kaersutite from The Pleiades, northern Victoria Land.

Major Elements (wt percent)		Structural Formula[+]			
SiO_2	38.75	Si	5.859		
Al_2O_3	12.78	Al	2.141		
TiO_2	5.20	Al	0.136		
Fe_2O_3[†]	5.35	Ti	0.591		
FeO	9.62	Fe^{3+}	0.608	Z	8.000
MnO	0.22	Fe^{2+}	1.217	Y	5.002
MgO	10.75	Mn	0.028	X	2.589
CaO	10.90	Mg	2.422		
Na_2O	2.68	Ca	1.637	Fe^{3+}/Fe^{2+}[†]	0.50
K_2O	0.87	Na	0.786		
P_2O_5	0.60	K	0.166	$\frac{100Mg}{Mg+Fe_T+Mn}$	56.6
Sum	97.72	OH	1.982		
		Sum	17.573		

Trace Elements (ppm)		Rare Earth Elements (ppm)	
Rb	8.2	La	30
Ba	404	Ce	67
Pb	10	Pr	11
Sr	657	Nd	58
Y*	69	Sm	15
Th	3.9	Eu	3.8
U	n.d.	Gd	14
Zr*	160	Tb	1.6
Hf	4.3	Dy	9.7
Sn	1.0	Ho	1.8
Nb	159	Er	4.6
Cu*	34	Yb	3.6
Co*	33	ΣREE	221
Ni	3		
Sc*	41		
V*	210		
Cr*	6		
Ga*	20		
B*	11		

[+] Analysis recalculated to 98% apatite-free and 2% water added to make total 100%. Structural formula based on 24(O,OH).

[†] Fe^{3+}/Fe^{2+} ratio determined by Mössbauer spectroscopy.

*Determined by B. P. Kohn (Victoria University) using emission spectroscopy, all other trace elements and REE by spark source mass spectrometry.

n.d. not detected.
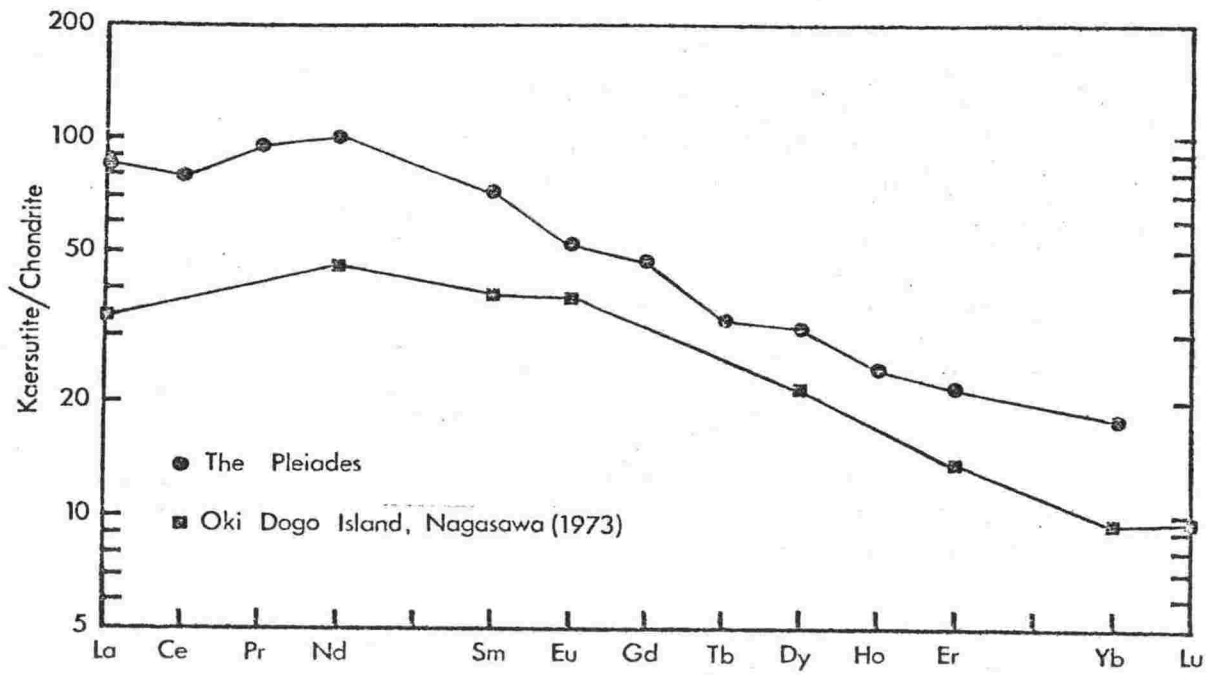
FIGURE 3. Chondrite normalised REE abundances in kaersutite.

uncertainties. Compared to the whole rock analyses, the kaersutite shows enrichment of the middle REE, hence with crystal fractionation of kaersutite residual liquids become depleted in the middle REE. This characteristic of kaersutite can be seen in the kaersutite/trachybasalt partition coefficients (Table 5), where the middle REE (Eu, Dy, Er) have a ratio greater than 1, whereas the light (Ce, Nd) and heavy (Yb) REE are less than 1.

Feldspar

Andesine $(An_{36}Ab_{52}Or_8)$ feldspar was separated from nepheline benmoreite (sample 13) and analysed (Table 4). The REE Gd to Yb were below the detection limits, however the data do show a large positive Eu anomaly (Eu/Eu* >9.9) typical of feldspars. (Fig. 4).

Anorthoclase $(An_{16}Ab_{66}Or_{18})$ from Mt Erebus summit contains higher REE abundances (Table 4) and a smaller Eu anomaly (Eu/Eu* = 4.5) than the andesine plagioclase.

Basanite - phonolite. Kaersutite lineage (Hut Point Peninsula and DVDP 1 and 2)

Chondrite normalised REE patterns for basanite-phonolite lavas from Hut Point Peninsula are shown in Fig. 5. Two lavas classified as basanite have parallel trends (Fig. 5) but one sample is enriched by a factor of about 2. The basanite with the lowest REE concentration is termed a primitive basanite, while the REE enriched sample is termed a fractionated basanite. Other lavas in the lineage generally show a continuous enrichment

TABLE 4.   Analyses of feldspar in lavas of the McMurdo Volcanic Group.

Major Elements (wt percent)	1	2	Structural Formulae On the basis of 32 (O)	1	2
SiO_2	58.31	61.61	Si	10.508	11.131
Al_2O_3	25.82	22.32	Al	5.486	4.754
TiO_2	0.18	0.19	Ti	0.024	0.026
Fe_2O_3*	0.36	0.75	Fe^{3+}	0.049	0.102
MnO	-	0.03	Mn	-	0.004
MgO	-	0.27	Mg	-	0.073
CaO	7.23	3.35	Ca	1.396	0.648
Na_2O	6.20	7.49	Na	2.166	2.623
K_2O	1.34	3.17	K	0.308	0.730
Total	99.44	99.18			
Rb	<1				
Ba	518		Z	15.994	16.090
Sr	2913		X	3.943	4.001
Zn	8		Σ	19.937	20.091
Cu	10				
			An	36.0	16.2
			Ab	56.0	65.6
			Or	8.0	18.2

Rare Earth Elements (ppm)

	1	2
La	(38)[+]	(45)
Ce	(68)	(90)
Pr	6.3	9.3
Nd	18	31
Sm	3.0	6.0
Eu	8.9	7.5
Gd	<3.0	4.9
Tb	<0.3	0.85
Dy	<1.0	(3.9)
Ho	<0.3	0.7
Er	<0.6	1.8
Yb	<1.0	1.7

* Total Fe as Fe_2O_3.

[+] Values in brackets estimated by extrapolation and interpolation of chondrite normalised trend (Fig. 4).

1. Andesine plagioclase from nepheline benmoreite (25748) (sample 15, Tables 1 and 2), Tent Island, McMurdo Sound.

2. Anorthoclase phenocrysts from anorthoclase phonolite, Mt Erebus summit.
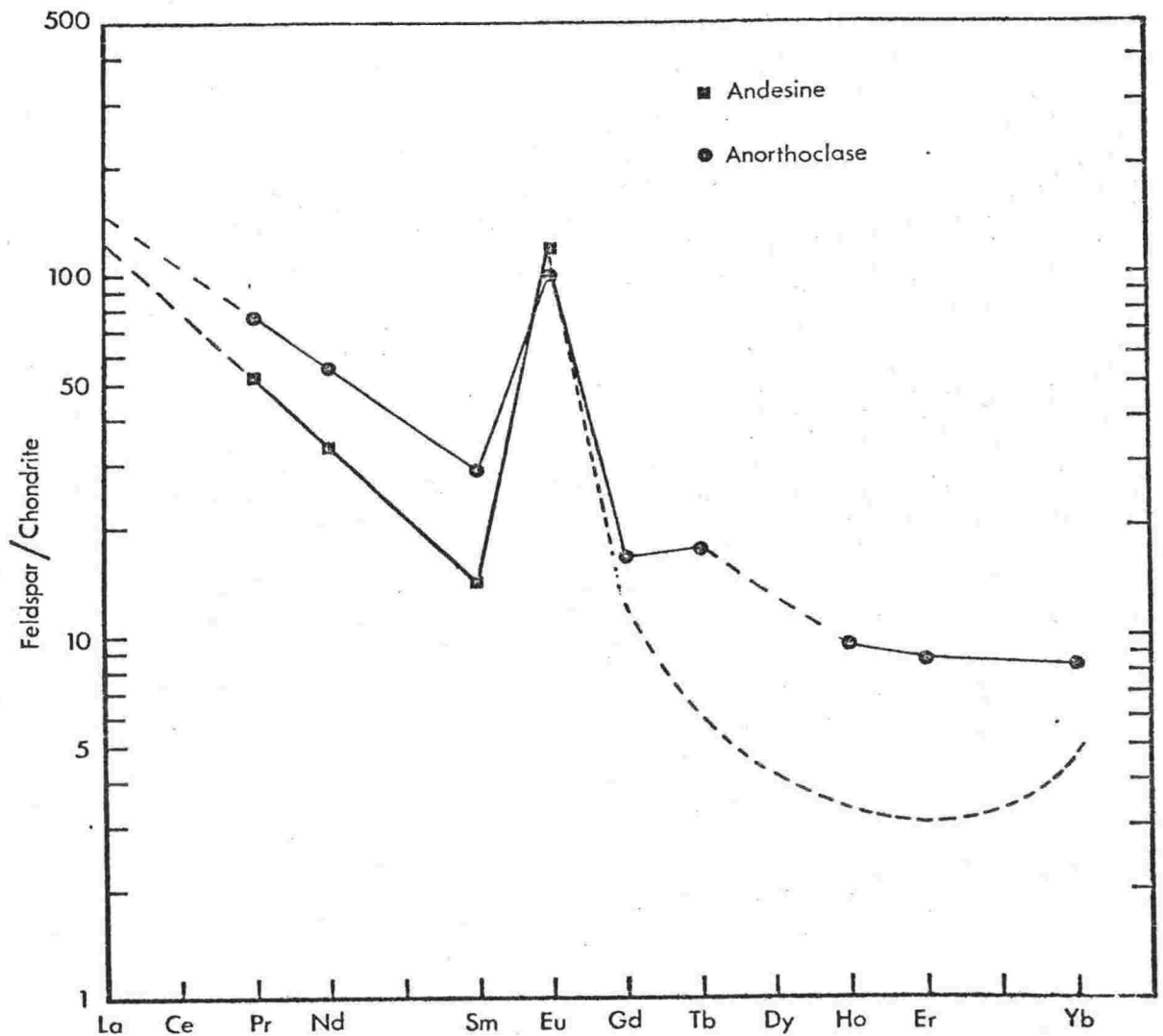
FIGURE 4. Chondrite normalised REE abundances in feldspar from Erebus volcanic province lavas. Anorthoclase (dots) from Mt Erebus summit. Andesine plagioclase (squares) from nepheline benmoreite (Table 1, sample 15), Tent Island. In the andesine sample elements from Gd to Yb were below the limit of detection, the short dashed line indicates approximately the lower limits of detection.
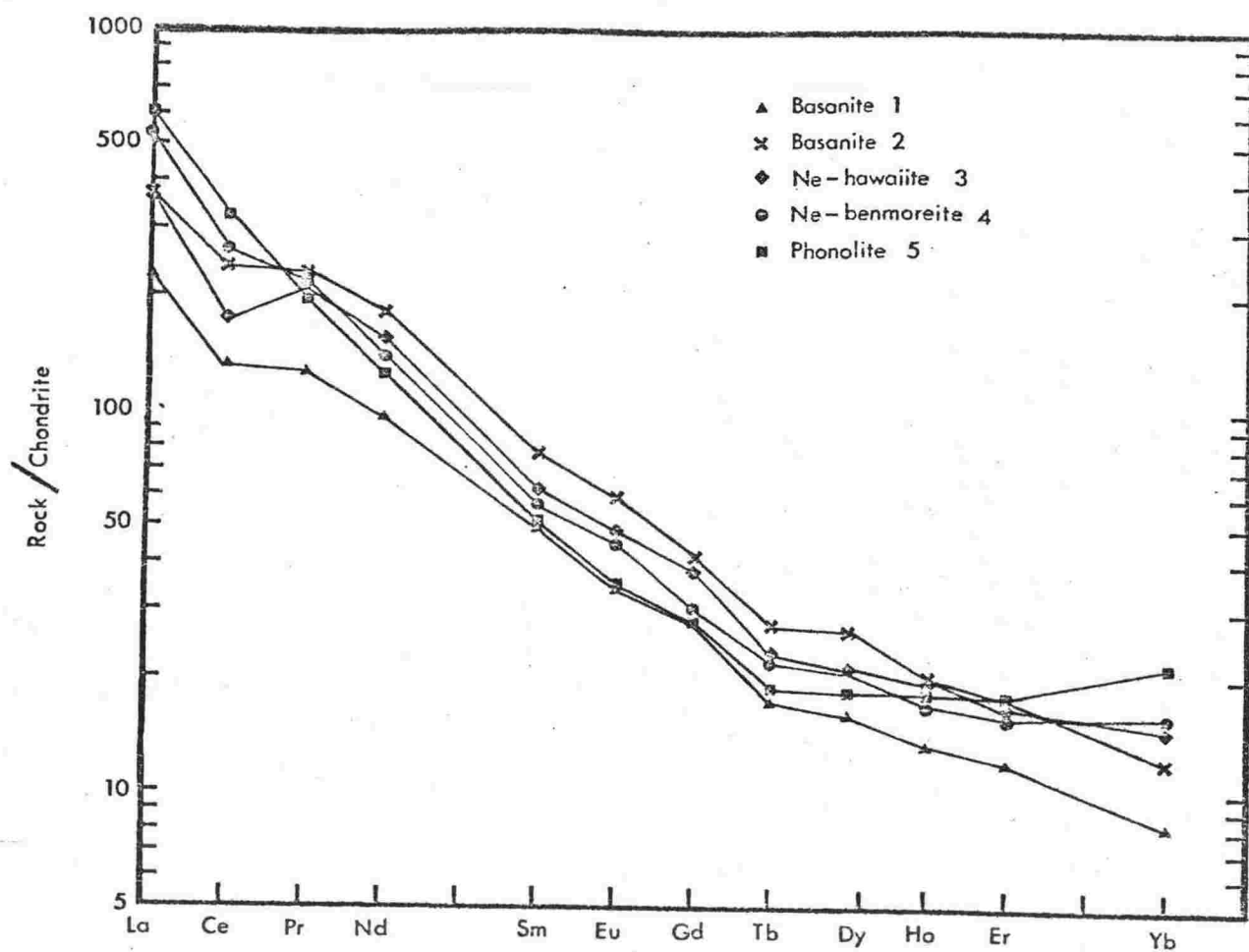
FIGURE 5. Chondrite normalised REE abundances in basanite-phonolite lavas from Hut Point Peninsula and DVDP holes 1 and 2, Erebus volcanic province.

of the light REE (La, Ce) and heavy REE (Er, Yb). The middle REE are depleted, decreasing in abundance with increased differentiation. Abundance of the middle REE (Sm to Tb) (Fig. 5) in the phonolite nearly equals that of the primitive basanite.

Basanite - nepheline benmoreite.   (The Pleiades)

The trends for the basanite - nepheline benmoreite lineage lavas from The Pleiades (Fig. 6) are very similar to Hut Point Peninsula and DVDP lavas (Fig. 5). Throughout the lineage, enrichment occurs in the light REE (La, Ce, Pr, Nd) and the heavy REE (Yb). The nepheline hawaiite is enriched in all REE relative to the basanite. However, the nepheline benmoreite shows a depletion of the middle REE (Sm to Er) relative to the nepheline hawaiite. All lavas have a small positive Eu anomaly.

Trachyandesite - peralkaline K-trachyte.   (The Pleiades)

The trachyandesites, tristanite and K-trachyte lavas have similar overlapping chondrite normalised patterns (Fig. 7). There is a regular pattern observed for the middle and heavy REE (Sm to Yb) where the trends of increasing REE content are from trachyandesite to K-trachyte to tristanite.

The most striking feature is the extreme enrichment of REE (except Eu) in the peralkaline K-trachyte, with La being enriched by a factor of 1350 over the chondrite abundances. The very large negative Eu anomaly (Eu/Eu* = 0.10) is also noteworthy.
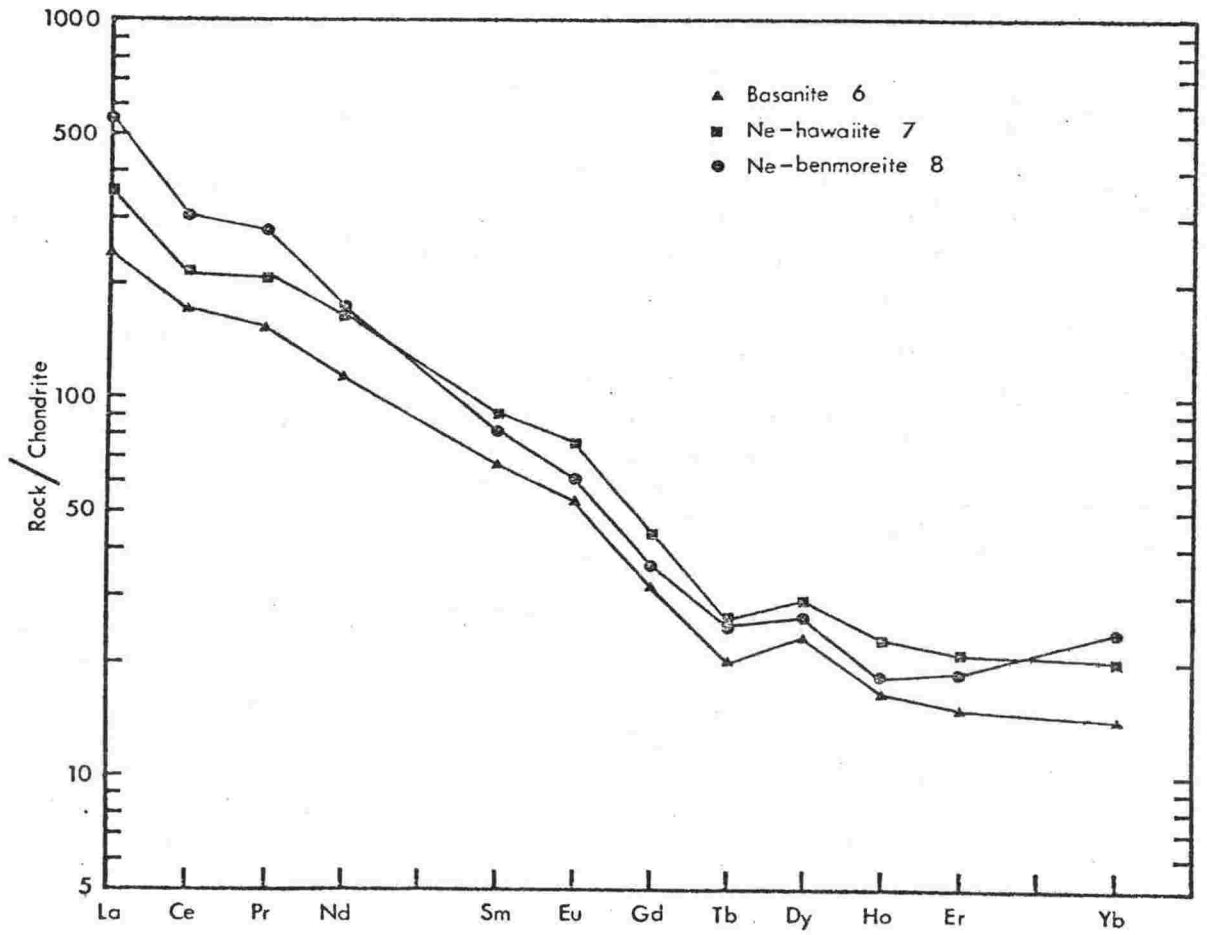
FIGURE 6. Chondrite normalised REE abundances in basanite-nepheline hawaiite — nepheline benmoreite lavas from The Pleiades, Melbourne volcanic province.
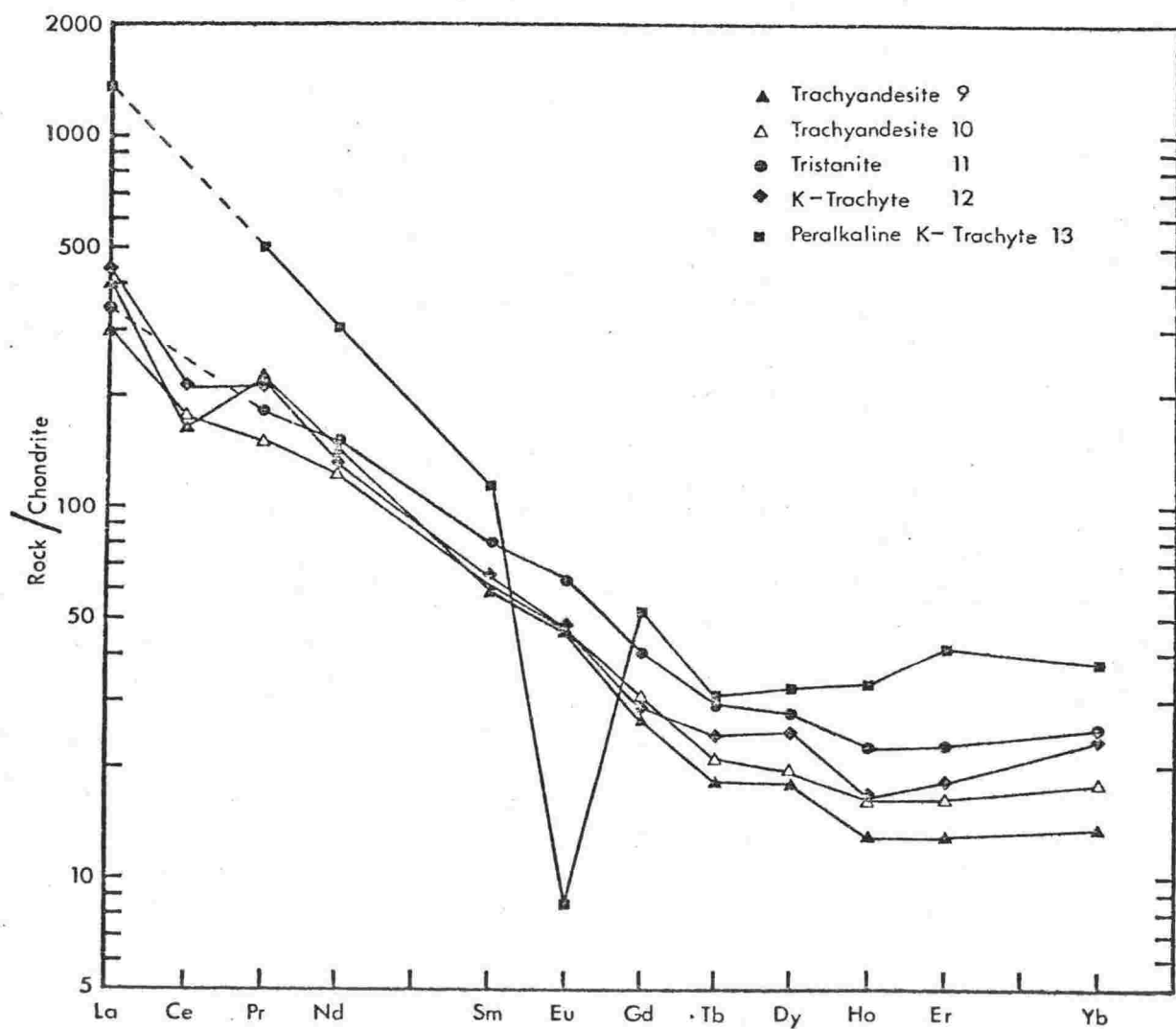
FIGURE 7. Chondrite normalised REE abundances in trachyandesite-peralkaline K-trachyte lavas from The Pleiades, Melbourne volcanic province.

Nepheline hawaiite - anorthoclase phonolite. Erebus lineage
(Erebus Centre)

Three Erebus Centre lavas, of the Erebus lineage, show
very similar chondrite normalised patterns with enrichment of
light REE (La to Nd) and heavy REE (Er to Yb) and some overlap
in the middle REE (Fig. 8). All samples have a negative Ce
anomaly. Anorthoclase phonolite has a strong positive Eu anomaly
(Eu/Eu* = 1.31) and the nepheline hawaiite a weak negative Eu
anomaly (Eu/Eu* = 0.91) (Fig. 8).

INTERPRETATION

Basanite - nepheline benmoreite - phonolite. (The Pleiades
and Hut Point Peninsula)

The basanite-phonolite lineage at Hut Point Peninsula (the
kaersutite lineage) and the basanite-nepheline benmoreite lineage
from The Pleiades are considered similar and are discussed
together.

There is a general enrichment in all REE from basanite to
nepheline hawaiite and fractionated basanite in The Pleiades
and Hut Point Peninsula lavas respectively. The mineralogy of
the basanites and an observed depletion of Cr and Ni with
differentiation, indicate olivine+augite+spinel have probably
fractionated. This is compatible with the overall increase in
REE abundances.

Other lavas in the two lineages generally show a continuous
enrichment of the light REE (La, Ce) and heavy REE (Er, Yb),
while the middle REE are depleted, decreasing in abundance with
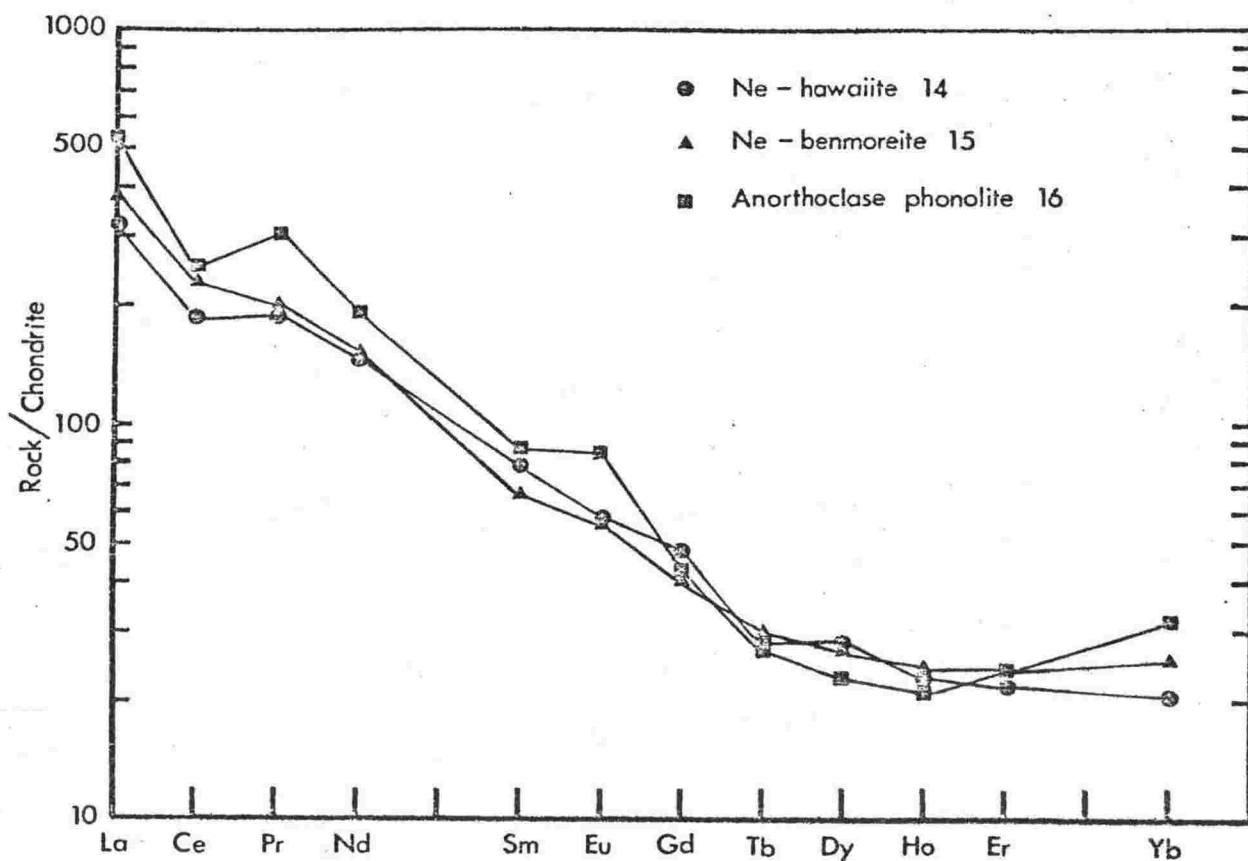
FIGURE 8. Chondrite normalised REE abundances in nepheline hawaiite-
nepheline benmoreite-anorthoclase phonolite (kenyte) lavas from
Mt Erebus and surrounds, Erebus volcanic province.

increased differentiation. Kaersutite and augite are the
dominant phenocrysts or microphenocryst phases in these lavas.
The depletion of the middle REE indicates that fractionation of
augite and kaersutite probably resulted in the observed trends.
The ability of kaersutite to deplete the middle REE has already
been discussed.

The nepheline hawaiite from Hut Point Peninsula has higher
Cr and lower Nb, Zr, Pb, La, Ce and Pr than the fractionated
basanite, indicating the two lavas probably cannot be related by
a simple crystal fractionation model. Trace element geochemistry
(Table 1) of the nepheline hawaiite is, however, compatible with
its derivation by crystal fractionation of olivine+augite+
kaersutite+spinel from the primitive basanite. The nepheline
benmoreite in the Hut Point Peninsula lineage is then derived by
fractionation of kaersutite+augite+apatite+spinel+feldspar from the
nepheline hawaiite, and similarly the phonolite from the nepheline
benmoreite.

In order to evaluate the role of kaersutite fractionation
in the Hut Point Peninsula lineage, a series of petrographic mixing
least squares mass balance calculations (Bryan et al., 1969)
were made using the whole rock major element analyses (Table 1)
and representative electron microprobe mineral analyses from the
DVDP lavas (Kyle, 1974). Using the solutions from these
calculations (Fig. 9), REE abundances were calculated in a similar
manner to Zielinski and Frey (1970) and Zielinski (1975).
Partition coefficients used are listed in Table 5, the partition
of REE by the spinel and ilmenite was assumed to be zero. In
general the calculated REE are within 30% of the measured value
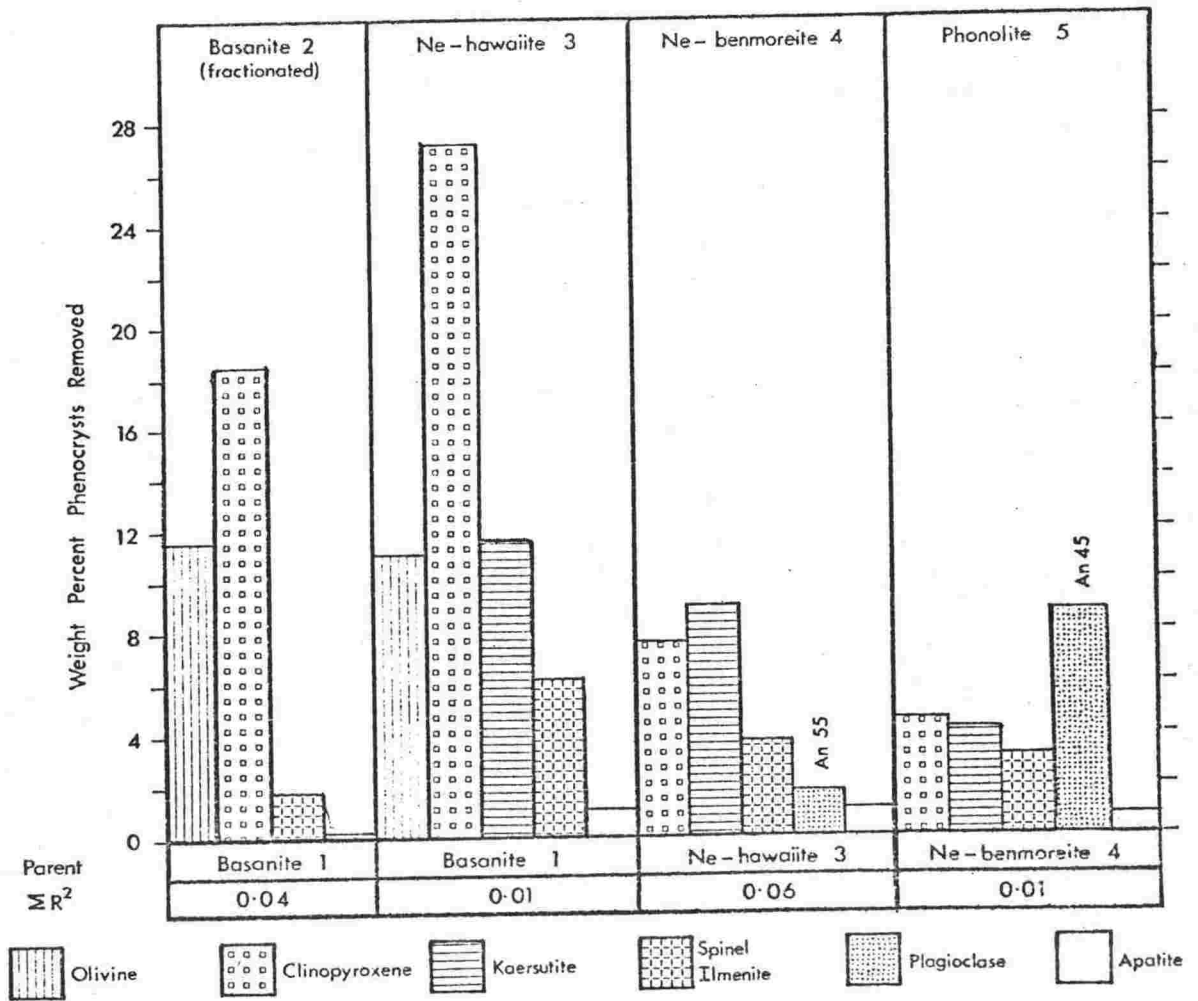
FIGURE 9. Weight percent of minerals removed to form each rock by crystal fractionation from a parent liquid. Lava type formed is shown along the top, while the parent liquid is listed at the bottom. Numbers refer to analyses in Table 1. Calculations were made using the computer program of Bryan *et al.*, (1969) and mineral data given in Kyle (1974). ΣR^2 is the sum of the residuals (measured concentration - calculated concentration) squared, for the major element mass balance.

TABLE 5.   Partition coefficients of REE

	Ol/liq	Cpx/Liq	Kaer/Liq	Ap/Liq	Plag/Liq (An$_{65}$)	Plag/Liq (An$_{46}$)
Ce	0.009	0.077	(0.43)	16.6	0.023	0.113
Pr	(0.010)*	(0.126)	(0.50)	18.0	(0.023)	(0.091)
Nd	0.010	0.174	0.63	21.0	0.023	0.069
Sm	0.011	0.260	0.94	20.7	0.024	0.035
Eu	0.010	0.273	1.02	14.5	0.232	0.392
Gd	0.012	(0.325)	(1.05)	21.7	(0.017)	(0.026)
Tb	(0.013)	(0.326)	(1.1)	(19.8)	(0.018)	(0.023)
Dy	0.014	0.351	1.19	16.9	0.018	0.019
Ho	(0.016)	(0.340)	(1.12)	(15.5)	(0.019)	(0.010)
Er	0.017	0.330	1.05	14.1	0.020	0.010
Yb	(0.023)	0.294	0.88	9.4	0.030	0.006
Source	1	1	2	3	1	1

1. Schnetzler and Philpotts (1970).

2. Nagasawa (1973)

3. Nagasawa and Schnetzler (1971).

* Values in brackets determined by interpolation and extrapolation.

(Table 6). There is considerable uncertainty in the partition coefficients, so that errors in the calculated REE concentrations are a function of both analytical error and partition uncertainties, ±30% is therefore a minimum uncertainty. The data clearly indicate the importance of crystal fractionation of kaersutite and augite in the formation of the sodic basanite-phonolite lineage from Hut Point Peninsula. By analogy, fractionation of kaersutite+augite must have occurred to give the observed REE in the nepheline benmoreite at The Pleiades.

Trachyandesite - peralkaline K-trachyte. (The Pleiades)

In the potassic trachyandesite-tristanite-K-trachyte-peralkaline K-trachyte lineage the light REE are scattered when plotted on chondrite normalised diagrams and any interpretation of their abundances is ambiguous. The continuous enrichment of incompatible elements Rb, Pb, Th, U and Sn indicates the lava sequence is probably a result of crystal fractionation. Plots of the individual REE against the residual liquid fraction (f) of Barberi et al., (1975) show two trends (Fig. 10):

1.   The light REE La and Pr decrease from trachyandesite (sample 9) to trachyandesite (sample 10) and then increase throughout the lineage. Nd is similar except it remains nearly constant from tristanite to K-trachyte (Fig. 10).

2.   Ce and remaining REE from Sm to Yb, excluding Eu, all show the same trend of increasing REE from trachyandesite to tristanite and then a decrease to K-trachyte followed by a rapid increase to the peralkaline K-trachyte. Eu is similar

TABLE 6. Calculated and observed REE abundances in lavas from Hut Point Peninsula (ppm)

	Basanite (Fractionated)		Nepheline hawaiite		Nepheline benmoreite		Phonolite	
	Calc	Obs	Calc	Obs	Calc	Obs	Calc	Obs
Ce	151	201	185	142	193	215	205	273
Pr	18	28	24	25	24	26	25	24
Nd	76	104	68	89	65	82	65	70
Sm	13.8	16.3	11.4	13.2	10.4	11.8	10.3	10.7
Eu	3.4	4.4	3.3	3.6	3.2	3.3	3.2	2.6
Gd	10.2	12.6	9.0	11.4	8.0	9.1	7.8	8.4
Tb	1.2	1.3	1.0	1.1	0.9	1.1	0.9	0.9
Dy	6.6	7.7	6.1	6.5	5.6	6.4	5.7	5.7
Ho	1.3	1.4	1.4	1.5	1.3	1.3	1.3	1.4
Er	2.7	2.6	3.3	3.5	3.2	3.2	3.4	3.7
Yb	2.2	2.4	2.6	2.9	2.8	3.4	3.1	4.4

FIGURE 10   Individual REE plotted against C^O_{Rb}/C_{Rb} (the residual liquid fraction of Barberi *et al.*, 1975) for the potassic trachyandesite-peralkaline K-trachyte lineage from The Pleiades. C^O_{Rb} = 36, was calculated from a plot of Cr versus Rb, for all lavas from The Pleiades. arrows above two values for Ce, indicate the concentration is greater than 220 ppm. All values in ppm.
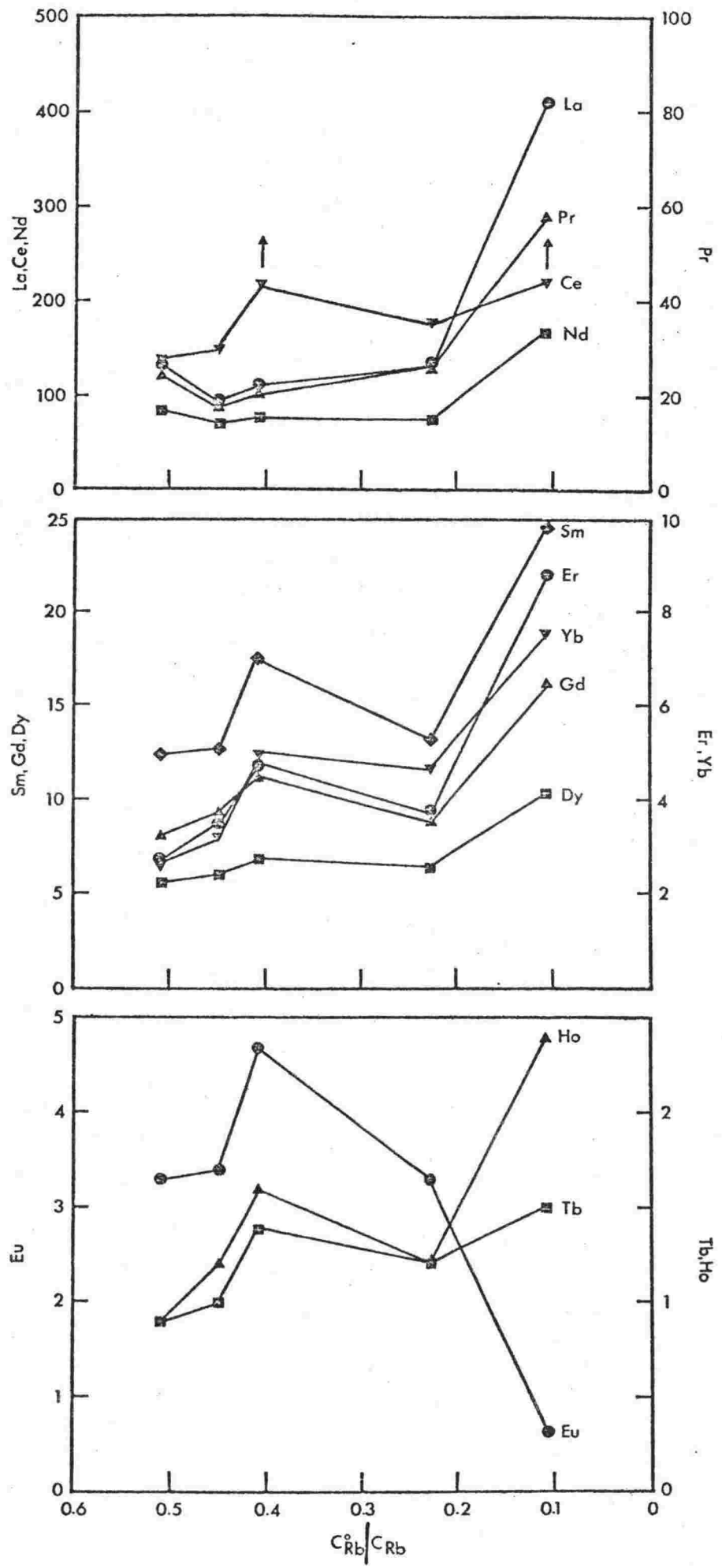
except it is depleted from K-trachyte to peralkaline K-trachyte (Fig. 10).

The lavas contain phenocrysts and microphenocrysts of olivine, augite, magnetite, feldspar (minor), kaersutite (rare) and apatite. Cognate plutonic inclusions with cumulate textures indicate fractionation of olivine, augite and magnetite. It is therefore suggested that the enrichment of REE shown by trend 2 above from trachyandesite to tristanite is compatible with the fractionation of the cumulus phases found in the inclusions. REE abundances decrease from tristanite to K-trachyte, indicating fractionation of a REE rich phase, for which apatite appears to be the probable source. This is supported by the rapid decrease in P_2O_5 content (Table 1) from 0.60% in the tristanite to 0.24% in the K-trachyte. The fractionated phases will therefore be similar to those involved in the trachyandesite-tristanite transition, except for a higher proportion of apatite. The large Eu depletion in the peralkaline K-trachyte must be the result of feldspar fractionation (Philpotts and Schnetzler, 1968; Weill and Drake, 1973). The above model of fractionation is supported by all REE except La, Pr and Nd, and the only inconsistency with these is the increase in La and Pr from tristanite to K-trachyte, when all other elements show a decrease (Fig. 10), and the high abundances of La, Pr and Nd in trachyandesite (sample 9).

The REE data clearly demonstrate the importance of feldspar fractionation in the formation of peralkaline lavas. Processes proposed for the formation of peralkaline lavas are partial melting of continental crust, contamination by volatile-rich

fluids and fractional crystallization of a basaltic magma.
Only rarely do a complete suite of basaltic to peralkaline lavas
exist at any one volcanic centre (Barberi et al., 1975), making
it difficult to demonstrate clearly the importance of fractional
crystallization processes. Although a basanite parent for the
potassic lineage at The Pleiades is assumed, the remaining
trachyandesite to tristanite lavas clearly demonstrate the
importance of fractional crystallization in the formation of
peralkaline lavas. Feldspar fractionation late in the differen-
tiation sequence gives rise to the peralkaline lavas.

Nepheline hawaiite - anorthoclase phonolite. (Erebus Centre)

Erebus Centre lavas (the Erebus lineage) are strongly
porphyritic. The nepheline hawaiite and nepheline benmoreite
contain abundant plagioclase phenocrysts and the anorthoclase
phonolite has large (up to 30 mm) anorthoclase phenocrysts.

The large positive Eu anomaly (Eu/Eu* = 1.31) in the
anorthoclase phonolite (sample 16) indicates a cumulate origin
for some anorthoclase, assuming the parental magma for the
lineage had no Eu anomaly (Eu/Eu* = 1.0). In order to make a
correction for the cumulus anorthoclase the whole rock REE
analysis of anorthoclase phonolite was adjusted by removing
anorthoclase (Table 4) until there was no Eu anomaly. The
REE data suggest 27% cumulus anorthoclase (Table 7).

No correction was applied to the nepheline benmoreite
(sample 15, Eu/Eu* = 1.04) as the REE data for the andesine
phenocrysts (Table 4) were incomplete and the Eu anomaly of the
nepheline benmoreite was only small.

TABLE 7. Whole rock REE analysis of anorthoclase phonolite (sample 16) and REE analysis after adjustment for 27% cumulus anorthoclase (Table 4, sample 2) (ppm).

	Whole Rock	Less 27% anorthoclase
La	159	(201)[+]
Ce	208	(252)
Pr	36	46
Nd	111	140
Sm	18.1	22
Eu	6.3	5.8
Gd	12.9	15.9
Tb	1.3	1.5
Dy	7.2	(8.4)
Ho	1.5	1.8
Er	5.1	6.3
Yb	6.4	8.1
ΣREE	576	708
Eu/Eu*	1.31	0.99
La/Yb	24.8	24.8

[+]Values in brackets indicate extropolated and interpolated REE for anorthoclase (Table 4) were used.
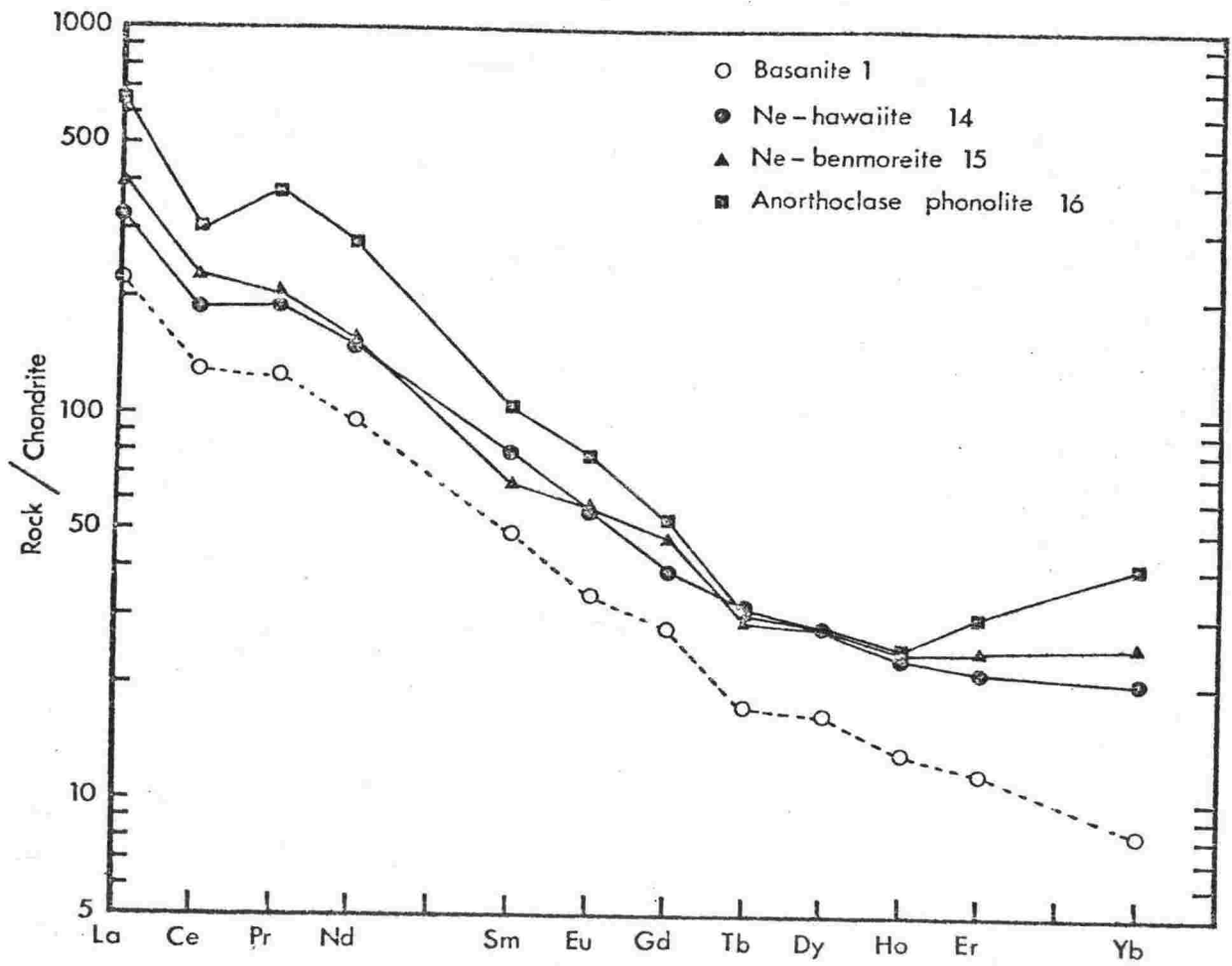
FIGURE 11. Chondrite normalised REE abundances in nepheline hawaiite, nepheline benmoreite and anorthoclase phonolite corrected for 27% cumulus anorthoclase (Table 7), from the Erebus Centre. Basanite (sample 1, Fig. 5) assumed to be similar to the parental magma for the lineage.

Chondrite normalised REE abundances in the recalculated anorthoclase phonolite (Table 7) and other lavas of the Erebus lineage are plotted in Fig. 11. In general there is an increase in REE from nepheline hawaiite to nepheline benmoreite to anorthoclase phonolite. There is some overlap in the middle REE and all three samples have very similar Tb, Dy and Ho abundances. A basanite, similar to that in the DVDP core (sample 1, Table 1) is assumed to be the parental magma for the lineage. The REE abundances in the Erebus lineage lavas are enriched relative to the basanite, mainly with a parallel trend, although the Erebus Centre lavas do show a progressive enrichment in Er and Yb (Fig. 11).

Comparing equivalent kaersutite lineage and Erebus lineage lavas (Table 2) it is obvious the latter contain higher middle and heavy REE. The depletion of middle REE in the kaersutite lineage has been attributed to kaersutite fractionation; this, however, is not the case in the Erebus lineage. Olivine, augite and magnetite are the main mafic phenocryst phases in the intermediate lavas of the Erebus lineage. Fractionation of these was probably responsible for the observed patterns of increasing REE abundances. Some apatite fractionation is indicated by the decrease in P_2O_5 through the lineage (Table 1) but this, however, did not result in any marked depletion in REE (cf. K-trachyte from The Pleiades).

BASANITE ORIGIN

DVDP basanite (Table 1, sample 1) has a high pressure mineralogy (chrome spinels and Ca-tschermak rich pyroxenes) and a high Mg number (Mg/Mg+Fe^{2+} atomic, Kesson, 1973) which suggests it is unlikely to have undergone fractionation ascending from the mantle. Kay and Gast (1973) reviewed REE abundances in alkali basaltic lavas and considered the lavas formed by small amounts of partial melting of hydrous garnet peridotite at the top of the asthenosphere. Shimizu and Arculus (1975) developed a model of 2-17% partial melting of a garnet lherzolite mantle (with chondrite REE abundances) to give the observed REE patterns in basanitoid and alkali basalt lavas from Grenada. DVDP basanite has a slightly more fractionated REE pattern than the Grenada lavas, but is similar (Fig. 12) to olivine nephelinites from Hawaii (sample K 17) and Fernando de Noronha (sample FN 8-1) (Kay and Gast, 1973). Kay and Gast (1973) developed partial melting models of garnet peridotite involving varying proportions of clinopyroxene and garnet, and varying degrees of partial melting, to explain the REE patterns in alkali basalts and nephelinites. Sun and Hanson (1975) have discussed REE abundances in basanites from Ross Island and believe they form from 3 to 7% melting, of a garnet-bearing mantle with a REE pattern in which La is enriched 14 times chondrite and Yb is about 3 times chondrite.

Until better information is available on mantle compositions and the distribution of REE in them, there will be a range of partial melt models. The results of Kay and Gast (1973) indicate, however, that the DVDP basanite probably formed by a low degree
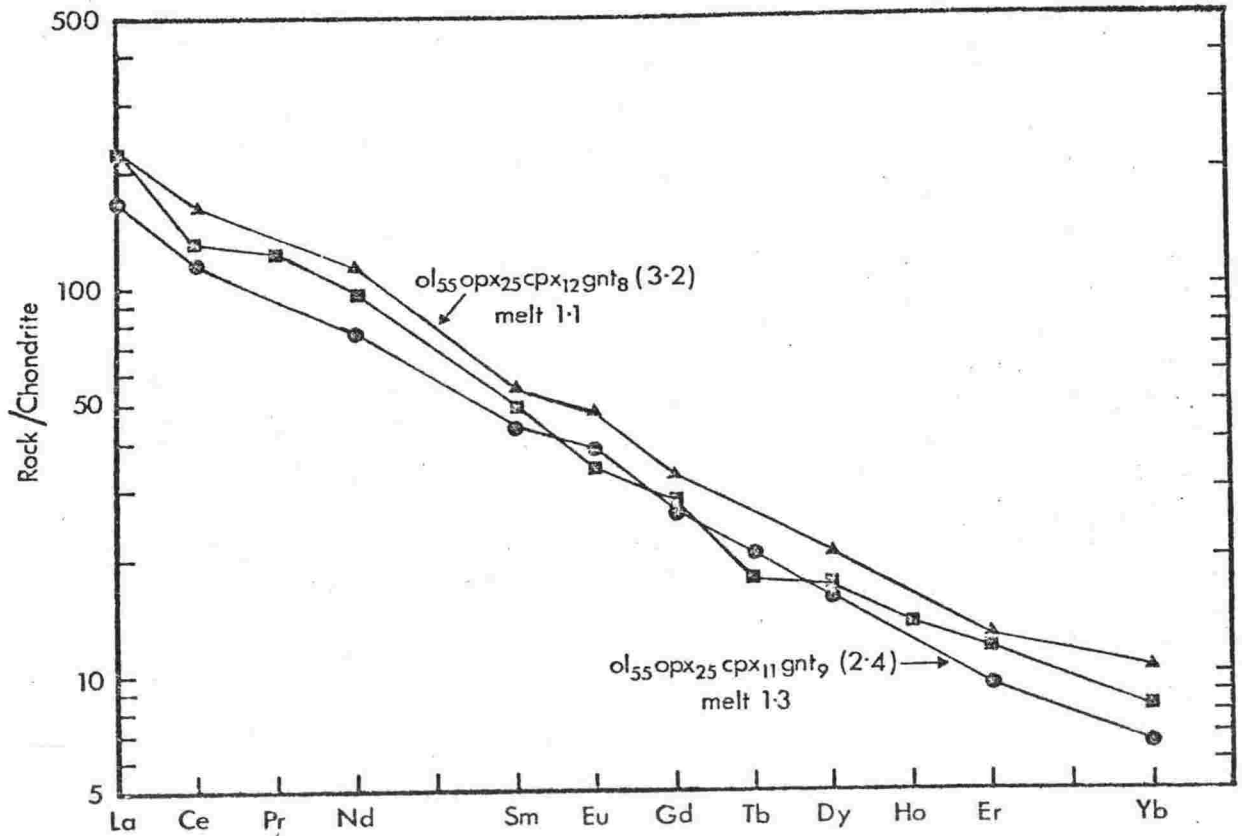
FIGURE 12. Comparison of chondrite normalised REE abundances in DVDP
basanite (Table 1, sample 1) (squares) with olivine nephelinites
from Kauai, Hawaii (sample K17) (dots) and Fernando de Noronha
(sample FN8-1) (triangles), from Kay and Gast (1973). Shown are
the assumed mantle compositions and (in parentheses) the REE-
enrichment of the mantle material over chondrite abundances used
in calculating partial melting mantle models for the generation
of the olivine nephelinites (Kay and Gast, 1973). Melt figures
indicate the degree of melting required to give the observed
REE abundances in the olivine nephelinites.

of partial melting (1-2%) of a hydrous garnet peridotite mantle which has a REE concentration 2 to 3 times chondrite.

CONCLUSIONS

REE data on four lava lineages from The Pleiades and Ross Island indicates they formed by crystal fractionation. Major element mass balance models have been used to show the importance of kaersutite as a fractionated phase in strongly undersaturated differentiation sequences.

Two basanite to nepheline benmoreite and phonolite lineages are depleted in middle REE as a result of kaersutite fractionation. A further basanite(?) - phonolite lineage, from Mt Erebus and vicinity, apparently fractionated under lower P_{H_2O} conditions without the appearance of kaersutite. Although the major element data are similar to the kaersutite-bearing lineages, the middle REE have higher concentrations as a result of olivine, augite, magnetite and minor apatite fractionation.

Mildly potassic trachyandesite to peralkaline K-trachyte lavas from The Pleiades have a scatter in REE, which are, however, considered consistent with crystal fractionation of olivine, augite, magnetite and apatite. Extensive apatite fractionation resulted in lower REE abundances in K-trachyte compared to a less differentiated tristanite. The development of peralkalinity by feldspar fractionation is conclusively demonstrated by a large depletion of Eu in the peralkaline K-trachyte.

REFERENCES

BARBERI F., SANTACROCE R., FERRARA G., TREUIL M. and VARET J. (1975) A transitional basalt-pantellerite sequence of fractional crystallization, the Boina Centre (Afar Rift, Ethiopia). J. Petrology 16, 22-56.

BRYAN W. B., FINGER L. W. and CHAYES F. (1970) Estimating proportions in petrographic mixing equations by least squares approximation. Science 163, 672-679.

COOMBS D. S. and WILKINSON J.F.G. (1969) Lineages and fractionation trends in undersaturated volcanic rocks from the East Otago Volcanic Province (New Zealand) and related rocks. J. Petrology 10, 440-501.

FLOWER M.F.J. (1971) Rare earth element distribution in lavas and ultramafic xenoliths from the Comores Archipelago, Western Indian Ocean. Contr. Mineral and Petrol. 31, 335-346.

GAST P. W. (1968) Trace element fractionation and the origin of tholeiitic and alkaline magma types. Geochim. Cosmochim. Acta 32, 1057-1086.

GOLDICH S. S., TREVES S. B., SUHR N. H. and STUCKLESS J. S. (1975) Geochemistry of the Cenozoic volcanic rocks of Ross Island and vicinity, Antarctica. J. Geology 83, 415-435.

HOWORTH R. and RANKIN P. C. (1975) Multi-element characterisation of glass shards from stratigraphically correlated rhyolitic tephra units. Chem. Geol. 15, 239-250.

ISHIKAWA H. (1974) Distribution of rare earths in volcanic rocks. In Physical Volcanology (ed. Civetta L., Gasparinni P., Luonga G. and Rapolla A.). Elsevier. p.241-253.

KAY R. W. and GAST P. W. (1973) The rare earth content and
    origin of alkali-rich basalts. J. Geology 81, 653-682.

KESSON S. E. (1973) The primary geochemistry of the Monaro
    alkaline volcanics, Southeastern Australia - Evidence for
    upper mantle heterogeneity. Contr. Mineral and Petrol. 42,
    93-108.

KYLE P. R. (1974) Electron microprobe analyses of minerals in
    core samples from Dry Valley Drilling Project (DVDP)
    holes 1 and 2, Ross Island, Antarctica. Antarctic Data
    Series 4, Publication of Department of Geology, Victoria
    University of Wellington 4: 27 pp.

KYLE P. R. and COLE J. W. (1974) Structural control of volcanism
    in the McMurdo Volcanic Group, Antarctica. Bull.
    Volcanologique 38, 16-25.

KYLE P. R. and TREVES S. B. (1974) Geology of DVDP 3, Hut Point
    Peninsula, Ross Island, Antarctica. Dry Valley Drilling
    Project (Northern Illinois University) Bulletin 3, 13-48.

MASUDA A. (1968) Geochemistry of lanthanides in basalts of
    Central Japan. Earth Planet. Sci. Lett. 4, 284-292.

MASUDA A., NAKAMURA N. and TANAKA T. (1971) Rare earth elements
    in metagabbros from the mid-Atlantic Ridge and their possible
    implications for the genesis of alkali olivine basalts as
    well as the Lizard peridotite. Contr. Mineral. and Petrol.
    32, 295-306.

NAGASAWA H. (1973) Rare-earth distribution in alkali rocks from
    Oki-Dogo Island, Japan. Contr. Mineral. and Petrol. 39,
    301-308.

NAGASAWA H. and SCHNETZLER C. C. (1971) Partitioning of rare
    earth, alkali and alkaline earth elements between

phenocrysts and acidic igneous magma. Geochim. Cosmochim. Acta 35, 953-968.

NORRISH K. and HUTTON J. T. (1969) An accurate X-ray spectrographic method for the analysis of a wide range of geological samples. Geochim. Cosmochim. Acta 33, 431-454.

PHILPOTTS J. A. and SCHNETZLER C. C. (1968) Europium anomalies and the genesis of basalt. Chem. Geol. 3, 5-13.

PRICE R. C. and TAYLOR S. R. (1973) The geochemistry of Dunedin Volcano, East Otago, New Zealand: Rare earth elements. Contr. Mineral. and Petrol. 40, 195-205.

SCHILLING J. G. and WINCHESTER J. W. (1969) Rare earth contribution to the origin of Hawaiian lavas. Contr. Mineral. and Petrol. 23, 27-37.

SCHNETZLER C. C. and PHILPOTTS J. A. (1970) Partition coefficients of rare-earth elements between igneous matrix material and rock-forming mineral phenocrysts - II. Geochim. Cosmochim. Acta 34, 331-340.

SHAPIRO L. and BRANNOCK W. W. (1962) Rapid analysis of silicate, carbonate and phosphate rocks. U.S. Geol. Survey Bull. 1144-A.

SHIMIZU N. and ARCULUS R. J. (1975) Rare earth element concentrations in a suite of basanitoids and alkali olivine basalts from Grenada, Lesser Antilles. Contr. Mineral. and Petrol. 50, 231-240.

SUN S. S. and HANSON G. N. (1975) Origin of Ross Island basanitoids and limitations upon the heterogeneity of mantle sources for alkali basalts and nephelinites. Contr. Mineral. and Petrol. 52, 77-106.

TAYLOR S. R. (1965) Geochemical analysis by spark source mass spectrography. Geochim. Cosmochim. Acta 29, 1243-1261.

TAYLOR S. R. (1971) Geochemical application of spark source mass
    spectrography - II. Photoplate data processing. Geochim.
    Cosmochim. Acta 35, 1187-1196.

TREVES S. B. and KYLE P. R. (1973) Geology of DVDP 1 and 2, Hut
    Point Peninsula, Ross Island, Antarctica. Dry Valley
    Drilling Project (Northern Illinois University) Bulletin
    2, 11-82.

WEILL D. F. and DRAKE M. J. (1973) Europium anomaly in plagioclase
    feldspar: experimental results and semiquantitative models.
    Science 180, 1059-1060.

ZIELINSKI R. A. (1975) Trace element evaluation of a suite of
    rocks from Reunion Island, Indian Ocean. Geochim.
    Cosmochim. Acta 39, 713-734.

ZIELINSKI R. A. and FREY F. A. (1970) Gough Island: Evaluation
    of a fractional crystallization model. Contr. Mineral. and
    Petrol. 29, 242-254.

CHAPTER EIGHT

"MINERALOGY AND GLASS CHEMISTRY OF RECENT

VOLCANIC EJECTA FROM MT EREBUS, ROSS ISLAND,

ANTARCTICA"

A paper presented here in manuscript form.

Electron microprobe analyses referred to
in this paper are given in Appendix B, Part 3.

Abstract

Bombs erupted in 1972 and recent flows of anorthoclase phonolite from Mt Erebus contain phenocrysts of anorthoclase and microphenocrysts of olivine ($Fa_{46}Te_3Fo_{51}$), pyroxene ($Wo_{48}Fs_{15}En_{37}$), titanomagnetite (Usp_{70}), pyrrhotite and apatite; the associated glass is peralkaline (agpaitic index = 1.06). Glass inclusions in large anorthoclase ($Ab_{65}An_{16}Or_{19}$) phenocrysts, which form a lag gravel on the summit cone of Mt Erebus, were analysed by electron micro-probe. Composition of the glass is generally similar to that found in recent flows and bombs, however small and systematic differences occur in inclusions between the core and rim of anorthoclase phenocrysts. The composition of recent flows and ejecta are similar to older (up to 1 m.y.) anorthoclase phonolite flows exposed around the base of Mt Erebus.

Introduction

Mt Erebus (3799 m), a composite volcano of anorthoclase phonolite, is the largest of four volcanoes forming Ross Island, Antarctica (Fig. 1) and constitutes part of the Erebus volcanic province (Kyle and Cole, 1974) of the McMurdo Volcanic Group (Harrington, 1958; Nathan and Schulte, 1968).

Mt Erebus was reported active by Ross in 1847 and observations since then have indicated continuing fumarolic activity (Berninghausen and van Padang, 1960). The first observations of lava in the inner crater were reported by Giggenbach *et al.*, (1973). They described small strombolian eruptions during the period December 1972 to January 1973. Lava continued to be present in November 1973 and a small flow about 20 m long fed a convecting lava lake 40 m in diameter (Kyle, 1975). The lava lake had grown in size by December 1974 when a combined French-New Zealand expedition attempted to sample the lava and volcanic gases, however frequent strombolian eruptions forced the project to be abandoned.

The unusual anorthoclase phonolite lavas from Mt Erebus are distinctive among the alkali volcanic rocks in the McMurdo Sound area. They are very porphyritic with large rhomb-shaped phenocrysts of anorthoclase and are also extremely alkaline in composition, occasionally peralkaline. The active lava lake in Mt Erebus crater is one of only three such features present in the world (the others are Nyiragongo, Zaire and Erta Ale, Ethiopa). Mt Erebus is the only phonolitic lava lake.
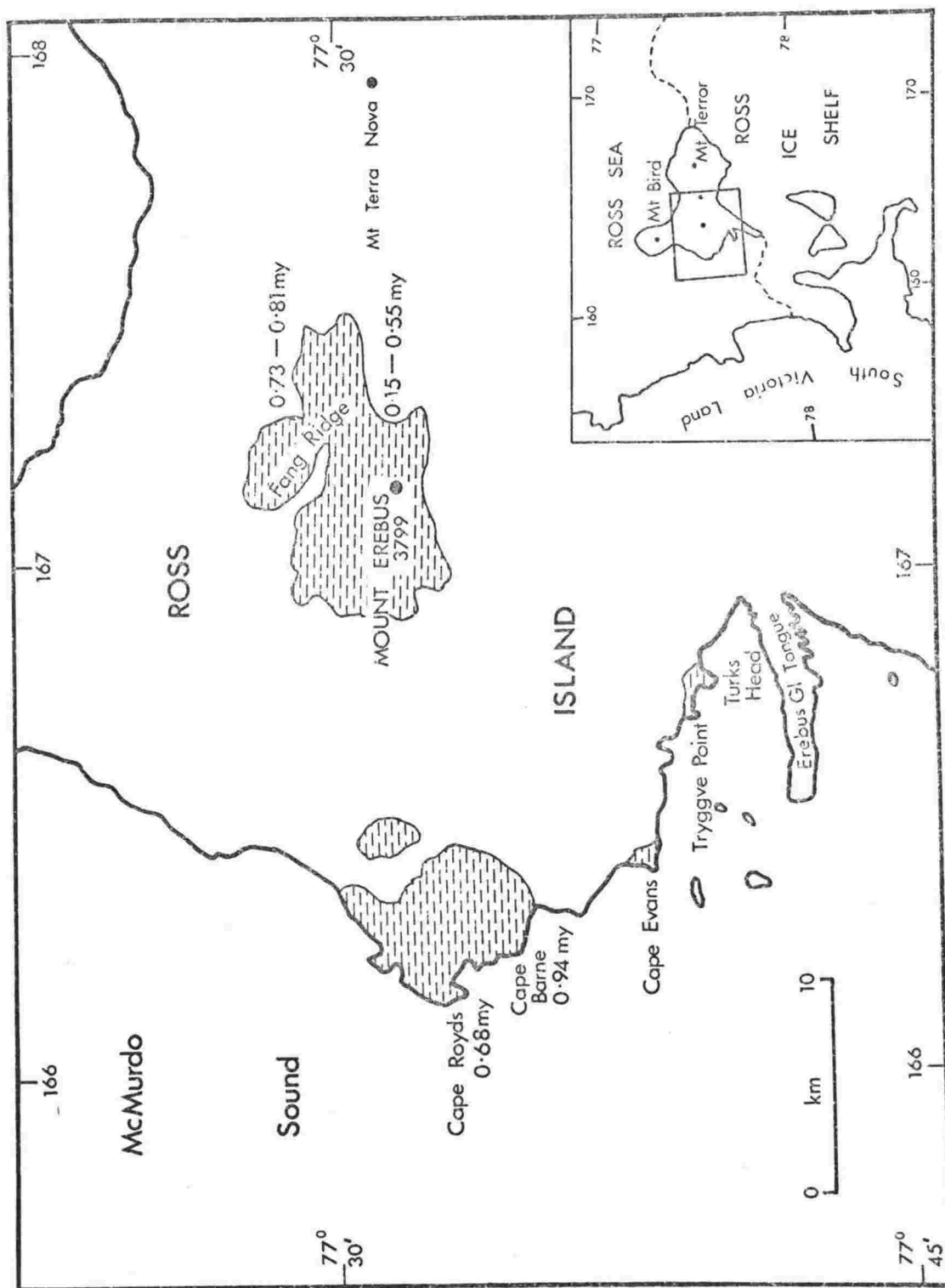
FIGURE 1. Geological and location map of Mt Erebus and Ross Island, 1967; Armstrong, 1975).

Fresh volcanic bombs erupted from the inner crater of Mt Erebus were collected in December 1972 on the crater rim and in December 1974 on both the crater rim and main crater floor.*

Large loose anorthoclase crystals were collected on the upper slopes of the active cone. The crystals form a lag gravel, which results from physical comminution of the weak glassy phonolite flows and pyroclastics. The crystals may also have been ejected as lapilli. This paper describes the petrology of two bombs erupted in 1972, two recent lava flows from the summit cone, and the chemistry of the anortho- clase phenocrysts and glass inclusions within them. A comparison is made with older anorthoclase phonolite flows exposed around the flanks of Mt Erebus.

Volcanic Geology

Most of the exposed rock on Mt Erebus is either above the 2000 m contour or around the base as isolated coastal outcrops. Anorthoclase trachyte (Ne <10%) and anorthoclase phonolite** (Ne >10%) are the dominant lithology, making up over 90% (by area) of the Mt Erebus lavas. Their K/Ar age is 0.94±0.05 m.y. at Cape Barne (Armstrong, 1975), and the

---

* Lava is confined to a 120 m deep pit (the inner crater) on the main crater floor.

** Early papers referred to the lavas from Mt Erebus as 'kenyte'. Smith (1954) argued this name was incorrect as the type kenyte from Mt Kenya contains nepheline phenocrysts, whereas the Erebus lavas do not. He thus named the Mt Erebus lavas 'Antarctic kenyte'. The present author uses the term 'anorthoclase phonolite'.

younger of three flows at Cape Royds is 0.68±0.14 m.y.
(Treves, 1967); the upper slopes of Mt Erebus are younger
than 0.5 m.y. (Armstrong, 1975) (Fig. 1).

Fang Ridge (Fig. 1) is a 0.7 to 0.8 m.y. old (Armstrong,
1975) remnant of a parasitic vent composed of porphyritic
plagioclase-rich nepheline hawaiite and nepheline benmoreite.
Similar lavas occur at Tryggve Point and Turks Head (Fig. 1),
25 km to the south-west of Mt Erebus summit.

Petrology of Recent Ejecta

The anorthoclase phonolite bombs are extremely delicate
and break up easily on handling. They consist of highly
pumiceous dark olive green to black glass with rhombic
phenocrysts of anorthoclase reaching up to 20 mm in length.
Usually the bombs are round to spindle-shaped ('fusiform')
and have hollow centres which are crossed by fine hairs or
strands of black glass. The size of vesicles increases from
1-2 mm on the rim of the bombs to over 30-40 mm on the inner
hollow surface. Winnowing of the glass on the outer surface
during the flight of the bomb exposes the anorthoclase
phenocrysts and gives an irregular rough exterior. Rarely
the outer surface of the bomb is covered with glass of olive
green colour which has a metallic lustre, and is drawn out in
long rounded ribbons and hairs.

Flow material on the upper slopes of the active cone
is similar to the bombs, consisting of black glassy
scoriaceous flows with ubiquitous anorthoclase phenocrysts.
Exposures in the crater wall indicate the flows vary in

thickness from less than 1 m up to 10 m.

It is difficult to determine the modal compositions of the bombs and flows because of their extremely pumiceous nature. Anorthoclase phenocrysts probably amount to 25 to 40% whereas microphenocrysts of olivine, pyroxene, magnetite, apatite and rare pyrrhotite combined, may amount to 5% by volume.

Analytical Techniques

Whole rock samples were analysed for major elements (except Na) by XRF (Seimens SRS-1 spectrometer) using the technique of Norrish and Hutton (1969). Na was determined by atomic absorption spectrometry. Trace element analyses were made by XRF (Philips PW 1220) at the University of Montreal.

Electron microprobe analyses were made on a JEOL JXA 5A instrument at Otago University. Instrumental conditions were 15 kv accelerating potential and 2.5×10^{-8} amps specimen current (on periclase). All glass analyses were made using a 50 μm defocused beam, no volatilisation of alkalies was noted and this is confirmed by some of the analyses summing close to 100%. Mineral analyses were made using both a 1-2 μm and 50 μm beam. Corrections were applied using the method of Bence and Albee (1968), and the alpha correction factors for a 40° takeoff angle, listed in Kushiro and Nakamura (1970). Standards used are given in Nakamura and Coombs (1973). Corrections for deadtime, background and drift were also made. Each complete analysis represents a minimum of 5 individual 10 second counts per element. Corrections for the feldspar partial analyses were made assuming the mineral was stoichiometric and consisted purely of the end members $KAlSi_3O_8$, $NaAlSi_3O_8$ and $CaAl_2Si_2O_8$. Precision (1σ), expressed as a relative standard deviation, based on repeated analysis of glass samples, is given in Table 1. Overall the accuracy is believed to be better than ±2% (relative) for the major components and up to ±5% (relative) for the elements less than 3%.

TABLE 1.   Precision of electron microprobe analyses based on
repeated analyses of glass samples.

	wt. percent	1σ	Relative std.dev. %
SiO_2	55	0.30	0.55
Al_2O_3	19	0.12	0.63
TiO_2	1	0.02	2.0
FeO	5.4	0.07	1.3
MnO	0.3	0.015	5.0
MgO	0.8	0.02	2.5
CaO	2.0	0.07	3.5
Na_2O	9.0	0.20	2.2
K_2O	5.4	0.04	0.75

Mineralogy

Representative* electron microprobe analyses of minerals in the recent volcanic ejecta are given in Table 2.

Olivine

Olivine is yellowish green in colour and occurs in minor amounts as subhedral microphenocrysts. It is often strongly resorbed and when it occurs as inclusions in anorthoclase phenocrysts, is rounded. The olivine is extremely uniform in composition, and shows no zoning; the maximum variation is from $Fa_{47.4}Te_{3.2}Fo_{49.4}$ to $Fa_{45.2}Te_{2.8}Fo_{52.0}$ (Fig. 2). The composition is similar to olivine in anorthoclase phonolite from Cape Royds on the lower slopes of Mt Erebus (Carmichael, 1967). CaO content of about 0.5% is slightly higher than olivines of similar composition from elsewhere in the McMurdo Volcanic Group (Kyle unpublished data), which is probably a reflection of differing silica activity (Stormer, 1973).

Pyroxene

The form of the pyroxene is similar to the olivine. Rare prismatic phenocrysts of pyroxene up to 10 mm long are found adhered to the outer surface of large anorthoclase phenocrysts. The pyroxene is salite in composition, showing no zoning and only minor variations in chemistry (Fig. 2). The range in composition is $Ca_{47.6}Fe_{16.3}Mg_{36.1}$ to $Ca_{49.1}Fe_{13.0}Mg_{37.9}$; there is a weak trend of decreasing Ca

---

*A complete listing of mineral analyses are available from the author on request.

TABLE 2. Representative analyses of minerals in bombs and lavas from Mt Erebus.

	Olivine 1	Olivine 2	Pyroxene 3	Pyroxene 4	Magnetite 5	Anorthoclase 6	Anorthoclase 7
SiO_2	34.6	34.8	50.2	50.4	0.06	64.7	62.9
Al_2O_3	-	-	2.64	2.80	2.33	21.7	23.0
TiO_2	0.05	0.02	1.45	1.32	25.3	0.13	0.13
FeO	38.6	38.3	9.19	9.75	65.5	0.15	0.20
MnO	2.52	2.35	0.63	0.65	1.80	-	-
MgO	23.6	24.4	12.1	12.2	2.94	-	-
CaO	0.50	0.49	22.0	21.1	-	2.75	3.80
Na_2O	0.03	-	0.85	1.07	-	7.48	7.39
K_2O	-	-	-	-	-	3.77	2.94
Sum	99.90	100.36	99.06	99.29	97.93	100.38	100.36
Fe_2O_3			2.43[a]	2.99[a]	18.8[b]		
FeO			7.00	7.06	48.6		
Total			99.30	99.59	99.75		

Pyrrhotite 8:

Fe	62.41	
S	37.56	
Sum	99.97	
	Molecular proportions	
Fe	1.117	
S	1.172	
	Mole fraction	
FeS	0.976	

	Olivine 1	Olivine 2	Pyroxene 3	Pyroxene 4	Anorthoclase 6	Anorthoclase 7
O	4	4	6	6	32	32
Si	0.994	0.990	1.897	1.897	11.440	11.185
Al	-	-	0.117	0.124	4.547	4.810
Ti	0.001	0.001	0.041	0.037	0.017	0.017
Fe^{3+}	-	-	0.069	0.085	-	-
Fe^{2+}	0.925	0.912	0.221	0.222	0.023	0.029
Mn	0.061	0.057	0.020	0.021	-	-
Mg	1.007	1.035	0.681	0.684	-	-
Ca	0.015	0.015	0.891	0.851	0.524	0.723
Na	0.002	-	0.062	0.078	2.577	2.546
K	-	-	-	-	0.854	0.667
Total	3.005	3.010	4.000	4.000	19.982	19.977

	Olivine 1	Olivine 2	Pyroxene 3	Pyroxene 4	Magnetite 5	Anorthoclase 6	Anorthoclase 7
Fe	46.4	45.5					
Mn	3.1	2.8					
Mg	50.5	51.7					
Ca			49.1	47.9		13.2	18.4
Mg			37.6	38.5			
Fe^{2+}+Mn			13.3	13.6			
Usp					69.5[b]		
Na						65.2	64.7
K						21.6	16.9

1, 25724 microphenocryst, grain 1.
2. Inclusion in anorthoclase 2, grain 2.
3. 25724 microphenocryst, grain 3.
4. Inclusion in anorthoclase 1, grain 12.
5, 25726, grain 1.
6. Anorthoclase 2, core.
7. Anorthoclase 2, rim.
8. 25724, grain 3.

[a] Fe_2O_3 in pyroxenes calculated by method of Papike et al., (1974).
[b] Fe_2O_3 in magnetites calculated by method of Carmichael (1967).

FIGURE 2. Composition of olivine and clinopyroxene in recent volcanic
ejecta, Mt Erebus, Antarctica. Lava and bomb samples 25724
(open triangles), 25725 (closed triangles), 25726 (open
squares) and inclusions in anorthoclase phenocrysts-
anorthoclase 1 (closed squares), anorthoclase 2 (circles).

with increasing Fe (Fig. 2).

Fe^{3+} was calculated using the charge balance procedure of Papike *et al.*, (1974); it appears that the number of Fe^{3+} cations is very similar to the number of Na cations, suggesting all the Na and Fe^{3+} is present as the acmite component. In terms of Na, Mg, Fe^{2+}+Mn, the enrichment of the acmite component is very small and amounts to only 6 to 8%. Nash and Wilkinson (1970) have shown that Na-rich pyroxenes in the Shonkin Sag laccolith do not form until olivine ceases crystallizing. They believe that the rate of change of oxygen fugacity, when olivine and magnetite are present (see equation 1, below), is too great to allow Na-rich pyroxenes to crystallize.

In the Mt Erebus pyroxenes the ratio of Ti and Al cations is nearly constant at 1:3; indicating there is excess Al, if it is assumed that all the Ti enters the theoretical Ca-Ti-tschermak molecule. The excess Al would probably form between 1 to 3% Ca-tschermak molecule.

Temperatures calculated using olivine-clinopyroxene geothermometry (Powell and Powell, 1974) are about $990^{\circ}C$ (Table 3).

Magnetite

Titanomagnetite is ubiquitous as resorbed cubic euhedral microphenocrysts of nearly constant composition, averaging $Usp_{69.5}$ (range $Usp_{70.7}$ to $Usp_{67.5}$). Weak zoning was noted in only one sample. Ilmenite is not present, so it is not possible to determine temperature and oxygen

TABLE 3. Temperature determinations using the olivine-clinopyroxene geothermometer of Powell and Powell (1974).

Sample	OL(MG/FE)	CPX(MI-MG/FE)	CPX(MI-AL)	Temperature ^{o}C
25725	1.118	2.520	0.109	989
25724	1.069	2.495	0.110	988
Anorth 2 Mineral inclusions	1.136	3.106	0.145	991

fugacity using magnetite-imenite geothermometry. However oxygen fugacity and silica activity may be buffered by the reaction (Nicholls *et al.*, 1971):

$$2/3Fe_3O_4 + SiO_2 = Fe_2SiO_4 + 1/3O_2 \qquad \ldots (1)$$

magnetite   glass   fayalite   gas
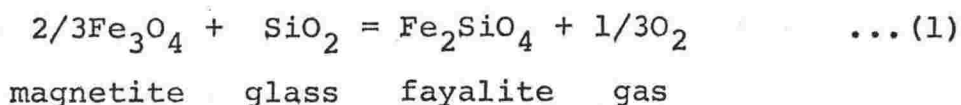
Silica activity of Mt Erebus lavas is unknown. In chemically and mineralogically similar anorthoclase phonolite lavas from Cape Royds, groundmass sanidine (0.464Ab) and nepheline (0.593Ne) occur (Carmichael, 1964) and log a_{SiO_2} = -0.71 was calculated at $1000^{o}C$, using equation 6 of Nicholls *et al.*, (1971). Silica activity of Mt Erebus lavas is unlikely to vary significantly from this value, therefore using equation 1 and the typical mineral chemistry of Mt Erebus samples log f_{O_2} = -12.2 at $1000^{o}C$. The oxygen fugacity is thus low, lying below the QFM buffer (as might be expected for under-saturated rocks) and within the upper part of the range for phonolites from Mt Suswa, Kenya (Nash *et al.*, 1969).

Pyrrhotite

Small, subcircular immiscible(?) blebs of pyrrhotite are found as inclusions in magnetite in most of the samples examined. Analyses of 4 grains in one sample all show a very similar and simple chemistry of $Fe_{1.11}S_{1.17}$; Cu, V and Ni were undetected in spectrometer scans. The pyrrhotite has an extremely high mole fraction FeS (0.977); greater than pyrrhotite reported in andesitic, dacitic and rhyolitic lavas by Heming and Carmichael (1973).
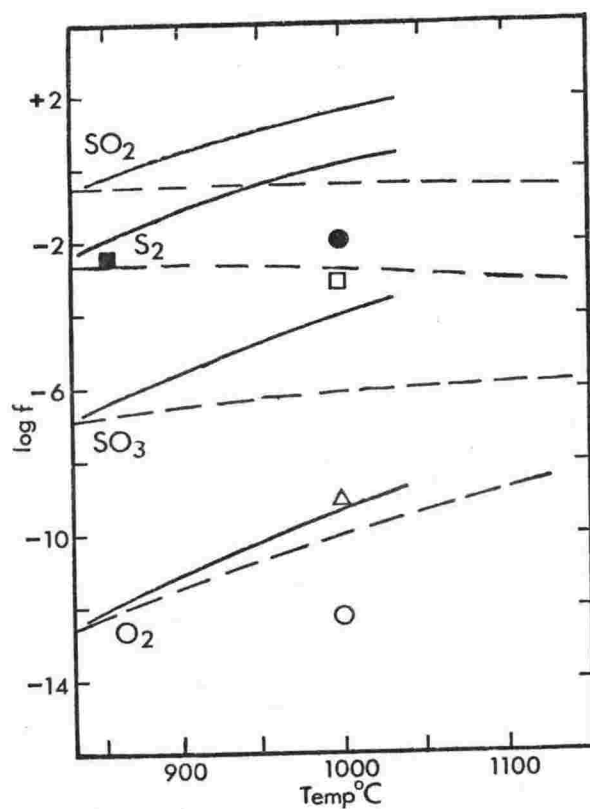
FIGURE 3. Calculated fugacity of various sulphur gases and oxygen for anorthoclase phonolite from Mt Erebus. Solid and dashed lines are trends for Rabaul lava samples and Kilauea magmatic gas respectively (from Heming and Carmichael, 1973). SO_2 (dot), S_2 (open square), SO_3 (triangle), O_2 (circle). f_{S_2} measured in magmatic gases from Mt Etna (filled square) (Sato and Moore, 1973).

The composition of pyrrhotite can be related to
sulfur fugacity, if the equilibrium temperature is known
(Heming and Carmichael, 1973). For the samples from Mt Erebus,
$\log f_{S_2}$ at $1000^{O}C$ is -2.7 which is nearly identical to volcanic
gases from Kilauea volcano, Hawaii (Heming and Carmichael,
1973) (Fig. 3). From the calculated values of f_{O_2} and f_{S_2}
fugacities of SO_2 and $SO_3 = 10^{-2.5}$ and $10^{-8.8}$ respectively
(Fig. 3).

Apatite

Hexagonal, euhedral needles and microphenocrysts of
apatite are common in all samples. No complete analyses were
made.

Anorthoclase

The large and well developed anorthoclase phenocrysts
have been studied by Mountain (1923) and Boudette and Ford (1966),
and their occurrence described briefly by David and Priestley
(1914) and others (see summary in Smith, 1954).

Crystals occur in a number of forms, of which rhombic
is the most common. The largest crystals are found loose on
the slopes of the active crater, where they form a lag gravel.
Some of the crystals may have been erupted as lapilli but most
have weathered from the weak pyroclastics and flows. Dimensions
rarely exceed 90x40x20 mm. Anorthoclase occurs in all the bombs
examined, but it is difficult to distinguish because it is
completely covered by black phonolitic glass. The maximum
length of any crystal found in a recent bomb is 40 mm.

Boudette and Ford (1966) have described the anorthoclase in thin section and noted it is optically homogeneous and extremely poikolitic. The inclusions are mainly light to dark brown glass, but all mineral phases that occur in the lavas are also found. In many of the large phenocrysts examined, a single or glomeroporphyritic clump of mafic minerals is found in the centre of the crystal.

An analysis of anorthoclase separated from a 1972 bomb (Table 4) and microprobe analyses from this study together with previously published analyses are shown in Figure 4. The range of microprobe analyses are extremely small; the main variation is in the An and Or component, while the Ab component is near constant varying from $Ab_{64.4}$ to $Ab_{65.8}$ (the spread is within analytical uncertainty). Minor zoning occurs; in three cases An increases slightly, while in one sample there is a progressive increase in Or (Fig. 4).

The agreement between the microprobe and published chemical analyses is good. The latter tend to be lower in Ab but show the same spread in An and Or content. The analyses indicate a consistent composition, except for one that is quite different from the rest (Fig. 4) and may be in error.

The anorthoclase crystals are believed to have grown extremely rapidly. Nucleation may have been slow, as indicated by the growth of anorthoclase around mafic minerals, but once nucleation was achieved growth could have been very rapid, if the magma was slightly super-cooled (Lofgren, 1974). Actual growth rates for the Erebus anorthoclase crystals are indeterminable, but some idea can be obtained from other

TABLE 4. Analyses of anorthoclase from anorthoclase phonolite

lavas, Mt Erebus.

	1	2	3	4
SiO_2	61.61	61.94	62.79	63.32
TiO_2	0.19	-	-	-
Al_2O_3	22.32	23.37	22.12	22.09
Fe_2O_3	0.75[a]	-	0.36	0.23
FeO	-	0.17	0.41	-
MnO	0.03	-	-	-
MgO	0.27	-	-	-
CaO	3.35	4.00	3.76	3.02
Na_2O	7.49	7.48	7.35	7.67
K_2O	3.17	2.89	2.98	3.35
H_2O+	-	0.11	0.19	0.09
H_2O-	-	0.09	0.07	0.07
Sum	99.18	100.05	100.03	99.84
Sr ppm	-	2700	-	2500
Ba "	-	2600	-	3000

Number of cations on the basis of 32 (O)

Si	11.131	11.090	11.257	11.335
Al	4.754	4.933	4.674	4.661
Ti	0.026	-	-	-
Fe^{3+}	0.102	-	0.049	0.031
Fe^{2+}	-	0.025	0.061	-
Mn	0.004	-	-	-
Mg	0.073	-	-	-
Ca	0.648	0.767	0.722	0.579
Na	2.623	2.597	2.555	2.661
K	0.730	0.660	0.681	0.766
Z	16.090	16.048	16.041	16.027
X	4.001	4.024	3.958	4.006
Ca	16.2	19.1	18.2	14.4
Na	65.6	64.5	64.6	66.4
K	18.2	16.4	17.2	19.1

[a] Total Fe as Fe_2O_3.

1. Anorthoclase from recent bomb 25726.

2. Anorthoclase, Cape Royds. Carmichael (1964). Trace elements Berlin and Henderson (1969).

3. Anorthoclase, summit Mt Erebus, Mountain (1925).

4. Anorthoclase, Cape Evans. Carmichael (1964). Trace elements Berlin and Henderson (1969).
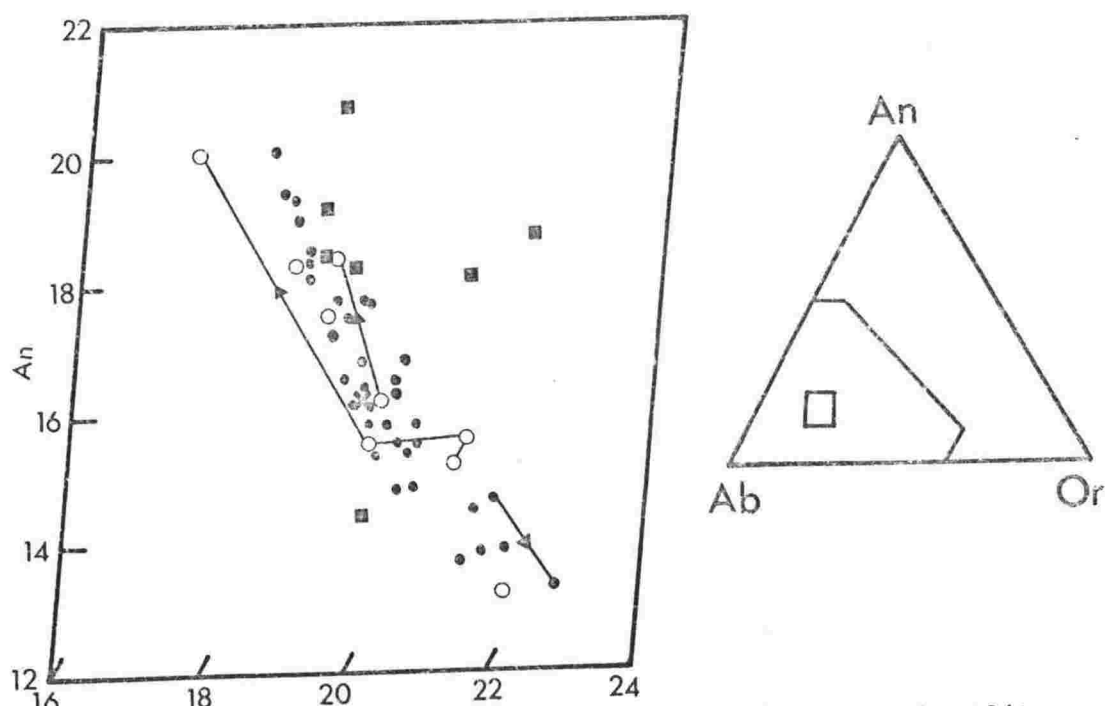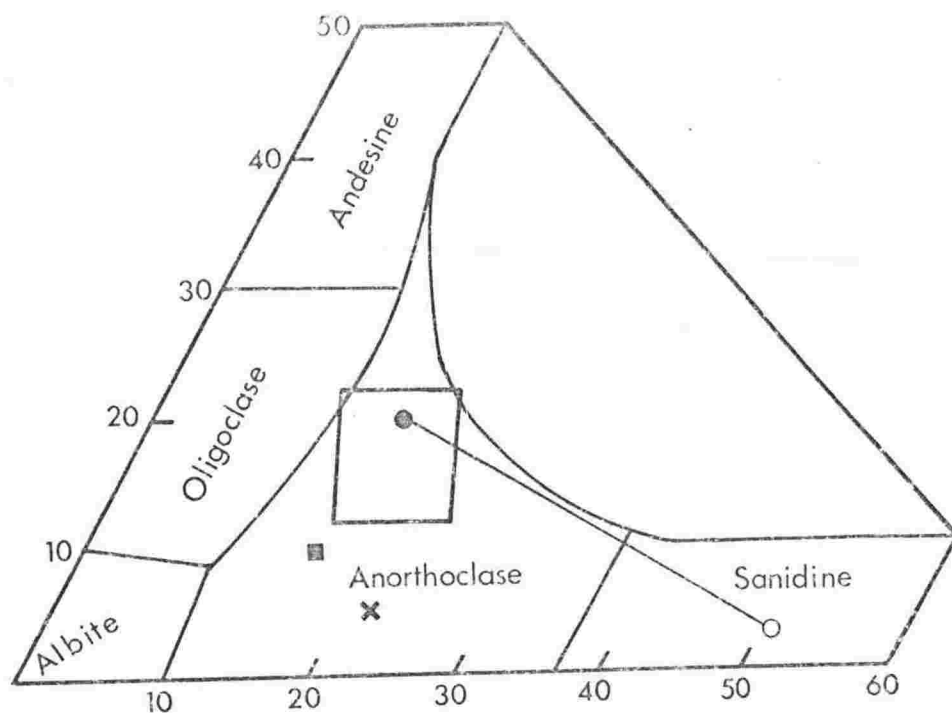
FIGURE 4. Composition of anorthoclase from anorthoclase phonolite
lavas and pyroclastics, Mt Erebus, Cape Evans and Cape
Royds, Antarctica.

(A) Feldspar triangle showing position of figure 3B.
Anorthoclase from summit of Mt Erebus (cross) (Carmichael and
McKenzie, 1963), anorthoclase phenocryst (dot) and groundmass
sanidine (circle) pair from Cape Royds (Carmichael, 1964),
anorthoclase phonolite Crary Mountains, Marie Byrd Land
(square), Antarctica (Boudette and Ford, 1966).

(B) Chemical analysis (Table 4) (cross), complete probe
analyses (circles) and partial probe analyses (dots) of
anorthoclase from the summit of Mt Erebus. Published chemical
analyses of anorthoclase (squares) from anorthoclase phonolite
at Cape Evans, Cape Royds and Mt Erebus (Jensen, 1916; Mountain,
1925; Carmichael, 1964; Boudette and Ford, 1966; Treves, 1967).

studies. Kirkpatrick (1974) has measured plagioclase growth
rates in Hawaiian tholeiitic lava lakes, and if the average of
his data is applied to Mt Erebus anorthoclase, then a 30 mm
crystal would grow in 600 days. In experimental studies rapid
crystal growth rates occur. Lofgren (1974) grew large unzoned
plagioclase, including An-poor compositions, in synthetic and
natural melts, at rates of 1-5 mm per day. Fenn (1972) reported
rates equivalent to 1 mm per 7 minutes in water undersaturated
synthetic melts at 2.5 kbars. Gutmann (1972) argued that giant
phenocrysts up to 100 mm in maximum dimension, from basaltic
lavas at Crater Eleganta, Mexico grew rapidly at shallow depths.

Glass Inclusions

Glass inclusions in the anorthoclase phenocrysts are
numerous and sufficiently large to allow them to be analysed
by electron microprobe, using a 50 μm defocused beam. As some
of the anorthoclase had an obvious growth pattern it was assumed
that the glass was included as the crystal grew, and therefore
represented a sequence of progressively younger inclusions from
core to rim.

Three loose anorthoclase crystals collected from the
lag gravel upper slopes were examined. The crystals may not
have been erupted at the same time, but any time differences
between their eruption are likely to be less than 1000 years.

Variation in glass chemistry with time is seen clearly
in one crystal (anorthoclase 1), poorly in another (anorthoclase
3), and in a third (anorthoclase 2) no regular variation was

observed. The significance of these results depend strongly
on the analytical reliability, as the differences observed
are small. Some of the variations discussed below are greater
than 2 standard deviations of the precision (Table 1) and must
be considered real.

Anorthoclase 1

Variations from core to rim are clearly shown by Al_2O_3
which increases from 18.7% to 19.5% (analyses were recalculated
to 100%), while FeO decreases from 5.38% to 4.91%. K_2O shows a
slight tendency to increase. FeO and Al_2O_3 vary regularly,
indicating that while the crystal grew the magma must have
remained a closed system. Any influxes of new magma would
cause discontinuities in the trend. The analytical uncertainties
in SiO_2, Na_2O and CaO are sufficiently high to account for any
variations, with the possible exception of two low values on the
CaO curve (Fig. 5).

Anorthoclase 2

Variations in the glass chemistry occur but show no
regular pattern from core to rim.

Anorthoclase 3

Sixteen inclusions were analysed, but because they were
spread over the whole crystal and did not lie on a transect,
it was difficult to relate their position relative to rim and
core and time of formation. The analyses when plotted on
variation diagrams (Fig. 6) show two sets of core to rim data.
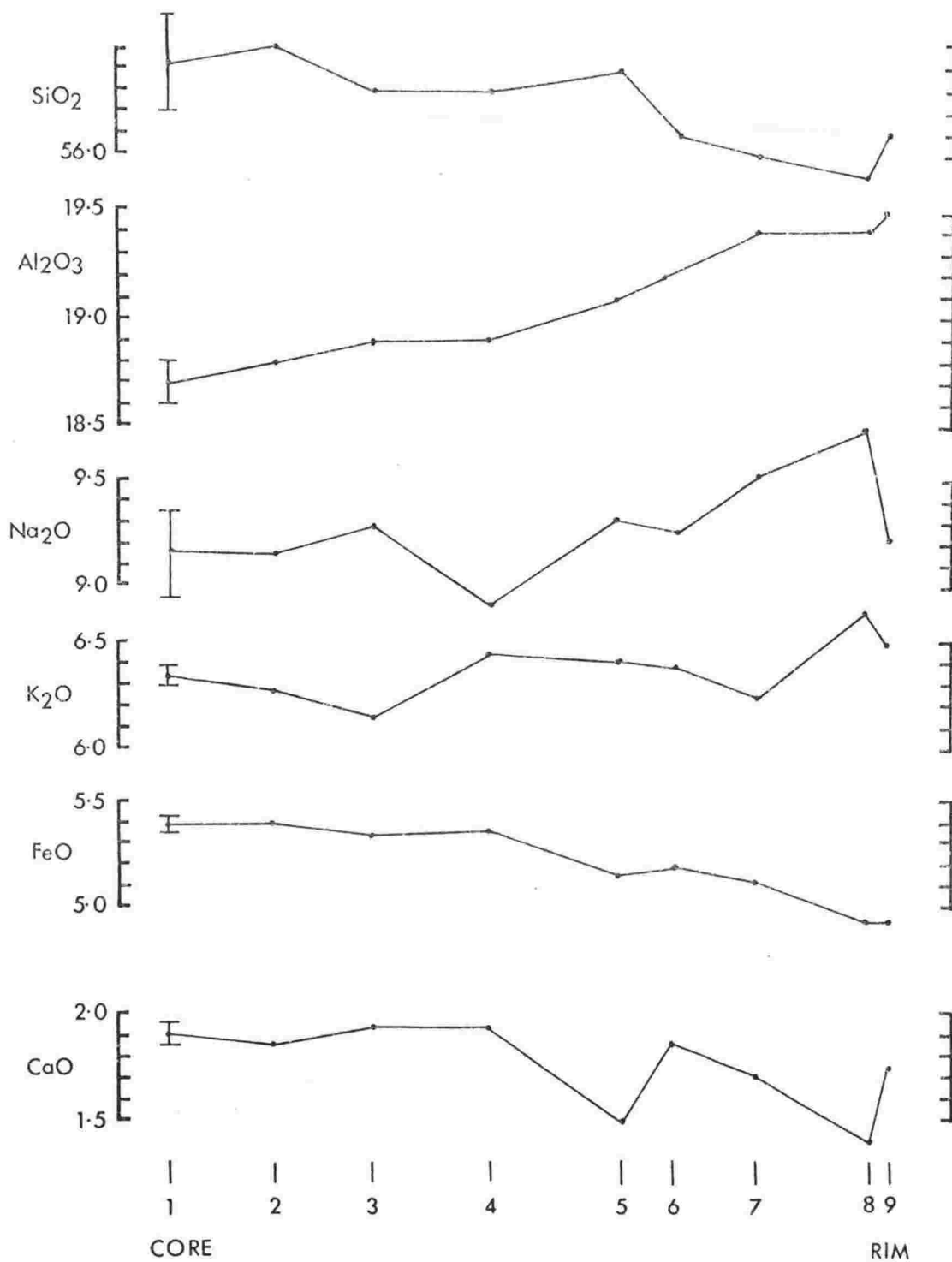
FIGURE 5. Variation in major element chemistry of glass inclusions in anorthoclase 1, plotted against position within phenocryst. Precision at one standard deviation is shown by error bar on the left. Analyses were recalculated to 100%.
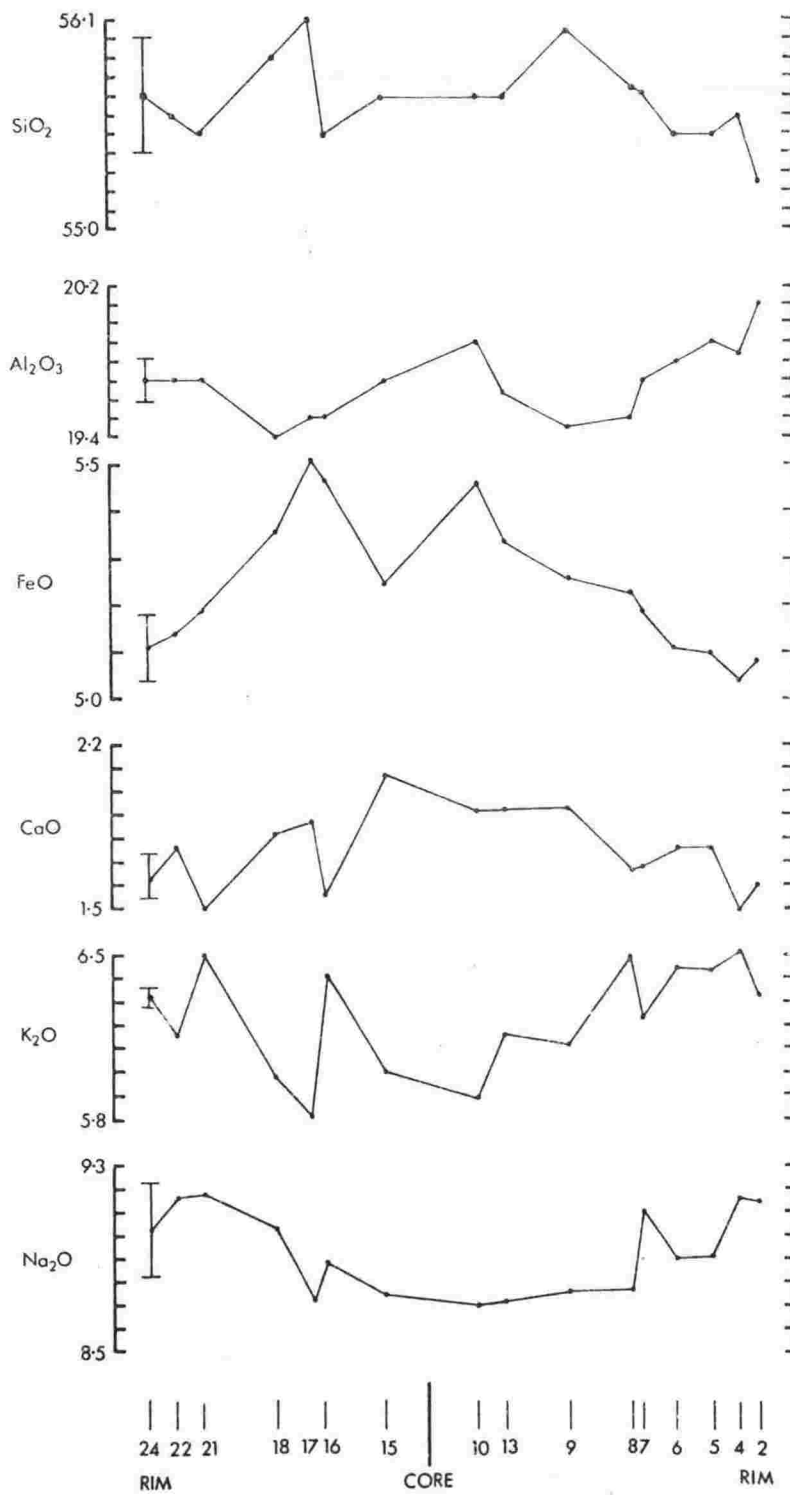
FIGURE 6.   Variation in major element chemistry of glass inclusions
in anorthoclase 3.   Analyses were recalculated to 100%.

Individual elements have a more scattered trend than anorthoclase 1. The variation on either side of the core should be a mirror image, if the crystal grew symmetrically. This is apparent in several elements particularly SiO_2, Al_2O_3, FeO, Na_2O and poorly in CaO. The symmetry in all these elements indicates the broad variations are real even though in many cases the variations are all within analytical uncertainty. FeO decreases steadily from core to rim, similar to the trend in anorthoclase 1.

Discussion

It is assumed that the glass chemistry is changing in response to crystal growth (i.e. it represents the residual in a fractional crystallization process). The increasing Al_2O_3 and decreasing FeO indicate that crystallization of the mafic minerals olivine, pyroxene and magnetite are having more effect on glass chemistry than the crystallization of anorthoclase. Even though Al_2O_3 increases this does not prohibit anorthoclase crystallization, obviously the crystal with the inclusions was growing, however mafic mineral crystallization is controlling the overall chemical trend.

Although the systematic variations of Al_2O_3 and FeO in anorthoclase 1 are small they do illustrate the continuous changes which occur during crystal fractionation. The changes from core to rim (Fig. 3) represent variations with time. If the anorthoclase crystallized rapidly, as suggested above, then crystal fractionation processes are rapid. This implies rapid crystallization of the mafic minerals.

Petrochemistry

Four new analyses of anorthoclase phonolite and three of associated glasses from two 1972 bombs and two flows near the summit of Mt Erebus and an analysis of a flow from near the summit by Goldich *et al.*, (1975), are given in Table 5. A rare earth element (REE) analysis of sample 25725 (Kyle and Rankin, in preparation) is plotted normalised to chondrite abundances in Fig. 9.

Analyses of whole rock, glass and glass inclusions in anorthoclase and all previously published analyses are plotted on a total alkalis versus silica diagram (Fig. 7) and oxide variation diagrams with silica as the abscissa (Fig. 8).

Although the glass inclusions show a regular variation in composition along a transect in the anorthoclase, they have a scatter on the oxide variation diagram (Fig. 8), the scatter being mainly due to the uncertainty in the electron microprobe silica analyses.

On the total alkalis versus silica diagram (Fig. 7) all the whole rock analyses fall below 13.5% total alkalis, whereas all the groundmass and glasses are above. The increase in alkalis and decrease in Al_2O_3 from whole rock to groundmass results in the groundmass and glass becoming peralkaline (Table 5) with agpaitic indexes (molecular Na_2O+K_2O/Al_2O_3) greater than 1. Carmichael (1964) pointed out that this illustrates the result of feldspar fractionation (the "plagioclase effect") to produce peralkalinity in undersaturated lavas.

TABLE 5. Analyses of whole rock and groundmass glass of recent volcanic ejecta and flows from the summit of Mt Erebus.

VUW	1 25726	2 25726G	3 25727	4 25724	5 25724G	6 25725	7 25725G	8
SiO_2	55.32	54.94	56.42	56.65	55.54	56.68	55.81	55.71
TiO_2	1.07	1.10	0.91	0.92	1.06	1.00	1.10	1.22
Al_2O_3	19.69	19.27	20.18	20.09	19.09	19.84	18.84	18.14
Fe_2O_3								1.83
FeO	5.17	4.89	4.36	4.52	4.88	4.66	4.96	4.90
MnO	0.25	0.30	0.21	0.22	0.31	0.22	0.28	0.25
MgO	1.09	0.85	0.95	0.97	0.80	1.06	0.87	1.37
CaO	2.68	2.03	2.80	2.79	1.95	2.92	2.06	3.35
Na_2O	7.92	8.85	7.88	7.75	9.05	7.88	8.27	7.92
K_2O	4.71	5.42	4.40	4.45	5.43	4.45	5.38	4.35
P_2O_5	0.45		0.37	0.38		0.40		0.49
H_2O+	0.05[a]					0.04[a]		0.11
H_2O-			0.02	0.02				0.00
CO_2								0.03
F								0.15
Cl								0.09
$-O=F,Cl$								0.08
Total	98.40	97.64	98.50	98.76	98.11	99.15	97.57	99.83

Trace elements (in ppm)

Rb	111		95	107		99		80
Ba	871		1133	876		1027		1200
Sr	735		1020	721		932		840
Y								66
Zr								540
Zn	135		112	132		119		135
Cu	4		6	5		5		24
Ni	<5		<5	<5		<5		13
V	5		4	4		4		32
Cr	<5		<5	<5		<5		<5
K%	3.91		3.65	3.69		3.71		3.61
K/Rb	352		384	345		375		431

CIPW Norms (Weight Percent)[b]

Hl	-	-	-	-	-	-	-	0.15
Or	27.83	32.03	26.00	26.30	32.09	26.30	31.79	25.70
Ab	36.78	24.20	41.46	41.94	23.60	41.18	30.54	37.97
An	4.26	-	6.70	6.89	-	5.62	-	1.45
Ne	16.38	24.24	13.66	12.80	24.03	13.81	19.73	15.38
Ac	-	5.24	-	-	7.23	-	2.67	-
Ns	-	-	-	-	0.10	-	-	-
Di-wo	2.54	4.20	2.00	1.87	4.04	2.61	4.27	4.46
Di-fs	1.04	2.49	0.41	0.50	2.67	0.72	2.20	2.88
Di-en	1.41	1.74	1.41	1.23	1.46	1.70	2.01	1.66
Fo	0.92	0.26	0.67	0.83	0.38	0.66	0.11	1.23
Fa	0.74	0.42	0.22	0.38	0.76	0.31	0.13	2.36
Mt	3.62	1.00	3.62	3.62	-	3.62	2.29	2.65
Il	2.03	2.09	1.73	1.75	2.01	1.90	2.09	2.32
Fl	-	-	-	-	-	-	-	0.31
Ap	1.04	-	0.86	0.88	-	0.93	-	1.14
Others	0.05	-	0.02	0.02	-	0.04	-	0.18
Total	98.66	97.91	98.75	99.01	98.36	99.40	97.82	99.83
Agpaitic Index	0.92	1.06	0.88	0.87	1.09	0.90	1.03	0.98

[a]Loss on ignition; [b]Norms for samples 1-7 calculated with standard value of Fe_2O_3 = 2.50.

Explanation of Table 5.   Analyses of whole rock and groundmass glass
              of volcanic ejecta and recent flows from the summit of
              Mt Erebus.

1.   25726* Anorthoclase phonolite bomb, erupted from Mt Erebus in
              December 1972. Collected on the northeast crater rim.

2.   25726G. Glass of above sample (Electron microprobe analysis).

3.   25727. Anorthoclase phonolite flow on west flank of Mt Erebus
              crater, older than 25725.

4.   25724. Anorthoclase phonolite bomb, erupted from Mt Erebus in
              late 1972. Collected on the north crater rim.   This
              bomb was erupted prior to 25726.

5.   25724G. Glass of above sample (Electron microprobe analysis).

6.   25725. Anorthoclase phonolite flow on southwest flank of Mt Erebus
              crater.

7.   25725G. Glass of above sample (Electron microprobe analysis).

8.   Anorthoclase phonolite, summit of Mt Erebus. Goldich *et al*., 1975.
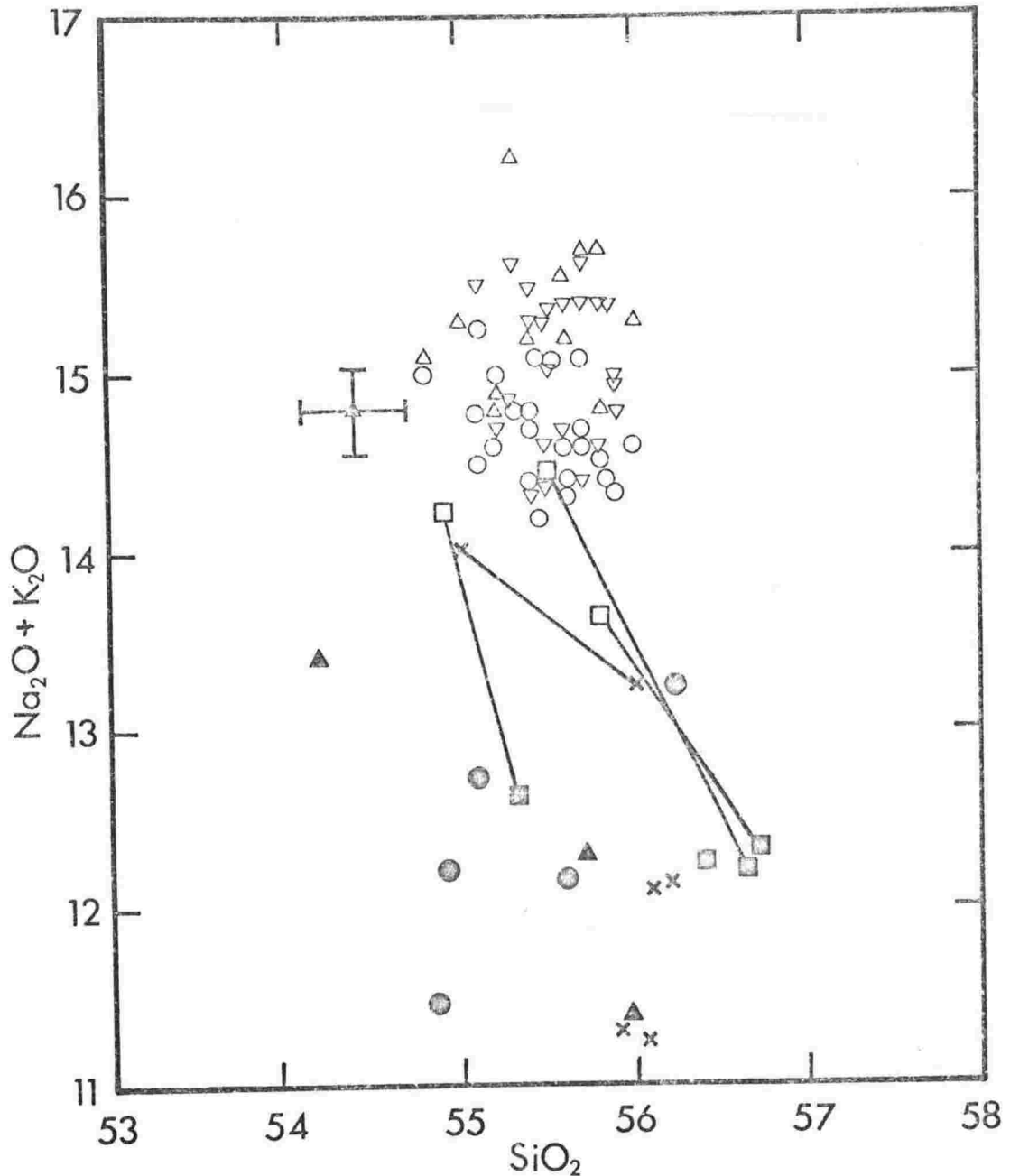
FIGURE 7. Total alkalis versus silica plot of whole rock and glass/
groundmass analyses of anorthoclase phonolite from Mt Erebus
and surrounds, Antarctica. Whole rock (filled squares) and
glass/groundmass (open squares) analyses; glass inclusions
in anorthoclase 1 (open triangle), anorthoclase 2 (circle),
anorthoclase 3 (inverted triangle), all from this study.
Published chemical analyses of anorthoclase phonolite from
Cape Royds (cross), Cape Evans (dot) and Mt Erebus (closed
triangle) from Prior (1907), Jensen (1916), Smith (1954),
Boudette and Ford (1966), Carmichael (1964) and Goldich
et al., (1975).
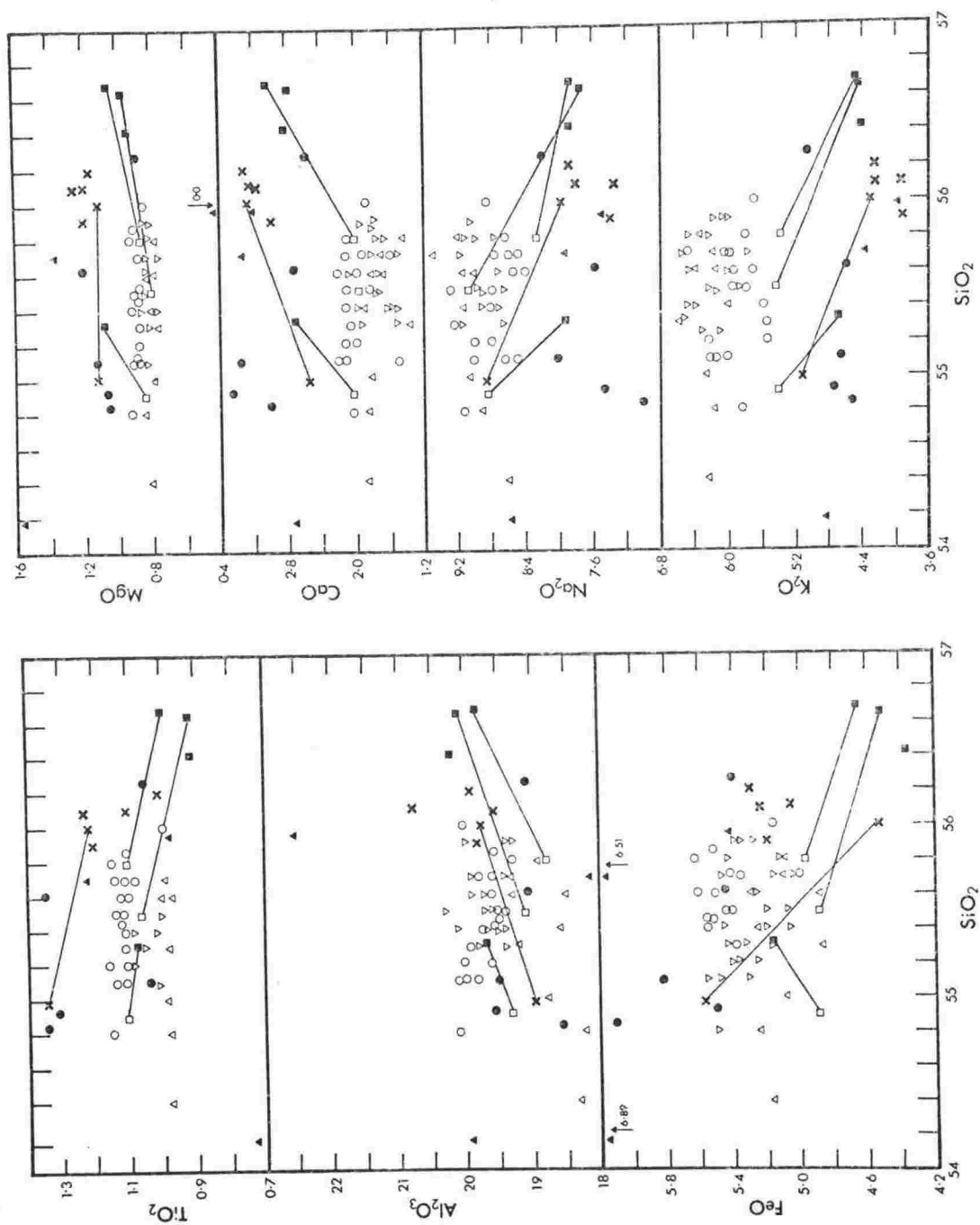
FIGURE 8. Variation of major element oxides plotted against silica for anorthoclase phonolite whole rock and groundmass/ glass analyses. Analyses and symbols same as Figure 7.
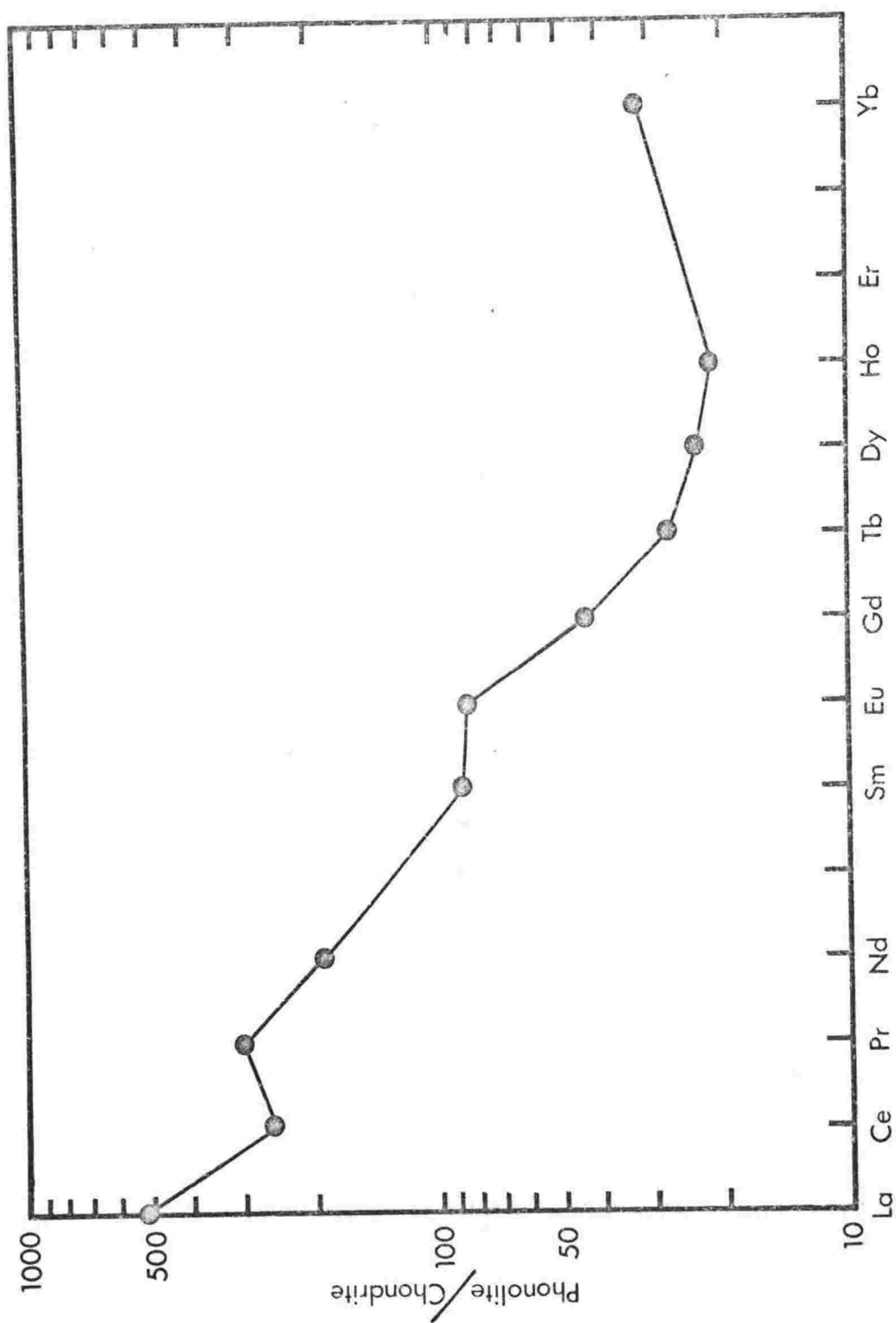
FIGURE 9. Chondrite normalised rare earth element abundances in anorthoclase phonolite sample 25725.

Discussion

The chemistry of the Mt Erebus glasses and the ground-mass of a flow, 0.68 m.y. old, from Cape Royds are similar to the glass inclusions in the anorthoclase (Fig. 8). Relative to the whole rock samples the glasses and groundmass sample show increased Na_2O, K_2O, TiO_2 and FeO (with the exception of one sample), and decreased CaO, MgO and Al_2O_3.

All whole rock major element analyses are very similar (Figs 7 and 8), even though the samples were collected from different localities up to 25 km apart, which vary from 0 to at least 0.7 m.y. in age. Many of the differences could be analytical resulting from varying analytical techniques and accuracies and the difficulty of obtaining representative samples from such porphyritic rocks. The glass and whole rock analyses suggest that the chemistry of Mt Erebus lavas has remained virtually unchanged for at least 0.7 m.y.

Details of the REE data will be discussed elsewhere (Kyle and Rankin, in preparation), however they have been included here to show the positive Eu anomaly (Eu/Eu* = 1.31) which is undoubtedly the result of feldspar accumulation (Philpotts and Schnetzler, 1968; Weill and Drake, 1973). The anorthoclase contains ~2600 ppm Sr and ~2800 ppm Ba (Table 4). Therefore the variable Sr and Ba contents of the whole rock samples (Table 5) probably reflects differences in the amount of cumulus anorthoclase.

Basaltic lavas do not occur on Mt Erebus, but in the surrounding centres basanites are the most abundant lavas. The anorthoclase phonolite probably differentiated from a

basanite (basanitoid) parent (Goldich *et al.*,1975), the
nepheline hawaiite and nepheline benmoreite lavas at The
Fang and other areas around Mt Erebus (Fig. 1) representing
the intermediate products in the process. Strontium isotope
ratios of anorthoclase phonolites (Jones and Walker, 1973)
overlap with the basanites indicating they may be comagnetic;
the average Sr^{87}/Sr^{86} of all analyses is 0.7035, thus crustal
contamination is unlikely. The data above suggests that the
chemistry of Mt Erebus lavas has remained unchanged for over
0.7 m.y. Therefore the differentiation processes must have
occurred repeatedly under identical conditions throughout the
life of Mt Erebus. The constant composition may be related to
the stable tectonic environment of the Antarctic continent,
as indicated by the absence of tectonic earthquakes.

Conclusions

1) Mineral chemistry indicates the anorthoclase
phonolites of Mt Erebus crystallized at temperatures of about
$1000^{O}C$ under low oxygen fugacity ($f_{O_2} = 10^{-12.2}$), although
within the expected limits of phonolitic lavas.

2) Anorthoclase phenocrysts from bombs, flows and a
lag gravel at Mt Erebus summit are similar in composition and
show only very minor zoning in terms of An and Or (Fig. 3).
Their composition is similar to those in older phonolite flows
around the flank of Mt Erebus.

3) Mafic minerals in a lava from Cape Royds (Carmichael,
1967) are identical to those analysed in bombs, flows and as

inclusions in anorthoclase phenocrysts from Mt Erebus summit.
Zoning is generally absent or only very minor.

4) Glass inclusions in large anorthoclase phenocrysts
from Mt Erebus summit show systematic variations in chemistry,
slightly larger than analytical error. FeO decreases and
Al_2O_3 increases indicating crystal fractionation of mafic
minerals (olivine, salite and magnetite) in a crustal magma
chamber. The changes are small and do not result in any major
modification of the magma composition.

5) Anorthoclase phonolite lavas from Mt Erebus and
surrounds have similar whole rock chemical compositions. Any
variations may be due to differences in analytical uncertainties.
A REE analysis shows a positive Eu anomaly due to cumulus
anorthoclase. Varying amounts of cumulus anorthoclase may also
account for small variations of whole rock chemistry.

6) Glass analyses and the groundmass of an anorthoclase
phonolite flow are also very similar in composition.

7) Mineral, glass and whole rock chemistry in
anorthoclase phonolite samples of differing ages from Mt Erebus
and surrounds are very similar. The anorthoclase phonolite
lavas presumably formed by crystal fractionation from a basanite
parent. The process has therefore occurred repeatedly under
identical conditions for at least the last 0.7 m.y.

8) The continued existence of the Mt Erebus lava lake
gives an ideal opportunity to search for short term variations
in magma chemistry similar to those found in glass inclusions
in anorthoclase phenocrysts.

References

Armstrong, R. L. 1975. K-Ar dating: McMurdo Volcanic Group
and Dry Valley Glacial History, Victoria Land, Antarctica.
(unpublished manuscript).

Bence, A. E., Albee, A. L. 1968. Empirical correction factors
for the electron microanalysis of silicates and oxides.
J. Geol. 76, 382-403.

Berlin, R., Henderson, C.M.B. 1969. The distribution of Sr
and Ba between the alkali feldspar, plagioclase and ground-
mass phases of porphyritic trachytes and phonolites.
Geochim. Cosmochim. Acta 33, 247-255.

Berninghausen, W. H., van Padang, M. N. 1960. Catalogue of
the active volcanoes of the world, including solfatara
fields; Pt. X, Antarctica. Internat. Volcan. Assoc.,
Naples, 32 p.

Boudette, E. J., Ford, A. B. 1966. Physical properties of
anorthoclase from Antarctica. Amer. Mineral. 51, 1374-1387.

Carmichael, I.S.E. 1964. Natural liquids and the phonolite
minimum. Geol. J. 4, 55-60.

_____ 1967. The iron-titanium oxides of salic volcanic
rocks and their associated ferromagnesian silicates.
Contr. Mineral. and Petrol. 14, 36-64.

_____ MacKenzie, W. S. 1963. Feldspar-liquid equilibria
in pantellerites: An experimental study. Amer. J. Sci.
261, 382-396.

David, T.W.E., Priestley, R. E. 1914. Glaciology, physiography,
stratigraphy, and tectonic geology of South Victoria Land.
Rep. Brit. Antarct. Exped. 1907-9, Geol. 1. 319 pp.

Fenn, P. M. 1972. Nucleation and growth of alkali feldspars from synthetic melts. (Abstract). Amer. Geophys. Union Trans. 53, 1127.

Giggenbach, W. F., Kyle, P. R., Lyon, G. L. 1973. Present volcanic activity on Mount Erebus, Ross Island, Antarctica. Geology 1, 135-136.

Goldich, S. S., Treves, S. B., Suhr, N. H., Stuckless, J. S. 1975. Geochemistry of the Cenozoic volcanic rocks of Ross Island and vicinity, Antarctica. J. Geol. 83, 415-435.

Gutmann, J. T. 1972. Giant phenocrysts from basaltic lavas at Crater Elegante: An argument for rapid growth of large crystals at shallow depth. (Abstract). Geol. Soc. Amer. Abstr. with Programs 4 (7), 522.

Harrington, H. J. 1958. Nomenclature of rock units in the Ross Sea region, Antarctica. Nature (London), 182, 290.

Heming, R. F., Carmichael, I.S.E. 1973. High-temperature pumice flows from the Rabaul Caldera, Papua, New Guinea. Contr. Mineral. and Petrol. 38, 1-20.

Jensen, H.I. 1916. Report on the petrology of the alkaline rocks of Mt Erebus, Antarctica. Rep. Brit. Antarct. Exped. 1907-9, Geol. 2, 89-92.

Jones, L. M., Walker, R. L. 1972. Geochemistry of the McMurdo volcanics, Victoria Land: Part 1, Strontium isotope composition. Antarctic Jour. U.S. 7, 142-144.

Kirkpatrick, R. J. 1974. Nucleation and growth of plagioclase in Hawaiian lava lakes. (Abstract). Amer. Geophys. Union Trans. 56, 1198.

Kushiro, I., Nakamura, Y. 1970. Petrology of some lunar crystalline rocks. Proc. Apollo 11 Lunar Science Conference, 1, 607-626.

Kyle, P. R. 1975. Volcanic activity of Mt Erebus, November 1973. N.Z. Volcanological Record 3 (N.Z. Geological Survey), 52-56.

_____, Cole, J. W. 1974. Structural control of volcanism in the McMurdo Volcanic Group, Antarctica. Bull. Volcanolog. 38, 16-25.

Lofgren, G. 1974. An experimental study of plagioclase crystal morphology: Isothermal crystallization. Amer. J. Sci. 274, 243-273.

Mountain, E. D. 1925. Potash-oligoclase from Mt Erebus, Antarctica and anorthoclase from Mt Kenya, East Africa. Mineral. Mag. 29, 331-345.

Nakamura, Y., Coombs, D. S. 1973. Clinopyroxenes in the Tawhiroko tholeiitic dolerite at Moeraki, North-Eastern Otago, New Zealand. Contr. Mineral. and Petrol. 42, 213-228.

Nash, W. P., Carmichael, I.S.E., Johnson, R. W. 1969. The mineralogy and petrology of Mount Suswa, Kenya. J. Petrol. 10, 409-439.

_____, Wilkinson, J.F.G. 1970. Shonkin Sag Laccolith, Montana. Part 1, Mafic minerals and estimates of temperature, pressure, oxygen fugacity and silica activity. Contr. Mineral and Petrol. 25, 241-269.

Nathan, S., Schulte, F. J. 1968. Geology and petrology of the Campbell-Aviator divide, northern Victoria Land, Antarctica. Part 1. Post-paleozoic rocks. N.Z. Jl Geol. Geophys. 11, 940-975.

Nicholls, J., Carmichael, I.S.E., Stormer, J. C. 1971.
Silica activity and P_{total} in igneous rocks. Contr.
Mineral. and Petrol. 33, 1-20.

Norrish, K., Hutton, J. T. 1969. An accurate x-ray
spectrographic method for the analysis of a wide range
of geological samples. Geochim. Cosmochim. Acta 33,
431-453.

Papike, J. J., Cameron, K. L., Baldwin, K. 1974. Amphiboles
and pyroxenes: Characterization of other than quadrilateral
components and estimates of ferric iron from microprobe
data. Geol. Soc. Amer. Abstr. with Programs 6, 1053-1054.

Philpotts, J. A., Schnetzler, C. C. 1968. Europium anomalies
and the genesis of basalt. Chem. Geol. 3, 5-13.

Powell, M., Powell, R. 1974. An olivine-clinopyroxene
geothermometer. Contr. Mineral. and Petrol. 48, 249-263.

Prior, G. T. 1907. Report on the rock-specimens collected
during the "Discovery" Antarctic Expedition, 1901-4.
Nat. Antarctic Exped. 1901-4. Natural History 1, 101-160.

Sato, M., Moore, J. G. 1973. Oxygen and sulphur fugacities
of magmatic gases directly measured in active vents of
Mount Etna. Phil. Trans. R. Soc. Lond. A. 274, 137-146.

Smith, W. C. 1954. The volcanic rocks of the Ross Archipelago.
Nat. Hist. Rep. Brit. Antarct. (Terra Nova) Exped. 1910.,
Geol. 1, 167-227.

Stormer, J. C. 1973. Calcium zoning in olivine and its
relationship to silica activity and pressure. Geochim.
Cosmochim. Acta 37, 1815-1821.

Treves, S. B. 1967. Volcanic rocks from the Ross Island, Marguerite Bay, and Mount Weaver areas, Antarctica. Japanese Antarctic Research Expedition (JARE). Scientific Reports 1, 136-149.

Weill, D. F., Drake, M. J. 1973. Europium anomaly in plagioclase feldspar: experimental results and semiquantitative model. Science 180, 1059-1060.

CHAPTER NINE

PETROGENESIS

Origin of the Basanites

Introduction

Basaltic lavas are predominant in the Balleny, Hallett
and Erebus volcanic provinces but are only minor in the
Melbourne volcanic province where salic lava types predominate.
In all provinces the basaltic lavas are mainly strongly
undersaturated and consist of basanites (basanitoids). A
few analyses of alkali basalt have been reported from the
Hallett volcanic province (page 185).

The parent magma from which most of the differentiation
sequences discussed below were derived is considered to have
the composition of basanite. The Mg number (page 212) shows
that most of the lava has been fractionated during its ascent
from the mantle. Fractionation probably involved removal of
olivine, clinopyroxene and lesser spinel, the main phases that
occur as phenocrysts and microphenocrysts in the lavas.
Basanite from DVDP holes is believed to be the best example
of unmodified mantle-derived basaltic material as it shows a
high pressure mineralogy, high Mg number (>67) and high Ni
concentrations (removal of olivine would cause a rapid
depletion of Ni - hence it is a sensitive guide to olivine
fractionation).

Experimental Studies

Basaltic magmas are believed to form by partial melting of
a peridotitic source rock under upper mantle conditions (Wyllie,
1971; Green, 1971). Experimental studies on natural and
synthetic basaltic systems are numerous (Yoder and Tilley, 1962;
Ito and Kennedy, 1967, 1968; O'Hara and Yoder, 1967; Green
and Ringwood, 1967; Green, 1968, 1971, 1973; O'Hara, 1968;
Kushiro, 1973; also see Boettcher, 1975, for a review of work

in the last five years). The studies are controversial with many disagreements between the various workers (O'Hara, 1968; Kushiro, 1969; and the discussion in Green, 1971).

Factors affecting the composition of a basaltic liquid at its source include (Wyllie, 1971 p. 190):

1) Mineralogical composition of the mantle, which varies with pressure and temperature.

2) Total pressure (depth).

3) Water pressure.

4) Degree of partial melting.

Recently Eggler (1974) has shown that P_{CO_2} plays an important role in the generation of strongly silica-undersaturated magmas (basanites, nephelinites, kimberlites) and must also be taken into consideration in experimental studies.

The origin of nepheline-normative basaltic magmas has been studied extensively by D. H. Green and his co-workers (Bultitude and Green, 1968, 1971; Green, 1968, 1970a, 1970b, 1971, 1973). They concluded that basanites similar in composition to those in the DVDP core (and most of the McMurdo Volcanic Group) are produced in an upper mantle composed of pyrolite (a model composition proposed for the upper mantle by Green and Ringwood, 1963; Ringwood, 1966), with 0.1-0.2% H_2O, by a low degree of partial melting at depths of 80-120 km (Bultitude and Green, 1968). Alkali basalt forms in a mantle of the same composition at a lower pressure by a larger degree of partial melting (Green, 1971).

Rare Earth Element Geochemistry

The concentration of rare earth elements (REE) in basaltic lavas, assumed to have ascended from the mantle without modification, can be used to develop models for magma generation in the upper mantle. Alkali-rich, silica-undersaturated basalts show a very strong enrichment of the light REE over the heavy REE (La/Yb>20) (see Chapter 7; Kay and Gast, 1973). If a mantle composition with a REE content 1-4 times chondrite enriched is assumed, then formation of alkali basaltic magma

requires substantial enrichment of the light REE. The strong partition of heavy REE over light REE into garnet (D^{Ce}=0.01-0.02, D^{Yb}=4.0; Shimizu and Arculus, 1975) indicates that separation of garnet would give REE patterns similar to those observed in alkali basaltic magmas. Models have been developed by Gast (1968), Kay and Gast (1973), Shimizu and Arculus (1975), and Sun and Hanson (1975).

A comparison of REE contents in the analysed DVDP basanite with those given for rocks of alkali basaltic compositions by Kay and Gast (1973) suggests they formed by 1-2% partial melting of a hydrous garnet peridotite mantle with REE concentrations 2 to 3 times chondrite. Sun and Hanson (1975) suggested two models for the generation of Ross Island basanite lavas. The first was similar to that discussed above, while the second involved about 5% partial melting of a garnet peridotite mantle with 3 times chondrite for heavy REE, 4 times for Sm, 6.4 times for Nd, Ce 10.5 times and La 13.7 times chondrite.

Discussion

Experimental studies, particularly those of Green, indicate a greater degree of partial melting than required by the REE models. Therefore the concentrations of the 'incompatible' elements (Green and Ringwood, 1967),which include K, Ti, P, Ba, Sr, Rb, Zr, Hf, U, Th, Pb and the light REE, in the experimental studies will be considerably lower than actually observed in nature. To account for this Green and Ringwood (1967) and subsequent papers by Green and others have suggested a process termed 'wall-rock reaction' by which the incompatible elements are concentrated in a magma. "In this process, it (is) envisaged that a body of magma could, under some conditions, cool by reaction with, and solution of, the lowest melting fraction of any wall-rock material with which it was in contact" (Green, 1970b, p.51) and hence concentrate the incompatible elements.

304.

The lower degree of partial melting required for most
REE models is difficult to conceive, as Carmichael et al.,
(1974 p.652) state "to restrict the alkali-basalt fraction
to about 1 percent (partial melting) - (is) a figure that
seems much too low to account for the volume of alkaline lavas
in many island provinces". Sun and Hanson's (1975) REE model
involving a light REE enriched mantle and 5% partial melting,
overcomes these difficulties.

Green and others in a recent abstract (Roy et al., 1975)
have explained the origin of several Australian SiO_2-under-
saturated alkali basalts by partial melting (<3%) of pyrolite
at 25-30 kbars (80-100 km) in the presence of 2-7 wt % H_2O.
The models were based on major element mass balance
calculations and were consistent with the basalt REE
abundances if an upper mantle source had a twice condrite
REE abundance. Therefore some agreement appears to have
been reached between the REE and experimental models without
relying on 'wall-rock reaction' or a REE-enriched mantle.

In the preceding sections different models developed
from the REE chemistry and high pressure and temperature
melting studies have been discussed. The composition of
basanites from the McMurdo Volcanic Group have been compared
to those used in the melting studies, and models have also
been developed from the REE data. From these it is concluded
that basanites, the typical basaltic lavas in the McMurdo
Volcanic Group, are formed by partial melting of a hydrous
garnet peridotite (pyrolite) upper mantle at pressures of
25-30 kbars (80-100 km).

Origin of the Lava Lineages

Introduction

For alkali rocks potential evolutionary mechanisms are
those of all magmatic suites, namely, liquid immiscibility,

differentiation, assimilation, magmatic mixing, crustal and
mantle anatexis (Sorensen, 1974, Chapter 6; Carmichael *et al.*,
1974, p.60). Addition mechanisms proposed specifically for
the formation of alkali rocks include volatile enrichment,
metasomatic processes and resorption of silicate minerals
(Sorensen, 1974, Chapter 6).

The origin of the basaltic magma has been ascribed to
partial melting processes in the upper mantle (i.e. partial
mantle anatexis). Basanite magma is considered to be the
parental magma for most of the lava lineages found in the
McMurdo Volcanic Group.

Differentiation probably accounts for most of the variation
observed in the non-basaltic or evolved lavas and was also
responsible for modifying most of the basanites on their
ascent to the surface. In the Melbourne and Erebus volcanic
provinces evidence in favour of differentiation include:

1) Sr isotopes which indicate that all lavas are
broadly comagmatic and preclude processes of assimilation
and crustal anatexis (pp.216)

2) A continuous variation in major and trace element
geochemistry. The variations are not linear (Figs. 7.6 to 7.8,
7.13, 1.14) as would be expected if magmatic mixing occurred.
Major and trace element variations are compatible with fractional
crystallization (fractionation) of mineral phases that occur as
phenocrysts in the lavas.

3) The mineralogy which shows well-developed fractionation
trends that are best explained by growth in a differentiating
magma (Figs. 5.1, 5.12, 5.31, 5.32).

Mixing Models

In recent years several computer programmes have been
developed to model magmatic processes (Bryan *et al.*, 1969;
Wright and Doherty, 1970; Reid *et al.*, 1973). Recently Wright
(1974) discussed the methods and results of such calculations
and outlined general procedures for their use.

Mass balance computer programmes solve a number of equations, equal to the number of elements being examined, by least square methods so as to minimize the sum of the squares of the residuals (i.e. the differences between the calculated and observed compositions). In order to illustrate the procedures a model for crystal fractionation in lavas from Hut Point Peninsula and DVDP holes will be examined.

In the following discussion reference should be made to Table 9.1. The suggested model indicates that kaersutite phonolite can form by removal of 8.7% (weight fraction = 0.0871) plagioclase, 3.2% magnetite, 0.8% apatite, 4.2% kaersutite and 4.6% clinopyroxene from DVDP nepheline benmoreite (2-54.72). The residual (phonolitic) liquid would amount to 78.7% (by volume) of the original nepheline benmoreite. Calculations are performed by adding phenocrysts to the phonolite in order to make an estimate of the nepheline benmoreite composition (i.e. the dependent vector). The estimated and observed nepheline benmoreite compositions are shown under Results (Table 9.1). A residual of about 0.1% is considered satisfactory.

Quantitative models such as that illustrated above can be made only when good analyses of the lavas and mineral phases are available.

Balleny volcanic province

The few available chemical analyses of rocks from the Balleny Islands indicate that basanite is the most common. Modification of these by fractional crystallization of olivine, clinopyroxene and minor spinel (the dominant phenocryst phases) probably gave rise to the rare hawaiite lavas. More field work and samples are needed before details of the processes can be discussed.

TABLE 9.1   Least squares mass balance model for the formation of kaersutite phonolite (25793) at Observation Hill, Hut Point Peninsula by crystal fractionation from DVDP nepheline benmoreite (2-54.72).

	Phonolite Observation Hill	Plagioclase**	Magnetite	Apatite	Kaersutite	Clinopyroxene	Nepheline benmoreite 2-54.72
SiO_2	54.82	57.1	0.04	0.36	38.2	47.35	51.90
TiO_2	1.16	-	17.5	-	6.49	2.64	1.85
Al_2O_3	20.41	26.9	1.79	-	14.3	5.60	19.31
$FeO*$	4.31	0.55	73.8	0.18	10.8	8.97	6.67
MnO	0.18	-	1.49	0.07	0.13	0.33	0.20
MgO	1.24	-	1.22	0.17	12.1	11.6	2.07
CaO	3.46	9.14	0.06	50.9	12.2	22.4	5.43
Na_2O	8.50	5.82	-	0.15	2.32	0.78	7.26
K_2O	4.57	0.62	-	-	1.57	-	3.70
P_2O_5	0.26	-	-	43.3	-	-	0.60

Solution

	Weight fraction	1σ
Phonolite	0.7869	0.0056
Plagioclase	0.0871	0.0054
Magnetite	0.0320	0.0008
Apatite	0.0081	0.0009
Kaersutite	0.0420	0.0052
Clinopyroxene	0.0457	0.0033

*** ΣR^2 = 0.0096

Results

	Estimated	Observed	Residuals
SiO_2	51.88	51.90	-0.0167
TiO_2	1.87	1.85	0.0162
Al_2O_3	19.32	19.31	0.0070
$FeO*$	6.67	6.67	-0.0040
MnO	0.21	0.20	0.0104
MgO	2.05	2.07	-0.0150
CaO	5.47	5.43	0.0385
Na_2O	7.33	7.26	0.0698
K_2O	3.72	3.70	0.0161
P_2O_5	0.55	0.60	-0.0453

* Total Fe as FeO
** Mineral analyses were made on phenocrysts and microphenocrysts in nepheline benmoreite (2-54.72) and other DVDP lavas (see Appendix B, Part 2).
*** ΣR^2 = sum of squares of residuals.
†Model was calculated using major element analyses as measured, recalculation of all phases to 100% as recommended by Wright (1974) makes no difference to the model.

Hallett volcanic province

Previously published data on Hallett volcanic province rocks are examined here for comparison with the chemistry of lavas from the other volcanic provinces.

Little has been written on the petrogenesis of the alkali basalt/basanite-trachyte-quartz trachyte sequence. Harrington *et al.*, (1967) noted that the analyses when plotted on an FMA ($FeO+Fe_2O_3$ - MgO - Na_2O+K_2O) diagram show a continuous differentiation series which is similar to differentiation curves of other basaltic provinces. Hamilton (1972) also discussed the Hallett rocks by reference to a FMA plot. He considered the chemical variations could be explained by models involving accumulation of magnesian crystals and the separation of calcic and ferromagnesian crystals combined with addition of volatile alkalis and ferric iron.

Melbourne volcanic province

PARENTAL MAGMA

Basaltic lavas are generally lacking in the Melbourne volcanic province and occur mainly in the volumetrically minor Local Suite. Several analyses show these lavas are basanites which have low concentrations of MgO and Ni and a low Mg number (61-64). The data suggest the lavas have been fractionated during their ascent from the mantle. Cognate olivine nodules (dunite) and the abundant glomeroporphyritic clumps of olivine observed in thin section probably result from accumulation at depth. Therefore it is probable that the lavas were fractionated in the lower crust or upper mantle by crystal fractionation of olivine, clinopyroxene and minor spinel. Removal of olivine has resulted in only minor modification of the original composition.

The Pleiades belong to the Central Suite and are composed of derivative lavas. Two basanite samples which belong to the basanite-nepheline benmoreite lineage were also analysed and have low MgO and Ni concentrations and a chemistry similar

to the Local Suite basanites. The parental magma for the sodic lineage is therefore believed to be similar to the Local Suite lavas.

No basaltic lavas have been found interbedded with the mildly potassic trachyandesite-peralkaline K-trachyte lineage at The Pleiades. The basanites at The Pleiades overlie potassic lineage lavas and show a close time, geochemical and spatial relationship with the sodic lineage lavas. Therefore the composition of a basaltic parent for the potassic lineage is somewhat speculative. Trends for the sodic and potassic lineages converge at the basaltic end of the major and trace element variation diagrams (Figs. 7.4 to 7.8). It is therefore inferred that a basaltic magma similar to that from which the basanites (both Local Suite and those at The Pleiades) differentiated, was also the parent for the potassic lineage lavas.

TRACHYANDESITE-PERALKALINE K-TRACHYTE LINEAGE

The mildly potassic lavas at The Pleiades consist of a trachyandesite-tristanite-K-trachyte-peralkaline K-trachyte lineage. Although there is some scatter within the lava lineage there is a continuous variation in chemistry. TiO_2, total iron (Fe_2O_3+FeO), MgO, CaO, P_2O_5, Sr, Cr, Ni, and Cu all decrease with increased SiO_2. Al_2O_3 increases to the K-trachyte then decreases in the peralkaline K-trachyte. Rb, K_2O and Na_2O are concentrated through the lineage. A genetic relationship is indicated for the trachyandesite-peralkaline K-trachyte lineage by these systematic variations in chemistry. The lineage is believed to form by a process of crystal fractionation. Rare earth element data is variable but it is also considered consistent with this model.

Cognate plutonic inclusions believed to be of cumulate origin, are found in the potassic lineage lavas. They contain olivine, augite, plagioclase, apatite, magnetite and ilmenite as well as late phase interstitial kaersutite and titanobiotite. The same phases with the exception of kaersutite and biotite occur as phenocrysts in the lavas.

Fractionation of the mafic minerals (olivine, augite and opaques) and minor apatite could account for much of the observed variations in the chemistry of the potassic series lavas. The decrease in REE and rapid reduction in P_2O_5 from 0.60% to 0.24% from tristanite to K-trachyte indicates a large amount of apatite was removed. Minor feldspar fractionation may have also occurred from tristanite to K-trachyte as Sr shows a moderate decrease and Eu concentrations go from a small positive Eu anomaly (Eu/Eu* = 1.05) to a small negative Eu anomaly (Eu/Eu* = 0.96).

The rapid decrease in Ba and Sr and the very large negative Eu anomaly (Eu/Eu* = 0.10) in the peralkaline K-trachyte clearly shows that fractionation of alkali and plagioclase feldspar was important in the transition K-trachyte to peralkaline K-trachyte. Preliminary mass balance calculations show that fractionation of 35-40% feldspar and 7% mafic minerals and apatite from a K-trachyte parent will give about 55% peralkaline K-trachyte liquid.

The chemistry of any one rock type is variable so it is likely that differentiation has occurred either in several upper crustal magma chambers or if only one magma chamber was present then different batches of magma were involved.

BASANITE-NEPHELINE BENMOREITE LINEAGE

The basanite-nepheline benmoreite lineage lavas show a systematic variation in major and trace element chemistry which is consistent with their formation by crystal fractionation. There is a general enrichment in all REE from basanite to nepheline hawaiite and a rapid depletion of Cr, V and Ni. Phenocryst phases found in the basanites are olivine (which contains inclusions of spinel) and clinopyroxene. Fractionation of these phases would be consistent with the observed chemistry.

REE chemistry of a nepheline benmoreite shows an enrichment of the light REE (La, Ce, Pr, Nd) and heavy REE (Yb) and a depletion of the middle REE, relative to the nepheline hawaiite. It is considered to result from fractionation of kaersutite. Phenocrysts of kaersutite and augite occur in the nepheline hawaiite and nepheline benmoreite. The observed

variations in chemistry are consistent with the fractionation
predominantly of kaersutite and augite. Fractionation of
minor amounts of feldspar, spinel and apatite may have occurred
to account for the observed small decreases in Sr, V and P_2O_5
respectively.

QUARTZ TRACHYANDESITE-QUARTZ TRACHYTE LINEAGE

The strongly potassic oversaturated lavas at Mt Melbourne
are unique among the McMurdo Volcanic Group. Only a few
chemical analyses are available but these do show a reasonably
systematic variation in chemistry from 56 to 65% SiO_2. It is
believed that the observed variations are the result of
fractional crystallization processes. If the lavas differentiated
from a basaltic parent then the basalt was probably saturated in
order to avoid the complication of crossing the thermal divide,
which is effective at low pressure, in the basalt tetrahedron
(Yoder and Tilley, 1962; Edgar, 1974).

Erebus volcanic province

KAERSUTITE LINEAGE

Lavas at Hut Point Peninsula including those penetrated
by the DVDP holes show the most complete geochemical and
petrographic sequence of any in the Erebus volcanic province.
They are examined here in some detail and used as a general
model for the formation of kaersutite lineage lavas.

An origin for the kaersutite lineage by crystal
fractionation from an initial basanite parental magma was
proposed on the basis of the continuous chemical changes
(see Chapter 7). To test this a series of mixing models were
developed. Results have been discussed briefly under the rare
earth elements (see page 244), but are discussed more fully
here.

Four models are developed:

1) parental basanite to fractionated basanite;

2) parental basanite to nepheline hawaiite;

3) nepheline hawaiite to nepheline benmoreite;

4) nepheline benmoreite to kaersutite phonolite.

Solutions for 1 to 3 are given in Appendix E, and 4 is given in Table 9.1.

Basanite (1-88.55) hereafter termed 'fractionated basanite' has a marked depletion of Cr, Ni and MgO and an enrichment of rare earth elements (REE) over what is considered the parental basanite (2-99.34). The data suggest fractionation of olivine, clinopyroxene and spinel. A successful mass balance model (Appendix E, Table 1) confirms this prediction and indicates it can be formed by crystallization and removal of 18.6% clino-pyroxene, 11.6% olivine, 1.3% spinel, 0.5% ilmenite and 0.3% apatite.

Nepheline hawaiite (2-70.41) has higher Cr and lower Nb, Zr, Pb, La, Ce and Pr than the fractionated basanite, indicating the two lavas cannot be related by a simple crystal fractionation model. Trace element chemistry is however compatible with the derivation of the nepheline hawaiite from parental basanite by fractionation of olivine+pyroxene+spinel+ kaersutite. A successful model (Appendix E, Table 2) indicates that crystallization and removal of 27.2% pyroxene, 11.1% olivine, 6.2% spinel, 11.6% kaersutite and 1.1% apatite from basanite (2-99.34) would yield 43.9% nepheline hawaiite. Some difficulty was encountered in finding a suitable spinel composition to satisfy the model. Spinels in the basanite are typically strongly zoned (see Chapter 5). The two spinels used in the model calculations represent two extreme compositions which are expected to account for any natural variation of the spinels during fractionation.

Nepheline benmoreite (2-54.72) can be derived from nepheline hawaiite by fractional crystallization involving the removal of 1.75% plagioclase, 0.2% ilmenite, 3.5% magnetite, 1.05% apatite, 9.0% kaersutite and 7.6% pyroxene (Appendix E, Table 3). The estimated model shows poor solutions for Na_2O and K_2O (with residuals of 0.14 and 0.13 respectively) although

the overall solution appears satisfactory ($\Sigma R^2 = 0.06$).
Kaersutite is now the main mafic phase removed and plagioclase
is beginning to crystallise and be removed.

The transition from nepheline benmoreite to kaersutite
phonolite (25793) has been discussed above (page 305 and Table
9.1). Plagioclase fractionation is the main feature of this
transition. Kaersutite and pyroxene are removed in nearly
equal amounts, the weight fraction of each being about half
that of plagioclase.

Apatite is removed in all steps of the basanite to
phonolite sequence and accounts for the regular decrease in
P_2O_5. In the basanite to fractionated basanite transition
apatite is only very slightly fractionated (the model indicates
0.3% apatite removed) In the same transition TiO_2 also shows
an increase. Goldich *et al.*, (1975) were puzzled by the
behaviour of P_2O_5, which increased in the basanites
(basanitoids) and 'trachybasalts'. The mass balance model
indicates this increase can be satisfactorily explained by
the lack of apatite crystallization, hence P is concentrated
in the liquid.

Rare earth element concentrations have been successfully
predicted using the mass balance solutions and published
rare earth element partition coefficients (see Chapter 7).
These calculations add confidence to the suggested models.

Prediction of trace element concentrations other than
REE are difficult due to a lack of data on partition
coefficients. Some elements are however concentrated in the
residual liquid and are not partitioned into any mineral phase.
These 'residual' or 'incompatible' elements include Rb, Cs,
Pb, Th and U.

The concentration of a trace element in a liquid can be
described by the equation (Shaw, 1970; Zielinski, 1975),

$$c_1/c_0 = \frac{1}{F + K(1-F)}$$

c_0 = concentration of trace element in initial system;
c_1 = concentration of trace element in remaining liquid;
F = fraction of liquid remaining;
K = distribution coefficient of trace element in mineral
phases removed.

For a perfectly residual element K = 0, therefore

$$C_1/C_0 = \frac{1}{F}$$

As F is known from the mass balance calculations and C_0 is the trace element concentration in the basanite (assumed parent) then C_1 can be calculated in the fractionated lavas. Results are shown in Table 9.2 and Figure 9.1.

Calculated values in the fractionated basanite are similar or higher than the observed concentrations, with the exception of Pb. Hence in satisfactory agreement with the fractionation crystallisation and mass balance models.

In the nepheline hawaiite, nepheline benmoreite and phonolite the calculated residual element concentrations are generally lower than the measured values. These discrepancies are difficult to explain as the differences are outside analytical error (Rb ±3%; Cs, Pb, Th, U ±15%). Assuming the analyses are correct this then implies that either

1) F the fraction of liquid remaining is incorrect; or 2) volatile elements (i.e. the residual elements) were added to the system.

Neither explanation is entirely satisfactory. If the first is accepted then the major element mass balance calculations are incorrect. Assuming the observed concentrations of residual elements in the parental basanite and phonolite are correct and if K = 0 then F may be calculated. K is likely to be >0 as minor partitioning would occur, therefore the calculated F is a maximum. Results are given in Table 9.3. Elements Cs, Pb and Th indicate that the phonolite would represent only 17% of the parent basanite liquid. This compares with 26% as derived by the major element mass balance calculations.

TABLE 9.2 Calculated and observed concentrations of the residual elements in lavas from Hut Point Peninsula.

	Parental basanite	Fractionated basanite		Nepheline hawaiite		Nepheline benmoreite		Phonolite	
	Co	Calc.	Obs.	Calc.	Obs.	Calc.	Obs.	Calc.	Obs.
F*	100	67.52		43.91		33.54		26.37	
Rb	30	44	41	68	72	89	97	114	139
Cs	0.3	0.4	0.4	0.7	0.5	0.9	1.3	1.14	1.7
Pb	4.3	6.4	11.5	9.8	7.6	12.8	15.2	16.3	24.2
Th	4.6	6.8	6.3	10.5	12.9	13.7	18.2	17.4	26.7
U	1.0	1.5	1.4	2.3	2.8	3.0	4.0	3.8	7.0

* F = % of parent basanite liquid remaining as calculated from major element mass balance computations.
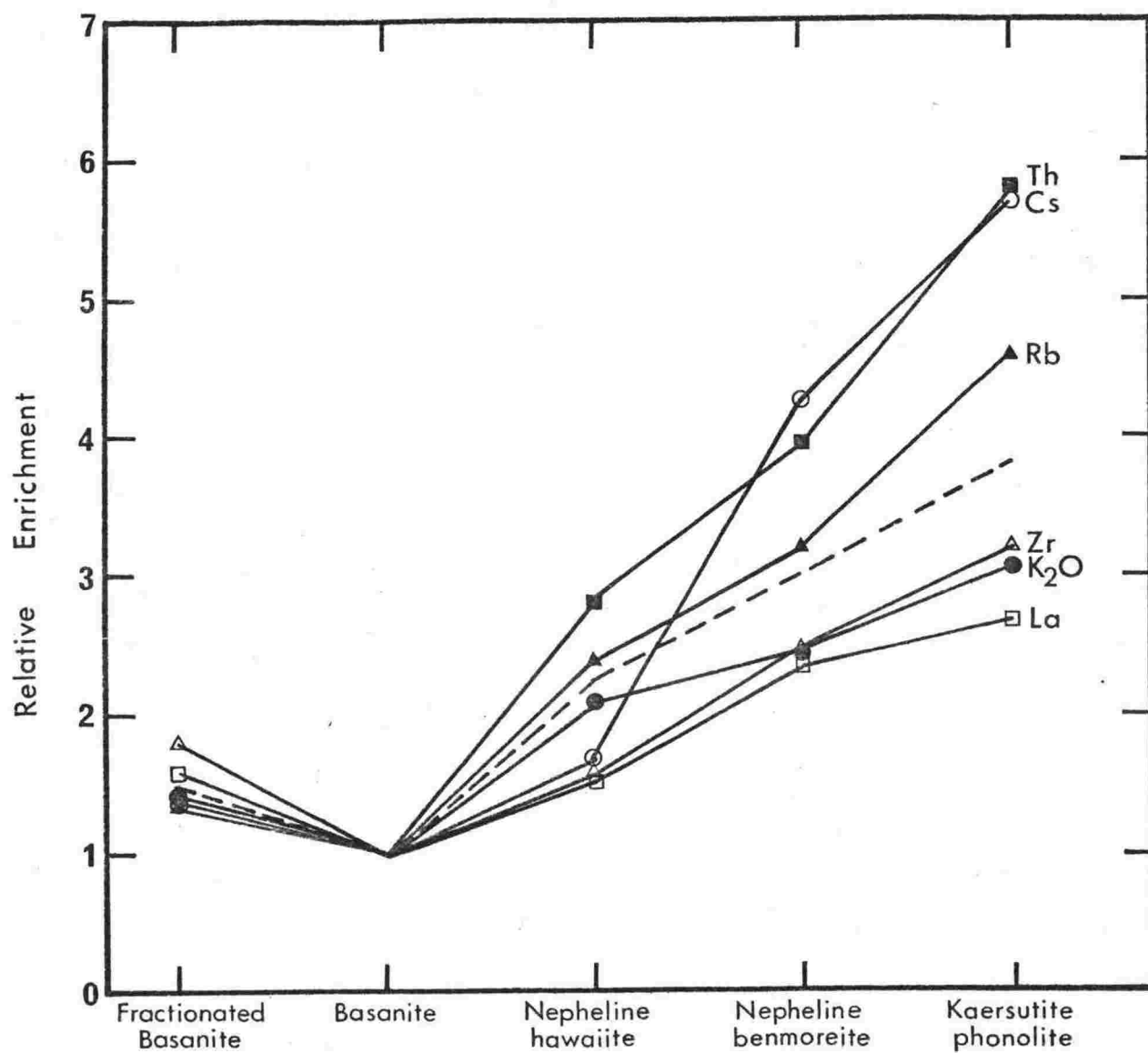
FIGURE 9.1 Enrichment of some incompatible elements in kaersutite
lineage lavas from Hut Point Peninsula and DVDP holes.
Abundances normalised relative to DVDP basanite 2-99.34.
Dashed line indicates enrichment of perfectly incompatible
element, as predicted by major element mass balance models.

TABLE 9.3 Fraction of phonolitic liquid derived from basanite
assuming pure residual behaviour of elements listed.

Element	C_o Basanite	C_ℓ Phonolite	F
Rb	30±3%	139±3%	0.2158
Cs	0.3±15%	1.7±15%	0.1765
Pb	4.3 "	24.2 "	0.1777
Th	4.6 "	26.7 "	0.1723
U	1.0 "	7.0 "	0.1428

F = fraction of phonolite liquid.

C_o = measured concentration in parental basanite.

C_ℓ = measured concentration in phonolite liquid.

If the second explanation of volatile enrichment is
accepted then it is possible that other volatile components
such as K, La, Ce, CO_2, F, H_2O and Cl would also be enriched.
The last four named would be presumably lost during degassing
of the magma column when the lava flows were erupted, as
there is no evidence of high concentrations of these components
in the rocks. Major element mass balance calculations appear
to be good for K_2O while the calculated abundance of Ce is
also satisfactory. Therefore it is unlikely that K, Ce and La
have also been enriched (Fig. 9.1).

Volatile enrichment appears to have affected the nepheline
hawaiite, nepheline benmoreite and kaersutite phonolite lavas
but not the fractionated basanite. It is noteworthy that the
first group of lavas all contain kaersutite, which requires
hydrous conditions for crystallization. High concentrations
of F and Cl would also help stabilize the crystallization
of kaersutite (Holloway and Ford, 1973). There is no
mineralogical evidence of hydrous conditions during crystal-
lization of the fractionated basanite, also there is little
or no evidence suggesting volatile enrichment.

Because of the consistent nature of the major element and
REE data, the fractionation crystallization models developed
from the major element mass balance calculations are adopted
here to explain the formation of the kaersutite lineage.

Volatile enrichment is also invoked to explain the concentrations of residual elements, Rb, Cs, Pb, Th and U. Volatile enrichment as a process has been used to explain the development of trends in alkaline magmas from several volcanic provinces (see summary in Sorensen, 1974, p.536). Price (1973) in his study of Dunedin Volcano noted 'some sort of "volatile transfer" process might be important in concentrating the incompatible elements' in the benmoreite and phonolite lavas.

The final step in the kaersutite trend is from kaersutite phonolite to pyroxene (aegirine-augite) phonolite. It is best exhibited in lavas from Post Office Hill and The Knoll, Cape Crozier. Pyroxene phonolite (The Knoll) is strongly depleted in Sr and to a lesser extent Ba, and is enriched in Rb, total alkalis and K_2O relative to the kaersutite phonolite (Post Office Hill). TiO_2 also decreases slightly. Fractional crystallization of anorthoclase (a microphenocryst phase) and minor kaersutite or titanomagnetite in the kaersutite phonolite would account for the observed changes in chemistry. In the phonolites, aegirine-augite may have crystallised as the main mafic phase instead of kaersutite due to an increase in the oxygen fugacity. Aegirine-augite has a high Fe^{3+} concentration and this is favoured under conditions of high or increasing oxygen fugacity.

Discussion

The fractional crystallization and volatile enrichment model developed for Hut Point Peninsula and DVDP lavas is believed to be applicable to other Erebus volcanic province lava sequences. Intermediate lavas described by Adams (1973) at Brown Peninsula are extremely similar both mineralogically and geochemically to those at Hut Point Peninsula and DVDP. Fractionation of the same mineral phases as indicated in the mass balance models for Hut Point Peninsula, probably in slightly different proportions, is therefore proposed to account for the intermediate lavas at Brown Peninsula.

Intermediate lavas are generally lacking at Cape Bird and Cape Crozier, but phonolite similar to that at Hut Point

Peninsula does occur. It would be special pleading to invoke any other process other than that discussed above for Hut Point Peninsula lavas for the petrogenesis of phonolites at Cape Bird and Cape Crozier.

EREBUS LINEAGE

No basaltic lavas are known from the Erebus Centre so it is assumed that basanite similar to that found at surrounding centres (e.g. Cape Crozier, Hut Point Peninsula) is the parent for the observed fractionation trend.

Conclusions on the petrogenesis of the Erebus lineage are difficult because of the almost complete lack of aphyric lavas. REE analyses of strongly porphyritic nepheline hawaiite and nepheline benmoreite lavas show small negative and positive Eu anomalies, $Eu/Eu^* = 0.91$ and 1.04 respectively. The nepheline hawaiite is unlikely therefore to contain cumulus feldspar while the nepheline benmoreite may contain minor cumulus feldspar. Anorthoclase phonolite from Mt Erebus has a large positive Eu anomaly ($Eu/Eu^* = 1.31$) resulting from up to 27% cumulus anorthoclase. Therefore whole rock analyses of the anorthoclase phonolite do not represent liquids in a liquid line of descent.

A qualitative fractional crystallization model has been discussed under the REE chemistry (see Chapter 7). The main mafic phenocryst phases of olivine, augite and opaques were probably fractionated and would account for the observed REE patterns and major and trace element chemistry. There is no strong depletion of the middle REE so kaersutite was unlikely to be of any importance during differentiation. Kaersutite is also not usually observed as a phenocryst phase.

A feature of the Erebus lineage lavas is the abundance of feldspar phenocrysts. Feldspar was not a major phase during fractional crystallization processes, as shown by the whole rock-groundmass trend lines (page 208) and the lack of large Eu anomalies. It is believed therefore that the feldspar crystallised at higher levels (i.e. lower pressure) than that at which differentiation occurred.

Conclusions

Differentiation by crystal fractionation of mantle-derived basaltic magma is believed to explain the evolution of most lava lineages within the McMurdo Volcanic Group. A generalised petrogenetic scheme is shown in Fig. 9.2. Although crystal fractionation could account for most of the observed variation in the lineages, volatile enrichment is also necessary, though less important, in the evolution of lineage B.

In the Erebus volcanic province two chemically similar lineages have been suggested (A and B, Fig. 9.2). Kaersutite is important in the evolution of lineage B, whereas it does not appear to be a major or important phase in lineage A (Fig. 9.2). What factors are therefore responsible for the appearance of kaersutite?

Two factors, P_{H_2O} and temperature, are considered to be responsible for the appearance of kaersutite and could explain the differences in the mineralogy of lineages A and B. Knutson and Green (1975), in experimental melts of a quartz normative hawaiite, found that amphibole crystallised when the H_2O content was 5%, at lower H_2O contents (2%) amphibole was not observed. Holloway and Burnham (1972) have discussed the difficulties of evaluating the effect of decreasing f_{H_2O} on the upper limit in stability of amphiboles. It is not possible at this stage to give a minimum estimate of P_{H_2O} in lineage B lavas, but the presence of kaersutite does imply hydrous conditions prevailed.

The Ti versus Al relationship of kaersutite in McMurdo Volcanic Group lavas (Fig. 5.24) suggests the kaersutite is not mantle-derived and also is unlikely to have a shallow crustal origin. Formation in the lower crust would seem most likely. From an examination of kaersutite stability (Fig. 5.25) it was suggested (page 131) that kaersutite in McMurdo Volcanic Group lavas crystallised at pressures below 12 kbars. At 12 kbars and lower pressures the upper stability limit of kaersutite is about 1050°C (Yagi et al., 1975) (Fig. 5.26). Holloway and Burnham (1972) found kaersutite in melts of tholeiitic basalt at 8 kbars and 1050°C. They suggested it

FIGURE 9.2   Generalised petrogenetic scheme for the evolution
             of lavas in the McMurdo Volcanic Group. The
             vertical scale shows in a general way the effects
             of decreasing pressure. Phases that may have been
             removed by fractional crystallization are shown in
             italics. When the proportions of phases removed
             are known they are listed in decreasing order. If
             the proportions are not known the possible phases
             are listed vertically. cpx - clinopyroxene,
             ol - olivine, sp - spinels (including magnetite and
             ilmenite), kaer - kaersutite, mt - magnetite
             (including ilmenite), ap - apatite, fsp - feldspar
             (undifferentiated), anorth - anorthoclase,
             plag - plagioclase, +vol - indicates volatile
             enrichment.

Increasing a_{SiO_2} of basaltic lavas

BASANITE (25-30 kb)

$cpx > ol > sp$

fractionated basanite

$cpx > ol > kaer > sp$?
$+ vol$ decreasing P_{H_2O}

increasing P_{H_2O}

increasing P_{H_2O}, f_{O_2}

ALKALI BASALT

TRANSITIONAL BASALT

? high pressure ?

QUARTZ TRACHYANDESITE → QUARTZ TRISTANITE → QUARTZ K-TRACHYTE

HAWAIITE → MUGEARITE → BENMOREITE → TRACHYTE → QUARTZ TRACHYTE

NEPHELINE HAWAIITE

$kaer > cpx > mt$
$> plag$
$+ vol$

NEPHELINE MUGEARITE

$kaer > cpx > mt$
$> plag$
$+ vol$

NEPHELINE BENMOREITE

$plag > cpx > kaer$
$> mt > ap$
$+ vol$

KAERSUTITE PHONOLITE

increasing f_{O_2}
ancrth

PYROXENE PHONOLITE

TRACHYANDESITE

decreasing f_{O_2}

ol
cpx
mt
ap

TRISTANITE decreasing f_{O_2}

ol
cpx
fsp
mt
ap

K-TRACHYTE increasing f_{O_2}

fsp

PERALKALINE K-TRACHYTE

NEPHELINE HAWAIITE

ol
cpx
mt
ap

NEPHELINE BENMOREITE

ol
cpx
mt
ap
fsp?
(?5 kb?)

ANORTHOCLASE PHONOLITE (Kenyte)

fsp cry.   Eruption

feldspar crystallization   Eruption

feldspar crystallization   Eruption

Decreasing depth (pressure) – not to scale

UPPER MANTLE

LOWER CRUST

UPPER CRUST

OCCURRENCE

A   Erebus Centre, Mt Discovery?

B   Ross Island (except Erebus Centre)
     Brown Peninsula
     The Pleiades (in part)

C   The Pleiades
     Mt Overlord?

D   Hallett volcanic province
     Balleny volcanic province?

E   Mt Melbourne
     Mt Cis?

was stable to about 1060°C at 8 kbars, in excellent agreement
with the stability determined by Yagi *et al.*, (1975). In the
experiments of Holloway and Burnham, olivine and clinopyroxene
continued to exist at temperatures above the stability of
kaersutite. Yagi *et al.*, (1975) showed that at pressures of
10 kbars and less and at temperatures greater than 1050°C,
kaersutite will break down to olivine and clinopyroxene.

It is therefore postulated that the occurrence of
kaersutite in the kaersutite lineage lavas and not in the
chemically similar Erebus lineage lavas results from lower
temperatures (<1060°C) and higher P_{H_2O} of the former.

The Mantle Plume Model

Recent and active volcanism in the McMurdo Sound area clearly indicates the region is the site of a "hot spot". The term "hot spot" is used here 'to describe localised volcanicity as a surface feature without implying what sub-surface phenomena are associated with it (Burke *et al.*, 1973)' (Chesworth, 1975). However Morgan (1972) assumed that hot spots are 'surface expressions of deep mantle plumes roughly 150 km in diameter' which consist of large convecting upwellings of mantle material. As the material rises from the mantle it apreads out in the asthenosphere causing stresses on the bottom of plates and so drives them apart. Diapiric upwelling of basalt magma would be associated with the plume, with larger volumes of magma upwelling at the centre of the plume than at the fringes.

Kyle and Cole (1974) (Chapter 2) recognised radial triplex symmetry of vents about Mt Erebus, Ross Island. They suggested the symmetry may have resulted from crustal doming with the development of radial fractures. Radial triplex symmetry occurred presumably because this is a least work configuration. The action of a plume impinging on the crust may account for the inferred radial triplex fractures, similar to, but on a smaller scale than, plume-generated triple junctions (Burke and Dewey, 1973).

All volcanic vents on Ross Island occur within a 50 km radius of Mt Erebus. Mt Bird and Mt Terror are two major vents on Ross Island, and are both 30 km from Mt Erebus (Fig. 3.10). Surface expression of volcanism on Ross Island therefore suggests a plume about 100 km in diameter, with the greatest amount of volcanism within a diameter of about 60 km.

Mt Erebus is composed predominantly of anorthoclase phonolite lavas. The differentiation model for anorthoclase phonolite (Fig. 9.2) implies a very large volume of basaltic and intermediate material underlying the volcano, presumably in crustal magma chambers. If the uplift model of Kyle and Cole (1974) is assumed then the centre of the postulated plume would be the region of greatest mantle upwelling and

crustal extension and hence a favourable site for large scale
magma chambers in which differentiation would occur.

Kaersutite lineage lavas are characteristic of the
eruptive centres surrounding Mt Erebus (i.e. Mt Bird,
Mt Terror and Hut Point Peninsula). The petrogenetic scheme
discussed above (Fig. 9.2) requires these to differentiate
from smaller, cooler and more hydrous batches of basaltic
magma. This therefore implies that the outer part of the
plume would be cooler and with a higher water pressure than
in the centre.

The model of a plume situated beneath Ross Island can
also be applied to the Mt Discovery area. Radial triplex
symmetry, similar to Ross Island, is also found at Mt Discovery
(Kyle and Cole, 1974). The main centres at Brown Peninsula
and Mt Morning (Fig. 3.10) are nearly 30 km from Mt Discovery,
similar to the vents on Ross Island. A plume 100 km in
diameter would include all volcanic vents on Brown Peninsula,
Minna Bluff, Mt Morning, Black Island and the Koettlitz
Glacier (Fig. 3.10). Eruptive centres in the Dry Valleys
and part of White Island would not be covered by either the
Erebus or Discovery plumes.

Porphyritic lavas similar to the Erebus lineage lavas
occur on Mt Discovery, while kaersutite lineage lavas occur
at Brown Peninsula and probably at Mt Morning. The geology
of Minna Bluff is unknown. Therefore Mt Discovery and its
surrounds are nearly identical in structure and petrology to
Mt Erebus and surrounds. These similarities are not likely
to be fortuitous.

It is concluded that McMurdo Sound is the site of two
hot spots each of which overlies a mantle plume. As the
plumes impinged on the crust they caused triplex radial
fractures. Large volumes of basaltic magma were intruded into
the crust at the centre of the plumes (i.e. the centre of the
triplex symmetry) and here it differentiated to give the large
volume of anorthoclase phonolite and associated porphyritic
intermediate lavas, which are common at Mt Erebus and
Mt Discovery. On the outer part of the plumes the basalt

magma differentiated in much smaller crustal magma chambers under cooler and more hydrous conditions.

The occurrence of hot spots and the implications of mantle plumes in the McMurdo Sound area have far reaching consequences if the model of Morgan (1972) is followed in the strict sense. Morgan suggested plumes were the driving force for moving plates apart, he also suggested the plumes had a diameter of 150 km. The plumes envisaged here are smaller than those of Morgan and the model has been used only to explain features of the volcanism. No conclusions are made on the implications of the plume model to the tectonic setting of the western Ross Sea area.

APPENDIX A

PALEOMAGNETIC DETERMINATIONS AND RESULTS

Paleomagnetic measurements were made on oriented one inch (25 mm) core samples collected using a portable gasoline-engine drill. Kerosene was used as a coolant and lubricant for the drill-bit. Remanent magnetism (RM) was measured using a fluxgate-spinner magnetometer (See Lienart (1971) for a fuller description of the equipment and analytical procedures). The samples were not cleaned by demagnetization techniques. McMahon and Spall (1974a,b) examined paleomagnetic core samples from DVDP hole 2 and stated 'during both alternating field (A.F.) and thermal demagnetization the major magnetic component continued to be vertical and very little migration of the magnetic vector was noted.' The normal and reverse paleomagnetic directions are almost parallel or antiparallel respectively to the present geomagnetic field, which again reflects an unlikely viscous component of magnetism. R.M. measurements therefore reflect the polarity at the time of solidification of the lavas.

Instrumental and field orientation errors may be of the following magnitudes:

$\pm 20^\circ$ for declination (D); $\pm 10^\circ$ for inclination (I); and $\pm 20\%$ for magnetic intensity (J).

TABLE A.1 Paleomagnetic measurements of lavas from Cape Bird, Ross Island.

Sample Number	Location	Rock Type	N	J	D	I	K	R	α_{95}	Polarity
CB1	Alexander Hill	Pyroxene-hornblende trachyte	7	0.6	147	64	114	6.96	6	R
CB2	Cinder Hill	Olivine basalt	3	0.8	198	38	96	2.98	13	R
CB4	Alexander Hill	Pyroxene-hornblende trachyte	4	0.7	238	70	384	3.99	5	R
CB5	Alexander Hill	Pyroxene trachyte	8	0.9	217	67	109	7.94	5	R
CB6	Trachyte Hill	Hornblende trachyte	9	5.5	40	44	202	8.96	4	R
CB7	Main Mt Bird Cone	Hornblende-augite-plagioclase basalt	1	0.3	144	-62	-	-	-	N
CB8	Inclusion Hill	Hornblende-pyroxene trachyte	7	0.003	55	79	4250	7.00	1	R
CB9	Main Mt Bird Cone	Olivine-augite plagioclase basalt	2	1.96	120	69	892	2.00	8	R

N = number of samples measured, J = mean intensity of magnetization ($\times 10^{-3}$ emu/cc),

D and I = mean declination and mean inclination of remanent magnetism respectively,

K = precision constant, R = resultant vector, α_{95} = semi-vertical angle of 95% conficence

cone, N = normal, R = reversed.

328.

TABLE A.2 Paleomagnetic measurements of lavas from Hut Point Peninsula, Ross Island.

Sample Number	Location	Rock Type	N[†]	J	D	I	K	R	α_{95}	Polarity
SB2	North side of Twin Crater	Olivine-augite basanite	6	6.5	322	-23	870	5.99	2.3	N(?)*
SB1	South end of Second Crater	Olivine-augite basanite	8	4.0	208	-80	537	7.99	2.4	N
SB4	South end of Half Moon Crater	Augite-kaersutite basanite	1	10.2	61	-78	-	-	-	N
SB3	Observation Hill near Nuclear Power Plant	Kaersutite phonolite	9	2.7	319	84	89	8.91	5.5	R
SB5	Flows, 250 m north of Scott Base	Olivine-augite basanite	9	8.7	196	-88	1836	9.00	1.2	N

†See Table A.1 for symbol identification,

*The low value of inclination suggests this sample may have acquired a viscous component of magnetization. However in the vicinity of the sample site extensive bulldozer scrapping has occurred and it is suggested that the site has been disturbed.

APPENDIX B

ELECTRON MICROPROBE ANALYSES OF GLASS AND MINERALS FROM

LAVAS AND INCLUSIONS OF THE MCMURDO VOLCANIC GROUP

Part 1.   The Pleiades

Table 1. Electron microprobe analyses of olivine in rocks from The Pleiades

| Sample | 25703 | | | | | | | 25668 | |
Grain	1C	1I	1R	3C	3R	2C	4-g	3	2C
SiO_2	39.7	39.6	38.3	39.4	39.6	39.1	39.4	34.1	33.9
Al_2O_3	0.05	0.05	0.04	0.05	0.04	0.04	0.04	0.03	–
TiO_2	–	–	0.05	–	–	0.03	0.04	0.03	0.04
FeO*	17.6	18.2	22.5	17.6	18.6	19.4	19.6	35.0	35.2
MnO	0.25	0.25	0.42	0.25	0.28	0.27	0.31	0.63	0.64
MgO	42.5	42.0	36.2	42.1	41.0	40.5	39.7	29.5	29.3
CaO	0.26	0.26	0.27	0.26	0.26	0.27	–	0.35	0.35
Cr_2O_3	–	n.d.	–	n.d.	n.d.	–	n.d.	–	–
NiO	0.12	n.d.	0.04	n.d.	n.d.	0.08	n.d.	n.d.	0.06
Total	100.48	100.36	97.82	99.66	99.78	99.69	99.09	99.64	99.49

Number of cations on the basis of 4 (O)

Si	1.004	1.005	1.020	1.005	1.012	1.006	1.019	0.959	0.956
Al	0.002	0.001	0.001	0.002	0.001	0.001	0.001	0.001	–
Ti	–	–	0.001	–	–	0.001	0.001	0.001	0.001
Fe	0.372	0.386	0.500	0.376	0.399	0.417	0.424	0.821	0.829
Mn	0.005	0.005	0.009	0.005	0.006	0.006	0.007	0.015	0.015
Mg	1.604	1.589	1.438	1.599	1.562	1.553	1.529	1.233	1.229
Ca	0.007	0.007	0.008	0.007	0.007	0.007	–	0.011	0.011
Cr	–	–	–	–	–	–	–	–	–
Ni	0.003	–	0.001	–	–	0.002	–	–	0.001
Z	1.004	1.005	1.020	1.005	1.012	1.006	1.019	0.959	0.956
X	1.993	1.988	1.958	1.989	1.975	1.987	1.962	2.082	2.086
Sum	2.997	2.993	2.978	2.994	2.989	2.993	2.981	3.041	3.042
Fe	18.8	19.5	25.8	19.0	20.4	21.2	21.7	40.0	40.3
Mg	81.2	80.5	74.2	81.0	79.6	78.8	78.3	60.0	59.7

Table 1 continued

Sample	25668 cont.				25671			25661	
Grain	2R	1C	1R	5	4-g	7	1	4	3C
SiO$_2$	33.6	33.8	33.85	33.85	37.5	37.3	37.5	35.7	34.5
Al$_2$O$_3$	–	–	0.03	–	0.04	–	–	–	–
TiO$_2$	0.06	0.03	0.03	0.04	0.03	–	0.03	0.03	–
FeO*	37.45	36.3	36.8	37.2	29.5	29.6	29.7	35.5	36.4
MnO	0.73	0.72	0.72	0.72	0.63	0.57	0.58	0.71	0.77
MgO	27.0	27.9	27.1	27.0	32.8	33.1	32.8	27.5	26.75
CaO	0.32	0.34	0.27	0.35	0.23	0.25	0.26	0.26	0.27
NiO	n.d.	0.06	n.d.	n.d.	n.d.	–	–	n.d.	n.d.
Total	99.16	99.15	98.80	99.16	100.73	100.82	100.87	99.70	98.69

Number of cations on the basis of 4 (O)

Si	0.961	0.961	0.967	0.966	1.004	0.998	1.002	0.999	0.983
Al	–	–	0.001	–	0.001	–	–	–	–
Ti	0.001	0.001	0.001	0.001	0.001	–	0.001	0.001	–
Fe	0.896	0.863	0.881	0.887	0.660	0.662	0.665	0.831	0.868
Mn	0.018	0.017	0.018	0.017	0.014	0.013	0.013	0.017	0.019
Mg	1.152	1.183	1.156	1.150	1.309	1.320	1.307	1.145	1.137
Ca	0.010	0.010	0.008	0.011	0.007	0.007	0.008	0.008	0.008
Ni	–	0.002	–	–	–	–	–	–	–
Z	0.961	0.961	0.967	0.966	1.004	0.998	1.002	0.990	0.983
X	2.077	2.076	2.065	2.066	1.992	2.002	1.994	2.002	2.032
Sum	3.038	3.037	3.032	3.032	2.996	3.000	2.996	2.992	3.015
Fe	43.8	42.2	43.3	43.5	33.5	33.4	33.7	42.1	43.3
Mg	56.2	57.8	56.7	56.5	66.5	66.6	66.3	57.9	56.7

Table 1 continued

Sample	25661 cont.				25666				
Grain	3R	2C	2R	6-g	1C	1R	4C	4R	5-X
SiO_2	35.9	34.9	35.2		38.6	38.9	38.0		34.6
Al_2O_3	–	–	0.17		0.05	n.d.	0.06		0.03
TiO_2	–	–	–		–	n.d.	–		–
FeO*	36.6	37.6	37.8	42.3	21.1	21.0	24.1	25.2	41.8
MnO	0.79	0.83	0.75		0.30	n.d.	0.36		1.31
MgO	26.6	26.1	27.3	20.9	40.1	40.3	38.0	36.9	22.1
CaO	0.24	0.27	0.25	0.43	0.22	0.22	0.20	0.19	0.33
NiO	n.d.	n.d.	n.d.		0.10	0.15	0.07		–
Total	100.13	99.70	101.47		100.47	100.57	100.79		100.17

Number of cations on the basis of 4 (O)

Si	1.004	0.989	0.989		0.994	0.999	0.991		0.998
Al	–	–	0.006		0.002	–	0.002		0.001
Ti	–	–	–		–	–	–		–
Fe	0.855	0.891	0.841		0.455	0.451	0.525		1.009
Mn	0.019	0.020	0.018		0.007	–	0.008		0.032
Mg	1.110	1.102	1.146		1.539	1.542	1.475		0.951
Ca	0.007	0.008	0.008		0.006	0.006	0.006		0.010
Ni	–	–	–		0.002	0.003	0.001		–
Z	1.004	0.989	0.989		0.994	0.999	0.991		0.998
X	1.991	2.021	2.019		2.011	2.002	2.017		2.003
Sum	2.995	3.010	3.008		3.005	3.001	3.008		3.001
Fe	43.5	44.7	42.3	53.2	22.8	22.6	26.2	27.7	51.5
Mg	56.5	55.3	57.7	46.8	77.2	77.4	73.8	72.3	48.5

Table 1 continued

Sample	25702	
Grain	4	2

SiO_2	33.5	33.4
Al_2O_3	0.03	-
TiO_2	-	-
FeO*	56.4	57.0
MnO	2.37	2.46
MgO	9.73	9.01
CaO	0.30	0.32
Total	102.33	102.19

Number of cations on the basis of 4 (O)

Si	1.022	1.025
Al	0.001	-
Ti	-	-
Fe	1,440	1.462
Mn	0.061	0.064
Mg	0.443	0.412
Ca	0.010	0.010
Z	1.022	1.025
X	1.955	1.948
Sum	2.977	2.973
Fe	76.5	78.0
Mg	23.5	22.0

Table 2. Electron microprobe analyses of pyroxenes in rocks from The Pleiades

Sample	25703							25668	
Grain	3C	3R	5C	5R	4C	4R	2	4C	7
SiO_2	46.8	46.9	44.8	45.5	50.2	45.0	52.0	48.9	49.2
Al_2O_3	7.82	8.22	10.1	8.50	3.44	9.04	2.06	3.02	3.06
TiO_2	2.68	1.77	2.97	3.05	0.95	3.31	0.52	1.45	1.53
FeO^*	8.24	8.26	8.73	8.21	12.0	8.41	13.3	7.94	8.41
MnO	0.14	0.16	0.15	0.15	0.44	0.15	0.74	0.19	0.19
MgO	12.2	13.5	10.7	11.8	12.2	11.6	11.2	14.0	14.4
CaO	21.4	21.3	20.6	21.2	19.4	21.1	20.2	21.5	21.5
Na_2O	0.50	0.61	0.91	0.63	0.67	0.66	0.69	0.46	0.52
Cr_2O_3	-	0.06	-	0.07	-	0.04	-	0.52	0.40
Sum	99.78	100.78	98.96	99.11	99.30	99.31	100.71	97.98	99.21
Fe_2O_3	1.66	5.48	2.58	2.59	1.41	2.83	0.49	2.47	2.65
FeO	6.75	3.33	6.40	5.88	10.7	5.86	12.86	5.72	6.02
Total	99.95	101.33	99.22	99.37	99.44	99.59	100.76	98.23	99.48

Number of cations on the basis of 6 (O)

Si	1.747	1.719	1.688	1.711	1.901	1.690	1.958	1.857	1.848
Al	0.253	0.281	0.312	0.289	0.099	0.310	0.042	0.135	0.135
Al	0.092	0.074	0.137	0.087	0.054	0.090	0.049	-	-
Ti	0.075	0.049	0.084	0.086	0.027	0.093	0.015	0.041	0.043
Fe^{3+}	0.047	0.151	0.073	0.073	0.040	0.080	0.014	0.071	0.075
Fe^{2+}	0.211	0.102	0.202	0.185	0.340	0.184	0.405	0.182	0.189
Mn	0.004	0.005	0.005	0.005	0.014	0.005	0.024	0.006	0.006
Mg	0.679	0.738	0.601	0.661	0.689	0.649	0.629	0.792	0.806
Ca	0.856	0.836	0.832	0.854	0.787	0.849	0.815	0.875	0.865
Na	0.036	0.043	0.066	0.046	0.049	0.048	0.050	0.034	0.038
Cr	-	0.002	-	0.002	-	0.001	-	0.016	0.012
Z	2.000	2.000	2.000	2.000	2.000	2.000	2.000	1.992	1.983
XY	2.000	2.000	2.000	2.000	2.000	2.000	2.000	2.016	2.034
Ca	48.9	49.8	50.7	50.1	43.0	50.3	43.5	47.2	46.4
Mg	38.8	43.9	36.7	38.8	37.6	38.5	33.6	42.7	43.2
Fe^{2+}+Mn	12.3	6.4	12.6	11.1	19.3	11.2	22.9	10.1	10.5
Na	3.9	4.9	7.6	5.1	4.5	5.4	4.6	3.3	3.6
Mg	73.0	83.1	68.8	73.7	63.1	73.3	56.8	78.2	77.6
Fe^{2+}+Mn	23.1	12.1	23.6	21.2	32.4	21.3	38.6	18.5	18.8

Calculated pyroxene molecules

Ca Ti Ts	7.5	4.9	8.4	8.6	2.7	9.4	1.5	4.1	4.3
Na Ti P	-	-	-	-	-	-	-	-	-
Ac	3.6	4.3	6.6	4.6	4.9	4.8	5.1	3.4	3.7
Ca Ts	9.7	12.9	14.0	10.2	5.0	10.7	3.1	2.6	2.4
Fe Ts	0.5	5.4	0.3	1.4	-	1.6	-	1.8	1.8
Wo	34.0	30.3	30.2	32.6	35.6	31.7	38.8	39.3	38.4
En	34.0	36.9	30.0	33.1	34.5	32.5	31.7	39.4	39.7
Fs	10.8	5.4	10.3	9.5	17.3	9.4	19.8	9.3	9.6
Wo	43.2	41.7	42.8	43.4	40.7	43.0	43.0	44.6	43.7
En	43.2	50.9	42.6	44.0	39.5	44.1	35.1	44.8	45.3
Fs	13.7	7.4	14.6	12.6	19.8	12.8	21.9	10.6	11.0

Table 2 continued

Sample	25668 cont.								25671
Grain	10C	10R	6	9	1C	1R	1R	2C	2
SiO_2	49.1	50.0	49.0	48.6	49.7	50.0	50.0	51.1	51.2
Al_2O_3	2.69	1.79	2.91	2.48	2.18	2.14	2.16	2.66	3.54
TiO_2	1.73	1.06	1.89	1.81	1.49	1.16	1.12	0.85	1.30
FeO*	8.52	8.79	8.73	8.76	8.98	8.48	8.76	9.30	8.72
MnO	0.21	0.23	0.19	0.21	0.19	0.21	0.18	0.19	0.25
MgO	14.3	13.6	14.2	14.3	13.8	13.6	13.1	13.5	14.0
CaO	21.5	22.1	21.5	21.6	21.5	22.3	22.1	21.5	21.2
Na_2O	0.44	0.65	0.51	0.50	0.47	0.70	0.71	0.51	0.56
Cr_2O_3	-	-	0.03	-	-	-	-	0.08	n.d.
Sum	98.49	98.22	98.96	98.26	98.31	98.59	98.13	99.69	100.77
Fe_2O_3	1.89	2.36	2.06	1.56	1.65	2.84	2.97	1.78	1.44
FeO	6.82	6.67	6.87	7.36	7.50	5.93	6.08	7.70	7.43
Total	98.68	98.46	99.17	98.42	98.48	98.87	98.43	99.87	100.92

Number of cations on the basis of 6 (O)

Si	1.860	1.901	1.850	1.853	1.889	1.890	1.899	1.910	1.887
Al	0.120	0.080	0.129	0.111	0.098	0.095	0.097	0.090	0.113
Al	-	-	-	-	-	-	-	0.027	0.041
Ti	0.049	0.030	0.054	0.052	0.043	0.033	0.032	0.024	0.036
Fe^{3+}	0.054	0.068	0.059	0.045	0.047	0.081	0.085	0.050	0.040
Fe^{2+}	0.216	0.212	0.217	0.235	0.238	0.187	0.193	0.241	0.229
Mn	0.007	0.007	0.006	0.007	0.006	0.007	0.006	0.006	0.008
Mg	0.808	0.771	0.799	0.813	0.782	0.766	0.742	0.752	0.769
Ca	0.873	0.900	0.870	0.883	0.876	0.903	0.899	0.861	0.837
Na	0.032	0.048	0.037	0.037	0.035	0.051	0.052	0.037	0.040
Cr	-	-	0.001	-	-	-	-	0.002	-
Z	1.980	1.982	1.979	1.965	1.987	1.986	1.995	2.000	2.000
XY	2.039	2.037	2.042	2.070	2.026	2.029	2.009	2.000	2.000
Ca	45.9	47.6	46.0	45.6	46.0	48.5	48.9	46.3	45.4
Mg	42.4	40.8	42.2	42.0	41.1	41.1	40.3	40.4	41.7
Fe^{2+}+Mn	11.7	11.6	11.8	12.5	12.9	10.4	10.8	13.3	12.9
Na	3.0	4.6	3.5	3.4	3.3	5.1	5.3	3.6	3.8
Mg	76.0	74.3	75.4	74.5	73.7	75.7	74.7	72.6	73.5
Fe^{2+}+Mn	21.0	21.1	21.1	22.1	23.0	19.2	20.0	23.8	22.7

Calculated pyroxene molecules

Ca Ti Ts	4.8	3.0	5.3	5.0	4.2	3.2	3.2	2.4	3.6
Na Ti P	-	-	-	-	-	-	-	-	-
Ac	3.2	4.7	3.7	3.6	3.4	5.1	5.2	3.7	4.0
Ca Ts	1.1	1.0	1.1	0.4	0.6	1.4	1.6	3.5	4.1
Fe Ts	1.1	1.0	1.0	0.4	0.6	1.4	1.6	0.6	-
Wo	39.3	41.8	38.9	39.8	40.5	41.5	41.5	39.8	38.0
En	39.6	37.8	39.1	39.3	38.6	37.8	36.9	37.6	38.5
Fs	10.9	10.8	10.9	11.7	12.1	9.6	9.9	12.4	11.8
Wo	43.8	46.2	43.7	43.8	44.4	46.7	47.0	44.4	43.0
En	44.1	41.9	44.0	43.3	42.3	42.5	41.8	41.9	43.6
Fs	12.1	11.9	12.3	12.9	13.2	10.8	11.2	13.7	13.4

Table 2 continued

Sample	25671 cont.			25661		25666			
Grain	4C	4R	3-g	1C	1R	6C	6C	6I	6R
SiO_2	49.6	49.5	50.6	48.9	49.2	47.4	45.9	47.1	
Al_2O_3	4.26	4.69	0.78	3.85	4.14	7.46	8.66	7.70	
TiO_2	1.52	1.72	0.33	1.33	1.35	2.02	2.46	1.99	
FeO*	8.86	8.70	20.7	12.1	10.85	6.97	7.49	7.30	10.05
MnO	0.26	0.21	1.03	0.41	0.32	0.13	0.11	0.13	
MgO	13.2	13.2	7.23	11.7	12.4	13.2	12.7	13.4	14.8
CaO	21.6	21.5	19.2	19.6	20.2	21.4	21.0	20.8	19.2
Na_2O	0.53	0.57	0.57	0.75	0.71	0.62	0.72	0.72	
Cr_2O_3	n.d.	n.d.	n.d.	n.d.	n.d.	0.44	0.21	0.32	
Sum	99.83	100.09	100.44	98.64	99.17	99.64	99.25	99.46	
Fe_2O_3	2.34	2.10	1.19	2.54	2.67	2.70	3.76	3.55	
FeO	6.76	6.81	19.6	9.81	8.45	4.54	4.11	4.11	
Total	100.07	100.30	100.53	98.89	99.44	99.91	99.63	99.82	

Number of cations on the basis of 6 (O)

Si	1.850	1.840	1.976	1.866	1.858	1.759	1.711	1.748	
Al	0.150	0.160	0.024	0.134	0.142	0.241	0.289	0.252	
Al	0.037	0.046	0.012	0.040	0.042	0.085	0.091	0.085	
Ti	0.043	0.048	0.010	0.038	0.038	0.056	0.069	0.056	
Fe^{3+}	0.066	0.059	0.035	0.073	0.076	0.075	0.105	0.099	
Fe^{2+}	0.211	0.212	0.641	0.313	0.267	0.141	0.128	0.127	
Mn	0.008	0.007	0.034	0.013	0.010	0.004	0.003	0.004	
Mg	0.734	0.731	0.421	0.666	0.698	0.730	0.706	0.741	
Ca	0.863	0.856	0.804	0.802	0.817	0.851	0.839	0.827	
Na	0.038	0.041	0.043	0.056	0.052	0.045	0.052	0.052	
Cr	–	–	–	–	–	0.013	0.006	0.009	
Z	2.000	2.000	2.000	2.000	2.000	2.000	2.000	2.000	
XY	2.000	2.000	2.000	2.000	2.000	2.000	2.000	2.000	
Ca	47.5	47.4	42.3	44.7	45.6	49.3	50.1	48.7	40.2
Mg	40.4	40.5	22.2	37.1	38.9	42.3	42.1	43.6	43.3
Fe^{2+}+Mn	12.1	12.1	35.5	18.2	15.5	8.4	7.8	7.7	16.5
Na	3.9	4.2	3.8	5.3	5.1	4.8	5.8	5.6	
Mg	74.0	73.8	36.9	63.5	68.0	79.4	79.4	80.2	
Fe^{2+}+Mn	22.1	22.0	59.3	31.2	26.9	15.8	14.8	14.2	

Calculated pyroxene molecules

Ca Ti Ts	4.3	4.8	1.0	3.8	3.8	5.6	6.9	5.6	
Na Ti P	–	–	–	–	–	–	–	–	
Ac	3.8	4.1	4.3	5.6	5.2	4.5	5.2	5.2	
Ca Ts	5.1	5.5	0.8	4.8	5.4	10.7	12.2	11.3	
Fe Ts	1.4	0.9	–	0.9	1.2	1.5	2.7	2.4	
Wo	37.8	37.2	39.4	35.3	35.7	33.7	31.1	31.8	
En	36.7	36.6	21.1	33.3	34.9	36.6	35.3	37.2	
Fs	11.0	10.9	33.4	16.3	13.8	7.3	6.6	6.6	
Wo	44.2	44.0	41.9	41.6	42.3	43.4	42.6	42.1	
En	43.0	43.2	22.5	39.2	41.3	47.2	48.4	49.2	
Fs	12.8	12.9	35.6	19.2	16.4	9.4	9.0	8.7	

Table 2 continued

Sample	25666 cont.								
Grain	12	1C	1I	1R	9-g	11C	11R	7C	7R
SiO_2	47.2	50.8			51.3	50.3		50.8	51.0
Al_2O_3	6.59	2.26			1.39	2.52		2.34	2.32
TiO_2	2.32	0.89			1.03	1.26		1.14	1.17
FeO*	8.23	10.0	11.1	9.72	11.2	11.3	10.9	11.6	11.2
MnO	0.15	0.28			0.43	0.40		0.34	0.39
MgO	13.3	13.6	13.5	14.0	13.3	13.4	13.6	13.5	13.6
CaO	21.0	21.2	19.6	20.4	20.5	19.8	19.5	19.3	19.4
Na_2O	0.62	0.45			0.43	0.64		0.62	0.60
Cr_2O_3	-	-			-	-		-	-
Sum	99.41	99.48			99.58	99.62		99.64	99.68
Fe_2O_3	3.71	2.48			1.23	2.94		2.04	1.60
FeO	4.89	7.77			10.1	8.66		9.76	9.76
Total	99.78	99.73			99.71	99.92		99.84	99.84

Number of cations on the basis of 6 (O)

Si	1.760	1.906			1.936	1.890		1.910	1.915
Al	0.240	0.094			0.062	0.110		0.090	0.085
Al	0.050	0.006			-	0.002		0.013	0.018
Ti	0.065	0.025			0.029	0.036		0.032	0.033
Fe^{3+}	0.104	0.070			0.035	0.083		0.058	0.045
Fe^{2+}	0.152	0.244			0.319	0.272		0.307	0.307
Mn	0.005	0.009			0.014	0.013		0.011	0.012
Mg	0.739	0.761			0.748	0.751		0.756	0.761
Ca	0.839	0.852			0.829	0.797		0.777	0.780
Na	0.045	0.033			0.031	0.047		0.045	0.044
Cr	-	-			-	-			
Z	2.000	2.000			1.998	2.000		2.000	2.000
XY	2.000	2.000			2.005	2.000		2.000	2.000
Ca	48.4	45.7	41.6	42.9	43.4	43.5	41.5	42.0	42.0
Mg	42.6	40.8	40.0	41.1	39.2	41.0	40.4	40.9	40.9
Fe^{2+}+Mn	9.0	13.6	18.4	16.0	17.4	15.5	18.1	17.2	17.1
Na	4.8	3.1			2.8	4.3		4.0	3.9
Mg	78.5	72.7			67.3	69.4		67.6	67.7
Fe^{2+}+Mn	16.7	24.2			29.9	26.3		28.4	28.4

Calculated pyroxene molecules

Ca Ti Ts	6.5	2.5			2.9	3.6		3.2	3.3
Na Ti P	-	-			-	-		-	-
Ac	4.5	3.3			3.1	4.7		4.5	4.4
Ca Ts	8.0	2.5			0.2	2.0		2.0	1.8
Fe Ts	3.0	1.9			0.2	1.8		0.6	0.1
Wo	33.2	39.2			39.7	36.2		36.0	36.4
En	37.0	38.0			37.3	37.5		37.8	38.1
Fs	7.9	12.6			16.6	14.2		15.9	16.0
Wo	42.6	43.6			42.4	41.1		40.1	40.3
En	47.4	42.3			39.9	42.7		42.2	42.1
Fs	10.1	14.1			17.7	16.2		17.7	17.6

Table 2 continued

Sample	25687								
Grain	8C	5C	5R	1C	1R	4-a	2C-g	2R-g	7
SiO_2	48.7	48.6	48.9	45.4	50.4	51.1	51.4	51.4	50.7
Al_2O_3	5.74	5.99	4.95	8.55	3.10	2.16	1.40	0.96	2.17
TiO_2	1.87	1.85	1.54	3.44	0.77	0.61	0.54	0.32	0.64
FeO*	10.1	10.3	12.8	11.1	14.3	13.5	15.6	17.2	16.6
MnO	0.24	0.27	0.54	0.32	0.74	0.88	0.88	1.25	0.88
MgO	11.5	11.4	9.28	9.54	9.11	9.97	8.98	6.47	8.10
CaO	21.2	21.1	20.7	21.2	21.1	21.4	21.0	20.1	20.9
Na_2O	0.77	0.77	0.80	0.91	0.78	0.99	0.60	1.63	0.71
Sum	100.12	100.28	99.51	100.46	100.30	100.61	100.40	99.34	100.70
Fe_2O_3	1.84	1.91	0.29	2.70	1.09	2.80	0.26	2.06	0.92
FeO	8.44	8.58	12.54	8.67	13.3	11.0	15.4	15.3	15.8
Total	100.30	100.47	99.54	100.73	100.39	100.91	100.46	99.49	100.82

Number of cations on the basis of 6 (O)

Si	1.823	1.817	1.870	1.708	1.922	1.931	1.971	2.003	1.946
Al	0.177	0.183	0.130	0.292	0.078	0.069	0.029	-	0.054
Al	0.076	0.081	0.093	0.087	0.061	0.027	0.035	0.044	0.044
Ti	0.053	0.052	0.044	0.097	0.022	0.017	0.016	0.009	0.018
Fe^{3+}	0.052	0.054	0.008	0.076	0.031	0.080	0.008	0.060	0.027
Fe^{2+}	0.264	0.268	0.401	0.273	0.425	0.347	0.493	0.500	0.506
Mn	0.008	0.009	0.017	0.010	0.024	0.028	0.029	0.041	0.029
Mg	0.642	0.635	0.529	0.535	0.518	0.562	0.513	0.376	0.463
Ca	0.850	0.845	0.848	0.855	0.862	0.866	0.863	0.839	0.859
Na	0.056	0.056	0.059	0.066	0.058	0.073	0.045	0.123	0.053
Z	2.000	2.000	2.000	2.000	2.000	2.000	2.000	2.003	2.000
XY	2.000	2.000	2.000	2.000	2.000	2.000	2.000	1.994	2.000
Ca	48.2	48.1	47.2	51.1	47.1	48.1	45.5	47.8	46.3
Mg	36.4	36.2	29.5	32.0	28.3	31.1	27.0	21.4	24.9
Fe^{2+}+Mn	15.4	15.7	23.3	16.9	24.5	20.8	27.5	30.8	28.8
Na	5.8	5.8	5.9	7.5	5.6	7.2	4.1	11.8	5.2
Mg	66.2	65.6	52.5	60.5	50.6	55.6	47.6	36.1	44.0
Fe^{2+}+Mn	28.0	28.6	41.6	32.0	43.8	37.2	48.3	52.0	50.8

Calculated pyroxene molecules

Ca Ti Ts	5.3	5.2	4.5	9.7	2.2	1.7	1.6	1.0	1.9
Na Ti P	-	-	-	-	-	-	-	-	-
Ac	5.6	5.6	6.0	6.6	5.8	7.2	4.5	12.6	5.5
Ca Ts	7.4	8.0	6.8	9.2	4.8	3.1	1.6	1.3	3.1
Fe Ts	-	-	-	0.5	-	0.4	-	-	-
Wo	36.2	35.7	37.3	33.0	39.9	40.7	42.0	41.6	40.8
En	32.1	31.8	26.8	26.8	26.1	28.1	25.9	19.2	23.3
Fs	13.4	13.8	18.6	14.2	21.2	18.8	24.4	24.4	25.5
Wo	44.3	43.9	45.1	44.6	45.7	46.5	45.4	48.9	45.5
En	39.3	39.1	32.4	36.2	29.9	32.1	28.1	22.5	26.0
Fs	16.4	17.0	22.5	19.2	24.4	21.4	26.5	28.6	28.5

Table 2 continued

Sample	25702							25699	
Grain	2	3	9-g	4	5	8-g	6	1C	1R
SiO_2	51.6	51.8	50.8	50.9	49.2	50.4	50.8	47.5	48.4
Al_2O_3	1.33	1.31	1.22	1.13	2.17	0.95	1.09	0.63	0.11
TiO_2	0.33	0.31	0.38	0.29	0.70	0.26	0.29	0.25	0.50
FeO*	17.5	17.9	18.5	19.0	19.0	21.9	22.1	26.7	31.4
MnO	0.90	0.87	1.10	0.91	0.96	1.01	1.10	1.59	2.17
MgO	8.71	8.44	8.04	7.51	7.60	5.26	5.37	1.48	0.13
CaO	20.0	19.9	19.8	20.4	19.2	19.8	19.8	19.8	10.2
Na_2O	0.60	0.65	0.46	0.64	0.71	0.65	0.68	1.20	5.00
K_2O	–	0.03	0.07	–	0.05	–	–	–	–
Sum	100.97	101.21	100.37	100.78	99.59	100.23	101.23	99.15	97.91
Fe_2O_3	0.38	0.15	0.46	1.43	2.21	0.20	0.34	3.58	12.1
FeO	17.2	17.8	18.1	17.7	17.0	21.70	21.8	23.5	20.6
Total	101.05	101.26	100.42	100.91	99.80	100.23	101.27	99.53	99.21

Number of cations on the basis of 6 (O)

Si	1.977	1.983	1.972	1.969	1.924	1.992	1.987	1.951	1.984
Al	0.023	0.017	0.028	0.031	0.076	0.008	0.013	0.030	0.005
Al	0.037	0.043	0.027	0.021	0.024	0.036	0.037	–	–
Ti	0.010	0.009	0.011	0.008	0.021	0.008	0.009	0.008	0.015
Fe^{3+}	0.011	0.004	0.013	0.042	0.065	0.006	0.010	0.111	0.372
Fe^{2+}	0.550	0.569	0.587	0.573	0.556	0.718	0.713	0.806	0.705
Mn	0.029	0.028	0.036	0.030	0.032	0.034	0.036	0.055	0.075
Mg	0.497	0.482	0.465	0.433	0.443	0.310	0.313	0.091	0.008
Ca	0.821	0.816	0.823	0.846	0.804	0.839	0.830	0.871	0.448
Na	0.045	0.048	0.035	0.048	0.054	0.050	0.052	0.096	0.397
K	–	0.001	0.003	–	0.002	–	–	–	–
Z	2.000	2.000	2.000	2.000	2.000	2.000	2.000	1.981	1.990
XY	2.000	2.001	2.002	2.000	2.001	2.000	2.000	2.037	2.021
Ca	43.3	43.1	43.1	44.9	43.8	44.1	43.8	47.8	36.2
Mg	26.2	25.4	24.3	23.0	24.1	16.3	16.5	5.0	0.6
Fe^{2+}+Mn	30.5	31.5	32.6	32.0	32.0	39.6	39.6	47.2	63.1
Na	4.0	4.4	3.4	4.4	5.2	4.5	4.6	9.1	33.5
Mg	44.4	42.7	41.3	40.0	40.7	27.9	28.1	8.6	0.7
Fe^{2+}+Mn	51.6	52.9	55.3	55.6	54.1	67.6	67.3	82.2	65.8

Calculated pyroxene molecules

Ca Ti Ts	1.0	0.9	1.1	0.8	2.1	0.8	0.9	0.8	0.3
Na Ti P	–	–	–	–	–	–	–	–	2.5
Ac	4.5	5.0	3.8	4.8	5.6	5.0	5.2	9.4	36.8
Ca Ts	2.1	2.1	1.7	1.7	2.9	1.5	1.7	0.7	–
Fe Ts	–	–	–	–	0.4	–	–	0.7	–
Wo	39.9	39.8	40.0	41.0	37.5	41.3	40.7	41.6	22.0
En	25.1	24.3	23.4	21.7	22.1	15.7	15.8	4.4	0.1
Fs	27.5	27.9	30.1	29.9	29.4	35.8	35.8	42.3	38.3
Wo	43.1	43.2	42.8	44.3	42.1	44.5	44.1	47.1	36.5
En	27.1	26.5	25.0	23.4	24.9	16.9	17.1	5.0	0.1
Fs	29.7	30.3	32.2	32.3	33.0	38.6	38.8	47.8	63.4

Table 2 continued

Sample	25699 cont.					
Grain	5	3	8	9	6	7
SiO_2	47.6	50.7	50.9	50.7	50.0	47.9
Al_2O_3	0.38	0.14	0.30	0.13	0.13	0.15
TiO_2	0.23	1.30	0.83	0.64	0.48	0.23
FeO*	28.1	28.7	28.7	29.6	29.9	29.9
MnO	1.55	1.09	1.68	1.35	1.46	2.18
MgO	1.83	-	-	-	-	0.43
CaO	18.8	2.43	1.33	1.88	2.38	16.8
Na_2O	1.50	11.7	12.7	12.0	11.1	1.85
K_2O	-	0.03	0.04	0.03	0.03	-
Sum	99.99	96.09	96.48	96.33	95.48	99.44
Fe_2O_3	4.00	27.8	31.5	29.8	27.8	4.54
FeO	24.5	3.72	0.33	2.75	4.85	25.8
Total	100.39	98.91	99.61	99.28	98.23	99.88

Number of cations on the basis of 6 (O)

Si	1.945	1.989	1.975	1.983	1.987	1.977
Al	0.018	0.006	0.014	0.006	0.006	0.007
Al	-	-	-	-	-	-
Ti	0.007	0.038	0.024	0.019	0.014	0.007
Fe^{3+}	0.123	0.820	0.921	0.878	0.833	0.141
Fe^{2+}	0.837	0.122	0.011	0.090	0.161	0.891
Mn	0.054	0.036	0.055	0.045	0.049	0.076
Mg	0.111	-	-	-	-	0.026
Ca	0.823	0.102	0.055	0.079	0.101	0.743
Na	0.119	0.890	0.955	0.910	0.855	0.148
K	-	0.002	0.002	0.001	0.002	-
Z	1.963	1.995	1.989	1.989	1.993	1.984
XY	2.074	2.010	2.023	2.022	2.015	2.032
Ca	45.1	39.2	45.7	36.9	32.5	42.8
Mg	6.1	-	-	-	-	1.5
Fe^{2+}+Mn	48.8	60.8	54.3	63.1	67.5	55.7
Na	10.6	84.9	93.6	87.1	80.3	13.0
Mg	9.9	-	-	-	-	2.3
Fe^{2+}+Mn	79.5	15.1	6.4	12.9	19.7	84.7

Calculated pyroxene molecules

Ca Ti Ts	0.7	0.3	0.7	0.3	0.3	0.4
Na Ti P	-	7.0	3.4	3.1	2.2	0.7
Ac	11.5	81.7	91.2	87.0	82.8	13.9
Ca Ts	0.2	-	-	-	-	-
Fe Ts	0.2	-	-	-	-	-
Wo	39.1	4.9	2.4	3.8	4.9	36.4
En	5.4	-	-	-	-	1.2
Fs	43.0	6.1	2.3	5.8	9.8	47.5
Wo	44.8	44.9	51.0	39.3	33.2	42.8
En	6.1	-	-	-	-	1.4
Fs	49.1	55.1	49.0	60.7	66.8	55.8

Table 3. Electron microprobe analyses of amphiboles in rocks from The Pleiades

Sample	25703			25668	25671	25687		25702	
Grain	1-mp	3-mp	2-mp	4	1	1C	1R	3	1
SiO_2	39.6	40.0	39.3	41.0	40.8	40.8	40.05	39.7	40.3
Al_2O_3	13.3	12.8	13.1	9.95	12.55	11.6	11.2	12.9	13.0
TiO_2	6.34	6.15	6.40	4.77	6.43	5.30	4.63	5.95	5.97
FeO^*	12.1	12.1	12.2	12.4	12.3	16.7	19.8	13.2	13.3
MnO	0.19	0.18	0.21	0.19	0.20	0.37	0.48	0.21	0.20
MgO	11.6	11.7	11.6	12.8	12.1	9.37	7.82	11.9	11.2
CaO	11.6	11.5	11.3	11.6	11.7	11.1	11.1	10.9	11.3
Na_2O	2.75	2.64	2.68	2.95	2.69	2.67	2.90	2.82	2.69
K_2O	0.96	1.04	1.00	1.56	0.96	1.38	1.42	0.81	0.94
Cr_2O_3	n.d.	n.d.	n.d.	0.08	n.d.	n.d.	n.d.	n.d.	n.d.
NiO	n.d.	n.d.	n.d.	0.04	n.d.	n.d.	n.d.	n.d.	n.d.
Sum	98.44	98.11	97.79	97.34	99.73	99.29	99.40	98.39	98.90
Fe_2O_3	0.76	1.06	1.09	4.03	1.32	2.06	3.74	2.60	1.19
FeO	11.4	11.1	11.2	8.77	11.1	14.85	17.0	10.9	12.2
Total	98.50	98.17	97.88	97.74	99.85	99.50	99.74	98.69	98.99

Number of cations on the basis of 23 (O)

Si	5.855	5.928	5.854	6.172	5.958	6.110	6.097	5.893	5.944
Al	2.145	2.072	2.146	1.766	2.042	1.890	1.903	2.107	2.056
Al	0.171	0.163	0.154	–	0.116	0.150	0.107	0.148	0.207
Ti	0.705	0.686	0.717	0.540	0.705	0.597	0.530	0.664	0.662
Fe	1.493	1.502	1.520	1.561	1.496	2.094	2.523	1.635	1.638
Mn	0.024	0.023	0.027	0.024	0.025	0.047	0.061	0.026	0.025
Mg	2.567	2.594	2.575	2.872	2.623	2.091	1.776	2.629	2.469
Ca	1.836	1.823	1.804	1.871	1.823	1.774	1.808	1.731	1.787
Na	0.788	0.758	0.773	0.861	0.762	0.776	0.855	0.811	0.769
K	0.181	0.197	0.190	0.300	0.178	0.263	0.275	0.153	0.177
Cr	–	–	–	0.010	–	–	–	–	–
Ni	–	–	–	0.004	–	–	–	–	–
Z	8.000	8.000	8.000	7.938	8.000	8.000	8.000	8.000	8.000
Y	4.960	4.968	4.993	5.011	4.965	4.979	4.996	5.102	5.001
X	2.805	2.778	2.767	3.032	2.763	2.813	2.938	2.695	2.733
Sum	15.765	15.746	15.760	15.981	15.728	15.792	15.934	15.797	15.734
$\dfrac{Mg}{Mg+Fe+Mn}$	0.63	0.63	0.62	0.64	0.73	0.50	0.41	0.62	0.60
$\dfrac{Fe^{2+}}{Fe^{3+}}$	16.8	11.6	11.5	2.4	9.4	8.0	6.0	4.6	11.4

Table 3 continued

Sample	25702 cont.	
Grain	5	4
SiO_2	40.8	41.5
Al_2O_3	12.2	11.8
TiO_2	5.12	4.83
FeO*	17.05	17.6
MnO	0.37	0.39
MgO	9.44	9.37
CaO	10.7	10.6
Na_2O	2.89	2.80
K_2O	0.95	1.11
Cr_2O_3	n.d.	n.d.
NiO	n.d.	n.d.
Sum	99.52	100.00
Fe_2O_3	2.42	2.78
FeO	14.9	15.1
Total	99.79	100.28

Number of cations on the basis of 23 (O)

Si	6.081	6.162
Al	1.919	1.838
Al	0.219	0.228
Ti	0.574	0.539
Fe	2.126	2.189
Mn	0.047	0.049
Mg	2.098	2.073
Ca	1.704	1.681
Na	0.835	0.806
K	0.181	0.210
Cr	–	–
Ni	–	–
Z	8.000	8.000
Y	5.064	5.078
X	2.720	2.697
Sum	15.784	15.775

$\dfrac{Mg}{Mg+Fe+Mn}$	0.49	0.49
$\dfrac{Fe^{2+}}{Fe^{3+}}$	6.8	6.0

Table 4.   Electron microprobe analyses of biotite in rocks from The Pleiades

Sample	25668				25702		
Grain	2	1C	1R	3	1	3	2
SiO_2	36.65	36.7	38.0	36.4	35.9	35.7	34.8
Al_2O_3	13.2	12.7	12.4	13.0	13.8	13.5	13.85
TiO_2	6.07	6.49	5.37	5.88	7.00	6.69	6.90
FeO*	12.9	13.2	12.7	13.2	23.9	24.95	26.25
MnO	0.13	0.11	0.13	0.05	0.29	0.33	0.36
MgO	16.1	15.6	16.6	15.4	7.81	7.36	5.96
CaO	-	-	0.05	0.04	-	0.03	-
Na_2O	0.66	0.78	0.42	0.62	0.74	0.72	0.72
K_2O	8.97	8.79	8.62	9.16	8.16	8.26	8.11
Cr_2O_3	-	-	-	-	n.d.	n.d.	n.d.
NiO	0.05	0.04	0.07	-	n.d.	n.d.	n.d.
Sum	94.73	94.41	94.36	93.75	97.60	97.54	96.95

Number of cations on the basis of 22 (O)

Si	5.484	5.515	5.676	5.518	5.467	5.475	5.410
Al	2.324	2.251	2.168	2.321	2.472	2.442	2.538
Ti	0.192	0.234	0.156	0.161	0.061	0.083	0.052
Ti	0.491	0.499	0.447	0.509	0.740	0.689	0.775
Fe	1.612	1.661	1.580	1.671	3.041	3.199	3.415
Mn	0.017	0.014	0.017	0.006	0.037	0.043	0.048
Mg	3.588	3.488	3.694	3.480	1.772	1.683	1.382
Ca	-	-	0.008	0.006	-	0.004	-
Na	0.191	0.228	0.123	0.181	0.219	0.213	0.217
K	1.713	1.685	1.642	1.770	1.584	1.615	1.608
Ni	0.007	0.005	0.008	-	-	-	-
Z	8.000	8.000	8.000	8.000	8.000	8.000	8.000
Y	5.715	5.667	5.746	5.666	5.590	5.614	5.620
X	1.904	1.913	1.765	1.957	1.803	1.832	1.825

Table 5. Electron microprobe analyses of magnetite and maghemite in rocks from The Pleiades

Sample	25703				25668				
Grain	4-i	3-i	1	2	3-Xg	11	14	10	13
SiO_2	0.11	0.14	0.11	0.12	n.d.	n.d.	n.d.	n.d.	n.d.
TiO_2	17.9	17.35	18.7	20.3	19.4	15.0	14.6	13.5	12.5
Al_2O_3	8.93	8.17	6.33	4.66	2.88	2.69	2.65	2.60	3.10
Cr_2O_3	0.60	0.06	0.15	−	n.d.	n.d.	n.d.	n.d.	n.d.
FeO*	60.5	64.5	65.3	65.9	71.7	76.2	76.6	77.5	77.6
MnO	0.22	0.39	0.36	0.39	0.69	0.52	0.44	0.45	0.45
MgO	6.49	6.37	6.24	6.14	1.90	1.37	1.15	1.47	1.13
CaO	−	0.12	−	−	−	−	−	−	−
NiO	−	−	−	−	n.d.	n.d.	n.d.	n.d.	n.d.
Sum	94.75	97.05	97.19	97.51	96.58	95.78	95.47	95.54	94.81
Fe_2O_3	24.7	29.0	28.4	27.6	28.7	37.3	37.7	40.3	41.0
FeO	38.3	38.4	39.8	41.1	45.8	42.6	42.6	41.2	40.7
Total	97.25	99.95	100.09	100.31	99.38	99.48	99.17	99.54	98.91
Usp %	48.1	43.0	46.8	50.6	54.4	41.6	41.2	36.9	35.2

Sample	25661							25666	
Grain	3C	3R	1	2C	2R	5	4	5-i	1
SiO_2	0.09	0.10	0.09	0.09	0.11	0.08	0.10	0.06	0.09
TiO_2	21.2	21.05	20.8	21.0	20.7	20.6	21.5	5.26	4.81
Al_2O_3	4.24	3.84	4.44	4.18	3.61	3.98	2.87	3.13	2.17
Cr_2O_3	n.d.	n.d.	n.d.	n.d.	n.d.	n.d.	n.d.	0.15	0.13
FeO*	67.7	69.1	67.8	68.4	69.6	69.0	69.4	82.9	84.5
MnO	0.67	0.76	0.74	0.72	0.81	0.86	0.88	0.49	0.42
MgO	3.61	2.81	3.24	3.13	2.55	2.81	2.15	0.68	0.70
CaO	−	−	−	−	−	−	−	0.05	−
NiO	n.d.	n.d.	n.d.	n.d.	n.d.	n.d.	n.d.	0.04	−
Sum	97.51	97.66	97.11	97.52	97.38	97.33	96.90	92.76	92.82
Fe_2O_3	24.8	25.2	24.9	25.0	25.9	25.9	24.7	54.0	56.1
FeO	45.4	46.4	45.4	45.8	46.3	45.8	47.2	34.3	34.0
Total	100.01	100.16	99.61	99.92	99.98	100.03	99.40	98.16	98.42
Usp %	58.4	58.7	58.2	58.3	57.9	57.4	60.6	13.8	12.5

Table 5 continued

Sample	25666 cont.		25687					25702	
Grain	2	6-a	3	2	4-g	5	6-g	1	3
SiO_2	0.12	0.16	0.13	0.07	0.08	0.18	0.10	0.10	0.12
TiO_2	5.31	1.57	19.6	22.4	16.7	16.6	16.0	20.7	19.2
Al_2O_3	1.42	0.63	1.91	2.15	1.59	1.16	1.13	1.91	1.75
Cr_2O_3	0.03	−	n.d.	n.d.	n.d.	n.d.	n.d.	n.d.	n.d.
FeO*	85.0	88.6	70.2	70.5	72.6	73.4	74.0	72.4	73.8
MnO	0.19	0.35	1.63	1.91	1.80	2.08	1.77	1.12	1.25
MgO	0.45	0.52	0.80	0.97	0.54	−	0.29	0.81	0.82
CaO	−	0.08	n.d.	n.d.	n.d.	0.09	n.d.	n.d.	n.d.
NiO	−	−	n.d.	n.d.	n.d.	−	n.d.	n.d.	n.d.
Sum	92.52	91.91	94.27	98.00	93.31	93.51	93.29	97.04	96.94
Fe_2O_3	55.7	64.0	26.9	24.0	32.6	33.0	34.4	26.7	30.1
FeO	34.9	31.1	46.0	48.9	43.2	43.7	43.1	48.3	46.8
Total	98.12	98.41	96.97	100.4	96.52	96.81	96.29	99.64	100.04
Usp %	15.0	3.1	57.3	62.9	48.3	48.6	46.4	59.2	54.2

Sample	25702 cont.	25699	
Grain	2	8	9
SiO_2	0.13	0.12	0.27
TiO_2	20.0	10.75	7.96
Al_2O_3	1.50	0.08	0.09
Cr_2O_3	n.d.	n.d.	n.d.
FeO*	73.9	79.02	80.42
MnO	1.11	0.66	0.70
MgO	0.71	−	−
CaO	n.d.	−	0.03
Na_2O	n.d.	0.08	0.74
K_2O	n.d.	−	0.14
Sum	97.35	90.71	90.35
Fe_2O_3	28.9	87.8[1]	89.4[1]
FeO	47.9	0.00	0.00
Total	100.25	99.49	99.33
Usp %	56.6		

[1]Total Fe as Fe_2O_3

Table 6. Electron microprobe analyses of ilmenite in rocks from The Pleiades

Sample	25668						25666		
Grain	2	11	1	10	3	5	2-i	5	4
SiO_2	–	–	–	n.d.	–	–	0.05	0.08	0.03
TiO_2	51.7	51.5	51.6	51.6	51.9	52.1	48.9	46.5	47.0
Al_2O_3	0.06	0.07	0.06	–	0.05	0.06	0.15	0.11	0.07
Cr_2O_3	n.d.	n.d.	n.d.	n.d.	n.d.	n.d.	–	–	0.18
FeO*	43.8	43.9	44.1	44.2	44.3	44.4	45.1	47.0	48.1
MnO	0.64	0.78	0.68	0.79	0.66	0.67	0.84	0.89	0.95
MgO	3.40	3.37	3.28	2.96	3.21	3.08	3.43	3.16	2.22
CaO	–	–	–	n.d.	–	–	0.05	–	–
NiO	0.06	n.d.	–	n.d.	–	n.d.	0.05	–	0.03
Sum	99.66	99.62	99.72	99.55	100.12	100.31	98.57	97.74	98.58
Fe_2O_3	4.48	4.8	4.71	4.25	4.46	4.08	9.00	12.9	11.9
FeO	39.7	39.5	39.9	40.3	40.3	40.7	37.0	35.3	37.3
Total	100.04	100.02	100.23	99.90	100.58	100.69	99.47	98.94	99.68
Hm %	4.9	5.3	5.1	4.6	4.8	4.4	10.1	14.3	11.9

Sample	25687
Grain	1
SiO_2	–
TiO_2	49.4
Al_2O_3	0.21
Cr_2O_3	n.d.
FeO*	45.5
MnO	1.66
MgO	2.36
CaO	–
NiO	n.d.
Sum	99.13
Fe_2O_3	7.7
FeO	38.6
Total	99.93
Hm %	8.6

Table 7. Electron microprobe analyses of feldspars in rocks from The Pleiades

Sample	25703						25671		
Grain	4	1C-g	1R-g	10-g	3C-x	3I-x	17	1C	1R
SiO_2	53.2	54.7	55.0	55.7	59.8	58.3	54.3	54.4	55.1
Al_2O_3	27.9	26.8	25.8	26.2	23.7	24.7	27.9	27.4	26.7
TiO_2	–	0.18	0.20	–	0.04	0.04	–	–	–
FeO*	0.53	0.70	0.74	0.66	0.23	0.25	0.60	0.62	0.40
MgO	–	0.12	0.09	–	0.02	–	–	–	–
CaO	11.9	10.7	10.1	10.2	6.65	7.70	11.7	11.6	10.9
Na_2O	4.59	4.98	5.16	5.24	7.15	6.69	4.97	5.02	5.36
K_2O	0.36	0.56	0.60	0.58	0.94	0.73	0.42	0.38	0.42
Sum	98.48	98.74	97.69	98.58	98.53	98.41	99.89	99.42	98.88

Number of cations on the basis of 32 (O)

Si	9.808	10.035	10.183	10.209	10.850	10.620	9.872	9.933	10.083
Al	6.061	5.789	5.627	5.654	5.059	5.294	5.975	5.896	5.755
Ti	–	0.024	0.027	–	0.006	0.005	–	–	–
Fe	0.082	0.108	0.115	0.102	0.035	0.037	0.092	0.095	0.062
Mg	–	0.033	0.024	–	0.005	–	–	–	–
Ca	2.350	2.106	2.005	2.001	1.294	1.502	2.278	2.264	2.141
Na	1.638	1.772	1.851	1.864	2.515	2.362	1.753	1.775	1.900
K	0.083	0.130	0.142	0.136	0.218	0.169	0.097	0.089	0.098
Z	15.951	15.989	15.976	15.965	15.955	15.956	15.847	15.829	15.838
X	4.071	4.008	3.998	4.001	4.027	4.033	4.220	4.223	4.201
Σ	20.022	19.997	19.974	19.966	19.982	19.989	20.067	20.052	20.039

Mole %									
Ca	57.7	52.5	50.1	50.0	32.1	37.2	55.2	54.8	51.7
Na	40.2	44.2	46.3	46.6	62.5	58.6	42.5	43.0	45.9
K	2.1	3.3	3.6	3.4	5.4	4.2	2.3	2.2	2.4

Table 7 continued

Sample	25671 cont.						25687		
Grain	19-g	20	15-g	10	16-g	18	10-g	15	22
SiO_2	55.7	56.3	56.0	56.2	56.7	56.1	66.5	66.8	65.8
Al_2O_3	26.7	26.5	26.3	26.1	25.6	26.4	18.8	19.9	19.1
FeO*	0.54	0.55	0.52	0.65	0.56	0.70	0.28	0.79	0.31
CaO	10.5	10.4	10.4	9.83	10.1	9.70	0.42	0.67	0.71
Na_2O	5.61	5.65	5.65	5.98	5.98	6.01	5.65	5.78	6.21
K_2O	0.37	0.42	0.47	0.43	0.27	0.34	7.38	6.34	6.39
Sum	99.42	99.82	99.34	99.19	99.21	99.25	99.03	100.28	98.52

Number of cations on the basis of 32 (O)

Si	10.130	10.187	10.192	10.239	10.308	10.206	12.010	11.879	11.934
Al	5.723	5.656	5.642	5.597	5.495	5.662	4.011	4.183	4.073
Fe	0.083	0.084	0.079	0.099	0.085	0.106	0.043	0.117	0.047
Ca	2.041	2.018	2.020	1.920	1.970	1.890	0.082	0.128	0.138
Na	1.978	1.983	1.996	2.112	2.109	2.119	1.978	1.992	2.183
K	0.086	0.097	0.109	0.101	0.062	0.079	1.701	1.440	1.479
Z	15.853	15.843	15.834	15.836	15.803	15.868	16.021	16.062	16.007
X	4.188	4.182	4.204	4.232	4.226	4.194	3.804	3.680	3.847
Σ	20.041	20.025	20.038	20.068	20.029	20.062	19.825	19.742	19.854

Mole %

Ca	49.7	49.2	49.0	46.5	47.6	46.2	2.2	3.6	3.6
Na	48.2	48.4	48.4	51.1	50.9	51.8	52.6	56.0	57.4
K	2.1	2.4	2.6	2.4	1.5	2.0	45.2	40.4	39.0

Table 7 continued

Sample	25687 cont.						25699		
Grain	1C	1R	21	28	29	6	3C	3R	1C
SiO_2	57.9	66.4	65.6	56.6	66.5	63.9	65.5	66.7	65.7
Al_2O_3	25.4	18.8	19.1	26.2	19.5	21.5	19.0	18.1	19.5
FeO*	0.27	0.30	0.20	0.31	0.27	0.22	0.20	0.86	0.16
CaO	8.08	0.45	0.82	8.65	7.81	4.00	0.42	0.15	0.55
Na_2O	6.36	6.04	6.50	6.66	6.84	7.68	6.55	7.08	6.75
K_2O	0.79	7.33	6.70	0.44	0.77	2.50	7.24	6.41	6.48
Sum	98.80	99.31	98.92	98.86	101.69	99.80	98.91	99.30	99.15

Number of cations on the basis of 32 (O)

Si	10.499	11.988	11.890	10.301	11.617	11.406	11.901	12.045	11.856
Al	5.442	3.993	4.074	5.627	4.014	4.517	4.065	3.850	4.154
Fe	0.041	0.045	0.030	0.047	0.040	0.033	0.030	0.130	0.024
Ca	1.571	0.087	0.159	1.687	1.463	0.766	0.081	0.029	0.106
Na	2.237	2.114	2.287	2.349	2.316	2.659	2.305	2.480	2.361
K	0.182	1.690	1.551	0.102	0.171	0.570	1.676	1.477	1.493
Z	15.941	15.981	15.964	15.928	15.631	15.923	15.966	15.895	16.010
X	4.038	3.936	4.027	4.185	3.990	4.028	4.092	4.116	3.984
Σ	19.979	19.917	19.991	20.113	19.621	19.951	20.058	20.011	19.994

Mole %									
Ca	39.4	2.2	4.0	40.8	37.1	19.2	2.0	0.7	2.7
Na	56.0	54.3	57.2	56.8	58.6	66.6	56.7	62.2	59.6
K	4.6	43.5	38.8	2.4	4.3	14.2	41.3	37.1	37.7

Table 7 continued

Sample	25699 cont.								
Grain	1I	1I	1R	5C	5R	7	4	13	12
SiO_2	65.2	65.2	66.5	66.3	67.0	68.6	66.7	66.4	66.8
Al_2O_3	19.8	19.8	20.1	19.0	18.3	19.1	18.3	19.1	18.5
FeO*	0.16	0.15	0.38	0.34	0.72	0.85	0.77	0.67	0.30
CaO	1.23	1.07	0.76	0.32	0.13	0.33	0.15	0.25	0.48
Na_2O	7.19	7.79	7.77	6.95	7.12	7.07	7.16	7.29	7.54
K_2O	5.41	4.93	5.24	6.80	6.15	5.72	6.19	5.71	5.51
Sum	98.99	98.94	100.75	99.71	99.42	100.67	99.27	99.42	99.13

Number of cations on the basis of 32 (O)

Si	11.776	11.766	11.791	11.927	12.046	12.030	12.032	11.933	12.020
Al	4.203	4.204	4.192	4.028	3.886	3.941	3.883	4.040	3.916
Fe	0.024	0.023	0.056	0.052	0.108	0.125	0.117	0.101	0.048
Ca	0.238	0.207	0.145	0.062	0.025	0.062	0.029	0.048	0.093
Na	2.518	2.726	2.671	2.421	2.483	2.405	2.507	2.542	2.633
K	1.247	1.135	1.186	1.559	1.409	1.280	1.427	1.310	1.264
Z	15.979	15.970	15.983	15.955	15.932	15.971	15.915	15.973	15.936
X	4.027	4.091	4.058	4.094	4.025	3.872	4.080	4.001	4.038
Σ	20.006	20.061	20.041	20.049	19.957	19.843	19.995	19.974	19.974

Mole %

Ca	5.9	5.1	3.6	1.5	0.6	1.7	0.7	1.2	2.3
Na	62.9	67.0	66.8	59.9	63.4	64.2	63.3	65.2	66.0
K	31.2	27.9	29.6	38.6	36.0	34.1	36.0	33.6	31.7

Table 7 continued

Sample	25699 cont.		
Grain	21	20	19
SiO_2	66.9	66.7	66.6
Al_2O_3	18.5	18.6	19.0
FeO*	0.57	0.36	0.50
CaO	0.24	0.67	0.44
Na_2O	7.56	7.75	7.85
K_2O	5.70	4.87	5.58
Sum	99.47	98.95	99.97

Number of cations on the basis of 32 (O)

Si	12.010	11.991	11.918
Al	3.920	3.950	4.003
Fe	0.085	0.055	0.075
Ca	0.046	0.129	0.085
Na	2.631	2.702	2.724
K	1.306	1.118	1.274
Z	15.930	15.941	15.921
X	4.068	4.004	4.158
Σ	19.998	19.945	20.079

Mole %

Ca	1.2	3.3	2.1
Na	66.1	68.4	66.7
K	32.7	28.3	31.2

Table 8. Electron microprobe analyses of apatite in rocks from
The Pleiades

Sample	25668		25661	
Grain	2	1	1-i	2
SiO_2	0.20	0.24	0.20	0.27
Al_2O_3	0.03	0.03	0.03	-
TiO_2	-	-	0.27	-
FeO*	0.09	0.11	1.72	0.70
MnO	-	-	0.06	0.09
MgO	0.06	0.05	0.18	0.28
CaO	52.1	52.4	50.8	51.2
Na_2O	0.16	0.09	0.15	0.08
P_2O_5	43.45	43.8	44.0	43.5
Sum	96.09	96.72	97.41	96.12

APPENDIX B continued

Part 2.   DVDP 1 and 2

"Electron microprobe analyses of minerals in core samples from Dry Valley Drilling Project (DVDP) holes 1 and 2, Ross Island, Antarctica"

Antarctic Data Series 4, Department of Geology Publication 4, Victoria University of Wellington.

VICTORIA UNIVERSITY OF WELLINGTON

ELECTRON MICROPROBE ANALYSES OF MINERALS IN CORE SAMPLES FROM DRY VALLEY DRILLING PROJECT (DVDP) HOLES 1 AND 2, ROSS ISLAND, ANTARCTICA.

Philip R. Kyle

N. Z. ANTARCTIC RESEARCH PROGRAMME
(WORKING GROUP IN GEOLOGY)

ERRATA

Electron Microprobe Analysis of Minerals in
Core Samples from Dry Valley Drilling Project
(DVDP) Holes 1 and 2, Ross Island, Antarctica.

by Philip R. Kyle

Sample 1-88.55 was incorrectly labelled during thin section
preparation at the Thiel Earth Sciences Laboratory, McMurdo
Station, Antarctica. It is a nepheline benmoreite from an
unknown depth in DVDP 1. The sample should be labelled
DVDP 1-A.

Page 1 paragraph 3. Add to the end of first sentence 'or
else small grain size'.

Page 1 paragraph 5. Delete sentence - 'For the feldspars it
was usual only to accumulate a single 10 second count'.

Page 1 paragraph 5. Add to end 'Detection limit was 0.03% for
all elements except SiO_2 which was 0.07%.

Page 2. Below references give key to tables:
n.d. not determined.
—   below limit of detection.

Page 5. Sample 1-57.94, grain 1 delete partial analysis.

Page 5. Grain number 2R listed under sample 1-85.35 should
be under sample 1-88.55 (i.e. sample DVDP 1-A).

Page 15. Sample 1-57.64 should be 1-57.94.

Page 24. Grain 5-i Cr = 0.181, Fe^{3+} = 6.004.

ELECTRON MICROPROBE ANALYSES OF MINERALS IN CORE SAMPLES
FROM DRY VALLEY DRILLING PROJECT (DVDP) HOLES 1 AND 2,
ROSS ISLAND, ANTARCTICA

Philip R. Kyle
Antarctic Research Centre
Department of Geology
Victoria University of Wellington
Private Bag
WELLINGTON, NEW ZEALAND

CONTENTS

INTRODUCTION

This paper presents quantitative electron microprobe analyses of minerals in core samples from the Dry Valley Drilling Project (DVDP) holes 1 and 2. Preliminary petrographic descriptions of some of the samples and detailed core logs are given elsewhere (Treves and Kyle, 1973).

In the tables contained herein the analysed samples are listed in order of increasing depth within each hole. The sample number refers firstly to the hole and this is followed by the depth in metres. Analyses for all ferromagnesium minerals are listed in order of increasing FeO. Felspars and apatites are listed by increasing Na_2O and CaO respectively. Where there is more than one analysis per grain the core is always listed first. To designate the position of analysis the following symbols are used:

    C - core
    R - rim
    I - intermediate between core and rim

Scans were made to determine the homogeneity of grains and where only one analysis is presented this usually indicates no zoning or only weak zoning. In such grains the analysis was made near the centre.

The following lower case symbols were used where applicable to denote the type of crystal analysed:

    a - alteration product
    g - groundmass; used only when the sample was porphyritic
    i - inclusion within another mineral
    x - xenocryst
  (010) - sector when crystal showed sector zoning.

Analytical Method

Analyses were made using a Japanese Electron Optics Laboratory electron probe X-ray microanalyser Model JXA-5A at the Department of Geology, University of Otago. Instrumental settings were: 15kV accelerating potential, 2.0 to 3.0 $\times 10^{-8}$ amps specimen current on periclase and a 1-2 μm beam size. Corrections for absorption, fluorescence and atomic number were applied using the method of Bence and Albee (1968) and the alpha correction factors, for a 40° takeoff angle, listed in Kushiro and Nakamura (1970). Corrections for dead-time, background and drift were made. Each complete analysis and also the partial analyses of pyroxenes and olivines represents a minimum of 5 individual 10 second counts per element. For the feldspars it was usual only to accumulate a single 10 second count. Corrections for the partial analyses were made assuming the mineral was stoichometric and consisted purely of the end members $CaSiO_3$, $MgSiO_3$, $FeSiO_3$ for the pyroxenes, Fe_2SiO_4, Mg_2SiO_3 for the olivines and $KAlSi_3O_8$, $NaAlSi_3O_8$, $CaAl_2Si_2O_8$ for the feldspars. Data was reduced at the Computer Centre, University of Canterbury.

Standard materials were as follows: natural albite from Amelia (Na), adularia from Gotthard (K), hematite from Sennin Mine (Fe), maganosite from Nodatamagawa Mine (Mn); synthetic corundum (Al), wollastonite (Ca, Si), NiO(Ni), Cr_2O_3 (Cr), periclase (Mg), rutile (Ti).

In all analyses total iron was determined as FeO, in the pyroxenes however Fe_2O_3 was calculated by allotting equivalent amounts of Fe_2O_3 to Na_2O.

Recalculation of magnetite and ilmenite analyses were made using the methods of Carmichael (1967). For the spinels total Fe has been assigned to Fe^{2+} and Fe^{3+} on the assumption of a formula $R^{2+} R_2^{3+}O_4$ with dissolved Fe_2TiO_4.

Acknowledgements

References

Bence, A.E., Albee, A.L. (1968) : Empirical correction factors for the electron microanalysis of silicates and oxides. J. Geol. 76, 382-403.

Carmichael, I.S.E., (1967) : The iron-titanium oxides of salic volcanic rocks and their associated ferro-magnesian silicates. Contr. Mineral Petrol, 14, 36-64.

Kushiro, I., Nakamura, Y., (1970) : Petrology of some lunar crystalline rocks. Proc. Apollo 11 Lunar Science Conference 1, 607-626.

Treves, S.B., Kyle, P.R., (1973) : Geology of DVDP 1, and 2, Hut Point Peninsula, Ross Island, Antarctica. Dry Valley Drilling Project Bulletin no. 2, 11-82.

TABLE 1

Electron Microprobe Analyses of Olivines in DVDP 1 and 2 Core Samples

Sample	1-121.88									
Grain	1C	1R	6C	6R	4	2C	2R	8	7-g	3-g
SiO2	39.5	39.4	39.2		38.8	38.0	37.1	38.4	38.2	36.8
Al2O3	0.05	0.06	0.03		0.07	0.06	0.05	0.04	0.06	0.03
TiO2	0.03	0.03	0.02		0.05	0.03	0.06		0.02	0.05
FeO	13.2	14.3	14.3	20.1	15.1	16.3	22.2	18.8	20.3	23.2
MnO	0.17	0.19	0.19		0.19	0.20	0.44	0.31	0.25	0.49
MgO	46.1	44.8	44.6	39.7	44.3	42.7	37.8	40.6	40.2	37.7
CaO	0.26	0.30	0.29	0.33	0.28	0.34	0.38	0.20	0.19	0.36
NiO	0.21	0.15	0.15		0.08	0.15	0.11	0.13	0.09	0.06
Cr2O3	0.03	-	-		-	-	-	-	-	-
Sum	99.55	99.23	98.78		98.87	97.78	98.14	98.48	99.31	98.69

Number of Ions on the Basis of 4(0)

	1C	1R	6C	6R	4	2C	2R	8	7-g	3-g
Si	0.991	0.997	0.996		0.989	0.986	0.989	0.999	0.992	0.980
Al	0.001	0.002	0.001		0.002	0.002	0.001	0.001	0.002	0.001
Ti	-	-	-		0.001	-	0.001	-	-	0.001
Fe	0.277	0.302	0.304		0.322	0.355	0.495	0.410	0.442	0.517
Mn	0.004	0.004	0.004		0.004	0.004	0.010	0.007	0.006	0.011
Mg	1.723	1.686	1.687		1.682	1.652	1.501	1.575	1.558	1.497
Ca	0.007	0.008	0.008		0.008	0.010	0.011	0.006	0.005	0.010
Ni	0.004	0.003	0.003		0.002	0.003	0.002	0.003	0.002	0.001
Cr	0.004	-	-		-	-	-	-	-	-
Z	0.991	0.997	0.996		0.989	0.986	0.989	0.999	0.992	0.980
X	2.020	2.005	2.007		2.021	2.026	2.021	2.002	2.015	2.038
Sum	3.001	3.002	3.003		3.010	3.012	3.010	3.001	3.007	3.018
Fo	86.2	84.8	84.7	77.9	83.9	82.3	75.2	79.4	77.9	74.3
Fa	13.8	15.2	15.3	22.1	16.1	17.7	24.8	20.6	22.1	25.7

Sample	1-131.36	1-187.64								
Grain	1	1C	1I	1I	1I	1R	3	5C	5R	6
SiO2	37.8	39.5			39.6	39.7	40.1	39.9	39.8	
Al2O3	0.06	0.11			0.05	0.04	0.06	0.06	0.04	
TiO2	0.04	0.03			0.04	0.03	0.03	-	-	
FeO	22.2	16.3	16.7	15.4	16.2	13.2	13.6	13.7	13.8	14.0
MnO	1.05	0.25			0.23	0.20	0.20	0.17	0.21	
MgO	38.0	44.3	43.9	45.3	44.4	46.3	46.4	46.2	45.9	46.1
CaO	0.43	0.31	0.30	0.32	0.30	0.36	0.34	0.36	0.41	0.38
NiO	nd	0.09			0.11	0.17	0.21	0.21	0.22	
Cr2O3	nd	-			-	0.03	0.03	0.03	-	
Sum	99.58	100.79			100.93	100.03	100.97	100.63	100.38	

Number of Ions on the Basis of 4(0)

	1	1C	1I	1I	1I	1R	3	5C	5R	6
Si	0.993	0.991			0.992	0.990	0.992	0.991	0.992	
Al	0.002	0.003			0.002	0.001	0.002	0.002	0.001	
Ti	0.001	-			0.001	-	-	-	-	
Fe	0.489	0.342			0.339	0.276	0.281	0.284	0.288	
Mn	0.023	0.005			0.005	0.004	0.004	0.004	0.004	
Mg	1.486	1.655			1.658	1.723	1.712	1.712	1.705	
Ca	0.012	0.008			0.008	0.010	0.009	0.010	0.011	
Ni	-	0.002			0.002	0.003	0.004	0.004	0.004	
Cr	-	-			-	0.001	0.001	0.001	-	
Z	0.993	0.991			0.992	0.990	0.992	0.991	0.992	
X	2.013	2.015			2.015	2.018	2.013	2.019	2.013	
Sum	3.006	3.006			3.007	3.008	3.005	3.008	3.005	
Fo	75.2	82.9	82.4	84.0	83.0	86.2	85.9	85.8	85.6	85.4
Fa	24.8	17.1	17.6	16.0	17.0	13.8	14.1	14.2	14.4	14.6

TABLE 1   Continued

Sample	1-187.64 cont.			2-39.28					2-62.41
Grain	4C-g	4R-g	2	2-x	4-x	1C-x	1R-x	3-x	1-x
SiO_2	40.1			38.8	38.6	39.1		38.5	35.1
Al_2O_3	0.05			-	-	-		-	0.03
TiO_2	0.05			-	0.03	-		0.05	-
FeO	14.3	16.4	15.0	16.4	17.15	17.2	22.5	17.9	34.1
MnO	0.22			0.24	0.27	0.24	0.56	0.24	1.45
MgO	45.4	43.6	45.1	43.2	43.0	42.8	38.4	42.1	28.7
CaO	0.47	0.54	0.38	0.29	0.30	0.30		0.27	0.26
NiO	0.20			n.d.	n.d.	n.d.		n.d.	-
Cr_2O_3	-			n.d.	n.d.	n.d.		n.d.	-
Sum	100.79			98.93	99.35	99.64		99.06	99.64

Number of Ions on the Basis of 4 (0)

	4C-g	4R-g	2	2-x	4-x	1C-x	1R-x	3-x	1-x
Si	0.998			0.993	0.989	0.997		0.990	0.982
Al	0.001			-	-	-		-	0.001
Ti	0.001			-	0.001	-		0.001	-
Fe	0.298			0.351	0.367	0.367		0.386	0.797
Mn	0.005			0.005	0.006	0.005		0.005	0.034
Mg	1.682			1.650	1.640	1.625		1.618	1.195
Ca	0.013			0.008	0.008	0.008		0.007	0.008
Ni	0.004			-	-	-		-	-
Cr	-			-	-	-		-	-
Z	0.998			0.993	0.989	0.997		0.990	0.982
X	2.004			2.014	2.022	2.005		2.017	2.035
Sum	3.002			3.007	3.011	3.002		3.007	3.017
Fo	85.0	82.6	84.3	82.5	81.7	81.6	75.3	80.8	60.0
Fa	15.0	17.4	15.7	17.5	18.3	18.3	24.7	19.2	40.0

Sample	2-99.34				2-103.15				
Grain	1	3	4-i	2	1	5-i	4	2	3
SiO_2	40.0	40.0	39.5	39.3	39.9	39.0	38.2	38.3	38.5
Al_2O_3	0.09	0.07	0.08	0.09	0.08	0.06	0.07	0.05	0.07
TiO_2	-	-	0.03	0.05	0.03	0.03	-	0.03	-
FeO	11.9	13.2	14.9	16.5	12.6	17.5	17.6	20.3	20.6
MnO	0.16	0.17	0.20	0.23	0.20	0.24	0.39	0.28	0.32
MgO	47.9	47.0	45.1	44.2	46.35	42.3	41.9	39.8	39.5
CaO	0.25	0.18	0.39	0.35	0.29	0.31	0.32	0.24	0.22
NiO	0.21	0.28	0.15	0.10	0.24	0.09	0.16	0.06	0.04
Cr_2O_3	0.05	0.06	0.03	-	-	-	-	-	-
Sum	100.56	100.96	100.38	100.82	99.69	99.53	98.64	99.06	99.25

Number of Ions on the Basis of 4 (0)

	1	3	4-i	2	1	5-i	4	2	3
Si	0.986	0.988	0.989	0.988	0.995	0.997	0.989	0.998	1.001
Al	0.003	0.002	0.002	0.003	0.002	0.002	0.002	0.001	0.002
Ti	-	-	-	0.001	0.001	0.001	-	0.001	-
Fe	0.246	0.273	0.313	0.346	0.264	0.374	0.381	0.442	0.448
Mn	0.003	0.004	0.004	0.005	0.004	0.005	0.008	0.006	0.007
Mg	1.761	1.731	1.684	1.656	1.724	1.611	1.617	1.544	1.533
Ca	0.007	0.005	0.010	0.009	0.008	0.009	0.009	0.007	0.006
Ni	0.004	0.006	0.003	0.002	0.005	0.002	0.003	0.001	0.001
Cr	0.001	0.001	0.001	-	-	-	-	-	-
Z	0.986	0.988	0.989	0.988	0.995	0.997	0.989	0.998	1.001
X	2.025	2.022	2.017	2.022	2.008	2.004	2.020	2.002	1.997
Sum	3.011	3.010	3.006	3.010	3.003	3.001	3.009	3.000	2.998
Fo	87.3	86.4	84.3	82.7	86.7	81.2	80.9	77.7	77.4
Fa	12.3	13.6	15.7	17.3	13.3	18.8	19.1	22.3	22.6

TABLE 2

Electron Microprobe Analyses of Pyroxene in DVDP 1 and 2 Core Samples

Sample	1-57.94		1-85.35				1-88.55		
Grain	1	2	1C	1I	1R	2R	5-g	1R-g	4-g
SiO_2		48.3	46.0	45.1	46.0	48.9	48.7	48.6	48.4
Al_2O_3		4.14	6.79	7.17	7.20	3.59	3.24	4.27	3.44
TiO_2		1.65	2.15	1.89	2.37	1.54	1.76	1.64	1.69
FeO	8.29	9.12	15.5	16.0	13.5	8.65	8.66	8.85	10.3
MnO		0.41	0.59	0.58	0.48	0.44	0.40	0.42	0.42
MgO	12.3	12.4	6.22	5.99	7.58	12.2	12.5	12.1	12.1
CaO	25.2	22.8	21.0	20.8	21.2	22.5	22.7	22.3	22.7
Na_2O		0.79	1.17	1.22	1.13	0.74	0.69	0.81	0.70
Cr_2O_3		n.d.	n.d.	n.d.	n.d.	n.d.	n.d.	n.d.	n.d.
Sum		99.61	99.42	98.75	99.46	98.56	98.65	98.99	99.75
Fe_2O_3		2.04	3.01	3.14	2.91	1.91	1.78	2.09	1.80
FeO		7.28	12.8	13.2	10.9	6.93	7.06	6.97	8.68
Total		99.81	99.73	99.09	99.77	98.75	98.83	99.20	99.93

Number of Ions on the Basis of 6(O)

	1	2	1C	1I	1R	2R	5-g	1R-g	4-g
Si		1.825	1.784	1.766	1.767	1.859	1.853	1.840	1.837
Al		0.175	0.216	0.234	0.233	0.141	0.145	0.160	0.154
Ti		-	-	-	-	-	0.002	-	0.009
Al		0.009	0.094	0.097	0.092	0.019	-	0.031	-
Ti		0.047	0.063	0.056	0.068	0.044	0.048	0.047	0.039
Fe^{3+}		0.058	0.088	0.093	0.084	0.055	0.051	0.060	0.051
Fe^{2+}		0.230	0.415	0.432	0.350	0.220	0.225	0.221	0.276
Mn		0.013	0.019	0.019	0.016	0.014	0.013	0.014	0.014
Mg		0.698	0.360	0.350	0.434	0.692	0.709	0.683	0.684
Ca		0.923	0.872	0.873	0.872	0.917	0.926	0.905	0.923
Na		0.058	0.088	0.093	0.084	0.055	0.051	0.060	0.052
Cr		-	-	-	-	-	-	-	-
Z		2.000	2.000	2.000	2.000	2.000	2.000	2.000	2.000
XY		2.036	1.999	2.013	2.002	2.016	2.024	2.018	2.038
Ca	51.7	48.0	49.7	49.4	49.7	48.3	48.1	48.1	47.4
Mg	35.0	36.3	20.5	19.8	24.7	36.5	36.9	36.3	35.1
$*Fe_T$+Mn	13.3	15.7	29.8	30.8	25.6	15.2	15.0	15.6	17.5
Na		5.8	10.0	10.4	9.5	5.6	6.1	6.1	5.0
Mg		69.9	40.8	39.1	49.1	70.5	71.1	69.9	66.8
Fe^{2+}+Mn		24.3	49.2	50.5	41.4	23.9	23.8	24.0	28.2

$*Fe_T = Fe^{2+} + Fe^{3+}$

TABLE 2 continued

Sample	1-121.88								
Grain	6C	6I	6I	6I	6R	5C	5I	5R	2
SiO_2	45.2				45.7				45.7
Al_2O_3	10.2				7.45				8.78
TiO_2	4.28				4.05				2.71
FeO	6.00	6.64	5.64	6.54	6.69	5.75	5.52	7.15	6.94
MnO	0.05				0.08				0.09
MgO	12.2	12.1	12.5	11.1	12.4	12.6	12.8	10.8	12.2
CaO	22.2	22.7	22.6	22.7	22.6	21.9	22.1	22.9	21.0
Na_2O	0.57				0.44				0.94
Cr_2O_3	0.40				-				0.24
Sum	101.10				99.41				98.60
Fe_2O_3	1.47				1.13				2.42
FeO	4.68				5.67				4.76
Total	101.25				99.52				98.84

Number of Ions on the Basis of 6(0)

	6C				6R				2
Si	1.659				1.715				1.717
Al	0.341				0.285				0.283
Al	0.100				0.095				0.106
Ti	0.118				0.114				0.077
Fe^{3+}	0.041				0.032				0.068
Fe^{2+}	0.144				0.178				0.150
Mn	0.002				0.002				0.003
Mg	0.668				0.694				0.683
Ca	0.873				0.909				0.846
Na	0.041				0.032				0.068
Cr	0.012				-				0.007
Z	2.000				2.000				2.000
XY	1.997				2.006				2.008
Ca	50.6	50.8	50.8	52.4	50.1	49.9	49.9	49.9	48.3
Mg	38.7	37.6	39.3	35.8	38.2	39.9	40.3	40.3	39.1
Fe_T+Mn	10.7	11.6	9.9	11.8	11.7	10.2	9.8	9.8	12.6
Na	4.8				3.5				7.6
Mg	78.2				76.6				75.6
Fe^{2+}+Mn	17.0				19.9				16.8

TABLE 2 continued

Sample	1-121.88 cont.					1-131.36			
Grain	4C	4I	4R	3C	3R	1	2	4	3
SiO_2	46.0	44.3	42.0	43.5	45.6	47.6	47.5	49.9	47.6
Al_2O_3	7.30	9.47	10.4	8.53	8.98	4.85	5.43	3.07	4.66
TiO_2	2.28	3.90	5.02	1.99	4.32	2.38	2.38	1.31	2.06
FeO	10.7	6.37	7.42	17.6	6.35	7.68	7.79	8.14	8.80
MnO	0.34	0.06	0.07	0.54	0.11	0.38	0.33	0.45	0.39
MgO	9.20	12.0	10.8	4.90	12.8	13.4	13.2	13.6	12.3
CaO	21.6	22.5	22.5	20.4	22.6	21.1	20.6	22.4	21.8
Na_2O	1.44	0.55	0.52	1.64	0.46	0.81	0.85	0.56	0.79
Cr_2O_3	0.05	0.34	0.03	-	0.20	n.d.	n.d.	n.d.	n.d.
Sum	98.91	99.49	98.76	99.10	101.42	98.20	98.08	99.43	98.40
Fe_2O_3	3.71	1.42	1.34	4.23	1.19	2.09	2.19	1.44	2.04
FeO	7.36	5.09	6.21	13.8	5.28	5.80	5.82	6.84	6.96
Total	99.28	99.63	98.89	99.53	101.54	98.41	98.30	99.57	98.60

Number of Ions on the Basis of 6(O)

Si	1.755	1.661	1.600	1.710	1.674	1.805	1.800	1.874	1.814
Al	0.245	0.339	0.400	0.290	0.326	0.195	0.200	0.126	0.186
Al	0.083	0.079	0.067	0.105	0.063	0.022	0.042	0.010	0.023
Ti	0.065	0.110	0.144	0.059	0.119	0.068	0.068	0.037	0.059
Fe^{3+}	0.106	0.040	0.038	0.125	0.033	0.060	0.062	0.041	0.058
Fe^{2+}	0.235	0.160	0.198	0.454	0.162	0.184	0.184	0.215	0.222
Mn	0.011	0.002	0.002	0.018	0.003	0.012	0.011	0.014	0.013
Mg	0.523	0.671	0.614	0.287	0.701	0.757	0.746	0.762	0.699
Ca	0.883	0.904	0.919	0.859	0.889	0.857	0.836	0.902	0.890
Na	0.106	0.040	0.038	0.125	0.033	0.060	0.062	0.041	0.058
Cr	0.002	0.010	0.001	-	0.006	-	-	-	-
Z	2.000	2.000	2.000	2.000	2.000	2.000	2.000	2.000	2.000
XY	2.015	2.015	2.022	2.033	2.009	2.019	2.011	2.021	2.022
Ca	50.2	50.9	51.9	49.3	49.7	45.8	45.5	46.6	47.3
Mg	29.8	37.8	34.6	16.5	39.2	40.5	40.5	39.4	37.1
Fe_T+Mn	20.0	11.3	13.5	34.2	11.1	13.7	14.0	14.0	15.6
Na	12.2	4.6	4.5	14.1	3.6	5.9	6.2	4.0	5.9
Mg	57.8	76.9	72.0	32.5	78.0	74.8	74.3	73.8	70.5
Fe^{2+}+Mn	28.0	18.5	23.5	53.4	18.4	19.3	19.5	22.2	23.6

TABLE 2 continued

Sample	1-187.64					2-39.28			
Grain	2	1C	1R	3	4	5-x	4C-x	4R-x	3C
SiO_2	43.2	42.9	42.3			51.2	51.0	51.0	49.55
Al_2O_3	8.56	10.2	9.93			3.93	4.37	3.75	4.31
TiO_2	4.52	5.17	5.48			0.82	1.04	0.92	2.24
FeO	6.85	6.96	7.58	6.04	7.32	6.20	6.58	6.66	7.18
MnO	0.10	0.09	0.10			0.16	0.16	0.14	0.24
MgO	11.4	11.4	10.6	14.2	11.5	14.1	14.1	14.0	13.4
CaO	22.6	22.6	22.2	22.5	22.4	22.2	21.45	22.4	22.4
Na_2O	0.48	0.45	0.59			1.01	1.21	0.89	0.56
Cr_2O_3	0.31	0.24	0.04			n.d.	n.d.	n.d.	n.d.
Sum	98.02	100.01	98.82			99.62	99.91	99.76	99.88
Fe_2O_3	1.24	1.16	1.52			2.60	3.12	2.29	1.44
FeO	5.73	5.92	6.21			3.86	3.77	4.60	5.88
Total	98.14	100.13	98.97			99.88	100.22	99.99	100.02

Number of Ions on the Basis of 6(0)

Si	1.655	1.610	1.610			1.888	1.874	1.885	1.842
Al	0.345	0.390	0.390			0.112	0.126	0.115	0.158
Al	0.041	0.061	0.056			0.059	0.063	0.048	0.031
Ti	0.130	0.146	0.157			0.023	0.029	0.026	0.063
Fe^{3+}	0.036	0.033	0.044			0.072	0.086	0.064	0.040
Fe^{2+}	0.184	0.186	0.198			0.119	0.116	0.142	0.183
Mn	0.003	0.003	0.003			0.005	0.005	0.004	0.008
Mg	0.651	0.638	0.602			0.775	0.772	0.772	0.743
Ca	0.928	0.909	0.906			0.877	0.844	0.887	0.892
Na	0.036	0.033	0.044			0.072	0.086	0.064	0.040
Cr	0.009	0.007	0.001			-	-	-	-
Z	2.000	2.000	2.000			2.000	2.000	2.000	2.000
XY	2.017	2.015	2.009			2.003	2.001	2.007	2.000
Ca	51.5	51.4	51.7	47.9	50.8	47.5	46.3	47.5	47.8
Mg	36.1	36.1	34.3	42.1	36.2	41.9	42.3	41.3	39.8
Fe_T+Mn	12.4	12.5	14.0	10.0	13.0	10.6	11.4	11.2	12.4
Na	4.1	3.8	5.1			7.4	8.8	6.5	4.1
Mg	74.5	74.2	71.1			79.8	78.9	78.6	76.3
Fe^{2+}+Mn	21.4	22.0	23.8			12.8	12.3	14.9	19.6

TABLE 2 continued

Sample	2-39.28 cont.		2-54.72					
Grain	3I	3R	11-a	10-a	4	2	3	1
SiO_2	48.3	43.8	46.6	49.9	49.3	49.1	46.2	44.8
Al_2O_3	4.45	8.01	6.73	3.83	3.76	4.17	6.90	7.57
TiO_2	2.06	4.32	3.26	1.86	1.69	1.94	2.99	3.96
FeO	7.17	8.28	7.31	7.51	8.09	9.03	9.07	9.70
MnO	0.25	0.22	0.30	0.39	0.37	0.37	0.31	0.27
MgO	13.2	10.9	12.7	13.3	13.0	12.0	11.0	10.3
CaO	22.8	22.3	21.3	21.6	22.6	22.4	22.3	22.3
Na_2O	0.64	0.80	0.99	0.70	0.70	0.66	0.89	0.86
Cr_2O_3	n.d.	n.d.	n.d.	n.d.	n.d.	n.d.	n.d.	n.d.
Sum	98.97	98.63	99.19	99.09	99.51	99.67	99.66	99.76
Fe_2O_3	1.65	2.06	2.55	1.80	1.80	1.70	2.29	2.22
FeO	5.69	6.43	5.02	5.89	6.47	7.50	7.01	7.70
Total	99.04	98.84	99.45	99.27	99.69	99.84	99.89	99.98

Number of Ions on the Basis of 6(O)

	3I	3R	11-a	10-a	4	2	3	1
Si	1.821	1.673	1.747	1.868	1.851	1.847	1.744	1.699
Al	0.179	0.327	0.253	0.132	0.149	0.153	0.256	0.301
Al	0.019	0.034	0.044	0.037	0.017	0.032	0.051	0.037
Ti	0.058	0.124	0.092	0.052	0.048	0.055	0.085	0.113
Fe^{3+}	0.047	0.059	0.072	0.051	0.051	0.048	0.065	0.063
Fe^{2+}	0.179	0.205	0.157	0.184	0.203	0.236	0.221	0.244
Mn	0.008	0.007	0.010	0.012	0.019	0.012	0.010	0.009
Mg	0.742	0.621	0.710	0.742	0.728	0.673	0.619	0.582
Ca	0.921	0.913	0.856	0.866	0.909	0.903	0.902	0.906
Na	0.047	0.059	0.072	0.051	0.051	0.048	0.065	0.063
Z	2.000	2.000	2.000	2.000	2.000	2.000	2.000	2.000
XY	2.021	2.022	2.013	1.996	2.018	2.006	2.018	2.019
Ca	48.5	50.6	47.4	46.7	47.8	48.2	49.6	50.2
Mg	39.1	34.4	39.3	40.0	38.2	26.0	34.1	32.3
Fe_T+Mn	12.4	15.0	13.2	13.3	14.0	15.8	16.3	17.3
Na	4.8	6.6	7.6	5.1	5.1	5.0	7.1	7.0
Mg	76.0	69.6	74.8	75.0	73.3	69.4	67.6	64.8
Fe^{2+}+Mn	19.2	23.8	17.6	19.9	21.6	25.6	25.3	28.2

TABLE 2 continued

Sample	2-62.41								
Grain	2C	2R	13C	13R	23-x	16C	16R	20-x	4C-x
SiO_2	45.5	45.0	44.3	44.2	50.4	44.4	43.4	50.2	50.8
Al_2O_3	8.50	8.90	9.47	9.48	4.66	9.50	9.95	4.99	4.64
TiO_2	3.11	3.20	3.66	3.57	0.88	3.50	3.49	1.07	0.95
FeO	7.26	7.80	7.26	7.67	7.40	7.61	8.65	7.61	7.62
MnO	0.14	0.19	0.11	0.09	0.24	0.14	0.16	0.30	0.31
MgO	12.4	11.6	11.8	11.5	13.5	11.4	10.65	13.2	13.3
CaO	21.8	21.7	22.0	22.05	21.9	22.1	21.85	21.6	21.8
Na_2O	0.83	0.70	0.76	0.85	0.88	0.87	0.97	1.08	1.04
Cr_2O_3	-	-	-	-	-	-	-	0.04	0.03
Sum	99.54	99.09	99.36	99.41	99.86	99.52	99.12	100.09	100.49
Fe_2O_3	2.14	1.80	1.96	2.19	2.27	2.24	2.50	2.78	2.68
FeO	5.33	6.18	5.50	5.70	5.36	5.59	6.40	5.11	5.21
Total	99.75	99.27	99.56	99.63	100.09	99.74	99.37	100.37	100.76

Number of Ions on the Basis of 6(0)

	2C	2R	13C	13R	23-x	16C	16R	20-x	4C-x
Si	1.703	1.697	1.665	1.663	1.866	1.668	1.646	1.854	1.869
Al	0.297	0.303	0.335	0.337	0.134	0.332	0.354	0.146	0.131
Al	0.078	0.093	0.085	0.083	0.069	0.089	0.091	0.071	0.070
Ti	0.088	0.091	0.103	0.101	0.024	0.099	0.100	0.030	0.026
Fe^{3+}	0.060	0.051	0.055	0.062	0.063	0.063	0.071	0.077	0.074
Fe^{2+}	0.167	0.195	0.173	0.179	0.166	0.176	0.203	0.158	0.160
Mn	0.004	0.006	0.004	0.003	0.008	0.004	0.005	0.009	0.010
Mg	0.692	0.652	0.661	0.645	0.745	0.638	0.602	0.727	0.729
Ca	0.874	0.877	0.886	0.889	0.869	0.890	0.888	0.855	0.859
Na	0.060	0.051	0.055	0.062	0.063	0.063	0.071	0.077	0.074
Cr	-	-	-	-	-	-	-	0.001	0.001
Z	2.000	2.000	2.000	2.000	2.000	2.000	2.000	2.000	2.000
XY	2.022	2.015	2.022	2.025	2.008	2.023	2.032	2.007	2.002
Ca	48.6	49.2	49.8	50.0	46.9	50.2	50.2	46.8	46.9
Mg	38.5	36.6	37.2	36.3	40.3	36.1	34.0	39.8	39.8
Fe_T+Mn	12.9	14.2	13.0	13.7	12.8	13.7	15.8	13.4	13.3
Na	6.5	5.7	6.2	7.0	6.4	7.2	8.1	8.0	7.6
Mg	74.9	72.1	74.0	72.5	75.9	72.4	68.3	74.8	74.9
Fe^{2+}+Mn	18.6	22.2	19.8	20.5	17.7	20.4	23.6	17.2	17.5

TABLE 2 continued

Sample	2-62.41	cont.						
Grain	21-x	15C	15R	14C	14R	22-x	10C	10R
SiO_2	50.4	43.8	44.5	41.7	41.7	50.1	45.6	46.4
Al_2O_3	4.49	10.0	9.58	11.6	12.5	3.47	7.07	5.06
TiO_2	0.92	3.54	3.41	3.85	4.12	0.71	1.91	2.64
FeO	7.69	8.14	7.78	8.89	8.63	11.7	15.1	7.99
MnO	0.29	0.14	0.12	0.16	0.15	0.56	0.62	0.26
MgO	13.2	10.75	11.6	9.57	9.53	10.4	6.75	13.0
CaO	22.1	22.05	22.15	21.7	21.8	21.4	20.9	22.8
Na_2O	0.97	0.90	0.88	0.95	0.90	1.20	1.43	0.57
Cr_2O_3	0.03	-	-	-	-	0.03	-	-
Sum	100.09	99.32	100.02	98.42	99.33	99.57	99.38	98.72
Fe_2O_3	2.50	2.32	2.27	2.45	2.32	3.09	3.68	1.47
FeO	5.44	6.05	5.74	6.69	6.54	8.92	11.8	6.67
Total	100.34	99.55	100.25	98.67	99.56	99.88	99.76	98.87

Number of Ions on the Basis of 6(0)

Si	1.866	1.654	1.664	1.597	1.580	1.897	1.766	1.767
Al	0.134	0.346	0.336	0.403	0.420	0.103	0.234	0.227
Ti	-	-	-	-	-	-	-	0.006
Al	0.062	0.099	0.056	0.121	0.138	0.052	0.089	-
Ti	0.026	0.100	0.096	0.111	0.117	0.020	0.056	0.070
Fe^{3+}	0.070	0.066	0.064	0.071	0.066	0.088	0.107	0.042
Fe^{2+}	0.168	0.191	0.180	0.214	0.207	0.282	0.382	0.212
Mn	0.009	0.004	0.004	0.005	0.005	0.018	0.020	0.008
Mg	0.728	0.605	0.647	0.546	0.538	0.587	0.390	0.738
Ca	0.877	0.892	0.888	0.891	0.885	0.868	0.867	0.930
Na	0.070	0.066	0.064	0.071	0.066	0.088	0.107	0.042
Cr	0.001	-	-	-	-	0.001	-	-
Z	2.000	2.000	2.000	2.000	2.000	2.000	2.000	2.000
XY	2.010	2.023	2.028	2.030	2.023	2.005	2.018	2.044
Ca	47.3	50.7	49.8	51.6	52.0	47.1	49.1	48.2
Mg	39.3	34.4	36.3	31.6	31.6	31.8	22.1	38.2
Fe_T+Mn	13.4	14.9	13.9	16.8	16.4	21.1	28.8	13.6
Na	7.1	7.6	7.1	8.4	8.1	9.0	11.9	4.2
Mg	74.7	69.8	72.4	65.3	65.9	60.2	43.3	73.7
Fe^{2+}+Mn	18.2	22.6	20.5	26.3	2 6.0	30.8	44.8	22.1

TABLE 2 continued

Sample	2-70.41						2-99.34	
Grain	3	4	5	2	1C	1R	1	3C
SiO_2	43.7	43.4	44.8	44.7	47.2	44.6	44.3	45.1
Al_2O_3	10.1	9.99	6.98	9.16	5.75	7.76	10.1	9.27
TiO_2	3.73	3.67	3.67	3.00	1.90	3.85	4.11	3.29
FeO	7.96	7.97	8.11	9.20	14.5	8.23	6.45	8.34
MnO	0.14	0.13	0.20	0.22	0.70	0.18	0.07	0.14
MgO	10.8	10.9	11.5	10.35	7.32	11.5	12.1	10.7
CaO	22.0	22.1	22.5	21.4	20.5	22.4	22.1	22.3
Na_2O	0.89	0.90	0.67	1.13	1.86	0.73	0.56	1.04
Cr_2O_3	-	-	-	-	-	-	0.03	-
Sum	99.32	99.06	98.43	99.16	99.73	99.25	99.82	100.18
Fe_2O_3	2.29	2.32	1.73	2.91	4.79	1.88	1.44	2.68
FeO	5.90	5.88	6.55	6.58	10.2	6.54	5.15	5.93
Total	99.55	99.29	98.60	99.45	100.22	99.44	99.96	100.45

Number of Ions on the Basis of 6(0)

	3	4	5	2	1C	1R	1	3C
Si	1.649	1.644	1.712	1.692	1.808	1.690	1.652	1.686
Al	0.351	0.356	0.288	0.308	0.192	0.310	0.348	0.314
Al	0.098	0.090	0.026	0.101	0.068	0.037	0.096	0.094
Ti	0.106	0.104	0.106	0.085	0.055	0.110	0.115	0.092
Fe^{3+}	0.065	0.066	0.050	0.083	0.138	0.054	0.040	0.075
Fe^{2+}	0.186	0.186	0.209	0.208	0.327	0.207	0.161	0.185
Mn	0.004	0.004	0.006	0.007	0.023	0.006	0.002	0.004
Mg	0.607	0.615	0.655	0.584	0.418	0.650	0.673	0.596
Ca	0.889	0.897	0.922	0.868	0.841	0.910	0.883	0.893
Na	0.065	0.066	0.050	0.083	0.138	0.054	0.041	0.075
Cr	-	-	-	-	-	-	0.001	-
Z	2.000	2.000	2.000	2.000	2.000	2.000	2.000	2.000
XY	2.021	2.029	2.025	2.019	2.008	2.027	2.011	2.017
Ca	50.7	50.7	50.0	49.6	48.2	49.8	50.2	50.9
Mg	34.7	34.8	35.6	33.4	23.9	35.6	38.2	34.0
Fe_T+Mn	14.6	14.5	14.4	17.0	27.9	14.6	11.6	15.1
Na	7.5	7.6	5.4	9.4	15.2	5.9	4.6	8.8
Mg	70.4	70.6	71.2	66.2	46.2	70.9	76.8	69.2
Fe^{2+}+Mn	22.1	21.8	23.4	24.4	38.6	23.2	18.6	22.0

TABLE 2 continued

Sample	2-99.34 cont.			2-103.15				
Grain	3R	4C	4R	16	3C	3I	3R	4(010)
SiO_2	45.7	46.8	44.7	46.3	48.4		46.9	46.1
Al_2O_3	8.93	8.18	8.29	8.26	6.72		8.02	7.30
TiO_2	3.38	2.72	3.69	3.23	1.98		2.35	4.05
FeO	6.88	9.07	6.49	5.43	5.71	6.17	6.81	6.34
MnO	0.12	0.16	0.08	0.08	0.13		0.12	0.11
MgO	12.5	10.8	13.1	12.4	13.9	13.8	12.6	12.5
CaO	22.3	22.0	23.0	22.7	21.75	21.8	21.4	22.8
Na_2O	0.60	1.17	0.38	0.61	0.75		0.95	0.53
Cr_2O_3	0.03	-	0.24	0.66	0.64		0.59	-
Sum	100.44	100.90	99.97	99.67	99.98		99.74	99.73
Fe_2O_3	1.55	3.01	0.98	1.57	1.93		2.45	1.37
FeO	5.48	6.36	5.61	4.02	3.97		4.61	5.11
Total	100.59	101.20	100.07	99.83	100.17		99.99	99.87

Number of Ions on the Basis of 6(0)

	3R	4C	4R	16	3C	3I	3R	4(010)
Si	1.694	1.735	1.673	1.721	1.784		1.742	1.721
Al	0.306	0.265	0.327	0.279	0.216		0.258	0.279
Al	0.084	0.093	0.039	0.081	0.076		0.093	0.042
Ti	0.094	0.076	0.104	0.090	0.055		0.066	0.114
Fe^{3+}	0.043	0.084	0.028	0.044	0.054		0.068	0.038
Fe^{2+}	0.170	0.197	0.176	0.125	0.122		0.143	0.160
Mn	0.004	0.005	0.002	0.002	0.004		0.004	0.004
Mg	0.691	0.597	0.731	0.687	0.764		0.698	0.696
Ca	0.886	0.874	0.922	0.904	0.859		0.852	0.912
Na	0.043	0.084	0.028	0.044	0.054		0.068	0.038
Cr	0.001	-	0.007	0.019	0.019		0.017	-
Z	2.000	2.000	2.000	2.000	2.000		2.000	2.000
XY	2.016	2.010	2.037	1.998	2.006		2.008	2.004
Ca	49.4	49.7	49.6	51.3	47.6	47.5	48.3	50.4
Mg	38.5	34.0	39.3	39.0	42.4	42.0	39.5	38.5
Fe_T+Mn	12.1	16.3	11.1	9.7	10.0	10.5	12.2	11.1
Na	4.8	9.5	2.9	5.1	5.7		7.5	4.3
Mg	76.1	67.6	78.1	80.0	80.9		76.4	77.5
Fe^{2+}+Mn	19.1	22.9	19.0	14.9	13.4		16.1	18.2

TABLE 2 continued

Sample	2-103.15 cont.							
Grain	4(010)	4(100)	4(100)	5C	5R	6C	6I	6R
SiO_2	45.3	42.3	40.1	44.1	44.1	47.0	46.2	46.7
Al_2O_3	7.63	10.15	11.75	10.5	10.4	5.66	6.14	7.22
TiO_2	3.76	4.84	6.60	4.21	3.88	1.08	3.22	2.60
FeO	6.82	7.09	7.19	6.40	6.23	15.6	6.62	6.39
MnO	0.13	0.09	0.10	0.08	0.08	0.70	0.12	0.09
MgO	12.5	11.0	10.3	11.9	11.8	6.54	12.3	13.0
CaO	22.7	22.9	22.8	21.6	22.4	20.8	23.1	22.6
Na_2O	0.53	0.54	0.55	0.81	0.66	1.94	0.65	0.54
Cr_2O_3	-	-	0.05	-	0.11	-	0.26	0.38
Sum	99.37	98.91	99.44	99.60	99.66	99.32	98.61	99.52
Fe_2O_3	1.37	1.39	1.42	2.09	1.70	5.00	1.67	1.39
FeO	5.59	5.84	5.91	4.52	4.70	11.10	5.12	5.14
Total	99.51	99.05	99.58	99.81	99.83	99.82	98.78	99.66

Number of Ions on the Basis of 6(0)

	4(010)	4(100)	4(100)	5C	5R	6C	6I	6R
Si	1.704	1.608	1.524	1.644	1.646	1.819	1.750	1.745
Al	0.296	0.392	0.476	0.356	0.354	0.181	0.250	0.255
Al	0.042	0.063	0.050	0.105	0.104	0.077	0.024	0.063
Ti	0.106	0.138	0.189	0.118	0.109	0.031	0.092	0.073
Fe^{3+}	0.039	0.040	0.041	0.059	0.048	0.146	0.048	0.039
Fe^{2+}	0.176	0.186	0.188	0.141	0.147	0.359	0.162	0.161
Mn	0.004	0.003	0.003	0.002	0.002	0.023	0.004	0.003
Mg	0.701	0.624	0.584	0.661	0.657	0.377	0.695	0.724
Ca	0.915	0.933	0.928	0.863	0.896	0.862	0.938	0.905
Na	0.039	0.040	0.040	0.058	0.048	0.146	0.048	0.039
Cr	-	-	0.002	-	0.003	-	0.008	0.011
Z	2.000	2.000	2.000	2.000	2.000	2.000	2.000	2.000
XY	2.021	2.026	2.024	2.007	2.014	2.021	2.017	2.018
Ca	49.9	52.3	53.2	50.0	51.2	48.8	50.8	49.4
Mg	38.2	34.9	33.5	38.3	37.5	21.3	37.6	39.5
Fe_T+Mn	11.9	12.8	13.3	11.7	11.3	29.9	11.6	11.1
Na	4.2	4.7	5.0	6.8	5.6	16.1	5.3	4.2
Mg	76.2	73.2	71.6	76.6	76.9	41.7	76.5	78.1
Fe^{2+}+Mn	19.6	22.1	23.4	16.6	17.5	42.2	18.2	17.7

TABLE 3

Electron Microscope Analyses of Amphiboles in DVDP 1 and 2 Core Samples

Sample 1-57.64

Grain	3C	3R	4I	4R	5g	1C	1R	2C	2R
SiO_2	38.5	38.7	39.7	39.0	38.8	38.8	38.9	38.1	38.9
Al_2O_3	13.6	13.1	12.8	13.2	13.6	13.3	12.8	13.3	13.0
TiO_2	6.19	5.40	6.02	5.22	6.34	5.90	5.35	4.91	5.15
FeO	10.5	11.9	10.8	12.2	11.2	11.4	11.5	15.4	11.9
MnO	0.14	0.22	0.16	0.22	0.17	0.19	0.22	0.34	0.22
MgO	13.0	12.3	13.0	12.15	12.35	12.2	12.5	9.93	12.2
CaO	11.9	11.6	11.6	11.6	11.7	11.7	11.8	11.5	11.7
Na_2O	2.71	2.80	2.72	2.94	2.78	2.79	2.86	2.68	2.79
K_2O	1.38	1.43	1.26	1.39	1.38	1.37	1.34	1.42	1.38
Cr_2O_3	-	-	-	-	-	-	-	-	0.04
Sum	97.92	97.45	98.06	97.92	98.32	97.65	97.27	97.58	97.28

Number of Ions on the Basis of 23(0)

	3C	3R	4I	4R	5g	1C	1R	2C	2R
Si	5.724	5.812	5.875	5.834	5.745	5.789	5.842	5.811	5.847
Al	2.276	2.188	2.125	2.166	2.255	2.211	2.158	2.189	2.153
Al	0.104	0.134	0.108	0.152	0.116	0.135	0.108	0.203	0.150
Ti	0.691	0.610	0.670	0.586	0.706	0.662	0.604	0.563	0.582
Fe	1.303	1.491	1.332	1.526	1.390	1.426	1.441	1.958	1.496
Mn	0.018	0.028	0.020	0.028	0.021	0.024	0.029	0.044	0.028
Mg	2.868	2.745	2.874	2.708	2.726	2.722	2.801	2.256	2.734
Ca	1.888	1.864	1.826	1.863	1.853	1.873	1.895	1.872	1.884
Na	0.782	0.816	0.780	0.851	0.799	0.809	0.833	0.791	0.813
K	0.261	0.274	0.239	0.264	0.260	0.261	0.257	0.276	0.265
Cr	-	-	-	-		-	-	-	
Z	8.000	8.000	8.000	8.000	8.000	8.000	8.000	8.000	8.000
Y	4.984	5.008	5.004	5.000	4.959	4.969	4.983	5.024	4.990
X	2.931	2.954	2.845	2.978	2.912	2.943	2.985	2.939	2.962
Sum	15.915	15.962	15.849	15.978	15.871	15.912	15.968	15.963	15.952
$\frac{100\ Fe}{Fe+Mg}$	31.2	35.2	31.7	36.0	33.8	34.3	34.0	46.5	35.3

Sample	1-85.35						1-88.55		
Grain	4C	4I	6	2	1I	1R	1C	1I	1R
SiO_2	40.3	39.3	38.0	35.8	36.7	36.6	37.8	37.8	38.3
Al_2O_3	10.1	10.8	13.2	12.9	12.2	12.6	13.9	13.4	12.9
TiO_2	3.45	3.58	4.82	5.57	5.09	5.27	6.23	5.75	5.26
FeO	9.16	9.26	10.2	11.7	11.7	11.9	10.4	11.8	12.1
MnO	0.21	0.19	0.12	0.18	0.19	0.18	0.16	0.17	0.23
MgO	9.88	9.85	13.0	12.2	12.3	12.4	12.7	11.9	12.0
CaO	21.9	21.9	11.9	11.8	11.6	11.7	11.9	11.8	11.7
Na_2O	0.98	0.97	2.96	2.87	2.90	3.08	2.63	2.67	2.78
K_2O	-	-	1.16	1.31	1.23	1.23	1.27	1.28	1.36
Sum	95.98	95.85	95.36	94.33	93.91	94.96	96.99	96.57	96.63

Number of Ions on the Basis of 23(0)

	4C	4I	6	2	1I	1R	1C	1I	1R
Si	6.153	6.021	5.790	5.594	5.744	5.683	5.666	5.732	5.810
Al	1.812	1.950	2.210	2.381	2.249	2.297	2.334	2.268	2.190
Al	-	-	0.164	-	-	-	0.115	0.124	0.116
Ti	0.396	0.413	0.552	0.655	0.600	0.615	0.703	0.656	0.601
Fe	1.171	1.188	1.301	1.524	1.534	1.539	1.307	1.494	1.532
Mn	0.027	0.025	0.015	0.024	0.026	0.024	0.021	0.022	0.029
Mg	2.252	2.251	2.950	2.843	2.874	2.873	2.849	2.682	2.712
Ca	3.589	3.597	1.938	1.975	1.943	1.939	1.909	1.923	1.905
Na	0.289	0.290	0.875	0.869	0.880	0.926	0.764	0.784	0.817
K	-	-	0.226	0.261	0.246	0.244	0.243	0.248	0.263
Z	7.965	7.971	8.000	7.975	7.993	7.980	8.000	8.000	8.000
Y	3.846	3.877	4.982	5.046	4.991	5.051	4.995	4.978	4.990
X	3.878	3.887	3.039	3.105	3.069	3.109	2.916	2.955	2.985
Sum	15.689	15.735	16.021	16.126	16.096	16.140	15.911	15.933	15.975
$\frac{100\ Fe}{Fe+Mg}$	34.2	34.5	30.6	43.6	44.1	44.2	31.4	35.8	36.1

TABLE 3 Continued

Sample 1-88.55 cont.

Grain	3	8C	8R	9	6C	6I	6R	2I	2I	7
SiO_2	37.8	38.0	37.9	36.8	38.1	38.2	38.3	38.4	38.6	37.9
Al_2O_3	13.8	13.8	13.5	14.9	14.0	14.3	13.2	13.5	13.0	13.5
TiO_2	6.50	5.98	5.95	7.05	6.23	6.24	5.48	5.46	5.23	5.66
FeO	10.8	10.9	11.0	11.4	11.4	11.5	12.8	12.2	13.4	13.0
MnO	0.17	0.15	0.15	0.15	0.13	0.11	0.19	0.17	0.23	0.24
MgO	12.4	12.4	12.6	11.5	11.6	11.6	11.4	11.9	11.1	11.4
CaO	11.5	11.6	11.8	11.6	11.9	11.8	11.4	11.6	11.5	11.2
Na_2O	2.64	2.59	2.67	2.43	2.41	2.43	2.70	2.79	2.75	2.88
K_2O	1.38	1.35	1.36	1.41	1.30	1.33	1.30	1.23	1.29	1.44
Sum	96.99	96.77	96.93	97.24	97.07	97.51	96.77	97.25	97.10	97.22

Number of Ions on the Basis of 23(0)

	3	8C	8R	9	6C	6I	6R	2I	2I	7
Si	5.674	5.717	5.701	5.535	5.724	5.701	5.808	5.783	5.855	5.733
Al	2.326	2.283	2.299	2.465	2.276	2.299	2.192	2.217	2.145	2.267
Al	0.121	0.158	0.099	0.166	0.206	0.225	0.168	0.176	0.174	0.147
Ti	0.734	0.677	0.674	0.797	0.703	0.701	0.625	0.618	0.596	0.645
Fe	1.361	1.376	1.383	1.434	1.431	1.438	1.621	1.539	1.694	1.645
Mn	0.021	0.019	0.019	0.019	0.017	0.015	0.025	0.022	0.030	0.030
Mg	2.771	2.780	2.827	2.573	2.587	2.591	2.577	2.659	2.499	2.574
Ca	1.845	1.867	1.903	1.873	1.914	1.887	1.850	1.863	1.869	1.814
Na	0.767	0.757	0.779	0.707	0.702	0.705	0.795	0.815	0.808	0.845
K	0.265	0.260	0.261	0.271	0.249	0.254	0.250	0.236	0.249	0.278
Z	8.000	8.000	8.000	8.000	8.000	8.000	8.000	8.000	8.000	8.000
Y	5.008	5.010	5.002	4.989	4.944	4.970	5.016	5.014	4.993	5.041
X	2.877	2.884	2.943	2.851	2.865	2.846	2.895	2.914	2.926	2.937
Sum	15.885	15.894	15.945	15.840	15.809	15.816	15.911	15.928	15.919	15.978

100 Fe

$\frac{Fe}{Fe + Mg}$	32.9	33.1	32.9	35.8	35.6	35.7	38.6	36.7	40.4	39.0

	Sample 1-88.55 cont.		1-131.36						2-39.28	
Grain	10C	10R	1C	1I	1I	1R	1R	2	2	1
SiO_2	37.6	37.5	38.5	39.3	39.1	38.8	38.8	38.8	39.6	39.1
Al_2O_3	14.1	14.1	12.8	12.6	12.8	12.9	12.8	13.4	12.7	12.7
TiO_2	5.88	5.81	5.31	5.40	5.29	5.33	5.29	5.56	5.81	5.61
FeO	13.0	13.7	11.2	11.3	12.6	12.7	12.8	11.4	9.79	10.2
MnO	0.22	0.26	0.21	0.20	0.22	0.24	0.24	0.20	0.13	0.16
MgO	11.1	10.6	12.9	12.5	11.8	11.6	11.8	12.4	13.6	13.5
CaO	11.4	11.4	11.6	11.5	11.4	11.6	11.6	11.6	11.6	11.4
Na_2O	2.72	2.69	2.94	2.82	2.84	2.86	2.83	2.86	2.90	2.78
K_2O	1.23	1.35	1.07	1.07	1.01	1.01	1.01	1.05	1.29	1.38
Sum	97.25	97.41	96.53	96.69	97.06	97.04	97.17	97.27	97.42	96.83

Number of Ions on the Basis of 23(0)

	10C	10R	1C	1I	1I	1R	1R	2	2	1
Si	5.685	5.684	5.819	5.909	5.892	5.863	5.851	5.808	5.874	5.853
Al	2.315	2.316	2.181	2.091	2.108	2.137	2.149	2.192	2.126	2.147
Al	0.197	0.200	0.091	0.140	0.162	0.151	0.130	0.172	0.097	0.098
Ti	0.668	0.662	0.603	0.611	0.600	0.605	0.600	0.626	0.648	0.631
Fe	1.640	1.731	1.410	1.424	1.593	1.602	1.614	1.422	1.213	1.273
Mn	0.028	0.033	0.027	0.025	0.028	0.030	0 031	0.025	0.016	0.021
Mg	2.492	2.400	2.894	2.794	2.643	2.610	2.657	2.774	3.007	3.003
Ca	1.850	1.844	1.884	1.858	1.835	1.876	1.867	1.852	1.847	1.833
Na	0.796	0.790	0.861	0.822	0.829	0.836	0.826	0.828	0.832	0.806
K	0.238	0.262	0.206	0.206	0.195	0.195	0.195	0.200	0.244	0.263
Z	8.000	8.000	8.000	8.000	8.000	8.000	8.000	8.000	8.000	8.000
Y	5.025	5.026	5.025	4.994	5.026	4.998	5.032	5.019	4.981	5.026
X	2.884	2.896	2.951	2.886	2.859	2.907	2.888	2.880	2.923	2.902
Sum	15.909	15.922	15.976	15.880	15.885	15.905	15.920	15.899	15.904	15.928

100 Fe

$\frac{Fe}{Fe + Mg}$	39.7	41.9	32.8	33.8	37.6	38.0	37.8	33.9	28.7	29.8

- 16 -

TABLE 3 continued

Sample 2-62.41

Grain	6	8	10C	10R	7	11-g	5	23	2	1
SiO_2	38.7	38.6	38.2	38.8	37.8	39.0	38.1	38.6	40.2	40.2
Al_2O_3	13.0	14.3	13.6	13.2	13.2	12.4	13.9	12.9	13.2	13.2
TiO_2	6.39	6.65	6.64	6.37	6.83	5.86	6.32	5.96	3.85	4.00
FeO	9.24	9.33	10.0	9.51	10.4	10.6	10.8	11.1	12.9	13.6
MnO	0.12	0.11	0.12	0.14	0.13	0.19	0.14	0.19	0.28	0.36
MgO	13.65	13.2	12.9	13.3	13.0	12.95	12.2	12.7	11.7	11.1
CaO	12.2	12.1	12.3	12.0	11.9	11.9	12.1	12.0	11.6	11.5
Na_2O	2.46	2.31	2.17	2.57	2.61	2.74	2.37	2.70	3.22	3.16
K_2O	1.38	1.52	1.66	1.38	1.24	1.24	1.46	1.27	0.97	0.98
Cr_2O_3	0.17	-	-	0.13	-	-	-	-	0.08	0.09
Sum	97.31	98.12	97.59	97.40	97.11	96.88.	97.39	97.42	98.00	98.19

Number of Ions on the Basis of 23(0)

	6	8	10C	10R	7	11-g	5	23	2	1
Si	5.734	5.662	5.685	5.765	5.653	5.845	5.679	5.780	5.996	5.994
Al	2.266	2.338	2.315	2.235	2.322	2.155	2.231	2.220	2.004	2.006
Al	0.011	0.142	0.075	0.071	-	0.045	0.116	0.048	0.312	0.316
Ti	0.712	0.734	0.744	0.712	0.768	0.661	0.708	0.671	0.432	0.449
Fe	1.144	1.146	1.249	1.181	1.298	1.334	1.350	1.394	1.612	1.704
Mn	0.015	0.013	0.015	0.018	0.017	0.024	0.018	0.024	0.036	0.046
Mg	3.014	2.893	2.855	2.949	2.886	2.896	2.715	2.838	2.595	2.480
Ca	1.937	1.896	1.965	1.916	1.903	1.919	1.937	1.927	1.856	1.835
Na	0.707	0.658	0.626	0.740	0.756	0.795	0.684	0.784	0.930	0.915
K	0.261	0.284	0.316	0.261	0.237	0.237	0.278	0.242	0.184	0.187
Cr	0.020	-	-	0.015	-	-	-	-	0.009	0.011
Z	8.000	8.000	8.000	8.000	7.975	8.000	8.000	8.000	8.000	8.000
Y	4.916	4.928	4.938	4.946	4.946	4.960	4.907	4.975	4.996	5.006
X	2.905	2.838	2.907	2.917	2.896	2.951	2.899	2.953	2.970	2.937
Sum	15.821	15.766	15.845	15.863	15.840	15.911	15.806	15.928	15.966	15.943
$\frac{100\ Fe}{Fe + Mg}$	27.5	28.4	30.4	28.6	31.0	31.5	33.2	32.9	38.3	40.7

Sample	2-62.41			2-70.41					
Grain	9C	9R	21	1	10-i	4	3	2C	2R
SiO_2	38.6	39.0	38.3	38.3	38.2	38.2	38.5	38.4	38.7
Al_2O_3	14.1	13.5	11.7	14.0	14.3	14.3	13.8	13.2	13.5
TiO_2	6.20	5.78	4.98	6.52	6.49	6.36	6.24	6.05	6.41
FeO	14.1	11.1	17.8	10.7	10.8	11.8	11.9	15.0	12.9
MnO	0.29	0.21	0.57	0.14	0.13	0.17	0.16	0.38	0.26
MgO	10.3	12.6	8.53	12.1	12.1	11.5	11.4	9.38	10.8
CaO	11 7	11.8	11.2	12.3	12.2	12.0	12.1	11.5	11.5
Na_2O	2.68	2.72	2.93	2.35	2.32	2.52	2.63	2.71	2.81
K_2O	1.09	1.28	1.47	1.54	1.57	1.38	1.45	1.17	0.99
Sum	99.06	97.99	97.48	97.95	98.11	98.23	98.18	97.79	97.87

Number of Ions on the Basis of 23(0)

	9C	9R	21	1	10-i	4	3	2C	2R
Si	5.724	5.796	5.968	5.694	5.676	5.679	5.741	5.819	5.789
Al	2.276	2.204	2.032	2.306	2.324	2.321	2.259	2.181	2.211
Al	0.188	0.153	0.088	0.146	0.172	0.191	0.161	0.176	0.172
Ti	0.691	0.646	0.575	0.729	0.724	0.711	0.701	0.690	0.720
Fe	1.745	1.384	2.289	1.331	1.342	1.464	1.486	1.897	1.610
Mn	0.036	0.027	0.075	0.018	0.017	0.022	0.021	0.049	0.033
Mg	2.272	2.783	1.953	2.680	2.675	2.553	2.529	2.120	2.417
Ca	1.856	1.874	1.837	1.961	1.939	1.918	1.933	1.869	1.847
Na	0.771	0.782	0.873	0.676	0.668	0.728	0.761	0.797	0.815
K	0.207	0.243	0.288	0.292	0.297	0.261	0.276	0.226	0.189
Z	8.000	8.000	8.000	8.000	8.000	8.000	8.000	8.000	8.000
Y	4.932	4.993	4.980	4.904	4.930	4.941	4.898	4.932	4.952
X	2.834	2.899	2.998	2.929	2.904	2.907	2.970	2.892	2.851
Sum	15.766	15.892	15.978	15.833	15.834	15.848	15.868	15.824	15.803
$\frac{100\ Fe}{Fe + Mg}$	43.4	33.2	54.0	33.2	33.4	36.4	37.0	47.2	40.0

TABLE 4

Electron Microprobe Analyses of Rhönite from DVDP 1 and 2 Core Samples

Sample	1-121.88			2-99.34			2-103.15			
Grain	2	3	1	1	4	2	2	3	1	1
SiO_2	23.6	23.8	23.4	23.7	23.6	23.8	23.2	23.7	23.4	23.6
Al_2O_3	16.6	17.0	17.1	16.8	16.7	17.1	17.4	17.4	17.2	17.45
TiO_2	11.4	11.6	12.1	11.9	11.9	12.2	12.0	11.7	11.8	11.7
FeO	20.8	21.3	21.5	21.0	21.0	21.4	20.9	20.9	21.5	21.9
MnO	0.15	0.19	0.12	0.16	0.16	0.18	0.18	0.17	0.20	0.20
MgO	13.4	12.7	13.1	13.05	13.1	12.4	12.7	12.45	12.3	12.2
CaO	11.8	11.8	12.0	12.05	12.3	12.4	12.2	12.3	12.3	12.1
Na_2O	1.00	0.96	0.90	0.97	0.92	0.88	0.89	0.91	0.89	0.96
Cr_2O_3	0.05	-	-	0.06	0 13	0.05	0.15	0.19	0.17	0.08
NiO	0.07	0.10	0.04	0.04	0.06	-	0.03	0.06	0.07	0.06
Sum	98.87	99.45	100.26	99.73	99.87	100.41	99.65	99.78	99.83	100.25

Number of Ions on the Basis of 40(0)

Si	6.514	6.536	6.385	6.489	6.460	6.480	6.360	6.481	6.422	6.450
Al	5.400	5.464	5.499	5.421	5.388	5.487	5.622	5.519	5.564	5.550
Al	-	0.038	-	-	-	-	-	0.089	-	0.071
Ti	2.366	2.396	2.483	2.450	2.450	2.498	2.474	2.406	2.436	2.405
Fe	4.801	4.892	4.906	4.808	4.808	4.873	4.792	4.780	4.935	5.006
Mn	0.035	0.044	0.028	0.037	0.037	0.042	0.042	0.039	0.047	0.046
Mg	5.514	5.199	5.329	5.326	5.346	5.033	5.190	5.075	5.033	4.971
Ca	3.490	3.472	3.508	3.535	3.608	3.617	3.583	3.604	3.617	3.543
Na	0.535	0.511	0.476	0.515	0.488	0.465	0.473	0.483	0.474	0.509
Cr	0.011	-	-	0.013	0.028	0.011	0.033	0.041	0.037	0.017
Ni	0.016	0.022	0.009	0.009	0.013	-	0.007	0.013	0.016	0.013
Z	11.914	12.000	11.884	11.910	11.848	11.967	11.982	12.000	11.986	12.000
Y	12.743	12.591	12.755	12.643	12.682	12.457	12.538	12.443	12.504	12.529
X	4.025	3.983	3.984	4.050	4.096	4.082	4.056	4.087	4.091	4.052
Sum	28.682	28.574	28.623	28.603	28.626	28.506	28.576	28.530	28.581	28.581

TABLE 5

Electron Microprobe Analyses of Spinels in DVDP 1 and 2 Core Samples

Sample	1-57.94			1-88.55	1-121.88				
Grain	1C	1R	2	2	3C	3R	6-i	7-i	2
SiO_2	0.12	0.12	0.14	0.04	0.11	-	0.11	0.08	-
TiO_2	0.66	14.9	19.1	17.5	2.21	15.6	6.01	8.03	22.2
Al_2O_3	15.1	3.14	2.40	1.79	28.1	11.2	28.3	22.9	5.13
Cr_2O_3	45.6	5.64	n.d.	n.d.	29.3	11.2	9.14	8.35	5.39
FeO	30.5	68.3	71.0	73.8	30.0	52.9	42.3	47.6	59.4
MnO	1.01	1.36	1.47	1.49	0.51	0.65	0.29	0.32	0.74
MgO	5.69	2.33	2.09	1.22	9.21	6.11	11.6	9.64	5.02
CaO	-	-	0.17	0.06	-	0.05	-	-	-
NiO	n.d.	n.d.	n.d.	n.d.	0.10	0.04	0.21	0.22	0.06
Sum	98.68	95.79	96.37	95.90	99.54	97.75	97.96	97.14	97.94
Fe_2O_3	5.96	31.0	29.7	33.2	6.83	17.3	20.8	22.6	17.1
FeO	25.2	40.4	44.2	44.0	23.9	37.4	23.5	27.2	44.0
Total	99.34	98.89	99.27	99.30	100.27	99.55	99.96	99.34	99.64

Number of Ions on the Basis of 32(0)

	1C	1R	2	2	3C	3R	6-i	7-i	2
Si	0.032	0.036	0.041	0.012	0.027	-	0.027	0.020	-
Ti	0.133	3.311	4.245	3.936	0.409	3.206	1.104	1.537	4.723
Al	4.780	1.094	0.836	0.631	8.158	3.607	8.149	6.871	1.710
Cr	9.683	1.318	-	-	5.706	2.420	1.766	1.681	1.206
Fe^{3+}	1.205	6.893	6.605	7.473	1.266	3.558	3.824	4.330	3.641
Fe^{2+}	5.660	9.984	10.924	11.007	4.924	8.548	4.802	5.791	10.410
Mn	0.230	0.340	0.368	0.378	0.106	0.150	0.060	0.069	0.177
Mg	2.278	1.026	0.921	0.544	3.382	2.489	4.225	3.658	2.117
Ca	-	-	0.054	0.019	-	0.015	-	-	-
Ni	-	-	-	-	0.020	0.009	0.041	0.045	0.014
Usp%*	-	43.6	52.2	48.2	-	-	-	-	66.2

Recalculated Spinel End Members

	1C	1R	2	2	3C	3R	6-i	7-i	2
Usp	2.1	41.8	53.5	50.2	5.4	40.0	14.1	19.4	59.0
Ch	28.5	8.2	-	-	35.7	15.2	11.0	10.5	7.5
Sp	-	4.6	5.2	4.0	6.9	16.2	42.3	35.8	10.7
Hc	29.9	2.2	-	-	44.1	6.4	8.6	7.2	-
Mf	-	-	7.0	3.1	-	-	-	-	8.5
Mt	7.5	43.1	34.3	42.7	7.9	22.1	23.9	27.1	14.3
Pc	32.0	-	-	-	-	-	-	-	-

Usp	-Ulvospinel	$2FeO \cdot TiO_2$	Mf-Magnesioferrite	$MgO \cdot Fe_2O_3$
Ch	-Chromite	$MgO \cdot Cr_2O_3$	Mt-Magnetite	$FeO \cdot Fe_2O_3$
Sp	-Spinel	$MgO \cdot Al_2O_3$	Pc-Picrochromite	$FeO \cdot Cr_2O_3$
Hc	-Hercynite	$FeO \cdot Al_2O_3$		

* Calculated by method of Carmichael (1967)

TABLE 5 continued

Sample	1-121-88 cont.			1-131.36	1-187.64				
Grain	4	1C	1R	1	6-i	5-i	2	4	3C
SiO_2	0.05	0.06	0.05	0.12	0.07	0.09	0.10	0.09	0.17
TiO_2	23.3	18.4	18.5	20.0	3.34	3.24	3.54	3.25	3.51
Al_2O_3	4.49	4.96	6.27	2.34	22.95	23.0	25.8	23.45	23.5
Cr_2O_3	4.97	-	-	n.d.	31.8	31.15	27.8	31.2	31.2
FeO	59.7	69.5	67.9	69.9	28.3	28.7	28.8	29.2	29.3
MnO	0.71	0.57	0.60	1.42	0.29	0.30	0.28	0.26	0.34
MgO	5.11	3.96	3.14	2.39	13.3	13.3	13.9	13.0	13.1
CaO	-	-	-	0.12	-	-	-	-	0.03
Ni O	0.06	-	-	n.d.	0.18	0.18	0.20	0.15	0.17
Sum	98.39	97.45	96.46	96.29	100.23	99.96	100.42	100.60	101.32
Fe_2O_3	16.3	30.0	27.0	28.0	11.1	11.8	11.9	11.4	11.2
FeO	45.0	42.5	43.6	44.7	18.3	18.1	18.1	18.9	19.2
Total	99.99	100.45	99.16	99.09	101.33	101.16	101.62	101.70	102.42

Number of Ions on the Basis of 32(O)

Si	0.014	0.017	0.014	0.035	0.017	0.022	0.024	0.022	0.041
Ti	4.950	3.941	4.006	4.442	0.611	0.594	0.637	0.593	0.636
Al	1.495	1.665	2.128	0.815	6.582	6.604	7.273	6.704	6.671
Cr_{3+}	1.110	-	-	-	6.118	6.001	5.257	5.984	5.942
Fe^{3+}	3.465	6.430	5.850	6.224	2.033	2.164	2.142	2.081	2.030
Fe^{2+}	10.631	10.123	10.499	11.042	3.724	3.688	3.620	3.834	3.868
Mn	0.170	0.138	0.146	0.355	0.060	0.062	0.057	0.053	0.069
Mg	2.152	1.681	1.348	1.052	4.825	4.831	4.956	4.701	4.704
Ca	-	-	-	0.038	-	-	-	-	0.008
Ni	0.014	-	-	-	0.035	0.035	0.038	0.029	0.033
Usp%	68.7	48.7	52.7	54.7	-	-	-	-	-

Recalculated Spinel End-Members

Usp	62.1	49.4	50.3	56.0	7.9	7.7	8.3	7.7	8.4
Ch	6.9	-	-	-	38.2	37.5	32.9	37.4	37.2
Sp	9.3	10.4	13.3	5.1	22.3	23.4	29.4	21.7	22.1
Hc	-	-	-	-	18.8	17.9	16.0	20.2	19.6
Mf	10.8	10.7	3.5	8.6	-	-	-	-	-
Mt	10.9	29.5	32.9	30.3	12.8	13.5	13.4	13.0	12.7

TABLE 5 continued

| Sample | 1-187.64 cont. | | | 2-39.28 | 2-54.72 | | | | |
Grain	3R	1	1	1	1	1	11-g	6-a	12-g
SiO_2	0.09	0.13	0.11	0.10	0.10	0.09	0.12	0.24	0.14
TiO_2	25.0	13.35	13.7	16.9	26.5	26.9	21.9	21.5	21.9
Al_2O_3	5.52	16.65	16.5	8.02	2.37	2.28	2.80	2.05	2.48
Cr_2O_3	2.08	3.62	3.63	n.d.	n.d.	n.d.	n.d.	n.d.	n.d.
FeO	59.7	52.9	52.9	66.2	64.0	64.1	68.6	68.8	69.2
MnO	0.63	0.27	0.31	0.90	1.47	1.47	1.43	1.29	1.50
MgO	4.07	10.5	10.4	4.82	3.67	3.54	2.03	1.36	1.57
CaO	0.10	-	-	-	-	0.07	0.07	0.30	0.08
NiO	0.06	0.23	0.17	n.d.	n.d.	n.d.	n.d.	n.d.	n.d.
Sum	97.25	97.65	97.72	96.94	98.11	98.45	96.95	95.54	98.87
Fe_2O_3	13.2	25.4	25.0	29.2	16.6	16.1	23.8	23.9	23.7
FeO	47.9	30.05	30.4	39.9	49.0	49.6	47.2	47.3	47.8
Total	98.65	100.20	100.22	99.84	99.71	100.05	99.35	97.94	99.17

Number of Ions on the Basis of 32(0)

Si	0.026	0.034	0.028	0.028	0.029	0.026	0.035	0.072	0.042
Ti	5.385	2.592	2.662	3.565	5.762	5.836	4.845	4.862	4.878
Al	1.863	5.067	5.025	2.652	0.808	0.775	0.971	0.726	0.866
Cr	0.471	0.739	0.742	-	-	-	-	-	-
Fe^{3+}	2.845	4.935	4.861	6.164	3.612	3.495	5.269	5.408	5.283
Fe^{2+}	11.474	6.489	6.569	9.361	11.848	11.967	11.612	11.895	11.842
Mn	0.153	0.059	0.068	0.214	0.360	0.359	0.356	0.329	0.376
Mg	1.738	4.042	4.006	2.016	1.582	1.522	0.890	0.610	0.693
Ca	0.031	-	-	-	-	0.022	0.022	0.097	0.025
Ni	0.014	0.048	0.035	-	-	-	-	-	-
Usp%	75.8	18.5	20.5	44.6	72.8	73.8	61.7	62.1	62.3

Recalculated Spinel End-members

Usp	67.7	32.8	33.5	44.9	72.4	73.3	61.0	61.7	61.5
Ch	2.9	4.6	4.6	-	-	-	-	-	-
Sp	11.6	31.7	31.5	16.6	5.0	4.8	6.1	4.5	5.4
Hc	-	-	-	-	-	-	-	-	-
Mf	7.7	14.7	14.5	8.6	14.7	14.5	5.3	4.3	3.5
Mt	10.1	16.2	15.9	29.9	7.8	7.4	27.6	29.5	29.5

TABLE 5 continued

Sample	2-62.41					2-70.41		
Grain	15C	15R	10	7	5	4	5	1
SiO_2	0.07	0.12	0.14	0.11	0.10	0.13	0.12	0.12
TiO_2	2.07	15.8	18.0	17.5	17.8	18.45	16.5	16.6
Al_2O_3	49.15	11.7	10.7	10.1	7.58	7.17	7.71	7.22
Cr_2O_3	-	-	0.13	0.07	0.04	0.08	-	-
FeO	33.9	61.9	60.4	61.3	63.3	65.3	66.1	66.4
MnO	0.26	0.45	0.35	0.32	0.54	0.71	0.66	0.62
MgO	13.4	6.95	8.26	8.34	6.43	5.66	6.00	5.80
CaO	-	0.03	-	-	-	-	0.03	0.03
NiO	-	-	-	0.04	-	n.d.	n.d.	n.d.
Sum	98.85	96.95	97.98	97.78	95.79	97.50	97.12	96.79
Fe_2O_3	14.4	28.0	26.1	27.8	27.9	27.8	31.1	31.25
FeO	20.7	36.7	37.0	36.25	38.2	40.3	38.1	38.3
Total	100.05	99.75	100.68	100.53	98.59	100.30	100.22	99.94

Number of Ions on the Basis of 32(O)

Si	0.016	0.033	0.038	0.030	0.028	0.036	0.033	0.034
Ti	0.346	3.229	3.627	3.542	3.761	3.864	3.447	3.489
Al	12.881	3.747	3.379	3.203	2.510	2.353	2.524	2.379
Cr	-	-	0.028	0.015	0.009	0.018	-	-
Fe^{3+}	2.410	5.726	5.262	5.630	5.898	5.826	6.502	6.574
Fe^{2+}	3.850	8.340	8.296	8.158	8.975	9.386	8.852	8.953
Mn	0.049	0.104	0.079	0.073	0.128	0.168	0.155	0.147
Mg	4.442	2.816	3.299	3.346	2.693	2.350	2.485	2.417
Ca	-	0.009	-	-	-	-	0.009	0.009
Ni	-	-	-	0.009	-	-	-	-
Usp%	-	38.7	42.9	39.8	44.6	47.6	41.2	40.5

Recalculated Spinel End-members

Usp	4.5	40.8	45.8	44.7	47.0	48.8	43.6	44.0
Ch	-	-	0.2	0.1	0.1	0.1	-	-
Sp	55.9	23.5	21.2	20.0	15.7	14.7	15.8	14.9
Hc	24.4	-	-	-	-	-	-	-
Mf	-	11.8	19.9	21.8	17.9	14.6	15.4	15.4
Mt	15.2	23.9	13.0	13.4	19.3	21.8	25.2	25.7

TABLE 5 continued

Sample	2-70.41 cont.		2-99.34					
Grain	3	7	3	12	10-i	2	11-i	1
SiO_2	0.16	0.08	0.14	0.12	0.17	0.09	0.59	0.10
TiO_2	20.2	16.8	1.62	1.42	3.36	18.3	14.5	24.0
Al_2O_3	3.70	5.89	32.6	29.5	41.7	7.43	11.7	3.67
Cr_2O_3	0.07	-	29.6	31.6	5.35	10.9	3.50	3.44
FeO	66.6	68.2	20.2	22.0	31.6	52.3	57.0	60.8
MnO	1.26	0.63	0.29	0.26	0.21	0.68	0.32	0.69
MgO	4.67	5.18	15.5	15.1	15.1	5.90	8.54	4.90
CaO	0.06	0.03	-	-	0.03	0.06	-	0.04
NiO	n.d.	n.d.	0.21	0.13	0.24	0.05	0.17	0.04
Sum	96.72	96.81	100.16	100.13	97.76	95.71	96.32	97.68
Fe_2O_3	27.4	32.3	6.05	7.9	15.3	14.9	26.15	16.8
FeO	42.0	39.2	14.8	14.8	17.8	38.9	33.5	45.7
Total	99.52	100.11	100.81	100.83	99.26	97.21	98.97	99.38

Number of Ions on the Basis of 32(0)

Si	0.046	0.023	0.032	0.028	0.039	0.026	0.159	0.029
Ti	4.361	3.566	0.282	0.251	0.575	3.911	2.945	5.156
Al	1.252	1.959	8.898	8.173	11.191	2.489	3.724	1.236
Cr	0.016	-	5.420	5.873	0.963	2.449	0.747	0.777
Fe^{3+}	5.919	6.861	1.054	1.397	2.622	3.187	5.314	3.612
Fe^{2+}	10.083	9.253	2.866	2.909	3.390	9.246	7.566	10.919
Mn	0.306	0.151	0.057	0.052	0.040	0.164	0.073	0.167
Mg	1.999	2.180	5.351	5.291	5.126	2.500	3.438	2.087
Ca	0.018	0.009	-	-	0.007	0.018	-	0.012
Ni	-	-	0.039	0.025	0.044	0.011	0.037	0.009
Usp%	52.4	41.3	-	-	-	62.0	33.4	69.1

Recalculated Spinel End-members

Usp	55.1	44.8	3.9	3.5	7.7	49.2	38.8	64.8
Ch	0.1	-	33.9	36.7	6.0	15.3	4.7	4.8
Sp	7.8	12.2	33.6	29.7	58.7	15.5	23.3	7.7
Hc	-	-	22.0	21.3	11.1	-	-	-
Mf	17.3	15.1	-	-	-	0.8	15.5	13.8
Mt	19.6	27.8	6.6	8.8	16.4	19.1	17.7	8.8

TABLE 5 continued

Sample	2-103.15		
Grain	10-i	3	5-i
SiO_2	0.11	0.12	0.12
TiO_2	4.11	21.3	15.2
Al_2O_3	32.3	4.25	10.7
Cr_2O_3	10.6	5.14	0.83
FeO	38.1	58.7	63.0
MnO	0.28	0.68	0.34
MgO	12.6	5.85	6.25
CaO	0.06	0.06	0.04
NiO	0.19	0.10	0.08
Sum	98.35	96.20	96.56
Fe_2O_3	19.0	19.2	29.0
FeO	21.0	41.4	36.9
Total	100.25	98.1	99.46

Number of Ions on the Basis of 32(0)

Si	0.026	0.034	0.033
Ti	0.736	4.592	3.145
Al	9.069	1.436	3.470
Cr	1.997	1.165	6.004
Fe^{3+}	3.406	4.142	0.181
Fe^{2+}	4.184	9.926	8.490
Mn	0.056	0.165	0.079
Mg	4.475	2.500	2.564
Ca	0.015	0.018	0.012
Ni	0.036	0.023	0.018
Usp%	-	61.3	38.0

Recalculated Spinel End-members

Usp	9.6	57.8	39.7
Ch	12.5	7.3	1.1
Sp	44.0	9.0	21.7
Hc	12.6	-	-
Mf	-	15.5	9.6
Mt	21.3	10.4	27.9

TABLE 6

Electron Microprobe Analyses of Ilmenite in DVDP 1 and 2 Core Samples

Sample	1-121.88		2-54.72		2-62.41		
Grain	2	1	2	1	1	2	6
SiO_2	-	0.06	0.04	-	-	-	-
Al_2O_3	0.10	0.12	0.38	0.38	0.38	0.35	1.01
TiO_2	51.8	53.1	50.3	50.4	50.8	50.5	47.3
FeO	38.2	38.5	42.6	42.9	40.1	40.5	44.1
MnO	0.80	0.71	1.34	1.34.	0.84	1.12	0.45
MgO	7.01	7.07	4.96	4.95	7.19	6.63	6.47
CaO	0.17	0.12	-	-	-	0.06	-
Cr_2O_3	0.23	0.24	n.d.	n.d.	0.04	0.03	-
NiO	0.03	-	n.d.	n.d.	0.03	-	-
Sum	98.34	99.92	99.62	99.97	99.38	99.19	99.33
Fe_2O_3	5.71	4.60	8.41	8.69	8.94	9.01	15.0
FeO	33.1	34.3	35.1	35.1	32.1	32.4	30.6
Total	98.95	100.32	100.53	100.86	100.32	100.10	100.83
Mole%							
$FeTiO_3$	67.0	68.6	71.1	71.0	64.1	65.1	61.1
$RTiO_3$	27.4	26.9	20.7	20.6	27.3	26.2	24.0
R_2O_3	5.6	4.5	8.2	8.4	8.6	8.7	14.9
Hm%*	7.7	6.2	10.3	10.6	11.8	11.8	19.6

Sample	2-70.41			2-99.34	2-103.15
Grain	2	3	1	1	1
SiO_2	-	0.07	-	0.12	0.14
Al_2O_3	1.04	0.74	0.90	0.19	0.10
TiO_2	47.9	47.9	46.6	51.9	51.1
FeO	41.6	43.7	44.0	39.5	41.6
MnO	0.42	0.72	0.44	0.72	0.69
MgO	7.39	5.96	6.29	5.98	4.91
CaO	0.06	0.04	0.05	0.17	0.14
Cr_2O_3	-	-	-	-	-
NiO	n.d.	n.d.	n.d.	-	-
Sum	98.41	99.13	98.28	98.58	98.68
Fe_2O_3	13.5	13.35	15.4	4.79	5.70
FeO	29.4	31.7	30.2	35.2	36.5
Total	99.71	100.48	99.88	99.07	99.28
Mole%					
$FeTiO_3$	58.9	63.8	61.1	71.7	74.8
$RTiO_3$	27.4	23.0	23.7	23.6	19.8
R_2O_3	13.5	13.2	15.2	4.7	5.4
Hm%*	18.6	17.1	19.9	6.1	6.7

*Calculated by method of Carmichael (1967)

- 25 -

TABLE 7

Electron Microprobe Analyses of Feldspars in DVDP 1 and 2 Core Samples

Sample	1-57.94		1-131.36	2-54.72			2-103.15	
Grain	1	2	1-a	3-a	1	2	1	3
SiO_2	57.8	59.4	57.9	56.5	57.5	56.7	50.4	51.7
Al_2O_3	26.0	24.6	25.3	26.7	26.9	26.9	30.9	29.9
TiO_2	0.11	0.15	0.19	0.22	0.15	0.13	0.28	0.28
FeO	0.41	0.48	0.47	0.60	0.50	0.60	0.73	0.53
MgO	0.03	-	0.03	0.04	0.04	0.29	0.03	0.05
CaO	8.27	6.59	7.96	9.58	8.79	9.48	14.6	12.3
Na_2O	6.61	7.36	6.88	5.74	5.75	5.90	3.14	4.21
K_2O	0.64	0.68	0.76	0.51	0.71	0.54	0.18	0.24
Sum	99.87	99.26	99.49	99.89	100.34	100.54	100.26	99.21

Number of Ions on the Basis of 32(O)

Si	10.407	10.699	10.471	10.199	10.299	10.177	9.200	9.469
Al	5.510	5.230	5.394	5.680	5.676	5.690	6.650	6.464
Ti	0.015	0.021	0.026	0.030	0.020	0.017	0.039	0.039
Fe	0.061	0.072	0.071	0.091	0.074	0.091	0.111	0.081
Mg	0.008	-	0.007	0.011	0.009	0.078	0.009	0.013
Ca	1.594	1.273	1.542	1.853	1.686	1.821	2.853	2.416
Na	2.307	2.571	2.412	2.008	1.996	2.052	1.110	1.497
K	0.147	0.157	0.176	0.118	0.163	0.123	0.042	0.056
Z	15.917	15.929	15.865	15.879	15.975	15.867	15.850	15.933
X	4.132	4.094	4.234	4.111	3.948	4.182	4.164	4.102
Sum	20.049	20.023	20.099	19.990	19.923	20.049	20.014	20.035
An	39.4	31.8	37.3	46.6	43.9	45.6	71.2	60.9
Ab	57.0	64.3	58.4	50.5	51.9	51.3	27.7	37.7
Or	3.6	3.9	4.3	2.9	4.2	3.1	1.1	1.4

TABLE 8

Electron Microprobe Analyses of Apatite in DVDP 1 and 2 Core Samples

Sample	2-54.72	2-62.41		2-70.41	
Grain	1	1-i	2	2-i	1
SiO_2	0.36	0.36	0.29	0.50	0.28
Al_2O_3	-	0.04	-	0.03	0.03
TiO_2	-	-	-	0.05	-
FeO	0.18	0.39	0.26	0.40	0.25
MnO	0.07	0.03	0.04	0.05	-
MgO	0.17	0.47	0.36	0.38	0.36
CaO	50.9	51.2	51.6	51.4	51.7
Na_2O	0.15	0.16	0.15	0.12	0.16
K_2O	-	-	-	-	-
P_2O_5	43.3	43.3	43.6	42.5	43.7
Total	95.13	95.95	96.30	95.43	96.48

APPENDIX B continued

Part 3.   Mt Erebus

Electron microprobe analyses of glass and minerals in recent volcanic ejecta from Mt Erebus, Ross Island, Antarctica.

Data to accompany paper;

"Mineralogy and Glass Chemistry of Recent Volcanic Ejecta from Mt Erebus, Ross Island, Antarctica"

Table 1. Electron microprobe analyses of olivine

Sample	25726			25725			25724		
Grain	3	1	2	2	1-C	1-R	2	1	4
SiO_2	34.0	34.1	33.8	34.1	33.9	33.7	35.2	34.6	34.7
Al_2O_3	–	–	–	0.02	–	–	–	–	0.03
TiO_2	0.03	0.03	0.05	0.10	0.04	0.04	0.03	0.05	0.02
FeO*	37.9	38.1	38.1	37.35	38.3	38.1	38.5	38.6	38.6
MnO	2.38	2.44	2.31	2.28	2.37	2.36	2.57	2.52	2.51
MgO	24.3	24.0	24.4	23.7	23.7	23.9	23.1	23.6	23.0
CaO	0.51	0.48	0.44	0.53	0.48	0.49	0.49	0.50	0.53
Na_2O	–	–	–	0.03	0.03	–	–	0.03	0.03
Sum	99.12	99.15	99.10	98.11	98.82	98.59	99.89	99.90	99.42

Number of cations on the basis of 4 (O)

Si	0.980	0.985	0.978	0.993	0.984	0.981	1.008	0.994	1.000
Al	–	–	–	0.001	–	–	–	–	0.001
Ti	0.001	0.001	0.001	0.002	0.001	0.001	0.001	0.001	0.001
Fe	0.915	0.921	0.920	0.908	0.930	0.926	0.921	0.925	0.930
Mn	0.058	0.060	0.057	0.056	0.058	0.058	0.062	0.061	0.061
Mg	1.048	1.032	1.050	1.026	1.025	1.036	0.984	1.007	0.990
Ca	0.016	0.015	0.014	0.017	0.015	0.015	0.015	0.015	0.016
Na	–	–	–	0.002	0.002	–	–	0.002	0.002
Z	0.980	0.985	0.978	0.993	0.984	0.981	1.008	0.994	1.000
X	2.038	2.029	2.042	2.012	2.031	2.036	1.983	2.011	2.001
Sum	3.018	3.014	3.020	3.005	3.015	3.017	2.991	3.005	3.001
Fe	45.3	45.7	45.4	45.6	46.2	45.8	46.8	46.4	46.9
Mn	2.9	3.0	2.8	2.8	2.9	2.9	3.2	3.1	3.1
Mg	51.8	51.3	51.8	51.6	50.9	51.3	50.0	50.5	50.0

Table 1. continued

Sample	25724 cont	An 2 1[a]	2[a]	3[a]	C[b]
Grain	3				
SiO$_2$	35.1	35.1	34.8	34.8	
Al$_2$O$_3$	0.03	-	-	-	
TiO$_2$	0.04	0.06	0.02	0.05	
FeO*	38.85	38.1	38.3	39.0	34.2
MnO	2.58	2.34	2.35	2.37	2.18
MgO	22.75	24.65	24.4	24.1	27.1
CaO	0.50	0.50	0.49	0.49	0.41
Sum	99.85	100.75	100.36	100.81	

Number of cations on the basis of 4 (O)

Si	1.007	0.992	0.990	0.988	
Al	0.001	-	-	-	
Ti	0.001	0.001	0.001	0.001	
Fe	0.932	0.902	0.912	0.928	
Mn	0.063	0.056	0.057	0.057	
Mg	0.973	1.039	1.035	1.021	
Ca	0.015	0.015	0.015	0.015	
Z	1.007	0.992	0.990	0.988	
X	1.985	2.013	2.020	2.022	
Sum	2.992	3.005	3.010	3.010	
Fe	47.4	45.2	45.5	46.3	48.5
Mn	3.2	2.8	2.8	2.8	3.1
Mg	49.4	52.0	51.7	50.9	47.3
Ca					0.6

[a] Analysed using 50 μ defocused beam.

[b] Sample 1910-199, Cape Royds, Carmichael 1967.

Table 2. Electron microprobe analyses of clinopyroxene

VUW no.	25725			25724					An 1
Grain	1C	1R	2[a]	3	4	1C	1R	2	1
SiO_2	51.7	51.5	51.6	50.2	50.3	50.4	49.8	49.7	51.1
Al_2O_3	2.72	2.85	2.98	2.64	2.99	2.71	2.72	2.77	2.79
TiO_2	1.38	1.43	1.42	1.45	1.65	1.32	1.35	1.32	1.29
$FeO*$	9.30	9.34	9.39	9.19	9.32	9.70	9.30	9.81	9.46
MnO	0.62	0.62	0.58	0.63	0.63	0.64	0.65	0.71	0.65
MgO	11.9	12.1	12.1	12.1	12.0	11.7	11.8	11.8	12.2
CaO	21.8	21.7	22.0	22.0	22.0	21.3	21.6	21.4	21.6
Na_2O	0.94	0.96	0.98	0.85	0.86	1.00	0.99	1.05	1.04
Sum	100.36	100.51	101.05	99.06	99.75	98.77	98.21	98.56	100.13
Fe_2O_3	0.40	1.02	1.44	2.43	2.09	1.86	2.77	3.59	2.33
FeO	8.94	8.42	8.09	7.00	7.44	8.03	6.81	6.58	7.37
Total	100.40	100.60	101.19	99.30	99.97	98.96	98.49	98.92	100.36

Number of cations on the basis of 6 (O)

Si	1.930	1.918	1.911	1.897	1.889	1.912	1.897	1.888	1.907
Al	0.070	0.082	0.089	0.103	0.111	0.088	0.103	0.112	0.093
Al	0.049	0.043	0.041	0.014	0.021	0.033	0.019	0.012	0.030
Ti	0.039	0.040	0.040	0.041	0.047	0.038	0.039	0.038	0.036
Fe^{3+}	0.011	0.029	0.040	0.069	0.059	0.053	0.079	0.103	0.065
Fe^{2+}	0.279	0.262	0.251	0.221	0.234	0.255	0.217	0.209	0.230
Mn	0.020	0.020	0.018	0.020	0.020	0.021	0.021	0.023	0.021
Mg	0.662	0.672	0.668	0.681	0.672	0.661	0.670	0.668	0.679
Ca	0.872	0.866	0.873	0.891	0.885	0.866	0.882	0.871	0.864
Na	0.068	0.069	0.070	0.062	0.063	0.074	0.073	0.077	0.075
Z	2.000	2.000	2.000	2.000	2.000	2.000	2.000	2.000	2.000
X+Y	2.000	2.000	2.000	2.000	2.000	2.000	2.000	2.000	2.000
Ca	47.6	47.6	48.2	49.1	48.9	48.0	49.3	49.2	48.2
Mg	36.1	36.9	36.9	37.6	37.1	36.7	37.4	37.7	37.8
Fe^{2+}+Mn	16.3	15.5	14.9	13.3	14.0	15.3	13.3	13.1	14.0
Na	6.6	6.7	7.0	6.3	6.4	7.3	7.4	7.9	7.5
Mg	64.3	65.7	66.3	69.2	67.9	65.4	68.3	68.4	67.6
Fe^{2+}+Mn	29.1	27.6	26.7	24.5	25.7	27.3	24.3	23.7	24.9

[a] Analysed using 50 μ defocused beam.

Table 2 continued

VUW no.	An 1 cont.							An 2	C[b]
Grain	9	2	12	6	13	8	7	1[a]	
SiO_2	50.6	50.5	50.4	51.1	50.3	50.7	50.5	50.75	(52.3)
Al_2O_3	2.28	2.25	2.80	2.87	2.16	2.59	2.62	2.71	2.68
TiO_2	1.19	1.22	1.32	1.38	1.16	1.21	1.33	1.39	1.52
FeO*	9.50	9.68	9.75	9.81	9.83	9.85	9.95	10.0	9.1
MnO	0.64	0.65	0.65	0.63	0.65	0.65	0.70	0.66	0.52
MgO	12.3	12.15	12.2	12.0	12.1	11.9	11.9	12.2	12.5
CaO	21.2	21.7	21.1	21.4	21.8	21.7	21.6	21.55	20.5
Na_2O	0.89	0.96	1.07	1.11	0.93	1.01	1.04	1.06	0.92
Sum	98.60	99.11	99.29	100.30	98.93	99.61	99.64	100.32	100.00
Fe_2O_3	1.98	3.07	2.99	2.28	3.45	2.77	3.09	3.34	
FeO	7.72	6.92	7.06	7.76	6.72	7.36	7.17	7.00	
Total	98.80	99.42	99.59	100.53	99.28	99.89	99.95	100.65	

Number of cations on the basis of 6 (O)

Si	1.920	1.907	1.897	1.906	1.904	1.906	1.899	1.893	
Al	0.080	0.093	0.103	0.094	0.096	0.094	0.101	0.107	
Al	0.022	0.007	0.021	0.032	-	0.021	0.015	0.012	
Ti	0.034	0.035	0.037	0.039	0.033	0.034	0.038	0.039	
Fe^{3+}	0.057	0.087	0.085	0.064	0.098	0.078	0.087	0.094	
Fe^{2+}	0.245	0.218	0.222	0.242	0.213	0.231	0.225	0.218	
Mn	0.021	0.021	0.021	0.020	0.021	0.021	0.022	0.021	
Mg	0.695	0.684	0.684	0.667	0.683	0.667	0.667	0.678	
Ca	0.862	0.878	0.851	0.855	0.884	0.874	0.870	0.861	
Na	0.065	0.070	0.078	0.080	0.068	0.074	0.076	0.077	
Z	2.000	2.000	2.000	2.000	2.000	2.000	2.000	2.000	
X+Y	2.000	2.000	2.000	2.000	2.000	2.000	2.000	2.000	
Ca	47.3	48.8	47.9	47.9	49.1	48.8	48.8	48.4	45.2
Mg	38.1	38.0	38.5	37.4	37.9	37.2	37.4	38.1	38.3
Fe^{2+}+Mn	14.6	13.2	13.6	14.7	13.0	14.0	13.8	13.5	16.5
Na	6.3	7.0	7.8	7.9	7.9	6.9	7.7	7.7	
Mg	67.7	68.9	68.1	66.1	66.1	69.3	67.4	68.2	
Fe^{2+}+Mn	25.9	24.1	24.1	26.0	26.0	23.8	24.9	24.1	

[a] Analysed using defocused 50 μ beam.

[b] Sample 1910-199, Cape Royds, Carmichael (1967)

Table 3. Electron microprobe analyses of magnetite

VUW no.	25726				25725				
Grain	2	3C	3R	1	1	2	4	3C	3R
SiO_2	0.06	0.05	0.07	0.06	0.03	0.04	0.06	0.05	0.09
Al_2O_3	2.28	2.43	2.34	2.33	2.39	2.44	2.46	2.34	2.31
TiO_2	25.5	25.2	25.3	25.3	25.4	25.4	25.7	25.6	24.7
FeO*	65.4	65.4	65.4	65.5	65.1	65.2	65.2	65.3	65.0
MnO	1.76	1.76	1.76	1.80	1.71	1.77	1.75	1.76	1.78
MgO	2.90	3.01	2.98	2.94	2.95	2.99	3.04	3.02	3.11
CaO	-	-	-	-	-	-	-	-	0.05
Sum	97.90	97.85	97.85	97.93	97.58	97.84	98.21	98.07	97.04
Fe_2O_3	18.3	18.9	18.7	18.8	18.3	18.4	18.0	18.3	19.4
FeO	48.9	48.5	48.6	48.6	48.7	48.9	49.0	48.8	47.6
Total	99.70	99.85	99.75	99.75	99.48	99.94	100.01	99.87	99.04
Usp %[a]	70.3	69.3	69.6	69.5	70.2	70.0	70.7	70.3	68.1

[a] Calculated by the method of Carmichael (1967).

VUW no.	25724			An 1				An 2	
Grain	3	2	1	1	9	14	11	1[a]	3[a]
SiO_2	0.06	0.08	0.07	0.07	0.09	0.09	0.08	0.10	0.08
Al_2O_3	2.24	2.23	2.31	2.60	2.30	2.27	2.40	2.43	2.50
TiO_2	24.9	24.7	25.3	25.15	25.2	25.0	25.3	25.2	25.4
FeO*	65.4	65.9	66.2	65.4	65.5	65.7	66.0	65.5	65.6
MnO	1.85	1.84	1.81	1.74	1.72	1.70	1.70	1.73	1.70
MgO	2.85	3.00	2.76	2.84	2.81	2.79	2.87	3.14	3.05
CaO	0.24	0.03	-	-	-	0.13	0.05	-	-
Sum	97.54	97.78	98.45	97.80	97.62	97.68	98.40	98.10	98.33
Fe_2O_3	19.3	20.0	18.9	18.5	18.6	19.1	18.9	18.95	18.6
FeO	48.1	47.9	49.1	48.7	48.7	48.6	48.9	48.4	48.9
Total	99.54	99.78	100.25	99.60	99.42	99.68	100.20	99.95	100.23
Usp %	68.5	67.5	69.6	69.9	69.8	69.1	69.5	69.1	69.9

[a] Analysed using defocused 50 μ beam.

Table 3 continued

| VUW no. | An 2 cont. | | Carmichael[b] | | |
Grain	2[a]		A	B	C
SiO_2	0.07	SiO_2	0.04	0.06	0.09
Al_2O_3	2.59	TiO_2	26.3	27.5	26.1
TiO_2	25.2	Al_2O_3	1.81	0.26	0.17
$FeO*$	65.7	V_2O_3	0.09	-	-
MnO	1.66	FeO	65.3	67.1	67.8
MgO	3.02	MnO	1.62	2.05	2.21
CaO	0.03	MgO	3.15	0.24	0.16
		CaO	-	0.04	0.06
Sum	98.27	ZnO	0.09	0.18	0.17
		Sum	98.4	97.4	96.6
Fe_2O_3	19.0	Fe_2O_3	17.7	14.8	17.3
FeO	48.7	FeO	49.4	53.7	52.3
Total	100.27	Total	100.2	98.9	98.4
Usp %	69.2	Usp %	71.9	78.8	75.2

[a] Analysed using defocused 50 μ beam.

[b]
A Phenocryst Sample 1910-199, Cape Royds Carmichael (1967).
B Phenocryst Sample 1930-218, Cape Evans Carmichael and Nicholls. (1967).
C Groundmass Sample 1930-218, Cape Evans Carmichael. and Nicholls (1967).

Table 4. Electron microprobe analyses of pyrrhotite

VUW no. Grain	25724 5	2	1	3
Fe	62.14	62.19	62.22	62.41
S	37.27	37.32	37.60	37.56
Sum	99.41	99.51	99.82	99.97
Molecular proportions				
Fe	1.113	1.114	1.114	1.117
S	1.162	1.164	1.173	1.172
Mole fraction FeS	0.979	0.978	0.975	0.976

Table 5. Electron microprobe analyses of anorthoclase

VUW no.	25724	An 1 C^a	I^a	I^a	R^a	An 2 C^a	I^a	I^a	R^a
Grain	1								
SiO_2	62.7	63.6	62.4	63.2	62.8	64.4	62.5	63.7	62.9
Al_2O_3	21.5	20.8	21.1	21.1	22.0	21.7	23.1	22.4	23.0
TiO_2	0.12	0.13	0.12	0.12	0.14	0.13	0.11	0.13	0.13
FeO^*	0.19	0.18	0.21	0.21	0.16	0.15	0.18	0.19	0.20
CaO	3.54	3.14	3.25	3.23	4.26	2.75	3.79	3.36	3.80
Na_2O	7.32	7.42	7.52	7.55	7.54	7.48	7.49	7.46	7.39
K_2O	2.94	3.47	3.32	3.27	2.51	3.77	2.86	3.22	2.94
Sum	98.31	98.75	97.92	98.68	99.41	100.38	100.03	100.46	100.36

Number of cations on the basis of 32 (O)

Si	11.369	11.498	11.393	11.431	11.268	11.440	11.155	11.317	11.185
Al	4.591	4.418	4.531	4.496	4.655	4.547	4.858	4.679	4.810
Ti	0.017	0.018	0.016	0.016	0.018	0.017	0.015	0.017	0.017
Fe	0.028	0.028	0.031	0.032	0.024	0.023	0.027	0.028	0.029
Ca	0.689	0.609	0.636	0.626	0.820	0.524	0.724	0.638	0.723
Na	2.573	2.600	2.660	2.647	2.625	2.577	2.592	2.568	2.546
K	0.679	0.800	0.772	0.755	0.574	0.854	0.650	0.729	0.667
Z	15.960	15.916	15.924	15.927	15.923	15.987	16.013	15.996	15.995
X	3.986	4.055	4.115	4.076	4.061	3.995	4.008	3.980	3.982
Sum	19.946	19.971	20.039	20.003	19.984	19.982	20.021	19.976	19.977
An	17.5	15.2	15.6	15.5	20.4	13.2	18.3	16.2	18.4
Ab	65.3	64.8	65.4	65.7	65.3	65.2	65.3	65.3	64.7
Or	17.2	20.0	20.0	18.7	14.3	21.6	16.4	18.5	16.9

[a] Analysed using defocused 50 μ beam.

Table 6.   Partial analyses of anorthoclase.

Sample	Position	CaO	Na$_2$O	K$_2$O	Sum	An	Ab	Or
An 1	8	2.72	7.30	3.84	13.86	13.3	64.4	22.3
	4	3.02	7.33	3.58	13.93	14.7	64.5	20.8
	3	3.20	7.40	3.48	14.08	15.4	64.6	20.0
	6	3.20	7.44	3.37	14.01	15.5	65.1	19.4
	2	3.44	7.55	3.12	14.11	16.5	65.6	17.9
An 3	53	3.44	7.34	3.21	13.98	16.8	64.6	18.6
	31	3.12	7.35	3.45	13.92	15.2	64.8	20.0
	42	4.00	7.38	2.72	14.10	19.4	64.9	15.7
	50	2.87	7.38	3.68	13.93	13.9	64.8	21.3
	40	4.17	7.39	2.66	14.22	20.1	64.6	15.3
	45	3.61	7.40	2.96	13.97	17.6	65.2	17.2
	47	3.46	7.43	3.12	14.01	16.8	65.2	18.0
	51	3.68	7.44	3.08	14.20	17.7	64.7	17.6
	26	3.83	7.44	2.88	14.15	18.5	65.0	16.5
	55	3.95	7.45	2.80	14.20	19.0	64.9	16.1
	41	4.01	7.45	2.78	14.24	19.3	64.8	15.9
	37	3.02	7.45	3.58	14.05	14.5	64.9	20.6
	35	3.82	7.46	2.88	14.16	18.4	65.1	16.5
	43	3.29	7.46	3.26	14.01	15.9	65.3	18.8
	46	3.41	7.47	3.24	14.12	16.4	65.0	18.6
	48	3.05	7.48	3.40	13.93	14.8	65.6	19.6
	25	3.75	7.48	2.90	14.13	18.1	65.2	16.7
	54	3.40	7.49	3.17	14.06	16.4	65.4	18.2
	36	3.65	7.49	3.07	14.21	17.5	65.0	17.5
	27	3.35	7.49	3.22	14.06	16.1	65.4	18.5
	38	3.25	7.50	3.33	14.08	15.6	65.3	19.1
	44	2.84	7.50	3.63	13.97	13.7	65.5	20.8
	49	3.57	7.51	3.04	14.12	17.2	65.4	17.4
	32	3.21	7.51	3.29	14.01	15.5	65.6	18.9
	28	3.40	7.52	3.29	14.21	16.3	65.0	18.7
	39	3.30	7.52	3.38	14.20	15.8	65.0	19.2
	30	2.89	7.54	3.69	14.12	13.8	65.2	21.0
	52	3.29	7.54	3.22	14.05	15.8	65.7	18.5
	34	3.37	7.59	3.18	14.14	16.1	65.8	18.1
	33	3.11	7.62	3.42	14.15	14.8	65.8	19.4
	29	3.22	7.62	3.30	14.14	15.4	65.8	18.8

Table 7. Electron microprobe analyses of glass inclusions in anorthoclase 1.

Position	1	2	3	4	5	6	7	8	9
SiO_2	54.8	55.6	55.4	54.4	55.8	55.0	55.7	55.3	55.6
Al_2O_3	18.2	18.5	18.6	18.3	18.9	18.8	19.3	19.2	19.3
TiO_2	0.98	1.00	1.00	0.98	1.00	0.99	0.99	0.98	0.97
FeO*	5.23	5.30	5.26	5.17	5.09	5.09	5.10	4.86	4.88
MnO	0.27	0.26	0.27	0.26	0.27	0.25	0.27	0.23	0.27
MgO	0.84	0.80	0.80	0.81	0.79	0.79	0.80	0.77	0.80
CaO	1.85	1.82	1.91	1.86	1.46	1.81	1.70	1.37	1.72
Na_2O	8.91	9.02	9.14	8.62	9.21	9.08	9.48	9.63	9.14
K_2O	6.16	6.17	6.03	6.22	6.35	6.25	6.20	6.57	6.41
Sum	97.24	98.47	98.41	96.62	98.87	98.06	99.54	98.91	99.09

Recalculated to 100%

	1	2	3	4	5	6	7	8	9
SiO_2	56.4	56.5	56.3	56.3	56.4	56.1	56.0	55.9	56.1
Al_2O_3	18.7	18.8	18.9	18.9	19.1	19.2	19.4	19.4	19.5
TiO_2	1.01	1.02	1.02	1.01	1.01	1.01	0.99	0.99	0.98
FeO	5.38	5.38	5.34	5.35	5.15	5.19	5.12	4.91	4.92
MnO	0.28	0.26	0.27	0.27	0.27	0.25	0.27	0.23	0.27
MgO	0.86	0.81	0.81	0.84	0.80	0.81	0.80	0.78	0.81
CaO	1.90	1.85	1.94	1.93	1.48	1.85	1.71	1.39	1.74
Na_2O	9.16	9.16	9.29	8.92	9.32	9.26	9.52	9.74	9.22
K_2O	6.33	6.27	6.13	6.44	6.42	6.37	6.23	6.64	6.47

Table 8. Electron microprobe analyses of glass inclusions in anorthoclase 3.

Position	2	4	5	6	7	8	9	13
SiO_2	55.25	55.7	55.6	55.8	55.8	55.4	55.9	55.2
Al_2O_3	20.1	19.9	19.9	19.9	19.7	19.4	19.4	19.45
TiO_2	1.02	0.96	0.99	0.98	0.98	1.09	0.96	1.06
FeO*	5.08	5.05	5.11	5.14	5.20	5.20	5.25	5.29
MnO	0.28	0.24	0.27	0.26	0.27	0.27	0.23	0.24
MgO	0.82	0.81	0.81	0.83	0.82	0.82	0.82	0.80
CaO	1.59	1.50	1.76	1.77	1.68	1.66	1.94	1.91
Na_2O	9.15	9.18	8.92	8.95	9.12	8.72	8.74	8.64
K_2O	6.33	6.54	6.45	6.48	6.27	6.45	6.09	6.10
P_2O_5	0.37	0.36	0.34	0.40	0.35	0.38	0.40	0.40
Sum	99.99	100.24	100.15	100.51	100.19	99.39	99.73	99.09

Recalculated to 100%

	2	4	5	6	7	8	9	13
SiO_2	55.25	55.6	55.5	55.5	55.7	55.75	56.05	55.7
Al_2O_3	20.1	19.85	19.9	19.8	19.7	19.5	19.45	19.65
TiO	1.02	0.96	0.99	0.98	0.98	1.10	0.96	1.07
FeO	5.08	5.04	5.10	5.11	5.19	5.23	5.26	5.34
MnO	0.28	0.24	0.27	0.26	0.27	0.27	0.23	0.24
MgO	0.82	0.81	0.81	0.83	0.82	0.82	0.82	0.81
CaO	1.59	1.50	1.76	1.76	1.68	1.67	1.94	1.92
Na_2O	9.15	9.16	8.91	8.90	9.10	8.77	8.76	8.72
K_2O	6.33	6.52	6.44	6.45	6.26	6.49	6.11	6.16
P_2O_5	0.37	0.36	0.34	0.40	0.35	0.38	0.40	0.40

Table 8 continued

Position	10	15	16	17	18	21	22	24
SiO_2	55.5	55.6	55.4	55.7	55.9	55.3	55.55	55.5
Al_2O_3	19.8	19.7	19.5	19.4	19.4	19.6	19.7	19.6
TiO_2	1.00	0.99	1.08	1.01	1.03	0.98	1.00	1.00
FeO*	5.44	5.24	5.46	5.47	5.36	5.17	5.14	5.09
MnO	0.27	0.27	0.25	0.26	0.27	0.26	0.25	0.29
MgO	0.82	0.81	0.87	0.78	0.83	0.83	0.84	0.84
CaO	1.90	2.07	1.56	1.86	1.82	1.50	1.76	1.62
Na_2O	8.67	8.73	8.86	8.67	9.02	9.14	9.16	8.99
K_2O	5.87	5.99	6.40	5.77	5.97	6.48	6.16	6.31
P_2O_5	0.38	0.41	0.42	0.36	0.41	0.39	0.41	0.40
Sum	99.65	99.81	99.80	99.28	100.01	99.65	99.97	99.64

Recalculated to 100%

	10	15	16	17	18	21	22	24
SiO_2	55.7	55.7	55.5	56.1	55.9	55.5	55.6	55.7
Al_2O_3	19.9	19.7	19.5	19.5	19.4	19.7	19.7	19.7
TiO_2	1.00	0.99	1.08	1.02	1.03	0.98	1.00	1.00
FeO	5.46	5.25	5.47	5.51	5.36	5.19	5.14	5.11
MnO	0.27	0.27	0.25	0.26	0.27	0.26	0.25	0.29
MgO	0.82	0.81	0.87	0.78	0.83	0.83	0.84	0.84
CaO	1.91	2.07	1.56	1.87	1.82	1.50	1.76	1.62
Na_2O	8.70	8.75	8.88	8.73	9.02	9.17	9.16	9.02
K_2O	5.89	6.00	6.41	5.81	5.97	6.50	6.16	6.33
P_2O_5	0.38	0.41	0.42	0.36	0.41	0.39	0.41	0.40

APPENDIX C

ANALYTICAL TECHNIQUES

Crushing

A 100 cc tungsten-carbide "TEMA' swing mill was used for crushing all samples. In order to determine time and sample size requirements a test sample (25706) was crushed using different sample sizes and varying grinding times. A pipette analysis was made of the crushed sample to determine the size distribution.

Run	Sample Weight grams	Crushing Time seconds	Mean Size phi	σ
1	50	45	6.9	1.6
2	95	60	6.8	1.6
3	95	45	6.8	1.6

In all three runs the mean grain size was the same. For routine work 90-100 grams of sample was crushed for 60 seconds.

X-ray Fluorescence Analysis

Most major and all trace element analyses were made using x-ray fluorescence spectroscopy.

Major element analyses were made at Victoria University using a Seimens SRS-1 spectrometer. Instrumental settings are given in Table 1. Most samples were analysed in duplicate and often each were analysed in duplicate for SiO_2 and Al_2O_3. Calibration was made using synthetic oxide mixtures and a large suite of international rock standards. The method is extremely precise and accurate judging from replicate determinations and analyses of international rock standards (Table 2). X-ray fluorescence (XRF) determinations of magnesium (MgO) are difficult because of the low count rate (Table 1), high background and interferences due to fluorescence of the ADP crystal.

TABLE 1   Instrumental settings for x-ray fluorescence.

A. Major Elements[a]

Oxide	Tube	kV	mA	Crystal	Collimator[b]	Time	cs/%
MgO[c]	Cr	55	46	ADP	C	160	17
Al_2O_3	Cr	55	46	PET	C	80	160
SiO_2	Cr	55	46	PET	C	80	160
P_2O_5	Cr	55	46	PET	C	80	200
K_2O	Cr	55	26	PET	C	40	4400
Fe_2O_3	Cr	55	26	LiF_{200}	C	40	1200
CaO	Cr	55	22	LiF_{200}	F	40	2800
TiO_2	Cr	55	16	LiF_{200}	C	40	7000
MnO	Au	45	35	LiF_{200}	C	40	3900

B. Trace Elements

Element	Tube	Crystal	Collimator[b]	Vacuum	Counter[d]	Counting Time Peak	Counting Time Background	Counts cs/ppm	Std	Adopted Value ppm
B-1 University of Montreal										
Cr	W	LiF_{200}	C	On	F+S	200	100	16	W1	120
Ni	W	LiF_{200}	F	On	F+S	200	100	16	W1	78
Cu	W	LiF_{200}	F	On	F+S	200	100	14	W1	110
Zn	W	LiF_{200}	F	On	F+S	200	100	9	W1	82
Sr	Mo	LiF_{200}	F	Air	S	100	100	26	G2	481
Rb	Mo	LiF_{200}	F	Air	S	100	100	20	G2	174
B-2 Victoria University of Wellington										
Cr	Au	LiF_{110}	F	On	F	200	100	2	W1	120
V	Au	LiF_{110}	F	On	F	200	100	1	W1	240
Zr	W	LiF_{200}	C	Air	S	200	100	2	Zr	300

[a] All major element determinations made at Victoria University of Wellington using a Seimens SRS-1 spectrometer. Vacuum and flow proportional counter were used throughout.

[b] C = coarse (0.4°), F = fine (0.15°)

[c] Pulse height analyser was run 25% off the symmetrical position to reduce background due to crystal fluorescence.

[d] F = flow proportional counter, S = scintillation counter.

TABLE 2. Major element analyses of international rock standards and a phonolite (P22973) showing precision and accuracy of analytical methods.

Sample		Number of determinations	SiO_2	TiO_2	Al_2O_3	Fe_2O_{3T}	MnO	MgO	CaO	K_2O	P_2O_5	Na_2O	FeO
G2		4	69.02	0.48	15.37	2.69	0.03	0.75	1.90	4.48	0.14	4.13	1.17
G2	*		69.11	0.50	15.40	2.65	0.03	0.76	1.94	4.51	0.14	4.07	1.45
AGV		7	58.97	1.04	17.14	6.80	0.10	1.50	4.90	2.94	0.51	4.34[b]	1.85[b]
AGV	*		59.00	1.04	17.25	6.76	0.10	1.53	4.90	2.89	0.49	4.26	2.05
GSP		4	67.40	0.66	15.16	4.32	0.04	0.95	1.99	5.51	0.28	2.75[a]	2.20[a]
GSP	*		67.38	0.66	15.25	4.33	0.04	0.96	2.02	5.53	0.28	2.80	2.31
P22973	A		57.33	0.38	20.05	5.27	0.23	0.15	2.05	5.42	0.06	8.46	2.12
P22973	B		56.81	0.38	19.99	5.22	0.22	0.11	2.03	5.43	0.05	8.49	
P22973	C		56.84	0.38	20.22	5.19	0.23	0.14	2.06	5.49	0.06	9.02	
P22973			56.71	0.38	20.21	5.28	0.23	—	2.16	5.48	0.06		
P22973	Mean		56.92	0.38	20.12	5.24	0.23	0.13	2.08	5.45	0.06	8.66	
P22973	Chem.Div.**		57.0	0.40	20.4	5.17	—	—	2.25	5.35	0.03	8.65	1.95
BR	A		38.07	2.67	10.05	12.96	0.21	13.42	13.80	1.39	1.09	3.04	5.93
BR	B		37.75	2.65	10.06	12.90	0.21	13.18	13.77	1.37	1.09		
BR	C		38.22	2.67	10.11	12.99	0.21	13.70	13.85	1.39	1.10		
BR	D		37.92	2.66	10.04	12.96	0.21	13.43	13.75	1.38	1.10		
	Mean		37.99	2.66	10.06	12.95	0.21	13.43	13.79	1.38	1.08		
	Accepted*		38.20	2.60	10.20	12.88	0.20	13.28	13.80	1.40	1.04	3.05	6.57
DR		1	52.77	1.06	17.78	9.67	0.22	4.31	7.03	1.71	0.26		
DR	*		52.65	1.11	17.42	9.91	0.21	4.50	7.08	1.70	0.27		
GA		1	69.71	0.35	14.85	2.76	0.09	0.92	2.44	4.06	0.14	3.50	
GA	*		69.90	0.38	14.50	2.83	0.09	0.95	2.45	4.03	0.12	3.55	
T1		1	62.86	0.56	16.56	5.90	0.11	1.81	5.07	1.21	0.17		
T1	†		62.69	0.59	16.57	5.94	0.11	1.86	5.11	1.24	0.14		
JG		3	72.06	0.25	14.21	2.13	0.07	0.73	2.17	3.98	0.09		
JG	*		72.24	0.26	14.21	2.21	0.06	0.73	2.18	3.96	0.10		

[a] single determination; [b] Average of 4 analyses
* Best values for international rock standards given by Flanagan (1973)
** Chemical analysis made by Chemistry Division, D.S.I.R.
† Bowden and Luena (1966)

Selected samples were analysed by XRF and atomic absorption spectroscopy and show excellent agreement (Table 3), they give confidence to the XRF determinations.

TABLE 3. X-ray fluorescence (XRF) spectroscopy and atomic absorption (AA) spectroscopy determinations of MgO.

Sample	XRF	AA
22879	6.42	6.29
22884	5.40	5.60
22888	0.56	0.52
22896	6.78	6.74
22952	0.41	0.41
22962	0.98	0.96
25261	1.65	1.59
25283	0.18	0.14
25290	1.29	1.28
25291	1.22	1.20
25704	1.13	1.14
P22971	0.17	0.17
P22973	0.13	0.13

Trace element determinations were made, with the exception of V and Zr, at the University of Montreal using a Philips 1220 x-ray fluorescence spectrometer. U.S. Geological Survey rock standards were used for calibration (Table 1). Mass absorption coefficients were calculated from the major element composition and mass absorption tables. Cr analyses were performed both at Victoria University using a Seimens spectrometer and at the University of Montreal. Excellent agreement, in general better than 5%, is shown between the two laboratories (Fig. 1). Victoria University determinations show a bias to slightly higher values above the 200 ppm level. Trace element analyses for U.S. Geological Survey rock standards are given in Table 4 and show good agreement with determinations made in other laboratories.
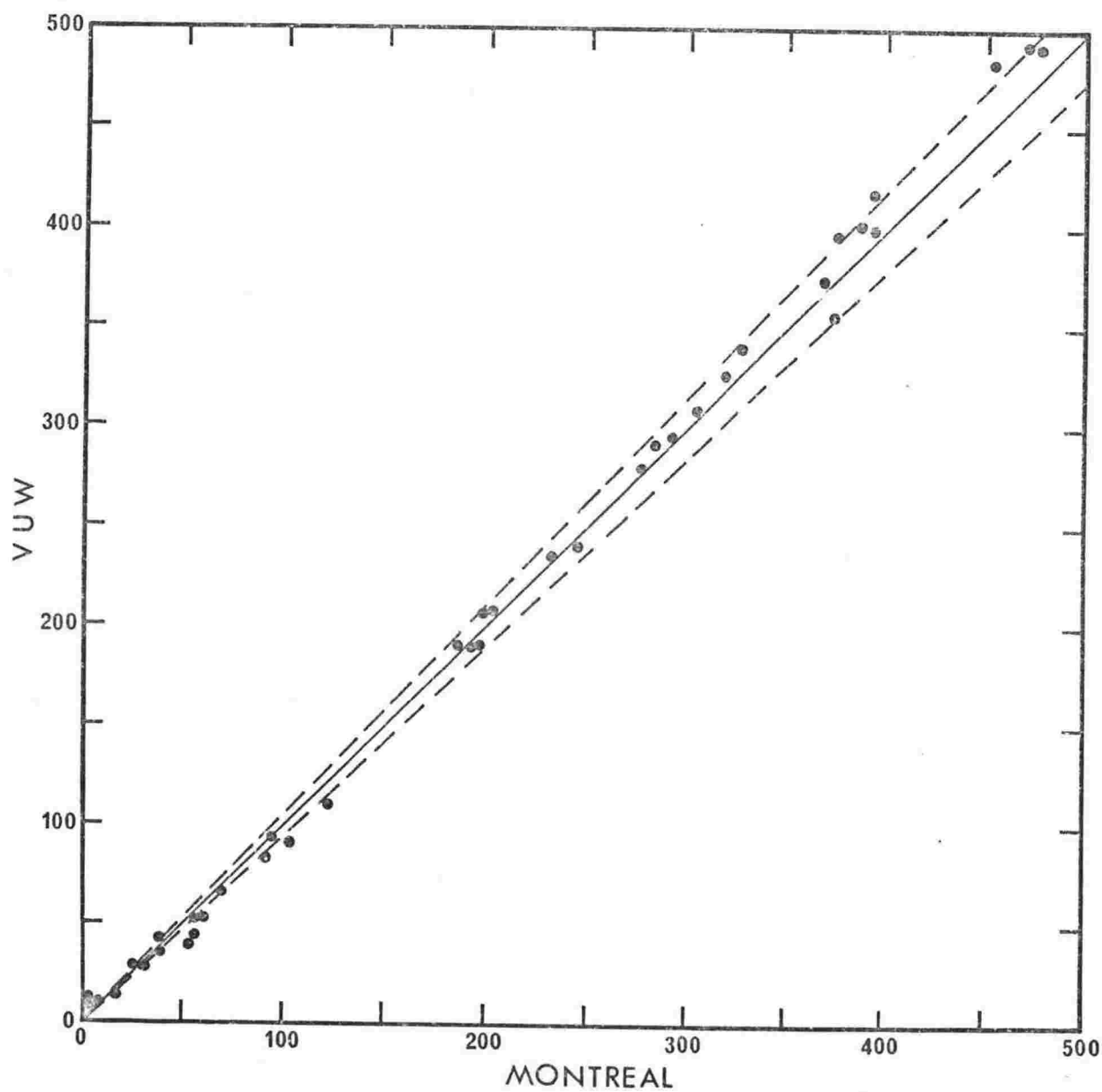
FIGURE 1 Plot of Cr determinations made at Victoria University against determinations made at the University of Montreal. Dashed lines indicate 5% difference about the line of equal values.

TABLE 4. Comparative values for trace elements in U.S. Geological Survey rock standards.

Element	Laboratory[a]	AGV	BCR	G1	G2	GSP	W1
Ba	This study			(1080)[b]	1910	1214	134
	Flanagan			1200	1870	1300	160
Rb	This study-VUW	78	42		(169)	254	
	This study-UM		49	220	(174)	260	22
	UCT	70	47	210	174		21
	Flanagan	67	47	220	168	254	21
Sr	This study-VUW	655	325	245	(461)	228	
	This study-UM		333	256	(481)	235	192
	UCT		328	249			188
	Flanagan	657	330	250	479	233	190
Zr	This study-VUW	218	180	201	(300)	523	
	UCT		192	219			
	ANU		180	210	305		
	Flanagan	225	190	210	300	500	
Zn	This study-UM				87	112	(82)
	Flanagan				85	98	86
Cu	This study-UM	61			11	41	(110)
	Flanagan	60			12	33	110
Ni	This study-UM	18			6		(78)
	Flanagan	18			5		76
V	This study-UM	104	366		33	44	(240)
	UCT	99	370			41	(240)
	ANU	104	370			41	240
	Flanagan	125	399		35	53	264
Cr	This study-VUW	9	14			9	(120)
	UCT	11	16			12	(120)
	ANU	10	13			13	111
	Flanagan	12	18			12	114

[a] This study VUW - determinations made by Seimens and Philips XRF at Victoria University of Wellington.

This study UM - determinations made by Philips XRF at the University of Montreal.

U.C.T. - XRF determinations, University of Cape Town (D. Reid pers. comm.).

A.N.U. - XRF determinations, Australian National University.

Flanagan - average values Flanagan (1973).

[b] Sample used as calibration standard with assumed value shown in brackets.

APPENDIX D

Tables 7.1 to 7.15

Compilation of major and trace element analyses
and CIPW norms for rocks of the McMurdo Volcanic
Group, excluding the Hallett volcanic province.

TABLE 7.1   Analyses of rocks from the Balleny
             volcanic province.

	1	2	3	4	5	6
VUW No.	24591	24583				
SiO_2	43.29	44.74	44.99	45.06	47.73	55.93
TiO_2	2.54	3.00	2.70	2.69	2.39	0.64
Al_2O_3	14.60	16.34	15.51	18.76	16.87	19.61
Fe_2O_3	4.24	3.72	3.43	0.23	2.52	1.75
FeO	6.38	7.72	7.27	9.94	8.78	6.32
MnO	0.18	0.19	0.19	0.19	0.18	0.13
MgO	10.25	7.53	9.29	7.33	5.80	0.50
CaO	10.37	10.60	9.63	9.72	8.64	3.53
Na_2O	3.41	3.86	4.32	4.19	4.90	7.75
K_2O	1.27	1.28	1.13	1.57	1.99	3.67
P_2O_5	0.60	0.63	0.70	0.65	0.65	0.12
H_2O+	0.52	0.35	0.32	0.12	0.14	0.19
H_2O-	0.60		0.01	0.02	0.02	0.10
CO_2			0.13			
S			0.05	0.05	0.09	
-O=S			0.02	0.01	0.02	
Total	98.25	99.96	99.65	100.57[1]	100.74[1]	100.24
Rb	31	32	14	-	-	
Ba	275	279	450	540	540	
Sr	621	688	800	-	-	
Y	-	-	50	-	-	
Zr	-	-	350	-	-	
Zn	72	79	-	-	-	
Cu	78	56	-	-	-	
Ni	258	106	200	-	-	
V	197	227	300	-	-	
Cr	362	196	200	-	-	
K%	1.05	1.06	-	-	-	
K/Rb	339	331	-	-	-	
Mg No.	68.7	59.8	66.2	61.2	53.4	-

CIPW Norms (Weight Percent)

	1	2	3	4	5	6
Or	7.50	7.56	6.68	9.28	11.76	21.69
Ab	12.10	15.33	17.59	11.00	20.61	39.47
An	20.78	23.48	19.59	27.74	18.16	7.88
Ne	9.08	9.39	10.28	13.25	11.30	14.14
Di-wo	11.17	10.44	9.52	6.78	8.54	3.69
Di-fs	1.46	2.47	1.88	2.83	3.44	3.57
Di-en	8.54	7.14	6.79	3.70	4.76	0.48
Fo	11.90	8.14	11.45	10.20	6.78	0.54
Fa	2.24	3.11	3.50	8.60	5.40	4.46
Mt	6.15	5.39	4.97	0.33	3.65	2.54
Il	4.82	5.70	5.13	5.11	4.54	1.22
Ap	1.39	1.46	1.62	1.51	1.51	0.28
Cc	-	-	0.30	-	-	-
Others	1.12	0.35	0.36	0.24	0.29	0.29
Total	98.25	99.96	99.65	100.57	100.74	100.24
D.I.	28.7	32.3	34.5	33.5	43.7	75.3
$\frac{An \times 100}{An+Ab}$	63.2	60.5	52.7	71.6	46.8	16.6

[1]Includes BaO=0.06.

Explanation of Table 7.1. Analyses of rocks from the Balleny
volcanic province.

1. 24591. Basanite. Dredge sample, New Zealand Oceanographic
            Institute (NZOI) Station 220B, approx. 3 km northeast
            of Sabrina Island. Collected by B. C. Waterhouse.

2. 24583. Basanite. Sabrina Island. Approximately 1 km north
            of southernmost end. Collected by B. C. Waterhouse.

3. Basanite (Porphyritic olivine basalt). Off Balleny Islands
            67° 09.6'S, 163° 27.7'E. Dredge sample collected
            21/1/38 by Discovery Expedition Station no. 2200,
            depth 512-532 m. (Analysts. C. J. Elliott, V. K. Din,
            A. J. Easton). Kempe, 1974.

4. Basanite (olivine-trachybasalt). Borradaile Island.
            (Analyst: A. P. Wymond). Mawson, 1950.

5. Nepheline hawaiite (olivine-trachybasalt). Buckle Island.
            (Analyst: R. B. Wilson). Mawson, 1950.

6. Phonolite (Trachydolerite). Scott Island, about 315 miles
            northeast of Cape Adare, Victoria Land.
            (Analyst: G. T. Prior). Prior, 1907.

TABLE 7.2   Analyses of rocks from The Pleiades, Melbourne volcanic province, Antarctica.

VUW No.	1 25679	2 25682	3 25685	4 25664	5 25663	6 25703	7 -Gmass	8 25700
SiO_2	44.26	46.11	47.58	48.44	48.93	49.26	53.1	49.46
TiO_2	3.66	2.41	2.96	2.85	1.90	2.63	2.75	2.01
Al_2O_3	14.82	14.35	16.97	16.19	13.55	16.10	17.0	18.01
Fe_2O_3	4.01	3.30	3.53	5.11	2.51	4.67	3.79	3.90
FeO	8.70	8.35	8.08	6.33	8.86	6.49	5.27	6.36
MnO	0.20	0.21	0.24	0.20	0.19	0.20	0.21	0.24
MgO	7.21	8.94	3.51	4.72	8.66	5.09	3.05	2.81
CaO	10.98	10.04	8.15	7.82	8.16	8.14	7.13	7.05
Na_2O	3.80	3.84	5.80	4.41	3.42	4.24	5.14	6.72
K_2O	1.74	1.48	2.67	2.33	1.71	2.25	3.11	2.80
P_2O_5	0.78	0.59	0.99	0.89	0.35	0.73		0.76
H_2O+				0.20[1]	0.95[1]	0.19		
H_2O-								
Total	100.16	99.62	100.48	99.49	99.19	99.99	100.55[2]	100.12
Rb	40	37	73	62	53	71		80
Ba	356	416	555	483	289	396		660
Sr	795	745	1052	873	430	758		1102
Zn	96	97	112	104	93	105		111
Cu	52	60	21	40	40	41		30
Ni	78	190	6	30	121	45		13
V	252	185	115	151	142	156		2
Cr	194	317	8	32	324	94		21
K%	1.44	1.23	2.22	1.93	1.42	1.87		2.32
K/Rb	360	332	304	311	268	263		290

CIPW Norms (Weight Percent)

Q	-	-	-	-	-	-	-	-
Or	10.28	8.75	15.78	13.77	10.10	13.30	18.38	16.55
Ab	11.57	16.37	20.64	30.95	27.36	30.98	33.67	25.03
An	18.24	17.55	12.38	17.50	16.57	18.25	14.13	10.71
Ne	11.15	8.74	15.41	3.45	0.86	2.66	5.32	17.24
Ac	-	-	-	-	-	-	-	-
Ns	-	-	-	-	-	-	-	-
Di-wo	13.00	11.86	9.01	6.46	9.03	7.25	8.87	8.06
Di-fs	3.37	3.17	4.04	1.22	2.94	1.62	1.95	3.46
Di-en	8.67	7.84	4.72	4.66	5.56	5.03	6.18	4.33
Wo	-	-	-	-	-	-	-	-
Hy-en	-	-	-	-	-	-	-	-
Hy-fs	-	-	-	-	-	-	-	-
Fo	6.51	10.11	2.82	4.97	11.22	5.36	0.99	1.87
Fa	2.79	4.51	2.66	1.43	6.54	1.90	0.34	1.64
Mt	5.81	4.78	5.12	7.41	3.64	6.77	5.50	5.66
Hm	-	-	-	-	-	-	-	-
Il	6.95	4.58	5.62	5.41	3.61	5.00	5.22	3.82
Ap	1.81	1.37	2.29	2.06	0.81	1.69	-	1.76
Others	-	-	-	0.20	0.95	0.19	-	-
Total	100.16	99.62	100.48	99.49	99.19	99.99	100.55	100.12
D.I.	33.0	33.8	51.8	48.2	38.3	46.9	57.4	58.8
$\frac{100An}{An+Ab}$	61.2	51.7	37.5	36.1	37.7	37.1	29.6	30.0

[1]Loss on ignition.

[2]Total iron as FeO=8.68, Fe_2O_3 calculated using same Fe_2O_3/FeO as the whole rock.

TABLE 7.2 Analyses of rocks from The Pleiades, Melbourne volcanic province, Antarctica (continued).

VUW No.	9 25668	10 25671	11 25691	12 25690	13 25704	14 25661	15 25675	16 25662
SiO_2	49.83	51.72	51.76	52.77	53.74	55.12	55.26	55.36
TiO_2	2.00	2.23	1.15	1.23	1.17	1.29	1.26	1.31
Al_2O_3	14.43	16.97	18.96	19.10	18.23	17.39	17.57	17.57
Fe_2O_3	2.56	7.17	4.39	5.15	5.16	3.07	3.24	3.24
FeO	8.40	3.26	3.86	3.45	4.24	5.66	5.50	5.55
MnO	0.19	0.20	0.25	0.25	0.28	0.23	0.23	0.23
MgO	7.68	3.50	1.22	1.29	1.13	1.65	1.60	1.63
CaO	7.81	5.97	4.58	4.72	4.82	4.11	3.96	4.14
Na_2O	3.75	4.86	8.34	8.03	7.47	7.31	6.88	6.69
K_2O	1.91	2.78	3.85	3.90	3.35	3.52	3.61	3.53
P_2O_5	0.38	0.79	0.39	0.41	0.48	0.59	0.57	0.60
H_2O+						0.00		0.00
H_2O-						0.02		0.03
Total	98.94	99.45	98.75	100.30	100.07	99.96	99.68	99.88
Rb	60	80	126	126	101	88	88	87
Ba	324	587	763	745	794	899	935	914
Sr	459	782	971	988	1050	643	613	637
Zn	87	101	117	101	131	110	125	121
Cu	47	27	12	13	9	13	12	12
Ni	100	17	<4	<4	<4	5	<4	<5
V	131	90	16	22	6	6	4	8
Cr	176	18	<5	<5	<5	5	<5	<5
K%	1.59	2.31	3.20	3.24	2.78	2.92	3.00	2.93
K/Rb	265	289	254	257	275	332	341	337

CIPW Norms (Weight Percent)

Q	-	-	-	-	-	-	-	-
Or	11.29	16.43	22.75	23.05	19.80	20.80	21.33	7.49
Ab	29.66	41.12	28.64	31.98	39.14	41.52	43.10	20.86
An	16.90	16.28	2.93	4.55	6.32	4.24	6.40	43.98
Ne	1.12	-	22.72	19.48	13.04	11.01	8.19	6.84
Ac	-	-	-	-	-	-	-	-
Ns	-	-	-	-	-	-	-	-
Di-wo	8.08	3.42	5.30	4.17	5.12	5.13	3.98	3.81
Di-fs	2.68	-	2.03	0.51	2.11	3.10	2.37	2.25
Di-en	4.95	2.95	3.04	3.21	2.82	2.07	1.64	1.58
Wo	-	-	1.90	2.59	0.92	-	-	-
Hy-en	-	1.75	-	-	-	-	-	-
Hy-fs	-	-	-	-	-	-	-	-
Fo	9.94	2.82	-	-	-	1.43	1.65	1.74
Fa	5.93	-	-	-	-	2.36	2.63	2.72
Mt	3.71	4.70	6.36	7.47	7.48	4.45	4.70	4.70
Hm	-	3.93	-	-	-	-	-	-
Il	3.80	4.24	2.18	2.34	2.22	2.45	2.39	2.49
Ap	0.88	1.83	0.90	0.95	1.11	1.37	1.32	1.39
Other	-	-	-	-	-	-	-	0.03
Total	98.94	99.45	98.75	100.30	100.07	99.96	99.68	99.88
D.I.	42.1	57.6	74.1	74.5	72.0	73.3	72.6	71.7
$\dfrac{100An}{An+Ab}$	36.3	28.4	9.3	12.5	13.9	9.3	12.9	14.5
Agpaitic Index	-	-	-	-	-	-	-	-

TABLE 7.2   Analyses of rocks from The Pleiades, Melbourne volcanic
             province, Antarctica (continued).

VUW No.	17 25684	18 25670	19 25666	20 25667	21 25674	22 25683	23 25687	24 25665
SiO_2	55.50	55.58	55.81	57.10	59.04	59.79	59.94	59.98
TiO_2	1.58	1.29	1.66	1.22	0.88	0.21	0.60	0.70
Al_2O_3	16.97	17.61	16.58	18.52	17.83	18.83	18.19	17.67
Fe_2O_3	2.71	3.41	3.77	5.65	2.15	3.54	4.03	5.57
FeO	5.38	5.44	4.18	2.51	4.76	1.89	1.34	0.98
MnO	0.18	0.23	0.16	0.11	0.18	0.20	0.18	0.17
MgO	2.66	1.65	2.98	0.77	1.06	0.16	0.57	0.75
CaO	4.98	4.09	5.04	3.20	3.02	1.34	2.13	2.47
Na_2O	6.28	6.61	5.35	5.89	6.79	8.68	7.29	7.09
K_2O	3.50	3.56	3.52	4.70	4.38	5.26	5.22	4.74
P_2O_5	0.55	0.59	0.53	0.67	0.35	0.09	0.17	0.24
H_2O+								
H_2O-								
Total	100.29	100.06	99.58	100.34	100.44	99.99	99.66	100.36
Rb	128	87	164	200	138	183	224	154
Ba	600	913	482	448	930	633	869	986
Sr	628	631	512	354	495	97	415	386
Zn	106	125	109	141	93	115	81	90
Cu	23	12	17	24	13	8	6	8
Ni	16	<5	24	5	<5	<5	<5	<5
V	69	8	143	65	0	0	8	<4
Cr	25	<5	24	10	<5	10	<5	<5
K%	2.91	2.96	2.92	3.90	3.64	4.37	4.33	3.93
K/Rb	227	340	178	195	264	239	193	255

CIPW Norms (Weight Percent)

	17	18	19	20	21	22	23	24
Q	-	-	-	-	-	-	-	-
Or	7.78	7.86	10.83	10.21	5.24	-	1.49	2.39
Ab	20.68	21.04	20.80	27.77	25.83	31.08	30.85	28.01
An	41.56	44.71	45.27	48.64	48.69	41.47	49.35	52.70
Ne	6.27	6.08	-	0.65	4.75	14.14	6.68	3.95
Ac	-	-	-	-	-	5.18	-	-
Ns	-	-	-	-	-	-	-	-
Di-wo	5.57	3.58	4.47	0.54	3.12	2.27	1.64	2.16
Di-fs	2.41	2.04	0.91	-	2.22	2.05	-	-
Di-en	2.98	1.54	3.18	0.46	1.00	0.40	1.42	0.87
Wo	-	-	-	-	-	0.26	1.68	1.30
Hy-en	-	-	0.29	-	-	-	-	-
Hy-fs	-	-	1.01	-	-	-	-	-
Fo	2.56	1.80	2.27	1.02	1.15	-	-	-
Fa	2.28	2.64	0.71	-	2.80	-	-	-
Mt	3.93	4.94	5.47	4.91	3.12	2.54	3.17	1.68
Hm	-	-	-	2.26	-	-	1.85	4.41
Il	3.00	2.45	3.15	2.32	1.67	0.40	1.14	1.33
Ap	1.27	1.37	1.23	1.55	0.81	0.21	0.39	0.56
Other	-	-	-	-	-	-	-	-
Total	100.29	100.06	99.58	100.34	100.44	99.99	99.66	100.36
D.I.	68.5	71.8	66.1	77.1	79.3	86.7	86.9	84.7
$\frac{100An}{An+Ab}$	15.8	15.0	19.3	17.4	9.7	0.0	2.9	4.3
Agpaitic Index	-	0.84	0.76	0.80	0.89	1.06	0.97	0.95

TABLE 7.2   Analyses of rocks from The Pleiades, Melbourne volcanic
province, Antarctica (continued).

VUW No.	25 25702	26 25701	27 25705	28 25696	29 25706	30 25699	31 25680	32 25698
SiO_2	62.71	63.84	63.86	63.90	64.36	64.56	64.83	65.16
TiO_2	0.46	0.29	0.28	0.15	0.14	0.15	0.15	0.17
Al_2O_3	17.56	16.52	16.59	15.77	16.85	16.95	15.99	16.70
Fe_2O_3	1.55	2.00	3.12	2.82	2.34	3.28	2.33	4.06
FeO	3.21	2.88	1.65	1.12	1.52	0.74	2.38	0.00
MnO	0.15	0.17	0.17	0.15	0.15	0.15	0.23	0.15
MgO	0.51	0.14	0.20	0.05	0.08	0.07	0.06	0.04
CaO	1.94	1.30	1.27	0.95	0.93	0.94	1.08	0.89
Na_2O	7.02	7.21	7.46	7.57	8.26	7.81	7.53	7.96
K_2O	5.07	5.32	5.36	5.12	5.24	5.18	5.26	5.21
P_2O_5	0.17	0.07	0.07	0.02	0.03	0.02	0.05	0.03
H_2O+				0.45				
H_2O-								
Total	100.35	99.74	100.03	99.07	99.90	99.85	99.89	100.37
Rb	184	255	254	317	321	315	254	316
Ba	792	444	445	20	12	26	74	22
Sr	310	48	49	4	3	7	7	3
Zn	80	106	101	150	146	139	141	125
Cu	6	9	11	<5	<5	<5	8	<5
Ni	<5	<5	<5	<5	<5	<5	<5	<5
V	<4	<4	<4	<4	<4	<4	<4	<4
Cr	<5	<5	<5	<5	<5	<5	<5	<5
K%	4.21	4.42	4.45	4.25	4.35	4.30	4.37	4.33
K/Rb	229	173	175	134	136	136	172	137

CIPW Norms (Weight Percent)

Q	-	-	-	0.04	-	-	1.18	0.35
Or	1.43	-	-	-	-	-	31.08	30.79
Ab	29.96	31.44	31.67	30.26	30.96	30.61	52.96	56.89
An	55.56	54.65	53.65	57.75	54.41	57.72	-	-
Ne	2.08	0.38	1.00	-	1.67	0.34	-	-
Ac	-	4.98	6.73	5.55	6.77	6.82	6.74	9.22
Ns	-	-	-	-	1.10	-	0.72	-
Di-wo	2.96	2.50	2.44	1.33	1.84	0.75	2.10	0.12
Di-fs	2.39	2.60	2.14	1.34	1.92	0.63	2.29	-
Di-en	0.74	0.18	0.48	0.12	0.14	0.17	0.08	0.10
Wo	-	-	-	0.59	-	1.14	-	1.64
Hy-en	-	-	-	-	-	-	2.26	-
Hy-fs	-	-	-	-	-	-	0.07	-
Fo	0.38	0.12	0.01	-	0.04	-	-	-
Fa	1.34	1.78	0.07	-	0.71	-	-	-
Mt	2.25	0.40	1.15	1.31	-	1.34	-	-
Hm	-	-	-	-	-	-	-	0.87
Il	0.87	0.55	0.53	0.28	0.27	0.28	0.28	0.32
Ap	0.39	0.16	0.16	0.05	0.07	0.05	0.12	0.07
Other	-	-	-	0.45	-	-		
Total	100.35	99.74	100.03	99.07	99.90	99.85	99.89	100.37
D.I.	87.6	86.5	86.3	88.0	87.0	88.7	85.2	88.0
100An An+Ab	2.5	0.0	0.0	0.0	0.0	0.0	0.0	0.0
Agpaitic Index	0.97	1.07	1.09	1.07	1.14	1.09	1.13	1.12

Explanation of Table 7.2. Analyses of rocks from The Pleiades, Melbourne volcanic province, Antarctica.

1. 25679   Basanite. Crater 4.

2. 25682   Basanite. Crater 7.

3. 25685   Nepheline hawaiite. Crater 5.

4. 25664   Trachyandesite. Cone 4, south of Mt Atlas.

5. 25663   Essexite inclusion. Cone 4, south of Mt Atlas.

6. 25703   Trachyandesite. Northern slope, Aleyone Cone.

7. 25703G   Glassy groundmass of above sample - electron microprobe analysis.

8. 25700   Nepheline mugearite. South flank of small crater on Taygete Cone.

9. 25668   Essexite inclusion. Eastern rim of Cone 1, Mt Atlas.

10. 25671   Trachyandesite. Dike, west flank of Cone 3, Mt Atlas.

11. 25691   Nepheline benmoreite. Dike, Crater 2.

12. 25690   Nepheline benmoreite. Crater 2.

13. 25704   Nepheline benmoreite. Crater 1.

14. 25661   Nepheline tristanite. Western base of Cone 2, Mt Atlas.

15. 25675   Tristanite. Southwestern flank of Cone 2, Mt Atlas.

16. 25662   Tristanite. West base of Cone 2, Mt Atlas.

17. 25688   Tristanite. Cone 6.

18. 25670   Tristanite. North side of Cone 3, Mt Atlas.

19. 25666   Tristanite. Summit of Mt Atlas.

20. 25667   K-trachyte. Northeast of summit, Mt Atlas.

21. 25674   K-trachyte. Southwestern flank of Cone 2, Mt Atlas.

22. 25683   Phonolite. Cone 7.

23. 25687 K-trachyte. Cone 6.

24. 25665 K-trachyte. Cone 4, south of Mt Atlas.

25. 25702 K-trachyte. Summit Aleyone Cone.

26. 25701 K-trachyte. Summit Aleyone Cone.

27. 25705 K-trachyte. West side of Crater 1.

28. 25696 Peralkaline K-trachyte. North side of Taygete Cone.

29. 25706 Peralkaline K-trachyte. Southwest flank of Taygete Cone.

30. 25699 Peralkaline K-trachyte. Southwest side of Taygete Cone.

31. 25680 Peralkaline K-trachyte. Crater 4.

32. 25698 Peralkaline K-trachyte. Southwest side of Taygete Cone.

TABLE 7.3 Analyses of volcanic rocks from Mt Overlord, Webb
Névé and Victory Plateau, Melbourne volcanic
province.

	1 25708	2 P34988	3 25718	4 25719	5 25720
SiO_2	41.37	42.76	49.57	56.89	58.57
TiO_2	3.55	3.17	2.42	1.15	0.80
Al_2O_3	14.18	13.72	17.52	18.74	18.93
Fe_2O_3	3.02	3.63	10.89	6.29	5.20
FeO	9.10	7.84			
MnO	0.19	0.20	0.21	0.14	0.13
MgO	8.52	8.99	3.66	1.43	0.90
CaO	10.80	11.91	6.89	3.55	2.78
Na_2O	3.55	3.61	5.42	6.70	6.82
K_2O	1.91	1.70	2.32	3.78	4.23
P_2O_5	0.67	0.76	1.03	0.42	0.26
Loss	0.20[1]		0.08	0.17	0.55
Total	97.06	98.29	100.01	99.26	99.17
Rb	44	50	61	129	147
Ba	397	486	444	801	908
Sr	772	863	924	807	714
Zn	97	81	107	88	90
Cu	59	70	33	14	9
Ni	124	147	21	6	<5
V	276	262	95	28	14
Cr	204	309	34	7	5
K%	1.59	1.41	1.93	3.14	3.51
K/Rb	361	282	316	243	239
Mg No.	61.2	63.9	44.9	35.6	29.6

CIPW Norms (Weight Percent)

	1	2	3	4	5
Or	11.29	10.05	13.71	22.34	25.00
Ab	2.31	3.89	32.52	47.79	50.95
An	17.12	16.21	16.62	9.90	8.55
Ne	15.02	14.44	7.23	4.82	3.66
Di-wo	13.40	15.83	4.52	2.08	1.48
Di-fs	3.62	3.27	2.08	0.83	0.52
Di-en	8.82	11.19	2.32	1.16	0.38
Fo	8.69	7.85	4.76	1.68	0.95
Fa	3.93	2.52	4.72	1.33	0.62
Mt	4.38	5.26	3.62	3.62	3.62
Il	6.74	6.02	4.60	2.18	1.52
Ap	1.55	1.76	2.39	0.97	0.60
Others	0.20	−	0.08	0.17	0.55
Total	97.06	98.29	99.17	98.88	98.90
D.I.	28.6	28.4	53.5	75.0	79.7
$\frac{100An}{An+Ab}$	88.1	80.6	33.8	17.2	14.4

[1] H_2O

Explanation of Table 7.3.   Analyses of volcanic rocks from
          Mt Overlord, Webb Neve and Victory Plateau,
          Melbourne volcanic province, Antarctica.

1.   25708   Basanite.   Scoria cone, western Webb Neve, 1600 m.a.s.l.

2.   P34988 Basanite.   Malta Plateau, Victoria Mountains.
             Collected by Riddolls and Hancox (1968).

3.   25718   Hawaiite.   Mt Overlord.

4.   25719   Tristanite.   Mt Overlord.

5.   25720   Tristanite.   Mt Overlord.

TABLE 7.4   Analyses of volcanic rocks from Mt Melbourne.

	1 25713	2 P34913	3 P35582	4 25714	5 25715	6 25712	7 P34911	8 P35581
SiO_2	56.06	56.4	58.2	60.86	64.18	65.06	65.2	68.7
TiO_2	1.63	1.60	0.94	0.86	0.33	0.41	0.38	0.79
Al_2O_3	15.64	17.6	17.2	15.56	15.32	15.35	16.0	10.1
Fe_2O_3	10.98	0.5	1.6	9.22	6.41	6.02	2.4	2.3
FeO_2		8.2	7.2				3.2	1.0
MnO	0.22	0.23	0.22	0.22	0.16	0.17	0.17	0.05
MgO	1.60	2.1	1.3	0.61	0.02	0.10	0.7	1.1
CaO	4.68	5.0	3.6	3.51	1.18	1.66	1.7	2.6
Na_2O	5.26	3.2	5.2	5.18	6.52	5.94	4.6	3.1
K_2O	3.2	2.0	3.7	3.59	5.13	4.82	3.7	1.6
P_2O_5	0.63	0.71	0.37	0.22	0.03	0.05	0.09	0.30
H_2O+	0.00[1]	0.14	0.17	0.00[1]	0.42[1]	0.18[1]	0.56	2.23
H_2O-		0.06	0.15				0.06	0.75
S		0.05	0.02				0.03	0.03
F		0.22						7.0
$-O=F$		0.09						2.9
Total	99.96	97.92	99.87	99.83	99.70	99.76	98.7a	98.75
Rb	91	90	80	108	142	130	130	65
Ba	682	500	1000	852	79	1570	1000	400
Sr	484	1000	800	405	4	100	70	600
Zn	128	–	–	150	175	144	–	–
Cu	10							

Explanation of Table 7.4. Analyses of rocks from Mt Melbourne,
Melbourne volcanic province, Antarctica.

1. 25313   Quartz trachyandesite. Small crater on south rim of
             summit caldera.

2. P34913   Quartz trachyandesite. (Glassy trachyandesite). Small
             cone on the east side of the main crater. (Analyst:
             Inorganic Section, Chemistry Division, D.S.I.R.).
             Nathan and Schulte, 1968.

3. P35582   Quartz tristanite. (Feldspathic trachyandesite). Sea
             cliffs near the Adelie penguin rookery. (Analyst:
             Inorganic Section, Chemistry Division, D.S.I.R.).
             Nathan and Schulte, 1968.

4. 25314   Quartz tristanite. Small parasitic cone on north
             flank of mountain, 1900 m.

5. 25315   Quartz K-trachyte. Outcrop north of small parasitic
             cone on north flank of mountain, 1800 m.

6. 25312   Quartz K-trachyte. Cliffs in the summit caldera below
             summit.

7. P34911   Quartz K-trachyte. (Trachyte). Cliffs in the summit
             caldera below summit. (Analyst: Inorganic Section,
             Chemistry Division, D.S.I.R.). Nathan and Schulte, 1968.

8. P35581. Hydrothermally altered trachyandesite scoria, northern
             side of the volcano near the summit. (Analyst:
             Inorganic Section, Chemistry Division, D.S.I.R.).
             Nathan and Schulte, 1968.

TABLE 7.5   Analyses of volcanic rocks from Cape Bird and
             Mt Bird, Ross Island.

	1 P23044	2 P23023	3	4	5	6 P23048	7
SiO_2	42.6	43.2	44.1	48.26	52.54	53.8	55.0
TiO_2	3.7	3.9	2.70	0.88	1.44	1.25	0.70
Al_2O_3	14.1	14.5	14.6	22.67	19.41	17.2	19.6
Fe_2O_3	5.7	6.7	3.57	3.22	2.90	5.8	3.79
FeO	7.8	6.3	8.77	4.56	5.31	1.9	2.04
MnO	0.3	0.3	0.22	0.11	0.23	0.25	0.12
MgO	6.15	6.5	8.71	3.73	1.91	1.60	1.17
CaO	11.7	11.45	9.07	8.68	4.60	4.4	3.65
Na_2O	4.3	4.0	4.45	4.03	7.50	8.25	7.76
K_2O	0.95	1.8	1.96	2.15	3.49	3.85	4.46
P_2O_5	0.4	0.4	0.71	1.01	0.26	0.35	0.23
H_2O+	1.16	0.60	0.15	0.32	0.16	0.28	0.43
H_2O-	0.52	0.22	0.04	0.30	0.08	0.12	0.38
CO_2			0.03		0.20		0.06
Total	99.38	99.87	99.08	99.92	100.03	99.05	99.39
Rb			33				112
Ba			560				750
Sr			950				640
Y			24				37
Zr			490				960
Zn			104				124
Cu			63				30
Ni			170				12
V			190				43
Cr			360				10
K%			1.63				3.70
K/Rb			493				311

CIPW Norm (Weight Percent)

C	—	—	—	0.35	—	—	—
Or	5.61	10.64	11.58	12.70	20.62	22.75	26.36
Ab	11.77	9.52	10.63	27.65	31.82	34.54	35.91
An	16.36	16.29	14.07	36.46	8.99	—	5.48
Ne	13.34	13.18	14.64	3.49	17.14	17.60	16.12
Ac	—	—	—	—	—	2.44	—
Di-wo	16.31	15.82	10.90	—	4.54	4.61	3.37
Di-fs	3.11	0.13	3.00	—	2.39	—	—
Di-en	11.73	13.58	7.14	—	2.10	3.98	2.91
Wo	—	—	—	—	—	3.55	1.12
Fo	2.52	1.83	10.20	6.51	1.86	—	—
Fa	0.73	0.02	4.72	3.45	2.33	—	—
Mt	8.26	9.71	5.18	4.67	4.20	3.32	4.94
Hm	—	—	—	—	—	2.67	0.38
Il	7.03	7.41	5.13	1.67	2.74	2.37	1.33
Cc	—	—	0.07	—	0.46	—	0.14
Ap	0.93	0.93	1.64	2.34	0.60	0.81	0.53
Others	1.68	0.82	0.15	0.62	0.24	0.40	0.81
Total	99.38	99.87	99.08	99.92	100.03	99.05	99.39
D.I.	30.7	33.3	36.8	43.8	69.6	74.9	78.4
$\frac{100An}{An+Ab}$	58.2	63.1	57.0	56.9	22.0	0.0	13.2

Explanation of Table 7.5. Analyses of volcanic rocks from Cape
Bird and Mt Bird, Ross Island, Antarctica.

1. P23044 Basanite. '30 ft basalt flow in cliffs adjacent to
           Caughley Beach, approximately 1 mile south of northern
           penguin rookery. Collected by H. J. Harrington.
           (Analyst: Mrs M. G. Rundle)'. Cole and Ewart, 1968.

2. P23023 Basanite. 'Basalt flow at top of scree slope leading
           to summit of Alexander Hill, from cliff at southern
           end of Romanes Beach. Collected by H. J. Harrington.
           (Analyst: Mrs M. G. Rundle)'. Cole and Ewart, 1968.

3. Basanite. Summit of Mt Bird, Ross Island. Goldich *et al.*, 1975.

4. Alkali basalt. (Kulaitic basalt). (Analyst: G. J. Burrows
           and A. B. Walkom). Jensen, 1916. It would appear as if
           the TiO_2 and Al_2O_3 analyses are in error. The TiO_2 is
           too low and the Al_2O_3 is excessively high.

5. Nepheline benmoreite. (Phyrohornblende trachyte). (Analyst:
           G. J. Burrows and A. B. Walkom). Jensen, 1916.

6. P23048 Nepheline benmoreite. 'Core of small trachyte plug,
           150 yd east of Trachyte Hill. Collected by H. J. Harrington.
           (Analyst: Mrs M. G. Rundle)'. Cole and Ewart, 1968.

7. Phonolite. Mt Bird, Ross Island. Goldich *et al.*, 1975.

TABLE 7.6 Analyses of volcanic rocks from Cape Crozier, Ross Island.

	1 22970	2	3 22977	4 22964	5	6 22954	7 P22981	8 22951	9 22958	10
SiO_2	42.11	43.47	43.54	43.60	44.0	44.50	44.8	45.53	46.38	47.40
TiO_2	4.01	3.28	2.84	4.07	2.83	3.48	3.75	2.95	3.18	0.63
Al_2O_3	15.05	12.85	14.08	14.28	14.2	15.27	15.7	17.12	17.09	20.27
Fe_2O_3	4.08	3.18	3.20	2.97	3.12	4.43	7.25	5.08	6.67	5.38
FeO	8.96	9.67	8.16	9.58	7.38	7.41	5.2	5.76	4.63	5.48
MnO	0.21	0.19	0.21	0.20	0.19	0.20	0.11	0.23	0.23	0.17
MgO	6.92	11.78	9.33	7.10	10.8	6.82	6.55	3.87	4.38	2.94
CaO	11.58	10.60	11.05	10.35	10.5	10.69	11.9	8.22	8.97	7.59
Na_2O	3.78	2.93	4.5	3.73	4.38	4.05	3.05	4.3	4.65	5.78
K_2O	1.42	1.09	1.55	1.83	1.77	1.82	1.60	2.74	2.36	2.73
P_2O_5	1.12	0.58	0.90	1.11	0.65	0.85	0.38	1.37	1.05	0.85
H_2O+		0.07			0.23		0.22	2.06[2]		0.23[2]
H_2O-		0.00			0.07		0.16			
CO_2		0.09			0.02					
Total	99.24	99.80[1]	99.36	98.82	100.14	99.52	100.67	99.23	99.59	99.45
Rb	27	26	49	30	56	34	35	45	51	
Ba	339	280	395	341	510	467	450	551	530	
Sr	1264	840	995	1151	950	1203	1228	1893	1426	
Y		31			31					
Zr		290	304		330	302		423	385	
Zn	96	112	92	105	78	92	101	127	110	
Cu	44	57	54	50	44	68	49	33	26	
Ni	56	210	156	74	170	98	115	14	26	
V	311	280	236	266	210	227	249	95	206	
Cr	121	760	390	186	430	199	245	17	56	
K%	1.18	0.90	1.29	1.52	1.45	1.51	1.33	2.27	1.96	
K/Rb	437	354	263	507	262	444	380	504	384	
Mg No.	54.5	67.2	64.9	55.9	69.8	56.7	55.0	45.0	47.4	38.4

CIPW Norms (Weight Percent)

	1	2	3	4	5	6	7	8	9	10
Or	8.39	6.44	9.16	10.81	10.46	10.76	9.46	16.19	13.95	16.13
Ab	9.25	10.90	6.04	13.03	4.83	13.57	15.11	23.97	23.66	21.26
An	19.90	18.69	13.64	16.82	13.86	18.11	24.42	19.32	18.79	21.30
Ne	12.32	7.52	17.35	10.04	17.46	11.21	5.80	6.73	8.50	14.98
Ac	-	-	-	-	-	-	-	-	-	-
Di-wo	12.62	12.21	14.74	11.39	14.14	12.26	13.42	5.22	7.87	4.51
Di-fs	3.33	2.87	3.49	3.55	2.54	2.37	-	0.79	-	1.73
Di-en	8.37	8.37	10.08	7.14	10.28	8.30	11.59	3.92	6.80	2.58
Wo	-	-	-	-	-	-	-	-	-	-
Fo	6.21	14.70	9.22	7.39	11.64	5.74	3.31	4.01	2.88	3.32
Fa	2.72	5.56	3.52	4.05	3.18	1.70	-	0.89	-	2.45
Mt	5.92	4.61	4.64	4.31	4.52	6.42	6.25	7.37	6.46	7.80
Ilm	-	-	-	-	-	-	2.94	-	2.22	-
Il	7.62	6.23	5.39	7.73	5.38	6.61	7.12	5.60	6.04	1.20
Ap	2.60	1.34	2.08	2.57	1.51	1.97	0.88	3.17	2.43	1.97
Others	-	0.35	-	-	0.34	-	0.38	2.06	-	0.23
Total	99.24	99.80	99.36	98.82	100.14	99.52	100.67	99.23	99.59	99.45
D.I.	30.0	24.9	32.6	33.9	32.8	35.5	30.4	46.9	46.1	52.4
$\frac{100An}{An+Ab}$	68.3	63.2	69.3	56.3	74.2	57.2	61.8	44.6	44.3	50.1
Agpaitic Index	-	-	-	-	-	-	-	-	-	-

[1]Includes F=0.04, less O=F=0.02; [2]Loss on ignition.

TABLE 7.6 Analyses of volcanic rocks from Cape Crozier (continued)

	11 22962	12 P22984	13 P22973	14 P22974	15 P22986	16 P22971	17 P22985	18	19	20 22952
SiO_2	54.28	57.04	57.07	57.16	57.2	57.40	57.79	57.9	57.95	58.27
TiO_2	0.84	0.25	0.38	0.38	0.25	0.29	0.27	0.44	0.40	0.42
Al_2O_3	20.01	19.79	20.02	20.03	19.6	19.92	19.74	19.6	20.43	19.38
Fe_2O_3	2.25	4.76	2.88	4.93	2.75	3.60	2.50	5.16	3.43	3.67
FeO	3.04	0.17	2.12	0.20	2.25	1.30	2.34	0.58	1.35	1.78
MnO	0.21	0.21	0.22	0.22	0.05	0.20	0.20	0.21	0.07	0.22
MgO	0.98	0.15	0.12	0.17	0.50	0.17	0.16	0.44	0.26	0.41
CaO	3.26	1.29	2.04	1.76	1.85	1.57	1.57	2.17	1.90	1.95
Na_2O	8.45	9.3	8.65	8.6	8.25	8.5	8.2	8.18	8.32	8.1
K_2O	4.81	5.72	5.43	5.40	5.85	5.83	5.79	4.97	5.96	5.15
P_2O_5	0.27	0.04	0.05	0.06	0.03	0.05	0.06	0.11	0.07	0.12
H_2O+	1.22^2	0.87^2	0.61^2	0.84^2	0.36	0.63^2	0.51^2	0.01	0.39	0.46^2
H_2O-					0.36			0.03	0.23	
CO_2								0.04		
Total	99.62	99.59	99.59	99.75	99.30	99.46	99.13	99.84	100.76	99.93
Rb	131	146	130	129	132	142	136	125		134
Ba	568	514	1306	1393	690	593	655	990		928
Sr	626	156	512	538	164	143	163	520		481
Y									26	
Zr	813	813	713	708		781	754	580		789
Zn	126	118	113	107	105	104	107	111		105
Cu	29	7	8	8	7	7	6	25		7
Ni	10	< 5	< 5	< 5	< 5	< 5	< 5	< 10		< 5
V	36	0	0	0	0	0	0	< 10		0
Cr	22	< 5	< 5	< 5	< 5	< 5	< 5	< 5		< 5
K%	3.99	4.75	4.51	4.48	4.86	4.84	4.81	4.12		4.28
K/Rb	304	325	347	347	368	341	354	330		319

CIPW Norms (Weight Percent)

	11	12	13	14	15	16	17	18	19	20
Or	28.42	33.80	32.09	31.91	34.57	34.45	34.22	29.37	35.22	30.43
Ab	28.81	29.60	35.96	38.72	32.50	35.58	36.84	43.20	36.03	43.73
An	2.46	-	-	0.10	-	-	-	2.08	0.80	1.31
Ne	23.13	21.86	19.93	18.45	19.37	18.65	17.58	14.09	18.62	13.44
Ac	-	7.71	0.40	-	1.38	1.69	0.08	-	-	-
Di-wo	4.99	0.43	1.59	0.49	3.14	0.49	2.38	1.27	0.75	1.18
Di-fs	2.60	-	1.41	-	1.93	-	2.18	-	-	-
Di-en	2.33	0.37	0.30	0.42	1.24	0.42	0.40	1.10	0.65	1.02
Wo	-	2.13	2.50	2.95	0.61	2.63	0.71	1.95	2.66	1.98
Fo	0.08	-	-	-	-	-	-	-	-	-
Fa	0.10	-	-	-	-	-	-	-	-	-
Mt	3.26	0.51	3.98	0.16	3.30	4.00	3.59	1.28	3.42	5.24
Hm	-	1.74	-	4.85	-	0.26	-	4.28	1.07	0.06
Il	1.60	0.48	0.72	0.72	0.48	0.55	0.51	0.84	0.76	0.80
Ap	0.63	0.09	0.12	0.14	0.07	0.12	0.14	0.26	0.16	0.28
Others	1.22	0.87	0.61	0.84	0.72	0.63	0.51	0.13	0.62	0.46
Total	99.62	99.59	99.59	99.75	99.30	99.46	99.13	99.84	100.76	99.93
D.I.	80.4	85.3	88.0	89.1	86.4	88.7	88.6	86.7	89.9	87.6
$\dfrac{100An}{An + Ab}$	7.9	0.0	0.0	0.3	0.0	0.0	0.0	4.6	2.2	2.9
Agpaitic Index	0.96	1.09	1.00	1.00	1.02	1.02	1.00	0.96	0.99	0.98

Explanation of Table 7.6.   Analyses of volcanic rocks from Cape
              Crozier, Ross Island.

1.   22970   Basanite. 1 km northeast of Post Office Hill.

2.   Basanite. Younger sequence, Cape Crozier. Goldich *et al.*, 1975.

3.   22977   Basanite. Coastal cliffs 1.5 km south of Discovery II pole.

4.   22964   Basanite. Scoria cone, 3 km NNE of The Knoll.

5.   Basanite. Older sequence, Cape Crozier, Goldich *et al.*, 1975.

6.   22954   Basanite. Small flow on southwest rim of The Knoll.

7.   P22981   Basanite. Flow on north rim of The Knoll. Collected by
              H. J. Harrington. (Analyst: Chemistry Division, D.S.I.R.).

8.   22961   Hawaiite. Flow, 50 m west of summit of Topping Peak.

9.   22958   Hawaiite. Western base of Kyle Peak.

10. Basanite. (Hornblende basalt), Foot of Mt Terror. (Analyst.
              G. T. Prior), Prior, 1902. TiO_2 is low and Al_2O_3 is high
              and appear to be in error.

11. 22962   Kaersutite phonolite. Dike west of Topping Peak summit.

12. P22984   Pyroxene phonolite. '100 ft below the top of the trachyte
              "cone" (Kyle Cone) between The Knoll and Mt Terror about
              2½ miles west of The Knoll'. Collected by H. J. Harrington.

13. P22973   Kaersutite phonolite. 'Flows from north side (seaward)
              of Post Office Hill, 500 ft below summit'. Collected by
              H. J. Harrington.

14. P22974   Kaersutite phonolite. As for P22973. Collected by
              H. J. Harrington.

15. P22986   Pyroxene phonolite. 'Sea cliff southwest corner, The
              Knoll'. Collected by H. J. Harrington. (Analyst: Chemistry
              Division, D.S.I.R.).

16. P22971   Pyroxene phonolite. 'Top of crater rim, The Knoll on north
              side at 1100 ft'. Collected by H. J. Harrington.

17. P22985   Pyroxene phonolite. As for P22986. Collected by
              H. J. Harrington.

18. Kaersutite phonolite. Post Office Hill, Cape Crozier. Goldich
              et al., 1975.

19. Phonolite. (Phonolitic trachyte). Cape Crozier. Prior, 1907.

20. 22952. Kaersutite phonolite. Southeast of Post Office Hill.

TABLE 7.7   Analyses of rocks from Hut Point Peninsula.

	1	2	3 22884	4	5	6	7	8
SiO_2	39.78	41.98	41.35	41.56	41.56	41.64	41.78	42.10
TiO_2	0.07	1.10	4.16	4.54	4.50	4.36	4.58	4.93
Al_2O_3	0.28	4.00	15.21	15.50	15.55	13.80	15.72	14.87
Fe_2O_3	2.73	4.17	3.35	13.48	13.10	7.93	13.55	3.26
FeO	10.51	10.52	9.08			5.41		9.76
MnO			0.22	0.21	0.20	0.19	0.21	0.07
MgO	45.29	27.17	5.40	5.83	5.81	8.78	6.07	8.88
CaO	tr	9.62	9.71	8.76	8.90	11.16	9.34	10.63
Na_2O	0.45	0.47	4.18	4.12	3.77	2.14	3.76	3.20
K_2O	0.06	0.03	1.92	1.90	1.78	1.40	1.79	1.80
P_2O_5			1.46	1.00	1.01	0.96	1.00	0.58
H_2O+	0.29	0.19	2.70	2.56^3	3.20^3	0.47	1.67^3	0.12
H_2O-	0.21	0.23				0.62		0.11
CO_2			0.10			0.05		
Total	100.11^1	99.99^2	98.84	99.46	99.38	100.61^4	99.47	100.31
Rb			40		22			
Ba			397		348			
Sr			1347		1133			
Zn			110		104			
Cu			30		33			
Ni			13		31			
V			224		267			
Cr			17		26			
K%			1.59		1.48			
K/Rb			398		673			
Mg No.	88.4	80.6	49.4	51.2	51.8	60.5	52.1	60.4

CIPW Norms (Weight Percent)

	1	2	3	4	5	6	7	8
Or		0.18	11.35	11.23	10.52	8.27	10.58	10.64
Ab		2.62	13.14	12.45	14.32	15.72	12.32	5.74
An		8.72	17.07	18.19	20.25	23.91	20.73	20.89
Ne		0.74	12.04	12.14	9.52	1.29	10.56	11.56
Ac		-	-	-	-	-	-	-
Di-wo		16.29	8.74	7.82	7.23	10.38	7.96	11.71
Di-fs		2.46	2.94	3.10	2.76	-	3.08	2.65
Di-en		12.21	5.32	4.40	4.14	8.97	4.54	8.11
Wo		-	-	-	-	-	-	-
Fo		38.87	5.70	7.09	7.24	9.04	7.41	9.82
Fa		8.62	3.48	5.49	5.31	-	5.54	3.53
Mt		6.05	4.86	2.90	2.90	5.42	2.90	4.73
Cm		0.75	-	-	-	-	-	-
Hm		-	-	-	-	4.19	-	-
Il		2.09	7.90	8.62	8.55	8.28	8.70	9.36
Cc		-	0.23	-	-	0.11	-	-
Ap		-	3.38	2.32	2.34	2.22	2.32	1.34
Others		0.42	2.70	2.56	3.20	2.79	1.67	0.23
Total		99.99	98.84	98.31	98.27	100.61	98.32	100.31
D.I.		3.5	36.5	35.8	34.4	25.3	33.5	27.9
$\frac{100An}{An+Ab}$		76.9	56.5	59.4	58.6	60.3	62.7	78.4

[1]Includes Cr_2O_3=0.44;   [2]Includes Cr_2O_3=0.51;   [3]Loss on ignition;
[4]Includes SO_3=1.70.

TABLE 7.7 Analyses of rocks from Hut Point Peninsula (continued).

	9	10	11 22887	12 22879	13 22899	14	15	16 22896
SiO_2	42.14	42.49	42.51	42.51	42.70	42.81	43.15	43.30
TiO_2	4.90	4.63	4.26	4.54	4.26	4.63	4.09	4.15
Al_2O_3	14.95	15.98	13.78	15.58	13.61	15.96	12.33	15.10
Fe_2O_3	2.90	14.06	2.62	2.72	3.76	13.74	4.66	3.52
FeO	9.71		9.86	9.94	9.10		9.56	9.52
MnO	0.12	0.21	0.19	0.20	0.18	0.22	0.19	0.21
MgO	9.47	6.36	8.73	6.42	9.15	5.93	9.05	6.78
CaO	10.32	9.24	10.86	8.90	10.87	9.35	10.75	9.97
Na_2O	3.27	3.61	3.54	3.79	3.49	3.90	3.17	4.12
K_2O	1.80	1.78	1.76	1.67	1.74	1.93	1.57	1.61
P_2O_5	0.40	1.01	0.87	1.02	0.86	1.03	0.82	1.30
H_2O+	0.16	1.52[3]	0.20	2.30	0.09	0.38[3]	0.48	0.29
H_2O-	0.12						0.29	
CO_2				0.10				
Total	100.26	100.89	99.18	99.69	99.81	99.88	100.14[5]	99.87
Rb			33	30	32			33
Ba			321	333	320			366
Sr			1004	1140	1015			1238
Zn			90	111	93			109
Cu			52	57	52			37
Ni			125	57	126			53
V			304	282	309			244
Cr			275	47	282			104
K%			1.46	1.39	1.44			1.34
K/Rb			442	463	450			406
Mg No.	62.7	52.3	60.9	53.1	61.6	51.2	59.0	53.9

CIPW Norm (Weight Percent)

	9	10	11	12	13	14	15	16
Or	10.64	10.52	10.40	9.87	10.28	11.40	9.28	9.51
Ab	4.68	13.80	6.33	17.02	7.57	13.10	11.90	15.36
An	20.80	22.14	16.51	20.57	16.33	20.34	14.78	17.95
Ne	12.46	9.07	12.80	8.15	11.90	10.78	8.08	10.56
Ac	-	-	-	-	-	-	-	-
Di-wo	11.60	7.14	13.23	6.80	13.35	8.06	13.86	9.61
Di-fs	2.58	2.81	3.68	2.30	2.84	3.22	3.10	2.92
Di-en	8.06	4.04	8.63	4.13	9.38	4.52	9.62	6.08
Wo	-	-	-	-	-	-	-	-
Fo	10.88	8.27	9.19	8.31	9.40	7.18	9.06	7.57
Fa	3.85	6.34	4.31	5.09	3.14	5.63	3.22	4.01
Mt	4.20	2.90	3.80	3.94	5.45	2.90	6.76	5.10
Cm	-	-	-	-	-	-	0.04	-
Hm	-	-	-	-	-	-	-	-
Il	9.31	8.79	8.09	8.62	8.09	8.79	7.77	7.88
Cc	-	-	-	0.23	-	-	-	-
Ap	0.93	2.34	2.02	2.36	1.99	2.39	1.90	3.01
Others	0.28	1.52	0.20	2.30	0.09	0.38	0.77	0.29
Total	100.26	99.68	99.18	99.69	99.81	98.70	100.14	99.87
D.I.	27.8	33.4	29.5	35.0	29.7	35.3	29.3	35.4
$\dfrac{100An}{An+Ab}$	81.6	61.6	72.3	54.7	68.3	60.8	55.4	53.9

[5]Includes $Cr_2O_3=0.03$.

TABLE 7.7 Analyses of rocks from Hut Point Peninsula (continued)

	17	18	19	20 25793	21	22	23 22888
SiO_2	43.55	43.7	43.92	54.82	55.47	55.9	56.89
TiO_2	3.86	3.64	4.19	1.16	1.32	0.76	0.56
Al_2O_3	15.37	11.9	17.42	20.41	20.67	20.5	20.82
Fe_2O_3	3.06	1.89	4.09	1.99	2.83	2.65	2.37
FeO	8.71	9.04	8.83	2.52	1.86	1.58	1.16
MnO	0.18	0.19	0.09	0.18	0.02	0.20	0.17
MgO	8.16	12.9	4.89	1.24	1.43	0.87	0.56
CaO	9.48	10.0	9.53	3.46	3.43	2.98	2.33
Na_2O	4.23	3.52	4.60	8.50	8.33	9.04	9.70
K_2O	2.17	1.28	2.17	4.57	4.86	4.26	4.83
P_2O_5	0.93	0.82	0.67	0.26	0.03	0.17	0.13
H_2O+	0.44	0.19	0.11	0.49[3]	0.12	0.35	0.12
H_2O-	0.21	0.01	0.06		0.08	0.04	
CO_2		0.01				0.01	
Total	100.35	99.09	100.57	99.60	100.46[6]	99.31	99.64
Rb		42		139		137	146
Ba		390		709		860	797
Sr		880		782		780	758
Zn		79		105		108	102
Cu		42		14		34	8
Ni		290		8		12	<5
V		260		55		48	18
Cr		570		8		10	9
K%		1.06		3.79		3.54	4.01
K/Rb		253		273		258	275
Mg No.	60.9	72.4	46.1	–	–	–	–

CIPW Norms (Weight Percent)

	17	18	19	20	21	22	23
Or	12.82	7.56	12.82	27.01	28.72	25.17	28.54
Ab	9.20	9.86	12.13	30.90	30.44	37.61	34.92
An	16.54	12.89	20.47	4.04	4.66	2.78	–
Ne	14.41	10.80	14.52	22.22	21.69	21.07	24.53
Ac	–	–	–	–	–	–	1.66
Di-wo	10.19	13.07	9.36	4.77	4.12	2.51	1.65
Di-fs	2.52	2.70	2.93	1.39	–	–	0.04
Di-en	6.89	9.24	5.86	3.06	3.56	2.17	1.40
Wo	–	–	–	–	0.96	2.02	2.83
Fo	9.41	16.04	4.43	0.02	–	–	–
Fa	3.79	5.16	2.44	0.01	–	–	–
Mt	4.44	2.74	5.93	2.88	2.23	3.54	2.61
Cm	–	–	–	–	–	–	–
Hm	–	–	–	–	1.29	0.21	–
Il	7.33	6.91	7.96	2.20	2.51	1.44	1.06
Cc	–	0.02	–	–	–	0.02	–
Ap	2.16	1.90	1.55	0.60	0.07	0.39	0.30
Others	0.65	0.20	0.17	0.49	0.21	0.39	0.12
Total	100.35	99.09	100.57	99.60	100.46	99.31	99.64
D.I.	36.4	28.2	39.5	80.1	80.8	83.8	88.0
$\frac{100An}{An+Ab}$	64.3	56.7	62.8	11.6	13.3	6.9	0.0

[6]Includes SrO=0.01.

Explanation of Table 7.7. Analyses of rocks from Hut Point
            Peninsula, Ross Island.

1. Dunite Inclusion. Forbes, 1963.

2. Peridotite Inclusion. Forbes, 1963.

3. 22884   Basanite. 1 km north of Castle Rock.

4. Basanite. Clast in hyaloclastite base of Castle Rock. Luckman, 1974.

5. Basanite. Clast in hyaloclastite, Castle Rock. Luckman, 1974.

6. Basanite (Leucite tephrite). Top of Crater Hill. (Analyst Hogarth).
            Jensen, 1916. Smith (1954) re-examined this sample and
            found only nepheline and no leucite.

7. Basanite. Clast in hyaloclastite, Castle Rock. Luckman, 1974.

8. Basanite. (Limburgite-like basalt). Ridge Road, Winter Quarters.
            (Analyst: G. T. Prior). Prior, 1907.

9. Basanite. (Olivine basalt). The Gap. (Analyst: G. T. Prior).
            Prior, 1907.

10. Basanite. Clast in hyaloclastite, Castle Rock. Luckman, 1974.

11. 22887   Basanite. 2. 1 km west-southwest of Crater Hill.

12. 22879   Basanite. Dike Castle Rock.

13. 22899   Basanite. Fortress Rock.

14. Basanite. Summit Castle Rock. Luckman, 1974.

15. Basanite. (Basanitoid). Hut Point Peninsula. (Analyst:
            M. Chiba). Forbes and Kuno, 1965.

16. 22896   Basanite. First Crater.

17. Basanite. (Basanitoid). Hut Point Peninsula. (Analyst: M. Chiba).
            Forbes and Kuno, 1965.

18. Basanite. Older sequence, Cape Armitage. Goldich *et al.*, 1975.

19. Basanite. (Hornblende basalt). Sulphur Cones. (Analyst: G. T. Prior).
            Prior, 1907.

20. 25793   Kaersutite phonolite. Observation Hill.

21. Kaersutite phonolite. (Hornblende trachyte). Observation Hill.
            (Analyst: G. T. Prior). Prior, 1907.

22. Kaersutite phonolite. Observation Hill. Goldich *et al.*, 1975.

23. 22888   Kaersutite phonolite. Flow north side of The Gap.

TABLE 7.8 Analyses of volcanic core samples from Dry Valley Drilling Project Holes 1 and 2.

	1 2-152.07	2 2-99.34	3 1-121.88	4 2-112.72	5 2-103.15	6 1-88.55	7 1-91.45	8 1-187.64	9 2-81.63
SiO_2	41.34	41.68	41.68	41.69	41.80	42.15	42.73	43.26	47.27
TiO_2	4.12	4.06	4.34	4.17	4.15	4.66	4.51	3.60	3.00
Al_2O_3	13.18	12.92	13.32	12.96	12.84	15.84	15.85	12.93	17.65
Fe_2O_3	5.81	3.06	3.77	3.92	4.29	4.73	4.68	2.50	3.64
FeO	6.06	8.48	8.24	8.05	7.74	8.27	8.21	9.04	6.04
MnO	0.18	0.18	0.18	0.18	0.18	0.22	0.21	0.19	0.21
MgO	11.65	12.13	11.85	11.99	12.12	5.54	5.85	11.72	3.84
CaO	10.94	11.32	11.56	11.40	11.53	10.60	10.54	11.81	7.79
Na_2O	3.00	3.16	2.90	3.09	3.03	4.51	4.19	3.00	5.82
K_2O	1.66	1.48	1.50	1.53	1.50	2.09	2.05	1.38	2.91
P_2O_5	0.83	0.84	0.89	0.85	0.83	1.30	1.13	0.78	0.80
Loss	0.24	-	0.06	0.08	-	0.10	0.11	0.10	0.09
Total	99.01	99.31	100.29	99.91	100.01	100.01	100.06	100.31	99.06
Rb	31	30	29	29	30	41	41	28	68
Ba	284	277	268	269	268	348	347	253	543
Sr	868	829	853	854	834	1242	1224	777	1408
Zn	86	82	89	79	82	109	103	90	101
Cu	63	52	48	55	54	42	48	73	26
Ni	250	276	249	253	259	25	42	253	19
V	296	300	316	292	330	291	281	264	148
Cr	370	469	382	477	451	31	62	536	31
K%	1.38	1.23	1.24	1.27	1.24	1.74	1.70	1.15	2.42
K/Rb	445	410	429	438	415	423	415	411	356
Mg No.	69.3	70.2	69.0	69.3	69.5	49.1	50.7	69.4	47.4

CIPW Norms (Weight Percent)

	1	2	3	4	5	6	7	8	9
Or	9.81	8.75	8.86	9.04	8.86	12.35	12.11	8.16	17.20
Ab	6.03	2.42	3.42	3.09	3.48	9.32	10.74	4.68	19.44
An	17.59	16.70	18.90	16.97	17.00	16.80	18.38	17.74	13.44
Ne	10.49	13.17	11.44	12.49	12.00	15.63	13.39	11.22	16.15
Di-wo	13.05	14.18	13.63	14.21	14.52	11.40	11.07	14.93	8.34
Di-fs	-	2.32	1.82	1.82	1.56	2.34	2.24	3.21	2.07
Di-en	11.28	10.50	10.39	10.89	11.36	8.07	7.86	10.46	5.63
Wo	-	-	-	-	-	-	-	-	-
Fo	12.43	13.82	13.40	13.29	13.19	4.01	4.70	13.12	2.76
Fa	-	3.36	2.60	2.45	2.00	1.28	1.48	4.43	1.12
Mt	8.18	4.44	5.47	5.68	6.22	6.86	6.79	3.62	5.28
Hm	0.17	-	-	-	-	-	-	-	-
Il	7.82	7.71	8.24	7.92	7.88	8.85	8.56	6.84	5.70
Ap	1.92	1.95	2.06	1.97	1.92	3.01	2.62	1.81	1.85
Others	0.24	-	0.06	0.08	-	0.10	0.11	0.10	0.09
Total	99.01	99.31	100.29	99.91	100.01	100.01	100.06	100.31	99.06
D.I.	26.3	24.3	23.7	24.6	24.3	37.3	36.2	24.0	52.8
$\frac{100An}{An+Ab}$	74.5	87.3	84.7	84.6	83.0	64.3	63.1	79.1	40.9

TABLE 7.8   Analyses of volcanic core samples from Dry Valley Drilling Project
Holes 1 and 2 (continued).

	10 2-70.41	11 2-47.42	12 2-28.37	13 2-39.28	14 2-13.49	15 2-54.72	16 1-85.35	17 1-57.94	18 1-131.36
SiO_2	47.27	49.28	49.36	50.76	51.32	51.90	52.32	53.08	55.78
TiO_2	2.95	2.68	2.49	2.23	2.03	1.85	1.62	1.58	1.29
Al_2O_3	17.61	18.41	18.18	18.88	18.82	19.31	19.55	19.77	19.00
Fe_2O_3	3.35	2.98	2.47	2.58	3.00	3.01	4.45	2.70	3.59
FeO	6.06	5.48	5.18	4.72	3.65	3.96	2.15	3.45	2.46
MnO	0.21	0.20	0.18	0.19	0.18	0.20	0.20	0.20	0.20
MgO	3.72	3.19	3.39	2.67	2.78	2.07	1.81	1.67	1.76
CaO	7.76	6.84	6.71	5.99	5.73	5.43	4.99	4.69	4.33
Na_2O	6.07	6.37	6.58	6.78	6.84	7.26	7.48	7.58	7.00
K_2O	3.11	3.43	3.49	3.65	3.88	3.70	3.95	4.15	3.64
P_2O_5	0.81	0.65	0.65	0.49	0.52	0.60	0.47	0.42	0.40
Loss	0.40[1]	0.31	0.31	0.27	0.47		0.65	0.34	0.09
Total	99.32	99.82	98.99	99.21	99.22	99.29	99.64	99.63	99.54
Rb	72	85	94	96	111	97	98	110	113
Ba	545	577	564	617	599	695	739	716	728
Sr	1374	1160	998	1062	860	1194	1256	1049	912
Zn	111	106	96	100	94	109	97	112	108
Cu	29	24	14	17	22	15	14	16	14
Ni	22	14	26	14	19	8	7	6	15
V	208	139	126	115	100	77	68	73	54
Cr	45	20	92	24	44	15	17	13	33
K%	2.58	2.85	2.90	3.03	3.22	3.07	3.28	3.44	3.02
K/Rb	358	335	308	316	290	316	335	313	267
Mg No.	47.2	46.1	50.0	45.3	48.9	40.4	39.1	38.3	40.3

CIPW Norms (Weight Percent)

	10	11	12	13	14	15	16	17	18
Or	18.40	20.27	20.62	21.57	22.93	21.86	23.34	24.52	21.51
Ab	17.31	21.29	20.55	24.49	25.67	28.79	29.61	29.14	43.23
An	11.62	11.51	9.76	10.30	9.19	9.17	8.10	7.66	9.67
Ne	18.45	17.67	19.03	17.81	17.45	17.68	18.25	18.96	8.67
Di-wo	9.01	7.59	8.05	6.77	6.61	5.78	5.22	5.37	3.84
Di-fs	2.47	2.19	2.28	2.06	0.88	1.56	−	1.55	−
Di-en	5.91	4.90	5.22	4.28	5.05	3.81	4.51	3.46	3.32
Wo	−	−	−	−	−	−	0.46	−	−
Fo	2.35	2.14	2.26	1.66	1.32	0.94	−	0.49	0.75
Fa	1.09	1.05	1.09	0.88	0.25	0.42	−	0.24	−
Mt	4.86	4.32	3.58	3.74	4.35	4.36	2.89	3.92	4.84
Hm	−	−	−	−	−	−	2.46	−	0.25
Il	5.60	5.09	4.73	4.24	3.86	3.51	3.08	3.00	2.45
Ap	1.88	1.51	1.51	1.14	1.20	1.39	1.09	0.97	0.93
Others	0.40	0.31	0.31	0.27	0.47	−	0.65	0.34	0.09
Total	99.32	99.82	98.99	99.21	99.22	99.29	99.64	99.63	99.54
D.I.	54.1	59.2	60.2	63.9	66.0	68.3	71.2	72.6	73.4
$\frac{100An}{An+Ab}$	40.2	35.1	32.2	29.6	26.4	24.2	21.5	20.8	18.3

[1] H_2O.

Explanation of Table 7.8. Analyses of volcanic core samples from Dry
Valley Drilling Project   Holes 1 and 2.

1.	2-152.07 m	Basanite.
2.	2-99.34 m	Basanite.
3.	1-121.88 m	Basanite.
4.	2-112.72 m	Basanite.
5.	2-103.15 m	Basanite.
6.	1-88.55 m	Basanite.
7.	1-91.45 m	Basanite.
8.	1-187.64 m	Basanite.
9.	2-81.63 m	Nepheline hawaiite.
10.	2-70.41 m	Nepheline hawaiite.
11.	2-47.42 m	Nepheline hawaiite.
12.	2-28.37 m	Nepheline mugearite.
13.	2-39.28 m	Nepheline mugearite.
14.	2-13.49 m	Nepheline benmoreite.
15.	2-54.72 m	Nepheline benmoreite.
16.	1-85.35 m	Nepheline benmoreite-dike.
17.	1-57.94 m	Nepheline benmoreite.
18.	1-131.36 m	Benmoreite.

TABLE 7.9. Analyses of volcanic rocks from the Dellbridge Islands, Tryggve Point and Turks Head

	1	2	3	4 25754	5 -Gmass	6 25758	7 -Gmass	8
SiO_2	45.36	46.98	47.0	47.27	44.99	47.44	45.70	47.56
TiO_2	2.68	2.94	2.7	2.43	3.20	2.49	3.21	2.60
Al_2O_3	17.26	16.75	17.5	19.31	16.72	19.30	16.83	18.77
Fe_2O_3	10.43	2.80	11.0	9.35	12.16	9.49	12.31	1.66
FeO		8.18						7.13
MnO	0.21	0.29	0.25	0.22	0.26	0.20	0.26	0.20
MgO	3.29	3.99	2.6	2.50	3.35	2.65	3.26	2.82
CaO	7.79	8.41	6.95	7.78	6.92	7.75	6.85	7.82
Na_2O	5.27	4.81	5.85	5.61	5.78	5.68	5.75	5.15
K_2O	2.66	1.97	3.4	2.52	2.95	2.66	3.20	2.68
P_2O_5	1.01	1.48	1.2	1.19	1.40	1.21	1.45	0.07
H_2O+	4.51[1]	1.28	1.4[1]	1.58[1]	1.81[1]	1.08[1]	1.24[1]	1.27
H_2O-		0.31						
CO_2								0.82
Total	100.47	100.23[2]	99.85	99.76	99.54	99.95	100.06	98.82[3]
Rb			62	51	63	52		
Ba		350	573	483	529	563		
Sr			1018	1375	991	1378	~1800	
Y								
Zr								
Zn			117	100	123	102		
Cu			33	41	52	44		
Ni			<5	<5	<5	<5		
V				52	68	51		
Cr			6	30	12	5		
K%			2.82	2.09	2.45	2.21		
K/Rb			455	410	389	425		

CIPW Norms (Weight Percent)

	1	2	3	4	5	6	7	8
Or	15.72	11.64	20.09	14.89	17.43	15.72	18.91	15.84
Ab	19.31	28.03	19.69	24.98	18.73	23.97	18.90	18.89
An	15.58	18.29	11.45	20.06	10.96	19.31	10.66	20.18
Ne	13.69	6.86	16.15	12.18	16.35	13.05	16.12	13.37
Di-wo	6.88	5.78	6.34	4.49	5.94	4.69	5.78	7.82
Di-fs	3.08	2.57	3.49	2.08	3.06	2.12	3.06	4.07
Di-en	3.60	3.04	2.83	2.30	2.80	2.44	2.67	3.66
Fo	3.22	4.84	2.56	2.75	3.88	2.92	3.82	2.36
Fa	3.03	4.50	3.47	2.75	4.66	2.80	4.84	2.88
Mt	3.62	4.06	3.62	3.62	3.62	3.62	3.62	2.41
Il	5.09	5.58	5.13	4.62	6.08	4.73	6.10	4.94
Ap	2.34	3.43	2.78	2.76	3.24	2.80	3.36	0.16
Others	4.51	1.59	1.40	1.58	1.81	1.08	1.24	2.15
Total	99.67	100.21	99.00	99.08	98.58	99.25	99.08	98.73
D.I.	48.7	46.5	55.9	52.1	52.5	52.7	53.9	48.1
$\frac{100An}{An + Ab}$	44.6	39.5	36.8	44.5	36.9	44.6	36.1	51.6

[1]Loss on ignition; [2]Includes BaO=0.04; [3]Includes SO_3=0.06, SrO=0.21.

TABLE 7.9   Analyses of volcanic rocks from the Dellbridge Islands,
Tryggve Point and Turks Head (continued)

	9	10	11	12 25742	13 25748	14 -Gmass	15 25749	16 25745
SiO_2	48.56	49.29	50.36	51.17	53.09	52.52	54.00	57.49
TiO_2	2.10	2.02	1.93	1.86	1.66	1.64	1.40	0.63
Al_2O_3	19.32	18.41	19.59	19.49	20.09	18.63	19.18	19.40
Fe_2O_3	8.16	8.58	2.82	8.01	7.10	7.96	7.90	6.36
FeO			5.16					
MnO	0.19	0.24	0.20	0.20	0.19	0.24	0.22	0.23
MgO	2.44	2.01	2.14	1.87	1.66	2.02	1.58	0.65
CaO	6.43	5.10	6.46	5.52	4.81	3.78	3.81	2.52
Na_2O	6.45	6.79	6.57	6.70	6.80	7.29	7.00	7.59
K_2O	3.01	3.91	3.32	3.71	3.88	4.88	4.35	4.66
P_2O_5	0.88	0.97	0.85	1.12	0.84	1.02	0.54	0.18
H_2O+			0.23	0.25[1]			0.16	0.13[1]
H_2O-			0.03					
CO_2			0.07					
Total	97.54	97.32	99.86[4]	99.90	100.12	99.98	100.14	99.84
Rb	87	85	68	74	84	113	101	107
Ba	807	703	760	740	789	658	791	1073
Sr	1087	1054	1180	1111	1194	568	610	536
Y			37					
Zr			470					
Zn	125	99	89	92	99	121	108	100
Cu	10	15	12	28	11	15	10	7
Ni	<5	<5	<10	<5	<5	<5	<5	<5
V	47		39	36	<3	14	24	0
Cr	<5	<5	<5	12	9	14	7	11
K%	2.50	3.25	2.76	3.08	3.22	4.05	3.61	3.87
K/Rb	287	382	408	416	382	383	358	362

CIPW Norms (Weight Percent)

	9	10	11	12	13	14	15	16
Or	17.79	23.10	19.62	21.92	22.93	28.84	25.70	27.54
Ab	25.51	25.04	26.99	30.08	34.40	27.97	34.09	42.32
An	14.87	8.21	14.16	12.15	12.83	3.70	8.06	5.10
Ne	15.75	17.56	15.50	14.42	12.54	18.26	13.62	11.87
Di-wo	4.71	4.49	4.97	3.31	2.31	3.50	3.05	2.60
Di-fs	1.84	2.23	2.16	1.56	0.96	1.65	1.70	1.87
Di-en	2.67	2.19	2.65	1.67	1.27	1.77	1.35	0.82
Fo	2.39	1.98	1.88	2.09	2.01	2.28	1.81	0.56
Fa	1.80	2.21	1.68	2.15	1.69	2.35	2.52	1.41
Mt	3.62	3.62	4.09	3.62	3.62	3.62	3.62	3.62
Il	3.99	3.84	3.66	3.53	3.15	3.12	2.66	1.20
Ap	2.04	2.25	1.97	2.60	1.95	2.36	1.25	0.42
Others	–	–	0.55	0.25	–	–	0.16	0.13
Total	96.98	96.71	99.86	99.35	99.66	99.44	99.60	99.46
D.I.	59.0	65.7	62.1	66.4	69.9	75.1	73.4	81.7
$\frac{100An}{An + Ab}$	36.8	24.7	34.4	28.8	27.2	11.7	19.1	10.8

[4] Includes F=0.14, Cl=0.06, less O≡Cl,F=0.07.

Explanation of Table 7.9. Analyses of volcanic rocks from the
Dellbridge Islands, Tryggve Point and Turks Head.

1. Nepheline hawaiite. Palagonitic breccia, Tryggve Point. Luckman, 1974.

2. Hawaiite (Basalt). Summit Little Razorback Island. Smith, 1954.

3. Nepheline hawaiite. (Plagioclase basalt). Pillow lava, Tryggve Point.
    Major element analyses, Luckman, 1974. Mean of 5 major
    element analyses and 3 trace element analyses from
    centre to margin of pillow. Interval   6 inches (15 cm).
    Major elements recalculated to 100%.

4. 25754. Nepheline hawaiite, pillow lava. Turks Head.

5. 25754G. Groundmass of above sample.

6. 25758. Nepheline hawaiite, dike. Tryggve Point.

7. 25758G. Groundmass of above sample.

8. Basanite (Plagioclase kenyte). Turks Head. Jensen, 1916.

9. Nepheline hawaiite. Turks Head. Major element analysis, Luckman, 1974.

10. Nepheline benmoreite. Tryggve Point. Major element analysis,
    Luckman, 1974.

11. Nepheline hawaiite (Trachybasalt). Tryggve Point. Goldich *et al.*, 1975.

12. 25742. Nepheline benmoreite. Inaccessible Island.

13. 25748. Nepheline benmoreite. Tent Island.

14. 25748G. Groundmass of above sample.

15. 25749. Nepheline benmoreite. Big Razorback Island.

16. 25745. Phonolite. Inaccessible Island.

TABLE 7.10   Analyses of volcanic rocks from Cape Royds, Cape Barne and Cape Evans.

	1	2	3	4	5	6	7	8	9
SiO_2	43.54	45.26	45.5	54.84	54.92	55.1	55.62	55.80	55.9
TiO_2	5.03	3.09	3.11	1.34	1.31	1.04	1.35	1.01	1.2
Al_2O_3	16.08	16.93	17.0	18.57	19.53	19.5	19.07	18.22	19.8
Fe_2O_3	2.63	2.85	3.81	6.26	4.19	1.91	6.06	5.99	1.9
FeO	10.14	8.79	8.41	0.47	1.74	4.12	0.00	0.85	3.5
MnO	0.20	0.29	0.24	0.21	0.21	0.21	0.20	0.24	0.14
MgO	6.44	3.98	3.74	1.06	1.07	1.13	1.20	1.17	1.2
CaO	8.09	9.32	9.30	3.00	3.48	3.30	2.72	2.78	3.0
Na_2O	3.61	4.58	5.07	6.96	7.48	8.03	7.56	8.13	7.4
K_2O	1.67	2.04	2.13	4.51	4.73	4.68	4.59	4.58	3.9
P_2O_5	1.29	1.66	1.56	0.85	0.26	0.42	0.57	0.50	1.3
H_2O+	0.36	0.77	0.26	1.20	0.41	0.22	0.12	0.00	0.53
H_2O-	0.08	0.20	0.10	0.62	0.04	0.17	0.14	tr	0.13
CO_2	0.15		0.01	0.05		0.01	0.03	0.04	<0.05
Cl					0.26			0.20	
F					0.07				
-O=F,Cl					0.14			0.07	
Total	100.77[1]	99.81[2]	100.24	100.70[3]	99.90[4]	99.84	100.63[5]	99.81[6]	99.95

CIPW Norms (Weight Percent)

	1	2	3	4	5	6	7	8	9
Q	–	–	–	–	–	–	–	–	–
C	–	–	–	–	–	–	–	–	1.18
Or	9.87	12.06	12.59	26.65	27.95	27.66	27.12	27.06	23.05
Ab	23.98	21.59	20.74	44.24	35.73	32.65	43.34	40.68	48.87
An	22.74	19.61	17.34	6.11	6.76	3.34	4.54	0.48	6.07
Ne	3.56	9.30	12.01	7.94	13.89	19.12	11.18	14.43	7.45
Ac	–	–	–	–	–	–	–	–	–
Hl	–	–	–	–	0.43	–	–	0.33	–
Di-wo	3.35	6.63	7.74	0.37	3.08	4.27	0.78	3.37	–
Di-fs	1.09	3.12	3.37	–	–	2.70	–	–	–
Di-en	2.06	3.35	4.13	0.32	2.66	1.63	0.68	2.91	–
Wo	–	–	–	–	0.50	–	–	0.87	–
Hy-fs	–	–	–	–	–	–	–	–	–
Hy-en	–	–	–	–	–	–	–	–	–
Fo	9.79	4.60	3.64	1.63	–	0.83	1.62	–	2.09
Fa	5.73	4.71	3.27	–	–	1.51	–	–	2.42
Mt	3.81	4.13	5.52	–	2.50	2.77	–	0.60	2.76
Hm	–	–	–	6.26	2.47	–	6.06	5.58	–
Il	9.55	5.87	5.91	1.44	2.49	1.98	0.43	1.92	2.28
Pf	–	–	–	–	–	–	1.91	–	–
Fl	–	–	–	–	0.14	–	–	–	–
Cc	0.34	–	0.02	0.11	–	0.02	0.07	0.09	0.11
Ap	2.99	3.85	3.61	1.97	0.60	0.97	1.32	1.16	3.01
Others	1.90	0.97	0.36	2.68	0.67	0.39	1.45	0.26	0.66
Total	100.77	99.81	100.24	100.70	99.88	99.84	100.50	99.74	99.95
D.I.	37.4	42.9	45.3	78.8	77.6	79.4	81.6	82.2	79.4
$\frac{100An}{An+Ab}$	48.7	47.6	45.5	12.1	15.9	9.3	9.5	1.2	11.1
Agpaitic Index	–	–	–	0.88	0.89	0.94	0.91	1.01	0.83

[1]Includes SrO=1.46; [2]Includes BaO=0.05; [3]Includes ZrO_2=0.20, SO_3=0.56;
[4]Includes ZrO_2=0.03, S=0.12, BaO=0.035, SrO=0.08, $(Ce,Y)_2O_3$=0.06;
[5]Includes ZrO_2=0.15, SO_3=0.97, SrO=0.28, [6]Includes ZrO =0.12, S=0.06.
BaO=0.10, SrO=0.07, $(Ce,Y)_2O_3$=0.02.

TABLE 7.10   Analyses of volcanic rocks from Cape Royds, Cape Barne and
Cape Evans (continued)

	10	11	12	13	14	15	16	17	18
SiO_2	56.00	54.98	56.09	56.10	56.2	56.27	58.1	58.90	58.94
TiO_2	1.22	1.34	1.23	1.10	1.01	1.06	1.00	1.29	1.40
Al_2O_3	19.74	18.97	20.79	19.57	19.9	19.08	15.9	16.24	16.33
Fe_2O_3	1.37	2.14	1.54	1.78	1.91	1.49	2.72	3.56	2.48
FeO	3.30	3.65	3.84	3.46	3.59	3.96	5.06	4.43	5.54
MnO	0.20	0.26	0.05	0.19	0.19	0.28	0.23	0.18	0.21
MgO	1.12	1.11	1.26	1.19	1.16	0.89	0.90	0.77	1.03
CaO	3.26	2.54	3.18	3.24	3.32	2.58	2.40	2.27	2.10
Na_2O	7.97	8.86	7.33	7.80	7.89	8.20	5.28	5.60	5.54
K_2O	4.28	5.13	3.91	4.26	4.24	5.05	4.98	5.85	5.25
P_2O_5	0.50	0.35	0.38	0.45	0.46	0.35	0.22	0.12	0.57
H_2O+	0.58	0.44	0.39	0.30	0.13	0.44	0.93	0.28	0.42
H_2O-	0.17	0.10	0.19	0.14	0.06	0.18	1.26	0.54	0.44
CO_2				0.07	0.02		0.06		0.05
Cl	0.20	0.20	0.17	0.06		0.25		0.07	
F				0.09				0.04	
$-O=F,Cl$	0.04	0.04	0.03	0.05		0.06		0.03	
Total	99.87	100.03	100.32	99.75	100.08	100.02	99.04	100.32[7]	100.68[8]

CIPW Norms (Weight Percent)

	10	11	12	13	14	15	16	17	18
Q	−	−	−	−	−	−	1.08	−	−
C	−	−	−	−	−	−	−	−	−
Or	25.29	30.32	23.10	25.17	25.06	29.84	29.43	34.57	31.02
Ab	39.43	26.90	42.95	40.50	39.19	35.27	44.68	45.49	46.88
An	6.23	−	12.94	6.04	6.36	1.32	4.98	2.17	4.18
Ne	14.37	22.82	9.65	13.58	14.94	17.48	−	0.75	−
Ac	−	3.94	−	−	−	−	−	−	−
Hl	0.33	0.33	0.28	0.10	−	0.41	−	0.12	−
Di-wo	2.79	4.31	0.15	2.50	2.91	3.84	2.14	3.39	0.92
Di-fs	1.50	2.66	0.08	1.33	1.63	2.72	1.61	2.21	0.67
Di-en	1.27	1.70	0.06	1.15	1.28	1.25	0.62	1.25	0.28
Wo	−	−	−	−	−	−	−	−	−
Hy-fs	−	−	−	−	−	−	4.21	−	5.17
Hy-en	−	−	−	−	−	−	1.62	−	2.14
Fo	1.06	0.75	2.15	1.27	1.13	0.68	−	0.47	0.10
Fa	1.38	1.29	2.90	1.62	1.60	1.62	−	0.92	0.27
Mt	1.99	1.13	2.23	2.58	2.77	2.16	3.94	5.16	3.60
Hm	−	−	−	−	−	−	−	−	−
Il	2.32	2.54	2.34	2.09	1.92	2.01	1.90	2.45	2.66
Pf	−	−	−	−	−	−	−	−	−
Fl	−	−	−	0.18	−	−	−	0.08	
Cc	−	−	−	0.16	0.04	−	0.14	−	0.11
Ap	1.16	0.81	0.88	1.04	1.07	0.81	0.51	0.28	1.32
Others	0.75	0.54	0.58	0.44	0.19	0.62	2.19	0.94	1.35
Total	99.87	100.03	100.31	99.75	100.08	100.03	99.04	100.24	100.68
D.I.	79.1	80.0	75.7	79.2	79.2	82.6	75.2	80.8	77.9
$\dfrac{100An}{An+Ab}$	13.6	0.0	23.2	13.0	14.0	3.6	10.0	4.6	8.2
Agpaitic Index	0.90	1.06	0.78	0.89	0.88	0.99	0.88	0.96	0.91

[7] Includes $ZrO_2=0.02$, $BaO=0.057$, $(Ce,Y)_2O_3=0.09$; [8] Includes $ZrO_2=0.22$, $SO_3=0.16$.

Explanation of Table 7.10. Analyses of volcanic rocks from Cape Royds,
            Cape Barne and Cape Evans.

1. Hawaiite (Olivine basalt). Cape Barne, Jensen, 1916.

2. Hawaiite (Basalt). Middle Dome, Cape Barne. Smith, 1954.

3. Nepheline hawaiite (Trachybasalt). Cape Barne. Goldich et al., 1975.

4. Anorthoclase trachyte (Vitrophyric kenyte). The Skuary, Cape Evans.
            Jensen, 1916.

5. Anorthoclase phonolite (Kenyte). Deviation Hill, Cape Evans.
            (Analyst: D. I. Bothwell). Smith, 1954.

6. Anorthoclase phonolite. Cape Evans. Goldich et al., 1975.

7. Anorthoclase phonolite (Kenyte). Cape Evans. Jensen, 1916.

8. Anorthoclase phonolite inclusion. The Ramp, Cape Evans.
            (Analyst: K. Chaperlin). Smith, 1954.

9. Anorthoclase phonolite (Anorthoclase trachyte). Cape Royds.
            Boudette and Ford, 1966.

10. Anorthoclase phonolite (Kenyte). Cape Royds (BM 1910-199(34)).
            Carmichael, 1964.

11. Groundmass of above sample. Carmichael, 1964.

12. Anorthoclase trachyte (Leucite kenyte). Cape Royds.   Prior, 1907.

13. Anorthoclase phonolite. Youngest flow, Cape Royds. Goldich et al., 1975.

14. Anorthoclase phonolite. Youngest flow, Cape Royds. Goldich et al., 1975.

15. Anorthoclase phonolite. Cape Evans. Carmichael, 1964.

16. Quartz K-trachyte. Mt Cis. Goldich et al., 1975.

17. K-trachyte. (Phonolitic trachyte). Mt Cis. Smith, 1954.

18. K-trachyte. (Trachyphonolite). Mt Cis. Jensen, 1916.

TABLE 7.11   Whole rock, groundmass and glass analyses of rocks from Fang
Ridge and Mt Erebus.

	1	2 25774	3 25782	4 25777	5 25778	6 -Gmass	7	8 25781
SiO$_2$	45.63	47.49	48.83	4°.37	49.64	48.94	54.17	55.32
TiO$_2$	2.42	2.71	2.50	2.26	2.02	2.53	0.73	1.29
Al$_2$O$_3$	10.43	18.63	18.52	18.35	19.58	18.23	19.92	19.13
Fe$_2$O$_3$	1.20	9.94	9.77	10.09	9.03	10.96	2.13	7.26
FeO	8.93						4.97	
MnO	0.17	0.22	0.22	0.23	0.22	0.26	0.26	0.22
MgO	15.01	3.41	2.99	2.09	2.12	2.10	1.57	1.42
CaO	12.89	7.41	6.41	5.01	6.63	5.19	2.72	3.93
Na$_2$O	2.04	5.73	6.05	6.66	6.10	6.68	8.57	6.54
K$_2$O	0.74	2.92	3.14	4.18	3.04	3.87	4.85	3.95
P$_2$O$_5$	0.43	1.12	1.18	1.10	0.88	0.82	0.06	0.46
H$_2$O+	0.16	0.06[1]	0.11[1]	0.14[1]	0.05[1]	0.07[1]	0.20	0.24[1]
H$_2$O-	0.21							
CO$_2$	0.12							
F							0.17	
-O=F							0.08	
Total	100.38	99.64	99.72	99.48	99.31	99.65	100.28[2]	99.76
Rb		61	70	93	56			81
Ba		549	595	722	754			993
Sr		1262	1146	830	1560			834
Y								
Zr								
Zn		102	102	125	104			97
Cu			18	38	21			10
Ni		10	<5	<5	<5			<5
V		111	66	25	17			11
Cr		31	<5	13	33			<5
K%		2.42	2.61	3.47	2.52			3.28
K/Rb		397	373	373	450			405

CIPW Norms (Weight Percent)

	1	2	3	4	5	6	7	8
C	-	-	-	-	-	-	-	-
Or	4.37	17.26	18.56	24.70	17.96	22.87	28.66	23.34
Ab	7.80	21.69	26.42	23.35	27.59	22.34	26.81	41.43
An	17.12	16.49	14.10	7.83	17.07	8.33	1.56	11.18
Ne	5.12	14.51	13.42	17.88	13.02	18.52	24.76	7.54
Ac	-	-	-	-	-	-	-	-
Ns	-	-	-	-	-	-	-	-
Di-wo	18.06	5.41	4.17	4.11	4.21	5.04	4.31	2.22
Di-fs	3.95	2.18	1.84	2.39	2.18	3.12	2.76	1.18
Di-en	12.60	3.01	2.20	1.73	1.98	1.98	1.63	1.02
Fo	17.37	3.84	3.68	2.43	2.31	2.28	1.60	1.76
Fa	6.00	3.07	3.39	3.69	2.80	3.94	3.00	2.24
Mt	1.74	3.62	3.62	3.62	3.62	3.62	3.09	3.62
Il	4.60	5.15	4.75	4.29	3.84	4.80	1.39	2.45
Fl	-	-	-	-	-	-	0.35	-
Cc	0.27	-	-	-	-	-	-	-
Ap	1.00	2.60	2.73	2.55	2.04	1.90	0.14	1.07
Others	0.37	0.06	0.11	0.14	0.05	0.07	0.20	0.24
Total	100.38	98.90	98.99	98.72	98.66	98.80	100.26	99.29
D.I.	17.3	53.5	58.4	65.9	58.6	63.7	80.2	72.3
$\frac{100An}{An+Ab}$	68.7	43.2	34.8	25.1	38.2	27.2	5.5	21.2
Agpaitic Index	-	-	-	0.84	-	0.83	0.97	0.79

[1]Loss of ignition;   [2]Includes S=0.004, BaO=0.03.

TABLE 7.11 Whole rock, groundmass and glass analyses of rocks from Fang Ridge and Mt Erebus (continued).

	9 25726	10 -Gmass	11	12	13 25727	14 25724	15 -Gmass	16 25725	17 -Gmass
SiO_2	55.32	54.94	55.71	55.95	56.42	56.65	55.54	56.68	55.81
TiO_2	1.07	1.10	1.22	1.98	0.91	0.92	1.06	1.00	1.10
Al_2O_3	19.69	19.27	18.14	22.53	20.18	20.09	19.09	19.84	18.84
Fe_2O_3	5.75	5.44	1.83	0.99	4.84	5.02	5.42	5.18	5.51
FeO			4.90	4.54					
MnO	0.25	0.30	0.25	tr	0.21	0.22	0.31	0.22	0.28
MgO	1.09	0.85	1.37	tr	0.95	0.97	0.80	1.06	0.87
CaO	2.68	2.03	3.35	3.21	2.80	2.79	1.95	2.92	2.06
Na_2O	7.92	8.85	7.92	7.42	7.88	7.75	9.05	7.88	8.27
K_2O	4.71	5.42	4.35	3.97	4.40	4.45	5.43	4.45	5.38
P_2O_5	0.45		0.49		0.37	0.38		0.40	
H_2O+	0.05[1]		0.11	0.00				0.04	
H_2O-			0.00	0.09	0.02	0.02			
CO_2			0.03	0.02					
F			0.15						
-O=F,Cl			0.08						
Total	98.98	98.20	99.83[3]	99.70	98.98	99.26	98.65	99.67	98.12
Rb	111		80		95	107		99	
Ba	871		1200		1133	876		1027	
Sr	735		840		1020	721		932	
Y			56						
Zr			540						
Zn	135		135		112	132		119	
Cu	4		24		6	5		5	
Ni	<5		13		<5	<5		<5	
V	5		32		4	<5		<5	
Cr	<5		<5		<5	<5		<5	
K%	3.91		3.61		3.65	3.69		3.71	
K/Rb	352		431		384	345		375	

CIPW Norms (Weight Percent)

C	-	-	-	0.24	-	-	-	-	-
Or	27.83	32.03	25.70	23.46	26.00	26.30	32.09	26.30	31.79
Ab	36.78	24.20	37.97	39.72	41.46	41.94	23.60	41.18	30.54
An	4.26	-	1.45	15.80	6.70	6.89	-	5.62	-
Ne	16.38	24.24	15.38	12.50	13.66	12.80	24.03	13.81	19.73
Hl	-	-	0.15	-	-	-	-	-	-
Ac	-	5.24	-	-	-	-	7.23	-	2.67
Ns	-	-	-	-	-	-	0.10	-	-
Di-wo	2.54	4.20	4.46	-	2.00	1.87	4.04	2.61	4.27
Di-fs	1.04	2.49	2.88	-	0.41	0.50	2.67	0.72	2.20
Di-en	1.41	1.74	1.66	-	1.41	1.23	1.46	1.70	2.01
Fo	0.92	0.26	1.23	-	0.67	0.83	0.38	0.66	0.11
Fa	0.74	0.42	2.36	4.56	0.22	0.38	0.76	0.31	0.13
Mt	3.62	1.00	2.65	1.44	3.62	3.62	-	3.62	2.29
Il	2.03	2.09	2.32	1.86	1.73	1.75	2.01	1.90	2.09
Fl	-	-	0.31	-	-	-	-	-	-
Cc	-	-	0.07	0.04	-	-	-	-	-
Ap	1.04	-	1.14	-	0.86	0.88	-	0.93	-
Others	0.05	-	0.11	0.09	0.02	0.02	-	0.04	-
Total	98.66	97.91	99.83	99.70	98.75	99.01	98.36	99.40	97.82
D.I.	81.0	80.5	79.0	75.7	81.1	81.0	79.7	81.3	82.1
$\frac{100An}{An+Ab}$	10.4	0.0	3.68	28.5	13.9	14.1	0.0	12.0	0.0
Agpaitic Index	0.92	1.06	0.98	0.73	0.88	0.87	1.09	0.90	1.03

[3] Includes Cl=0.09

Explanation of Table 7.11. Whole rock, groundmass and glass analyses
of rocks from Fang Ridge and Mt Erebus,

1. Limburgite. Mt Erebus. (Analyst: Burrows and Walkom).
Jensen, 1916,

2, 25774, Nepheline hawaiite, Fang Ridge,

3, 25782, Nepheline hawaiite, South of Abbott Peak,

4, 25777, Nepheline benmoreite, Fang Ridge.

5, 25778, Nepheline hawaiite. Fang Ridge.

6, 25778G, Groundmass of above sample.

7, Anorthoclase phonolite (Leucite-kenyte). Recent cinder cone of
Mt Erebus, (Analyst: J, D, Easton), Smith, 1954,

8, 25781, Mugearite, Abbott Peak,

9. 25726, Anorthoclase phonolite, Bomb, erupted from Mt Erebus in 1972.

10, 25726G. Glassy groundmass of above sample. (Electron microprobe
analysis),

11, Anorthoclase phonolite, Summit of Mt Erebus, Goldich et al,, 1975,

12. Anorthoclase phonolite, 'Pumice, groundmass of kenyte. Mt Erebus',
(Analyst: Burrows and Walkom), Mawson, 1916,

13. 25727. Anorthoclase phonolite. Flow upper slopes of present active
cone, Mt Erebus.

14, 25724, Anorthoclase phonolite. Bomb erupted in December, 1972.

15, 25724G, Glassy groundmass of above sample. (Electron microprobe
analysis).

16, 25725, Anorthoclase phonolite. Camp flow. Summit area of Mt Erebus.

17, 25725G. Glassy groundmass of above sample. (Electron microprobe
analysis).

TABLE 7.12   Analyses of volcanic rocks from Brown Peninsula.

	1	2 24085	3 24087	4 24086	5	6 24088A	7 24088B	8 24091	9 24089	10 24090	11
SiO_2	41.3	41.88	42.03	42.52	43.8	48.46	48.55	52.14	52.60	52.87	58.64
TiO_2	4.08	3.72	3.82	3.80	3.47	2.56	2.56	1.40	1.38	1.26	0.28
Al_2O_3	12.9	13.37	14.19	14.50	14.5	18.17	18.07	19.72	20.02	20.04	22.55
Fe_2O_3	4.87	13.11	13.86	13.09	4.56	9.53	9.56	6.43	6.44	6.09	0.97
FeO	7.39				7.85						0.99
MnO	0.20	0.20	0.22	0.21	0.23	0.20	0.19	0.19	0.19	0.20	tr
MgO	10.2	9.88	8.16	7.98	7.75	3.91	3.95	1.97	2.10	1.79	0.16
CaO	11.0	11.70	10.63	11.54	10.3	7.24	7.29	4.68	4.46	4.41	1.43
Na_2O	3.59	3.46	3.99	3.74	4.11	6.37	6.38	8.01	7.77	8.05	9.87
K_2O	0.63	1.33	1.77	1.69	1.78	3.04	3.02	3.90	4.04	3.97	4.98
P_2O_5	0.82	0.85	1.07	0.91	0.98	0.74	0.74	0.45	0.44	0.41	tr
H_2O+	1.19	0.60[1]	0.67[1]		0.36	0.07[1]	0.07[1]	0.78[1]	0.56[1]	0.67[1]	0.35
H_2O-	0.72				0.07						0.08
CO_2	0.82				0.03						
Total	99.71	100.10	100.41	99.98	99.79	100.29	100.38	99.67	100.00	99.76	100.30
Rb	24	30	37	32	49	77	76	105	110	101	
Ba	290	287	338	287	580	493	498	652	638	645	
Sr	880	930	1250	1062	1200	1063	1063	912	896	892	
Y	31				49						
Zr	330				370						
Zn	110	100	107	102	113	112	111	102	107	107	
Cu	41	58	42	58	32	28	27	15	16	14	
Ni	200	184	119	131	140	34	34	13	18	15	
V	280	272	241	265	260	143	141	56	59	55	
Cr	460	356	233	292	350	70	71	31	53	27	
K%	0.52	1.10	1.47	1.40	1.48	2.52	2.51	3.24	3.35	3.30	
K/Rb	218	367	397	438	302	327	330	308	304	327	
Mg No.	65.4	64.7	58.8	59.7	58.6	49.9	50.1	–	–	–	

CIPW Norms (Weight Percent)

	1	2	3	4	5	6	7	8	9	10	11
Or	3.72	7.86	10.46	9.99	10.52	17.96	17.85	23.05	23.87	23.46	29.43
Ab	16.32	3.02	4.78	4.05	12.86	19.42	19.54	27.06	28.05	28.99	39.01
An	17.22	17.02	15.58	17.78	15.86	12.01	11.75	6.33	7.82	6.82	2.52
Ne	7.62	14.22	15.70	14.95	11.87	18.68	18.66	22.06	20.42	21.19	24.11
Di-wo	11.19	14.81	12.60	14.00	11.96	7.96	8.18	5.82	4.78	5.17	0.95
Di-fs	1.11	4.25	4.45	4.65	2.36	2.79	2.85	1.83	1.45	1.58	0.55
Di-en	8.83	9.56	7.50	8.56	8.54	4.76	4.90	3.64	3.02	3.26	0.40
Wo	–	–	–	–	–	–	–	–	–	–	0.96
Fo	11.61	10.54	8.98	7.93	7.54	3.49	3.46	0.89	1.55	0.84	–
Fa	1.60	5.16	5.87	4.74	2.30	2.25	2.22	0.49	0.82	0.45	–
Mt	7.06	2.90	2.90	2.90	6.61	3.63	3.62	3.62	3.62	3.62	1.41
Il	7.75	7.06	7.26	7.22	6.59	4.86	4.86	2.66	2.62	2.39	0.53
Ap	1.90	1.97	2.48	2.11	2.27	1.72	1.72	1.04	1.02	0.95	–
Others	3.77[2]	0.60	0.67	–	0.50	0.07	0.07	0.78	0.56	0.67	0.43
Total	99.71	98.99	99.22	98.87	99.79	99.59	99.68	99.28	99.61	99.40	100.30
D.I.	27.7	25.1	30.9	29.0	35.2	56.1	56.0	72.2	72.3	73.6	92.6
$\frac{100An}{An+Ab}$	51.4	84.9	76.5	81.5	55.2	38.2	37.5	19.0	21.8	19.0	6.1

[1]Loss on ignition;   [2]Includes Cc=1.86%.

Explanation of Table 7.12.   Analyses of volcanic rocks from Brown Peninsula.

1.   Basanite.   Younger flow contains minor carbonate and altered olivine.
                 Goldich et al., 1975.

2.   24085.   Basanite.   Rainbow Ridge.   Major element analysis, Adams (1973).

3.   24087.   Basanite.   Rainbow Ridge.   Major element analysis, Adams (1973).

4.   24086.   Basanite.   Rainbow Ridge.   Major element analysis, Adams (1973).

5.   Basanite.   Core of pillow, older flow on Brown Peninsula.   Goldich
                 et al., 1975.

6.   24088A.   Nepheline hawaiite.   Rainbow Ridge. Major element analysis,
               Adams (1973).

7.   24088B.   Duplicate sample of above.

8.   24091.   Nepheline benmoreite.   Rainbow Ridge.   Major element analysis,
              Adams (1973).

9.   24089.   Nepheline benmoreite.   Rainbow Ridge.   Major element analysis,
              Adams (1973).

10.   24090.   Nepheline benmoreite.   Rainbow Ridge.   Major element analysis.
               Adams (1973).

11.   Phonolite (Phonolitic trachyte).   (Analyst: G. T. Prior).   Prior, 1907.

TABLE 7.13   Analyses of volcanic rocks from Mt Discovery and miscellaneous localities in the McMurdo Sound area.

	1 P23010	2	3	4	5	6	7	8 P23006	9
SiO_2	41.2	42.1	42.5	42.7	44.5	44.6	45.0	45.0	45.61
TiO_2	5.35	3.57	3.12	3.27	3.91	3.46	3.07	3.3	3.48
Al_2O_3	12.0	13.0	13.3	12.8	16.6	16.9	13.3	16.6	15.70
Fe_2O_3	5.4	3.37	3.00	3.10	6.09	11.8	5.30	5.65	6.17
FeO	9.0	8.90	10.0	7.96	6.01	0.09	6.38	5.85	7.29
MnO	0.25	0.19	0.20	0.19	0.25	0.22	0.19	0.11	tr
MgO	9.45	11.8	12.1	12.7	4.78	3.78	9.50	4.9	4.84
CaO	12.75	11.5	10.4	12.5	9.74	9.44	12.5	9.25	6.34
Na_2O	2.7	3.70	2.85	2.85	4.35	5.37	2.61	5.0	5.06
K_2O	1.05	0.90	1.17	0.96	1.92	2.01	1.03	2.3	2.67
P_2O_5	0.45	0.81	0.68	0.63	1.53	1.39	0.54	0.4	
H_2O+	0.82	0.45	0.13	0.13	0.20	0.14	0.23	1.06	2.34[1]
H_2O-	0.20	0.04	0.03	0.04	0.06	0.06	0.30	0.84	
CO_2		0.02	0.03	0.00	0.03	0.02	0.08		
Total	100.62	100.35	99.51	99.83	99.97	99.28	100.03	100.26	99.50
Rb	25	36	33	30	50	60	36		
Ba	212	380	390	300	630	630	240		
Sr	1038	960	1000	740	1270	1270	640		
Y		35	31	25	37	33	23		
Zr		310	230	240	340	410	260		
Zn	94	84	84	120	109	111	126		
Cu	52	57	37	56	34	25	85		
Ni	157	170	170	300	14	<10	150		
V	344	290	250	280	190	120	300		
Cr	303	600	540	870	<5	<5	510		
K%	0.87	0.75	0.97	0.80	1.59	1.67	0.86		
K/Rb	348	208	294	266	319	278	238		
Mg No.	59.8	68.4	67.5	72.1	47.6	43.5	65.0	49.5	45.2

CIPW Norms (Weight Percent)

Or	6.20	5.32	6.91	5.67	11.35	11.88	6.09	13.59	15.78
Ab	5.74	5.20	7.79	3.49	23.19	28.94	15.74	15.08	21.57
An	17.52	16.20	20.04	19.30	20.10	16.07	21.53	16.06	12.24
Ne	9.27	14.14	8.84	11.18	7.38	8.94	3.44	14.75	11.51
Ac	-	-	-	-	-	-	-	-	-
Ns	-	-	-	-	-	-	-	-	-
Di-wo	17.87	14.79	11.24	16.12	7.53	4.47	15.22	11.36	8.02
Di-fs	2.17	2.89	2.80	2.64	0.01	-	1.34	0.64	1.26
Di-en	13.79	10.59	7.59	11.92	6.50	3.87	12.13	9.34	5.97
Wo	-	-	-	-	-	-	-	-	-
Fo	6.83	13.18	15.80	13.81	3.79	3.89	8.08	2.01	4.26
Fa	1.18	3.96	6.42	3.37	0.01	-	0.99	0.15	0.99
Mt	7.83	4.89	4.35	4.50	8.83	-	7.68	8.19	8.95
Hm	-	-	-	-	-	11.80	-	-	-
Il	10.16	6.78	5.93	6.21	7.43	0.66	5.83	6.27	6.61
Pf	-	-	-	-	-	5.30	-	-	-
Cc	-	0.04	0.07	-	0.07	0.04	0.18	-	-
Ap	1.04	1.88	1.58	1.46	3.54	3.22	1.25	0.93	-
Others	1.02	0.49	0.16	0.17	0.26	0.20	0.53	1.90	2.34
Total	100.62	100.35	99.51	99.83	99.97	99.28	100.03	100.26	99.50
D.I.	21.2	24.7	23.5	20.3	41.9	49.8	25.3	43.4	48.9
$\frac{100An}{An+Ab}$	75.3	75.7	72.0	84.7	46.4	35.7	58.8	51.6	36.2

[1]Loss on ignition

TABLE 7.13   Analyses of volcanic rocks from Mt Discovery and miscellaneous localities in the McMurdo Sound area (continued).

	10 P23018	11	12 P23015	13 -Gmass	14	15	16	17 P23014
SiO_2	48.92	49.5	52.29	53.23	54.0	56.8	57.3	59.52
TiO_2	2.65	2.64	1.81	1.34	1.42	0.27	0.26	0.29
Al_2O_3	17.90	17.2	19.71	19.06	19.8	21.7	21.6	19.70
Fe_2O_3	10.36	2.98	7.68	6.54	2.51	2.80	1.70	4.27
FeO		6.38			3.83	0.64	0.80	
MnO	0.26	0.21	0.21	0.21	0.22	0.20	0.17	0.23
MgO	3.24	2.98	1.97	1.96	1.39	0.07	0.29	0.25
CaO	7.50	7.95	5.06	4.16	4.33	0.90	1.26	0.87
Na_2O	5.46	5.02	6.82	7.81	7.18	10.95	10.00	8.66
K_2O	2.26	2.57	3.49	4.75	3.85	5.56	5.00	5.61
P_2O_5	1.33	1.08	0.94	0.92	0.55	0.01	0.03	0.07
H_2O+	0.07[1]	0.73	0.03[1]		0.37	0.07	0.65	0.28[1]
H_2O-		0.14			0.22	0.13	0.15	
CO_2		0.02			0.03	0.01	0.03	
Total	99.95	99.40	100.01	99.98	99.70	100.11	99.24	99.75

	10	11	12	13	14	15	16	17
Rb	48	54	74	115	68	156	173	168
Ba	583	710	882	590	1430	~15	580	134
Sr	1867	1000	1754	687	1440	<30	420	24
Y		37			46	43	39	
Zr		400			510	620	510	
Zn	118	95	86	92	87	120	98	115
Cu	13	36	12	11	8	24	19	<5
Ni	<5	<10	<5	<5	<10	25	<10	<5
V	11	130	24	76	16	<10	<10	<5
Cr	6	<5	10	6	<5	<5	<5	<3
K%	1.88	2.13	2.90	3.94	3.20	4.62	4.15	4.66
K/Rb	392	395	392	343	470	296	227	277
Mg No.	43.2	41.8	-	-	-	-	-	-

CIPW Norms (Weight Percent)

	10	11	12	13	14	15	16	17
Or	13.36	15.19	20.62	28.07	22.75	32.86	29.55	33.15
Ab	31.69	31.08	34.53	27.84	36.58	23.92	36.30	40.87
An	17.66	16.81	12.86	2.92	10.42	-	-	-
Ne	7.86	6.18	12.56	20.72	13.10	30.74	25.44	15.83
Ac	-	-	-	-	-	8.10	1.19	2.80
Ns	-	-	-	-	-	0.65	-	-
Di-wo	4.54	6.45	2.55	4.89	3.04	1.17	1.09	1.61
Di-fs	2.05	2.58	1.09	1.68	1.38	1.10	0.29	1.21
Di-en	2.36	3.62	1.37	2.94	1.58	0.17	0.72	0.47
Wo	-	-	-	-	-	0.64	1.36	-
Fo	4.00	2.67	2.48	1.36	1.32	-	-	-
Fa	3.84	2.09	2.17	0.85	1.27	-	-	0.11
Mt	3.62	4.32	3.62	3.62	3.64	-	-	0.31
Hm	-	-	-	-	-	-	1.87	2.22
Il	5.03	5.01	3.44	2.54	2.70	-	-	-
Pf	-	-	-	-	-	0.51	0.49	0.55
Cc	-	0.04	-	-	0.07	-	-	-
Ap	3.08	2.50	2.18	2.13	1.27	0.02	0.07	-
Others	0.07	0.87	0.03	-	0.59	0.20	0.80	0.16
Total	99.17	99.40	99.49	99.58	99.70	100.11	99.24	99.58
D.I.	52.9	52.4	67.7	76.6	72.4	87.5	91.3	89.9
$\dfrac{100An}{An+Ab}$	35.8	35.1	27.1	9.5	22.2	0.0	0.0	0.0

Explanation of Table 7.13. Analyses of volcanic rocks from Mt Discovery
and miscellaneous localities in the McMurdo Sound area.

1. P23010. Basanite (Basalt). 'Minna Bluff survey station, 7 miles east
of Minna Saddle, and 9 miles east of foot of Mt Discovery'.
Collected by H. J. Harrington (N.Z. Geological and
Survey Antarctic Expedition 1958-59). (Major element
analyst: Chemistry Division, D.S.I.R.).

2. Basanite. Mt Hayward, White Island. Goldich et al., 1975.

3. Basanite. Summit Mt Morning. Goldich et al., 1975.

4. Basanite. North of Mt Heine, White Island. Goldich et al., 1975.

5. Hawaiite (Trachybasalt). Mt Terra Nova, Ross Island, Goldich et al.,
1975.

6. Hawaiite (Trachybasalt). Mt Terra Nova, Ross Island. Goldich et al.,
1975.

7. Alkali basalt. Mt Melania, Black Island. Goldich et al., 1975.

8. P23006. Nepheline hawaiite, (Basalt). Beaufort Island. Cliff at
north end of penguin rookery. Collected by H. J. Harrington
(N.Z. Geological and Survey Antarctic Expedition 1958-59).
(Analyst: Chemistry Division, D.S.I.R.).

9. Nepheline hawaiite (Basalt). Franklin Island. (Analyst: G. T. Prior).
Prior, 1898.

10. P23018. Hawaiite (Basalt). 'Mt Discovery 500 feet below top rock and
1500 feet below summit - at survey station'. Collected
by H. J. Harrington (N.Z. Geological and Survey Expedition
1958-59).
11. Hawaiite (Trachybasalt). Mt Melania, Black Island. Goldich et al., 1975.

12. P23015. Nepheline benmoreite. 'Mt Discovery 2500 feet below summit
on east side, 1000 feet below survey station.' Collected
by H. J. Harrington (N.Z. Geological and Survey Expedition
1958-59).

13. P23015G. Phonolitic groundmass of above sample.

14. Nepheline benmoreite (Phonolite). Near the summit of Mt Discovery.
Goldich et al.,1975.

15. Phonolite. Mt Aurora, Black Island. Goldich et al., 1975.

16. Phonolite. Minna Bluff (near Minna Saddle). Goldich et al., 1975.

17. P23014. Phonolite. Mt Discovery. Same as analysis no. 12.

TABLE 7.14   Analyses of McMurdo Volcanic Group samples from the Koettlitz
              Glacier area, Taylor Valley and tephra layers in the Skelton
              Névé.

	1	2	3	4	5	6	7
SiO_2	41.47	41.73	42.48	42.55	42.92	42.93	43.1
TiO_2	5.19	3.35	3.34	3.32	3.77	3.29	3.32
Al_2O_3	14.31	12.82	12.88	14.60	15.34	14.29	14.3
Fe_2O_3	3.96	13.68	3.75	12.82	3.71	12.95	4.89
FeO	11.48		7.87		10.39		8.55
MnO	0.22	0.19	0.19	0.19	0.23	0.19	0.21
MgO	7.07	10.25	10.88	7.19	7.25	7.71	8.30
CaO	10.03	11.08	11.08	11.92	10.98	11.61	10.0
Na_2O	3.13	3.20	2.52	3.29	3.15	3.38	4.31
K_2O	1.59	1.06	1.12	1.24	1.30	1.23	1.51
P_2O_5	0.49	0.59		0.60	tr	0.62	0.63.
H_2O+	0.57		0.94[2]	0.55[2]	0.35	0.01[2]	0.20
H_2O-	0.36				0.00		0.46
CO_2					0.08		0.02
Total	100.51[1]	97.92	97.15[3]	98.27	100.02[4]	98.21	99.97[5]

CIPW Norms (Weight Percent)

	1	2	3	4	5	6	7
Or	9.40	6.26	6.62	7.33	7.68	7.27	8.92
Ab	9.98	5.41	8.21	7.29	8.83	8.31	10.78
An	20.30	17.49	20.52	21.41	23.88	20.19	15.21
Ne	8.94	11.74	7.10	11.13	9.66	10.99	13.92
Di-wo	10.96	14.12	14.38	14.12	12.56	13.93	12.59
Di-fs	3.66	4.35	2.42	5.14	4.29	4.91	2.78
Di-en	6.69	8.90	10.59	8.29	7.59	8.30	8.76
Fo	7.65	11.65	11.57	6.74	7.34	7.64	8.35
Fa	4.62	6.27	2.91	4.60	4.57	4.98	2.92
Mt	5.74	2.90	5.44	2.90	5.38	2.90	7.09
Il	9.86	6.36	6.34	6.30	7.16	6.25	6.30
Cc	–	–	–	–	0.18	–	0.04
Ap	1.14	1.30	–	1.39	–	1.44	1.46
Others	1.57	–	–	0.55	0.90	0.01	0.66
Total	100.51	96.75	97.15	97.19	100.02	97.12	99.80
D.I.	28.3	23.4	21.9	25.7	26.2	26.6	33.6
$\frac{100An}{An+Ab}$	67.0	76.4	71.4	74.6	73.0	70.8	58.5
Mg No.	50.7	64.5	67.9	57.6	53.6	59.1	58.3

[1]Includes ZrO_2=0.005, SrO=0.08, BaO=0.04; [2]Loss on ignition;
[3]Includes NiO=0.02, Cr_2O_3=0.08; [4]Includes ZrO_2=0.03, SrO=0.06,
BaO=0.057, S=0.10, Cl=0.10, F=0.20; [5]Includes SrO=0.12, BaO=0.05.

TABLE 7.14 Analyses of McMurdo Volcanic Group samples from the Koettlitz Glacier area, Taylor Valley and tephra layers in the Skelton Névé (continued).

	8	9	10	11	12	13	14
SiO_2	43.13	43.13	43.15	43.3	43.37	45.0	50.0
TiO_2	3.43	3.36	3.41	3.42	3.23	2.9	2.36
Al_2O_3	14.69	13.44	14.57	12.8	13.53	14.8	18.7
Fe_2O_3	13.17	2.44	13.31	3.19	12.94		2.85
FeO		8.59		9.33		13.0[8]	5.42
MnO	0.19	0.18	0.19	0.19	0.19	0.22	0.20
MgO	7.61	9.17	7.82	10.9	9.83	7.1	2.58
CaO	11.98	11.90	11.72	12.9	11.25	9.3	6.37
Na_2O	3.27	2.69	3.41	2.62	3.00	4.3	6.35
K_2O	1.23	1.18	1.24	0.93	1.13	1.7	3.43
P_2O_5	0.63		0.64	0.55	0.55	0.65	0.99
H_2O+		0.90		0.07		0.8	0.21
H_2O-				0.03			0.15
CO_2				0.03		0.16	0.03
Total	99.33	97.04[6]	99.46	100.38[7]	99.02	99.93	99.86[9]

CIPW Norms (Weight Percent)

	8	9	10	11	12	13	14
Or	7.27	6.97	7.33	5.50	6.68	10.05	20.27
Ab	7.68	7.01	7.77	5.96	9.18	14.35	26.82
An	21.77	21.11	20.79	20.42	20.11	16.06	12.39
Ne	10.83	8.53	11.42	8.78	8.78	11.94	14.58
Di-wo	14.01	15.84	13.85	16.62	13.40	10.36	5.24
Di-fs	5.02	3.98	4.95	3.87	3.99	4.53	1.94
Di-en	8.28	10.65	8.20	11.42	8.54	5.51	3.06
Fo	7.48	8.54	7.90	11.02	11.17	8.53	2.36
Fa	5.00	3.52	5.26	4.12	5.75	7.73	1.65
Mt	2.90	3.54	2.90	4.62	2.90	2.90	4.13
Il	6.51	6.38	6.48	6.50	6.13	5.51	4.48
Cc	-	-	-	0.07	-	0.36	0.07
Ap	1.46	-	1.48	1.27	1.27	1.51	2.29
Others	-	0.96	-	0.10	-	0.80	0.36
Total	98.21	97.04	98.33	100.26	97.93	100.13	99.64
D.I.	25.8	22.5	26.5	20.2	24.6	36.3	61.7
$\frac{100An}{An+Ab}$	73.9	75.1	72.8	77.4	68.7	52.8	31.6
Mg No.	58.4	65.0	58.8	66.1	64.8	54.4	41.4

[6]Includes NiO=0.02, Cr_2O_3=0.04; [7]Includes SrO=0.09, BaO=0.03;
[8]Total iron as FeO; [9]SrO=0.15, BaO=0.07.

Explanation of Table 7.14. Analyses of McMurdo Volcanic Group samples
from the Koettlitz Glacier area, Taylor Valley and
tephra layers in the Skelton Névé and Mt Kempe area.

1, Basanite (Olivine basalt). Lava flow, Black Hill, Taylor Valley.
(Analyst: D. I. Bothwell). Smith, 1954.

2, Basanite. Tephra layer composed mainly of lapilli sized material,
Mt Kempe area. (Analyst: M. Schafer). Keys (pers. comm.).

3, Basanite. Vesicular basalt from vent on ridge between Radian and
Pipecleaner Glacier (Analyst: I. H. Wright). McIver and
Gevers, 1970. The analysis total as given was 99.15.

4, Basanite. Tephra layer in Skelton Neve, near Mt Metschel. (Analyst:
M. Schafer). Keys (pers. comm.).

5, Basanite (Olivine basalt). Taylor Valley. (Analyst: N. E. Butcher
and D. I. Bothwell). Smith, 1954.

6, Basanite. Tephra layer, Mt Kempe area. (Analyst: M. Schafer).
Keys (pers. comm.),

7, Basanite. Small vent on the south side of Taylor Valley at western
edge of Sollas Glacier. Goldich et al., 1975,

8, Basanite. Tephra layer in Skelton Neve, near Alligator Peak.
(Analyst: M. Schafer). Keys (pers. comm.).

9. Basanite. Massive basalt from dike within Brandau Vent (Analyst:
I. H. Wright). McIver and Gevers, 1970. The analysis
total as given was 99.04.

10, Basanite. Tephra layer, Mt Kempe area. (Analyst: M. Schafer).
Keys (pers. comm.).

11, Basanite. Brandau Vent, Royal Society Range. Goldich et al., 1975.

12. Basanite. Scoria cone, Mt Kempe area. (Analyst: M. Schafer).
Keys (pers. comm.),

13. Basanite. (Basalt). Average of 4 analyses, Taylor Valley.
Armstrong et al., 1968.

14, Nepheline hawaiite. (Trachybasalt). Miers Valley. Goldich et al., 1975.

TABLE 7.15   Analyses of unaltered samples from the Hallett volcanic province

	1 Hm*31	2 Hm 26	3 Hm 16	4 Hm 15	5 Hm 2	6 Hm 34	7 Hm 32	8 Hm 5
SiO_2	41.18	41.77	43.12	44.89	45.86	46.21	46.65	48.51
TiO_2	3.47	3.73	3.45	2.31	2.56	2.90	2.80	2.47
Al_2O_3	13.52	14.28	13.20	13.20	17.99	16.41	15.64	17.71
Fe_2O_3	3.57	4.64	2.87	2.40	4.06	3.88	3.24	4.85
FeO	8.86	8.26	9.09	8.26	7.13	7.16	7.61	6.25
MnO	0.22	0.21	0.20	0.19	0.24	0.21	0.21	0.24
MgO	9.46	8.56	11.51	12.86	4.07	6.01	7.32	3.45
CaO	12.25	11.74	11.41	9.67	9.17	9.61	9.86	8.00
Na_2O	4.43	3.41	2.80	3.11	5.37	4.30	4.27	5.07
K_2O	1.69	1.39	1.30	1.15	1.84	1.55	1.53	1.80
P_2O_5	0.99	0.68	0.57	0.54	1.14	0.74	0.60	1.16
H_2O+	0.09	0.74	0.18	0.79	0.33	0.34	0.11	0.27
H_2O-	0.07	0.47	0.10	0.25	0.10	0.27	0.05	0.10
CO_2	0.02	0.14	0.02	0.38	0.02	0.01	0.02	0.16
Cl	0.34	0.08	0.05	0.04	0.13	0.20	0.10	0.03
F	0.11	0.10	0.10	0.07	0.14	0.10	0.09	0.09
$-O=F,Cl$	0.13	0.06	0.05	0.04	0.09	0.08	0.06	0.05
Total	100.14	100.14	99.92	100.07	100.06	99.82	100.05	100.11
Mg No.	63.1	60.1	68.3	71.0	45.2	55.2	60.3	41.5

CIPW Norms (Weight Percent)

	1	2	3	4	5	6	7	8
Q	-	-	-	-	-	-	-	-
Or	2.58	8.21	7.68	6.80	10.87	9.16	9.04	10.64
Ab	-	6.41	6.28	15.33	21.00	22.00	19.35	35.10
An	12.01	19.55	19.61	18.66	19.55	20.90	19.99	20.25
Lc	5.81	-	-	-	-	-	-	-
Ne	20.31	12.16	9.43	5.95	13.24	7.79	9.09	4.23
Ac	-	-	-	-	-	-	-	-
Di-wo	17.60	13.93	13.84	9.76	7.67	9.14	10.81	4.53
Di-fs	4.10	2.62	3.03	2.08	2.69	2.28	2.79	1.30
Di-en	12.09	10.04	9.66	6.85	4.58	6.16	7.22	2.92
Wo	-	-	-	-	-	-	-	-
Hy-fs	-	-	-	-	-	-	-	-
Hy-en	-	-	-	-	-	-	-	-
Fo	8.04	7.90	13.32	17.64	3.89	6.17	7.72	3.97
Fa	3.01	2.27	4.61	5.90	2.52	2.52	3.29	1.96
Mt	5.18	6.73	4.16	3.48	5.89	5.63	4.70	7.03
Hm	-	-	-	-	-	-	-	-
Il	6.59	7.08	6.55	4.39	4.86	5.51	5.34	4.69
Cc	0.04	0.32	0.04	0.86	0.04	0.02	0.04	0.36
Ap	2.29	1.58	1.32	1.25	2.64	1.72	1.39	2.69
Others	0.48	1.33	0.38	1.11	0.61	0.83	0.29	0.44
Total	100.14	100.14	99.92	100.07	100.06	99.82	100.05	100.11
D.I.	28.7	26.8	23.4	28.1	45.1	39.0	37.5	50.0
$\frac{Anx100}{An+Ab}$	100.0	75.3	75.7	54.9	48.2	48.7	49.5	36.6

* Hm refers to Hamilton (1972)   ) Numbers refer to those in the
  H refers to Harrington et al., (1967).) tables of the references.

TABLE 7.15   Analyses of unaltered samples from the Hallett volcanic province (continued).

	9 H 8	10	11 H 10	12 H 11	13 Hm 14	14 Hm 19
SiO_2	50.5	61.01	62.3	62.8	67.75	69.6
TiO_2	2.8	0.00	0.30	0.30	0.24	0.17
Al_2O_3	13.7	16.62	19.6	16.5	14.88	14.7
Fe_2O_3	4.6	3.55	0.3	3.3	3.77	1.8
FeO	9.1	2.81	2.7	2.6	0.31	1.5
MnO	0.16	0.55	0.02	0.19	0.14	0.11
MgO	5.0	0.06	0.3	0.3	0.02	0.00
CaO	8.5	3.27	1.3	1.7	1.01	0.62
Na_2O	3.2	5.92	7.7	7.1	5.80	6.5
K_2O	0.6	5.22	4.4	4.8	5.25	4.5
P_2O_5	0.45	0.01	0.07	0.45	0.01	0.02
H_2O+	0.8	1.13	0.5	0.4	0.29	0.30
H_2O-	0.15		0.55		0.08	0.07
CO_2					0.34	0.05
Cl					0.03	
F					0.25	
-O=F,Cl					0.11	
Total	99.56	100.15	100.04	100.44	100.06	99.94
Mg No.	-	-	-	-	-	-

CIPW Norms (Weight Percent)

Q	5.17	0.80	-	0.85	13.69	13.97
Or	3.55	30.85	26.00	28.36	31.02	26.59
Ab	27.08	50.09	58.39	58.15	47.31	50.56
An	21.24	3.36	5.92	-	-	-
Lc	-	-	-	-	-	-
Ne	-	-	3.66	-	-	-
Ac	-	-	-	1.70	1.56	3.92
Di-wo	7.51	3.04	0.03	2.29	0.06	1.10
Di-fs	2.93	3.25	0.03	1.85	-	1.25
Di-en	4.26	0.15	-	0.58	0.05	-
Wo	-	2.34	-	-	1.11	-
Hy-fs	5.65	-	-	0.54	-	1.06
Hy-en	8.20	-	-	0.17	-	-
Fo	-	-	0.52	-	-	-
Fa	-	-	3.26	-	-	-
Mt	6.67	5.15	0.44	3.93	0.76	0.65
Hm	-	-	-	-	2.71	-
Il	5.32	-	0.57	0.57	0.46	0.32
Cc	-	-	-	-	0.77	0.11
Ap	1.04	-	0.16	1.04	0.02	0.05
Others	0.95	1.13	1.05	0.40	0.54	0.37
Total	99.56	100.14	100.04	100.44	100.06	99.94
D.I.	35.8	81.7	88.1	87.4	92.0	91.1
$\frac{Anx100}{An+Ab}$	44.0	6.3	9.2	0.0	0.0	0.0

Explanation of Table 7.15. Analyses of unaltered samples from the
Hallett volcanic province.

1. Basanite, (Basanite). Possession Island. Hamilton, 1972.

2. Basanite, (Olivine basalt). North end, Adare Peninsula.
Hamilton, 1972.

3. Basanite. (Olivine basalt). Near Trafalgar Glacier. Hamilton, 1972.

4. Basanite, (Olivine-diopside basalt). West side Moubray Bay.
Hamilton, 1972.

5. Nepheline hawaiite. (Nepheline trachybasalt), Hallett Peninsula.
Hamilton, 1972.

6. Hawaiite. (Olivine basalt). Foyn Island. Hamilton, 1972.

7. Hawaiite, (Olivine basalt). McCormick Island. Hamilton, 1972.

8. Hawaiite, (Olivine-andesine trachybasalt). Arneb Glacier, Hallett
Peninsula. Hamilton, 1972.

9. Hawaiite, (Plagioclase-olivine basalt). Bomb, Cape Hallett District.
Harrington *et al.*, 1967.

10. Quartz trachyte. (Trachyte). Waterworn pebble, Cape Adare.
David *et al.*, 1896.

11. K-trachyte, (Leucite trachyte). Salmon Cliff, Cape Hallett
District. Harrington *et al.*, 1967.

12. Quartz trachyte. (Alkali trachyte). Cape Hallett District.
Harrington *et al.*, 1967.

13. Quartz trachyte, (Quartz trachyte (or quartz-poor rhyolite)).
East Side Hallett Peninsula. Hamilton, 1972.

14. Quartz trachyte, (Quartz trachyte). Near Trainer Glacier.
Hamilton, 1972.

APPENDIX E

Least squares mass balance models for differentiation
in lavas from DVDP and Hut Point Peninsula

For explanation of tables see Table 9.1 and text
of Chapter 9.

TABLE 1 Crystal fractionation model for the transition basanites (2-99.34) to fractionated basanite (1-88.55).

	Basanite-fractionated DVDP 1-88.55	Pyroxene	Olivine	Spinel	Ilmenite	Apatite	Basanite DVDP 2-99.34
SiO_2	42.73	44.3	40.0	0.17	0.12	0.50	41.69
TiO_2	4.51	4.11	-	3.51	51.9	0.05	4.17
Al_2O_3	15.85	10.1	0.09	23.5	0.19	0.03	12.96
FeO^*	12.28	6.45	11.9	29.3	39.5	0.40	11.36
MnO	0.21	0.07	0.16	0.34	0.72	0.05	0.18
MgO	5.85	12.1	47.9	13.1	5.98	0.38	12.00
CaO	10.54	22.1	0.25	0.03	0.17	51.4	11.40
Na_2O	4.19	0.56	-	-	-	0.12	3.00
K_2O	2.05	-	-	-	-	-	1.50
P_2O_5	1.13	-	-	-	-	42.5	0.86

Solution

	Weight fraction	1σ
Basanite-fractionated	0.6752	0.0083
Pyroxene	0.1856	0.0088
Olivine	0.1161	0.0024
Spinel	0.0128	0.0033
Ilmenite	0.0050	0.0016
Apatite	0.0027	0.0018

Results

	Estimated	Observed	Residual
SiO_2	41.72	41.69	0.0297
TiO_2	4.11	4.17	-0.0583
Al_2O_3	12.89	12.96	-0.0707
FeO^*	11.44	11.36	0.0838
MnO	0.18	0.18	0.0014
MgO	11.95	12.00	-0.0454
CaO	11.39	11.40	-0.0142
Na_2O	2.93	3.00	-0.0667
K_2O	1.38	1.50	-0.1158
P_2O_5	0.88	0.86	0.0168

$\Sigma R^2 = 0.0367$

TABLE 2   Crystal fractionation model for the transition basanite (2-99.34) to nepheline hawaiite (2-70.41)

	Nepheline hawaiite DVDP 2-70.41	Pyroxene	Olivine	Spinel A	Spinel B	Kaersutite	Apatite	Basanite DVDP 2-99.34
SiO_2	47.27	44.3	40.0	0.17	0.09	38.2	0.50	41.69
TiO_2	2.95	4.11	-	3.51	25.0	6.49	0.05	4.17
Al_2O_3	17.61	10.1	0.07	23.5	5.52	14.3	0.03	12.96
FeO^*	9.07	6.45	13.2	29.3	59.7	10.8	0.40	11.36
MnO	0.21	0.07	0.17	0.34	0.63	0.13	0.05	0.18
MgO	3.72	12.1	47.0	13.1	4.07	12.1	0.38	12.00
CaO	7.76	22.1	0.18	0.03	0.10	12.2	51.4	11.40
Na_2O	6.07	0.56	-	-	-	2.32	0.12	3.00
K_2O	3.11	-	-	-	-	1.57	-	1.50
P_2O_5	0.81	-	-	-	-	-	42.5	0.86

Solution

	Weight fraction	1σ
Nepheline hawaiite	0.4391	0.0070
Pyroxene	0.2721	0.0100
Olivine	0.1106	0.0020
Spinel A	0.0257	0.0035
Spinel B	0.0362	0.0015
Kaersutite	0.1158	0.0185
Apatite	0.0111	0.0012

Results

	Estimated	Observed	Residual
SiO_2	41.67	41.69	-0.0157
TiO_2	4.16	4.17	-0.0097
Al_2O_3	12.95	12.96	-0.0104
FeO^*	11.36	11.36	0.0042
MnO	0.18	0.18	-0.0028
MgO	12.01	12.00	0.0121
CaO	11.43	11.40	0.0280
Na_2O	3.09	3.00	0.0881
K_2O	1.55	1.50	0.0476
P_2O_5	0.83	0.86	-0.0340

$\Sigma R^2 = 0.0126$

TABLE 3   Crystal fractionation model for transition nepheline hawaiite (2-70.41) to nepheline benmoreite (2-54.72).

	Nepheline benmoreite DVDP 2-54.72	Plagioclase An$_{55}$	Ilmenite	Magnetite	Apatite	Kaersutite	Pyroxene	Nepheline hawaiite DVDP 2-70.41
SiO$_2$	51.90	53.0	–	0.12	0.50	38.2	43.4	47.27
TiO$_2$	1.85	–	46.6	16.5	0.05	6.49	3.67	2.95
Al$_2$O$_3$	19.31	29.55	0.90	7.71	0.03	14.3	9.99	17.61
FeO*	6.67	–	44.0	66.1	0.40	10.8	7.97	9.07
MnO	0.20	–	0.44	0.66	0.05	0.13	0.13	0.21
MgO	2.07	–	6.29	6.00	0.38	12.1	10.9	3.72
CaO	5.43	12.0	0.05	0.03	51.4	12.2	22.1	7.76
Na$_2$O	7.26	4.70	–	–	0.12	2.50	0.90	6.07
K$_2$O	3.70	0.70	–	–	–	1.57	–	3.11
P$_2$O$_5$	0.60	–	–	–	42.5	–	–	0.81

Results

	Estimated	Observed	Residual
SiO$_2$	47.32	47.27	0.0484
TiO$_2$	2.95	2.95	-0.0031
Al$_2$O$_3$	17.58	17.61	-0.0251
FeO*	9.07	9.07	0.0033
MnO	0.20	0.21	-0.0112
MgO	3.72	3.72	0.0048
CaO	7.68	7.76	-0.0799
Na$_2$O	5.93	6.07	-0.1440
K$_2$O	2.98	3.11	-0.1305
P$_2$O$_5$	0.91	0.81	0.0965

Solution

	Weight fraction	1σ
Nepheline benmoreite	0.7638	0.0132
Plagioclase	0.0175	0.0110
Ilmenite	0.0020	0.0040
Magnetite	0.0349	0.0035
Apatite	0.0105	0.0026
Kaersutite	0.0899	0.0225
Pyroxene	0.0761	0.0155

$\Sigma R^2 = 0.0566$

REFERENCES

Abbott, M. J. (1969) Petrology of the Nandawar volcano, N.S.W. Australia. Contr. Mineral. and Petrol. 20, 115-134.

Adams, J. (1973) Petrology and petrochemistry of an alkaline cone, McMurdo Sound. Unpubl. B.Sc. (Hons.) Project, Dept. of Geology, Victoria University of Wellington. 36p.

Adie, R. J. (1969) Sheet 1, Northern Antarctic Peninsula. "Geological Map of Antarctica 1:1,000,000 Antarctic Map Folio Series (Bushnell, V. C. ed.) American Geographical Society, New York.

_____ (1972) Evolution of volcanism in the Antarctic Peninsula. In "Antarctic Geology and Geophysics" (ed. R. J. Adie), Universitetsforlget, Oslo, 137-141.

Akella, J. and Boyd, F. R. (1973) Partitioning of Ti and Al between coexisting silicates, oxides and liquids. Proc. 4th Lunar Sci. Conf. (Supplement 4, Geochim. Cosmochim. Acta) 1, 1049-1059.

Allen, J. C. and Boettcher, A. L. (1973) Phase relations and the stability of amphiboles in an olivine nephelinite at high pressure (Abstract). Trans. Amer. Geophys. Un. (Eos) 54, 481.

Anderson, A. T. (1968) The oxygen fugacity of alkaline basalt and related magmas, Tristan da Cunha. Amer. J. Sci. 266, 704-727.

Aoki, K. (1964) Clinopyroxenes from alkaline rocks of Japan. Amer. Mineral. 49, 1199-1223.

_____ (1968) Petrogenesis of ultrabasic and basic inclusions in alkali basalts, Iki Island, Japan. Amer. Mineral. 53, 241-256.

_____ (1970) Petrology of kaersutite-bearing ultramafic and mafic inclusions in Iki Island, Japan. Contr. Mineral. and Petrol. 25, 270-283.

Aoki, K. and Kushiro, I. (1968) Some clinopyroxenes from ultramafic inclusions in Dreiser Weiher, Eifel. Contr. Mineral. and Petrol. 18, 326-337.

Aoki, K. and Prinz, M. (1974) Chromian spinels in lherzolite
inclusions from Itinome-gata, Japan. Contr. Mineral. and
Petrol. 46, 249-256.

Arculus, R. J. (1974) Solid solution characteristics of spinels:
Pleonaste-chromite-magnetite compositions in some island-
arc basalts. Ann. Rept. Geophys. Lab. (Carnegie Inst.
Yrbk 73), 322-327.

Armstrong, R. L. (1975) K-Ar dating: McMurdo Volcanics and
Dry Valley glacial history, Victoria Land, Antarctica.
Unpublished manuscript.

Armstrong, R. L., Hamilton, W. and Denton, G. H. (1968)
Glaciation in the Taylor Valley, Antarctica, older than
2.7 million years. Science 159, 187-189.

Bacon, C. R. and Carmichael, I.S.E. (1973) Stages in the P-T
path of ascending basalt magma: An example from San Quintin,
Baja California. Contr. Mineral. and Petrol. 41, 1-22.

Bailey, D. K. and Schairer, J. F. (1966) The system $Na_2O-Al_2O_3-Fe_2O_3-SiO_2$ at 1 atmosphere, and the petrogenesis of
alkaline rocks. J. Petrol. 7, 114-170.

Baker, I. (1968) Compositional variation of minor intrusions
and the form of a volcanic magma chamber. Quart. Jl.
Geol. Soc. Lond. 124, 67-79.

Baker, P. E. (1972) Recent volcanism and magmatic variation
in the Scotia Arc In "Antarctic Geology and Geophysics"
(ed. R. J. Adie). Universitetsforlget, 57-60.

Barberi, F., Bizouard, H. and Varet, J. (1971) Nature of the
clinopyroxene and iron enrichment in alkalic and
transitional basaltic magmas. Contr. Mineral. and Petrol.
33, 93-107.

Barth, T.F.W. (1931) The crystallization process of basalt.
Amer. J. Sci. 31, 321-351.

Basu, A. R. and MacGregor, I. D. (1975) Chromite spinels from
ultramafic xenoliths. Geochim. Cosmochim. Acta 39, 937-945.

Beck, A. C. (1965) A note on Mount Erebus, Ross Island, Antarctica. N.Z. J. Geol. Geophys. 8, 180-185.

Best, M. G.(1974) Mantle-derived amphibole within inclusions in alkalic-basaltic lavas. J. Geophys. Res. 79, 2107-2113.

_____ (1975) Amphibole-bearing cumulate inclusions, Grand Canyon, Arizona and their bearing on silica-undersaturated hydrous magmas in the upper mantle. J. Petrol. 16, 212-236.

Blank, H. R., Cooper, R. A., Wheeler, R. H. and Willis, I.A.G. (1963) Geology of the Koettlitz-Blue Glacier region, southern Victoria Land, Antarctica. Trans. Roy. Soc. N.Z. Geol. 2, 79-100.

Boettcher, A. L. (1975) Experimental igneous petrology. Review Geophys. Space Phys. 13, 75-81.

Borley, G. D. (1974) Oceanic islands. In "The alkaline rocks" (ed. H. Sorensen) John Wiley and Sons. p.311-330.

Borley, G. D., Suddaby, P. and Scott, P. (1971) Some xenoliths from the alkalic rocks of Teneriffe, Canary Islands. Contr. Mineral. and Petrol. 31, 102-114.

Boudette, E. L. and Ford, A. B. (1966) Physical properties of anorthoclase from Antarctica. Amer. Mineral. 51, 1374-1387.

Bowden, P. and Luena, G. (1966) The use of T-1 as a geochemical standard. Geochim. Cosmochim. Acta 30, 361.

Brooks, C. K. and Rucklidge, J. C. (1973) A Tertiary lamprophyre dike with high pressure xenoliths and megacrysts from Wiedemanns Fjord, East Greenland. Contr. Mineral. and Petrol. 42, 197-212.

Brown, F. H. and Carmichael, I.S.E. (1971) Quaternary volcanoes of the Lake Rudolf region. II. The lavas of North Island, South Island, and the Barrier. Lithos 4, 305-323.

Brown, G. M. (1967) Mineralogy of basaltic rocks. In "Basalts" vol. 1 (eds. H. H. Hess and A. Poldervaart). Interscience, New York, 103-162.

Browne, P.R.L. (1974) Secondary minerals from Ross Island
     drillholes. (Abstract). Dry Valley Drilling Project
     (Northern Illinois University) Bulletin 4, Paper 3.

Bryan, W. B., Finger, L. W. and Chayes, F. (1970) Estimating
     proportions in petrographic mixing equations by least
     squares approximation. Science 163, 672-679.

Buddington, A. F. and Lindsley, D. H. (1964) Iron-titanium oxide
     minerals and synthetic equivalents. J. Petrol. 5, 310-357.

Bull, C. and Webb, P. N. (1973) Some recent developments in the
     investigation of the glacial history of Antarctica.
     In "Paleoecology of Africa": Scient. Comm. Antarct. Res.
     Conf. Quat. Studies (ed. E. M. van Zinderen Bakker).
     Balkema (Cape Town/Ritterdam), 55-84.

Bultitude, R. J. and Green, D. H. (1968) Experimental study at
     high pressures on the origin of olivine nephelinite and
     olivine melitite nephelinite magmas. Earth Planet. Sci.
     Lett. 3, 325-337.

_____ (1971) Experimental study of crystal-liquid relation-
     ships at high pressures in olivine nephelinite and basanite
     compositions. J. Petrology 12, 121-147.

Burke, K. and Dewey, J. F. (1973) Plume-generated triple
     junctions : Key indicators in applying plate tectonics
     to old rocks. J. Geology 81, 406-433.

Burke, K., Kidd, W.S.F. and Wilson, J. T. (1973) Plumes and
     concentric plume traces of the Eurasian plate. Nature 241,
     128-129.

Calkin, P. E. and Bull, C. (1972) Interaction of the East
     Antarctic Ice Sheet, alpine glaciations and sea level in
     the Wright Valley area, southern Victoria Land. In
     "Antarctic Geology and Geophysics" (ed. R. J. Adie).
     Universitetsforlaget, Oslo, 435-440.

Carmichael, I.S.E. (1962) Pantelleritic liquids and their
     phenocrysts. Mineral. Mag. 33, 86-113.

Carmichael, I.S.E. (1964) Natural liquids and the phonolite
minimum. Geol. J. 4, 55-60.

_____ (1967) The iron-titanium oxides of salic volcanic rocks
and their associated ferromagnesian silicates. Contr.
Mineral. and Petrology 14, 36-64.

Carmichael, I.S.E. and Nicholls, J. (1967) Iron-titanium oxides
and oxygen fugacities in volcanic rocks. J. Geophys. Res.
72, 4665-4687.

Carmichael, I.S.E., Nicholls, J.and Smith, A. L. (1970) Silica
activity in igneous rocks. Amer. Mineral. 55, 246-263.

Carmichael, I.S.E., Spera, F. J. and Wood, B. J. (in preparation)
Source to surface: Calculations for basic magmas.

Carmichael, I.S.E., Turner, F. J. and Verhoogen, J. (1974)
"Igneous petrology" McGraw-Hill, New York. 739p.

Cawthorn, R. G. and Collerson, K. D. (1974) The recalculation
of pyroxene end-member parameters and the estimation of
ferrous and ferric iron content from electron microprobe
analyses. Amer. Mineral. 59, 1203-1208.

Chayes, F.(1960) On correlation between variables of constant
sum. J. Geophys. Res. 65, 4185-4193.

_____ (1962) Numerical correlation and petrographic
variation. J. Geology 70, 440-452.

Chesworth, W. (1975) Mantle plumes, plate tectonics, and the
Cenozoic volcanism of the Massif Central. J. Geology 83,
579-588.

Cole, J. W. and Ewart, A.(1968) Contributions to the volcanic
geology of the Black Island, Brown Peninsula and Cape Bird
areas, McMurdo Sound, Antarctica. N.Z. J. Geol. Geophys.
11, 793-828.

Cole, J. W., Kyle, P. R. and Neall, V. E. (1971) Contributions
to the Quaternary geology of Cape Crozier, White Island
and Hut Point Peninsula, McMurdo Sound region, Antarctica.
N.Z. J. Geol. Geophys. 14, 528-546.

Coombs, D. S. and Wilkinson, J.F.G. (1969) Lineages and
        fractionation trends in undersaturated volcanic rocks from
        the East Otago Volcanic Province (New Zealand) and related
        rocks. J. Petrol. 10, 440-501.

Cox, A. (1969) Geomagnetic reversals. Science 163, 237-245.

Craddock, C. (1972) Geologic map of Antarctica 1:5,000,000
        Amer. Geographic Society, New York.

David, T.W.E., Smeeth, W. F. and Schofield, J. A. (1896)
        Notes on Antarctic rocks collected by Mr C. E. Borchgrevink
        Proc. R. Soc. N.S.W. 29, 461-492.

Dawson, E. W. (1970) Balleny bathymetry. N.Z. Oceanogr. Inst.
        Chart, Oceanic Series, 1:1,000,000.

Debenham, F. (1923) The physiography of the Ross Archipelago.
        Brit. Antarctic ("Terra Nova") Exped. 1910-1913. 40pp.,
        Harrison, London.

Deer, W. A., Howie, R. A. and Zussman, J. (1963) Rock-forming
        minerals. Vol. 1 Ortho- and ring silicates. Longman,
        London.

Eggler, D. H. (1974) Effect of CO_2 on the melting of peridotite.
        Ann. Rept. Geophys. Lab. (Carnegie Inst. Yrbk. 73), 215-224.

Evans, B. W. and Moore, J. G. (1968) Mineralogy as a function
        of depth in the prehistoric Makaopuhi tholeiitic lava lake,
        Hawaii. Contr. Mineral. and Petrol. 17, 85-115.

Evans, B. W. and Wright, T. L. (1972) Composition of liquidus
        chromite from the 1959 (Kilauea Iki) and 1965 (Makaopuhi)
        eruptions of Kilauea Volcano, Hawaii. Amer. Mineral. 57,
        217-230.

Falconer, R.K.H. (1972) The Indian-Antarctic-Pacific triple
        junction. Earth Planet. Sci. Lett. 17, 151-158.

Faure, G. and Powell, J. L. (1972) "Strontium isotope geology"
        Springer. Berlin-Heidelberg-New York. 188p.

Fitton, J. G. and Gill, R.C.O. (1970) The oxidation of ferrous
        iron in rocks during mechanical grinding. Geochim.
        Cosmochim. Acta 34, 518-524.

Flanagan, F. J. (1973) 1972 values for international geochemical reference samples. Geochim. Cosmochim. Acta 37, 1189-1200.

Fleck, R. J., Jones, L. M. and Behling, R. E. (1972) K-Ar dates of the McMurdo volcanics and their relation to the glacial history of Wright Valley. Antarctic J. of the U.S. 7, 244-246.

Forbes, R. B. (1963) Ultrabasic inclusion from the basalts of the Hut Point area, Ross Island. Bull. volcanologique 26, 13-21.

Forbes, R. B. and Banno, S. (1966) Nickel-iron content of peridotite inclusion and cognate olivine from an alkali-olivine basalt. Amer. Mineral. 51: 130-139.

Forbes, R. B. and Kuno, H. (1965) The regional petrology of peridotite inclusions and basaltic host rocks. Proc. 22nd Inter. Geol. Cong., Upper Mantle Symp., 161-179.

Forbes, R. B., Turner, D. L. and Carden, J. R. (1974) Age of trachyte from Ross Island, Antarctica. Geology 2, 297-298.

Frisch, T. and Schmincke, H. U. (1968) Petrology of clinopyroxene-amphibole inclusions from the Roque Nublo volcanics, Gran Canaria, Canary Islands. (Petrology of Roque Nublo Volcanics 1) Bull. Volcanologique 33, 1073-1088.

Gair, H. S. (1964) Geology of the upper Rennick, Campbell, and Aviator Glaciers, Victoria Land, Antarctica. In 'Antarctic Geology' (ed. R. J. Adie) North Holland, Amsterdam. p.188-198.

_____ (1967) The geology from the upper Rennick Glacier to the coast, northern Victoria Land, Antarctica. N.Z. J. Geol. Geophys. 10, 309-344.

Gair, H. S., Sturm, A., Carryer, S. J. and Grindley, G. W. (1969) The geology of northern Victoria Land. "Geological Map of Antarctica 1:1,000,000" Antarctic Map Folio Series (Bushnell, V. C. ed.) American Geographical Society, New York.

Gast, P. W. (1968) Trace element fractionation and the origin of tholeiitic and alkaline magma types. Geochim. Cosmochim. Acta 32, 1057-1086.

Gibb, F.G.F. (1973) The zoned clinopyroxenes of the Shiant Isles sill, Scotland. J. Petrol. 14, 203-230.

Giggenbach, W. F., Kyle, P. R. and Lyon, G. (1973) Present volcanic activity on Mt Erebus, Ross Island, Antarctica. Geology 1, 135-136.

Gilbert, M. C. (1969) High-pressure stability of acmite. Amer. J. Sci. (Schairer Vol.) 267-A, 145-159.

Goldich, S. S., Stuckless, J. S., Suhr, N.H. and Treves, S. B. (1973) Geochemistry of volcanic rocks of the Ross Island area, Antarctica (Abstract). Geol. Soc. Amer. Abs. with Prog. 5, 638-639.

Goldich, S. S., Treves, S. B., Suhr, N. H. and Stuckless, J. S. (1975) Geochemistry of the Cenozoic volcanic rocks of Ross Island and vicinity, Antarctica. J. Geology 83, 415-435.

Gomes, C. de B., Moro, S. L. and Dutra, C. V. (1970) Pyroxenes from the alkaline rocks of Itapirapua, Sao Paulo, Brazil. Amer. Mineral. 55, 224-230.

Green, D. H. (1968) Origin of basaltic magmas. In "The Poldervaart treatise on rocks of basaltic composition" (eds. Hess, H. H. and Poldervaart, A.). Interscience, New York. Vol. 2, 835-862.

_____ (1970a) A review of experimental evidence on the origin of basaltic and nephelinitic magmas. Phys. Earth Planet. Interiors 3, 221-235.

_____ (1970b) The origin of basaltic and nephelinitic magmas. Trans. Leicester Literary Philosophical Society 64, 26-54.

_____ (1971) Composition of basaltic magmas as indicators of conditions of origin: application to oceanic volcanism. Phil. Trans. Roy. Soc. Lond. A. 268, 707-725.

_____ (1973) Conditions of melting of basanite magma from garnet peridotite. Earth Planet. Sci. Lett. 17, 456-465.

Green, D. H. and Ringwood, A. E. (1963) Mineral assemblages in a model mantle composition. J. Geophys. Res. 68, 937-945.

Green, D. H. and Ringwood, A. E. (1967) The genesis of basaltic magmas. Contr. Mineral. and Petrol. 15, 103-190.

Gunn, B. (1972) The fractionation effect of kaersutite in basaltic magmas. Canadian Mineral. 11, 840-850.

Gunn, B. M., Coy-yll, R., Watkins, N. D., Abranson, C. E. and Nougier, J. (1970) Geochemistry of an oceanite-ankaramite-basalt suite from East Island, Crozet Archipelago. Contr. Mineral. and Petrol. 28, 319-339.

Gunn, B.M. and Warren, G. (1962) The geology of Victoria Land between the Mawson and Mulock Glaciers, Ross Dependency, Antarctica. Bull. Geol. Surv. N.Z. n.s.71.

Gupta, A. K., Onuma, K., Yagi, K. and Lidiak, E. G. (1973) Effect of silica concentration on the diopsidic pyroxenes in the system diopside-$CaTiAl_2O_6$-SiO_2. Contr. Mineral. and Petrol. 41, 333-344.

Haggerty, S. E. (1972) Luna 16: an opaque mineral study and a systematic examination of compositional variations of spinels from Mare Fecunditatis. Earth Planet. Sci. Lett. 13, 328-352.

Haggerty, S. E. and Baker, I. (1967) The alteration of olivine in basaltic and associated lavas. Part 1 High temperature alteration. Contr. Mineral. and Petrol. 16, 233-257.

Halpern, M. (1969) Sr^{87}/Sr^{86} ratios of ultramafic nodules and host basalt from the McMurdo area and Ford Ranges, Antarctica. Antarctic J. of the U.S. 4, 206-207.

Hamilton, W. (1972) The Hallett Volcanic Province, Antarctica. U.S. Geol. Surv. Prof. Paper. 456-B.

Harrington, H. J. (1958) Nomenclature of Rock Units in the Ross Sea Region, Antarctica. Nature 182, 290.

Harrington, H. J., Wood, B. L., McKellar, I. C. and Lensen, G. J. (1967) Topography and geology of the Cape Hallett district, Victoria Land, Antarctica. N.Z. Geol. Surv. Bull. ns. 80.

Hatherton, T., Dawson, E. W. and Kinsky, F. C. (1965) Balleny Island reconnaissance expedition, 1964. N.Z. J. Geol. Geophys. 8, 164-179.

Heming, R. F. and Carmichael, I.S.E. (1973) High-temperature pumice flows from the Rabaul Caldera, Papua New Guinea. Contr. Mineral. and Petrol. 38, 1-20.

Hill, R. and Roeder, P. (1974) The crystallization of spinel from basaltic liquid as a function of oxygen fugacity. J. Geology 82, 709-729.

Hollister, L. S. and Gancarz, A. J. (1971) Compositional sector-zoning in clinopyroxene from the Narce area, Italy. Amer. Mineral. 56, 959-979.

Holloway, J. R. and Burnham, C. W. (1972) Melting relations of basalt with equilibrium water pressure less than total pressure. J. Petrol. 13, 1-29.

Holloway, J. R. and Ford, C. E. (1973) The effect of fluorine on hornblende: fluid-absent melting of F-OH pargasite to 35 kb (Abstract). Trans. Amer. Geophys. Un (EOS) 54, 478.

Huang, T-C., Watkins, N. D. and Shaw, D. M. (1974) Atmospherically transported volcanic ash in Eltanin deep sea sedimentary cores. Antarctic J. of the U.S. 9, 257.

Huckenholz, H. G. (1973) The origin of fassaitic augite in the alkali basalt suite of the Hocheifel area, West Germany. Contr. Mineral. and Petrol. 40, 315-326.

Irvine, T. N. (1967) Chromian spinel as petrogenetic indicator. Part 2. Petrologic applications. Can. J. Earth Sci. 4, 71-103.

Irvine, T. N. and Baragar, W.R.A. (1971) A guide to the chemical classification of the common volcanic rocks. Canad. J. Earth Sci. 8, 523-548.

Ito, K. and Kennedy, G. C. (1967) Melting and phase relations in a natural peridotite to 40 kilobars. Amer. J. Sci. 265, 519-538.

_____ (1968) Melting and phase relations in the plane tholeiite-lherzolite-nepheline basanite at 40 kilobars with geological implications. Contr. Mineral. and Petrol. 19, 177-211.

Jackson, E. D. (1969) Chemical variation in coexisting chromite and olivine in chromitite zones of the Stillwater Complex. In 'Magmatic Ore Deposits' (ed. Wilson, H.D.B.) Econ. Geol. Mono. 4, 41-71.

Jensen, H. I. (1916) Report on the petrology of the alkaline rocks of Mt Erebus, Antarctica. Rep. Brit. Antarctic Exped. 1907-9, Geol. 2, 93-128.

Johannsen, A. (1939) A descriptive petrography of igneous rocks Vol. 1: Introduction, Textures, Classifications and Glossary. Univ. Chicago Press, Chicago.

Jones, L. M. and Walker, R. L. (1972) Geochemistry of the McMurdo volcanics, Victoria Land: Part 1, Strontium isotope composition. Antarctic J. of the U.S. 7: 142-144.

Kay, R. W. and Gast, P. W. (1973) The rare earth content and origin of alkali-rich basalts. J. Geology 81, 653-682.

Keil, K., Fodor, R. V. and Bunch, T. E. (1972) Contributions to the mineral chemistry of Hawaiian Rocks. II. Feldspars and interstitial material in rocks from Haleakala and West Maui Volcanoes, Maui, Hawaii. Contr. Mineral. and Petrol. 37, 253-276.

Keil, K. and Fricker, P. E. (1974) Baddeleyite (ZrO_2) in gabbroic rocks from Axel Heiberg Island, Canadian Arctic Archipelago Amer. Mineral. 59, 249-253.

Kempe, D.R.C. (1973) Rocks from Antarctica; The Discovery collection in the British Museum (Natural History). Bull. Brit. Mus. Nat. Hist. (Mineralogy), 2 (7), 338-376.

Kesson, S. E. (1973) The primary geochemistry of the Monaro alkaline volcanics, Southeastern Australia - Evidence for Upper Mantle Heterogeneity. Contr. Mineral. and Petrol. 42, 93-108.

Kesson, S. E. and Price, R. C. (1972) The major and trace element chemistry of kaersutite and its bearing on the petrogenesis of alkaline rocks. Contr. Mineral. and Petrol. 35, 119-124.

Knutson, J. and Green, T. H. (1975) Experimental duplication of a high-pressure megacryst/cumulate assemblage in a near-saturated hawaiite. Contr. Mineral. and Petrol. 52, 121-132.

Kudo, A. M. and Weill, D. F. (1970) An igneous plagioclase thermometer. Contr. Mineral. and Petrol. 25, 52-65.

Kurasawa, H. (1974) Strontium isotope studies of the Ross Island volcanics (Abstract). Dry Valley Drilling Project (Northern Illinois University) Bulletin 4: Paper 13.

_____ (1975) Strontium isotopic studies of the Ross Island volcanics, Antarctica. Mem. Nat. Inst. Polar Research (Japan) Spec. Issue 4: 67-74.

Kushiro, I. (1960) Si-Al relation in clinopyroxenes from igneous rocks. Amer. J. Sci. 258, 548-554.

_____ (1962) Clinopyroxene solid solutions. Part 1. The $CaAl_2SiO_6$ component. Japan J. Geol. and Geog. 33, 213-220.

_____ (1969) Discussion of the paper "The origin of basaltic and nephelinitic magmas in the earth's mantle" by D. H. Green. Tectonophysics 7, 427-436.

_____ (1973) Origin of some magmas in oceanic and circum-oceanic regions. Tectonophysics 17, 211-222.

Kyle, P. R. (1971) The geology and geochemistry of Cape Crozier, Ross Island, Antarctica. Unpubl. B.Sc. (Hons.) Project, Dept. of Geology, Victoria University of Wellington.

_____ (1974a) Petrology and mineralogy of DVDP 1 and 2 core samples. (Abstract). Dry Valley Drilling Project (Northern Illinois University) Bulletin 4: Paper 15.

_____ (1974b) Electron microprobe analyses of minerals in core samples from Dry Valley Drilling Project (DVDP) holes 1 and 2, Ross Island, Antarctica. Antarctic Data Series 4, Publication of Department of Geology, Victoria University of Wellington 4: 27pp.

_____ (1975) Volcanic activity of Mt Erebus, Antarctica. N.Z. Volcanological Record 3, 52-56.

Kyle, P. R. and Cole, J. W. (1974) Structural control of
    volcanism in the McMurdo Volcanic Group, Antarctica.
    Bull. Volcanologique 38, 16-25.

Kyle, P. R. and Treves, S. B. (1973) Review of the geology of
    Hut Point Peninsula, Ross Island, Antarctica. Dry Valley
    Drilling Project (Northern Illinois University) Bulletin 2, 1-10.

_____ (1974a) Geology of DVDP 3, Hut Point Peninsula, Ross
    Island, Antarctica. Dry Valley Drilling Project (Northern
    Illinois University) Bulletin 3, 13-48.

_____ (1974b) Geology of DVDP 3, Hut Point Peninsula, Ross
    Island. Antarctic J. of the U.S. 9, 127-129.

_____ (1974c) Geology of Hut Point Peninsula, Ross Island.
    Antarctic J. of the U.S. 9, 232-234.

Le Bas, M. J. (1962) The role of aluminium in igneous clino-
    pyroxenes with relation to their parentage. Amer. J. Sci.
    260, 267-288.

LeMaitre, R. W. (1969) Kaersutite-bearing plutonic xenoliths
    from Tristan da Cunha, S. Atlantic. Mineral. Mag. 37,
    185-197.

Leung, I. S. (1974) Sector-zoned titanaugites: Morphology,
    crystal chemistry, and growth. Amer. Mineral. 59, 127-138.

Lienart, B. R. (1971) Construction of a spinner magnetometer
    and paleomagnetic measurements on a Pliocene-Miocene
    sedimentary section. Unpublished M.Sc. thesis, Victoria
    University of Wellington.

Lindsley, D. H., Carmichael, I.S.E. and Nicholls, J. (1968)
    Iron-titanium oxides and oxygen fugacities in volcanic
    rocks: A correction. J. Geophys. Res. 73, 3351-3352.

Loney, R. A., Himmelberg, G. R. and Coleman, R. G. (1971)
    Structure and petrology of the Alpine-type peridotite at
    Burro Mountain, California, U.S.A. J. Petrol. 12, 245-309.

Luckman, P. (1974) Products of submarine and subglacial
    volcanism in the McMurdo Sound region, Ross Island,
    Antarctica. Unpubl. B.Sc.(Hons) Project, Dept of Geology,
    Victoria University of Wellington. 115p.

Lyon, G. L. and Giggenbach, W. F. (1974) Geothermal activity
    in Victoria Land, Antarctica. N.Z. J. Geol. Geophys.
    17, 511-521.

Macdonald, G. A. (1960) Dissimilarity of continental and oceanic
    rock types. J. Petrol. 1, 172-177.

_____ (1968) Composition and origin of Hawaiian lavas.
    Geol. Soc. Amer. Mem. 116, 477-522.

Macdonald, G. A. and Katsura, T. (1964) Chemical composition
    of Hawaiian lavas. J. Petrol. 5, 82-133.

Mathez, E. A. (1973) Refinement of the Kudo-Weill plagioclase
    and its application to basaltic rocks. Contr. Mineral. and
    Petrol. 41, 61-72.

Mawson, D. (1916) Petrology of rocks collected from the mainland
    of south Victoria Land. Rep. Brit. Antarctic Exped. 1907-9,
    Geol. 2, 201-237.

_____ (1950) Basaltic lavas of the Balleny Islands,
    A.N.A.R.E. Report. Trans. R. Soc. S. Aust.73, 223-231.

McDougall, I. and Aziz-Ur-Rahman (1972) Age of the Gauss-
    Matuyama boundary and of the Kaena and Mammoth events.
    Earth. Planet. Sci. Lett. 14, 367-380.

McGinnis, L. D. (1973) McMurdo Sound - A key to the Cenozoic
    of Antarctica. Antarctic J. of the U.S. 8, 157.

McGinnis, L. D., Clark, C. C., Pederson, D. R., Wong, H. K.,
    Ervin, C. P. and Montgomery, G. E. (1974). Aeromagnetic
    and refraction seismic studies for the Dry Valley Drilling
    Project (DVDP). (Abstract). Dry Valley Drilling Project
    (Northern Illinois University) Bull. 4, 34-36.

McGinnis, L. D., Torii, T. and Webb, P. N. (1972) Dry Valley
    Drilling Project - three nations are studying the subsurface
    in the McMurdo Sound region. Antarctic J. of the U.S.
    7, 53-56.

McIver, J. R. and Gevers, T. W. (1970) Volcanic vents below the
    Royal Society Range, Central Victoria Land. Trans. Geol.
    Soc. South Africa. 73, 65-88.

McMahon, B. E. and Spall, H. (1974a) Results of paleomagnetic
   investigation of selected cores recovered by Dry Valley
   Drilling Project (Abstract). Dry Valley Drilling Project
   (Northern Illinois University) Bulletin 4, Paper 17.

_____ (1974b) Paleomagnetic data from unit 13, DVDP hole 2,
   Ross Island. Antarctic J. of the U.S. 9, 229-232.

McSaveney, M. J. and McSaveney, E. R. (1972) A reappraisal of
   the Pecten glacial episode, Wright Valley, Antarctica.
   Antarctic J. of the U.S. 7, 235-240.

Morgan, W. J. (1972) Deep mantle convection plumes and plate
   motions. Bull. Am. Assoc. Pet. Geol. 56, 203-213.

Muñoz, M. and Sagredo, J. (1974) Clinopyroxenes as geobarometric
   indicators in mafic and ultramafic rocks from Canary
   Islands. Contr. Mineral. and Petrol. 44, 139-147.

Mysen, B. (1974) The oxygen fugacity (f_{O_2}) as a variable during
   partial melting of peridotite in the upper mantle.
   Ann. Rept. Geophys. Lab. (Carnegie Inst. Yrbk. 73), 237-240.

Nakamura, Y. (1973) Origin of sector-zoning of igneous
   clinopyroxenes. Amer. Mineral. 58, 986-990.

Nash, W. P., Carmichael, I.S.E. and Johnson, R. W. (1969)
   The mineralogy and petrology of Mount Suswa, Kenya.
   J. Petrol. 10, 409-439.

Nash, W. P. and Wilkinson, J.F.G. (1970) Shonkin Sag Laccolith,
   Montana I. Mafic minerals and estimates of temperature,
   pressure, oxygen fugacity and silica activity.
   Contr. Mineral. and Petrol. 25, 241-269.

Nathan, S. and Schulte, F. J. (1967) Recent thermal and volcanic
   activity on Mt Melbourne, northern Victoria Land, Antarctica.
   N.Z. J. Geol. Geophys. 10, 504-511.

_____ (1968) The geology and petrology of the area between
   the Campbell and Aviator Glaciers. N.Z. J. Geol. Geophys.
   11, 940-975.

Nicholls, J. and Carmichael, I.S.E. (1972) The equilibration temperature and pressure of various lava types with spinel- and garnet-peridotite. Amer. Mineral. 57, 941-959.

Nicholls, J., Carmichael, I.S.E. and Stormer·Jr, J. C. (1971) Silica activity and P_{total} in igneous rocks. Contr. Mineral. and Petrol. 33, 1-20.

Nolan, J. and Edgar, A. D. (1963) An x-ray investigation of synthetic pyroxenes in the system acmite-diopside-water at 1000 kg/cm^2 water vapour pressure. Mineral. Mag. 33, 625-634.

Norrish, K. and Chappell, B. W. (1967) X-ray fluorescence spectrography In "Physical methods in determinative mineralogy" (edit. by J. Zussman) London and New York Academic Press. p.161-214.

Norrish, K. and Hutton, J. T. (1969) An accurate x-ray spectrographic method for the analysis of a wide range of geological samples. Geochim. Cosmochim. Acta 33, 431-453.

Northey, D. J., Brown, C., Christoffel, D. A., Wong, H. K. and Barrett, P. J. (1975). A continuous seismic profiling survey in McMurdo Sound, Antarctica. Dry Valley Drilling Project (Northern Illinois University) Bulletin 5, 167-179.

O'Hara, M. J. (1968) The bearing of phase equilibria studies in synthetic and natural systems on the origin and evolution of basic and ultrabasic rocks. Earth Sci. Rev. 4, 69-133.

O'Hara, M. J. and Yoder, H. S. (1967) Formation and fractionation of basic magmas at high pressures. Scot. J. Geol. 3, 67-117.

Orville, P. M. (1972) Plagioclase cation exchange equilibria with aqueous chloride solution: results at 700°C and 2000 bars in the presence of quartz. Amer. J. Sci. 272, 234-272.

Papike, J. J., Cameron, K. L. and Baldwin, K. (1974) Amphiboles and pyroxenes: Characterization of other than quadrilateral components and estimates of ferric iron from microprobe data (Abstract). Geol. Soc. Amer. Abstr. with Programs 6, 1053-1054.

Powell, M. and Powell, R. (1974) An olivine-clinopyroxene
    geothermometer. Contr. Mineral. and Petrol. 48, 249-263.

Price, R. C. (1973) Geochemical investigations of the alkalic
    rocks of the Dunedin volcano, East Otago, New Zealand.
    Unpubl. Ph.D. thesis, University of Otago, Dunedin.

Prior, G. T. (1898) Petrographical notes on the rock-specimens
    collected in Antarctic regions during the voyage of HMS
    Erebus and Terror under Sir James Ross in 1839-43.
    Mineral. Mag. 12, 69-91.

_____ (1902) Report on rock specimens collected by the
    Southern Cross Antarctic Expedition. Rep. Southern Cross
    Collections (British Museum), 321-332.

_____ (1907) Report on the rock specimens collected during
    the Discovery Antarctic Expedition, 1901-4. National
    Antarctic Exped. 1901-4, Nat. Hist. 1, 101-160.

Quatermain, L. B. (1963) (Revised 1964) The Balleny Islands -
    a descriptive and historical outline. Antarctic Division,
    D.S.I.R. Wellington 42p.

Reid, M. J., Gancarz, A. J. and Albee, A. L. (1973) Constrained
    least-squares analysis of petrologic problems with an
    application to Lunar sample 12040. Earth Planet. Sci.
    Lett. 17, 433-445.

Riddolls, B. W. and Hancox, G. T. (1968) The geology of the upper
    Mariner Glacier region, north Victoria Land, Antarctica.
    N.Z. J. Geol. Geophys. 11, 881-899.

Ridley, W. I. (1970) The petrology of the Las Canadas volcanoes,
    Tenerife, Canary Islands. Contr. Mineral. and Petrol. 26,
    124-160.

Ridley, W. I., Rhodes, J. M., Reid, A. M., Jakes, P., Shih, C.
    and Bass, M. N. (1974) Basalts from Leg 6 of the Deep-Sea
    Drilling Project. J. Petrol. 15, 140-159.

Riley, J. P. (1958) Simultaneous determination of water and
    carbon dioxide in rocks and minerals. Analyst 83, 42-49.

Ringwood, A. E. (1966) The chemical composition and origin of the earth. In "Advances in Earth Sciences" (ed. P. M. Hurley). The M.I.T. Press, Cambridge, Mass., 287-356.

Roeder, P. L. (1974) Activity of iron and olivine solubility in basaltic liquids. Earth Planet. Sci. Lett. 23, 397-410.

Roeder, P. L. and Emslie, R. F. (1970) Olivine-liquid equilibrium. Contr. Mineral. and Petrol. 29, 275-289.

Ross, J. (1847) Voyage to the southern seas (Vol. 1). John Murray, London.

Roy, S. D., Frey, F. A. and Green, D. H. (1975) Models for alkaline basalt petrogenesis. Trans. Amer. Geophys. Un. (EOS) 56, 483-484.

Saggerson, E. P. and Williams, L.A.J. (1964) Ngurumanite from southern Kenya and its bearing on the origin of rocks in the northern Tanganyika alkaline district. J. Petrol. 5, 40-81.

Sato, M. and Moore, J. G. (1973) Oxygen and sulphur fugacities of magmatic gases directly measured in active vents of Mount Etna. Phil. Trans. R. Soc. Lond. A. 274, 137-146.

Schmincke, H-U. (1973) Magmatic evolution and tectonic regime in the Canary, Madeira, and Azores Island Groups. Geol. Soc. Amer. Bull. 84, 633-648.

Schwarzer, R. R. and Rogers, J.J.W. (1974) A worldwide comparison of alkali olivine basalts and their differentiation trends. Earth Planet. Sci. Lett. 23, 286-296.

Scott, P. W. (1969) Pyroxenes from the Tenerife volcanic suite (Abstract). IAVCEI Symposium, Oxford, England.

Shapiro, L. and Brannock, W. W. (1962) Rapid analysis of silicate, carbonate and phosphate rocks. U.S. Geol. Survey Bull. 1144-A.

Shaw, D. M. (1970) Trace element fractionation during anatexis. Geochim. Cosmochim. Acta 34, 237-243.

Shimizu, N. and Arculus, R. J. (1975) Rare earth element concentrations in a suite of basanitoids and alkali olivine basalts from Grenada, Lesser Antilles. Contr. Mineral. and Petrol. 50, 231-240.

Simkin, T. and Smith, J. V. (1970) Minor element distribution in olivine. J. Geology 78, 304-325.

Smith, W. C. (1954) The volcanic rocks of the Ross Archipelago. Brit. Antarctic ("Terra Nova") Exped. 1910, Nat. Hist. Rep., Geology 2, 1-107.

_____ (1959) The volcanic rocks of Cape Adare, south Victoria Land. Brit. Antarctic ("Terra Nova") Exped. 1910, Nat. Hist. Rep., Geology 2, 109-150.

Sorensen, H. (ed.) (1974) "The alkaline rocks" John Wiley and Sons. 622p.

Stephenson, D. (1972) Alkali clinopyroxenes from nepheline syenites of the South Qôroq Centre, south Greenland. Lithos 5, 187-201.

_____ (1974) Mn and Ca enriched olivines from nepheline syenites of the South Qôroq Centre, south Greenland. Lithos 7, 35-41.

Stewart, D. (1956) On the petrology of Antarctica. Geophys. Monograph Series (Amer. Geophys. Union) 1, 52-74.

Stormer, J. C. (1973) Calcium zoning in olivine and its relationship to silica activity and pressure. Geochim. Cosmochim. Acta 37, 1815-1821.

Stormer, J. C. and Carmichael, I.S.E. (1970) The Kudo-Weill plagioclase geothermometer and porphyritic acid glasses. Contr. Mineral. and Petrol. 28, 306-309.

Streckeisen, A. L. (1967) Classification and nomenclature of igneous rocks. Neues Jb. Miner. Abh. 107, 144-214.

Stuckless, J. S., Weiblen, P. W. and Schulz, K. J. (1974a) Magmatic evolution for the alkalic rocks of the Ross Island Area, Antarctica. (Abstract). Trans. Amer. Geophys. Un. (EOS) 55, 474.

Stuckless, J. S., Weiblen, P. W. and Goldich, S. S. (1974b) A petrogenetic model for the alkalic rocks from Ross Island area, Antarctica (Abstract). Dry Valley Drilling Project (Northern Illinois University) Bulletin 4, Paper 25.

Sun, S. S. and Hanson, G. N. (1974a) Genesis of Ross Island, Antarctica volcanic rocks based on rare earth element and Pb isotope studies. (Abstract). Trans. Amer. Geophys. (EOS) 55, 474.

_____ (1974b) Genesis of McMurdo volcanics on Ross Island. Antarctic J. of the U.S. 9, 234-236.

_____ (1974c) Genesis of Ross Island, Antarctica volcanic rocks based on rare earth element and Pb isotope studies (Abstract). Dry Valley Drilling Project (Northern Illinois University) Bulletin 4, Paper 26.

_____ (1975) Origin of Ross Island basanitoids and limitations upon the heterogeneity of mantle sources for alkali basalts and nephelinites. Contr. Mineral. and Petrol. 52, 77-106.

Thompson, R. N. (1972) The 1-atmosphere melting patterns of some basaltic volcanic series. Amer. J. Sci. 272, 901-932.

_____ (1973a) Titanian chromite and chromian titanomagnetite from a Snake River Plain basalt, a terrestrial analogue to lunar spinels. Amer. Mineral. 58, 826-830.

_____ (1973b) One-atmosphere melting behaviour and nomenclature of terrestrial lavas. Contr. Mineral. and Petrol. 41, 197-204.

_____ (1974) Some high-pressure pyroxenes. Min. Mag. 39, 768-87.

Thompson, R. N., Esson, J. and Dunham, A. C.(1972) Major element chemical variation in the Eocene lavas of the Isle of Skye, Scotland. J. Petrol. 13, 219-253.

Thomson, J. A. (1916) Report on the inclusions of the volcanic rocks of the Ross Archipelago (with Appendix by F. Cohen). Rep. Brit. Antarctic Exped. 1907-9, Geol. 2, 129-151.

Thornton, C. P. and Tuttle, O. F. (1960) Chemistry of igneous rocks. I. Differentiation index. Amer. J. Sci. 258, 664-684.

Tilley, C. E. and Thompson, R. N. (1972) Melting relations of some ultra alkali volcanics. Geol. J. 8, 65-70.

Tilley, C. E., Yoder, H. S. and Schairer, J. F. (1965) Melting relations of volcanic tholeiite and alkali rock series. Ann. Rept. Geophys. Lab. (Carnegie Inst. Yrbk. 64), 69-82.

Toulmin, P. III and Barton, P. B., Jr (1964) A thermodynamic study of pyrite and pyrrhotite. Geochim. Cosmochim. Acta 28, 641-671.

Treves, S. B. (1962) The geology of Cape Evans and Cape Royds, Ross Island, Antarctica. Geophys. Monograph Series (Amer. Geophys. Union) 7, 40-46.

_____ (1967) Volcanic rocks from the Ross Island, Marguerite Bay, and Mt Weaver areas, Antarctica. In Nagata, T. ed. Proceedings of the Symposium on Pacific-Antarctic sciences. JARE sci. Rep., Special Issue, No.1, 136-149.

Treves, S. B. and Ali, M. Z. (1974) Geology and petrography of DVDP 1, Hut Point Peninsula, Ross Island, Antarctica (Abstract). Dry Valley Drilling Project (Northern Illinois University) Bulletin 4, Paper 29.

Treves, S. B. and Kyle, P. R. (1973a) Geology of DVDP 1 and 2, Hut Point Peninsula, Ross Island, Antarctica. Dry Valley Drilling Project (Northern Illinois University) Bulletin 2, 11-82.

_____ (1973b) Geology of boreholes 1 and 2, Hut Point Peninsula, Antarctica. Antarctic J. of the U.S. 8, 157-159.

_____ (1973c) Renewed volcanic activity of Mt Erebus, Antarctica. Antarctic J. of the U.S. 8, 156.

Tyler, R. C. and King, B. C. (1967) The pyroxenes of the alkaline igneous complex of eastern Uganda. Mineral. Mag. 36, 5-21.

Uchimizu, M. (1966) Geology and petrology of alkali rocks from Dogo, Oki Islands. Journal Faculty of Science, University of Tokyo Sec. II 16, 85-159.

Vella, P. P. (1969) Surficial geological sequence, Black Island and Brown Peninsula, McMurdo Sound, Antarctica. N.Z. J. Geol. Geophys. 12, 761-770.

Verhoogen, J. (1962) Distribution of titanium between silicates and oxides in igneous rocks. Amer. J. Sci. 28, 91-136.

Wager, L. R. and Brown, G. M. (1967) Layered igneous rocks. Oliver and Boyd, Edinburgh, London. 588p.

Walker, G.P.L. (1973) Lengths of lava flows. Phil. Trans. Roy. Soc. Lond. A.274, 107-118.

Warren, G. (1969) Geology of the Terra Nova Bay - McMurdo Sound area, Victoria Land. "Geological Map of Antarctica 1:1,000,000" Antarctic Map Folio Series (Bushnell, V. C. ed.) American Geographical Society, New York.

Waterhouse, B. C. (1965) Western Ross Sea Balleny Islands expedition: January-March, 1965. N.Z. Geol. Survey (unpublished report).

Watkins, N. D. and Haggerty, S. E. (1967) Primary oxidation variation and petrogenesis in a single lava. Contr. Mineral. and Petrol. 15, 251-271.

Webb, P. N. (1972) Wright Fjord, Pliocene marine invasion of an Antarctic dry valley. Antarctic J. of the U.S. 7, 227-234.

Weiblen, P. W., Mudrey, M. G., Stuckless, J. S. and Schulz, K. J. (1974a) Reaction relations of clinopyroxenes in alkali basalts of the Ross Is. Area Antarctica. (Abstract). Trans. Amer. Geophys. Un. (EOS) 55, 475.

Weiblen, P. W., Schulz, K. J., Stuckless, J. S., Hunter, W. C. and Mudrey, M. G. (1974b) Clinopyroxenes in alkali basalts from the Ross Island area, Antarctica: Clues to stages of magma crystallization. (Abstract). Dry Valley Drilling Project (Northern Illinois University) Bulletin 4, Paper 33.

Wellman, H. W. (1964) Later geological history of Hut Point Peninsula, Antarctica. Trans. Roy. Soc. N.Z. 2, 149-154.

Wilkinson, J.F.G. (1957) The clinopyroxenes of a differentiated teschenite sill near Gunnedah, New South Wales. Geol. Mag. 94, 123-134.

Wilkinson, J.F.G. (1974) The mineralogy and petrography of alkali basaltic rocks. In "The alkaline rocks" (ed. H. Sorensen) John Wiley and Sons, p.67-95.

Wright, T. L. (1974) Presentation and interpretation of chemical data for igneous rocks. Contr. Mineral. and Petrol. 48, 233-248.

Wright, T. L. and Doherty, P. C. (1970) A linear programming and least squares computer method for solving petrologic mixing problems. Geol. Soc. Amer. Bull. 81, 1995-2008.

Wyllie, P. J. (1970) Ultramafic rocks and the upper mantle. Mineral. Soc. Amer. Special Paper 3, 3-32.

_____ (1971) "The Dynamic Earth" Wiley, New York. 416p.

Yagi, K. (1953) Petrochemical studies on the alkalic rocks of the Morotu district, Sakhalin. Bull. Geol. Soc. Amer. 64, 769-810.

_____ (1962) A reconnaissance of the systems acmite-diopside and acmite-nepheline. Ann. Rept. Geophys. Lab. (Carnegie Inst. Yrbk. 61), 98-99.

_____ (1966) The system acmite-diopside and its bearing on the stability relations of natural pyroxenes of the acmite-hedenbergite-diopside series. Amer. Mineral. 51, 976-1000.

Yagi, K., Hariya, Y., Onuma, K. and Fukushima, N.(1975) Stability relation of kaersutite. Jour. Fac. Sci. Hokkaido Univ., Ser. IV, 16, 331-342.

Yagi, K. and Onuma, K. (1967) The join $CaMgSi_2O_6$-$CaTiAl_2O_6$ and its bearing on the titanaugites. J. Fac. Sci. Hokkaido Univ., Ser. IV, 8, 463-483.

Yoder, H. S. and Tilley, C. E. (1962) Origin of basaltic magmas: An experimental study of natural and synthetic rock systems. J. Petrol. 3, 342-532.

Zielinski, R. A. (1975) Trace element evaluation of a suite of rocks from Reunion Island, Indian Ocean. Geochim. Cosmochim. Acta 39, 713-734.

EVANS NEVE

Cone 7
684 • • 682
683

Crater 4
679-81 678 • 677
676 •

Crater 5
685 •
686

Small basaltic cone ▲

Cliffs with slickensides ▲ 694-99
693
706 • TAYGETE CONE
0·003 my 700

707
Crater 3
689 •

Crater 2

661-2
0·01 m •

674-5 •
673 •

704 •
705 • Crater 1

690-1
692 Nepheline benmoreite dike

688 •

Cone 6
687 •

ALEYONE CONE
701-2 ▲
703 •

Cone 4 663 •
MT PLEIONES
3020 m
Cone 2
671 •
0·02 my
Cone 3
670 •
669 •

664-5

Cone 1
668,
672

666 •
0·04 my

MT ATLAS
3040 m

Cone 5

667

▦ Area of hydrothermal alteration

• 703 VUW sample number

0·04 my K-Ar age

Moraine

0   km (approx.)   2